



Technische Universität München
Fakultät für Chemie | Lehrstuhl für Organische Chemie II

Probing the catalytic activity and oligomeric assembly of *S. aureus* ClpXP

MARKUS LAKEMEYER

Vollständiger Abdruck der von der Fakultät für Chemie der Technischen Universität
München zur Erlangung des akademischen Grades eines

Doktors der Naturwissenschaften (Dr. rer. nat.)

genehmigten Dissertation.

Vorsitzender: Prof. Dr. Michael Groll
Prüfer der Dissertation: 1. Prof. Dr. Stephan A. Sieber
2. Prof. Dr. Kathrin Lang
3. Prof. Dr. Markus Kaiser (schriftliche Beurteilung)
Prof. Dr. Franz Hagn (mündliche Prüfung)

Die Dissertation wurde am 23.10.2018 bei der Technischen Universität München eingereicht
und durch die Fakultät für Chemie am 08.11.2018 angenommen.



Technische Universität München
Fakultät für Chemie | Lehrstuhl für Organische Chemie II

Probing the catalytic activity and oligomeric assembly of *S. aureus* ClpXP

MARKUS LAKEMEYER

Vollständiger Abdruck der von der Fakultät für Chemie der Technischen Universität
München zur Erlangung des akademischen Grades eines

Doktors der Naturwissenschaften (Dr. rer. nat.)

genehmigten Dissertation.

FÜR MEINE FREUNDE
FÜR MEINE FAMILIE

ABSTRACT

Antibiotic resistance poses a serious threat to human health and novel antibacterial strategies are urgently needed. The ClpXP protease is a global regulator of virulence in a variety of microorganisms, including *Staphylococcus aureus*. Hence, ClpXP is a promising target for antivirulence approaches. The protease consists of a barrel-like core, that is formed by 14 ClpP protomers. Hexameric ClpX chaperones stack on top of ClpP, resulting in the proteolytically active complex. The molecular basis of the ClpP-ClpX interaction, however, is only partially understood and efficient inhibitors of ClpXP are lacking.

This thesis provides novel chemical tools to manipulate the activity of *S. aureus* ClpXP and to study its oligomeric assembly. Phenyl esters are novel ClpXP inhibitors that were identified by a high-throughput screen of 137,000 compounds. Phenyl esters bind covalently to the active site of ClpP, and surpass previous β -lactone inhibitors in potency and selectivity. Extensive SAR studies led to compounds with improved stability, and identified a critical methyl position in the inhibitor structure. Depending on its stereochemistry, this “stereogenic switch” either retained the tetradecameric ClpP state or induced de-oligomerization into heptameric species.

Oxazoles are the second class of ClpP inhibitors identified by the high-throughput screen. A co-crystal structure of one oxazole compound and ClpP gave insights into an unprecedented binding mode. While the initial hit was only moderately potent in reducing the activity of ClpP, chemical synthesis led to improved inhibitors with low-micromolar IC_{50} -values. Additional studies revealed that ClpX exerts conformational control over ClpP, which revoked inhibition of the ClpXP complex.

Lastly, second-generation, amino acid-based phenyl esters were developed. Systematic screening of amino acids in P1 and P2 position of dipeptide phenyl esters revealed compounds that surpassed the potency of previous ClpXP inhibitors. Additionally, some derivatives stimulated, rather than inhibited ClpXP-mediated proteolysis. The compounds and various techniques were applied to probe the oligomerization of ClpP and ClpX as well as their affinity towards each other. In this regard, a novel ClpXP complex with an unprecedented stoichiometry was found, and its potential biological function was evaluated. Overall, the insights obtained set the foundation for future inhibitor design and will facilitate studies towards the cellular function of ClpXP.

ZUSAMMENFASSUNG

Antibiotikaresistenzen sind eine wesentliche Gefahr für die humane Gesundheit und neue antibakterielle Strategien werden dringend benötigt. Die ClpXP-Protease ist in vielen Mikroorganismen, darunter *Staphylococcus aureus*, ein globaler Regulator der Virulenz. Daher ist ClpXP ein vielversprechendes Angriffsziel für Antivirulenz-Ansätze. Die Protease besitzt eine fassartige Struktur, die aus 14 ClpP-Protomeren aufgebaut ist. Hexamere ClpX-Chaperone stapeln sich auf ClpP, wodurch der proteolytisch aktive Komplex gebildet wird. Die molekularen Grundlagen der ClpP-ClpX-Interaktion sind jedoch nur teilweise verstanden und effiziente Inhibitoren für ClpXP fehlen.

In dieser Dissertation werden neue chemische Schlüsselverbindungen vorgestellt, mit denen die Aktivität und die Oligomerisierung von *Staphylococcus aureus* ClpXP untersucht wurden. Phenylester sind neuartige ClpXP-Inhibitoren, die mithilfe eines High-Throughput Screens (HTS) aus 137.000 Verbindungen identifiziert wurden. Phenylester binden kovalent an das aktive Zentrum von ClpP und übertreffen β -Lacton-Inhibitoren bezüglich Potenz und Selektivität. Ausgiebige Studien zur Struktur-Aktivitäts-Beziehung führten zu neuen Verbindungen mit verbesserter Stabilität. Außerdem wurde eine entscheidende Methylgruppe in der Inhibitor-Struktur identifiziert. Abhängig von der Stereochemie dieses "stereogenen Schalters" wurde der tetradekamere Zustand von ClpP beibehalten oder die De-Oligomerisierung in heptamere Spezies induziert.

Oxazole sind die zweite Klasse von ClpP-Inhibitoren, die mittels des HTS gefunden wurden. Die Co-Kristallstruktur eines Oxazols mit ClpP ermöglichte einen direkten Einblick in einen neuartigen Bindungsmodus. Während die initiale Hit-Verbindung nur moderat aktiv war, konnten durch chemische Synthese verbesserte Inhibitoren mit IC_{50} -Werten im mikromolaren Bereich erhalten werden. Weiterführende Studien zeigten, dass ClpX konformationelle Kontrolle auf ClpP ausübt, weshalb der gesamte ClpXP-Komplex nicht inhibiert werden konnte.

Zuletzt wurde eine zweite Generation von Aminosäure-basierten Phenylestern entwickelt. Die systematische Untersuchung von Aminosäuren in P1 und P2-Position von Dipeptid-Phenylestern resultierte in Verbindungen, die die Potenz von früheren ClpXP-Inhibitoren übertrafen. Zusätzlich wurden Derivate gefunden, die die ClpXP

basierte Proteolyse aktivierten, statt zu inhibieren. Die Schlüsselverbindungen und zahlreiche Methoden wurden anschließend angewendet um die Oligomerisierung von ClpP und ClpX zu untersuchen und um zudem ihre Affinität zueinander zu bestimmen. In diesem Zusammenhang wurde ein ClpXP-Komplex mit beispielloser Stöchiometrie identifiziert und eine potentielle biologische Funktion des neuen Komplexes evaluiert.

Die in dieser Arbeit gewonnenen Erkenntnisse legen den Grundstein für zukünftige Inhibitor-Entwicklungen und werden außerdem Untersuchungen zur zellulären Funktionsweise von ClpXP unterstützen.

Parts of this thesis have been published in peer-reviewed journals as listed below:

Research articles

Phenyl Esters Are Potent Inhibitors of Caseinolytic Protease P and Reveal a Stereogenic Switch for Deoligomerization

Mathias W. Hackl,[#] Markus Lakemeyer,[#] Maria Dahmen, Manuel Glaser, Axel Pahl, Katrin Lorenz-Baath, Thomas Menzel, Sonja Sievers, Thomas Böttcher, Iris Antes, Herbert Waldmann, and Stephan A. Sieber
J. Am. Chem. Soc. **2015**, 137, 8475–8483

Reversible Inhibitors Arrest ClpP in a Defined Conformational State that Can Be Revoked by ClpX Association

Axel Pahl,[#] Markus Lakemeyer,[#] Marie-Theres Vielberg,[#] Mathias W. Hackl, Jan Vomacka, Vadim S. Korotkov, Martin L. Stein, Christian Fetzter, Katrin Lorenz-Baath, Klaus Richter, Herbert Waldmann, Michael Groll, and Stephan A. Sieber
Angew. Chem. Int. Ed. **2015**, 54, 15892–15896

[#]These authors contributed equally to this work.

Review article

Thinking Outside the Box – Novel Antibacterials To Tackle the Resistance Crisis

Markus Lakemeyer, Weining Zhao, Franziska A. Mandl, Peter Hammann, Stephan A. Sieber
Angew. Chem. Int. Ed. **2018**, 57, 14440–14475.

Research topics that are not covered in this thesis:

My individual contributions are described under the respective projects.

Quantitative map of β -lactone induced virulence regulation

Joanna Krysiak,[#] Matthias Stahl,[#] Jan Vomacka,[#] Christian Fetzer, Markus Lakemeyer,
Anja Fux, Stephan A. Sieber

J. Proteome Res. **2017**, 16, 1180–1192

Synthesis of β -lactone E2, and analytical activity-based protein profiling in
Staphylococcus aureus.

Design and synthesis of tailored human caseinolytic protease P inhibitors

Thomas F. Gronauer, Melanie M. Mandl, Markus Lakemeyer, Mathias W. Hackl,
Vadim S. Korotkov, Johanna Pachmayr, Stephan A. Sieber

Chem. Comm. **2018**, 54, 9833–9836.

Evaluation of compound stability in plasma, and activity assays for *Staphylococcus aureus* ClpP.

[#]These authors contributed equally to this work.

Parts of this thesis have been presented at conferences and workshops:

Gordon Research Seminar and Conference: High Throughput Chemistry & Chemical Biology

June 13 - June 19, 2015, New London (NH), USA

poster presentation

Doktorandenforum der Studienstiftung des deutschen Volkes

April 25 - April 28, 2016, Berlin, Germany

oral presentation

Activity-based protein profiling and bioorthogonal chemistry

April 19 - April 21, 2017, Leiden, The Netherlands

oral presentation

Gordon Research Seminar and Conference: High Throughput Chemistry & Chemical Biology

June 24 - June 30, 2017, Andover (NH), USA

oral and poster presentation

Helmholtz Drug Discovery Conference (HDDC)

April 26 - April 27, 2018, Neuberberg, Germany

poster presentation

SwitchSENSE User Meeting (Dynamic Biosensors)

June 06 - June 08, 2018, Munich, Germany

oral presentation

Contents

I Scientific Background

1 Introduction	3
1.1 The antibiotic crisis	4
1.1.1 History of antibiotic resistance	4
1.1.2 Antivirulence as an alternative antibacterial approach	5
1.2 Targeting ClpXP-regulated virulence of <i>Staphylococcus aureus</i>	6
1.2.1 Pathogenicity of <i>Staphylococcus aureus</i> (<i>S. aureus</i>)	7
1.2.2 The role of the ClpXP protease in the regulation of virulence	8
1.2.3 Structure and function of <i>S. aureus</i> ClpXP	9
1.2.4 Chemical modulators of ClpXP's activity	13
1.3 References	16

II Research

2 Phenyl esters are potent inhibitors of caseinolytic protease P and reveal a stereogenic switch for deoligomerization	25
3 Reversible inhibitors arrest ClpP in a defined conformational state that can be revoked by ClpX association	39
4 Amino acid-based phenyl esters as chemical tools for inhibition, activation and disintegration of the ClpXP protease	49
4.1 Introduction and objective	50
4.2 Results and discussion	51
4.2.1 Structure-activity relationship studies	51
4.2.2 A ClpXP complex with an unprecedented stoichiometry	58
4.2.3 Towards a biochemical function of de-oligomerization	63
4.3 Conclusion and outlook	65

4.4	Supporting figures	67
4.5	Author contributions	68
4.6	References	68
5	Research conclusion and outlook	71
 III Review		
6	Thinking outside the box – novel antibacterials to tackle the resistance crisis	77
 IV Appendix		
7	Experimental Section for Chapter 4	119
7.1	Chemical synthesis	120
7.1.1	Materials and methods	120
7.1.2	Synthetic protocols	121
7.2	Biochemical methods	154
7.2.1	Protein purification	154
7.2.2	Intact-protein mass spectrometry	156
7.2.3	<i>In vitro</i> activity assays	157
7.2.4	Analytical size-exclusion chromatography	158
7.2.5	Negative-stain electron microscopy	158
7.2.6	Determination of dissociation constants by swichSENSE	159
7.2.7	Intact-protein MS-based pulldown-assay	160
7.3	References	161
7.4	NMR spectra	162

Part I

SCIENTIFIC BACKGROUND



Introduction

1.1 THE ANTIBIOTIC CRISIS

In this introduction, the historical background of the current antibiotic crisis, its implications for today's medicine and methods for overcoming antibiotic resistance are discussed. For a comprehensive overview, the interested reader is kindly referred to Chapter 6 which reviews interdisciplinary approaches to address the antibiotic crisis.

1.1.1 HISTORY OF ANTIBIOTIC RESISTANCE

The spread of bacteria that are resistant to antibiotics is a growing problem to humanity. Apart from cancer, infection is the only disease that has been able to evolve resistance to chemotherapy. Importantly, pathogens not only develop their own resistances, but also borrow resistance genes from environmental organisms. Infections caused by resistant bacteria therefore threaten not only individuals but societies.^[1]

For bacterial infections, the groundbreaking discovery of penicillin by Alexander Fleming in 1928^[2] ushered in a new era. Historically uncontrollable and deadly infections were largely relegated to mild and conveniently treatable illnesses.^[3] In the following golden age of antibiotics (1940-1960s), numerous potent drugs were discovered from natural product screenings, and bacterial infections were easily contained with effective and low-priced medicine.^[4] Since then, antibiotic treatment has saved millions of lives worldwide. Over the last few years, however, society's most powerful weapons against bacterial infections are steadily losing efficacy. It is estimated that annually two million people in the United States suffer from largely untreatable infections caused by antibiotic-resistant bacteria, resulting in 23,000 fatalities.^[5] The world health organization (WHO) has recently even issued a warning concerning the current trajectory towards a post-antibiotic era.^[6]

Microorganisms produce a variety of antibiotic compounds in order to compete with their environmental opponents. Bacterial resistance has always been an expedient to succeed in this everlasting battle, and it far precedes the first therapeutic application of an antibiotic. Resistance is inherently connected to the antibiotic mode of action, *e.g.* the disruption of essential biological pathways that will eventually kill the pathogen. Therefore, the survival of these organisms that have evolutionarily found a way to evade the selec-

tive pressure is promoted. The short generation time of bacteria, their large population sizes, and their ability to horizontally interchange genes with environmental organisms make antibiotic resistance that predominant. In addition, current antibiotics only address a small selection of bacterial targets, namely the biosynthesis of (i) proteins, (ii) DNA/RNA, (iii) the cell wall, and (iv) folate. Alternatively, antibiotics act by disrupting bacterial membranes. Once a resistance is acquired, similarly acting drugs therefore often also lose their antibacterial effect.

Tragically, already from the beginning of antibiotic therapy, humanity largely promoted the development of resistances. Antibiotics were prescribed for patients with symptoms of an infection, regardless of whether it was bacterial or viral (for the latter antibiotics are ineffective). Patients stopped taking the drug prior to finishing the whole regimen, and hygiene in hospitals was at a lower standard. Very soon, antibiotics additionally became attractive in livestock feed as an inexpensive means to accelerate animal growth.^[7] Presently, the consequences of these practices are being realized by a spread of resistant bacteria not only in hospitals, but also in the community.

While there has been a rapid increase in multi-resistant bacterial strains, the number of novel antibiotics for clinical applications is low with only two new classes introduced in the past 20 years.^[8] The reasons for this discrepancy are manifold and include regulatory and economic aspects. More importantly, the identification of new antibiotics has become a substantial hurdle as natural product screenings, traditionally the richest source for new antibiotics, most frequently fail to discover novel chemical entities.^[4] In this regard, anti-infective research needs to devise alternative measures to manipulate pathogens using unprecedented mechanisms.

1.1.2 ANTIVIRULENCE AS AN ALTERNATIVE ANTIBACTERIAL APPROACH

Humans live in strong symbiosis with trillions of commensal microorganisms, which inhabit, for example, the skin and the digestive system, and are indispensable for our well-being.^[9] Unfortunately, not all microbes are this peaceful. To invade the host and to circumvent or evade the host immune system, pathogenic bacteria use an arsenal of virulence factors, which include toxins, adhesins or destructive enzymes.^[10] Bacteria are able to communicate with each other and determine their population density by using

small molecules in a process called quorum sensing. When in low numbers, pathogens are nonvirulent and are thereby able to remain undetected by the immune system. Once having reached a critical population, the pathogens use quorum sensing to coordinate the gene expression of virulence factors, and subsequently change over to form a joint attack.^[11,12]

Antivirulence approaches focus on manipulating these elaborate mechanisms by blocking bacterial communication and disposing of the harmful chemical weapons. Pathogens are thus rendered harmless without being killed. Antivirulence is a rather long-known concept. Already in the 1880s, von Behring and Shibasaburo developed antiserum therapies to neutralize bacterial toxins for the treatment of diphtheria and tetanus.^[13,14] Considering the current lack of novel antibacterials, antivirulence approaches have experienced a resurgence over the last few years. As the pathogens are not directly killed, it is at debate that antivirulence exerts a lower selective pressure over the development of resistances. Therefore, potential antivirulence agents might have an increased period of therapeutic efficacy, and could reduce the permanent need for novel antibacterial drugs. Additionally, due to distinct virulence mechanisms within different bacterial species, antivirulence strategies can be designed to specifically target pathogenic bacteria, while causing less collateral damage to the commensal microbiota.^[11,15]

1.2 TARGETING CLPXP-REGULATED VIRULENCE OF *STAPHYLOCOCCUS AUREUS*

In view of the emerging threat of antibiotic resistance, the WHO released a top priority list of 12 bacterial organisms, for which novel therapeutics are urgently needed. Among those pathogens, resistant *Staphylococcus aureus* (*S. aureus*) strains were ranked with “high priority.”^[16] The methicillin-resistant *S. aureus* (MRSA) has recently gained notoriety, as it is responsible for recurrent infections that are very difficult to treat.

1.2.1 PATHOGENICITY OF *STAPHYLOCOCCUS AUREUS* (*S. AUREUS*)

S. aureus is a Gram-positive bacterium that appears as a grape-like cluster of sphere-shaped cells in growing cultures. When incubated on agar plates, *S. aureus* produces colonies that turn buff-golden over time (due to the production of the pigment staphyloxanthin), which gave the pathogen its binomial name (*staphyle* = Greek for “grape-cluster berry”, *aureus* = Latin for golden).^[17]

S. aureus is an opportunistic pathogen that colonizes the skin and the mucosal microbiome in about 30% of the human population.^[18,19] The physical barrier of the skin usually holds off the pathogen efficiently. Upon breach of the host’s defenses, however, *S. aureus* can invade the body, dissimilate, and cause severe conditions, such as endocarditis, osteomyelitis, toxic shock syndrome or sepsis.^[20] In addition, the pathogen is able to form biofilms, which are robust, surface-attached encasements of bacterial cells in a biomolecular matrix. Biofilms are nearly inaccessible by the immune system and antibiotics, thus rendering the pathogen persistent. Prosthetic devices and other synthetic surfaces are especially prone to biofilm formation, which often results in difficult-to-treat, recalcitrant infections.^[20,21]

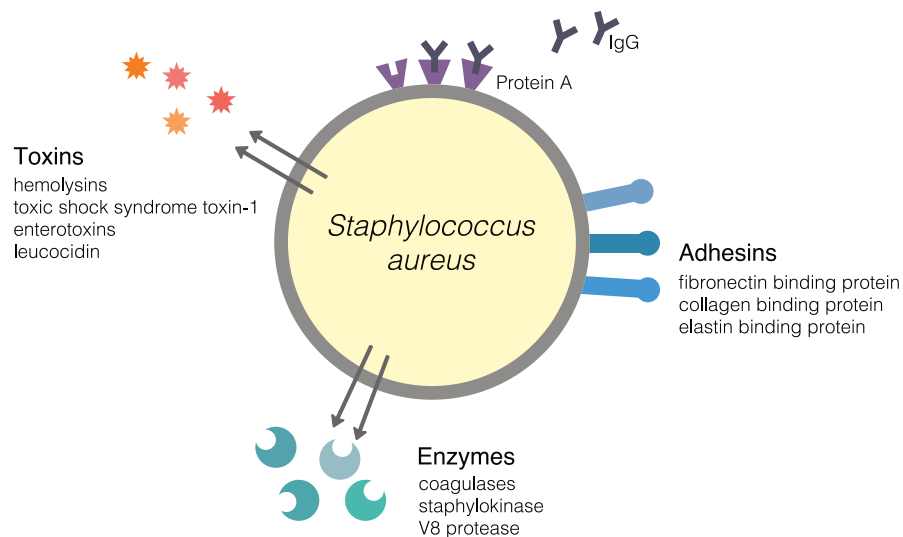


Figure 1.1. Schematic overview of representative membrane-bound and secreted virulence factors of *S. aureus*.

An extensive arsenal of virulence factors allows *S. aureus* to survive extreme conditions within the human host. Surface-associated proteins, like adhesins (*e.g.* fibrinogen-binding

proteins or clumping factors) bind to host extracellular matrix components (*e.g.* fibrinogen or collagen), and facilitate the internalization into host cells. Staphylococcal protein A (SpA), binds to the Fc region of immunoglobulins and thereby impedes opsonophagocytosis by neutrophils.^[22,23] Moreover, *S. aureus* secretes a variety of toxins, such as α -, β - and γ -hemolysins, which form pores in the membrane of host cells and trigger lysis.^[24,25] Further secreted virulence factors include, among others, additional toxins (*e.g.* toxic shock syndrome toxin-1) and exoenzymes (*e.g.* V8 protease) which all contribute to inflammation and cell death.^[23,26–28]

To efficiently apply this armamentarium during invasion of host tissue in a spatiotemporal manner, the expression of virulence factors is tightly controlled by a complex network of virulence regulators.^[23,29–31] The effective regulation and the plethora of virulence factors produced make *S. aureus* an emerging target for antivirulence therapies. Chapter 6 provides an overview of contemporary efforts to target virulence, not only in *S. aureus*, but for a variety of pathogens.

1.2.2 THE ROLE OF THE CLPXP PROTEASE IN THE REGULATION OF VIRULENCE

Proteolysis is a crucial element in eukaryotic and prokaryotic cells for various cellular functions, including homeostasis, stress response and virulence regulation. This process it is predominantly carried out by energy-dependent proteases. Targeting bacterial proteolysis has evolved to an emerging field for antibiotic and antivirulence strategies.^[32] In prokaryotes, a variety of ATP-dependent proteases are responsible for regulated protein degradation, including Lon,^[33,34] FtsH^[35] and HslUV.^[36,37] An additional member of this class is the caseinolytic protease complex (ClpXP), a structure involved in environmental adaptation and, more importantly, a key regulator of virulence in several pathogenic strains, including *S. aureus*,^[38–42] *Listeria monocytogenes*,^[43,44] and *Salmonella typhimurium*.^[45]

While a full understanding of the biochemical pathways that connect ClpXP to virulence is still lacking,^[46] the first animal studies have shown that small molecules targeting ClpXP-mediated virulence are indeed therapeutically valuable.^[47]

1.2.3 STRUCTURE AND FUNCTION OF *S. AUREUS* CLPXP

All Clp-containing degradation complexes share two functional elements: a barrel-like proteolytic core and one or two chaperone-units that act as caps of the former. The proteolytic core is formed by 14 ClpP protomers that are arranged into two heptameric rings that are stacked on top of each other. The catalytic residues (Ser⁹⁸-His¹²³-Asp¹⁷²) of each ClpP protomer are located within the sequestered space of the barrel. ClpP alone only shows moderate peptidase activity, as access to the active sites is limited to short peptides that are able to enter the barrel through axial pores with a diameter of 10 Å.^[48]

In order to exert its full proteolytic potential, ClpP associates with hexameric chaperones of the AAA+ (ATPases associated with various cellular activities) family. The chaperones recognize and unfold proteins marked for degradation and direct the proteins into the proteolytic chamber for digestion. In *S. aureus*, the two chaperones ClpX and ClpC are described to bind to one or both sides of the ClpP barrel, thereby forming active proteolytic complexes (ClpXP and ClpCP, respectively). Depending on the organisms, additional or different proteolytic ClpP complexes can be found (e.g. ClpAP or ClpEP).^[37,49]

Structural studies of *S. aureus* ClpP (SaClpP) have revealed several hotspots which are crucial for the heptamer-heptamer and protease-chaperone interactions. Until today, three distinct conformational states of wild-type *S. aureus* ClpP have been characterized, namely extended,^[48] compact,^[50] and compressed.^[51]

The extended form resembles the active, tetradecameric state in which the catalytic residues are assembled into a charge-relay system. Central α -helices in the handle region, called E-helices and antiparallel β -sheets (strands β_9) deviate from the head domain and form hydrogen bonds across the heptamer interface. Additionally, the so-called oligomerization sensor, located in the vicinity of the active site, interconnects the heptamers by a salt-bridge between the Arg¹⁷¹ of one ring and the Asp¹⁷⁰ of the adjacent heptamer (Figure 1.2a-d).^[48]

The compressed state, however, is catalytically inactive. The central E-helix is kinked and both the catalytic triad and the oligomerization sensor are misaligned (Figure 1.2e).^[51]

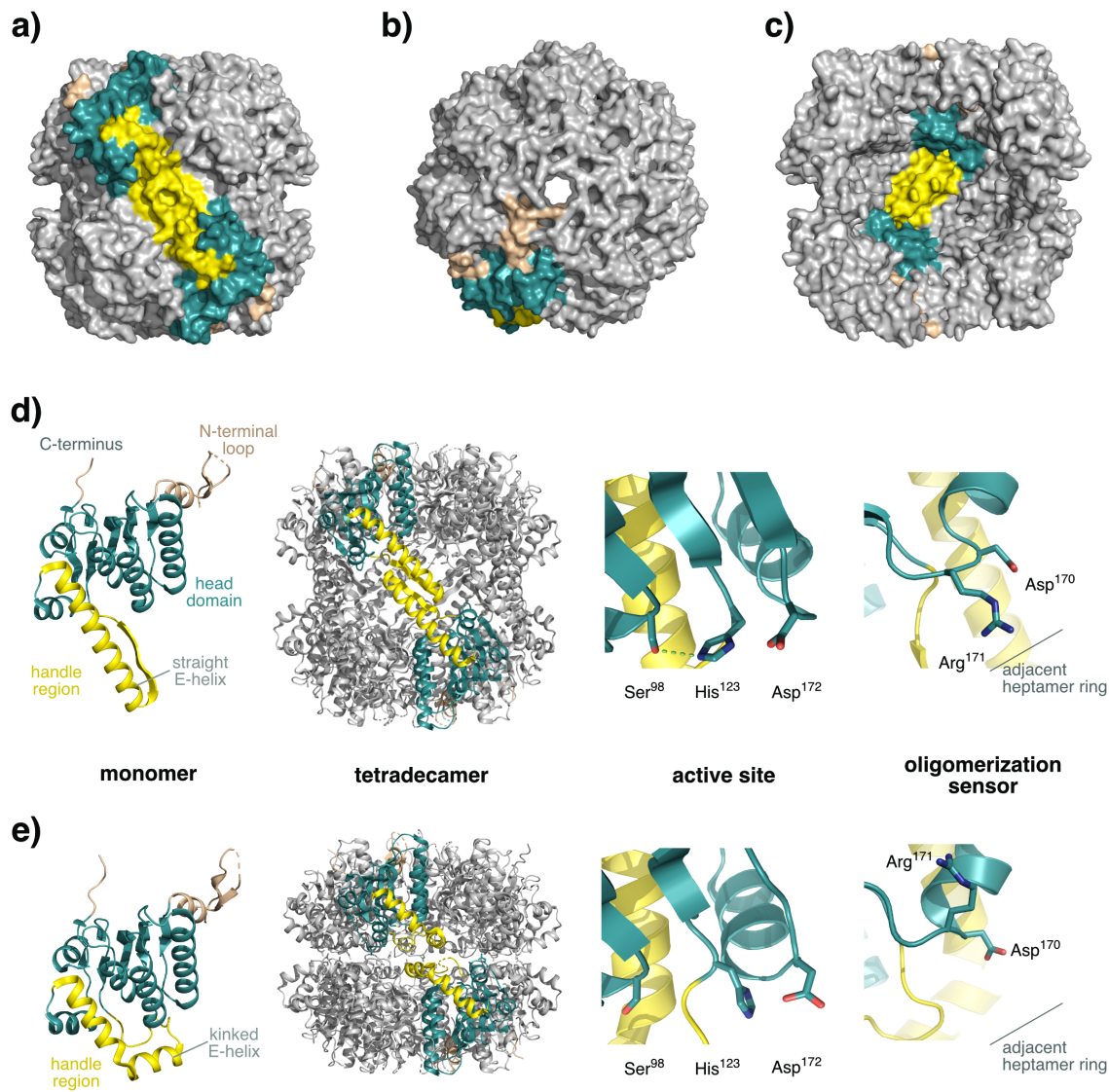


Figure 1.2. Insights into the structure of SaClpP in its catalytically active, extended state (a-d) (PDB ID: 3V5E)^[48] and (e) inactive, compressed form (PDB ID: 3QWD).^[51] a-c) Surface representations of extended ClpP in a) side- b) top- and c) profile-view. d-e) Comparison of functional hotspots: In the extended state, straight E-helices (colored in yellow) form well-defined interactions between the heptameric rings, but are kinked in the compressed state. Only the proper alignment of the catalytic triad and the oligomerization sensor residues result in a catalytically active complex.

A conserved hydrogen-bonding network links the geometry of ClpP's catalytic triad to the N-terminal loop segment in the apical area.^[51,52] Here, chaperones including ClpX bind to the barrel, resulting in a proteolytically active complex. Because the ClpX chaperone from *E. coli* is the best-characterized orthologue, it will be described here in detail.

Six protomers form an asymmetric ClpX ring with a diameter of 135 Å.^[53,54] Each subunit consists of an N-domain and an AAA+ module which is divided into a large and a small AAA+ domain (Figure 1.3a,b). The two AAA+ domains are connected by a short hinge region and together form the hexameric ring. Depending on the structure of the small domain, subunits can either adopt a loadable (L) or an unloadable (U) conformation.^[55,56] Only in L-subunits will nucleotides bind in a cleft, which is formed in the hinge region by conserved sequence motifs, including Walker A and Walker B. The Walker motifs are the motor of ClpX's hexameric conformational dynamics enabling ATP binding and hydrolysis.^[57] Already a single glutamate-to-alanine mutation in the Walker B motif (E185A) stalls ATP hydrolysis and leads to the formation of a static, ATP-bound conformation.^[58]

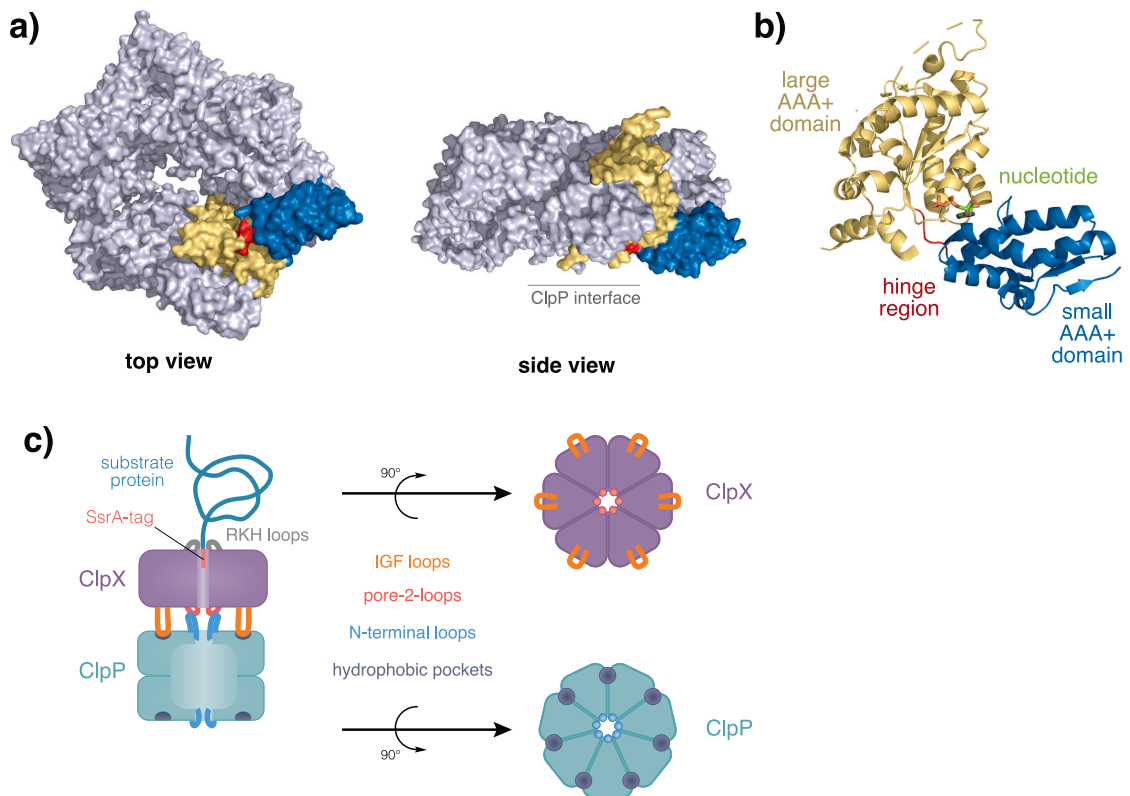


Figure 1.3. Structure of *E. coli* ClpX with a depleted N-domain (PBD ID: 3HWS).^[53] a) Top and side view of the hexameric chaperone structure. One ClpX protomer is highlighted in color. b) Structure of the ClpX monomer. The large and the small AAA+ domains are connected by the hinge region, which in the loadable position facilitates nucleotide binding. c) Schematic representation of the ClpP-ClpX interface with its characteristic hydrophobic interactions. Adapted from Martin *et al.*^[57]

The assembly of the full proteolytic ClpXP complex must overcome a symmetry mismatch between the heptameric ClpP rings and the hexameric ClpX chaperone. Because high-resolution structures of ClpXP have not been solved, a comprehensive understanding of this phenomenon does not exist. Nevertheless, crucial hydrophobic interaction hotspots between the apical sites of ClpP and ClpX have been identified. Conserved tripeptide IGF-loops of ClpX bind into clefts on the face of the ClpP barrel and are important for the ClpXP assembly.^[59,60] A second set of interactions is located at the axial pores of each ring: ClpP's flexible N-terminal loops, which in the absence of a chaperone act as a plug of the barrel, move up when ClpX is present. The N-terminal loops then bind to the pore-2 loops of ClpX, resulting in an axial channel (Figure 1.3c).^[57,61]

To avoid uncontrolled degradation, the proteolysis by ClpXP is highly regulated via limited access to the sequestered chamber.^[55] The N-domains of ClpX, flexibly tethered to the AAA+ ring, can bind adaptor proteins such as RssB and SspB which facilitate substrate recognition. Additionally, the N-domains can directly bind to selected substrates without adaptors, such as FtsZ and MuA.^[62-64] Importantly, ClpX alone, or the ensemble of ClpX and SspB, recognize proteins that are marked for degradation by a short SsrA-tag. This amino acid sequence is attached C-terminally to incomplete nascent proteins in order to rescue ribosomes stalled during translation.^[65-67]

Once recognized, conserved GYVG loops (pore-1-loops) in the axial channel unfold and translocate substrate proteins into the proteolytic chamber for degradation.^[68]

The catalytic activities of ClpP and ClpX are precisely coordinated. Binding of ClpP affects the rates of substrate unfolding and ATP hydrolysis by ClpX.^[57,59,69] The association of ClpX in turn boosts the peptidolytic activity of ClpP.^[70,71] Interestingly, in double-capped ClpX₆-ClpP₁₄-ClpX₆ complexes, the translocation of substrates at any given time appears to occur only from one of the two ClpX rings. This result indicates that the crosstalk between the distant chaperones is effective even through the full ClpP barrel.^[72]

1.2.4 CHEMICAL MODULATORS OF ClpXP'S ACTIVITY

Due to ClpXP's essential role in virulence regulation, various efforts have been made to manipulate its activity with the prospect of therapeutical application. These endeavors have been directed to the ClpP peptidase compartment, the ClpX chaperone or the interaction between the two.

In general, inhibition of ClpP has been focused on targeting the enzyme's active site. Peptide-based chloromethyl ketone^[73,74] and boronic acid^[75] inhibitors are able to bind to the catalytic site and thereby inhibit ClpP; however, the compounds hold only moderate selectivity. β -sultam compounds first covalently bind to the catalytic serine residue, and subsequently lead to the formation of a dehydroalanine unit by elimination.^[76]

The most studied class of ClpP inhibitors are β -lactones with aromatic or aliphatic chains, such as **E2**, **D3** and **U1** (Figure 1.4).^[77,78] The compounds covalently acylate the active site serine residues and form acyl-enzyme complexes of diverging durability. In *S. aureus*, a large hydrophobic S_I pocket is well-suited to accommodate the aliphatic side chains. Importantly, treatment of *S. aureus* with β -lactone compounds resulted in overall reduced virulence *in vitro* and *in vivo*, which was comparable to the phenotype of genetic ClpX and/or ClpP knockouts.^[46,47,78-80]

On the molecular level, application of β -lactones can either result in binding to all 14 active sites of ClpP while retaining the tetradecamer complex stoichiometry, or partial modification and disruption into heptameric ClpP species. In both cases, ClpP is catalytically inactive, and the proteolytic ClpXP complex can as well be inhibited at higher compound concentrations.^[48,70,76,81] Due to the low stability of the lactone moiety towards water and other biological nucleophiles, alternatives inhibitors of ClpP have been urgently sought.

The 5-arylmethylidenerhodanine **M21** (Figure 1.4) is a novel ClpP inhibitor that was recently identified by a reporter-strain based phenotypic high-throughput screen for compounds that reverse virulent *S. aureus* into its nonvirulent state.^[82] Treatment with the non-antibiotic compound suppressed the expression of multiple virulence factors in *S. aureus*. Further experiments revealed that the compound binds ClpP in a reversible manner with an IC₅₀ of about 40 μ M, while the closely-related compound, lacking the carboxylic acid moiety of **M21**, was inactive. Owing to several challenging properties,

including unspecific binding and photo-reactivity, rhodanine-based molecules, however, are generally considered to be pan assay interference compounds (PAINS). PAINS are often false positives in high-throughput screenings and therefore necessitate careful validation.^[83] Future studies are required to investigate the true therapeutic potential of **M21** as a selective ClpP inhibitor.

A very different approach to inhibit the ClpXP complex is undertaken by dihydrothiazepine compounds, such as **334**, which bind non-covalently to the ClpX chaperone, resulting in the disruption of the hexameric ring (Figure 1.4). In addition to its potent inhibition of the full ClpXP complex in the low- μ M range, treatment of *S. aureus* with the compound revealed a global reduction of virulence.^[84]

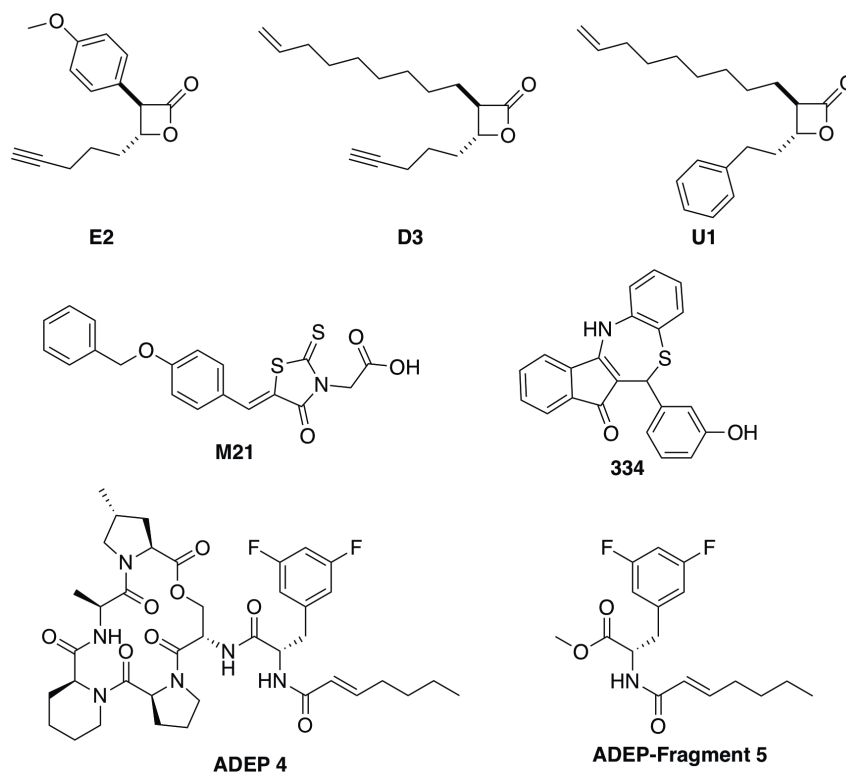


Figure 1.4. Small molecule modulators of ClpXP.

Aside from its potential as an antivirulence target, ClpP can also be addressed in an antibiotic fashion. Natural product acyldepsipeptides (ADEPs) act as activators, rather than inhibitors, of ClpP.^[85] ADEPs bind to the hydrophobic clefts in the apical face of ClpP, which are normally occupied by the IGF loops of ClpX. Binding leads to an opening of the axial pores by rearrangement of the N-terminal loops, allowing for the entrance of unfolded proteins into the proteolytic chamber. Additionally, the catalytic

activity of ClpP is enhanced.^[70] Unregulated proteolysis results in inhibition of cell division, and eventually cell death.^[86–88] Structure-activity-relationship (SAR) studies have revealed ADEPs with improved potency and stability, including **ADEP4** (Figure 1.4).^[89–91] Interestingly, small ADEP fragments, such as fragment **5** (Figure 1.4), were also sufficient for activating ClpP and showed antibacterial properties.^[92]

In summary, the insights provided emphasize that the ClpXP complex is a promising drug target for antibiotic and antivirulence therapy. However, additional research is urgently required in order to understand the molecular details of its catalytic function, which is a prerequisite for targeted inhibitor design.

This thesis provides novel chemical tools to manipulate the activity of ClpXP and to study its oligomeric assembly. In Chapter 2, phenyl esters are introduced as novel inhibitors for ClpP that surpass previous β -lactones in potency and selectivity. Chapter 3 describes the first noncovalent inhibitors of ClpP, the oxazoles. In Chapter 4, the manipulation of ClpXP by a second generation of amino acid-based phenyl esters is presented. Lastly, Chapter 6 gives a comprehensive overview of contemporary methods for the identification of novel antibacterials, and additionally discusses the current clinical pipeline.

1.3 REFERENCES

- [1] K. Lewis, *Biochemical Pharmacology* **2017**, *134*, 87–98.
- [2] A. Fleming, *Br. J. Exp. Pathol.* **1929**, *10*, 226–236.
- [3] S. E. Rossiter, M. H. Fletcher, W. M. Wuest, *Chem. Rev.* **2017**, *117*, 12415–12474.
- [4] K. Lewis, *Nat Rev Drug Discov* **2013**, *12*, 371–387.
- [5] Center for Disease Control and Prevention, *Antibiotic/Antimicrobial Resistance*, **2017**, <https://www.cdc.gov/drugresistance/index.html>, accessed: 10/15/2018.
- [6] World Health Organization, *Antimicrobial resistance: global report on surveillance*, **2014**, http://apps.who.int/iris/bitstream/handle/10665/112642/9789241564748_eng.pdf?sequence=1, accessed: 10/15/2018.
- [7] T. S. Crofts, A. J. Gasparrini, G. Dantas, *Nat. Rev. Microbiol.* **2017**, *15*, 422–434.
- [8] Center for Drug Evaluation, *New Drugs at FDA: CDER's New Molecular Entities and New Therapeutic Biological Products*, **2013**.
- [9] The Human Microbiome Project Consortium, *Nature* **2012**, *486*, 207–214.
- [10] A. Casadevall, L. A. Pirofski, *Infect. Immun.* **1999**, *67*, 3703–3713.
- [11] M. Garland, S. Loscher, M. Bogyo, *Chem. Rev.* **2017**, *117*, 4422–4461.
- [12] S. T. Rutherford, B. L. Bassler, *Cold Spring Harb Perspect Med* **2012**, *2*, a012427.
- [13] E. v. Behring, S. Kitasato, *Dtsch. Med. Wschr.* **1890**, 1113–1114.
- [14] F. Winau, R. Winau, *Microbes and Infection* **2002**, *4*, 185–188.
- [15] R. C. Allen, R. Popat, S. P. Diggle, S. P. Brown, *Nat. Rev. Microbiol.* **2014**, *12*, 300–308.
- [16] E. Tacconelli, E. Carrara, A. Savoldi, S. Harbarth, M. Mendelson, D. L. Monnet, C. Pulcini, G. Kahlmeter, J. Kluytmans, Y. Carmeli, M. Ouellette, K. Outtersson, J. Patel, M. Cavaleri, E. M. Cox, C. R. Houchens, M. L. Grayson, P. Hansen, N. Singh, U. Theuretzbacher, N. Magrini, WHO Pathogens Priority List Working Group, *Lancet. Infect. Dis.* **2018**, *18*, 318–327.
- [17] K. J. Ryan, C. G. Ray, J. C. Sherris, *Sherris Medical Microbiology: An Introduction To Infectious Diseases*, McGraw-Hill, New York, **2004**.

- [18] R. E. Williams, *Bacteriol. Rev.* **1963**, *27*, 56–71.
- [19] H. F. Wertheim, D. C. Melles, M. C. Vos, W. van Leeuwen, A. van Belkum, H. A. Verbrugh, J. L. Nouwen, *Lancet. Infect. Dis.* **2005**, *5*, 751–762.
- [20] S. Y. C. Tong, J. S. Davis, E. Eichenberger, T. L. Holland, V. G. Fowler, *Clin. Microbiol. Rev.* **2015**, *28*, 603–661.
- [21] K. B. Laupland, O. Lyytikäinen, M. Sgaard, K. J. Kennedy, J. D. Knudsen, C. Ostergaard, J. C. Galbraith, L. Valiquette, G. Jacobsson, P. Collignon, H. C. Schnheyder, for the International Bacteremia Surveillance Collaborative, *Clin. Microbiol. Infect.* **2013**, *19*, 465–471.
- [22] N. Harraghy, M. Hussain, A. Hagggar, T. Chavakis, B. Sinha, M. Herrmann, J.-I. Flock, *Microbiology* **2003**, *149*, 2701–2707.
- [23] G. Y. Liu, *Pediatric Research* **2009**, *65*, 71R–77R.
- [24] A. L. DuMont, V. J. Torres, *Trends in Microbiology* **2014**, *22*, 21–27.
- [25] B. K. Dhakal, M. A. Mulvey, *Cell Host and Microbe* **2012**, *11*, 58–69.
- [26] M. M. Dinges, P. M. Orwin, P. M. Schlievert, *Clin. Microbiol. Rev.* **2000**, *13*, 16–34.
- [27] K. Becker, G. Bierbaum, C. von Eiff, S. Engelmann, F. Götz, J. Hacker, M. Hecker, G. Peters, R. Rosenstein, W. Ziebuhr, *Int. J. Med. Microbiol.* **2007**, *297*, 483–501.
- [28] M. Fraunholz, B. Sinha, *Front Cell Infect Microbiol* **2012**, *2*, 43.
- [29] R. P. Novick, *Mol. Microbiol.* **2003**, *48*, 1429–1449.
- [30] M. Thoendel, J. S. Kavanaugh, C. E. Flack, A. R. Horswill, *Chem. Rev.* **2011**, *111*, 117–151.
- [31] A. L. Cheung, A. S. Bayer, G. Zhang, H. Gresham, Y.-Q. Xiong, *FEMS Immunol. Med. Microbiol.* **2004**, *40*, 1–9.
- [32] E. Culp, G. D. Wright, *J. Antibiot.* **2017**, *70*, 366–377.
- [33] V. Tsilibaris, G. Maenhaut-Michel, L. Van Melderren, *Res. Microbiol.* **2006**, *157*, 701–713.
- [34] E. Gur, R. T. Sauer, *Genes Dev.* **2008**, *22*, 2267–2277.

- [35] S. Langklotz, U. Baumann, F. Narberhaus, *Biochim. Biophys. Acta. Mol. Cell. Res.* **2012**, *1823*, 40–48.
- [36] S. Sundar, T. A. Baker, R. T. Sauer, *Protein Sci.* **2012**, *21*, 188–198.
- [37] R. T. Sauer, T. A. Baker, *Annu. Rev. Biochem.* **2011**, *80*, 587–612.
- [38] D. Frees, S. N. A. Qazi, P. J. Hill, H. Ingmer, *Mol. Microbiol.* **2003**, *48*, 1565–1578.
- [39] D. Frees, K. Sørensen, H. Ingmer, *Infect. Immun.* **2005**, *73*, 8100–8108.
- [40] D. Frees, A. Chastanet, S. Qazi, K. Sørensen, P. Hill, T. Msadek, H. Ingmer, *Mol. Microbiol.* **2004**, *54*, 1445–1462.
- [41] D. Frees, J. H. Andersen, L. Hemmingsen, K. Koskenniemi, K. T. Bæk, M. K. Muhammed, D. D. Gudeta, T. A. Nyman, A. Sukura, P. Varmanen, K. Savijoki, *J. Proteome Res.* **2011**, *11*, 95–108.
- [42] A. Michel, F. Agerer, C. R. Hauck, M. Herrmann, J. Ullrich, J. Hacker, K. Ohlsen, *J. Bacteriol.* **2006**, *188*, 5783–5796.
- [43] O. Gaillot, E. Pellegrini, S. Bregenholt, S. Nair, P. Berche, *Mol. Microbiol.* **2000**, *35*, 1286–1294.
- [44] O. Gaillot, S. Bregenholt, F. Jaubert, J. P. Di Santo, P. Berche, *Infect. Immun.* **2001**, *69*, 4938–4943.
- [45] T. Yamamoto, H. Sashinami, A. Takaya, T. Tomoyasu, H. Matsui, Y. Kikuchi, T. Hanawa, S. Kamiya, A. Nakane, *Infect. Immun.* **2001**, *69*, 3164–3174.
- [46] J. Krysiak, M. Stahl, J. Vomacka, C. Fetzer, M. Lakemeyer, A. Fux, S. A. Sieber, *J. Proteome Res.* **2017**, *16*, 1180–1192.
- [47] F. Weinandy, K. Lorenz-Baath, V. S. Korotkov, T. Böttcher, S. Sethi, T. Chakraborty, S. A. Sieber, *ChemMedChem* **2014**, *9*, 710–713.
- [48] M. Gersch, A. List, M. Groll, S. A. Sieber, *J. Biol. Chem* **2012**, *287*, 9484–9494.
- [49] W. Kress, Z. Maglica, E. Weber-Ban, *Res. Microbiol.* **2009**, *160*, 618–628.
- [50] F. Ye, J. Zhang, H. Liu, R. Hilgenfeld, R. Zhang, X. Kong, L. Li, J. Lu, X. Zhang, D. Li, H. Jiang, C. G. Yang, C. Luo, *J. Biol. Chem* **2013**, *288*, 17643–17653.
- [51] S. R. Geiger, T. Böttcher, S. A. Sieber, P. Cramer, *Angew. Chem. Int. Ed.* **2011**, *50*, 5749–5752.

- [52] T. Ni, F. Ye, X. Liu, J. Zhang, H. Liu, J. Li, Y. Zhang, Y. Sun, M. Wang, C. Luo, H. Jiang, L. Lan, J. Gan, A. Zhang, H. Zhou, C.-G. Yang, *ACS Chem. Biol.* **2016**, *11*, 1964–1972.
- [53] S. E. Glynn, A. Martin, A. R. Nager, T. A. Baker, R. T. Sauer, *Cell* **2009**, *139*, 744–756.
- [54] A. O. Olivares, T. A. Baker, R. T. Sauer, *Nat. Rev. Microbiol.* **2015**, *14*, 33–44.
- [55] T. A. Baker, R. T. Sauer, *Biochim. Biophys. Acta* **2012**, *1823*, 15–28.
- [56] B. M. Stinson, A. R. Nager, S. E. Glynn, K. R. Schmitz, T. A. Baker, R. T. Sauer, *Cell* **2013**, *153*, 628–639.
- [57] A. Martin, T. A. Baker, R. T. Sauer, *Mol. Cell.* **2007**, *27*, 41–52.
- [58] G. L. Hersch, R. E. Burton, D. N. Bolon, T. A. Baker, R. T. Sauer, *Cell* **2005**, *121*, 1017–1027.
- [59] Y. I. Kim, I. Levchenko, K. Fraczkowska, R. V. Woodruff, R. T. Sauer, T. A. Baker, *Nat. Struct. Biol.* **2001**, *8*, 230–233.
- [60] S. A. Joshi, G. L. Hersch, T. A. Baker, R. T. Sauer, *Nat. Struct. Mol. Biol.* **2004**, *11*, 404–411.
- [61] A. Gribun, M. S. Kimber, R. Ching, R. Sprangers, K. M. Fiebig, W. A. Houry, *J. Biol. Chem* **2005**, *280*, 16185–16196.
- [62] D. P. Haeusser, A. H. Lee, R. B. Weart, P. A. Levin, *J. Bacteriol.* **2009**, *191*, 1986–1991.
- [63] C. J. LaBreck, S. May, M. G. Viola, J. Conti, J. L. Camberg, *Front. Mol. Biosci.* **2017**, *4*, 26.
- [64] A. H. Abdelhakim, E. C. Oakes, R. T. Sauer, T. A. Baker, *Mol. Cell.* **2008**, *30*, 39–50.
- [65] K. C. Keiler, P. R. Waller, R. T. Sauer, *Science* **1996**, *271*, 990–993.
- [66] S. Gottesman, E. Roche, Y. Zhou, R. T. Sauer, *Genes Dev.* **1998**, *12*, 1338–1347.
- [67] S. D. Moore, R. T. Sauer, *Annu. Rev. Biochem.* **2007**, *76*, 101–124.
- [68] O. Iosefson, A. R. Nager, T. A. Baker, R. T. Sauer, *Nat. Chem. Biol.* **2015**, *11*, 201–206.
- [69] R. E. Burton, T. A. Baker, R. T. Sauer, *Protein Sci.* **2003**, *12*, 893–902.

- [70] M. Gersch, K. Famulla, M. Dahmen, C. Göbl, I. Malik, K. Richter, V. S. Korotkov, P. Sass, H. Rübsamen-Schaeff, T. Madl, H. Brötz-Oesterhelt, S. A. Sieber, *Nat. Commun.* **2015**, *6*, 6320.
- [71] A. Pahl, M. Lakemeyer, M. T. Vielberg, M. W. Hackl, J. Vomacka, V. S. Korotkov, M. L. Stein, C. Fetzer, K. Lorenz-Baath, K. Richter, H. Waldmann, M. Groll, S. A. Sieber, *Angew. Chem. Int. Ed. Engl.* **2015**, *54*, 15892–15896.
- [72] J. Ortega, H. S. Lee, M. R. Maurizi, A. C. Steven, *EMBO J.* **2002**, *21*, 4938–4949.
- [73] A. Szyk, M. R. Maurizi, *J. Struct. Biol.* **2006**, *156*, 165–174.
- [74] D. Balogh, M. Dahmen, M. Stahl, M. Poreba, M. Gersch, M. Drag, S. A. Sieber, *Chem. Sci.* **2017**, *8*, 1592–1600.
- [75] T. Akopian, O. Kandrór, C. Tsu, J. H. Lai, W. Wu, Y. Liu, P. Zhao, A. Park, L. Wolf, L. R. Dick, E. J. Rubin, W. Bachovchin, A. L. Goldberg, *J. Biol. Chem.* **2015**, *290*, 11008–11020.
- [76] M. Gersch, R. Kolb, F. Alte, M. Groll, S. A. Sieber, *J. Am. Chem. Soc.* **2014**, *136*, 1360–1366.
- [77] T. Böttcher, S. A. Sieber, *Angew. Chem. Int. Ed.* **2008**, *47*, 4600–4603.
- [78] T. Böttcher, S. A. Sieber, *J. Am. Chem. Soc.* **2008**, *130*, 14400–14401.
- [79] T. Böttcher, S. A. Sieber, *ChemBioChem* **2009**, *10*, 663–666.
- [80] E. Zeiler, V. S. Korotkov, K. Lorenz-Baath, T. Böttcher, S. A. Sieber, *Bioorg. Med. Chem.* **2012**, *20*, 583–591.
- [81] M. Gersch, F. Gut, V. S. Korotkov, J. Lehmann, T. Böttcher, M. Rusch, C. Hedberg, H. Waldmann, G. Klebe, S. A. Sieber, *Angew. Chem. Int. Ed. Engl.* **2013**, *52*, 3009–3014.
- [82] P. Gao, P. L. Ho, B. Yan, K. H. Sze, J. Davies, R. Y. T. Kao, *Proc. Natl. Acad. Sci. U.S.A.* **2018**, *115*, 8003–8008.
- [83] T. Tomašić, L. Peterlin Mašič, *Expert Opin. Drug Discov.* **2012**, *7*, 549–560.
- [84] C. Fetzer, V. S. Korotkov, R. Thänert, K. M. Lee, M. Neuenschwander, J. P. von Kries, E. Medina, S. A. Sieber, *Angew. Chem. Int. Ed.* **2017**, *56*, 15746–15750.

- [85] J. Kirstein, A. Hoffmann, H. Lilie, R. Schmidt, H. Rübsamen-Waigmann, H. Brötz-Oesterhelt, A. Mogk, K. Turgay, *EMBO Mol Med* **2009**, *1*, 37–49.
- [86] B.-G. Lee, E. Y. Park, K.-E. Lee, H. Jeon, K. H. Sung, H. Paulsen, H. Rübsamen-Schaeff, H. Brötz-Oesterhelt, H. K. Song, *Nat. Struct. Mol. Biol.* **2010**, *17*, 471–478.
- [87] D. H. S. Li, Y. S. Chung, M. Gloyd, E. Joseph, R. Ghirlando, G. D. Wright, Y.-Q. Cheng, M. R. Maurizi, A. Guarné, J. Ortega, *Chem. Biol.* **2010**, *17*, 959–969.
- [88] J. Alexopoulos, B. Ahsan, L. Homchaudhuri, N. Husain, Y.-Q. Cheng, J. Ortega, *Mol. Microbiol.* **2013**, *90*, 167–180.
- [89] B. Hinzen, S. Raddatz, H. Paulsen, T. Lampe, A. Schumacher, D. Häbich, V. Hellwig, J. Benet-Buchholz, R. Endermann, H. Labischinski, H. Brötz-Oesterhelt, *ChemMedChem* **2006**, *1*, 689–693.
- [90] D. W. Carney, K. R. Schmitz, J. V. Truong, R. T. Sauer, J. K. Sello, *J. Am. Chem. Soc.* **2014**, *136*, 1922–1929.
- [91] J. D. Goodreid, J. Janetzko, J. P. Santa Maria, K. S. Wong, E. Leung, B. T. Eger, S. Bryson, E. F. Pai, S. D. Gray-Owen, S. Walker, W. A. Houry, R. A. Batey, *J. Med. Chem.* **2016**, *59*, 624–646.
- [92] D. W. Carney, C. L. Compton, K. R. Schmitz, J. P. Stevens, R. T. Sauer, J. K. Sello, *ChemBioChem* **2014**, *15*, 2216–2220.

Part II

RESEARCH

2

Phenyl esters are potent inhibitors of caseinolytic protease P and reveal a stereogenic switch for deoligomerization

Published in *Journal of the American Chemical Society*, **2015**, *137*, 8475-8483
by Mathias W. Hackl,[#] Markus Lakemeyer,[#] Maria Dahmen, Manuel Glaser, Axel Pahl,
Katrín Lorenz-Baath, Thomas Menzel, Sonja Sievers, Thomas Böttcher, Iris Antes, Her-
bert Waldmann, and Stephan A. Sieber.

[#]equal contribution

Reprinted with permission. © American Chemical Society.

DOI: 10.1021/jacs.5b03084

SYNOPSIS

The barrel-shaped ClpXP protease is a key regulator of virulence in *S. aureus*, which renders it a promising target for antivirulence approaches. β -lactones are covalent inhibitors of ClpP and have been a valuable tool to chemically probe *S. aureus*' virulence. However, their limited stability and selectivity have hampered their application.

In this publication, we describe our endeavors to identify and characterize novel ClpP inhibitors with improved properties. A high-throughput screen of more than 137,000 compounds revealed the phenyl ester group as a privileged motif for covalent modification of the active site serine of ClpP. The six hit compounds from the screen surpassed β -lactones in inhibiting ClpP's peptidase and protease activity. We synthesized an alkyne-tagged derivative of the most potent phenyl ester, **AV170**, and applied the probe for activity-based protein profiling (ABPP) in live *S. aureus* cells. Gel-based and gel-free analyses confirmed ClpP to be a highly selective binding partner of the probe in these experiments. Next, we performed in-depth structure-activity-relationship studies, which led to derivatives with improved plasma stability and extended half-lives of the covalent acyl-enzyme state. In this context, an enantiomeric pair of α -methyl derivatives was identified which had - depending on the stereochemistry of the methyl group - distinctly different modes of inhibition. The (*R*)-enantiomer **ML89** led to partial modification of ClpP's 14 active sites and induced de-oligomerization of the tetradecameric complex into two heptameric species. For (*S*)-enantiomer **ML90**, all active sites were acylated, and the complex stoichiometry was retained. This was an important finding, as for the first time a "stereogenic switch" was found in an inhibitor structure, which could clearly influence the oligomerization state.

AUTHOR CONTRIBUTIONS

Markus Lakemeyer synthesized compounds, purified ClpP, tested the derivatives in peptidase assays and performed gel-based activity-based protein profiling (ABPP) experiments. Mathias W. Hackl tested the initial hit compounds in peptidase assays, purified ClpP, performed analytical size-exclusion chromatography, acyl-enzyme stability experiments and gel-free ABPP. Maria Dahmen tested the hit compounds for inhibition

of proteolysis. Manuel Glaser and Iris Antes performed quantum mechanics/molecular dynamics simulations. Axel Pahl, Thomas Menzel and Sonja Sievers conducted the high-throughput screen. Katrin Lorenz-Baath tested plasma stability. Markus Lakemeyer, Mathias W. Hackl and Stephan A. Sieber prepared the manuscript.

Phenyl Esters Are Potent Inhibitors of Caseinolytic Protease P and Reveal a Stereogenic Switch for Deoligomerization

Mathias W. Hackl,^{†,‡} Markus Lakemeyer,^{†,‡} Maria Dahmen,[†] Manuel Glaser,[‡] Axel Pahl,[†] Katrin Lorenz-Baath,[†] Thomas Menzel,[†] Sonja Sievers,[§] Thomas Böttcher,[⊥] Iris Antes,[‡] Herbert Waldmann,^{§,||} and Stephan A. Sieber^{*,†}

[†]Center for Integrated Protein Science at the Department of Chemistry, Technische Universität München, Lichtenbergstrasse 4, Garching, D-85747, Germany

[‡]Center for Integrated Protein Science at the Department of Life Sciences, Technische Universität München, Emil-Erlenmeyer-Forum 8, D-85354 Freising, Germany

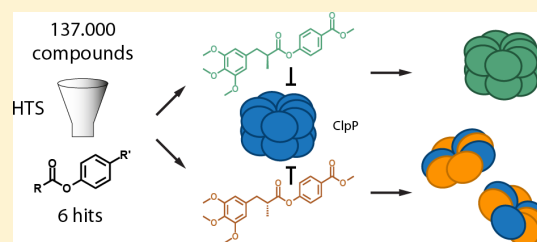
[§]Max-Planck-Institut für Molekulare Physiologie, Abteilung Chemische Biologie, Otto-Hahn-Strasse 11, D-44227 Dortmund, Germany

^{||}Technische Universität Dortmund, Fakultät für Chemie und Chemische Biologie, Otto-Hahn-Strasse 6, D-44221 Dortmund, Germany

[⊥]Department of Chemistry, Universität Konstanz, Universitätsstrasse 10, D-78457 Konstanz, Germany

Supporting Information

ABSTRACT: Caseinolytic protease P (ClpP) represents a central bacterial degradation machinery that is involved in cell homeostasis and pathogenicity. The functional role of ClpP has been studied by genetic knockouts and through the use of *beta*-lactones, which remain the only specific inhibitors of ClpP discovered to date. *Beta*-lactones have served as chemical tools to manipulate ClpP in several organisms; however, their potency, selectivity and stability is limited. Despite detailed structural insights into the composition and conformational flexibility of the ClpP active site, no rational efforts to design specific non-*beta*-lactone inhibitors have been reported to date. In this work, an unbiased screen of more than 137 000 compounds was used to identify five phenyl ester compounds as highly potent ClpP inhibitors that were selective for bacterial, but not human ClpP. The potency of phenyl esters largely exceeded that of *beta*-lactones in ClpP peptidase and protease inhibition assays and displayed unique target selectivity in living *S. aureus* cells. Analytical studies revealed that while phenyl esters are cleaved like native peptide substrates, they remain covalently trapped as acyl-enzyme intermediates in the active site. The synthesis of 36 derivatives and subsequent structure–activity relationship (SAR) studies provided insights into conserved structural elements that are important for inhibition potency and acylation reactivity. Moreover, the stereochemistry of a methyl-substituent at the *alpha* position to the ester, resembling amino acid side chains in peptide substrates, impacted ClpP complex stability, causing either dissociation into heptamers or retention of the tetradecameric state. Mechanistic insights into this intriguing stereo switch and the phenyl ester binding mode were obtained by molecular docking experiments.



INTRODUCTION

Proteolysis represents an essential physiological mechanism for diverse cellular functions including post-translational processing, signaling and protein degradation.^{1,2} This important process is catalyzed by a variety of proteases, which together constitute one of the largest enzyme classes in eukaryotic and prokaryotic cells. In prokaryotes, a variety of ATP-dependent proteases are responsible for protein degradation, including FtsH,³ Lon⁴ and HslUV.^{5–7} One additional member of this group is the caseinolytic protease P (ClpP), a tetradecameric, barrel-shaped serine protease that associates with AAA+ chaperones such as ClpA, ClpC and ClpX for protein degradation.^{8–13} The chaperones recognize, unfold and direct SsrA-tagged protein substrates into the proteolytic chamber of

ClpP in an ATP-dependent manner.¹⁴ ClpP is essential for the regulation of the cellular stress response, cell homeostasis and bacterial virulence.^{10,15,16} Virulence, i.e., the expression of bacterial toxins such as *alpha*-hemolysin, is regulated by the Agr signaling network wherein ClpP is believed to be involved in the degradation of Rot, a repressor of bacterial toxins.¹⁷ Genetic ClpP knockouts in *Listeria monocytogenes* and *Staphylococcus aureus* revealed a reduction in virulence, resulting in attenuated infections in murine abscess models.^{10,18} Similarly, the same phenotype was observed upon the chemical inhibition of ClpP with long-chain aliphatic *beta*-lactones (e.g., D3, Figure 1B), the

Received: March 24, 2015

Published: June 17, 2015

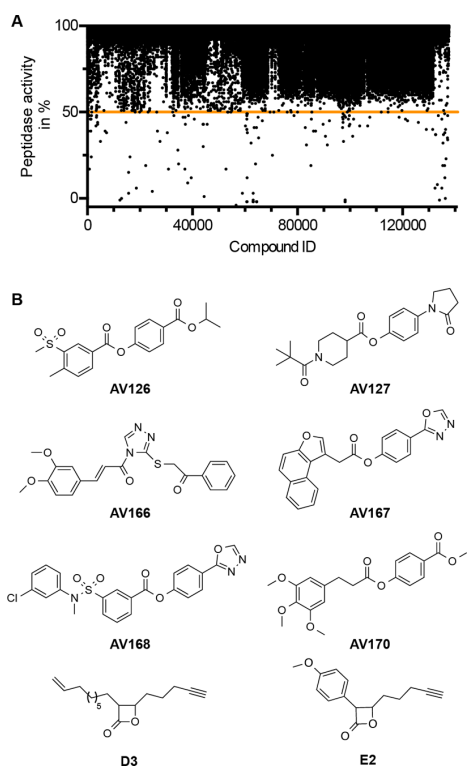


Figure 1. Identification of HTS primary hits. (A) A screen of more than 137 000 compounds identified 161 primary hits which reduced turnover of the fluorogenic substrate *N*-succinyl-Leu-Tyr-7-amido-4-methylcoumarin (SLY-AMC) by 50% at 12.5 μM concentration. (B) Structures of the six final hits that had suitable pharmacological properties and showed an $\text{IC}_{50} < 2 \mu\text{M}$, and structures of *beta*-lactone compounds D3 and E2.

only specific inhibitors reported for ClpP to date.^{19–21} Crystal structures of *S. aureus* ClpP revealed a deep hydrophobic channel next to the active site Ser98, which accommodates lactone side chains of maximum 8 atoms length.^{22–24} Ser98 nucleophilically attacks the 4-membered lactone ring resulting in a covalent acyl-enzyme intermediate. Depending on the *beta*-lactone C-4 substitution, the occupancy of ClpP varies from stoichiometric for aliphatic D3 to 50% for aromatic E2.²⁵ One reason for these differing ratios is the transient stability of the ClpP tetradecamer, which dissociates into heptamers via an unknown mechanism upon E2 binding.

The interaction of subunits in the tetradecameric complex is facilitated by a dynamic H-bond network of adjacent helices (E-helix), *beta*-sheets (Gly-rich loop) and oligomerization sensors (Asp170-Arg171).²² The E-helices exist in extended, compact and compressed conformations. While an extended helix supports an aligned and active catalytic triad (Ser98, His123 and Asp172), the compressed helix induces a rotation of the active site His123 and displaces the catalytic residues.²⁶ Moreover, in the compressed state all crucial interactions between the rings are abrogated leading to the formation of inactive heptamers. From a pharmacological perspective, inhibitor-induced heptamerization is advantageous as the corresponding enzyme, although not quantitatively acylated, is misaligned and inactive in all catalytic centers, effectively maximizing the sustainability of deactivation. Thus, drug

discovery efforts for ClpP and other multimeric enzymes need to consider deoligomerization as an attractive mode of action.

As *beta*-lactones are labile electrophiles which quickly hydrolyze in human plasma within minutes,¹⁹ previous rational attempts focused on replacing this group with more stable moieties. However, installation of lactam, carbamate, ester and oxetane moieties failed to inhibit the enzyme suggesting a restricted active site tolerance.²³ In order to expand the repertoire of ClpP inhibitors as chemical biology tools and to identify novel pharmacological leads we performed an unbiased high-throughput screen (HTS) of more than 137 000 compounds and identified six compounds as potent hits, which all contained activated ester or amide moieties. In-depth biochemical characterization and structure–activity relationship (SAR) studies revealed a new class of deoligomerizing ClpP inhibitors with superior potency, inhibition kinetics, plasma half-life, stability of the acyl-enzyme intermediate and specificity. The (*R*)- or (*S*)-configuration of a methyl substituent in the *alpha* position to the ester served as a switch of the oligomeric state which was further supported by molecular docking experiments.

RESULTS

High Throughput Screen for ClpP Inhibitors. For the discovery of novel, non-*beta*-lactone inhibitors of ClpP, we performed a HTS with more than 137 000 compounds, which were each tested for inhibition of *S. aureus* ClpP (SaClpP) peptidase activity. Compounds that inhibited turnover of the fluorogenic substrate *N*-succinyl-Leu-Tyr-7-amido-4-methylcoumarin (SLY-AMC) by 50% at 12.5 μM concentration were regarded as a hit. Dose–response behavior of the assay was validated using the ClpP inhibitor Palmostatin M, a *beta*-lactone, as a positive control (Figure S1). The overall Z' factor of the primary screen was calculated to be 0.69 ± 0.14 and the overall signal-to-background ratio was 25 ± 9 .

161 initial hits were identified (hit rate 0.017%) and their individual IC_{50} values determined (Figure 1A, Table S2). Compounds with an $\text{IC}_{50} < 2 \mu\text{M}$ and desirable pharmacological properties (see Supporting Information for details on filtering criteria) were selected for further studies. Given the large number of molecules screened, it is surprising that only six hits met these criteria, demonstrating a restricted structural access to the ClpP active site (Figure 1B, Table S1). Interestingly, five molecules contained a central phenyl ester (of respective aromatic acids: AV126, AV168 or aliphatic acids: AV127, AV167, AV170) and one compound a triazole amide motif (AV166). All compounds exhibited potent IC_{50} values between 0.3 and 1.3 μM which are even at the lower limit of the assay (requires 1 μM ClpP).

Although previous attempts to replace the lactone scaffold with open-chain esters and carbamates failed,²³ phenyl esters and triazole amides exhibit a stabilized aromatic leaving group that elevates electrophilicity, and thereby reactivity, toward Ser98. Remarkably, of the 1780 phenyl esters present in the library only five (0.3%) were identified as hits, emphasizing that not only reactivity, but also structural prerequisites, are important for binding and inhibition.

Customized Inhibitors of Bacterial and Human ClpP Peptidase and Protease Activity. The panel of inhibitors was tested for potency and selectivity against *S. aureus*, *Escherichia coli*, *L. monocytogenes* and human ClpP. First, inhibition of ClpP-catalyzed SLY-AMC peptide hydrolysis was

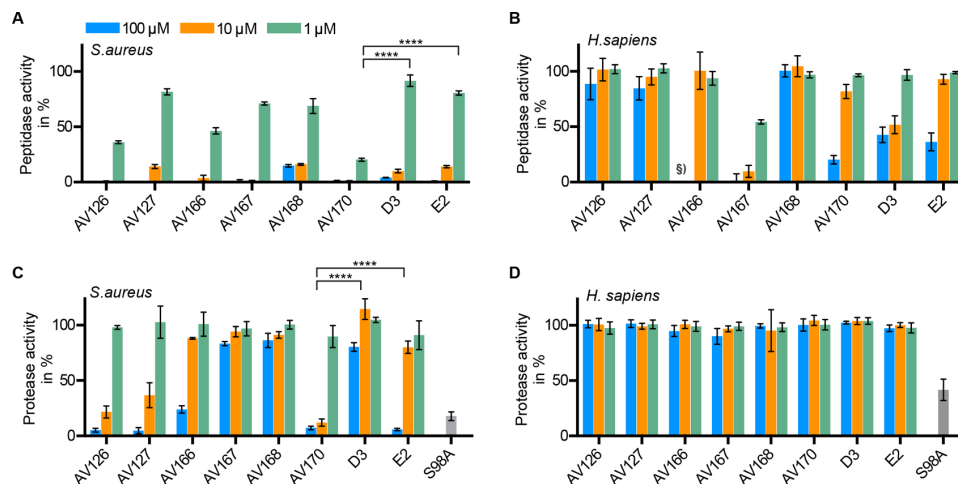


Figure 2. Inhibition of ClpP peptidase and ClpXP protease activity. Hit compounds and two lactone inhibitors (**E2** and **D3**) were tested at three concentrations for their inhibition of peptidase and protease activity. Data are normalized with respect to DMSO as a negative control (100% activity) (A) *S. aureus* ClpP peptidase assay (1 μM SaClpP in the presence of 200 μM SLY-AMC) (B) *H. sapiens* ClpP peptidase assay (1 μM HsClpP in the presence of 200 μM SLY-AMC). (C) *S. aureus* ClpP protease assay (0.2 μM SaClpP in the presence of 0.4 μM SaClpX and 0.4 μM GFP-SsrA) (D) *H. sapiens* ClpP protease assay (0.2 μM HsClpP in the presence of 0.4 μM EcClpX[§] and 0.4 μM GFP-SsrA). Each data set represents six replicates obtained from two independent experiments (mean \pm standard deviation). **** represent p -value ≤ 0.0001 determined by Student's t test. [§]EcClpX was used in place of HsClpX as the AAA+ Chaperone to recognize, unfold and translocate the substrate as described previously.²⁸ [§]Internal fluorescence of compound AV166 precluded measurements at 100 μM .

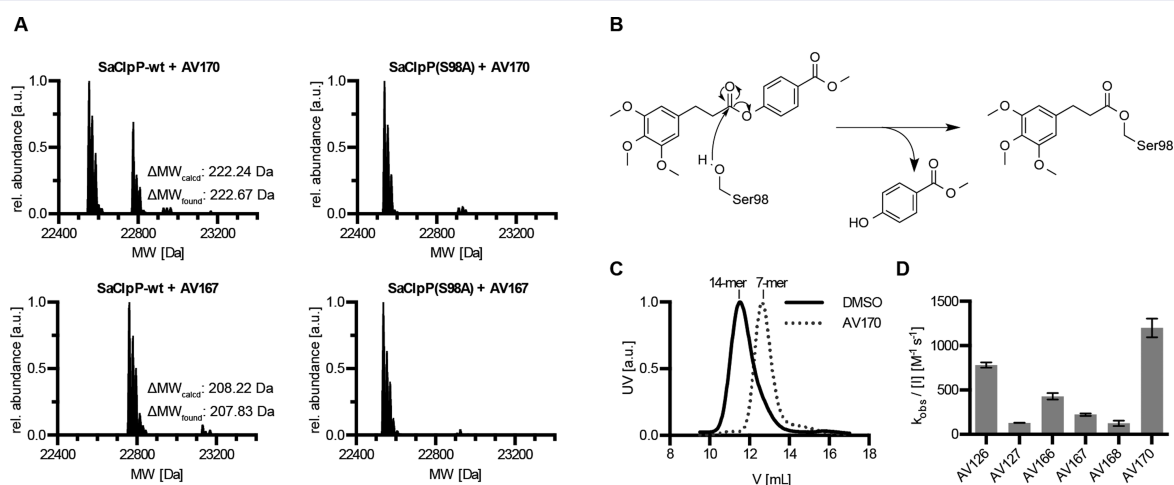


Figure 3. Phenyl esters covalently modify ClpP. (A) Intact protein mass spectrometry of SaClpP after compound treatment reveals incomplete (**AV170**) and full (**AV167**) modification whereas the respective active site mutant SaClpP(S98A) lacks binding. (B) Suggested mode of action, illustrated for **AV170**. (C) Size-exclusion chromatograms show SaClpP heptamer formation upon treatment with **AV170**. (D) SaClpP inactivation rates ($k_{\text{obs}}/[I]$ values) for the six hit compounds.

determined by the percent residual activity at 100, 10, and 1 μM compound concentration across the panel of enzymes. In prokaryotic ClpP, **AV170** exhibited the most pronounced reduction in peptide hydrolysis followed by **AV166** and **AV126** (Figure 2A and Figure S2). Importantly, at the lowest concentration tested (1 μM), **AV170** was four times more effective (for SaClpP) compared to the previously reported *beta*-lactone inhibitors **D3** and **E2**, which have served as a gold standard for ClpP inhibition so far.²¹ On the contrary, the best inhibitors of bacterial ClpP did not significantly reduce human ClpP (hClpP) peptidase activity even at low to moderate (1 to 10 μM) concentrations, pointing toward significant differences

in the binding sites (Figure 2B). Human and *S. aureus* ClpP share only a moderate sequence similarity of 37%. Since the inactivation of human ClpP has been linked to cancer and the Perrault syndrome²⁷ the observed discrimination between human and bacterial enzymes is beneficial for putative medicinal applications. In turn, **AV167**, with a large naphthofuran moiety, was the only compound that significantly reduced human ClpP peptidase activity even at low (1 μM) concentrations (Figure 2B).

To examine if the identified peptidase inhibitors also impair proteolysis, we monitored the digest of green fluorescent protein (GFP) tagged with a SsrA peptide sequence. Bacterial

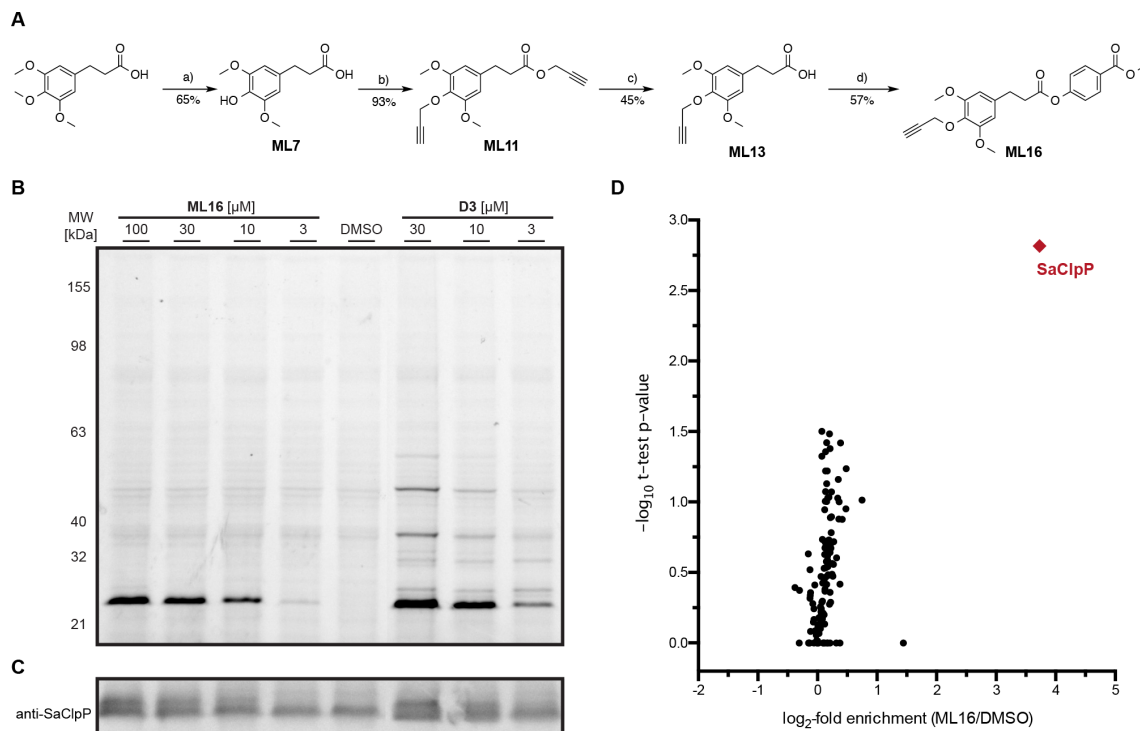


Figure 4. Synthesis of **ML16** and in situ target analysis. (A) Scheme for the synthesis of activity-based probe **ML16**. Reagents and conditions: (a) MgI_2 , *neat*, 80 °C, 1.5 h; (b) propargyl bromide, K_2CO_3 , KO^tBu , DMF, rt, 72 h; (c) 15% aq. NaOH, MeOH, 50 °C, 2 h; (d) methyl 4-hydroxybenzoate, EDC-HCl, DMAP, DCM, rt, 24 h. (B,C) ABPP-labeling of living *S. aureus* cells with **ML16** and **D3**. (B) Fluorescence SDS-PAGE of soluble fraction. (C) Western blot against SaClpP confirming the labeling of ClpP. See Figure S7 for full image and overlay of Western blot and fluorescence scan. Note: Probe binding slightly changes protein migration explaining the double band in Western Blots of treated samples. (D) Volcano plot representation of gel-free quantitative ABPP experiments with **ML16**. ClpP is identified as the only target of **ML16** (13-fold enrichment over DMSO, p -value of 0.0015). Data are derived from three independent experiments.

ClpX recognizes SsrA as a degradation signal, unfolds, and subsequently directs the protein into the ClpP proteolytic chamber.^{14,29} Proteolytic activity of the SaClpXP complex was effectively inhibited at 10 μM by phenyl esters **AV126** and **AV170** which is nearly 11-fold more potent compared to the lactones **D3** and **E2** (Figure 2C). In line with previous reports,²⁹ the proteolytically inactive ClpXP(S98A) complex reduced GFP fluorescence solely by ClpX-mediated unfolding (about 17%). However, no reduction of fluorescence was observed in ClpXP samples treated with phenyl esters, suggesting that compounds not only abolished GFP degradation but also impaired its unfolding. None of the phenyl ester compounds inhibited human ClpXP proteolysis, demonstrating the desired selectivity for bacterial ClpP species (Figure 2D).

Phenyl Esters Covalently Bind to the Active Site and Induce ClpP Deoligomerization. Given the compelling activity of phenyl esters in peptidase and protease assays, we next focused on elucidating the mechanism of inhibition of SaClpP as the biologically relevant target. Phenyl esters and triazole amides represent electrophilic molecules that can inhibit ClpP by either covalent or noncovalent binding. In order to investigate the binding mode and the degree of modification, we utilized intact protein mass spectrometry and determined the exact mass of SaClpP treated with inhibitor. All compounds active in *S. aureus* peptidase assays shifted the protein mass to higher molecular weights, confirming a covalent binding mechanism (Figure 3A, Figure S3). The extent of

modification ranged from 25% for **AV168** to 50% for **AV170**. Only the human ClpP inhibitor **AV167** achieved binding saturation (Figure 3A). None of the molecules were able to bind the SaClpP(S98A) mutant, reaffirming the role of active site Ser98 as the functional nucleophile (Figure 3A, Figure S3).

Moreover, the adduct mass corresponded to the attachment of only the carboxy part of the esters. These findings elucidate a mode of inhibition in which the inhibitor binds to the active site, undergoes nucleophilic attack by Ser98 at the ester or amide and releases the phenol or triazole as a stabilized leaving group (Figure 3B). Activated ester inhibitors thus act as substrate mimics which are cleaved like native peptides but remain trapped in the acyl-enzyme intermediate state.

Previous studies with *beta*-lactones **D3** and **E2** showed that binding to the active site of ClpP can either result in acylation of all sites (**D3**) under retention of the oligomeric state, or in partial modification and subsequent deoligomerization (**E2**).²⁵ Here, all phenyl esters and triazole amides followed the deoligomerization route leading to inactive heptamers (Figure 3C, Figure S4). This conformational change disassembles the ClpP barrel, stalls proteins at ClpX, and thus explains the surprising dual inhibition of unfolding and degradation activity with **AV170** and **AV126**.

In order to determine the potency of the covalent phenyl ester and triazole amide inhibitors, we measured the inactivation rates via $k_{\text{obs}}/[I]$ values. The highest $k_{\text{obs}}/[I]$ values, i.e., acylation velocities, were obtained with **AV170**

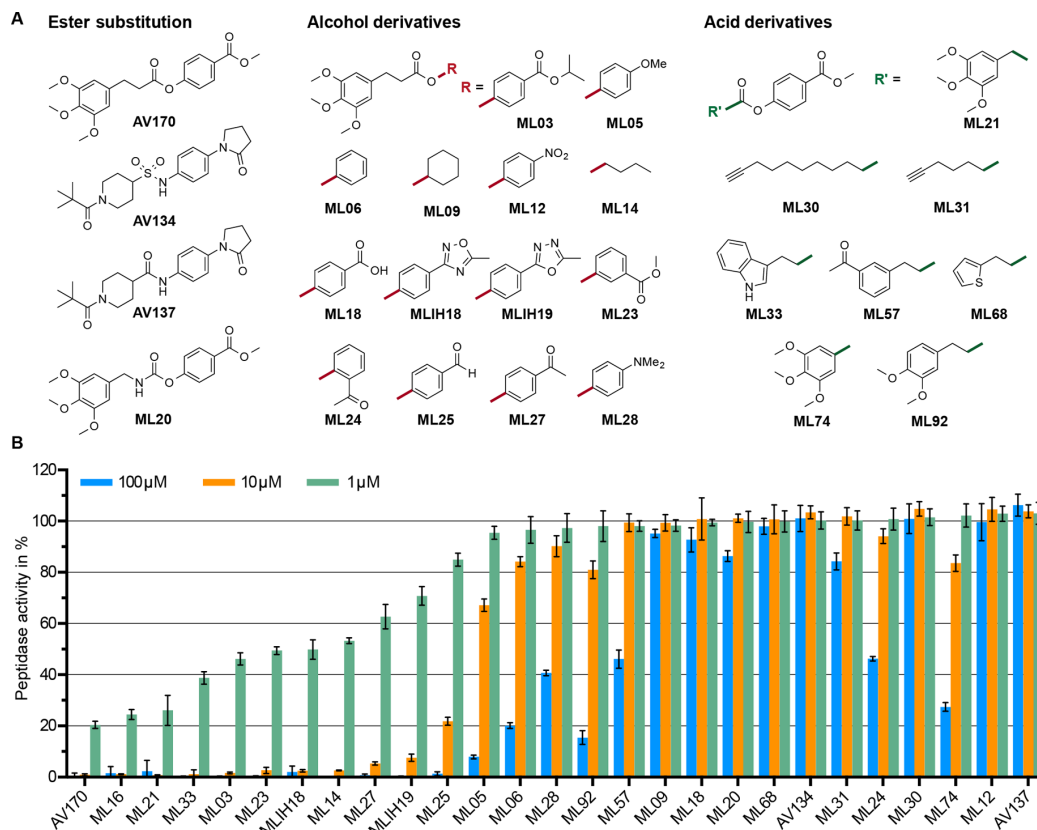


Figure 5. Structure–activity relationship studies. (A) Chemical structures of AV170 and its synthesized derivatives modified at the ester, alcohol or acid moiety. (B) Inhibition of SaClpP peptidase activity by the compounds. Each data set represents six replicates from two independent experiments (mean \pm standard deviation).

($1200 \pm 105 \text{ M}^{-1} \text{ s}^{-1}$) and AV126 ($781 \pm 31 \text{ M}^{-1} \text{ s}^{-1}$). This accounts for approximately 20 times faster reaction kinetics in the case of AV170, compared to the previous gold standard inhibitors D3 ($78 \pm 6 \text{ M}^{-1} \text{ s}^{-1}$) and E2 ($64 \pm 3 \text{ M}^{-1} \text{ s}^{-1}$) (Figure 3D, Figure S5).²⁵ On the basis of its superior activity, AV170 was selected as the most promising candidate for in situ target validation.

ClpP Is the Predominant Intracellular Target of Phenyl Esters in *S. aureus*. Prior to compound optimization, cell permeability and target selectivity of AV170 in living *S. aureus* cells were analyzed. We utilized a chemical proteomic strategy termed activity-based protein profiling (ABPP)^{30,31} wherein we synthesized an alkyne-tagged AV170 derivative which remains bound to the enzyme upon inhibition. The alkyne serves as a benign tag for subsequent conjugation to a functionalized azide via the Huisgen–Sharpless–Meldal cycloaddition (click chemistry).^{32–34} In brief, the synthesis started with 3-(3,4,5-trimethoxyphenyl)propanoic acid which was selectively demethylated in the *para* position by means of magnesium iodide (Figure 4A).³⁵ Global propargylation and ester hydrolysis, followed by esterification with methyl-4-hydroxybenzoate yielded the final probe ML16. The compound showed similar potency in SaClpP peptidase inhibition compared to AV170 (Figure 5B) and intact protein mass spectrometry confirmed covalent modification of the enzyme with about 22% (Figure S6). The probe was incubated with

intact *S. aureus* cells for 1h, followed by cell lysis, proteome separation into soluble and insoluble fractions, treatment with a rhodamine azide dye, separation on SDS-PAGE and visualization via fluorescent scanning. Importantly, only a single band appeared on the fluorescent SDS gel, which could be identified as ClpP by Western blotting (Figure 4B, C, Figure S7 for entire blot). The lack of any off-targets surpassed the selectivity of D3, which weakly labeled additional bands, and thereby establishes phenyl esters as selective ClpP inhibitors. Furthermore, the ClpP band in D3 treated samples could selectively be outcompeted by AV170 while all off-targets of D3 remained unchanged (Figure S8). Quantitative MS-based proteomic experiments further underlined the unprecedented selectivity of ML16 for ClpP as the predominant target in living *S. aureus* cells (Figure 4D). ClpP was the only identified target and was enriched about 13-times over the DMSO control with a *p*-value of 0.0015 (see Supporting Information for further experimental details).

Structure–Activity Relationship Studies. To explore the SAR of phenyl esters, we systematically varied the phenol group, the carboxylic acid moiety and the ester bond of AV170 and AV127 (Figure 5A, Scheme S1–S3). Substitution of the ester bond by carbamates (ML20), amides (AV137) or sulfonamides (AV134) led to inactive compounds (Figure 5B). Therefore, the ester was kept as an integral part of this inhibitor class. The phenol of AV170 is substituted with an

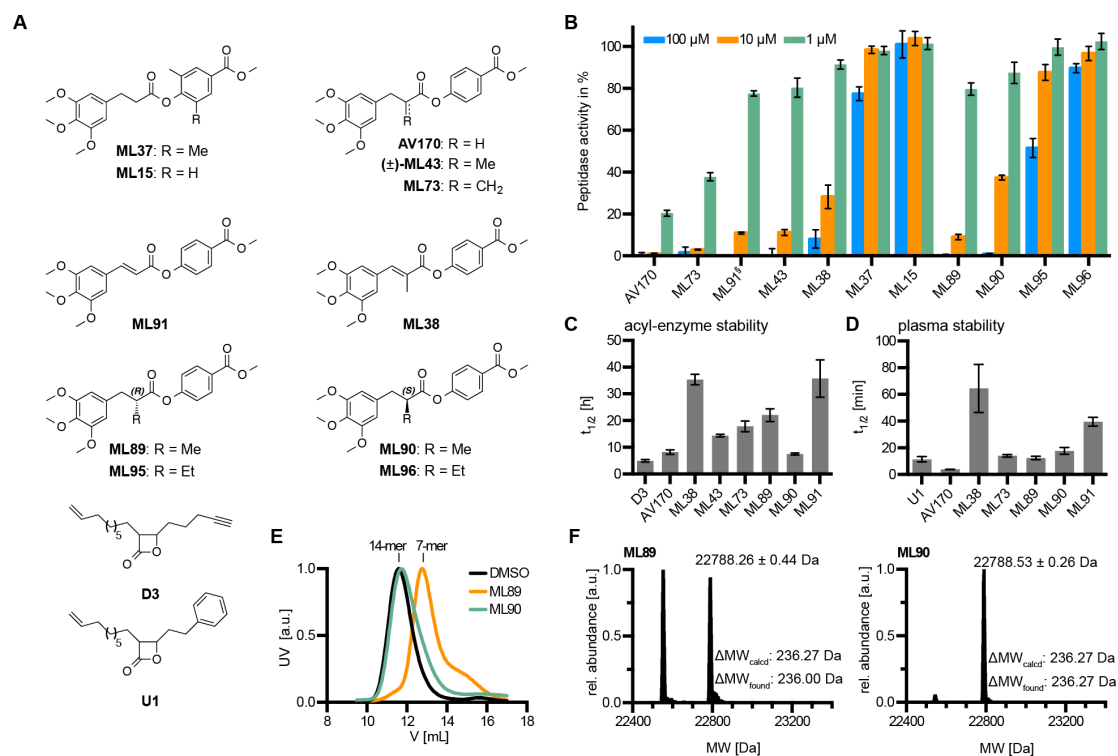


Figure 6. (A) Chemical structures of stabilized AV170 derivatives. (B) Inhibition of peptidase activity upon treatment with respective compounds. Each data set represents six replicates from two independent experiments (mean \pm standard deviation). (C) Stability of various acyl-SaClpP complexes at 32 °C as determined by time-dependent intact protein mass spectrometry. Half life refers to the time needed for a 50% reduction in the extent of protein modification (see Figure S9 for raw data). Each data set represents three biological replicates (mean \pm standard deviation). (D) Compound stability in human blood plasma. Each data set represents three independent experiments (mean \pm standard deviation). (E) Size-exclusion chromatograms illustrating heptamer formation upon treatment with the (*R*)-enantiomer ML89. (F) Intact protein mass spectrometry showing partial (ML89) and full (ML90) modification of SaClpP after compound treatment. [§]Internal fluorescence of compound ML91 precluded measurements at 100 μ M.

electron-withdrawing group in the *para* position, which increases its lability. Interestingly, all HTS hits contained electron-withdrawing phenol substituents such as esters (AV126, AV170), lactams (AV127) or oxadiazoles (AV167, AV168), suggesting that this electronic fine-tuning is a substantial driving force for reactivity and ClpP acylation. Accordingly, removal of the electron-withdrawing group (ML06) or exchange to electron donating groups such as methoxy (ML05) and *N,N'*-dimethylamine (ML28) resulted in a significant drop in potency (Figure 5B). In addition, an ester derivative of cyclohexanol (ML09) exhibited no activity. We thus increased the diversity of electron-withdrawing substituents and altered their position on the phenol ring. Aldehydes (ML25), ketones (ML27) and isopropylesters (ML03) in the *para* position were among the best inhibitors (Figure 5B). While the ester group was tolerated in the *meta* position (ML23), a keto-group in the *ortho* position (ML24) displayed almost no activity, suggesting that electronic and steric restrictions in the active site alter inhibitor potency. This is also supported by the observation that electron-withdrawing *p*-nitro (ML12) and *p*-carboxy (ML18) substituents were inactive, while the small, non-activated aliphatic butanol ester (ML14) retained moderate inhibitory activity.

Next, we explored the carboxylic acid moiety of AV170 and determined a very limited structural flexibility in this part of the

molecule. Variations of aromatic substituents (ML92, ML57) and replacement of the benzene ring by aliphatic residues (ML30 and ML31) were not tolerated for ClpP inhibition. Interestingly, ML33, bearing an indole moiety, was among the best inhibitors while ML68, with an aromatic thiophene, displayed no potency (Figure 5B).

In AV170, the trimethoxyphenyl moiety and the reactive ester are separated by two methylene groups. We successively removed both methylene groups to generate compounds ML21 and ML74. While ML21 was active, ML74 displayed only weak activity compared to AV170, suggesting that chain length is a crucial parameter for activity.

Chemical Modifications Increase Stability and Reveal a ClpP Deoligomerization Switch. *Beta*-lactones exhibit limited stability in acyl-enzyme complexes. Interestingly, the half-life of the AV170 acyl-enzyme intermediate was higher compared to the respective D3 acyl-enzyme complex ($t_{1/2} = 8.2 \pm 0.8$ h vs $t_{1/2} = 5.0 \pm 0.4$ h) (Figure 6C, Figure S9). To improve compound stability, we rationalized that substituents *alpha* to the carbonyl could sterically hinder hydrolysis. We therefore synthesized derivatives of AV170 containing either methyl (ML38, ML43, ML89, ML90), methylene (ML73) or ethyl substituents (ML95, ML96) at this position (Figure 6A). Moreover, methyl groups were installed in the *ortho* position of the phenol ring (ML15, ML37) to protect the ester from the

opposite side (Figure 6A). While incorporation of methyl groups in the phenyl ring abolished inhibitor activity, methylation at the *alpha* position (ML43, ML89, ML90) enhanced acyl-enzyme stability with a moderate reduction of potency compared to AV170 (Figure 6B,C). ML73, containing a methylene substituent, was the most potent compound in this series and also showed an improved half-life. Extended conjugated systems (ML38, ML91), leading to mesomeric stabilization, exhibited the most prominent prolongation of acyl-enzyme half lives. Similar trends were observed for compound stability in human blood plasma (Figure 6D, Figure S10). Mesomeric stabilization by the extended conjugated system exhibited the best stabilizing effects (ML38, ML91) with half lives of up to 65 ± 18 h. This corresponds to a 20-fold and 6-fold improvement compared to AV170 (3.7 ± 0.1 h) and *beta* lactone U1 (11 ± 2 h),¹⁹ respectively. Sterical shielding of the carbonyl via introduction of a methyl (ML89, ML90) or methylene group (ML73) had a less pronounced influence on stabilization.

ML43 was initially tested as a racemic mixture. To discriminate between the properties of each enantiomer, we stereoselectively synthesized both (*S*)-ML90 and (*R*)-ML89 using a chiral auxiliary (Figure 6A, Scheme S4, S5). (*R*)-ML89 is moderately more potent than (*S*)-ML90 (Figure 6B) and exhibited 3-fold enhanced acyl-enzyme stability (Figure 6C). In agreement with the mode of action of other phenyl esters, (*R*)-ML89 partially modified ClpP and induced dissociation into heptamers (Figure 6E,F). Surprisingly, unlike all other phenyl esters studied so far, the orientation of the methyl group in (*S*)-ML90 resulted in acylation of all 14 ClpP active sites and retention of the tetradecameric assembly (Figure 6E,F). It is an intriguing feature of these inhibitors that the orientation of the methyl substituent acts as a switch that either stabilizes or destabilizes the transient ClpP complex. Contrastingly, an ethyl group at this position ((*R*)-ML95 and (*S*)-ML96) abolished activity, demonstrating that longer chains are not tolerated (Figure 6B).

As ClpP activity is important for bacterial virulence the inhibitors were tested in a hemolysis assay. A reduction in hemolysis was observed with compounds AV170, ML21, ML89 and ML90 through dose–response curves, with EC_{50} values ranging from 60–200 μ M (Figure S11). However, upon prolonged incubation of bacterial supernatants with red blood cells, residual hemolytic activity could be detected, suggesting that *alpha*-hemolysin production was not completely attenuated. No cytotoxic effects were observed at a concentration of 100 μ M for AV170, ML21, ML89 and ML90 (Figure S12) against human epithelial lung cancer cells A549. This is in line with in situ labeling experiments which showed weak labeling of only two distinct bands in the soluble protein fraction of A549 cells upon incubation with the phenyl ester probe ML16 (Figure S13).

Molecular Docking Reveals the Binding Mode of Phenyl Esters. To elucidate the binding mode of phenyl esters to ClpP in more detail and to investigate the underlying cause of the (*R*),(*S*)-enantiomer switch, we completed molecular docking studies with compounds AV170, ML21, ML89, ML90, and nonbinding ML74. The docking solutions were filtered using pharmacophoric constraints to ensure the correct placement of the carbonyl oxygen in the oxyanion hole, which is a prerequisite for the nucleophilic attack to occur. Molecular dynamics (MD) simulations were subsequently performed for the three best poses of each compound. Figure

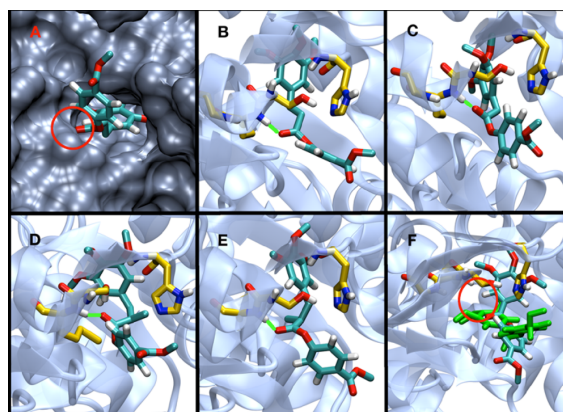


Figure 7. (A) Surface representation of the ClpP active site bound to AV170. (B–F) Conformations of five selected compounds after MD refinement. Important residues of the catalytic site and the oxyanion hole (M99, S98, H123), as well as bound ligands are shown in stick representation. (B) AV170. (C) ML21. (D) ML89. (E) ML90. (F) ML74. Final conformations of ML74 are given in green.

7 illustrates the most energetically favored conformations upon MD refinement. All inhibitors show the same general binding mode, as exemplified by AV170 in Figure 7A. The trimethoxyphenyl moiety of AV170 binds to a distinct hydrophobic channel extending from the catalytic center, while the reactive ester points toward the oxyanion hole (red circle).

Previous mutation experiments have validated this pocket as an integral part of the binding mode of *beta*-lactones.²³ Here, mutation of Leu154 to Tyr restricted the pocket size and strongly reduced binding of AV170, while the shorter ML21 derivative was unaffected (Figure S14). We calculated the equilibrated bound structures of AV170 as well as ML21 and ML74 within this binding pocket. In order to fully accommodate the trimethoxyphenyl moiety, a flexible linker is needed to span the constricted area between the catalytic center and the hydrophobic pocket. In the case of AV170, the two-carbon linker appears to have an optimal length to accommodate the trimethoxyphenyl ring. In ML21, the methylene linker still allows the ring to enter the pocket but its conformation is more constricted, whereas ML74, with its shorter linker, places the bulky trimethoxyphenyl ring directly at the pocket entrance and prohibits a stable conformation where the reactive ester group is close enough to the oxyanion hole for the reaction to occur (Figure 7F). Moreover, no hydrogen bond between the backbone amino group of the oxyanion hole and the ester groups of ML74 is formed. This leads to the release of compound out of the pocket during MD (final conformation given in green) for all three investigated poses, whereas all three poses of AV170 and ML21 remained in their bound conformation (Figure 7B–E).

Next, we looked into the strikingly different binding and deoligomerization behaviors of compounds ML89 and ML90 (Figure 7D,E). A comparison of these compounds with AV170 (same linker length, but no methyl group) revealed two main differences. First, the methyl group of ML89/ML90 strongly restricts possible binding conformations as it is located directly at the constricted area between the catalytic center and the hydrophobic binding pocket. Second, the relative orientation of the methyl group largely diverges in the two stereoisomers. In

ML90, the methyl group is located at the bottom of the constricted area. In the case of the **ML89** stereoisomer, the methyl group points to the top of the binding site toward the histidine of the catalytic triad. As there is more space in this direction, there seem to be less conformational restrictions compared to **ML90**. Importantly, this histidine has previously been identified as part of a hydrogen bonding network which plays a crucial role for the deoligomerization process.²⁶ Thus, the relative orientation of the inhibitor scaffold of **ML89** compared to **ML90** may trigger a steric rearrangement which causes the observed deoligomerization.

DISCUSSION

Functional and mechanistic analysis of the ClpXP proteolytic system represents an area of intense research. Recent reports have focused on mechanistic aspects of the whole ClpXP unfolding machinery.^{36–38} *Beta*-lactones, the only specific ClpP inhibitors reported to date, have been applied as tools to probe the binding pocket and mechanism of inhibition, as well as the transient stability of the ClpP tetradecamer and its conformational switching.^{23,25,39} One additional consequence of *beta*-lactone-based ClpP inhibition is the reduction of virulence in pathogenic bacteria such as MRSA and the eradication of *Mycobacteria* that express two essential ClpP isoforms.^{19,20,40} Here, we expand the set of ClpP tools through a novel class of phenyl esters that surpass *beta*-lactones in terms of potency in peptidase and protease inhibition, reaction kinetics, target selectivity in the soluble fraction of the proteome, plasma half-life, acyl-enzyme stability and deoligomerization as the preferred mechanism of inhibition. Contrary to *beta*-lactones, phenyl esters closely mimic the natural peptide substrate in which the acyl-enzyme intermediate is irreversibly trapped and the phenol released. Our SAR studies showed that an electron-deficient phenol moiety is important in maintaining a level of reactivity that facilitates the attack of the active site serine. The ester must be substituted with an aromatic system that is linked via at least one methylene bridge in order to pass a constricted area in the binding pocket.

Importantly, introduction of a methyl group in the *alpha* position not only enhances the acyl-enzyme stability but also yields a switch that, depending on the absolute configuration, retains the oligomeric state or induces dissociation into heptamers. Considering that the native peptide backbone branches at the same position, it is intriguing to speculate that this inhibitor-trapped intermediate may reflect a transition of ClpP-mediated substrate turnover.

It is worth noting that the HTS only revealed a very limited set of potent inhibitors and that all of these utilize a covalent mode of action. These potent inhibitors help to elucidate and dissect ClpP action; however, their translation into pharmacologically suitable virulence blockers still represents a major challenge. Inspired by the marketed phenyl ester protease inhibitor sivelestat, protection of the ester group by adjacent methyl substituents increased the ester stability, at the cost of ClpP reactivity. Thus, future studies have to consider the two opposing factors, stability and reactivity, in order to identify an optimal pharmacological candidate.

ASSOCIATED CONTENT

Supporting Information

Additional text, figures, tables and schemes giving biochemical data, labeling results, synthetic strategies, compound characterization data and ¹H and ¹³C NMR spectra. The Supporting

Information is available free of charge on the ACS Publications website at DOI: 10.1021/jacs.5b03084.

AUTHOR INFORMATION

Corresponding Author

*stephan.sieber@tum.de

Author Contributions

#M.W.H. and M.L. contributed equally to this work.

Notes

The authors declare no competing financial interest.

ACKNOWLEDGMENTS

The work was funded by the Deutsche Forschungsgemeinschaft, SFB749, SFB1035, FOR1406 and the ERC starting grant (250924-antibacterials). We would like to acknowledge Eilika Weber-Ban (ETH Zürich) for generously providing the EcClpX plasmid. We thank Malte Gersch and Matthias Stahl for providing purified EcClpX, EcClpP and hClpP proteins, as well as Ines Hübner for support in the synthesis of compounds MLIH18 and MLIH19. Furthermore, we would like to acknowledge Ernst Bernges, Burghard Cordes and Mona Wolff for technical assistance, Elena Kunold for help with analysis of quantitative mass spectrometry data and Vadim Korotkov and Annabelle Hoegl for critical revision of the manuscript.

REFERENCES

- (1) Ehrmann, M.; Clausen, T. *Annu. Rev. Genet.* **2004**, *38*, 709.
- (2) Walsh, C. T.; Garneau-Tsodikova, S.; Gatto, G. J., Jr. *Angew. Chem., Int. Ed. Engl.* **2005**, *44*, 7342.
- (3) Bieniossek, C.; Schalch, T.; Bumann, M.; Meister, M.; Meier, R.; Baumann, U. *Proc. Natl. Acad. Sci. U. S. A.* **2006**, *103*, 3066.
- (4) Botos, I.; Melnikov, E. E.; Cherry, S.; Khalatova, A. G.; Rasulova, F. S.; Tropea, J. E.; Maurizi, M. R.; Rotanova, T. V.; Gustchina, A.; Wlodawer, A. *J. Struct. Biol.* **2004**, *146*, 113.
- (5) Liu, K.; Ologbenla, A.; Houry, W. A. *Crit. Rev. Biochem. Mol. Biol.* **2014**, *49*, 400.
- (6) Ramachandran, R.; Hartmann, C.; Song, H. K.; Huber, R.; Bochtler, M. *Proc. Natl. Acad. Sci. U. S. A.* **2002**, *99*, 7396.
- (7) Bochtler, M.; Ditzel, L.; Groll, M.; Huber, R. *Proc. Natl. Acad. Sci. U. S. A.* **1997**, *94*, 6070.
- (8) Baker, T. A.; Sauer, R. T. *Biochim. Biophys. Acta* **2012**, *1823*, 15.
- (9) Katayama-Fujimura, Y.; Gottesman, S.; Maurizi, M. R. *J. Biol. Chem.* **1987**, *262*, 4477.
- (10) Frees, D.; Qazi, S. N.; Hill, P. J.; Ingmer, H. *Mol. Microbiol.* **2003**, *48*, 1565.
- (11) Thompson, M. W.; Maurizi, M. R. *J. Biol. Chem.* **1994**, *269*, 18201.
- (12) Battesti, A.; Gottesman, S. *Curr. Opin. Microbiol.* **2013**, *16*, 140.
- (13) Weber-Ban, E. U.; Reid, B. G.; Miranker, A. D.; Horwich, A. L. *Nature* **1999**, *401*, 90.
- (14) Gottesman, S.; Roche, E.; Zhou, Y.; Sauer, R. T. *Genes Dev.* **1998**, *12*, 1338.
- (15) Gaillot, O.; Pellegrini, E.; Bregenholt, S.; Nair, S.; Berche, P. *Mol. Microbiol.* **2000**, *35*, 1286.
- (16) Frees, D.; Andersen, J. H.; Hemmingsen, L.; Koskenniemi, K.; Baek, K. T.; Muhammed, M. K.; Gudeta, D. D.; Nyman, T. A.; Sukura, A.; Varmanan, P.; Savijoki, K. J. *Proteome Res.* **2012**, *11*, 95.
- (17) Frees, D.; Sorensen, K.; Ingmer, H. *Infect. Immun.* **2005**, *73*, 8100.
- (18) Gaillot, O.; Bregenholt, S.; Jaubert, F.; Di Santo, J. P.; Berche, P. *Infect. Immun.* **2001**, *69*, 4938.
- (19) Weinandy, F.; Lorenz-Baath, K.; Korotkov, V. S.; Böttcher, T.; Sethi, S.; Chakraborty, T.; Sieber, S. A. *ChemMedChem* **2014**, *9*, 710.
- (20) Böttcher, T.; Sieber, S. A. *J. Am. Chem. Soc.* **2008**, *130*, 14400.

- (21) Böttcher, T.; Sieber, S. A. *Angew. Chem., Int. Ed. Engl.* **2008**, *47*, 4600.
- (22) Gersch, M.; List, A.; Groll, M.; Sieber, S. A. *J. Biol. Chem.* **2012**, *287*, 9484.
- (23) Gersch, M.; Gut, F.; Korotkov, V. S.; Lehmann, J.; Böttcher, T.; Rusch, M.; Hedberg, C.; Waldmann, H.; Klebe, G.; Sieber, S. A. *Angew. Chem., Int. Ed. Engl.* **2013**, *52*, 3009.
- (24) Geiger, S. R.; Böttcher, T.; Sieber, S. A.; Cramer, P. *Angew. Chem., Int. Ed. Engl.* **2011**, *50*, 5749.
- (25) Gersch, M.; Kolb, R.; Alte, F.; Groll, M.; Sieber, S. A. *J. Am. Chem. Soc.* **2014**, *136*, 1360.
- (26) Zeiler, E.; List, A.; Alte, F.; Gersch, M.; Wachtel, R.; Poreba, M.; Drag, M.; Groll, M.; Sieber, S. A. *Proc. Natl. Acad. Sci. U. S. A.* **2013**, *110*, 11302.
- (27) Kang, S. G.; Ortega, J.; Singh, S. K.; Wang, N.; Huang, N. N.; Steven, A. C.; Maurizi, M. R. *J. Biol. Chem.* **2002**, *277*, 21095.
- (28) Jenkinson, E. M.; Rehman, A. U.; Walsh, T.; Clayton-Smith, J.; Lee, K.; Morell, R. J.; Drummond, M. C.; Khan, S. N.; Naeem, M. A.; Rauf, B.; Billington, N.; Schultz, J. M.; Urquhart, J. E.; Lee, M. K.; Berry, A.; Hanley, N. A.; Mehta, S.; Cilliers, D.; Clayton, P. E.; Kingston, H.; Smith, M. J.; Warner, T. T.; University of Washington Center for Mendelian Genetics; Black, G. C.; Trump, D.; Davis, J. R.; Ahmad, W.; Leal, S. M.; Riazuddin, S.; King, M. C.; Friedman, T. B.; Newman, W. G. *Am. J. Hum. Genet.* **2013**, *92*, 605.
- (29) Kim, Y. I.; Burton, R. E.; Burton, B. M.; Sauer, R. T.; Baker, T. A. *Mol. Cell* **2000**, *5*, 639.
- (30) Evans, M. J.; Cravatt, B. F. *Chem. Rev.* **2006**, *106*, 3279.
- (31) Fonovic, M.; Bogoyo, M. *Curr. Pharm. Des.* **2007**, *13*, 253.
- (32) Huisgen, R. *Proc. Chem. Soc.* **1961**, 357.
- (33) Rostovtsev, V. V.; Green, J. G.; Fokin, V. V.; Sharpless, K. B. *Angew. Chem., Int. Ed. Engl.* **2002**, *41*, 2596.
- (34) Tornøe, C. W.; Christensen, C.; Meldal, M. *J. Org. Chem.* **2002**, *67*, 3057.
- (35) Bao, K.; Fan, A.; Dai, Y.; Zhang, L.; Zhang, W.; Cheng, M.; Yao, X. *Org. Biomol. Chem.* **2009**, *7*, 5084.
- (36) Maillard, R. A.; Chistol, G.; Sen, M.; Righini, M.; Tan, J.; Kaiser, C. M.; Hodges, C.; Martin, A.; Bustamante, C. *Cell* **2011**, *145*, 459.
- (37) Iosefson, O.; Nager, A. R.; Baker, T. A.; Sauer, R. T. *Nat. Chem. Biol.* **2015**, *11*, 201.
- (38) Aubin-Tam, M. E.; Olivares, A. O.; Sauer, R. T.; Baker, T. A.; Lang, M. J. *Cell* **2011**, *145*, 257.
- (39) Gersch, M.; Famulla, K.; Dahmen, M.; Göbl, C.; Malik, I.; Richter, K.; Korotkov, V. S.; Sass, P.; Rubsamen-Schaeff, H.; Madl, T.; Brötz-Oesterheld, H.; Sieber, S. A. *Nat. Commun.* **2015**, *6*, 6320.
- (40) Compton, C. L.; Schmitz, K. R.; Sauer, R. T.; Sello, J. K. *ACS Chem. Biol.* **2013**, *8*, 2669.

**RightsLink®**[Home](#)[Account Info](#)[Help](#)

Title: Phenyl Esters Are Potent Inhibitors of Caseinolytic Protease P and Reveal a Stereogenic Switch for Deoligomerization

Author: Mathias W. Hackl, Markus Lakemeyer, Maria Dahmen, et al

Publication: Journal of the American Chemical Society

Publisher: American Chemical Society

Date: Jul 1, 2015

Copyright © 2015, American Chemical Society

Logged in as:
Markus Lakemeyer
Account #:
3001346301

[LOGOUT](#)**PERMISSION/LICENSE IS GRANTED FOR YOUR ORDER AT NO CHARGE**

This type of permission/license, instead of the standard Terms & Conditions, is sent to you because no fee is being charged for your order. Please note the following:

- Permission is granted for your request in both print and electronic formats, and translations.
- If figures and/or tables were requested, they may be adapted or used in part.
- Please print this page for your records and send a copy of it to your publisher/graduate school.
- Appropriate credit for the requested material should be given as follows: "Reprinted (adapted) with permission from (COMPLETE REFERENCE CITATION). Copyright (YEAR) American Chemical Society." Insert appropriate information in place of the capitalized words.
- One-time permission is granted only for the use specified in your request. No additional uses are granted (such as derivative works or other editions). For any other uses, please submit a new request.

[BACK](#)[CLOSE WINDOW](#)

Copyright © 2018 [Copyright Clearance Center, Inc.](#) All Rights Reserved. [Privacy statement.](#) [Terms and Conditions.](#) Comments? We would like to hear from you. E-mail us at customercare@copyright.com

3

Reversible inhibitors arrest ClpP in a defined conformational state that can be revoked by ClpX association

Published in *Angewandte Chemie International Edition*, **2015**, *54*, 15892-15896
by Axel Pahl,[#] Markus Lakemeyer,[#] Marie-Theres Vielberg,[#] Mathias W. Hackl, Jan Vomacka, Vadim S. Korotkov, Martin L. Stein, Christian Fetzer, Katrin Lorenz-Baath, Klaus Richter, Herbert Waldmann, Michael Groll, and Stephan A. Sieber.

[#]equal contribution

Reprinted with permission. © 2017 John Wiley and Sons.

DOI: 10.1002/anie.201507266

SYNOPSIS

Covalently acting drugs have experienced a resurgence in medicinal chemistry during the last few years. In antibacterial therapy, β -lactams have been successfully applied since the beginning of antibiotic development. However, covalent drugs often face the hurdle of non-specific reactivity towards cellular nucleophiles, including water, or enzymatic degradation of the reactive moiety. For β -lactams, the degradation by β -lactamases has been a reason for resistances. Structurally related β -lactones, and phenyl esters, two potent classes of covalent ClpP inhibitors, are even more susceptible to (enzymatic) hydrolysis, which thwarts their *in situ* and *in vivo* application.

In this study we present the first noncovalent inhibitors of *S. aureus* ClpP. Oxazole compounds stem from the same high-throughput screen which already yielded the phenyl ester inhibitors. Co-crystallization of ClpP and the original hit compound **AV145** provided insights into an unprecedented binding mode. The inhibitor arrests ClpP in a non-productive conformational state. Here, the active site is distorted, which, among others, is caused by a 180°-flip of a key proline residue. On the basis of the co-crystal structure and molecular modelling, extensive structure-activity relationship studies were performed. These efforts resulted in oxazole **AV286**, which inhibits ClpP's peptidase activity with an IC₅₀ in the sub-micromolar range.

All oxazoles, however, failed to efficiently inhibit the proteolytic degradation of GFP by the full ClpXP complex. Additionally, the compounds did not affect virulence in *S. aureus*. In-depth studies were performed to understand this behaviour and eventually revealed that the compound-induced conformational arrest of ClpP was revoked upon binding of its cognate chaperone ClpX.

These findings underline the conformational control of ClpX on the structure and catalytic activity of ClpP. Although oxazoles therefore do not have a direct therapeutical value, they unveiled that during inhibitor design it is important to focus on the full ClpXP complex.

AUTHOR CONTRIBUTIONS

Axel Pahl and Vadim S. Korotkov synthesized the inhibitors. Marie-Theres Vielberg and Martin L. Stein co-crystallized ClpP and **AV145**. Jan Vomacka performed activity-based protein profiling experiments. Katrin Lorenz-Baath tested the plasma stability and antivirulence properties of the compounds. Klaus Richter and Mathias Hackl performed analytical ultracentrifugation. Axel Pahl conducted the virtual screening. Markus Lakemeyer and Christian Fetzner performed biochemical assays. Markus Lakemeyer analyzed the data. Markus Lakemeyer and Stephan Sieber prepared the manuscript in collaboration with Axel Pahl, Marie-Theres Vielberg and Michael Groll.

Reversible Inhibitors Arrest ClpP in a Defined Conformational State that Can Be Revoked by ClpX Association

Axel Pahl, Markus Lakemeyer, Marie-Theres Vielberg, Mathias W. Hackl, Jan Vomacka, Vadim S. Korotkov, Martin L. Stein, Christian Fetzer, Katrin Lorenz-Baath, Klaus Richter, Herbert Waldmann, Michael Groll,* and Stephan A. Sieber*

Abstract: Caseinolytic protease P (ClpP) is an important regulator of *Staphylococcus aureus* pathogenesis. A high-throughput screening for inhibitors of ClpP peptidase activity led to the identification of the first non-covalent binder for this enzyme class. Co-crystallization of the small molecule with *S. aureus* ClpP revealed a novel binding mode: Because of the rotation of the conserved residue proline 125, ClpP is locked in a defined conformational state, which results in distortion of the catalytic triad and inhibition of the peptidase activity. Based on these structural insights, the molecule was optimized by rational design and virtual screening, resulting in derivatives exceeding the potency of previous ClpP inhibitors. Strikingly, the conformational lock is overturned by binding of ClpX, an associated chaperone that enables proteolysis by substrate unfolding in the ClpXP complex. Thus, regulation of inhibitor binding by associated chaperones is an unexpected mechanism important for ClpP drug development.

Caseinolytic protease P (ClpP), a member of the serine hydrolase enzyme family, is a major regulator of bacterial cell homeostasis.^[1] The enzymatic complex consists of two adjacent heptameric rings that are connected by central α -helices E, forming a tetradecameric barrel (Figure 1a–c). The E helix is linked to strand β 9, which forms crucial hydrogen bonds across the heptamer interface. Different conformations of ClpP have been observed. Whereas an extended E helix (Figure 1a, PDB ID: 3V5E)^[2] is important for peptidolytic activity and tetradecamer stability, a kink in this helix leads to either compact (Figure 1b, PDB ID: 4EMM)^[3] or compressed (Figure 1c, PDB ID: 3QWD)^[4] states with misaligned catalytic triads. This distortion of

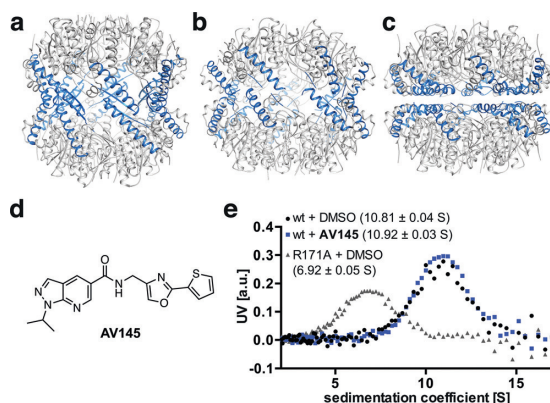


Figure 1. SaClpP in its a) extended (PDB ID: 3V5E), b) compact (PDB ID: 4EMM), and c) compressed (PDB ID: 3QWD) state. The E helices are shown in blue. d) Structure of AV145. e) Analytical ultracentrifugation of wild-type ClpP and the heptameric^[2] ClpP mutant R171A. DMSO served as a control. Sedimentation coefficient maxima are shown as the mean \pm standard deviation.

catalytic residues induces a rotation of the conserved Pro125 (in strand β 9), which in turn pulls at helix E, resulting in its collapse. ClpP requires associated chaperones, such as hexameric ClpX, to unfold and digest larger protein substrates.^[1] Moreover, ClpX binding is believed to induce conformational selection of the active and extended state.^[5]

Thus far, only β -lactones and phenyl esters have been reported as specific ClpP inhibitors in whole proteome studies.^[6] Both compound classes covalently acylate the active-site Ser98.^[7] Covalent, irreversible binding is beneficial for proteome-labeling experiments, mechanistic studies, and for achieving a prolonged target residence time. The in vitro^[5,6] and in vivo^[8] application of irreversible ClpP inhibitors, however, has been limited by the low stability of their electrophilic motifs owing to hydrolysis.^[9] Thus far, all attempts to design non-covalent inhibitors have failed.^[7a] Surprisingly, given the importance of ClpP inactivation and the need for rational design, only one complex crystal structure of the protease with a nonspecific chloromethyl ketone (CMK) peptide ligand is available (PDB ID: 2FZS).^[10] Herein, we report the first co-crystal structure of a specific ClpP inhibitor with a novel, reversible mode of action, which was further exploited to synthetically optimize the ligand by rational design and in silico screening.

[*] Dr. A. Pahl,^[4] M. Lakemeyer,^[4] M.-T. Vielberg,^[4] M. W. Hackl, J. Vomacka, Dr. V. S. Korotkov, Dr. M. L. Stein, C. Fetzer, Dr. K. Lorenz-Baath, Dr. K. Richter, Prof. Dr. M. Groll, Prof. Dr. S. A. Sieber
Center for Integrated Protein Science at the Department of Chemistry, Technische Universität München
Lichtenbergstrasse 4, 85747 Garching (Germany)
E-mail: michael.groll@tum.de
stephan.sieber@tum.de

Prof. Dr. H. Waldmann
Department of Chemistry and Chemical Biology
Technische Universität Dortmund
Otto-Hahn-Strasse 6, 44221 Dortmund (Germany)

[†] These authors contributed equally to this work.

Supporting information and ORCID(s) from the author(s) for this article are available on the WWW under <http://dx.doi.org/10.1002/anie.201507266>.

A previous high-throughput screen (HTS) with about 140 000 compounds from the COMAS library (MPI Dortmund) did not reveal a single non-covalently binding SaClpP inhibitor with an $IC_{50} < 2 \mu\text{M}$.^[6a] However, the low activity of ClpP with the standard Suc-Leu-Tyr-AMC substrate requires at least $1 \mu\text{M}$ ClpP to record significant turnover, so that the potencies of the best inhibitors are still in the micromolar concentration range. We therefore reinvestigated our previous HTS results by lowering the selection criteria to an $IC_{50} \leq 10 \mu\text{M}$.^[6a] Four compounds of the HTS fulfilled this prerequisite (Supporting Information, Figure S1). Mass-spectrometric analysis of the intact proteins revealed that **AV145** binds non-covalently (Figure 1 d, Figure S1), and medicinal-chemistry considerations made this compound the most promising candidate for further analysis. Compound **AV145** lacks any reactive groups and consists of three characteristic heterocycles, a pyrazolopyridine as well as a 2-(thiophen-2-yl)oxazole moiety. Time-dependent incubation of SaClpP with **AV145** did not change the IC_{50} (Figure S2), supporting the fact that the compound is a reversible inhibitor. Furthermore, analytical ultracentrifugation demonstrated that **AV145**, unlike most phenyl esters and lactones, did not induce dissociation of ClpP into heptamers (Figure 1 e).^[6a,7b]

To gain insights into the mechanism of inhibition, we co-crystallized **AV145** with SaClpP and solved the complex structure by molecular replacement at 3 \AA resolution ($R_{\text{free}} = 27.4\%$, Table S1, PDB ID: 5DL1). The asymmetric unit contains a ClpP tetradecamer with the compound bound to every subunit. Despite variations in occupancy, model building into the averaged $2F_o - F_c$ electron-density map allowed the unambiguous positioning of **AV145** near to the active site between α -helix E and strand $\beta 9$ (Figure 2 a). Surprisingly,

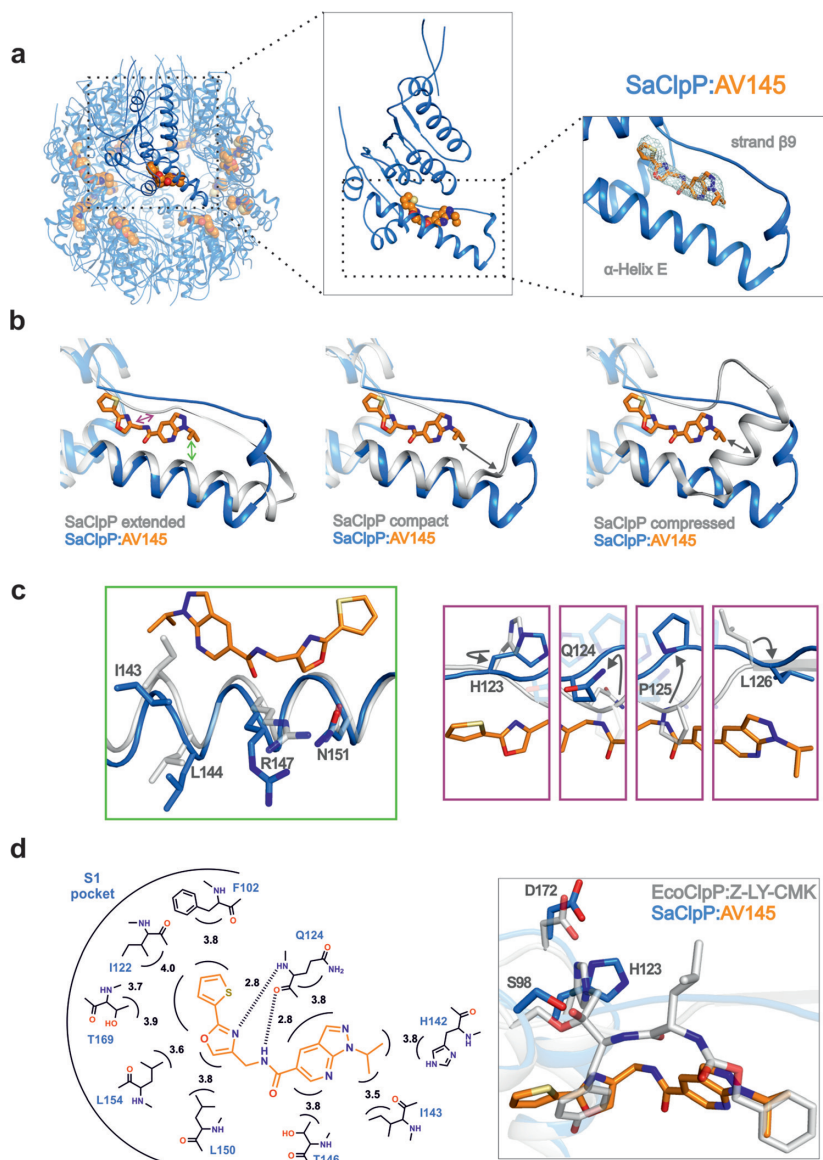


Figure 2. a) Binding of **AV145** to SaClpP (PDB ID: 5DL1). b) Structural superposition of SaClpP:**AV145** with the extended, compact, or compressed form of SaClpP. Structural changes between the extended and co-crystal structure are indicated by colored arrows. c) Detailed exploration of the structural changes of α -helix E and strand $\beta 9$ compared to the extended form. d) Analysis of the specific enzyme-inhibitor contacts and overlay with the EcoClpP:Z-LY-CMK structure (PDB ID: 2FZS), illustrating the non-covalent inhibition mechanism of **AV145**. Color code: SaClpP:**AV145** marine, **AV145** orange, SaClpP:extended/compact/compressed and EcoClpP:Z-LY-CMK gray; heteroatoms: O red, N blue, S yellow.

overlays with structures of the apo enzyme in its extended, compact, and compressed form revealed that the inhibitor binds in a non-substrate-like mode and induces an unprecedented conformational state (Figure 2 b). Although helix E is almost completely aligned as in the extended, active enzyme, binding of **AV145** displaces Ile143 and Arg147 because of

a steric clash (Figure 2c) leading to a shift of about 1.4 Å in the center of the helix (green arrow in Figure 2b). The majority of the structural alterations, however, are found in strand β 9 (purple arrow in Figure 2b). Formation of a β -sheet with the subunit in the opposite ring is impeded, as can be seen by the partial disorder of the two glycine residues 127 and 128. Notably, β 9 is mainly defined by a large inhibitor-induced flip of Pro125 of about 180°. The residue still retains its *trans* peptide bond and resides at a similar position as in the inactive form of the protease (Figure 2c). One direct consequence of this relocation is a shift of His123 out of the catalytic triad, leading to a distortion of the active site, which explains the inhibiting effect of AV145. The induced structural rearrangement of Pro125 also causes a major change to Gln124. Hereby, Gln124 is arrested in a position where it is able to form two hydrogen bonds between its peptide backbone and AV145, likely providing important protein–inhibitor interactions. Moreover, an extended network of van

der Waals contacts with Phe102, Ile122, His142, Ile143, Thr146, Leu150, and Leu154 as well as Thr169 stabilizes compound binding (Figure 2d). Overall, this novel mode of action explains why AV145 is a non-covalent SaClpP inhibitor. Superposition of our structure with the Z-LY-CMK bound EcClpP structure (PDB ID: 2FZS)^[10] reveals differences (Figure 2d). Unlike CMK, AV145 does not influence the catalytic center of SaClpP directly, but rather transmits its function through neighboring residues. Such a type of indirect binding has not been observed for this class of enzymes thus far.

The co-crystal structure of SaClpP in complex with AV145 provides key information for improving inhibitor potency. The two constituent parts of the molecule, namely the pyrazolopyridine (acid part) and 2-(thiophen-2-yl)oxazole (amine part) moieties, were substituted with different chemical groups to explore their structure–activity relationships (SARs; Figure 3a). Compounds were designed according to

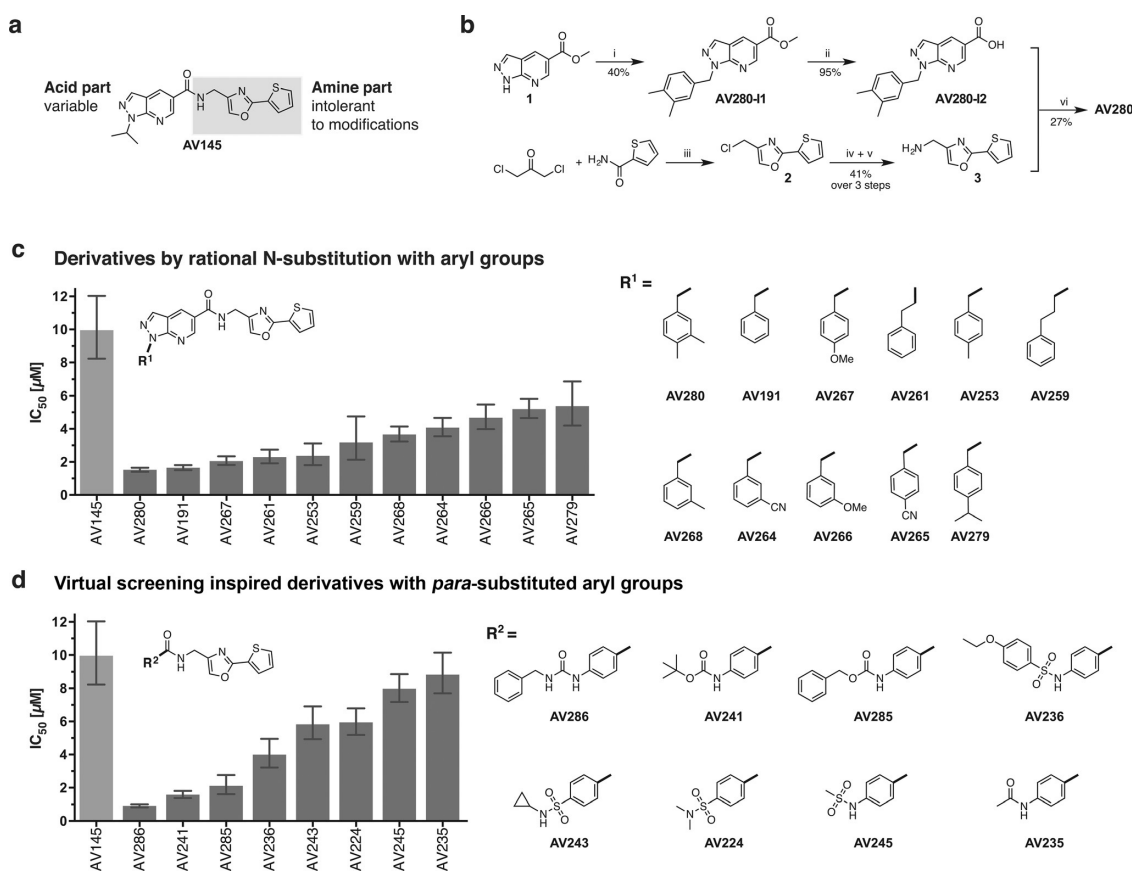


Figure 3. SAR studies. a) The amine part of AV145 is intolerant to modifications whereas the acid part can be modified to improve ClpP inhibition. b) Synthesis of AV280: Reagents and conditions: i) 3,4-dimethylbenzyl bromide, K₂CO₃, DMF, RT, 18 h; ii) LiOH, THF/H₂O (9:1), RT, 18 h; iii) neat, 120 °C, 16 h; iv) NaN₃, DMF, 60 °C, 16 h; v) PPh₃, THF/H₂O (9:1), RT, 16 h; vj) TBTU, NMM, DMF, 0 °C to RT, 18 h. Structures and IC₅₀ values for derivatives with c) *N*-aryl substituents and d) *para*-substituted aryl groups that were inspired by virtual screening. IC₅₀ values are derived from at least two biological experiments with three technical replicates per concentration and are shown as mean and 95 % confidence interval. See the Supporting Information for further details.

rational considerations or resulted from a virtual screen (see the Supporting Information). Alterations within the amine part, for example, by introduction of thiophene substituents and the replacement of the thiophene by a phenyl or oxazole group, resulted in inactive compounds (Figures S3, S4). However, modifications within the acid part were much more tolerated and led to improved inhibitors. Based on this, we explored the possibility of incorporating aromatic groups for π -stacking with His142 (part of the strand β 9) through the design of eleven derivatives with *N*-aryl substituents (Figure 3c).

The synthesis of these derivatives, exemplified for **AV280** in Figure 3b, involved *N*-alkylation of pyrazolopyridine **1** with 3,4-dimethylbenzyl bromide, followed by saponification of the ester with lithium hydroxide. Preparation of the oxazole amine part **3** started with the condensation of the appropriate aryl amide with dichloroacetone at 120 °C. The resulting chloromethyl-substituted oxazole **2** was converted into amine **3** in two steps. Standard amide coupling of the acid with the amine resulted in the final products.

AV191 and **AV280**, which bear a benzyl and a 3,4-dimethylbenzyl substituent, respectively, showed a sixfold increase in ClpP inhibition compared to **AV145**, with IC_{50} values of 1.7 and 1.5 μ M, respectively (Figure 3c). Based on results from the virtual screening, we next replaced the pyrazolopyridine moiety by aryl rings with a *para* urea or a *para* carbamate substituent, resulting in **AV286** with an IC_{50} value of 0.9 μ M (Figure 3d). Notably, this value shows that a stoichiometric amount of **AV286** (relative to the monomer concentration of the protease) is sufficient to inhibit 50% of SaClpP. An increase in substrate concentration did not influence inhibitor binding (Figure S5).

With potent and reversible ClpP inhibitors at hand, we investigated whether the best compound of this series exhibits cell permeability and target selectivity in situ. Therefore, an **AV286**-related activity-based protein profiling^[11] photoprobe (**AV321**) equipped with a diazirine photocrosslinker and an alkyne tag was prepared (Figure 4a).^[12] Pleasingly, the probe retained a low IC_{50} value (2 μ M) for SaClpP peptidase inhibition (Figure S6). Living *S. aureus* cells were incubated with **AV321**, irradiated with UV light to form a covalent link between target protein and diazirine, lysed, and clicked to a functionalized azide tag (fluorescent dye or biotin) via the alkyne; the labeled proteome was then analyzed by fluorescence SDS-PAGE analysis (Figure 4b) or mass spectrometry (MS; Figure 4c). A dominant fluorescent protein band at the molecular weight of ClpP appeared on SDS-PAGE (Figure 4b). To confirm ClpP binding in situ we performed quantitative gel-free MS by isotope labeling.^[13] MS-based target enrichment was visualized by volcano plots (Figure 4c, Figure S7). In all runs, ClpP was highly enriched, and only a few putative off-targets (significance level: $p \leq 0.05$), such as the 50S ribosomal protein L1 (Protein ID ID: Q2G0P0), were detected. We next examined whether cell-permeable inhibitors reduced the production of α -hemolysin (hla), a predominant *S. aureus* toxin regulated by ClpP. Surprisingly, the general level of hla was high, suggesting that inhibition of intracellular proteolysis was not as efficient as the reduction of in vitro peptidase activity.

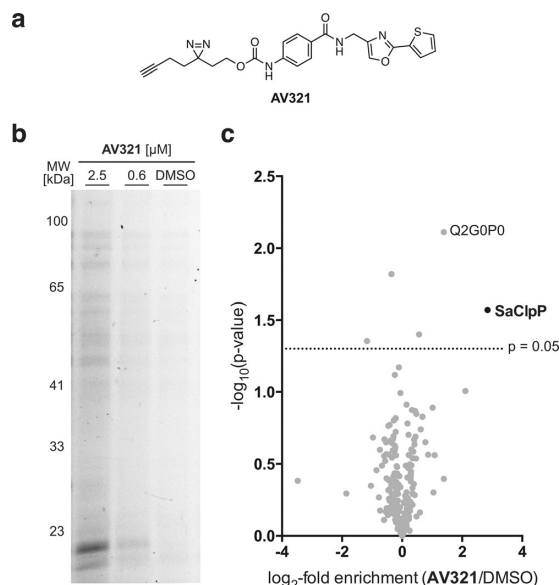


Figure 4. In situ target validation in living *S. aureus* cells with **AV321**. a) Chemical structure of the activity-based photoprobe **AV321**. b) Fluorescence SDS-PAGE analysis of the soluble fraction. c) Volcano plot representation of gel-free quantitative ABPP experiments measured on the Orbitrap XL. Data are derived from three biological replicates for DMSO and **AV321** (5 μ M), respectively. The \log_2 -fold enrichment values were z-score-normalized, and $\log_{10}(p$ values) were calculated using a two-sided one-sample Student's t-test. Protein enriched in addition to SaClpP: Protein ID Q2G0P0: 50S ribosomal protein L1. See the Supporting Information for further details and additional analysis.

To explore this finding in more detail, we tested the most potent peptidase inhibitors in a ClpXP protease assay with fluorescent GFP-SsrA (tagged for ClpXP degradation) as a substrate. Indeed, all inhibitors were largely inactive in this assay (Figure S8), demonstrating that ClpX overrides the inhibitor-induced conformational lock. To investigate the mechanistic basis of this unexpected behavior, we utilized a previously introduced activator of ClpP.^[14] This compound displaces ClpX in protease assays and was thus used as a surrogate for the chaperone (Figure S9). The molecule abolished **AV286** inhibition of ClpP in casein and peptidase assays in a concentration-dependent manner, which validates a conformational selection of the active enzyme state by ClpX or its surrogates (Figure S9).^[15] Our observation is in line with a recent study that showed a conformational switch to the active and extended state upon binding of acyldepsipeptides, which mimic ClpX binding.^[5] Thus, regulation by ClpX and other proteolytic activators represents an important and thus far neglected parameter for future ClpP inhibitor development.

In conclusion, **AV145** bound to ClpP arrested the enzyme in an unprecedented inactive conformational state by a significant rotation of Pro125 and an associated misalignment of the catalytic triad architecture. This binding mode was explored for the design of new compounds, which resulted in **AV286**, the first non-covalent inhibitor of ClpP with an

IC₅₀ value of < 1 μM. Importantly, ClpX revoked non-covalent binding of the examined inhibitors to ClpP, a counter-intuitive finding when compared to related complex proteolytic systems, such as the proteasome, where stable proteolytic inhibitors for individual subunits have been described.^[16] Our results therefore strongly imply that regulators such as the ATP-dependent ClpX orchestrate and modulate various distinct conformational stages in the hydrolytic chamber of ClpP. For the identification of non-covalent ClpP inhibitors that are also active in situ, it is thus important not to solely focus on the peptidase activity of the isolated ClpP complex, as this, although easy to monitor, does not accurately reflect the situation in live cells. We hypothesize that sustained ClpP inhibition may either be achieved by increasing the small-molecule-induced conformational lock by, for example, the incorporation of large ligands that block the proteolytic channel, or by inhibitor discovery with the intricate ClpXP proteolytic complex. Both would certainly represent attractive starting points for the future optimization of anti-virulence compounds against *S. aureus* and its antibiotic-resistant strains.

Acknowledgements

The work was funded by the Deutsche Forschungsgemeinschaft (SFB1035), the Bundesministerium für Bildung und Forschung (FKZ: 031A131), the European Community's Seventh Framework Programme (FP7/2007–2013) under BioStruct-X (283570), and the Center for Integrated Protein Science (CIPSM). M.L. was supported by the German National Academic Foundation. We thank the staff of the beamline X06SA at the Paul Scherrer Institute, Swiss Light Source (Villingen, Switzerland) for help with data collection. Furthermore, we would like to acknowledge Heike Hofmann, Ernst Bernges, Katja Bäumel, Burghard Cordes, and Mona Wolff for technical assistance. We are grateful to Elena Kunold for help with the analysis of quantitative mass spectrometry data, Pavel Kielkowski for synthesis of the ADEP fragment, and Megan Wright for critical revision of the manuscript.

Keywords: caseinolytic protease · conformational selection · non-covalent inhibition · protein crystallography · structural rearrangement

How to cite: *Angew. Chem. Int. Ed.* **2015**, *54*, 15892–15896
Angew. Chem. **2015**, *127*, 16121–16126

- [1] a) T. A. Baker, R. T. Sauer, *Biochim. Biophys. Acta Mol. Cell Res.* **2012**, *1823*, 15–28; b) J. Ortega, S. K. Singh, T. Ishikawa, M. R. Maurizi, A. C. Steven, *Mol. Cell* **2000**, *6*, 1515–1521; c) J. A. Alexopoulos, A. Guarne, J. Ortega, *J. Struct. Biol.* **2012**, *179*, 202–210.
- [2] M. Gersch, A. List, M. Groll, S. A. Sieber, *J. Biol. Chem.* **2012**, *287*, 9484–9494.
- [3] F. Ye, J. Zhang, H. Liu, R. Hilgenfeld, R. Zhang, X. Kong, L. Li, J. Lu, X. Zhang, D. Li, H. Jiang, C. G. Yang, C. Luo, *J. Biol. Chem.* **2013**, *288*, 17643–17653.
- [4] S. R. Geiger, T. Böttcher, S. A. Sieber, P. Cramer, *Angew. Chem. Int. Ed.* **2011**, *50*, 5749–5752; *Angew. Chem.* **2011**, *123*, 5867–5871.
- [5] M. Gersch, K. Famulla, M. Dahmen, C. Gobl, I. Malik, K. Richter, V. S. Korotkov, P. Sass, H. Rubsamen-Schaeff, T. Madl, H. Brotz-Oesterheld, S. A. Sieber, *Nat. Commun.* **2015**, *6*, 6320.
- [6] a) M. W. Hackl, M. Lakemeyer, M. Dahmen, M. Glaser, A. Pahl, K. Lorenz-Baath, T. Menzel, S. Sievers, T. Böttcher, I. Antes, H. Waldmann, S. A. Sieber, *J. Am. Chem. Soc.* **2015**, *137*, 8475–8483; b) T. Böttcher, S. A. Sieber, *Angew. Chem. Int. Ed.* **2008**, *47*, 4600–4603; *Angew. Chem.* **2008**, *120*, 4677–4680.
- [7] a) M. Gersch, F. Gut, V. S. Korotkov, J. Lehmann, T. Böttcher, M. Rusch, C. Hedberg, H. Waldmann, G. Klebe, S. A. Sieber, *Angew. Chem. Int. Ed.* **2013**, *52*, 3009–3014; *Angew. Chem.* **2013**, *125*, 3083–3088; b) M. Gersch, R. Kolb, F. Alte, M. Groll, S. A. Sieber, *J. Am. Chem. Soc.* **2014**, *136*, 1360–1366.
- [8] F. Weinandy, K. Lorenz-Baath, V. S. Korotkov, T. Böttcher, S. Sethi, T. Chakraborty, S. A. Sieber, *ChemMedChem* **2014**, *9*, 710–713.
- [9] A. Cole et al., *Cancer Cell* **2015**, *27*, 864–876.
- [10] A. Szyk, M. R. Maurizi, *J. Struct. Biol.* **2006**, *156*, 165–174.
- [11] a) M. J. Evans, B. F. Cravatt, *Chem. Rev.* **2006**, *106*, 3279–3301; b) P. P. Geurink, L. M. Prely, G. A. van der Marel, R. Bischoff, H. S. Overkleeft, *Top. Curr. Chem.* **2012**, *308-319*, 85–113.
- [12] a) Z. Li, P. Hao, L. Li, C. Y. J. Tan, X. Cheng, G. Y. J. Chen, S. K. Sze, H.-M. Shen, S. Q. Yao, *Angew. Chem. Int. Ed.* **2013**, *52*, 8551–8556; *Angew. Chem.* **2013**, *125*, 8713–8718; b) V. V. Rostovtsev, J. G. Green, V. V. Fokin, K. B. Sharpless, *Angew. Chem. Int. Ed.* **2002**, *41*, 2596–2599; *Angew. Chem.* **2002**, *114*, 2708–2711; c) C. W. Tornøe, C. Christensen, M. Meldal, *J. Org. Chem.* **2002**, *67*, 3057–3064; d) R. Huisgen, *Proc. Chem. Soc.* **1961**, 357–396.
- [13] P. J. Boersema, R. Raijmakers, S. Lemeer, S. Mohammed, A. J. Heck, *Nat. Protoc.* **2009**, *4*, 484–494.
- [14] D. W. Carney, C. L. Compton, K. R. Schmitz, J. P. Stevens, R. T. Sauer, J. K. Sello, *ChemBioChem* **2014**, *15*, 2216–2220.
- [15] M. Merdanovic, T. Mönig, M. Ehrmann, M. Kaiser, *ACS Chem. Biol.* **2013**, *8*, 19–26.
- [16] E. M. Huber, M. Groll, *Angew. Chem. Int. Ed.* **2012**, *51*, 8708–8720; *Angew. Chem.* **2012**, *124*, 8838–8850.

Received: August 4, 2015

Revised: September 15, 2015

Published online: November 13, 2015

**JOHN WILEY AND SONS LICENSE
TERMS AND CONDITIONS**

Oct 11, 2018

This Agreement between Lichtenbergstr 4 ("You") and John Wiley and Sons ("John Wiley and Sons") consists of your license details and the terms and conditions provided by John Wiley and Sons and Copyright Clearance Center.

License Number	4445891481823
License date	Oct 11, 2018
Licensed Content Publisher	John Wiley and Sons
Licensed Content Publication	Angewandte Chemie International Edition
Licensed Content Title	Reversible Inhibitors Arrest ClpP in a Defined Conformational State that Can Be Revoked by ClpX Association
Licensed Content Author	Axel Pahl, Markus Lakemeyer, Marie-Theres Vielberg, et al
Licensed Content Date	Nov 13, 2015
Licensed Content Volume	54
Licensed Content Issue	52
Licensed Content Pages	5
Type of use	Dissertation/Thesis
Requestor type	Author of this Wiley article
Format	Print and electronic
Portion	Full article
Will you be translating?	No
Title of your thesis / dissertation	Probing the catalytic activity and oligomeric assembly of S. aureus ClpXP
Expected completion date	Nov 2018
Expected size (number of pages)	160
Requestor Location	Lichtenbergstr 4 Organische Chemie II Lichtenbergstr. 4 Garching, Bavaria 85748 Germany Attn: Lichtenbergstr 4
Publisher Tax ID	EU826007151
Total	0.00 EUR
Terms and Conditions	

TERMS AND CONDITIONS

This copyrighted material is owned by or exclusively licensed to John Wiley & Sons, Inc. or one of its group companies (each a "Wiley Company") or handled on behalf of a society with which a Wiley Company has exclusive publishing rights in relation to a particular work

4

Amino acid-based phenyl esters as chemical tools for inhibition, activation and disintegration of the ClpXP protease

4.1 INTRODUCTION AND OBJECTIVE

As outlined in Chapter 2, the phenyl ester group is a novel, privileged warhead motif for covalent inhibition of the ClpXP protease of various species.^[1,2] On a mechanistic level, inhibition occurs via attack of ClpP's active site serine at the ester group of the inhibitor. In a transesterification reaction, a covalent acyl-enzyme complex is formed, as the phenolic leaving group is released (Figure 4.1a). For *S. aureus*, the stereochemistry of a methyl group in the α -position of the ester was identified as critical for the mode of action. Depending on the stereo-information at this chiral center, the compound either facilitated full modification of all active sites and retention of the 14-mer ClpP complex ((*S*)-**ML90**), or partial modification and de-oligomerization into two heptameric species ((*R*)-**ML89**).^[1]

The dissociation of ClpP into heptameric species has been previously observed upon binding to selected β -lactone inhibitors, but a clear structure-activity-relationship (SAR) for de-oligomerization could not be obtained. It remains to be seen if the inactive heptameric form of ClpP is only an artifact of inhibition with synthetic molecules, or if this state has a biological function; *e.g.* for the release of cleavage products after proteolysis or within the regulation of ClpP's catalytic activity. Previous studies have shown that ClpP and its cognate chaperones, such as ClpX substantially influence each other's structure, catalytic activity and susceptibility to inhibition.^[3-6] However, a detailed understanding of the exact communication within the proteolytic ClpXP complex and how it can efficiently be modulated by molecular probes is still lacking.

This work builds upon the first generation of phenyl ester inhibitors and the corresponding SAR data. Because the critical α -methyl group, which acts as a stereogenic switch for ClpP, corresponds to an amino group in structurally closely-related aromatic amino acids (Figure 4.1b), respective (*R*)- and (*S*)-amino acid-based phenyl esters were synthesized and evaluated for biochemical activity. Systematic screening of amino acids in the P1 and P2 positions of peptide phenyl esters revealed improved compounds that surpassed the potency of previous ClpXP inhibitors. Additionally, derivatives were found that stimulated, rather than inhibited ClpXP-mediated proteolysis. The compounds and various techniques were applied to probe the oligomerization of ClpP and ClpX, as well as their affinity for each other. In this regard, a novel ClpXP complex was

identified with an unprecedented stoichiometry and its potential biological function was evaluated.

4.2 RESULTS AND DISCUSSION

4.2.1 STRUCTURE-ACTIVITY RELATIONSHIP STUDIES

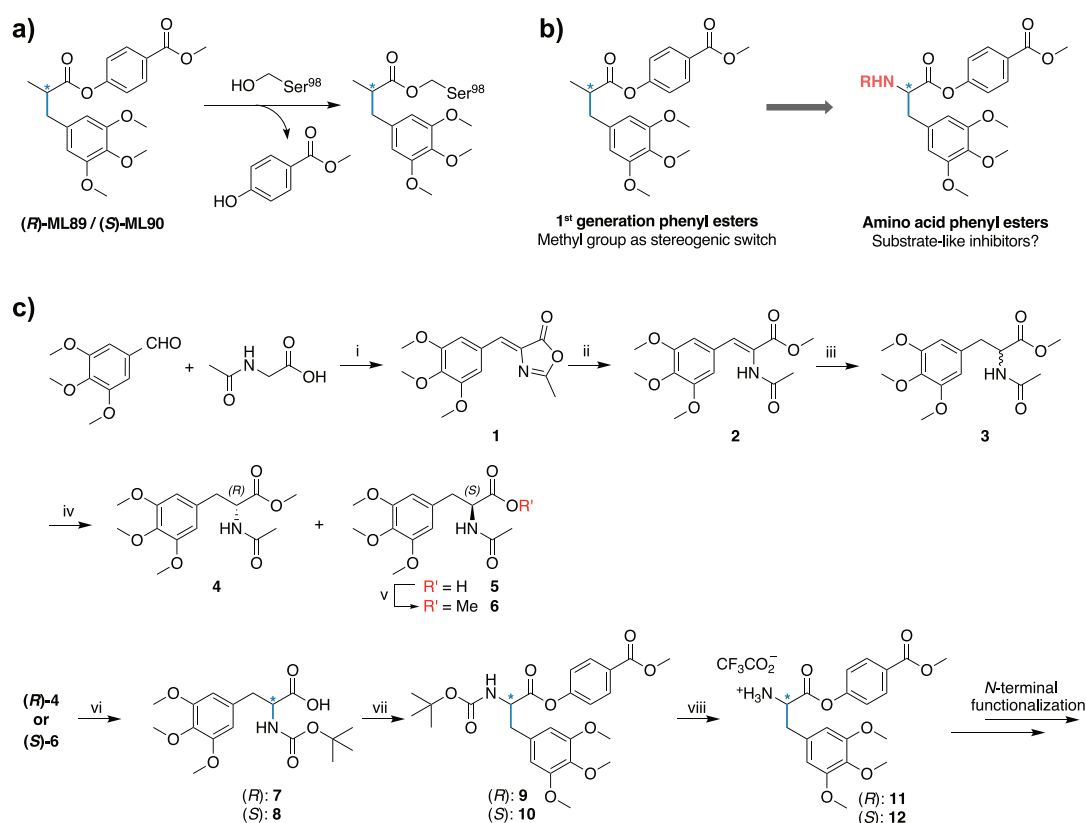


Figure 4.1. From 1st generation of phenyl esters to amino acid-based phenyl esters a) Reaction of phenyl esters (*R*)-ML89 or (*S*)-ML90 with the active site Ser⁹⁸ of ClpP leads to the formation of a stable acyl-enzyme complex. b) Replacement of the critical α -methyl group by a substituted amine generates amino acid-based phenyl esters. c) Stereoselective synthesis of unnatural 3,4,5-trimethoxy-phenylalanine (Tmo) phenyl ester derivatives. *Reagents and conditions:* i) NaOAc, Ac₂O, 125 °C, 5 h; ii) NaOMe, MeOH, rt, 1.5 h; iii) H₂, Pd/C, MeOH, rt, 16 h; iv) Alcalase, 0.2 M aq. NaHCO₃, rt, 6 h; v) *p*-TsOH, MeOH, 80 °C, 6 h; vi) Boc₂O, DMAP, 75 °C, 3 h, then 2 M aq. LiOH, rt, 3 h; vii) methyl-4-hydroxybenzoate, EDC · HCl, HOBT, DIPEA, DCM, 0 °C → rt, 18 h; viii) TFA, DCM, 0 °C, 5 h.

The first generation of phenyl esters surpassed previous β -lactone inhibitors in potency and hydrolytic stability. As a result of extensive SAR studies, the prominent 3,4,5-tri-

methoxyphenyl moiety was shown to be critical for good binding to ClpP and could only be poorly replaced.^[1] Thus, this motif was selected as the side chain decoration of the first amino acid phenyl esters, yielding the unnatural amino acid 3,4,5-trimethoxyphenylalanine (Tmo, Figure 4.1b).

Both enantiomers of the amino acid were synthesized, following the well-known Erlenmeyer-synthesis route, starting from 3,4,5-trimethoxybenzaldehyde and acetyl glycine (Figure 4.1c).^[7,8] After azlactone formation, the heterocycle **1** was opened with sodium methanolate and the double bond was reduced, affording the racemic *N*-acetyl methyl ester **3**. Enzymatic resolution allowed for separation of the enantiomers, as only the (*S*)-enantiomer was hydrolyzed and subsequently separated from the (*R*)-methyl ester **4** by extraction. To facilitate the following steps for both enantiomers analogously, the methyl ester was subsequently re-introduced. For each enantiomer, one-pot conversion of the acetyl-moiety to a Boc-group and ester hydrolysis yielded the respective (*R*)-**7** and (*S*)-**8** intermediates. Lastly, esterification with methyl-4-hydroxy benzoic acid generated the respective Boc-Tmo phenyl esters (*R*)-**9** and (*S*)-**10**. For the synthesis of *N*-terminally modified dipeptide phenyl esters, the compounds were first Boc-deprotected, yielding (*R*)-**11** as well as (*S*)-**12**, and were subjected to standard solution-phase peptide chemistry.

All phenyl ester compounds were initially tested in three concentrations (100, 10, 1 μ M) using two different assay setups: 1) inhibition of ClpP's peptidolytic activity towards the fluorogenic peptide Ac-Ala-hArg-(*S*)-2-aminooctanoic acid-7-amino-4-carbamoylmethylcoumarin (Ac-Ala-hArg-2-Aoc-ACC), which is an optimized substrate for ClpP-mediated degradation,^[9] and 2) inhibition of the full ClpXP complex by means of green fluorescent protein (GFP) that was tagged with a short SsrA-peptide sequence. ClpX recognizes the SsrA-sequence as a degradation signal, unfolds the protein and directs it into the proteolytic chamber where it is subsequently digested.^[10] Compared to previously reported *S. aureus* ClpP peptidase assays,^[1,4,11] the minimal buffer system was changed to the buffer of the protease assay, as we found that this increased the peptidase activity fourfold, and in some cases considerably altered the inhibition of ClpP by small molecules (compare to Supporting Figure 1).

The inhibition of ClpP and ClpXP by the first set of *N*-terminally modified Tmo phenyl esters is depicted in Figure 4.2a. From the new phenyl esters, the previously described stereo-preference of ClpP was confirmed, meaning that (*R*)-phenyl esters were generally better inhibitors than the respective (*S*)-enantiomers. The unmodified Tmo phenyl esters (*R*)-**11**/*(S)*-**12** behaved similarly to the α -methyl compounds (*R*)-**ML89**/*(S)*-**ML90** in peptidase and protease assays. Only the (*R*)- enantiomers showed moderate inhibition of the ClpXP system (full inhibition at 100 μ M) while the (*S*)-enantiomers were inactive. Capping the amine with a pivaloyl- (**13** and **14**) or Boc-(**9** and **10**) group led to significantly improved inhibitors. The best derivative, (*R*)-Boc-Tmo-OAr (**9**), had an apparent IC₅₀ of 0.37 μ M in the protease assay, representing the most potent ClpXP inhibitor, while its (*S*)-enantiomer (*S*)-Boc-Tmo-OAr (**10**) was 25-times weaker (Figure 4.2b). Importantly, the average grade of active-site modification for **9** at the IC₅₀ concentration was \approx 10% (Supporting Figure 2a-c). Hence, sub-stoichiometric binding of **9** facilitates an overall conformational rearrangement that leads to inhibition of all active sites. Lastly, we tested the sterically more demanding Cbz-protecting group, which was well-tolerated for the (*R*)-enantiomer **15** in the peptidase assay, but failed to inhibit the full ClpXP complex. The respective (*S*)-enantiomer **16** showed poor inhibition under peptidase and protease conditions (Figure 4.2a).

In general, the effective inhibition of ClpP's peptidolytic activity did not necessarily lead to efficient inhibition of the proteolytic ClpXP complex. This finding is in accordance with previous studies, confirming that ClpX exerts conformational control over ClpP and is able to boost peptidolysis and revoke inhibitor binding.^[3,4] This study was thus focused on the biologically more relevant ClpXP protease system for subsequent compound evaluation.

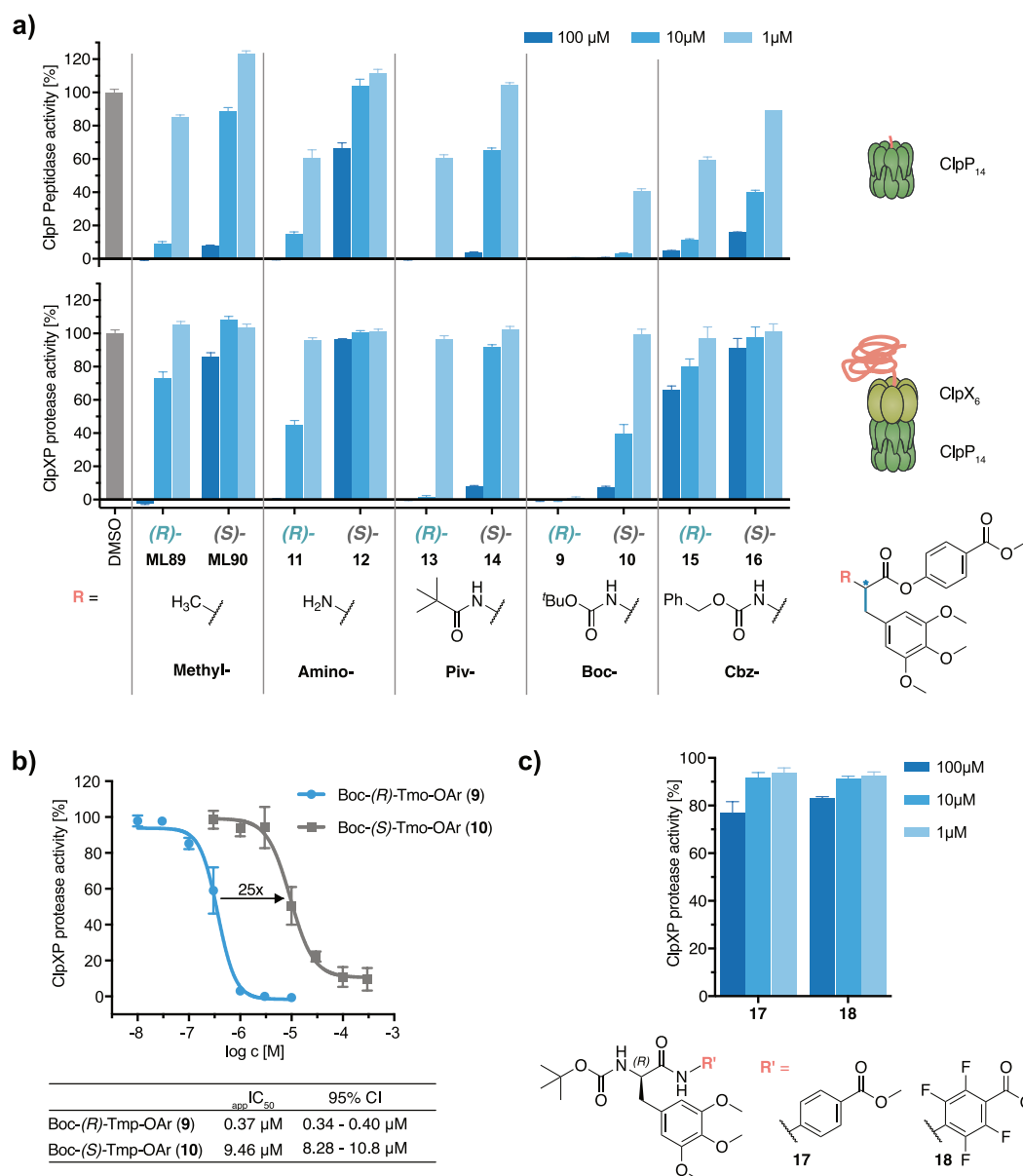


Figure 4.2. Biochemical evaluation of *N*-terminally capped Tmo phenyl esters. a) Inhibition of ClpP peptidase (10 nM ClpP₁₄, 200 μ M Ac-Ala-hArg-2-Aoc-ACC) and ClpXP protease (100 nM ClpP₁₄, 200 nM ClpX₆, 300 nM SsrA-GFP) activity by the respective enantiomers. b) Determination of the apparent IC_{50} of ClpXP protease activity for both enantiomers of Boc-Tmp-OAr. c) Inhibition of ClpXP protease activity by aryl amide derivatives. Data are normalized to the DMSO control (100% activity) and presented as mean and standard error of the mean (SEM). Each data set is derived from at least two independent experiments, which were measured in triplicates.

A key challenge for many covalent inhibitors is the susceptibility to cellular nucleophiles, especially water, which often hampers application *in vivo*. In previous studies the hydrolytically labile phenyl ester and lactone motifs of ClpP inhibitors were substituted

with more stable groups (*e.g.* amides or sulfone amides). All of these efforts, however, failed to deliver potent binders.^[1,12] Having identified phenyl ester **9** as a remarkable inhibitor of both ClpP and ClpXP, another attempt to replace the ester group was made. Unfortunately, the aryl amide derivative **17** did not show any inhibition of ClpXP, which is most likely attributed to the enhanced stability of the amide group. To further increase reactivity, a fluorinated aryl amide **18** was synthesized. However, this compound could not compete with substrate turnover even at 100 μM (Figure 4.2c). These findings indicate that the reactivity of the phenyl esters and/or its binding mode to ClpP is finely tuned and thus cannot be simply altered without losing efficacy.

Next, we investigated, if inhibition by (*R*)-amino acid phenyl esters was a general feature or if it was exclusive to the unnatural amino acid Tmo. A collection of thirteen diverse (*R*)-, *i.e.* D-, amino acid phenyl esters was synthesized and the effect on the proteolytic activity of ClpXP was evaluated (Figure 4.3a). Unfortunately, almost all derivatives were inactive, including phenyl esters of nonpolar alanine (**20**) and methionine (**22**), or polar serine (**27**) and glutamine (**29**). The aromatic phenylalanine (**23**) and tyrosine (**24**) derivatives, structurally closely related to **9**, also did not affect proteolysis. Only the leucine (**21**) and tryptophan (**25**) phenyl esters showed inhibition at high and medium concentrations, respectively. Nevertheless, compound **9** remained by far the most potent derivative.

Previous studies have shown that ClpP has a large hydrophobic S₁ pocket that can accommodate long alkyl chains.^[12] Covalently acting β -lactone compounds with alkyl chains of various lengths,^[13,14] as well as fluorogenic peptide substrates, containing the unnatural amino acid (*S*)-2-aminooctanoic acid (2-Aoc) in the P₁ position,^[9] were correspondingly good inhibitors and substrates, respectively. Contrarily, this preference could not be transferred to the phenyl esters, as the Boc-(*R*)-2-Aoc phenyl ester **31** did not inhibit ClpXP. The binding geometry of (*R*)-phenyl esters during inhibition must, therefore, be different than the geometry of β -lactone inhibitors and peptide substrates. For the first generation of phenyl esters, modeling predicted that the 3,4,5-trimethoxy phenyl moiety binds to the described hydrophobic pocket.^[1] The fact that only leucine (**21**) and tryptophan (**25**) phenyl esters, but not structurally related phenylalanine (**23**) and tyrosine (**24**) side chains induce inhibition highlights the special structural properties of the nonpolar, yet flexible 3,4,5-trimethoxyphenyl moiety.

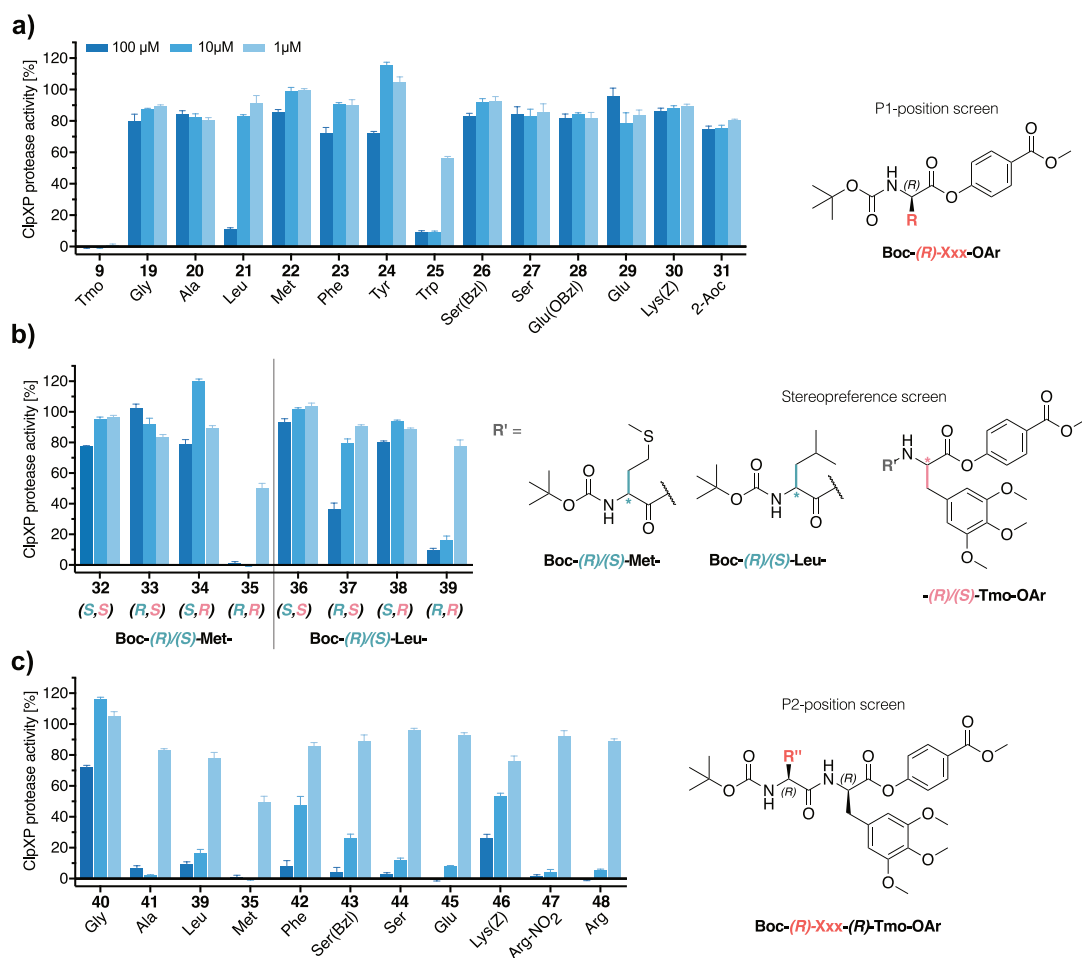


Figure 4.3. Inhibition of ClpXP (100 nM ClpP₁₄, 200 nM ClpX₆, 300 nM SsrA-GFP) by (a) a set of Boc-protected (*R*)-amino acid- and (b-c) dipeptide phenyl esters. ClpXP shows a strong preference for (*R,R*)-dipeptide phenyl esters with various amino acid side chains in the P₂ position. Each data set was derived from at least two independent experiments, which were measured in triplicates (mean and SEM).

To further converge to the natural peptide substrates of ClpXP, dipeptide Tmo-phenyl esters were next synthesized by standard solution phase peptide chemistry. To study the stereo-preference at the P₂ position, all four diastereomers of Boc-Met-Tmo-OAr and Boc-Leu-Tmo-OAr were synthesized and evaluated (Figure 4.3b). Both (*S,S*)-dipeptides **32** and **36** did not show any inhibition of the proteolytic activity of ClpXP. The (*R,S*)-diastereomers **33** and **37**, as well as the (*S,R*)-diastereomers **34** and **38** also failed to efficiently inhibit proteolysis. Conversely, the (*R,R*) phenyl esters **35** and **39** were potent inhibitors, with **35** showing full inhibition at 10 μ M and only about 50% residual ClpXP activity at 1 μ M.

Having identified the (*R*)-stereo-preference of ClpXP for the P₂-position as well, a representative set of (*R,R*)-dipeptide Tmo-phenyl esters was synthesized and tested to determine the effect on ClpXP-mediated GFP degradation (Figure 4.3c). In contrast to the P₁ position, ClpXP tolerated various amino acid side chains in P₂, ranging from non-polar groups, such as alanine (**41**) or methionine (**35**), to polar side chains including serine (**44**), glutamate (**45**) or arginine (**48**). This is in accordance with the lack of a well-defined S₂ pocket, which allowed ClpP to digest peptides with diverse amino acids in the P₂ position.^[9] However, as the Boc-Gly-Tmo-OAr dipeptide (**40**) did not inhibit ClpXP, a certain degree of sidechain interaction in the correct conformation was required for efficient binding to the protein. In conclusion, while ClpXP cleaves proteins in the natural L-conformation, it is well-inhibited by D-(*R*) dipeptide phenyl esters.

Notably, we also identified three structurally diverse compounds that did not inhibit, but rather stimulated the proteolytic activity of ClpXP. While **34** led to a moderate increase of proteolysis up to a maximum of 150% at 10 μM, the acetylated (*R*)-Tmo phenyl ester **49** and Boc-(*R*)-Glu(OBn)-(*R*)-Tmo-OAr **50** activated the ClpXP complex even more, achieving about 250% at 100 μM and 10 μM, respectively (Figure 4.4). Interestingly, compound **51**, the *S*-enantiomer of **49**, hardly affected ClpXP (Supporting Figure 2d), and the unprotected glutamic acid **45** was a potent inhibitor of ClpXP (Figure 4.3c). In stark contrast to the activation of proteolysis, the three compounds did not stimulate the peptidase activity of ClpP alone, but rather showed moderate-to-good inhibition (Supporting Figure 1b-c). A similar small molecule-induced enhancement of proteolysis was previously described for the ClpXP₂ complex from *Listeria monocytogenes*. In-depth studies revealed that partial binding of peptide chloromethylketones (CMK) stimulated the proteolytic turnover by increasing the affinity of ClpX and ClpP₂.^[15] Since the recognition of tagged substrates and ATP-dependent unfolding represent the rate-determining steps of proteolysis,^[16] a higher affinity of ClpX and ClpP₂ thus led to an increased degradation of GFP.^[15]

From this study's set of phenyl ester compounds, clear structural features that cause activation could unfortunately not be identified. Hence, the structural details of small molecule-induced activation remain subject to further investigation.

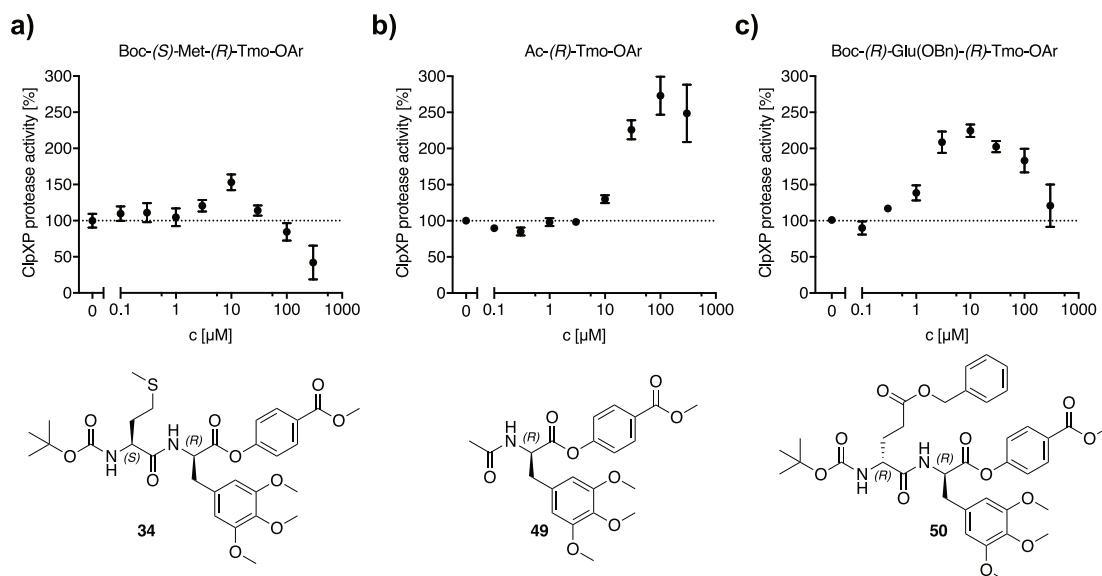


Figure 4.4. Stimulation of ClpXP-mediated proteolysis (100 nM ClpP₁₄, 200 nM ClpX₆, 900 nM SsrA-GFP) by phenyl esters **34** (a), **49** (b) and **50** (c). Each data set is derived from at least two independent experiments, which were measured in triplicates (mean and standard deviation).

4.2.2 A CLPXP COMPLEX WITH AN UNPRECEDENTED STOICHIOMETRY

The binding of previously identified inhibitors to ClpP either retained the tetradecameric state or led to de-oligomerization into heptameric species. To determine the oligomerization of the full ClpXP complex upon incubation with amino acid phenyl esters, analytical gel filtration was performed using a calibrated column. As expected for viable substrate turnover the strongly activating compounds **49** and **50** retained the native complex stoichiometry, namely ClpX₁₂P₁₄ (Supporting Figure 3a). In contrast, an unprecedented peak at a retention volume of 14.7 mL was detected after incubation with inhibitor **9** (Figure 4.5a). This value corresponds to a molecular weight of about 400 kDa. Intact-protein mass spectrometry of the peak fraction revealed the presence of ClpX and ClpP, which was almost quantitatively modified by the respective inhibitor fragment (Figure 4.5b). Incubation of ClpP alone with compound **9** led to the formation of heptameric ClpP species (Supporting Figure 3c). Hypothesizing that the new complex might correspond to a ClpX₆P₇ stoichiometry with a molecular weight of 435 kDa, we visualized the protein species of the peak fraction by negative-stain electron microscopy (EM). Indeed, 2D classification and 3D-reconstruction of the particles

unambiguously revealed the presence of a complex that consisted of one ClpX hexamer stacked on top of a ClpP heptamer (Figure 4.5c-d). The overall geometry and the molecular dimensions of the model coincided well with the crystal structures of compressed *S. aureus* ClpP (PDB ID: 3QWD)^[17] and hexameric *E. coli* ClpX (PDB ID: 3HWS).^[18] To the best of the author's knowledge, a corresponding interaction between a ClpX hexamer and a catalytically inactive ClpP heptamer has never been described before. Similarly, binding of ADEPs, which act as ClpX surrogates that share the same binding site with the IGF-loop of ClpX, was only observed for ClpP₁₄. In fact, hydrogen-deuterium-exchange mass spectrometry (HDX-MS) of *E. coli* ClpP revealed less exchange, *i.e.* a more rigid conformation, of the E-helices responsible for heptamer-heptamer interaction, upon ADEP binding.^[19] Therefore, ClpX/ADEP binding to ClpP was usually associated with a rigidification of the ClpP₁₄ complex.

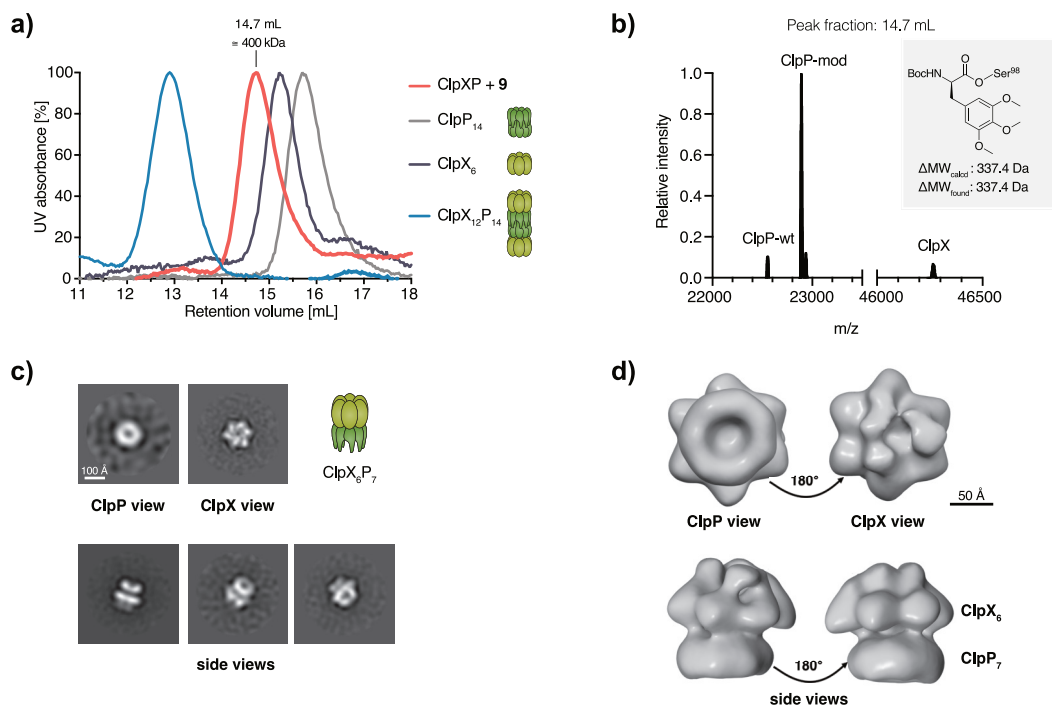


Figure 4.5. Discovery of an unprecedented ClpXP-state. a) Size-exclusion chromatography revealed the formation of a novel complex upon incubation of ClpX₁₂P₁₄ with phenyl ester **9** (0.72 μM ClpP₁₄, 2.86 μM ClpX(E183Q)₆, 50 μM compound **9**). b) Intact-protein mass spectrometry of the peak fraction verified the presence of ClpX and ClpP, which was covalently modified by the inhibitor. Negative-stain electron microscopy images of selected 2D class averages (c) and 3D reconstruction (d) unambiguously verified the presence of a ClpX₆P₇ complex.

The disruption of both the peptidolytic and proteolytic system was observed for all potent amino acid phenyl esters tested, including the (*S*)-Boc-Tmo-OAr (**10**), which - although 25 times weaker than its (*R*)-enantiomer **9** - also induced heptamerization of ClpP and partial formation of the ClpX₆P₇ complex (Supporting Figure 3b). This indicates that breakdown of the ClpXP complex is indispensable for full proteolytic arrest, as was also shown for a set of reversible inhibitors that disrupt ClpXP by de-oligomerizing the ClpX hexamer.^[20]

To further characterize the new ClpX₆P₇ complex, its dissociation constant was sought. Unfortunately, all our efforts to directly quantify the interaction between the chaperone and peptidase by various methods, *e.g.* isothermal titration calorimetry (ITC) and surface plasmon resonance (SPR), failed. Previous studies were only able to determine apparent dissociation constants of ClpX and ClpP via activity-based assays.^[6,15] Thus, the switchSENSE[®] technology was used, which is a label-free method for the analysis of the interaction of proteins with surface-tethered interacting partners (*e.g.* ligands, DNA, proteins). Short DNA levers are electrically actuated on microelectrodes by alternating current potentials, and the switching dynamics are measured in real-time by fluorescence energy transfer. Binding of proteins to binding partners attached to the top of the DNA levers can be detected by time-resolved measurements of the levers' dynamic motion.^[21,22]

For the study of the ClpP-ClpX interaction, ClpP₁₄ was coupled to a short DNA-strand and the conjugate was immobilized on a biochip by hybridization. ClpX was titrated to the immobilized complex and the dynamic response was measured for each concentration. An unmodified DNA double strand, which carried a different dye, acted as an online control for unspecific binding of ClpX (Figure 4.6a). Applying this technology allowed, for the first time, the direct determination of the K_d-value of ClpX and ClpP to be 19.5 ± 3.2 μM (Figure 4.6b). This rather low affinity becomes reasonable when considering that in the bacterial cell ClpP is required to dynamically exchange between various cognate chaperones (in *S. aureus*, ClpC and ClpX). Accordingly, the related hexameric HslUV protease complex, which does not have additional chaperone partners, has a lower K_d-value of 1 μM, as determined by SPR.^[23]

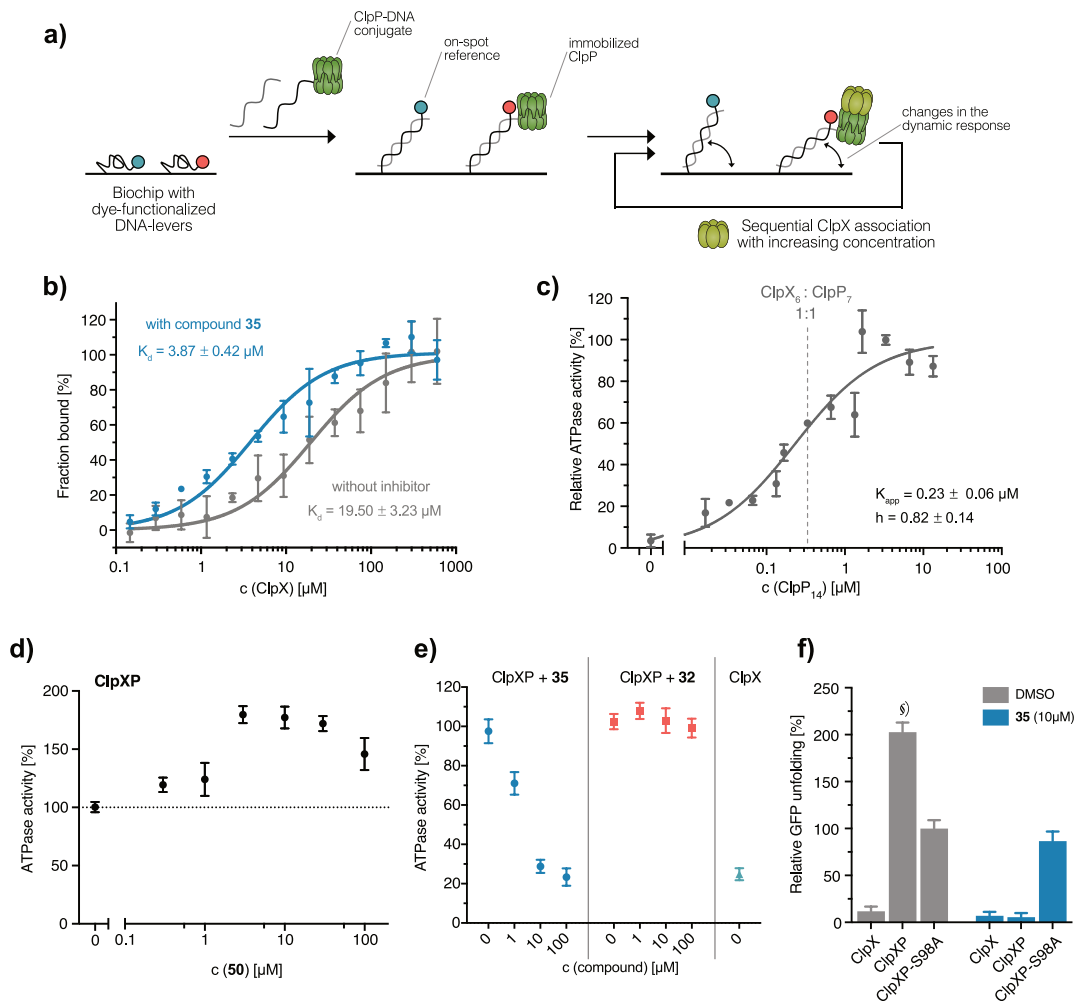


Figure 4.6. In-depth study of the novel ClpXP complex. a) Schematic representation of the experimental setup to determine the dissociation constants of ClpX and ClpP using SwitchSENSE[®]. A ClpP-DNA-conjugate was immobilized on the biochip by hybridization and the dynamic response was measured upon titration of increasing ClpX concentrations. An unmodified DNA-double strand (colored in green) acted as an on-line control for unspecific binding of ClpX. b) Determination of dissociation constants by titration of ClpX to immobilized unmodified ClpP in its 14-mer, as well as its 35-treated heptameric state (mean and standard deviation, $n = 5$). c) Stimulation of the ATPase activity of *S. aureus* ClpX₆ (0.33 μM) upon ClpP binding (mean and standard deviation, $n = 3$). d) Stimulation of the ATPase activity of ClpXP by 50, an activator of proteolysis. e) Incubation of ClpXP with 35 revoked the increased ATPase activity of ClpXP, while its (S,S)-enantiomer 32 did not have any effect. Assay conditions for d-e: 0.33 μM ClpX₆, 0.17 μM ClpP₁₄. Each data set was derived from two independent experiments, which were measured in triplicates (mean and standard deviation). f) Residual GFP-unfolding activity of 35-treated ClpXP as compared to unfolding by the proteolytically inactive ClpXP-S98A mutant (100% GFP unfolding) (protease assay conditions). [§] Increased value due to GFP-degradation by proteolysis, not solely unfolding.

Having established the switchSENSE® technology for this system, we proceeded with the study of the ClpX₆P₇ complex. The ClpP-DNA conjugate was treated with phenyl ester **35** to induce de-oligomerization and the resulting heptameric ClpP was immobilized. Interestingly, titration of ClpX revealed a dissociation constant ($K_d = 3.9 \pm 0.4 \mu\text{M}$) for ClpX₆P₇ that was five-times lower than the one for the native complex (Figure 4.6b). Thus, while disrupting the ClpP₇-ClpP₇ interaction, binding of the inhibitors increased the affinity of ClpX and ClpP.

The question of whether the increased affinity of ClpX to ClpP in the **35**-bound state influenced the ATPase activity of the chaperone arose. Turnover of ATP was monitored by an enzyme-coupled assay, which has been widely used for the study of *E. coli* ClpX (EcClpX). Previous comprehensive studies showed that the ATPase activity of EcClpX was markedly reduced upon binding of ClpP, and this effect has been used to monitor the association of ClpP and ClpX.^[5,6,24-27] This study, however, found that *S. aureus* ClpX itself only had a very low activity, which drastically increased in the presence of increasing equivalents of ClpP (Figure 4.6c). The apparent binding constant K_{app} for this interaction was determined to be $0.23 \pm 0.06 \mu\text{M}$ (ClpX₆-concentration in the assay: $0.33 \mu\text{M}$).

Previous discussions have indicated that a high EcClpX-mediated turnover of ATP, also in the absence of ClpP, is rather odd from the perspective of energy conservation in a cell.^[28] For SaClpX, a very low basal ATPase activity would save valuable ATP. A similar stimulation of ATP-turnover, rather than a reduction, upon association with a peptidase was previously described for the HslUV protease complex, among others.^[29] Hence, the catalytic activities of EcClpX and SaClpX seem to be regulated in a different manner.

The effect of phenyl ester compounds on the SaClpX-mediated turnover of ATP was then tested. Compound **50**, which stimulated ClpXP proteolysis, activated the ATPase activity of ClpX within the ClpXP complex in a similar way (Figure 4.6d). Interestingly, incubation of ClpXP with the inhibitor **35** reduced the ATPase activity of ClpX in a concentration-dependent manner, converging to the rate of ClpX alone (Figure 4.6e). Both compound-induced alterations in ATP-turnover were solely mediated by binding to ClpP, as the compounds did not have an effect on ClpX alone (Supporting Figure 2e). The respective (*S,S*)-enantiomer **32**, which was inactive in the protease assay, also did

not alter the ATPase activity (Figure 4.6e). Accordingly, the ClpXP complex inhibited by **35** did not show any residual GFP-unfolding activity beyond the background level, as compared to the proteolytically inactive complex of the active site mutant ClpP-S98A and ClpX. (Figure 4.6f).

As a result, covalent binding of phenyl esters corrupted the interplay of the heptameric ClpP rings and inhibited proteolysis, while at the same time reinforcing the ClpP-ClpX interaction. Although ClpXP complexes generally showed higher turnover of ATP than ClpX alone, the inhibitor bound ClpX₆P₇ complex only possessed the basal ATPase activity of ClpX.

4.2.3 TOWARDS A BIOCHEMICAL FUNCTION OF DE-OLIGOMERIZATION

Intrigued by the conformational arrest of ClpXP by compounds that are related to its natural substrates, it was hypothesized that the trapped ClpX₆P₇ complex resembled a state of biological relevance. While the pathway of substrate delivery is well understood, the mechanism by which cleaved peptide fragments are liberated after proteolytic digestion is still open for debate. Two main hypotheses for the release are proposed based on the temporal kinking of the central E-helices of ClpP: 1) formation of equatorial pores through which cleavage products can exit, or 2) opening of the sequestered ClpP barrel by the collapse of the ClpXP complex which would release all fragments simultaneously.^[26,30-32] The detection of the novel ClpX₆P₇ state demonstrates that only disassembly of the protease into ClpX₆P₇-species, and not full disruption, would be sufficient for release. ClpX could thus remain bound to each heptamer, which facilitates re-assembly of the catalytically active ClpX₁₂P₁₄ complex, making collapse of the complex less entropically unfavorable.

To investigate this possible mechanism, a pulldown-assay was established to determine, if the catalytic activity of ClpP or ClpXP was associated with a temporal collapse of the ClpP₇-ClpP₇ interaction. For this, in addition to the standard ClpP-construct, which contains a Strep-Tag, an untagged ClpP form was used. In this way, we obtained two different ClpP₁₄ complexes exclusively consisting of Strep-ClpP or untagged ClpP, respectively. The interchange of both ClpP forms was analyzed by Strep-Tactin-based affinity purification and subsequent intact-protein mass spectrometry (Figure 4.7a). Only in

the case of exchange between the ClpP₁₄ complexes should untagged ClpP be detected after Strep-pull-down by mass spectrometry (MS).

First, it was determined whether mixed ClpP complexes could actually be formed. For this purpose, both ClpP₁₄ variants were incubated together with phenyl ester compound **9** to induce full de-oligomerization and the acyl-enzyme intermediates were fully hydrolyzed overnight to allow for re-oligomerization into ClpP₁₄ species, as monitored by gel filtration chromatography (Figure 4.7b). Affinity-purification isolated all complexes that contained Strep-tagged ClpP subunits.

As depicted in Figure 4.7b, untagged ClpP co-eluted with Strep-ClpP, which confirms the interchange of the ClpP subunits. The DMSO-treated control also showed partial interchange of the ClpP forms, which can likely be ascribed to natural interchange over the long incubation time. While interchange between the two ClpP species could happen between all protomers, leading to mixed heptameric rings, the disruption of ClpP into smaller species than heptamers was rarely observed.^[32] This makes interchange within the heptamers rather unlikely and supports the fact that only heptamer-heptamer exchange occurred.

Experiments were then conducted on the potential temporal de-oligomerization of 1) ClpP upon incubation with the peptide substrate Ac-Ala-hArg-2-Aoc-ACC and 2) ClpXP during proteolysis of SsrA-tagged GFP. A mix of the two ClpP₁₄-constructs (and ClpX for the protease condition) were incubated with the respective substrates. After full consumption of substrates (amply estimated from previous activity assays), the mixtures were purified by affinity chromatography and measured by MS. DMSO-treatment acted as a control for both conditions. Figure 4.7d-e show, however, that untagged ClpP did not co-elute with Strep-ClpP, for the peptidase or protease assay conditions. Hence, a temporal collapse of Clp(X)P in the context of its catalytic activity could not be confirmed. This result points towards a partial disassembly of the E-helices, leading to the formation of equatorial pores. Nevertheless, the novel ClpX₆P₇ state indicates that kinking of the E-helix seems to be an energetic minimum of the protein at which it can be stalled. This is in agreement with the crystal structure of ClpP in its compressed form and compound-induced heptamerization of ClpP. Future investigation is necessary to unambiguously elucidate the mechanism of product release.

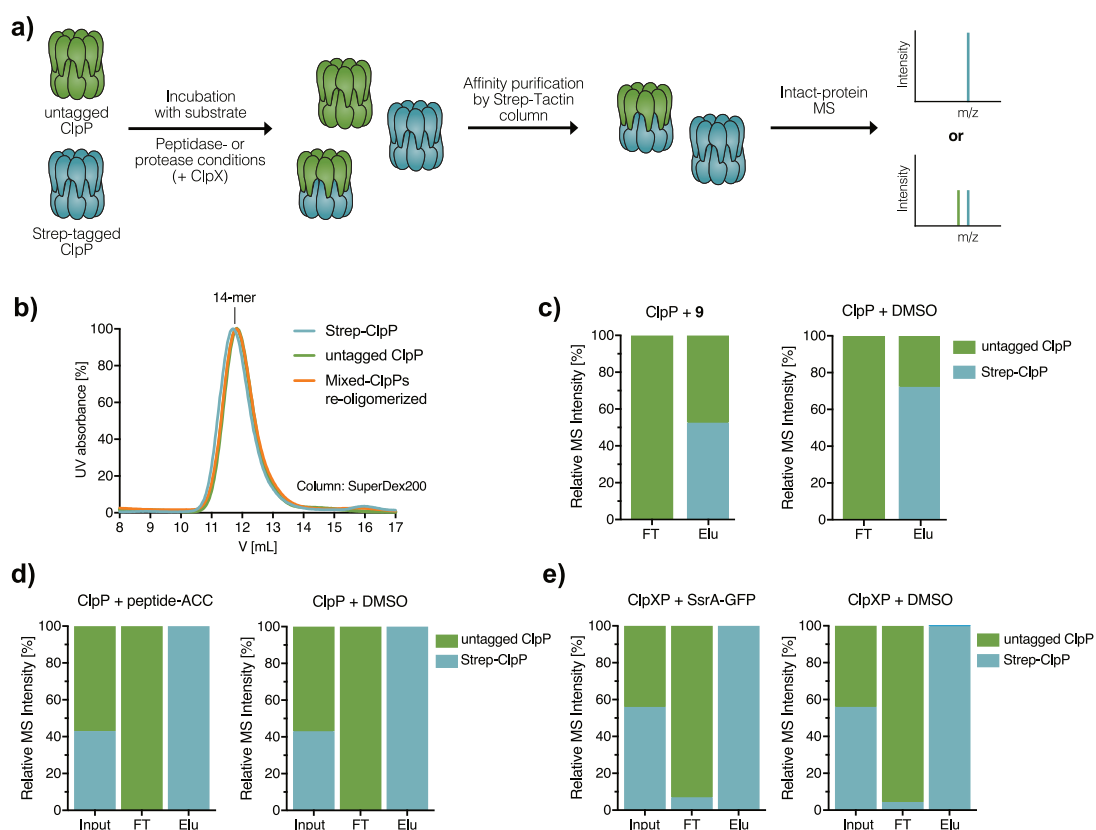


Figure 4.7. Study of potential temporal collapse of the $\text{Clp}(X_{12})P_{14}$ complex during its catalytic activity. a) Schematic representation of the experimental setup. Affinity-purification allowed co-elution of untagged ClpP if it had interchanged with Strep-tagged ClpP subunits. b) Size-exclusion chromatography of Strep-tagged ClpP and untagged ClpP, as well of a mix of both species that were de-oligomerized by treatment with phenyl ester **9** and subsequently re-oligomerized upon hydrolysis. c) Relative MS-intensities of the re-oligomerized complex after affinity purification showed significant interchange of the ClpP isoforms. d-e) Relative MS-intensities for the investigation of the temporal collapse of ClpP_{14} under peptidase (d) and protease (e) conditions. Both ClpP_{14} forms, and ClpX_6 for the protease conditions, were incubated with the substrate $\text{Ac-Ala-hArg-2-Aoc-ACC}$ and SsrA-GFP , respectively. After full consumption of substrates, ensuring completed catalytic activity, the mixtures were purified by affinity chromatography. No interchange of the ClpP_{14} forms was observed under these conditions. For each experiment, one representative dataset from at least two replicates is shown.

4.3 CONCLUSION AND OUTLOOK

ClpXP is a highly dynamic protease and its catalytic activity depends on the correct assembly of up to 26 subunits. This work yielded novel tool compounds that can interfere with specific aspects of the underlying equilibria. Amino acid and dipeptide phenyl esters were rationally designed on the basis of a first generation of phenyl ester inhibitors.

These compounds were able to efficiently modulate the activity and the oligomerization of the ClpXP protease complex. Comprehensive evaluation of a library of dipeptide phenyl esters revealed that the most potent compounds possessed a mirror-inverted stereochemistry, as compared to ClpXP's natural protein substrates. In addition, compounds that activated proteolytic turnover were identified. In-depth biochemical investigations revealed that inhibitor-binding induced the formation of an unprecedented ClpX₆P₇ complex. The active site modification of ClpP was linked to an abrogation of the ClpP₇-ClpP₇ interaction and, more importantly, to an increased affinity between ClpP and ClpX. The binding of *S. aureus* ClpX to ClpP was shown to increase its ATPase activity substantially and hence, is inversely regulated as compared to ClpX from *E. coli*. Significantly, binding by phenyl esters to ClpP subunits within the ClpXP complex not only stalled protein degradation, but also suppressed ClpX-mediated turnover of ATP. Lastly, it was evaluated whether the novel ClpX₆P₇ complex owns a biological function during the release of peptide fragments after protein degradation. While a full de-oligomerization of ClpP or ClpXP could not be verified during substrate turnover, it remains reasonable to assume that the monomers of ClpP separately run through dynamic motions, including the state observed. As only individual monomers would therefore lose their ClpP₇-ClpP₇ contacts, the complex would still remain intact. Figure 4.8 schematically summarizes the findings obtained within this study.

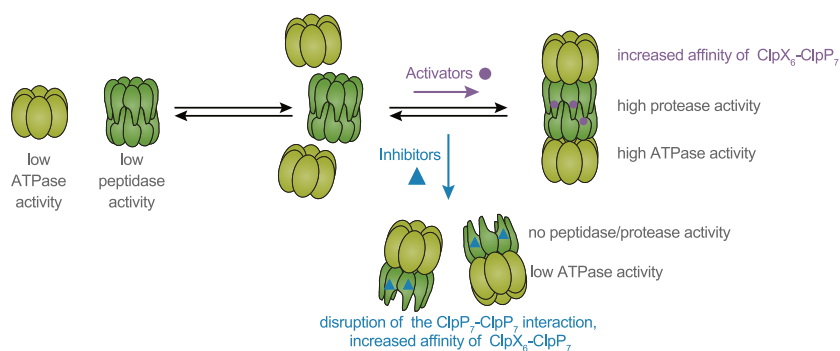
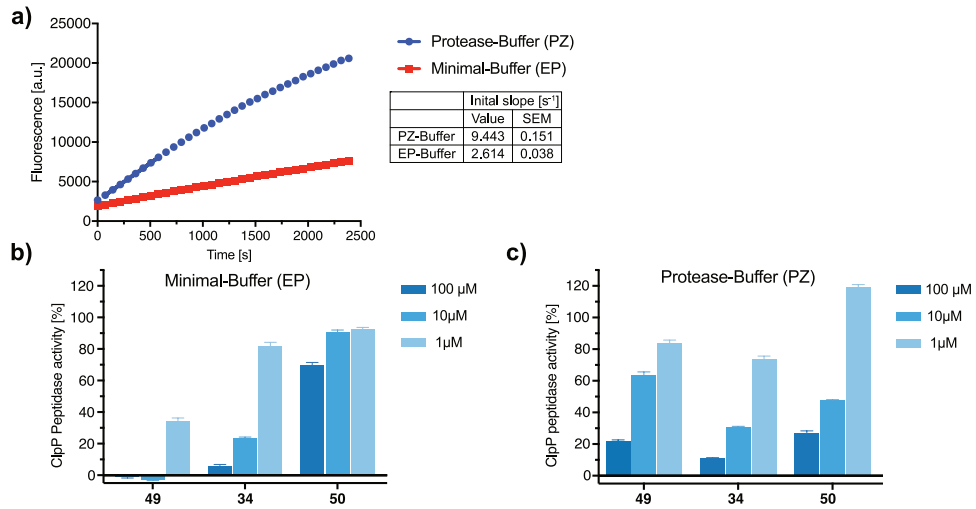


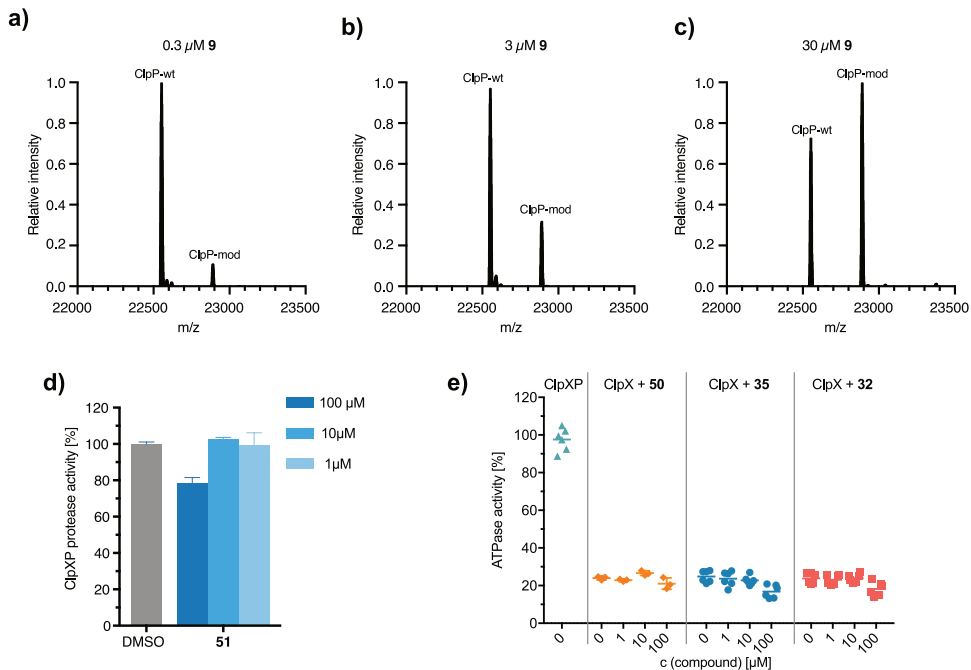
Figure 4.8. Schematic representation of the phenyl ester-induced structural and catalytic alterations of ClpXP.

Future studies will need to unveil the molecular details that result in the arrest of ClpXP in its inactive ClpX₆P₇ state, by using a variety of suitable techniques, including crystallography, HDX-MS or cryo-electron microscopy. Ideally, this input will also help to unravel the underlying mechanisms of protein turnover and subsequent peptide release.

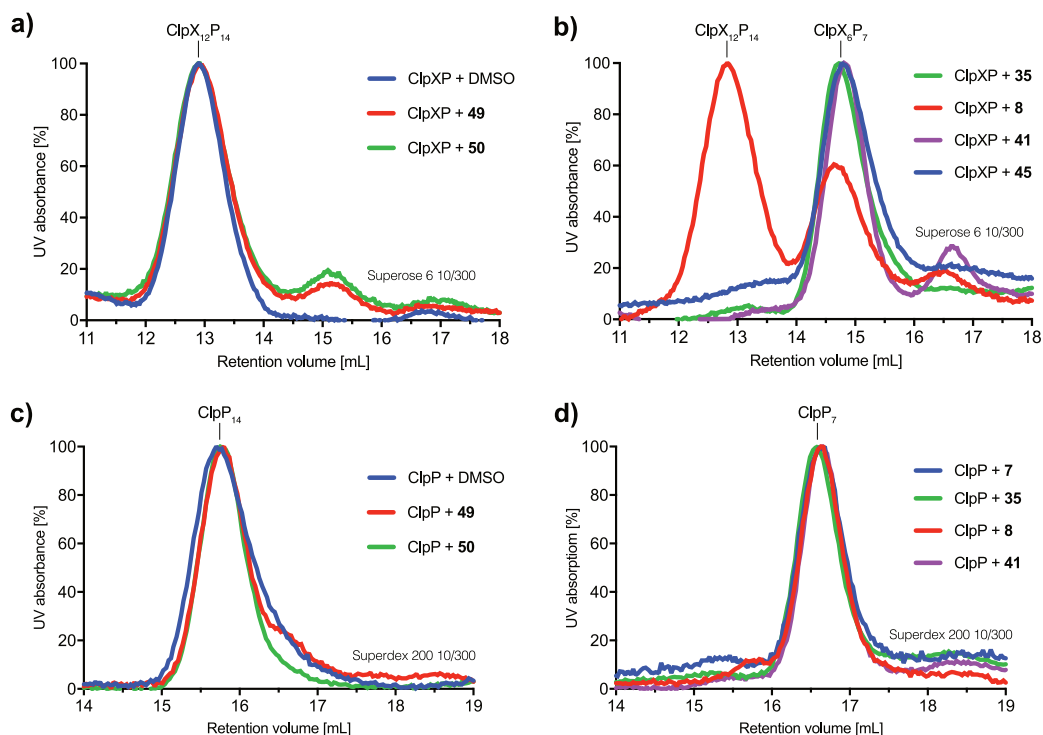
4.4 SUPPORTING FIGURES



Supporting Figure 1. a) Enhanced peptidase activity of ClpP (10 nM ClpP₁₄, 200 μM Ac-Ala-hArg-2-Aoc-ACC) in protease-buffer (PZ-buffer) as compared to minimal peptidase buffer (EP-buffer). b+c) ClpP peptidase activity with phenyl ester compounds is dependent on the buffer system used. EP-Buffer: 100 mM HEPES, pH = 7.0, 100 mM NaCl, Protease-buffer: 25 mM HEPES, pH = 7.6, 200 mM KCl, 5 mM MgCl₂, 1 mM DTT, 10% glycerol. Each data set was derived from at least two independent experiments, which were measured in triplicates (mean and SEM)



Supporting Figure 2. a-c) Intact-protein MS spectra of ClpXP (100 nM ClpP₁₄, 200 nM ClpX₆) incubated with increasing concentrations of compound **9** revealed only partial active-site modification (Representative datasets from two replicates, respectively). d) Proteolytic activity of ClpXP upon incubation with Ac-(S)-Tmo-OAr (**51**) (100 nM ClpP₁₄, 200 nM ClpX₆, 300 nM SsrA-GFP). e) ATPase activity of ClpX(P) upon treatment with activator **50** and inhibitors **35** and **32** (0.33 μM ClpX₆; 0.17 μM ClpP₁₄ or no ClpP added). Each dataset was derived from at least two independent experiments, which were measured in triplicates.



Supporting Figure 3. Size-exclusion chromatograms of ClpXP incubated with activators (a) and inhibitors (b), respectively. c+d) Size-exclusion chromatograms of ClpP incubated with activators (c) and inhibitors (d), respectively.

4.5 AUTHOR CONTRIBUTIONS

Markus Lakemeyer synthesized the compounds, expressed proteins, performed biochemical assays and analyzed the data. Dóra Balogh expressed proteins for SwitchSENSE experiments. Friederike Möller determined the dissociation constants by SwitchSENSE. Eva Bertosin recorded and analyzed the EM images. Markus Lakemeyer conceived the project with support from Stephan A. Sieber and wrote the manuscript.

4.6 REFERENCES

- [1] M. W. Hackl, M. Lakemeyer, M. Dahmen, M. Glaser, A. Pahl, K. Lorenz-Baath, T. Menzel, S. Sievers, T. Böttcher, I. Antes, H. Waldmann, S. A. Sieber, *J. Am. Chem. Soc.* **2015**, *137*, 8475–8483.

- [2] T. F. Gronauer, M. M. Mandl, M. Lakemeyer, M. W. Hackl, M. Meßner, V. S. Korotkov, J. Pachmayr, S. A. Sieber, *Chem. Commun. (Camb.)* **2018**, 54, 9833–9836.
- [3] M. Gersch, K. Famulla, M. Dahmen, C. Göbl, I. Malik, K. Richter, V. S. Korotkov, P. Sass, H. Rübsamen-Schaeff, T. Madl, H. Brötz-Oesterhelt, S. A. Sieber, *Nat. Commun.* **2015**, 6, 6320.
- [4] A. Pahl, M. Lakemeyer, M. T. Vielberg, M. W. Hackl, J. Vomacka, V. S. Korotkov, M. L. Stein, C. Fetzer, K. Lorenz-Baath, K. Richter, H. Waldmann, M. Groll, S. A. Sieber, *Angew. Chem. Int. Ed. Engl.* **2015**, 54, 15892–15896.
- [5] Y. I. Kim, I. Levchenko, K. Fraczkowska, R. V. Woodruff, R. T. Sauer, T. A. Baker, *Nat. Struct. Biol.* **2001**, 8, 230–233.
- [6] R. E. Burton, T. A. Baker, R. T. Sauer, *Protein Sci.* **2003**, 12, 893–902.
- [7] P. Furet, P. Imbach, M. Noorani, J. Koeppler, K. Laumen, M. Lang, V. Guagnano, P. Fuerst, J. Roesel, J. Zimmermann, C. García-Echeverría, *J. Med. Chem.* **2004**, 47, 4810–4813.
- [8] C. E. Humphrey, M. Furegati, K. Laumen, L. La Vecchia, T. Leutert, J. C. D. Müller-Hartweg, M. Vögtle, *Org. Process Res. Dev.* **2007**, 11, 1069–1075.
- [9] M. Gersch, M. Stahl, M. Poreba, M. Dahmen, A. Dziedzic, M. Drag, S. A. Sieber, *ACS Chem. Biol.* **2016**, 11, 389–399.
- [10] S. Gottesman, E. Roche, Y. Zhou, R. T. Sauer, *Genes Dev.* **1998**, 12, 1338–1347.
- [11] M. Gersch, R. Kolb, F. Alte, M. Groll, S. A. Sieber, *J. Am. Chem. Soc.* **2014**, 136, 1360–1366.
- [12] M. Gersch, F. Gut, V. S. Korotkov, J. Lehmann, T. Böttcher, M. Rusch, C. Hedberg, H. Waldmann, G. Klebe, S. A. Sieber, *Angew. Chem. Int. Ed. Engl.* **2013**, 52, 3009–3014.
- [13] T. Böttcher, S. A. Sieber, *Angew. Chem. Int. Ed.* **2008**, 47, 4600–4603.
- [14] T. Böttcher, S. A. Sieber, *J. Am. Chem. Soc.* **2008**, 130, 14400–14401.
- [15] D. Balogh, M. Dahmen, M. Stahl, M. Poreba, M. Gersch, M. Drag, S. A. Sieber, *Chem. Sci.* **2017**, 8, 1592–1600.
- [16] Y. I. Kim, R. E. Burton, B. M. Burton, R. T. Sauer, T. A. Baker, *Mol. Cell.* **2000**, 5, 639–648.

- [17] S. R. Geiger, T. Böttcher, S. A. Sieber, P. Cramer, *Angew. Chem. Int. Ed.* **2011**, *50*, 5749–5752.
- [18] S. E. Glynn, A. Martin, A. R. Nager, T. A. Baker, R. T. Sauer, *Cell* **2009**, *139*, 744–756.
- [19] M. A. Sowole, J. A. Alexopoulos, Y.-Q. Cheng, J. Ortega, L. Konermann, *J. Mol. Biol.* **2013**, *425*, 4508–4519.
- [20] C. Fetzer, V. S. Korotkov, R. Thänert, K. M. Lee, M. Neuenschwander, J. P. von Kries, E. Medina, S. A. Sieber, *Angew. Chem. Int. Ed.* **2017**, *56*, 15746–15750.
- [21] J. Knezevic, A. Langer, P. A. Hampel, W. Kaiser, R. Strasser, U. Rant, *J. Am. Chem. Soc.* **2012**, *134*, 15225–15228.
- [22] A. Langer, P. A. Hampel, W. Kaiser, J. Knezevic, T. Welte, V. Villa, M. Maruyama, M. Svejda, S. Jähner, F. Fischer, R. Strasser, U. Rant, *Nat. Commun.* **2013**, *4*, 2099.
- [23] M. K. Azim, W. Goehring, H. K. Song, R. Ramachandran, M. Bochtler, P. Goettig, *Protein Sci.* **2005**, *14*, 1357–1362.
- [24] S. A. Joshi, G. L. Hersch, T. A. Baker, R. T. Sauer, *Nat. Struct. Mol. Biol.* **2004**, *11*, 404–411.
- [25] A. Martin, T. A. Baker, R. T. Sauer, *Mol. Cell.* **2007**, *27*, 41–52.
- [26] M. S. Kimber, A. Y. H. Yu, M. Borg, E. Leung, H. S. Chan, W. A. Houry, *Structure* **2010**, *18*, 798–808.
- [27] J. A. Kenniston, T. A. Baker, J. M. Fernandez, R. T. Sauer, *Cell* **2003**, *114*, 511–520.
- [28] T. A. Baker, R. T. Sauer, *Biochim. Biophys. Acta* **2012**, *1823*, 15–28.
- [29] J. A. Yakamavich, T. A. Baker, R. T. Sauer, *J. Mol. Biol.* **2008**, *380*, 946–957.
- [30] R. Sprangers, A. Gribun, P. M. Hwang, W. A. Houry, L. E. Kay, *Proc. Natl. Acad. Sci. U.S.A.* **2005**, *102*, 16678–16683.
- [31] J. Zhang, F. Ye, L. Lan, H. Jiang, C. Luo, C.-G. Yang, *J. Biol. Chem* **2011**, *286*, 37590–37601.
- [32] M. Gersch, A. List, M. Groll, S. A. Sieber, *J. Biol. Chem* **2012**, *287*, 9484–9494.

5

Research conclusion and outlook

The continued success in treating infectious diseases will rely on the development of novel antibacterial strategies. In this regard, targeting the ClpXP protease, a gatekeeper of bacterial virulence, is a promising antivirulence approach.

This thesis provided novel chemical tools to manipulate the activity of ClpXP and to study its oligomeric assembly. Two novel classes of ClpP inhibitors which both derived from a high-throughput screen were presented. Phenyl esters are covalent ClpP inhibitors that surpass previous β -lactone inhibitors in potency and selectivity. Activity-based protein profiling experiments with the alkyne-tagged phenyl ester **ML16** identified ClpP as the only covalent target in live *S. aureus* cells. Extensive SAR led to compounds with improved stability, and identified a critical methyl position in the inhibitor structure. Depending on its stereochemistry, this “stereogenic switch” retained the tetradecameric ClpP state or induced de-oligomerization.

Oxazoles were the second class of ClpP inhibitors identified by the high-throughput screen. Until today, they remain the only noncovalent inhibitors of ClpP known. The co-crystal structure of ClpP and the hit compound **AV145** gave insights into the unprecedented binding mode. While **AV145** was only moderately potent in the reducing ClpP's peptidase activity, chemical synthesis generated improved inhibitors, including **AV286**, with low-micromolar IC_{50} -values. Unfortunately, association of ClpX to ClpP revoked the inhibitor binding, thus rendering oxazoles ineffective in cellular assays. Nevertheless, this study provided valuable information about the conformational control of ClpX over ClpP.

Lastly, we developed second-generation phenyl esters in which the critical methyl “switch” of the first generation was substituted with an amino group, resulting in amino acid-based phenyl esters. Applying the knowledge gained from the investigation of the oxazole inhibitors, the evaluation of the novel compounds focussed on the full ClpXP complex. Comprehensive screening of amino acids in P₁ and P₂ position showed that ClpXP is best inhibited by (*R*)-amino acid-based phenyl esters. Moreover, activators of ClpXP-mediated proteolysis were found. Significantly, inhibitor binding induced the formation of an unprecedented ClpX₆P₇ complex, which was characterized in detail using a variety of methods.

This work has shown that sub-stoichiometric binding of covalent inhibitors to the active site of ClpP can stall the activity not only of ClpP, but also of ClpX by formation of a stabilized ClpX₆P₇ complex. In addition to its role in proteolytic degradation, ClpX exerts cellular functions that are independent of ClpP.^[1] Recent studies, for example, indicated that ClpX is involved in coordination of the cell cycle and cell division.^[2,3] Hence, the trapping of ClpX in an unproductive ClpX₆P₇ complex might open up entirely new antibacterial possibilities.

Although phenyl esters are invaluable tools for the study of ClpXP, their hydrolytic stability hampers a translational application. Future research should therefore aim to find novel inhibitor classes that, while acting similarly to phenyl esters, show improved stability and duration of inhibition. As noncovalent inhibition of the highly dynamic ClpXP complex appears to be difficult, initial efforts could focus on alternative covalent warheads with improved stability. Although previous efforts to substitute the phenyl ester moiety, for example by aryl amides or carbamates, unfortunately failed, there is still large chemical space that can be explored. Boronic acids, previously already proven to be able to inhibit ClpP,^[4,5] might be suitable for this application. While selectivity over other serine hydrolases and proteolytic stability can be difficult for (*S*)-peptide boronic acids, boronic acid derivatives based on the unnatural amino acid (*R*)-Tmo might possibly overcome these hurdles.

On a cellular level, the molecular regulation of ClpXP and the release of peptide fragments after proteolysis remain interesting questions for future research. There even might be natural small molecule modulators that act similarly to the amino acid phenyl esters, and stall proteolysis by formation of an inactive ClpX₆P₇ complex. Moreover, the molecular interaction and the biological functions of additional ClpP complexes (*e.g.* ClpCP) are so far only poorly understood^[6,7] and small molecule modulators might help to elucidate the underlying mechanisms.

REFERENCES

- [1] A. O. Olivares, T. A. Baker, R. T. Sauer, *Nat. Rev. Microbiol.* **2015**, *14*, 33–44.
- [2] V. Vimberg, J. Lenart, J. Janata, G. Balikova Novotna, *Antimicrob Agents Chemother* **2015**, *59*, 3611–3614.
- [3] K. T. Baek, C. Jensen, C. Gallay, N. S. Fisker, I. Thalsoe-Madsen, A. R. Pereira, W. Paulander, J.-W. Veening, M. G. Pinho, D. Frees, *bioRxiv* **2018**.
- [4] T. Akopian, O. Kandror, C. Tsu, J. H. Lai, W. Wu, Y. Liu, P. Zhao, A. Park, L. Wolf, L. R. Dick, E. J. Rubin, W. Bachovchin, A. L. Goldberg, *J. Biol. Chem* **2015**, *290*, 11008–11020.
- [5] W. Moreira, G. J. Y. Ngan, J. L. Low, A. Poulsen, B. C. S. Chia, M. J. Y. Ang, A. Yap, J. Fulwood, U. Lakshmanan, J. Lim, A. Y. T. Khoo, H. Flotow, J. Hill, R. M. Raju, E. J. Rubin, T. Dick, *mBio* **2015**, *6*, e00253–15–13.
- [6] D. B. Trentini, M. J. Suskiewicz, A. Heuck, R. Kurzbauer, L. Deszcz, K. Mechtler, T. Clausen, *Nature* **2016**, 1–24.
- [7] J. Kirstein, N. Molière, D. A. Dougan, K. Turgay, *Nat. Rev. Microbiol.* **2009**, *7*, 1–11.

Part III

REVIEW

6

Thinking outside the box – novel antibacterials to tackle the resistance crisis

Published in *Angewandte Chemie International Edition*, **2018**

by Markus Lakemeyer, Weining Zhao, Franziska A. Mandl, Peter Hammann and
Stephan A. Sieber.

online version of record before inclusion in an issue

Reprinted with permission. © 2017 John Wiley and Sons.

DOI: 10.1002/anie.201804971

SYNOPSIS

The public view on antibiotics as reliable medicines changed when reports about "resistant superbugs" appeared in the news. While reasons for this resistance development are easily spotted, solutions for re-establishing effective antibiotics are still in their infancy. This Review encompasses several aspects of the antibiotic development pipeline from very early strategies to mature drugs. An interdisciplinary overview is given of methods suitable for mining novel antibiotics and strategies discussed to unravel their modes of action. Select examples of antibiotics recently identified by using these platforms not only illustrate the efficiency of these measures, but also highlight promising clinical candidates with therapeutic potential. Furthermore, the concept of molecules that disarm pathogens by addressing gatekeepers of virulence will be covered. The Review concludes with an evaluation of antibacterials currently in clinical development. Overall, this Review aims to connect select innovative antimicrobial approaches to stimulate interdisciplinary partnerships between chemists from academia and industry.

The synopsis is taken from the original publication.

AUTHOR CONTRIBUTIONS

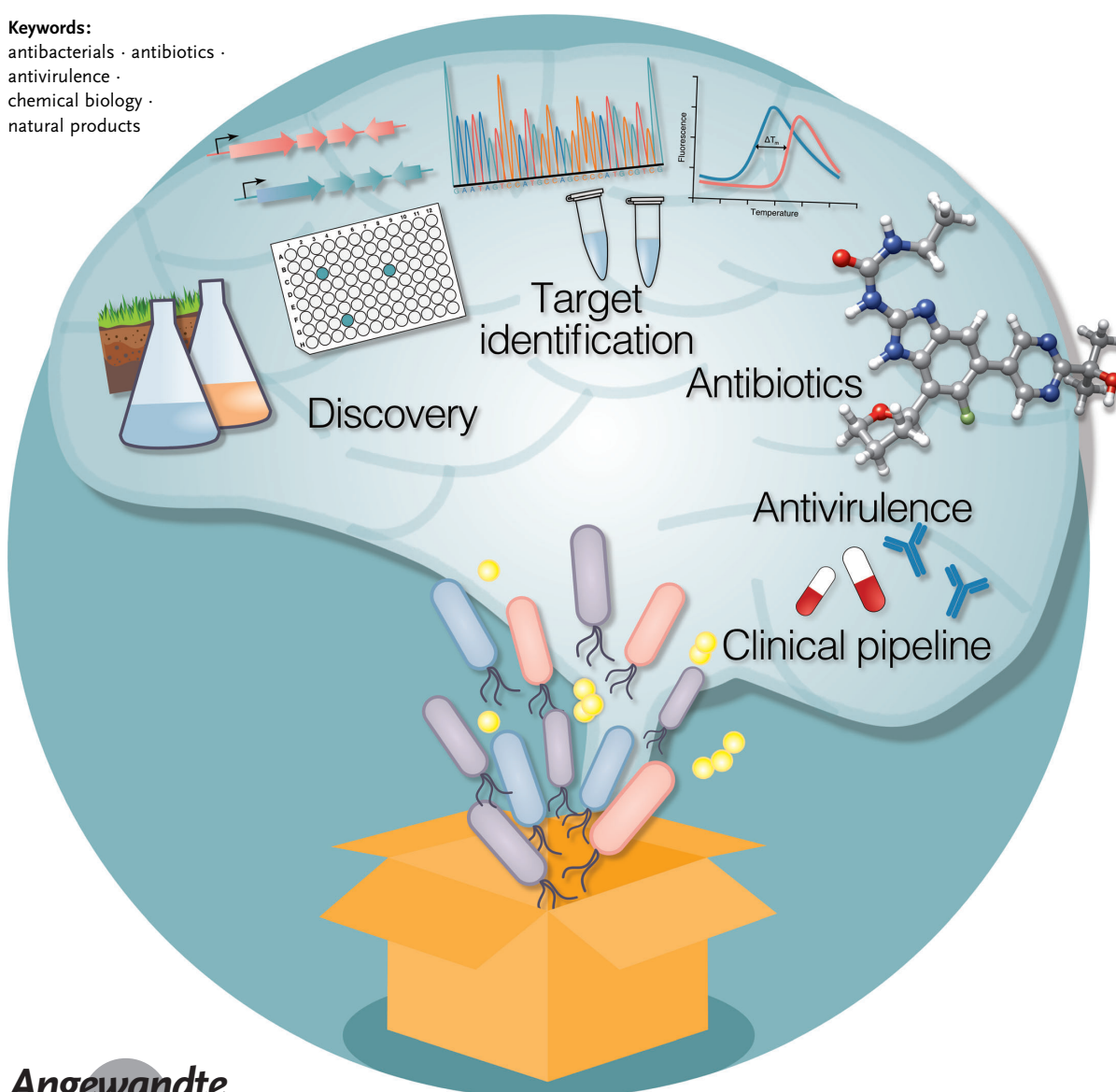
All authors outlined of the manuscript and performed literature research. Markus Lakemeyer wrote chapters 1-3 and chapters 5 in cooperation with Stephan A. Sieber and Peter Hammann. Weining Zhao and Stephan A. Sieber wrote chapter 4. Markus Lakemeyer created the figures. Franziska Mandl supported the other authors during composition of the manuscript and translated, in cooperation with Markus Lakemeyer, the article to German. Peter Hammann and Stephan Sieber supervised the process.

Thinking Outside the Box—Novel Antibacterials To Tackle the Resistance Crisis

Markus Lakemeyer, Weining Zhao, Franziska A. Mandl, Peter Hammann, and Stephan A. Sieber*

Keywords:

antibacterials · antibiotics ·
antivirulence ·
chemical biology ·
natural products



The public view on antibiotics as reliable medicines changed when reports about “resistant superbugs” appeared in the news. While reasons for this resistance development are easily spotted, solutions for re-establishing effective antibiotics are still in their infancy. This Review encompasses several aspects of the antibiotic development pipeline from very early strategies to mature drugs. An interdisciplinary overview is given of methods suitable for mining novel antibiotics and strategies discussed to unravel their modes of action. Select examples of antibiotics recently identified by using these platforms not only illustrate the efficiency of these measures, but also highlight promising clinical candidates with therapeutic potential. Furthermore, the concept of molecules that disarm pathogens by addressing gatekeepers of virulence will be covered. The Review concludes with an evaluation of antibacterials currently in clinical development. Overall, this Review aims to connect select innovative antimicrobial approaches to stimulate interdisciplinary partnerships between chemists from academia and industry.

From the Contents

1. Introduction	3
2. Methods for the Discovery and Validation of New Antibacterials	5
3. Novel Antibiotics with High Potential for Further Development	10
4. Antivirulence	15
5. Antibacterial Drugs in Clinical Development	19
6. Summary and Outlook	30

1. Introduction

“Antibiotic apocalypse”: doctors sound alarm over drug resistance,^[1] “We will miss antibiotics when they’re gone”^[2] are exemplary newspaper headlines referring to the threat of the antibiotic crisis on public health worldwide. Today, not only the scientific community, but also governments and the general public agree that novel antibacterial efforts are urgently needed to safeguard future therapeutic options.^[3] Although there is a rapid increase in multiresistant bacterial strains, the number of novel antibiotics for clinical applications remains low, with only two novel classes introduced in the past 20 years.^[4] The reasons for the onset of the current crisis are manifold and include aspects such as the careless prescription of antibiotics. On a molecular level, bacterial resistance is inherently associated with the antibiotic mode of action, that is, to block essential pathways and eventually kill the pathogen. Bacteria respond to this so called “selective pressure” by modifying the antibiotic target or finding other ways to impair the efficacy of the drug. This inevitable evolutionary process is based on cell division, which is prone to spontaneous mistakes that create random mutations in

DNA sequences. Those bacteria which by chance have acquired a lowered antibiotic susceptibility will survive while all other sensitive bacteria will die. This selection leads to the rapid evolution of resistant strains. Many of these genetic resistances are located on transferable plasmids which can be easily transmitted between different bacterial populations. The arsenal of resistance strategies reaches far beyond direct modifications of the binding sites but also includes elaborate strategies to chemically inactivate the antibiotic, pump it out of the cell, restrict its uptake, or bypass the target’s essentiality (Figure 1).

In fact, these evolutionarily driven mechanisms of resistance emphasize the necessity to limit antibiotic exposure and, if treatment is warranted, to ensure a full eradication of the pathogen. However, even if such measures would be strictly followed, it is still very challenging to fully eradicate dormant bacteria which reside in a metabolic resting state, so-called persisters, which can awaken and lead to a relapse of the infection. Moreover, bacteria from multicellular communities on surfaces are protected by a thick layer of extracellular polymeric substances (EPS) which prevent the access of

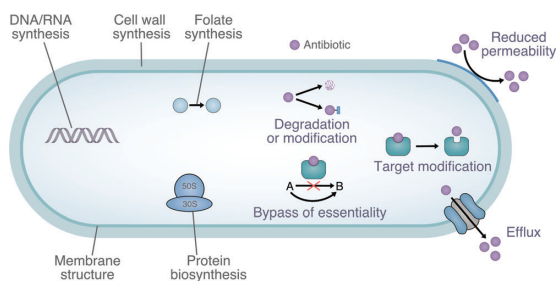


Figure 1. Schematic overview of common antibiotic targets and bacterial resistance mechanisms.

[*] M. Lakemeyer, Dr. W. Zhao, Dr. F. A. Mandl, Prof. Dr. S. A. Sieber
Department of Chemistry
Chair of Organic Chemistry II
Center for Integrated Protein Science (CIPSM)
Technische Universität München
Lichtenbergstrasse 4, 85747 Garching (Germany)
E-mail: stephan.sieber@tum.de
Prof. Dr. P. Hammann
R&D Therapeutic Area Infectious Diseases
Sanofi-Aventis (Deutschland) GmbH
Industriepark Höchst, 65926 Frankfurt am Main (Germany)
E-mail: peter.hammann@sanofi.com

ORCID The ORCID identification number(s) for the author(s) of this article can be found under:
<https://doi.org/10.1002/anie.201804971>.

antibiotics. These so-called biofilms are a major problem for implants, catheters, and stents, and represent a constant source of reoccurring infections. Persisters and biofilms, the latter of which are also composed of persister cells, represent natural mechanisms to withstand antibiotic treatment independent of acquired resistance.^[5] Thus, resistance is a general phenomenon which is impossible to avoid by traditional antibiotic therapies.

The antibiotic crisis is further triggered by the limited number of essential bacterial targets that are addressed by current antibiotics. These largely focus on inhibiting the biosynthesis of the cell wall, proteins, DNA/RNA, and folate or alternatively lead to membrane disruption. This is a surprising finding, as surveys predict that bacteria exhibit about 300 essential genes, which would provide plenty of opportunity to enlarge the scope to new and still resistance-free targets.^[6] However, the majority of antibiotics are derived from natural products which have been optimized towards a limited set of target hotspots by ancient evolutionary cycles of microbial combat for limited resources (Figure 1). Overall, this narrow spectrum of cellular target pathways has triggered multiple resistances, many of which date back to far earlier

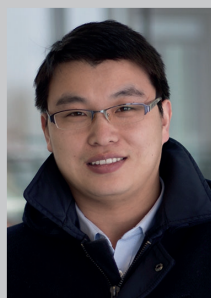
than their clinical use, as rescue mechanisms that protect the antibiotic-producing microbe. In fact, recently isolated bacteria which were buried in permafrost for 30 000 years showed broad resistance to common antibiotics.^[7] Although classical antibiotics and resistance development are major important topics to understand the origin of the crisis, they will not be the focus of this Review and the reader is pointed towards excellent articles covering this field.^[8–13]

In general, the development of antibacterial compounds is hampered by basic pharmacological challenges. Uptake represents a major obstacle that limits the success rate of such approaches. For Gram-positive strains, which bear only a single cell membrane, a few antibiotics of last resort are still available, including daptomycin, linezolid, and tigecycline. In contrast, Gram-negative bacteria are difficult to penetrate, as they have both an inner and an outer cell membrane. The treatment of patients infected by multiresistant Gram-negative strains such as colistin-resistant *Pseudomonas aeruginosa* becomes almost impossible—in some cases no therapeutic options remain. The WHO has released a priority list of bacteria, for which new antibiotics are desperately needed.^[14] The top priorities are summarized under the acronym ESKAPE, which describes the Gram-negative strains *Klebsiella pneumoniae*, *Acinetobacter baumannii*, *Pseudomonas aeruginosa*, and *Enterobacter*, as well as the Gram-positive strains *Enterococcus faecium* and *Staphylococcus aureus*.

This Review aims to give an interdisciplinary overview of the attempts and strategies to overcome the current antibiotic crisis and provides different facets of novel approaches to



Markus Lakemeyer received his BSc in chemistry from RWTH Aachen University in 2011 and his MSc in medicinal chemistry from Philipps-University Marburg, Germany, in 2014. During his master's project, he developed activity-based probes for human proteases in the group of Prof. Matthew Bogoy at Stanford University, USA. In 2014 he started his PhD under the supervision of Prof. Stephan Sieber at the Technical University of Munich, where he focuses on the inhibition and mechanistic studies of the bacterial protease ClpP.



Weining Zhao obtained his BSc in chemistry in 2009 and master's degree in organic chemistry in 2012 under the supervision of Prof. Francois Mathey and Prof. Zheng Duan from Zhengzhou University, China. He then carried out PhD research at the Technical University of Munich in the group of Prof. Stephan A. Sieber. After completing his doctoral studies in 2016, he started postdoctoral work in the Sieber group supported by a DFG grant.



Franziska Mandl studied chemistry at the Technical University Munich, with a special focus on organic and analytical chemistry. After her MSc, which she received in 2012, she started her PhD under the supervision of Prof. Stephan Sieber. Her work comprised the target evaluation of natural-derived compounds in Gram-negative bacteria. Since 2016 she has been a postdoctoral researcher in the Sieber group, working on the preclinical development of an MRSA-active antibiotic funded by the BMBF.



Peter Hammann studied chemistry at the Technical University of Darmstadt and received his PhD in organic chemistry from the University of Hannover, Germany. He joined Hoechst AG in 1986 and since had several leading positions in the field of lead discovery with a special focus on anti-infectives in Germany, India, and in USA. Since 2014 he has been responsible for the Sanofi–Fraunhofer Natural Product Center, with a major focus on the discovery of novel antibiotics for severe bacterial infections. He was appointed Honorary Professor at the University of Giessen (JLU) in 2016.



Stephan A. Sieber studied chemistry at the universities of Marburg (Germany) and Birmingham (England). He completed his PhD with Prof. Mohamed A. Marahel, University of Marburg, and Prof. Christopher T. Walsh, Harvard Medical School, Boston, USA. He then joined the group of Prof. Benjamin F. Cravatt for postdoctoral studies. In 2006 he started his independent research career at the University of Munich (LMU), Germany, funded by a DFG Emmy-Noether grant. In 2009 he was appointed full professor at the Technische Universität München. His research focuses on chemical biology and chemical proteomics.

combat pathogenic bacteria. We would also like to highlight promising strategies which have the potential to generate a next generation of antibiotic therapeutics.

We divide this Review into three main sections which reflect the development timeline at very different stages. For the early stage, we summarize innovative tools and methods that facilitate antibiotic discovery and are crucial for identifying innovative compounds acting beyond the classical targets. Next, recent innovative discoveries of antibiotics against Gram-positive and Gram-negative bacteria will be discussed and linked to the previous section by highlighting the corresponding discovery platform. We do not discuss anti-tuberculosis strategies, as this infection follows different development principles because of its special membrane composition and slow growth. We refer the interested reader to excellent recent reviews.^[15,16] Examples of antibacterial strategies will be highlighted that go beyond the classical killing paradigm. Here, strategies to eliminate bacterial pathogenicity represent a different approach that alleviates the pressure of resistance development. Finally, we discuss antibacterials which are currently in clinical development, with a critical evaluation from an industry perspective. As this Review focusses on selected recent examples, we are unable to discuss all notable work in this large research field and recommend outstanding review articles for further reading.^[8–13]

2. Methods for the Discovery and Validation of New Antibacterials

In this section, we present a selection of contemporary approaches for mining novel natural products and discuss screening methods that allow the assessment of their antibacterial properties. Additional methods have been well-summarized in previous reviews.^[17,18] Furthermore, we highlight approaches for the investigation of the mode of action of new compounds, an important parameter for translational antibiotic research.

2.1. Natural Products as a Resource of New Antibacterials

Natural products are produced by all kinds of microorganisms and have been the most important resource for antibiotic agents.^[19,20] They are evolutionarily optimized and thus have been selected for multiple beneficial properties: 1) structural diversity, 2) cell-wall penetration, including for Gram-negative bacteria, 3) potent cellular activity, and 4) selectivity. However, these molecules have not evolved for their drug-like properties but to act in bacterial physiology and ecology. Hence, while the identification of a novel antibiotic natural product is an essential first step, laborious research is required to transform a natural product into an effective antibiotic drug.^[21]

For the identification of bioactive natural product candidates, microbes have traditionally been cultivated and their metabolites screened for a phenotypic effect. Potent fractions are subsequently further investigated, and the exact chemical

structure of the active compound is elucidated by labour-intensive analytical work. This identification strategy has become well-known as the Waksman platform, in honor of the pioneering work of Nobel laureate Selman Waksman.^[17]

For many years, *Actinomycetes* were the most important resource in terms of number and diversity of natural products. However, over the last few decades, traditional natural product extract screenings failed to unravel new active antibiotics. In particular, the rediscovery of already known natural products has become a significantly hurdle which has dramatically increased the attrition rates of natural product discovery.^[22] As the “low-hanging fruits” of antibiotic natural products have already been picked, novel approaches are urgently needed. The adaptation of laboratory cultivation methods was shown to be an effective strategy to revive natural product discovery. In all natural environments (such as soil, plants, or the human gut), microbes live in association with a multitude of other organisms and interact with these through antagonism, commensalism, or mutualism.^[23] In contrast, laboratory cultivation was for a long time performed axenically, which means only a single organism was cultivated.^[24] Since microbes concomitantly faced optimal growth conditions (e.g. excess of nutrients, constant temperature, and pH value), they were not triggered to produce all the secondary metabolites they would use in a natural environment to interact with nearby organisms. Several authors have reviewed potential methods to induce the expression of the silent biosynthetic gene clusters (BGCs) of these metabolites, for example, by varying the cultivation conditions or by genomic engineering.^[23–26] The cocultivation of multiple bacterial species has proven to be very effective for the production of previously unknown secondary metabolites (Figure 2a).^[24,27,28] A recent successful example is the coculturing of two marine species, the producer *Micromonospora* together with *Rhodococcus* sp., to afford the bis-nitroglycosylated anthracycline keyicin (Figure 3). This antibiotic is active against Gram-positive bacteria and, importantly, does not share a common mode of action with other anthracycline compounds. Instead of inducing DNA damage, chemogenomic results indicate that keyicin instead interacts with bacterial metabolism of fatty acids.^[29]

To dive deep into the pool of uncharted, yet promising natural products, scientists have now shifted their focus towards exploring the “microbial dark matter”^[30] namely, the 85–99% of bacteria and archaea that defy cultivation in the laboratory.^[31] It is widely believed that these strains harbor a plethora of novel bioactive natural product classes. In this context, Lewis, Epstein, and co-workers pioneered the development of a diffusion growth chamber, which enables the cultivation of traditionally “uncultivable” bacteria in a simulated natural biosphere.^[32,33] In their approach, environmental samples (e.g. soil or marine sediments) are collected and diluted with agar, placed between two semi-permeable membranes, and put back into their natural habitat. The membranes allow free diffusion of nutrients and growth factors produced by fellow organisms, but restrict the movement of the trapped microbes (Figure 2b). This technology improves the number of cultivatable cells dramatically up to 50%, compared to 1% of cells from soil that

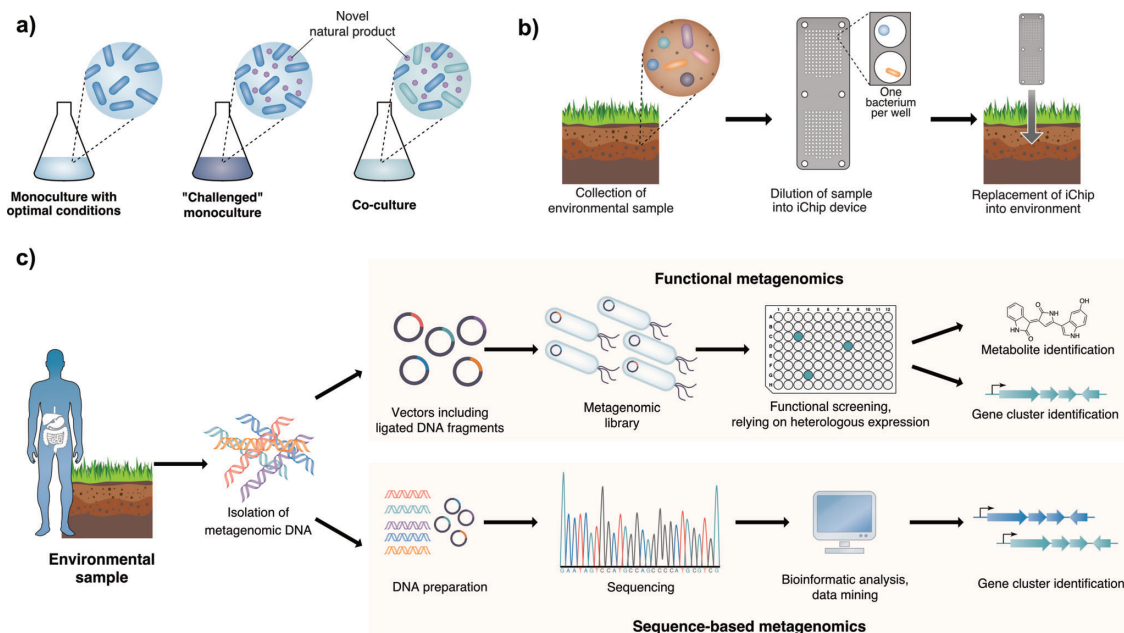


Figure 2. Methods for the discovery of novel natural products. a) Modified cultivation conditions, either by altered environmental cues or by co-cultivation, induce the microbial production of new natural products. b) Cultivation of microbes in their native environment by means of the isolation chip (iChip). Environmental samples are collected and diluted in agar to enable the (average) presence of one bacterial cell per hole. After covering with semipermeable membranes that allow the free diffusion of nutrient and metabolites while restricting bacterial movement, the iChip is placed back into the original environment. Once colonies are established, they can frequently be grown using traditional culture conditions and tested for the production of natural products. c) Schematic overview of functional and sequence-based metagenomic workflows. Metagenomic DNA is isolated from environmental samples (e.g. soil or the human microbiome). For functional metagenomics, DNA fragments are cloned and ligated into vectors, and then transformed into a suitable host to create a metagenomic library. This can be functionally screened for phenotypes of interest caused by the production of natural products from the corresponding encoded BGCs. Finally, the metabolites of interest can be structurally analyzed and responsible gene clusters can be identified by sequencing of the original eDNA insert. In sequence-based metagenomics, all the eDNA is directly sequenced and bioinformatically analyzed for the identification of BGCs and their natural products.

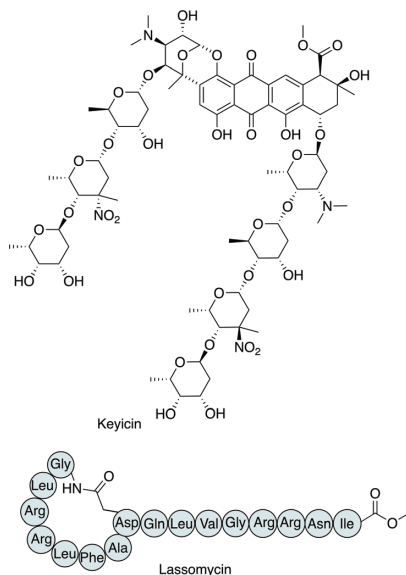


Figure 3. Antibiotic natural products keyicin and lassomycin.

will grow on a nutrient Petri dish.^[33,34] Importantly, once a colony is produced in situ, a substantial number of isolates can also be cultivated under laboratory conditions, thereby allowing the investigation of antibacterial natural products.^[35] The first antibiotic discovered using a miniaturized, multiwell diffusion chamber called iChip (isolation chip) was lassomycin (Figure 3), an inhibitor of the ATP-dependent protease complex ClpC1ClpP1P2 in *M. tuberculosis*.^[36]

Despite the advances described, the cultivation of many microbes is still a major obstacle. In this regard, metagenomic approaches offer a means for identifying new antibiotics and their respective biosynthetic gene clusters (BGCs) without the need to cultivate the original producer strain (Figure 3c).^[37,38] Metagenomic DNA (or environmental DNA, eDNA), that is, the collective DNA in a given environment, can be extracted from essentially every environmental source. eDNA can be directly sequenced and bioinformatically analyzed to identify BGCs (sequence-based metagenomics).^[39,40] Alternatively, DNA fragments are first cloned into a screening vector library, which is transformed into a suitable heterologous host, where the product of the metagenomic DNA is expressed. The resulting clones are screened for a specific phenotype (e.g. growth-inhibition of a pathogenic

strain) which is caused by the production of metabolites from eDNA-encoded BGCs. Subsequently, clones of interest can be further investigated, for example, to identify the accountable natural product or its BGC (functional metagenomics).^[41,42]

In addition to ecological environments, metagenomic and bioinformatic efforts point towards the human microbiome as a great resource for the discovery of new microbes and their natural products harboring a variety of biological activities, including immune modulation or antibiosis.^[43–47] A selection of fascinating examples of antibiotics identified by these methods will be discussed in Section 3.

2.2. Synthetic Libraries and Target-Based Screens

When the antibiotic pipeline started to dry out because of rediscoveries of already known natural products, the focus changed towards target-based screening of essential bacterial proteins by using synthetic compound libraries. Although screening recombinant proteins has been highly fruitful in drug discovery for multiple diseases, efforts towards novel antibiotic drugs were mostly disappointing.^[22,48,49] The main reason for this discrepancy is limited compound accumulation inside the bacterial cell. The compound libraries for antibacterial screenings mostly derived from previous screening approaches against human targets, thereby neglecting the substantially different physicochemical properties needed for antibacterial activity.^[50,51] In particular, the penetration of Gram-negative bacteria and circumventing drug efflux pose significant challenges to today's antibiotic discovery. Since we lack a clear understanding of the physicochemical properties needed to guarantee target engagement in Gram-negative pathogens, there is no defined set of properties that can be easily integrated into promising antibacterial candidates.^[52] Scientists have therefore tried to identify guidelines for bacterial penetration, equivalent to Lipinski's rule of five for orally available drugs. Retrospective analysis of various screening approaches^[51,53–55] and recent efforts to monitor and optimize cell penetration have so far only resulted in vague and sometimes contradicting guidelines.^[56–58] In a recent comprehensive study by the Hergenrother group, the accumulation of over 180 compounds inside *Escherichia coli* was quantified by mass spectrometry and correlated to their physicochemical properties. Computational analysis revealed that small molecules are most likely to accumulate if they contain an ionizable amine (primary amines preferred), are amphiphilic, rigid, and have low globularity.

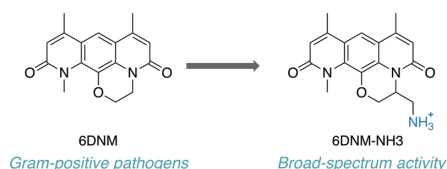


Figure 4. The addition of a primary amine to the deoxynymycin analogue 6DNM, potent solely against Gram-positive bacteria, leads to broad-spectrum antibacterial activity.

Application of these guidelines to an analogue of deoxynymycin (6DNM), an antibiotic active only against Gram-positive pathogens, indeed enabled the functionalized derivative 6DNM-NH₃ to act against a variety of Gram-negative bacteria (Figure 4).^[59,60]

In the meantime, the limitations of current compound libraries have been understood and contemporary approaches are being pursued to broaden the chemical space used for antibacterial screenings. New libraries are generated using combinatorial and diversity-oriented synthesis^[61–64] or small-molecule fragments.^[65–68] These libraries are mostly used for the targeted screening of purified proteins.

2.3. Screening Platforms

As long as the physicochemical compound properties needed to reach a cellular bacterial target are not fully understood, targeted screens with recombinant proteins are used, although with limited application. For this reason, industrial programs rely extensively on phenotypic screening for the identification of new antibacterials.^[17] The screening platform most widely applied in both industry and academia is antibiotic susceptibility testing (AST). In this screen, the incubation of pathogens with increasing concentrations of an antibiotic allows the determination of the minimal inhibitory concentration (MIC), that is, the lowest concentration of an antibiotic which prevents visible growth of the bacterial species. This value is the most important factor for the initial assessment of the potency of a compound. Antibiotics can be grouped into two categories, both of which are therapeutically efficient: bactericidal drugs immediately kill bacterial cells, for example, by cell-wall disruption, while bacteriostatic antibiotics merely stall their growth.

Similar to natural product identification, ASTs have for a long time overlooked the influence of the bacterial environment during host infection, which has occasionally resulted in inaccurate assertions of antibiotic susceptibility. There is a growing appreciation that antibiotic lethality is a complex, system-level process which is responsive to a variety of environmental cues.^[69,70] Several studies have shown that bacterial metabolism is sensitive to factors such as nutrient and oxygen availability, or the presence of environmental metabolites and bioactive compounds, for example, antimicrobial peptides (AMPs) produced by the host's immune system. All of these components modulate various pathways and are mainly causative for the altered in vivo efficiency of antibiotics.^[69,71–74] Efforts were made to mimic in vivo conditions during in vitro AST to account for this contextual antibiotic susceptibility. A straightforward and very effective approach is the substitution of common rich laboratory medium with minimal medium.^[75,76] A recent study by Ersoy et al. revealed that the antibiotic susceptibility of various clinical isolates strongly depends on the medium used for in vitro cultivation. Replacing the MHB medium for host-mimicking media such as DMEM, MLM, or LPM5.5 during the AST drastically improved the prediction accuracy for antibiotic efficacy in mouse infection models.^[77] Similarly, the addition of physiological concentrations of NaHCO₃ to

standard MHB medium resulted in a host-mimicking environment, which suggests that the salt is a key component that contributes to antibiotic susceptibility in vivo.^[77,78] Despite these advancements of in vitro AST, the full complexity of bacterial infections in vivo can hardly be simulated. Therefore, high-throughput infection screening has become a valuable tool, especially for secondary antibiotic screens.^[79] Suitable organisms for predicting drug efficacy against bacterial infections in mammalian systems with minimal ethical concerns are zebrafish embryos,^[80] silkworms,^[81,82] wax moths,^[83,84] and nematodes (e.g. *Caenorhabditis elegans*).^[85-87]

During the last few years, phenotypic screening has evolved from the empirical screening of AST to hypothesis-driven discovery approaches that focus on inhibiting defined bacterial pathways or functions. The underlying concept is to combine the advantages of target-based biochemical screens and cell-based phenotypic assays. Target-based whole-cell approaches allow the screening of inhibitors for promising novel bacterial targets directly in live cells. In contrast to assays on recombinant enzymes, the direct cellular activity of a compound is thereby guaranteed. Depending on the global distribution of the target of interest, these efforts aid, in particular, in the identification of potent antibiotic and antivirulence (see also Section 4) candidates which spare commensal bacteria and are likely less toxic to eukaryotic cells.^[17,18]

Target-based whole-cell screenings include comparative profiling of, for example, genetically modified versus wild-type bacterial strains or the rescue of an antibiotic effect upon external supplementation, for example, of a metabolite.^[88] Reporter strains are genetically engineered bacterial strains that allow the readout of a specific physiological perturbation by the altered expression of a reporter gene, such as GFP. Numerous HTS campaigns have been performed in various genetically modified *E. coli* reporter strains.^[89-92] In a comprehensive study, Tucker et al. established a sophisticated conjugate strategy that allowed the screening of a random library of 800000 genetically encoded antimicrobial peptides (AMPs) directly in *E. coli*, in which one peptide per cell was recombinantly expressed.^[93] Comparative next-generation sequencing of the mutant library (before and after induction) resulted in the identification of 2000 potent AMP hits. Importantly, AMP candidates were not biased to accompanying eukaryotic toxicity, which often limits the clinical application of cationic AMPs (see Section 5).^[93,94]

Although *E. coli* strains allow straightforward genetic modifications and antibiotic screening, they do not always accurately reflect bioactivity in clinically important pathogens. To account for the different physiologies of bacterial species, including specific cell-wall structure or virulence mechanisms, reporter-based assays are directly performed in the respective strain of interest. Screens of wild-type or multiresistant bacteria have for example been performed in *S. aureus*,^[95,96] *V. cholerae*,^[97] *K. pneumoniae*,^[98] and *P. aeruginosa*.^[99,100]

Bacterial cytological profiling (BCP) has proven itself as a valuable tool that exceeds simple cellular susceptibility tests. In particular, the automation of microscopic imaging nowadays allows not only the parallel monitoring of various

cellular characteristics and functions in bacterial cells, but also cellular bacterial infection models. BCP can not only be applied to phenotypic drug discovery screening, but also to cytological profiling experiments that allow the study of a drug's mode of action.^[101-104]

Additionally, computational methods have been a very valuable tool for the screening and analysis of potential antibiotics. The substantial advances in the “-omics” fields including genomics, proteomics, and metabolomics have resulted in a veritable explosion of (phenotypic) data. Bioinformatic approaches aim to take advantage of these huge data sets to identify new antibacterial compounds and potential new targets or to help clarify the mode of action of new compounds.^[105-109]

2.4. Target Identification and Validation

A major challenge after identifying an antibiotic hit compound is elucidating its molecular mode of action (MoA). This is often a key prerequisite for subsequent parameter optimization during lead development. Previous reviews have already presented overviews of both traditional (e.g. metabolic labeling of biological macromolecules with radioactive precursors) and current methods for identification of the target of new antibiotic compounds.^[110-112]

Many approaches for the identification of antibacterial targets are based on the generation of resistant mutants, which are subsequently sequenced to identify altered cellular targets. The advancement of sequencing technologies nowadays allows the cost-efficient analysis of DNA and RNA samples and has established chemical genomic methods as a widely applied method for the study of the MoA of new antimicrobial compounds. The generation of barcoded deletion mutant libraries in which each mutant is encoded by a specific DNA-sequence allows parallel resistance screening of all mutants directly in one vessel. This technology was first reported for yeast and since been applied also in *E. coli*. Resistant mutants are identified by comparative sequencing of the barcodes before and after compound treatment. This method will become especially powerful when libraries of barcoded deletion mutants are available for clinically important pathogenic strains.^[113-115] In the near future, application of the CRISPR-Cas technology to bacterial cells will most likely further enable cell-wide target assessment.^[116]

The prerequisite for these methods, however, is the identification of a bacterial clone that is resistant to the antibiotic of interest because of an alteration of the direct target, which is not always so straightforward. As already described, resistance does not necessarily rely on mutations of a cellular binding partner but can also derive from modified permeability or transport as well as up-regulation of a compensatory pathway, which complicates the analysis of the MoA of a compound. Therefore, we will focus on methods for the identification of protein targets that do not rely on the generation of resistant mutants, but instead are based on cellular profiling techniques.

Over the last few years, activity-based protein profiling (ABPP), pioneered by the groups of Cravatt and Bogoy, has



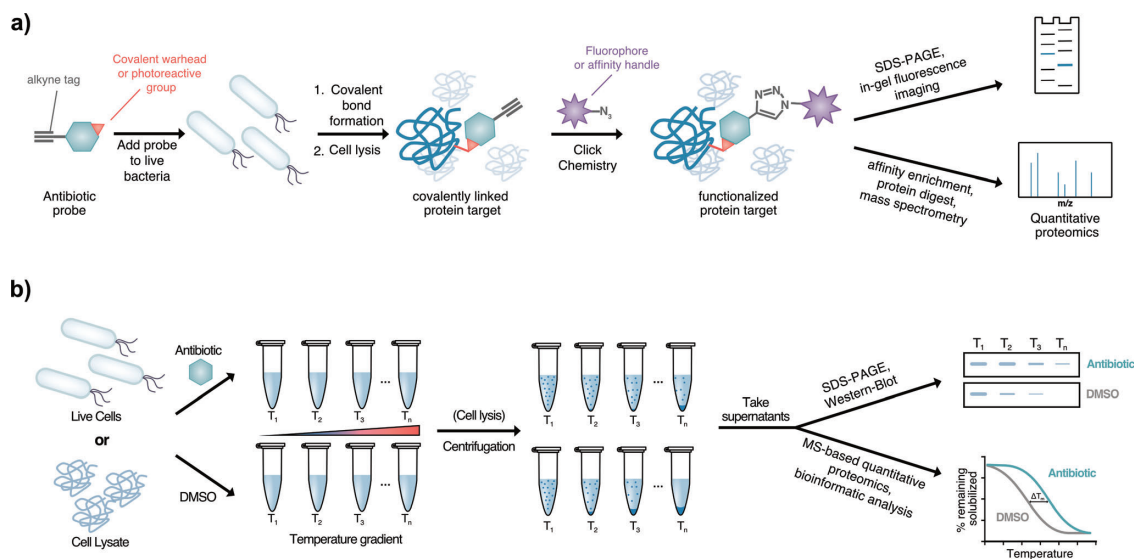


Figure 5. Methods for the identification of protein targets of antibiotics. a) For A(f)BPP, parent antibiotics are equipped with an alkyne tag and, if they are acting noncovalently, a photo-cross-linking group. Live cells are treated with the probe. After formation of the covalent bonds (either by reaction of the covalent warhead or by UV-mediated cross-linking for photo-cross-linkers), cells are lysed and functionalized with a tag by copper-catalyzed click chemistry. For conjugation to fluorophore azides, protein targets are separated by SDS-PAGE and visualized by in-gel fluorescence imaging. When an affinity handle (e.g. biotin azide) is attached, proteins can be enriched by affinity purification, proteolytically digested, and subjected to mass spectrometry to allow quantitative proteomic analysis. b) Alternatively, parent antibiotic compounds can be used for thermal profiling assays. Live cells or lysates are incubated with the antibiotic or DMSO (control) at increasing temperatures. The binding of the compound to the target proteins can lead to a change in the melting temperatures. After incubation, cells are lysed (if live cells were used) and the samples are centrifuged. The remaining soluble proteins of each temperature sample are either analyzed by SDS-PAGE and Western-Blot or alternatively by MS-based quantitative proteomics to identify compound-induced stabilization of the target protein.

emerged as a powerful method for target elucidation of small molecules in live cells.^[117–121] ABPP analyzes the direct interaction of ligands and their protein targets (Figure 5a). Cell-permeable small-molecule probes are applied which carry functionalities for covalent protein binding and subsequent bioorthogonal modification, for example, through an alkyne tag. After binding to cellular protein targets and cell lysis, the alkyne group allows conjugation with azide-functionalized fluorophore or affinity tags by the copper-catalyzed click reaction.^[122,123] For fluorophore conjugates, target proteins are analyzed by SDS-PAGE and in-gel fluorescence imaging. Alternatively, biotinylated samples are enriched by affinity purification, proteolytically digested, and subjected to mass spectrometric analysis, which allows the identification and quantification of target proteins. ABPP was originally developed for mapping protein targets of covalent probes. Additional functionalization with photo-cross-linking moieties (such as benzophenones, aryl azides, or diazirines) has extended the application to noncovalent parent compounds and is known as affinity-based protein profiling (AfBPP). Irradiation with UV light results in the generation of highly reactive intermediates, which react with proximal protein groups and covalently link the probe and the protein for downstream sample preparation.^[119] There are numerous examples in which A(f)BPP revealed the molecular targets of small molecules in eukaryotic and prokaryotic cells.^[124–126] An illustrative recent example is the target elucidation of the

Pseudomonad secondary metabolite promysalin in *P. aeruginosa*.^[127] Promysalin is an effective antibacterial compound in *P. aeruginosa*; however, its mode of action was poorly understood. Since the compound does not contain any apparent covalent warheads, an alkyne-containing photo-cross-linker^[128] was incorporated into the natural product. In addition, a closely related inactive promysalin photoprobe was synthesized as a control. Comparison of the enriched proteins of these two probes and additional competition experiments using unmodified promysalin allowed the identification of a succinate dehydrogenase as the molecular target, which could subsequently be verified by orthogonal methods.^[127] In addition to small molecules, A(f)BPP has also been applied for the target elucidation of antibacterial peptides by means of modified amino acids.^[129–131]

Recent advancements have established mass spectrometry as a widely used and very powerful tool for the analysis of cellular metabolic (metabolomics) or protein (proteomics) networks. This includes the identification of functional pathways that are affected upon treatment with antibacterial compounds. In a recent study by Zampieri et al., a non-targeted metabolomics approach was applied to monitor the immediate short-term metabolic response of *E. coli* to a variety of antibiotic perturbations.^[132] The authors quantified changes in about 750 metabolites upon exposure to the antibiotic and could see concentration- and compound-specific changes of distinct metabolic pathways. Importantly,

this profiling approach cannot only be used to predict the MoA of new compounds, it also aids the identification of novel druggable targets, as recently shown in *M. tuberculosis*.^[133]

Thermal proteome profiling allows an unbiased search of protein targets in live cells using parent drugs without the need for modification. It is based on ligand-induced changes in thermal protein stability, which have been studied in vitro for decades through thermal shift assays on recombinant proteins. The simultaneous analysis of the melting curves of a full proteome became widely known to the scientific community as the Cellular Thermal Shift Assay (CETSA).^[134,135] Protein stability is assessed by compound-induced changes in the protein precipitation temperatures which can either be analyzed for selected proteins by Western Blot, or in an unbiased way using MS-based proteomics (Figure 5b). Prerequisite for this method is that the protein or protein complex significantly changes its melting point upon compound binding. Although thermal proteome profiling has been widely applied in eukaryotic systems^[136,137] there are only a few examples of its use in microbes. However, initial studies show that this method can also be applied in live bacterial cells in a targeted way (through Western blot)^[138,139] and in an unbiased way in bacterial lysate (by MS-based proteomics).^[140] We believe that thermal profiling will, in the future, prove to be a powerful method for the identification of antibacterial protein targets.

3. Novel Antibiotics with High Potential for Further Development

Novel antibiotics and antibacterial targets are urgently needed to combat the rampant spread of resistance towards classic antibiotic agents. Academic research is a key driver in the advancement of known antibiotic classes and pursues a multitude of innovative antibacterial approaches, including light-controlled (de)activation of antibiotics or antibiotic-conjugation strategies.^[141–143] For example, the incorporation of siderophore moieties onto antibiotic structures facilitates Gram-negative penetration by using a “Trojan horse” approach, whereby antibiotics are taken up by natural siderophore transporters. Although a multitude of projects

would certainly deserve to be discussed in detail, this would go beyond the scope of this Review. We, therefore, focus on novel antibiotics which were largely discovered by the methods discussed above, review their MoAs, and comment on their antibacterial properties and potential for further development.

3.1. Teixobactin

The discovery of the nonribosomal depsipeptide teixobactin^[144] (Figure 6) in 2015 not only raised the attention of the scientific community, but also of the general media. Teixobactin was identified using the diffusion chamber device iChip (see Section 2), which allows the high-throughput cultivation of microbes in their natural environment. Extracts from 10000 isolates obtained by growth in iChips were screened for antibacterial activity against *S. aureus*.^[144] A previously unknown Gram-negative β -proteobacterium isolated from soil, *Eleftheria terrae*, was identified as the producer of teixobactin. Teixobactin displays remarkable activity against a variety of Gram-positive bacteria, including multiresistant strains (e.g. methicillin-resistant *S. aureus* (MRSA): MIC of $0.25 \mu\text{g mL}^{-1}$, vancomycin-resistant *Enterococci* (VRE): MIC of $0.5 \mu\text{g mL}^{-1}$) and is superior to vancomycin in killing late exponential phase populations. Additionally, *M. tuberculosis*, *Bacillus anthracis* and *C. difficile* are killed very efficiently. However, teixobactin is inefficient against Gram-negative pathogens, with the exception of outer membrane-defective *E. coli* mutants, thus indicating that the compound is unable to traverse the outer membrane of Gram-negative bacteria.^[144]

Teixobactin exhibited excellent in vivo potency in three different mouse infection models, equivalent to or even surpassing the approved antibiotics vancomycin and amoxicillin. For example, in a mouse septicemia model of intraperitoneal MRSA infection, the PD₅₀ (protective dose at which half the animals survive) for teixobactin was 0.2 mg per kg, in comparison to vancomycin with a PD₅₀ of 2.75 mg per kg. Importantly, all efforts to generate teixobactin-resistant *S. aureus* and *M. tuberculosis* mutants in the laboratory so far failed, thus encouraging its potential application as a therapeutic agent.^[144]

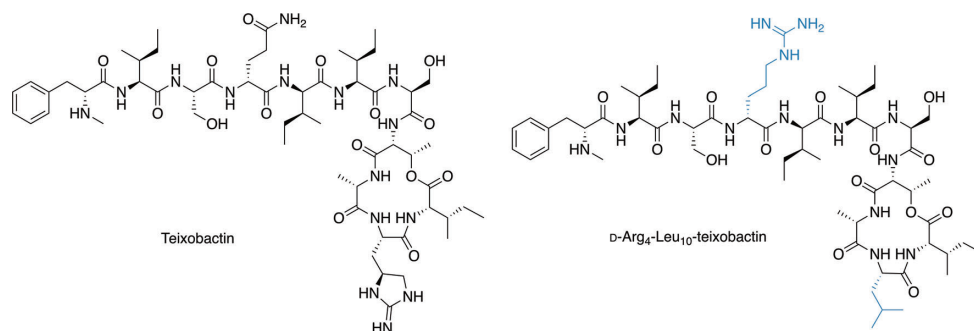


Figure 6. The natural product teixobactin and its synthetic analogue d-Arg₄-Leu₁₀-teixobactin.



The MoA of teixobactin was elucidated by macromolecular incorporation studies, which showed strong inhibition of peptidoglycan biosynthesis upon compound treatment. Subsequent *in vitro* analyses revealed that teixobactin binds to the highly conserved pyrophosphate motifs of multiple bacterial cell-wall substrates, for example, lipid II, a precursor of peptidoglycan, and lipid III, a precursor of cell-wall teichoic acid. Additionally, it also binds to the cytosolic lipid I, which, however, is not responsible for the antibiotic effect.^[144] Further comprehensive studies revealed that the synergistic inhibition of both peptidoglycan and teichoic acid synthesis results in cell-wall damage, delocalization of autolysins, and ultimately cell lysis.^[145] The lack of resistance development so far is a result of the multifaceted MoA, combined with the fact that teixobactin addresses a highly-conserved non-protein target.^[146]

Various groups have pursued the total synthesis of teixobactin and its corresponding analogues. Additionally, NMR and crystallographic studies have given insight into the structural details of the peptide and identified the macrolactone ring to be essential for pyrophosphate binding and thus the antibiotic effect (all of this is summarized excellently by Guo *et al.*^[147] and Fiers *et al.*^[148]). In-depth structure–activity relationship (SAR) studies, especially aiming to replace the synthetically inconvenient *L-allo*-enduracididine (*L-allo*-End) amino acid, led to the identification of various potent derivatives, including D-Arg₇-Leu₁₀-teixobactin (Figure 6).^[149–151] This peptide is readily available synthetically and shows excellent antibacterial activity against MRSA (MIC of 0.125 $\mu\text{g mL}^{-1}$) and 18 additional Gram-positive strains. Importantly, the peptide does not exhibit toxicity, neither *in vitro* nor *in vivo* (topical administration in a rabbit corneal damage model), and clears infections in a mouse-eye model of *S. aureus* keratitis as well as the approved antibiotic moxifloxacin.^[152]

3.2. Malacidin A + B

Malacidin A and B (Figure 7) are novel lipopeptide antibiotics that were recently discovered using a culture-

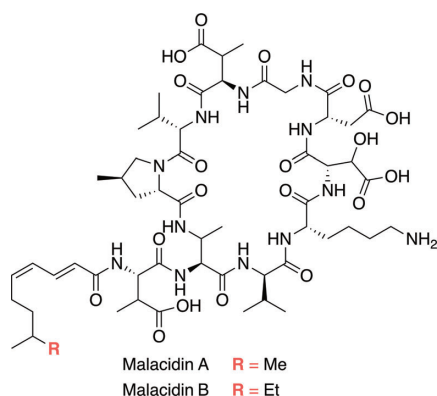


Figure 7. Chemical structures of malacidin natural products.

independent strategy.^[153] They belong to the family of calcium-dependent antibiotics. All previously known members of this group contain a conserved Asp-X-Asp-Gly motif that is thought to facilitate calcium binding, which is essential for antibacterial activity, but is absent in the malacidins. The most prominent member of this family is daptomycin, one of the last approved antibiotics with a novel MoA.

Hover *et al.* aimed to identify new calcium-dependent antibiotics by a metagenomics approach.^[153] By using a large eDNA collection isolated from >2000 unique soils, they performed a sequence-guided screen for BGCs similar to those of known calcium-dependent antibiotics. Bioinformatic analysis and phylogenetic mapping guided them to a very abundant, yet so far unknown, class of natural products, which they termed malacidins (metagenomics acidic lipopeptide antibiotic-cidins). Well-established metagenomic cloning methods were then applied to a desert soil sample especially rich in malacidin BGCs, which resulted in two new antibiotics: malacidin A and B which only differ in a single methylene group in the N-terminal lipid chain.^[153] Malacidins are the first members of a novel class of calcium-dependent antibiotics in which the canonical Asp-X-Asp-Gly calcium-binding motif is replaced by (Asp-OH)-Asp-Gly. Nevertheless, they still execute their antibacterial activity in a calcium-dependent manner. Malacidin A shows excellent antibiotic activity against a variety of Gram-positive pathogens, including multidrug-resistant strains (e.g. MRSA: MIC of 0.2–0.8 $\mu\text{g mL}^{-1}$, VRE: MIC of 0.8–2.0 $\mu\text{g mL}^{-1}$). However, it is inactive against Gram-negative bacteria. All efforts to generate malacidin A resistant *S. aureus* mutants in the laboratory have so far failed.^[153] Importantly, malacidin A is non-toxic to mammalian cells *in vitro* and does not induce hemolysis of sheep red blood cells. The *in vivo* efficacy was assessed in a rat cutaneous wound infection model, where topical administration of malacidin A successfully cured MRSA infections.^[153]

Previously known calcium-dependent antibiotics act either by 1) binding to cytosolic membrane phospholipids and oligomerizing in the membrane to diminish membrane integrity (daptomycin) or 2) by binding to the lipid II precursor undecaprenyl phosphate (C55-P) to inhibit cell-wall biosynthesis (e.g. laspartomycin, friulimicins).^[154,155] Comprehensive *in vitro* studies revealed that while malacidin also inhibits cell-wall biosynthesis, it does not bind to C55-P. Instead, it exerts its antibiotic activity by calcium-dependent binding to lipid II. Importantly, malacidin A shows no cross-resistance to vancomycin, which also targets lipid II, thus confirming a different binding site.^[153] Further studies are necessary to investigate if teixobactin and malacidin A share a common binding mode to lipid II.

3.3. Lysocins

Lysocins are depsipeptides produced by *Lysobacter* sp. which share a common skeletal backbone consisting of 12 amino acids. They were first identified by a phenotypic HTS for growth inhibition of *S. aureus* caused by culture supernatants from soil bacteria.^[81] To further prioritize the initial

hit candidates, a silkworm infection model was used as a secondary screen. This platform was previously proven to be a valuable tool for the assessment of toxicity and antibacterial efficacy of primary hits.^[156,157] The most potent analogue, lysocin E (Figure 8), exerts good antibacterial activity against

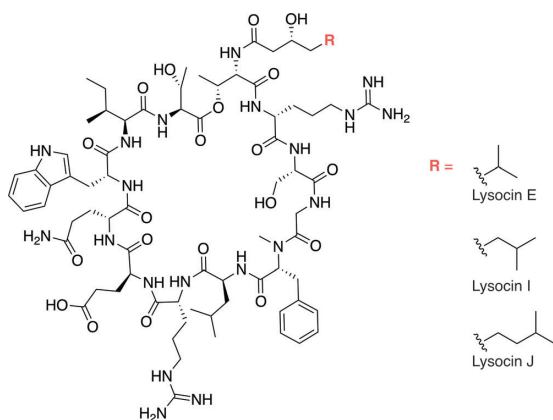


Figure 8. Chemical structure of lysocin E, I, and J.

Gram-positive pathogens, including methicillin-sensitive *S. aureus* (MSSA) and MRSA strains (MICs of $4 \mu\text{g mL}^{-1}$), but lacks potency against Gram-negative bacteria. The peptide shows low toxicity against mammals (intraperitoneal administration of 400 mg per kg body was tolerated in mice) as well as excellent *in vivo* effects in a mouse intraperitoneal infection model with *S. aureus* (subcutaneous administration, ED_{50} : 0.5 mg per kg body weight). Macromolecular incorporation assays were carried out in an attempt to identify the mode of action of lysocin E and showed immediate termination of all cellular biosynthesis pathways upon compound treatment. Together with the strong bactericidal activity, this directed the authors towards a mechanism of membrane disruption. The generation of *S. aureus* mutants resistant to lysocin E revealed altered menaquinone biosynthesis genes, and the addition of menaquinone was able to rescue wild-type bacteria. Subsequent studies suggested that lysocin E exerts its antibacterial effect by directly binding to menaquinone within the cytoplasmic membrane, thus promoting membrane disruption.^[81] This unusual mode of action was supported by the total synthesis and study of lysocin E as well as several derivatives.^[158,159] In a recent study, Santiago et al., however, found evidence that lipid II is a molecular binding partner of lysocins and is, therefore, likely responsible for the bacteriolytic phenotype.^[160] The authors developed a novel genome-wide mutant profiling approach that allows the identification of the MoAs of novel antibiotics. To validate their platform, they applied it to an uncharacterized natural product sample. Coincidentally, the isolated peptides included lysocin E and a new derivative lysocin J (Figure 8). Transposon mutant analysis revealed lipid II to be the molecular target of the peptides and subsequent peptidoglycan synthesis assays showed inhibition through an antibiotic/substrate binding stoichiometry of 2:1. Furthermore, an innovative affinity

capture assay allowed direct verification of binding between lipid II and lysocin E, whereas menaquinone did not compete with this interaction. As menaquinone-deficient *S. aureus* mutants were shown to have very low levels of lipid II, this might explain the previously observed menaquinone-dependent antibiotic susceptibility.^[160] Future studies will reveal if menaquinone and lipid II are both able to bind lysocin E simultaneously in a noncompetitive manner and will give further insights into the exact MoA of lysocin natural products.

3.4. Cystobactamids and Albicidins

Cystobactamids and albicidins (Figure 9) are closely related natural product classes which consist of a central amino acid motif, substituted *p*-aminobenzoic acid (pABA) chains—rare features in natural products—and an N-terminal group. The natural products and their respective BGCs were first independently identified in two unrelated species, *Cystobacter* sp.^[161] and *Xanthomonas albilineans*.^[162] Importantly, both compound classes have excellent activity in the low $\mu\text{g mL}^{-1}$ range not only against Gram-positive, but also against Gram-negative bacteria, including clinically relevant ESKAPE pathogens. Various members of both compound classes have been prepared synthetically, thereby unambiguously determining the configuration of the central amino acid. The different derivatives vary in their central amino acid motif, pABA-substituents, and N-terminal modifications. To date, 13 cystobactamids,^[161,163,164] including two analogues called coralmycin A/B, which were first identified from *Coralloccoccus* sp.,^[165] and numerous natural and synthetic albicidin derivatives^[166–169] have been reported. Cystobactamids and albicidins represent the first natural products that inhibit the subunit A of type II topoisomerases. This MoA was verified by the presence of resistance genes and by assays using recombinant enzyme.^[161] The antibacterial activities of the derivatives vary depending on the bacterial pathogens, which seems to be mostly a result of penetration and efflux since *in vitro* inhibition of DNA gyrase enzymes is often comparable in the low-nanomolar range.^[163] Cystobactamids and albicidins can be considered as natural analogues of

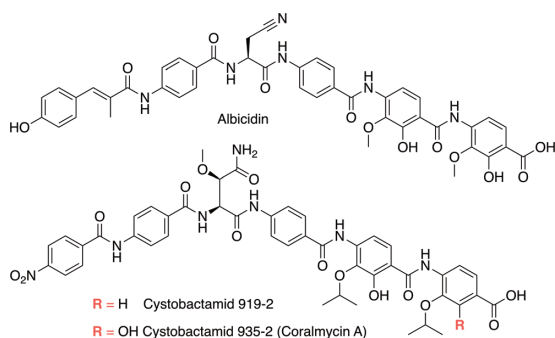


Figure 9. Representatives of the closely related natural product classes of the albicidins and cystobactamids.

synthetic quinolones, with whom they share their cellular target. Notably, quinolone-resistant pathogens are still partially susceptible towards cystobactamids and albicidins, which is attributed to their moderately different binding modes. If known limitations, such as the previously reported low solubility of the compounds, can be overcome, cystobactamids and albicidins may in the future open new possibilities to target bacterial DNA replication.

3.5. Retinoids

Persister cells pose a true challenge to infection therapy, as bacteria in this nongrowing, dormant state have a high antibiotic tolerance and often cause chronic and recurrent infections.^[5] In view of this obstacle, a new class of synthetic retinoid (vitamin A) antibiotics was recently discovered by Kim et al. using a high-throughput *C. elegans*-MRSA infection screen.^[170] Of the 82 000 small molecules screened, two retinoid compounds CD437 and CD1530 (Figure 10) exhib-

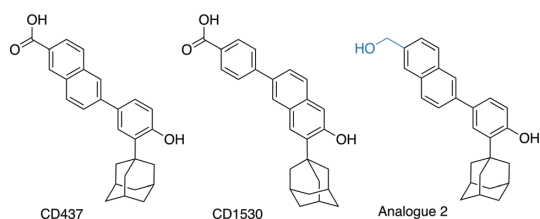


Figure 10. Retinoid antibiotics which are active against persister cells.

ited potent bactericidal activity against MRSA (MIC of $1 \mu\text{g mL}^{-1}$), completely eradicating persister cells formed by 13 clinical isolates. Additionally, they were active against persisters found in MRSA biofilms. Although showing high killing rates for Gram-positive bacteria, both compounds were inactive against Gram-negative pathogens. Resistance development towards these drug candidates is unlikely, as only a twofold greater resistance of MRSA to CD437 and CD1530 was observed after serial passaging for 100 days. Studies of the MoA showed that the compounds act by membrane permeabilization, although they do not directly lyse bacterial cells. Molecular dynamics simulations demonstrated the ability of the retinoids to become embedded in lipid bilayers, whereas closely related derivatives failed to insert. As a consequence of the significant cytotoxicity of the parent compounds, additional derivatives were synthesized. Analogue 2 (Figure 10), a retinoid in which the carboxylic acid of CD437 is substituted for a hydroxy group, retains anti-persister activity (MIC of $2 \mu\text{g mL}^{-1}$), while having an improved cytotoxicity profile both in vitro ($\text{LC}_{50} \geq 31 \mu\text{g mL}^{-1}$ in human primary hepatocytes and HepG2 cells) and in mice (no detectable hepatic or renal toxicity at intraperitoneal doses of up to 80 mg kg^{-1} (highest dose tested) every 12 h for 3 days). Importantly, a combination of gentamycin and analogue 2 or gentamycin with CD437 exhibited considerable efficacy in a mouse model of deep-seated thigh

MRSA infection. This efficacy most likely stems from increased passive diffusion of gentamycin upon retinoid-derived membrane permeabilization.^[170] A combination of retinoids and known antibiotics may, therefore, be an effective strategy in the treatment of chronic Gram-positive infections. Future studies will reveal if cytotoxicity, one of the remaining major obstacles, can be overcome by additional derivatives.

3.6. Oxadiazoles

Oxadiazoles are new, non- β -lactam antibiotics that inhibit penicillin binding protein 2a (PBP2a). Notably, the compound class was identified by in silico screening against the X-ray structure of PBP2a.^[171] Lead optimization and extensive SAR studies led to multiple promising derivatives, including oxadiazole 3 (Figure 11), which showed excellent potency

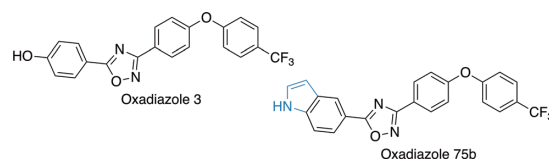


Figure 11. Chemical structures of oxadiazole antibiotics.

against a panel of Gram-positive bacteria (e.g. linezolid- and vancomycin-resistant MRSA, as well as VRE: MIC of $2 \mu\text{g mL}^{-1}$). However, all the compounds were inactive against Gram-negative pathogens.^[171] Macromolecular biosynthesis assays with radiolabeled precursors verified the antibiotic activity of oxadiazoles to be mediated by inhibition of the cell-wall biosynthesis. For detailed analysis, serial passaging of *S. aureus* in the presence of increasing levels of oxadiazole 3 led to two mutants that showed a twofold and > fourfold (limit of solubility) increase in the MIC value, respectively. In accordance with previous findings, the mutations were traced back to structural genes or promoters of the genes of the cell-wall stress stimulon.^[172] Additional comprehensive SAR studies revealed the oxadiazole 75b (Figure 11) to have a similar potency as oxadiazole 3 in vitro, while having a threefold reduced toxicity in HepG2 cells (IC_{50} of $25.8 \mu\text{g mL}^{-1}$ versus $75.7 \mu\text{g mL}^{-1}$, respectively).^[173] The in vivo efficacy was assessed using a mouse MRSA peritonitis model, in which per oral administration of a single dose of oxadiazole 75b was very effective (ED_{50} of 3.1 mg per kg body weight, compared to 2.8 mg per kg for linezolid).^[173] Furthermore, oxadiazole 75b showed equivalent or superior efficacy to linezolid in a mouse MRSA neutropenic thigh-infection model.^[174]

3.7. Antibiotic Natural Products from the Human Microbiome

During recent years, the clinical importance of the human microbiome has been scientifically recognized. Not only do bacteria, for example, in the intestinal tract, play a role during digestion, but they may also influence pathogenesis and convalescence of numerous diseases by metabolism of endogenous molecules as well as xenobiotics.^[47,175] As in every ecosystem, human microbes are in permanent interspecies competition for which they produce diverse, yet poorly investigated antibacterial compounds. Hence, the human microbiota might become a valuable source for the identification of novel antibiotic classes.^[45] In a process called *syn-BNP* (synthetic-bioinformatic natural product analysis), Chu et al. bioinformatically predicted the structures of natural products from primary sequences of human-derived eDNA and subsequently chemically synthesized the compounds for antibacterial testing. Their method led to the identification of two natural products, Humimycin A and B (Figure 12), which are N-acetylated linear peptides, comprising four L- and three D-amino acids.^[45] The peptides and their synthetic derivatives target the lipid II flippase MurJ of *S. aureus* and thereby sensitize resistant pathogens towards β -lactam antibiotics.^[45] Lactocillin (Figure 12) is a novel thiopetide antibiotic produced by a prominent member of the vaginal microbiota, *Lactobacillus sp.* It was identified by Fischbach and co-workers through sequence-based metagenome mining. Lactocillin shows activity in the nanomolar range against *S. aureus*, *E. faecalis*, and other Gram-positive pathogens. Its therapeutic application and its MoA, however, need to be further evaluated.^[44] Lugdunin (Figure 12) is a macrocyclic thiazolidine peptide antibiotic produced by *Staphylococcus lugdunensis*. It was identified by Zipperer et al. when screening *Staphylococcus* samples from the human nasal cavity for *S. aureus* antagonism.^[176] The authors found one strain, *S. lugdunensis*, that strongly antagonized the

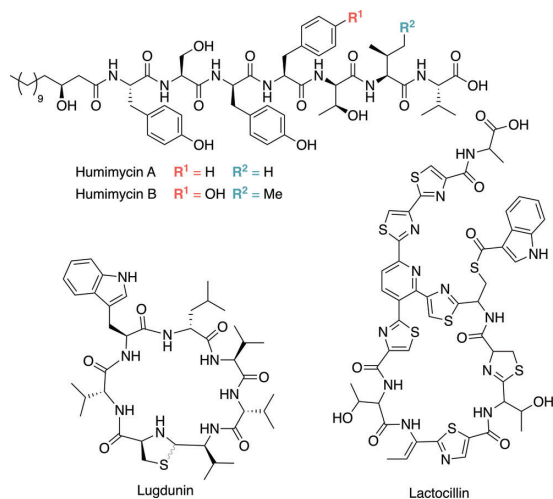


Figure 12. Natural product antibiotics derived from the human microbiome.

S. aureus growth and, after overcoming initial cultivation problems, they were able to generate *S. lugdunensis* mutants that lacked bioactivity. The mutation was traced back to an NRPS gene cluster, which was suggested to be responsible for the production of an NRP antibiotic. Recombinant expression led to the isolation and structural elucidation of lugdunin. Lugdunin is active against Gram-positive pathogens, including MRSA and VRE (MIC values of 1.5 and 12 $\mu\text{g mL}^{-1}$, respectively) and shows strong bactericidal activity in a mouse skin infection model. Importantly, neither the serial passaging with sub-inhibitory concentrations over 30 days nor the *in vivo* treatment with lugdunin led to the development of resistant *S. aureus* mutants. The MoA of lugdunin is not yet understood and requires future investigations.^[176]

3.8. Riboswitches as Novel Antibacterial Targets

RNA riboswitches are—in addition to the cell wall—promising non-protein targets for antibacterial agents. Bacterial riboswitches, usually found in the 5'-UTR (untranslated regions) of mRNA, act as intracellular sensors of different ligands, including amino acids, inorganic ions, purines, and coenzymes. The binding of a ligand to the aptamer domain of a cognate riboswitch induces a conformational change in the expression platform, thereby regulating transcription and translation of downstream genes (Figure 13a). Most riboswitches control the biosynthesis and transport of their respective ligands, which serves as a feedback mechanism to modulate metabolism.^[177] Although this mechanism is pre-

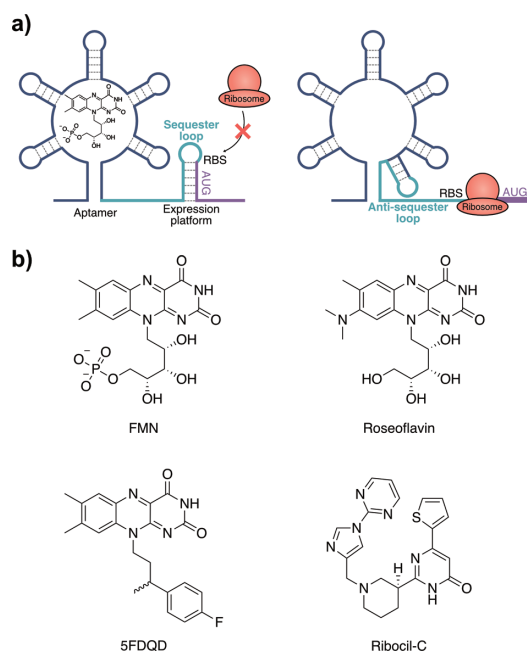


Figure 13. a) Regulation of transcription and translation by the FMN riboswitch and b) chemical structures of FMN and inhibitors of the FMN riboswitch.

alent in bacteria, no riboswitches have been found in humans to date. This observation, in combination with the prevalent essentiality of regulated genes for bacterial growth, makes riboswitches attractive antibiotic targets.^[178] One of the best-characterized antimetabolite inhibitors of a riboswitch is the natural product roseoflavin (Figure 13b). It is an analogue of riboflavin (vitamin B₂), from which flavin mononucleotide (FMN) and flavin adenine dinucleotide (FAD), two essential cofactors of numerous flavoenzymes, derive. Roseoflavin targets FMN riboswitches of multiple bacterial species. However, it simultaneously also inhibits more than 40 bacterial and eukaryotic flavoenzymes, thus resulting in toxicity issues.^[179]

Confirmation that bacterial riboswitches can indeed be selectively targeted was obtained from the identification of two novel inhibitors of the FMN riboswitch in 2015: 5FDQD and ribocil-C (Figure 13b). 5FDQD is a novel analogue of riboflavin and shows potent and rapid bactericidal activity against *Clostridium difficile* in vitro (MIC 0.5–1 µg mL⁻¹) and also in a mouse infection model (murine CDI model, peroral dosing), while sparing other bacteria found in the murine cecal flora.^[180] Ribocil-C is a “drug-like” small molecule that is chemically unrelated to FMN. It was first identified by comparative phenotypic screening of a synthetic small-molecule library.^[181] The screen was based on monitoring the growth inhibition of *E. coli*, which was completely suppressed in the presence of exogenous riboflavin. Target selectivity towards the FMN riboswitch was elucidated by generation of resistant *E. coli* mutants that showed mutations in the FMN biosynthesis genes. Furthermore, an X-ray cocrystal structure allowed insights into the binding mode of ribocil-C. Importantly, in addition to its in vitro activity (MIC 2 µg mL⁻¹ against *E. coli*), the compound also showed in vivo activity when applied subcutaneously in a murine systemic *E. coli* infection model.^[181, 182]

Whereas Gram-negative bacteria exclusively rely on the de novo biosynthesis of riboflavin, Gram-positive bacteria possess systems for both uptake and de novo synthesis which are regulated by two different FMN riboswitches. Effective treatment of *S. aureus* infections, therefore, requires inhibition of both riboswitches, as shown by a combination treatment with ribocil-C and roseoflavin.^[183] Although targeting riboswitches is a very promising approach which increases the number of new antibacterial targets, good in vivo inhibition without rapid development of resistance remain a challenge for future investigation.

4. Antivirulence

Despite their simple and effective use, antibiotics exhibit drawbacks beyond the problem of inherent development of resistance. For example, they usually do not distinguish between commensal bacteria in the gut and disease-causing pathogens, which results in side effects such as diarrhea. To avoid these limitations, the concept of antivirulence was put forward, which aims to selectively disarm, but not kill, the pathogen. By applying this approach, the commensal flora is preserved and bacteria are under less selective pressure with

the intriguing perspective of slower development of resistance.

Pathogens deploy a diverse arsenal of virulence factors tailored to not only colonize (pili, fimbriae, afimbrial adhesins, and invasins) and damage (toxins, hemolysins, and proteases) host cells, but also to evade the host immune system and to render themselves resistant to drug treatment (biofilm).^[184] Thus, disabling virulence factors disarms pathogenic bacteria, decreases the rate of infection, and eventually makes them vulnerable to clearance by the immune system. Despite these advantages, a practical antivirulence therapy faces several challenges. Virulence factors are often limited to several closely related pathogens and thus antivirulence agents are usually narrow in spectrum. Furthermore, the pathogen–host interaction is a complex and dynamic process that requires a precise understanding of pathogenic mechanisms during various infection and disease stages. As virulence factors play diverse roles during infection, a combination of several agents may be needed to enhance the scope and success of treatment. Furthermore, coadministration with established antibiotics may be needed to reduce bacterial burden in high-risk patients and to eradicate persistent pathogenic bacteria in immunocompromised patients. Although the argument for lack of resistance development in antivirulence strategies is debatable, especially for those virulence factors that are of immediate advantage to bacteria, the narrow spectrum of most approaches indeed impairs horizontal gene transfer, a major pathway for the transmission of resistance.^[185–187]

The infection process represents a finely tuned continuum that depends on environmental cues and bacterial population density, which are determined through intertwined regulatory systems such as quorum sensing, cyclic nucleotide signaling, two-component systems etc. (Figure 14). These virulence pathways are prevalent and exhibit versatile roles in bacteria which provide competitive advantages to the cell. For example, to cope with the hostile environment during an infection in host tissue, bacteria tightly control the expression of virulence factors to avoid premature recognition and elimination by the immune response.

Plenty of efforts have been devoted to develop innovative antivirulence strategies. These strategies usually target key virulence factors through their regulatory pathways, secretion systems, or direct function. A large number of small molecules have been investigated for their modulation of regulatory pathways and secretion systems. In addition, antibodies were specifically raised against toxins to eliminate their devastating function to host cells. As a consequence of their sheer number, we solely discuss selected examples of small-molecule approaches with a focus on the past five years. Excellent reviews covering different aspects of this topic have been published and are recommended for further reading.^[121, 184, 187–190]

4.1. Quorum Sensing

Small populations of pathogens can persist undetected for a long time on the human skin or nose without causing

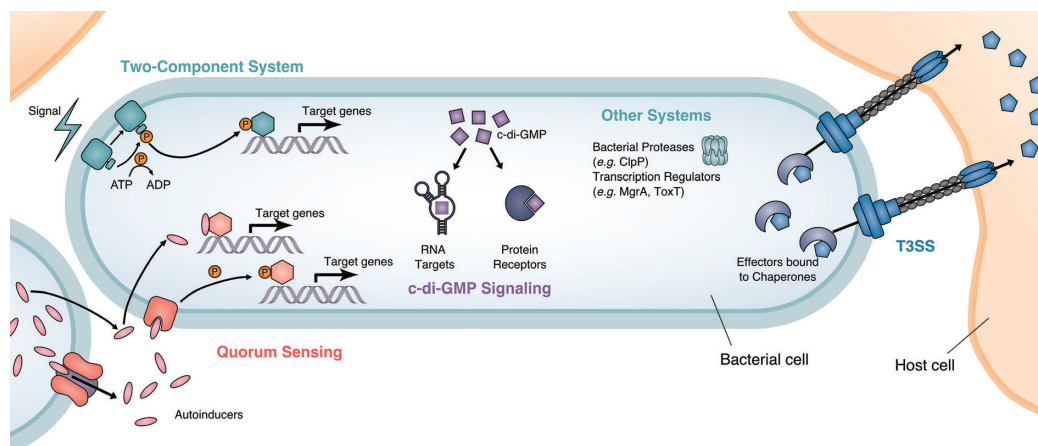


Figure 14. Schematic overview of the targets of antivirulence strategies discussed in this Review. Abbreviations: c-di-GMP: bis(3',5')-diguanosine monophosphate or cyclic diguanylate, T3SS: type III secretion system.

disease. However, when the immune system is weakened, for example, in hospitalized patients, bacteria have a unique opportunity to grow and overrun the host by virulence expression. To coordinate these attacks with a population that is strong enough, bacteria detect their population density through quorum sensing (QS). Here, bacteria secrete small molecules called autoinducers that are sensed by specific receptors of a growing population (Figure 15). Upon attainment of a certain quorum, signaling processes inside the bacteria initiate the expression of an arsenal of toxins which are secreted into the extracellular space.^[191,192] Targeting QS

represents an early intervention into bacterial pathogenesis by disruption of their elaborated communication and signaling pathways. Classical QS autoinducers can be mainly categorized into the Gram-negative-specific *N*-acylhomoserine lactones (AHLs), Gram-positive-specific autoinducing peptides (AIPs), and interspecies autoinducer 2 (AI-2). Synthetic analogues of these molecules have been tested for their ability to manipulate bacterial communication. For example, the binding of AHL derivatives to LasR, an receptor and transcriptional activator from *P. aeruginosa*, was explored, with antagonistic to agonistic effects observed.^[193]

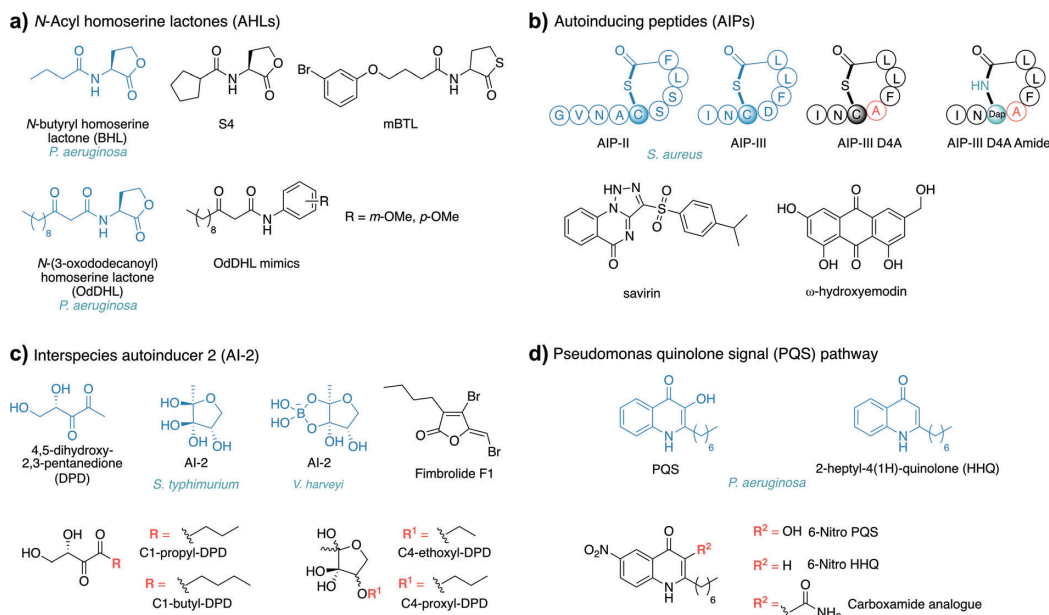


Figure 15. Chemical structures of representative autoinducers from four different QS systems (highlighted in blue) and examples of their corresponding modulators.

Interestingly, Blackwell and co-workers found one synthetic analogue S4 (Figure 15 a), which inhibited the production of two important virulence factors, pyocyanin and rhamnolipid, in *P. aeruginosa*. This regulation is believed to occur through an interconnection between Pqs and Rhl quorum sensing pathways.^[194] Other examples include mBTL^[195] and *N*-(3-oxododecanoyl)homoserine lactone (OdDHL) mimics which contain aromatic head groups.^[196]

The signaling pathways of autoinducer peptides (AIPs) are present in many Gram-positive bacteria and have been intensely investigated in *S. aureus*. They play a crucial role in the regulation of a number of key virulence factors, such as adhesins, hemolysins, and staphylocoagulase.^[197] This so-called *agr* (accessory gene regulator) system has four allelic variants and can thus be categorized into four subgroups based on the intraspecies AIPs (AIP-I to AIP-IV).^[198] Muir and co-workers developed AIP-II analogues as AgrA inhibitors^[199–201] and Blackwell and co-workers recently published a series of studies on AIP mimetics with a focus on AIP-III.^[202] A set of synthetic AIP-III analogues were found to be excellent inhibitors of all four AgrC receptors in both fluorescence reporter and hemolysis assays. The most potent inhibitor, D4A, exhibited picomolar IC₅₀ values.^[203] To avoid the hydrolytically labile thiolactone moiety, D4A was converted into its amide analogue (D4A amide), which exhibited high stability with only a slight reduction of activity (Figure 15 b).^[204] Besides employing AIP analogues to target AgrC, some active small molecules were discovered to interact with other gatekeepers of the Agr system.^[197,200] For example, savirin and ω-hydroxyemodin were shown to impede Agr signaling in *S. aureus* by targeting the response regulator AgrA, thereby resulting in bacterial clearance in a mouse infection model.^[95,205]

In view of the role of AI-2 for interspecies communication,^[206] various modifications on the AI-2 precursor 4,5-dihydroxy-2,3-pentanedione (DPD) have been carefully examined.^[207–209] Although possible sites for modification are limited, variations at C1 and C4 led to the discovery of C1-propyl- and butyl-DPDs as potent AI-2 QS antagonists in *S. typhimurium* and native DPD and C4-ethoxyl- and proxyl-DPDs as AI-2-based QS agonists in *V. harveyi* AI-2 (Figure 15 c).^[210,211] Further manipulation of this pathway was observed with fimbrolide natural products, which cause phenotypic changes in various bacterial strains. Chemical proteomics confirmed that fimbrolides inhibit AI-2 signaling by targeting LuxS.^[212,213]

In addition to interfering with these three classical QS pathways, some species-specific QS systems of important pathogens have also attracted attention. In particular, the *Pseudomonas* quinolone signal (PQS) pathway, in which both PQS and 2-heptyl-4(1*H*)-quinolone (HHQ) act as autoinducers, has to be mentioned here. In-depth SAR studies have led to various synthetic PQS/HHQ agonists or antagonists.^[193,214–216] One key discovery was that an antagonist of the PQS and HHQ receptor PqsR, 6-nitro-HHQ, can undergo in vivo conversion to 6-nitro-PQS, which turns out to be a potent PqsR modulator. Based on this finding, a carboxamide analogue was synthesized, which showed inhibition of pyocyanin production as well as protection of *C. elegans* from

P. aeruginosa PA14 infection in a nematode assay (Figure 15 d).^[217,218]

4.2. Type III Secretion Systems (T3SS)

Several pathogens utilize tailored secretion systems to inject destructive cargos such as toxins, adhesins, and effector proteins into host cells. The responsible type III secretion systems (T3SS), most common to Gram-negative bacteria, possess a needle-like structure that enables direct translocation of virulence factors into target cells through pore formation and transmembrane passage.^[219] After their injection, often guided by chaperones, these virulence factors subvert or weaken host cellular pathways and contribute to pathogenesis, disease, bacterial survival, and persistence.^[220] Defects in T3SS function and assembly were shown to abolish pathogenicity in many cases, thus making it an attractive target for inhibitor development.^[221] A number of T3SS inhibitors have been discovered which interfere with T3SS expression regulation, needle component synthesis and assembly as well as secretion and translocation of the effector protein (Figure 16).^[222–224] Salicylidene acylhydrazides

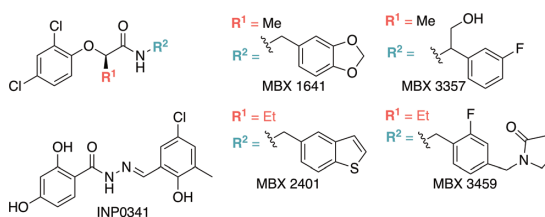


Figure 16. Overview of representative T3SS inhibitors.

(SAHs) represent a well-known class of T3SS inhibitors that have been extensively studied in various pathogens including *P. aeruginosa* and *Salmonella typhimurium*.^[224] Diverse SAH derivatives such as INP0341 have been synthesized and were found to attenuate bacterial pathogenesis.^[225–229] However, these SAHs seem to function through several mechanisms which need further elucidation.^[230] In a different approach, screening of compound libraries with a cellular reporter assay revealed phenoxyacetamide MBX 1641 to be a potent inhibitor of *P. aeruginosa* T3SS (IC₅₀ ≈ 10 μM) with a low toxicity against eukaryotic cells (Figure 16).^[231] Sequencing of inhibitor-resistant mutants unraveled that the molecules exert their antivirulence properties by binding to the needle apparatus PscF.^[232] Based on these promising results, selected phenoxyacetamides (MBX 2401, MBX 3357, and MBX 3459) were tested in a mouse model of *P. aeruginosa* abscess formation and, consistent with the in vitro data, significant reduction of the infected area could be observed.^[233,234] In addition to the intensive efforts centering around the development of the T3SS inhibitor, other secretion systems, such as T4SS, also play major roles in pathogenesis.^[219] Nevertheless, only a few small molecules have so far been reported to interfere with T4SS, thus rendering it an important area for future studies.^[235]

4.3. Biofilm Inhibitors

Many properties of biofilms, such as poor penetration of compounds and their composition of persister cells, greatly challenge antibiotic treatment.^[188] For example, a bacterial species embedded in a biofilm has been shown in some cases to be about 100–1000 times more tolerant to antimicrobials compared to the planktonic state.^[236] Typically, biofilm formation occurs in five well-organized steps: 1) reversible attachment on a surface, 2) irreversible adhesion, 3) microcolony development, 4) extracellular polymeric substance (EPS) secretion and three-dimensional biofilm maturation, and 5) dispersal. These steps are deliberately regulated by bacterial signaling systems such as QS,^[237,238] dicyclic-GMP signaling,^[239] and two-component system (TCS).^[240] Although interfering with these signaling systems represents a promising strategy to block biofilm formation as discussed in Section 4,^[241] some other approaches are also promising for biofilm treatment.

Biofilm formation is a reversible process and its partial transformation back to the free-floating planktonic state provides an opportunity to target bacteria by drug treatment or the immune system. Manipulating biofilm dispersal is thus one of the major routes towards biofilm treatment. Biofilm dispersal can be achieved by extracellular enzymes that are able to degrade EPS components. In this regard, various proteases, deoxyribonucleases, and glycoside hydrolases were shown to degrade the biofilm matrix.^[242,243] Interestingly, inspired by these enzymatic processes, a multinuclear metal complex which mimics DNase activity was designed to degrade extracellular DNA. This compound is not only environmentally stable and exhibits activity against biofilm formation, but also causes dispersion of established biofilms, thus suggesting a huge potential for further development of enzyme mimetics.^[244]

Moreover, several small molecules or peptides have been developed that show activity in the modulation of biofilms (Figure 17).^[245] Glycomimetic compound 7b, an inhibitor of the fucose binding lectin LecB with drug-like properties, was recently reported to reduce biofilm formation by 80–90% for *P. aeruginosa* at 100 μM , while no toxicity was observed for human cells. It exhibits great target selectivity and binds LecB 1000-fold more strongly than the cognate host lectin langerin. Moreover, glycomimetic 7b exhibited good metabolic stability in ADME (absorption, distribution, metabolism, and excretion) experiments as well as oral bioavailability during in vivo studies. The evaluation of this compound in animal models of infection will be needed to show its efficacy.^[246]

Halogenated phenazine (HP) analogue 14, inspired by marine antibiotic 2-bromo-1-hydroxyphenazine, is able to efficiently eradicate biofilms formed by MRSA, methicillin-resistant *S. epidermidis* (MRSE), and VRE with minimum biofilm eradication concentrations (MBECs) of 12.5 μM , 1.56 μM , and 0.20 μM , respectively. This excellent potency is promising for future development. Moreover, it also kills persister cells effectively without showing toxicity to mammalian cells.^[247] Cationic amphiphiles such as quaternary ammonium amphiphiles^[248] have also shown antibiofilm activity. Recently, cationic pillararenes (Figure 17) were revealed to inhibit biofilm formation effectively at sub-MIC concentrations in several clinically important Gram-positive pathogens including *S. aureus* and *E. faecalis*. Moreover, these compounds do not cause damage to human cells.^[249] In addition to synthetic molecules, nature has tailored a variety of small molecules to combat biofilm formation. Carolacton is a secondary metabolite of *Sorangium cellulosum* and was discovered to combat biofilm formation of *Streptococcus*. Subtle changes in four simplified analogues (C1, C3, D2, and D4) severely affected *S. mutans* biofilms at different stages, including adherence and microcolony for-

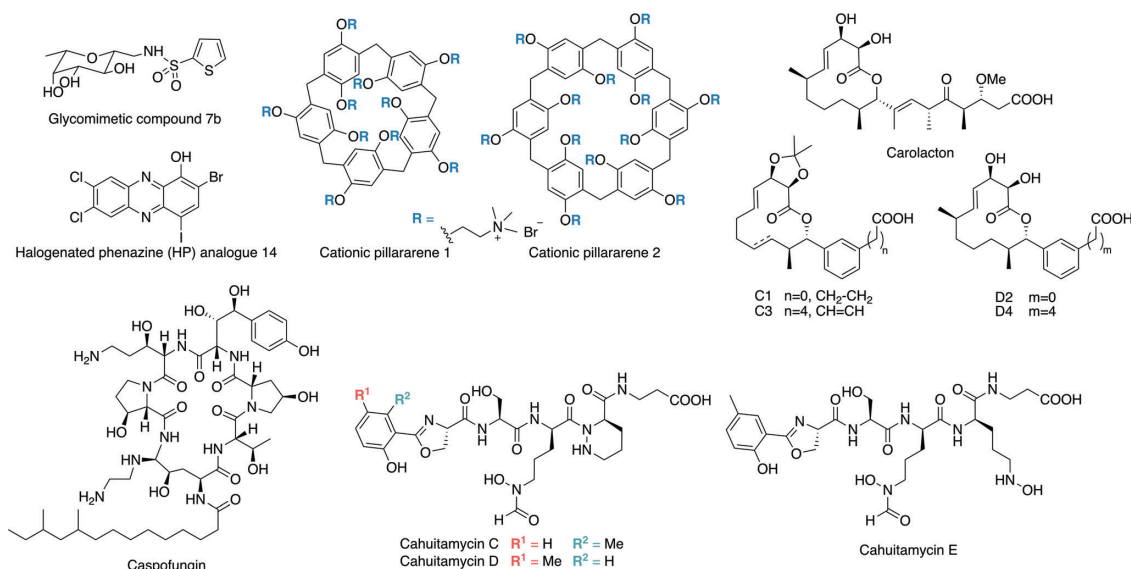


Figure 17. Overview of biofilm inhibitors discussed in this Review.

mation.^[250] A high-throughput screen of marine microbial extracts identified cahuitamycin C, a peptidic metabolite from *Streptomyces gandocaensis*, as inhibiting biofilm formation of *A. baumannii* with an IC_{50} value of 14.5 μM . Subsequent mutasynthetic studies revealed cahuitamycins D and E to have an even higher potency with IC_{50} values of 8.4 μM and 10.5 μM , respectively.^[251]

The antifungal natural product caspofungin attenuates poly-(1-6)-*N*-acetylglucosamine (PNAG) polymerization by inhibiting bacterial *N*-acetylglucosamine transferase (IcaA). As a consequence, the *S. aureus* biofilm matrix structure becomes vulnerable to fluoroquinolone treatment both in vitro and in vivo at clinically relevant doses.^[252] Several other excellent strategies based on synthetic and natural product derived compounds have been reported, including antimicrobial bridged bicyclic peptides^[253] and promysalin.^[254]

4.4. ClpP, ClpX, MgrA, and ToxT Modulators

In addition to the aforementioned general strategies, individual antivirulence targets with great potential against clinically important pathogens have received considerable attention. Here, a few examples with a focus on virulence regulation are discussed.

Caseinolytic protease P (ClpP), which is conserved in many prokaryotes, is involved in bacterial virulence regulation through a mechanism that is still incompletely characterized.^[255,256] Together with cognate chaperones such as ClpX, it recognizes, unfolds, and degrades certain protein substrates. Genetic knockouts of *S. aureus*,^[257] *Listeria monocytogenes*,^[258] and *Streptococcus pneumoniae*^[259] ClpPs exhibited reduced virulence and correspondingly lower infectivity in murine abscess or lung infection models.^[260,261] Similar results were observed for ClpX, thus making this system a prime target for antivirulence drug discovery.^[257] Inhibition of ClpP was achieved by small molecules such as β -lactone U1,^[262] phenyl esters AV170,^[263] and AV286^[264] by directly targeting the active tetradecamer of ClpP through irreversible or reversible binding (Figure 18). β -Lactones demonstrated a global reduction of *S. aureus* and MRSA toxin production and were promising in initial abscess models.^[265] However, alternative strategies are required because of their limited stability. Therefore, a specific inhibitor 334, which targets ClpX with sufficient plasma stability, was developed that also significantly attenuated production of the *S. aureus* toxin.^[266] Activation rather than inhibition of ClpP by natural products called acyldepsipeptides (ADEPs) led to killing of the cell by uncontrolled degradation of essential proteins.^[267] This strategy was also successful in the eradication of persister cells.^[268]

Transcriptional regulation represents another central mechanism which directly affects the expression of virulence genes. Here, the global transcriptional regulator A (MgrA) of the MarR family regulates more than 350 genes in *S. aureus* related to, for example, virulence, clumping, and antibiotic resistance.^[269,270] Thus, it is an intriguing antivirulence target. 5,5'-Methylenedisalicylic acid (MDSA) was found to disrupt the DNA-MgrA interaction by both directly blocking MgrA and enhancing MgrA phosphorylation.^[271-273] MDSA not only

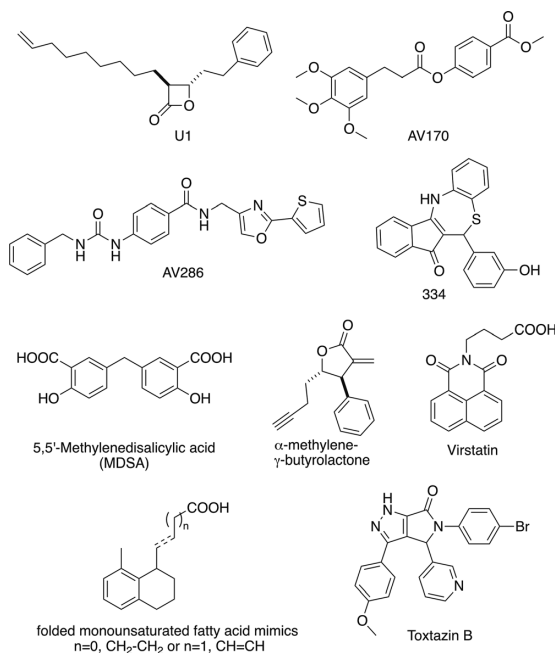


Figure 18. ClpP, ClpX, MgrA, and ToxT inhibitors.

decreased α -toxin expression in in vitro experiments, but also reduced abscess formation in a murine abscess model.^[273] Additionally, a natural product inspired α -methylene- γ -butyrolactone downregulated expression of the virulence factor by binding to transcriptional regulators, including MgrA and SarA (Figure 18).^[274]

The pathogenicity of *V. cholerae* mainly relies on two critical virulence determinants, cholera toxin (CT) and the toxin-co-regulated pilus (TCP).^[275] Their production is directly controlled by ToxT, which was identified as a promising target for the treatment of cholerae disease. In addition to the previously discovered ToxT inhibitor virsatin,^[276] bile and unsaturated fatty acids (UFAs)^[277,278] were reported recently to mimic folded monounsaturated fatty acid structures in ToxT. These mimics inhibit CT expression and TCP-mediated autoagglutination in the nanomolar range, thus demonstrating superior ToxT inhibition compared to virsatin and oleic acid.^[279] Toxtazin B, identified from high-throughput screening of a reporter assay, almost completely abolished CT expression in vitro at 10 μM . Moreover, a 100-fold decrease of *V. cholerae* CFU was observed in mice treated with toxtazin B compared to the DMSO control. Toxtazin B does not directly bind ToxT, but downregulates its expression by an unclear mechanism.^[280]

5. Antibacterial Drugs in Clinical Development

In the final section of our Review, we evaluate the current clinical antibiotic pipeline in terms of added value and medical need. Prior to this discussion, we will highlight some

of the special needs and challenges of industrial antibiotic development and start by analyzing the reasons for the current drought in antibiotic development.

After the golden age of antibiotics (1940s–1960s), many research activities were terminated as it was believed that the danger of pathogenic bacteria was permanently overcome. Industrial antibacterial research only peaked again at the turn of the millennium, after the complete DNA sequence of the bacterial genome of *Haemophilus influenzae* was described.^[48,281] All major pharmaceutical companies subsequently invested in genomic approaches and identified essential bacterial genes. For example, GlaxoSmithKline (GSK) spent seven years (1995–2001) genetically evaluating more than 300 genes for their suitability as novel antibacterial targets and showed that more than 160 of them are essential. GSK performed 70 HTS campaigns on individual targets, complete macromolecular biosynthetic pathways, as well as whole-cells using their synthetic chemical collection.^[48,51] Similar approaches were pursued in all major pharma enterprises around this time. Several companies additionally used natural products as a screening resource. Analysis of our current antibiotic pipeline, however, shows that these efforts failed to deliver. Potential explanations for this lack of success include the disconnect between the physicochemical properties of chemical libraries and potent antibiotics, as well as the

missing novelty of natural product structures originating from well-exploited microorganisms such as *Actinomyces*.^[282] This failure is also reflected in the mere numbers: since 2000, 17 systemic antibiotics have been approved and marketed in the US for community-acquired or nosocomial infections. Within this group, there are only two representatives of novel antibiotic classes, daptomycin (lipopeptide) and linezolid (oxazolidinone), as well as two novel β -lactamase inhibitors, avibactam (diazabicyclooctane (DBO)) and vaborbactam (boronic acid).^[4] All the remaining compounds are elaborations of already approved antibiotic classes (Table 1).^[11,22,283]

From our current point of view, the existing gap is a result of three major reasons:^[281]

1) The economic value of a novel antibacterial drug can be relatively low, although the developmental costs can reach up to €1000 Mio. Whereas innovative drugs with a significant improvement usually achieve reasonable prices, smaller margins can be expected for novel classes of antibiotics that overcome current resistances, since they are constrained as antibiotics of last resort. As a consequence of their ubiquitous application, antibiotics generally have to be rather cheap compared to, for example, cancer therapeutics. In addition, the period of reimbursement is limited by the eventual occurrence of antibiotic resistance.

Table 1: Summary of systemic antibiotic classes, their time of discovery, and number of them in clinical development.^[11,22,283]

Class	Target	Initial discovery reported/ patented	Important anti- biotics marketed glob- ally ^[c]	New compounds in the USA since 2000	Generations	Currently in clinical phase			
						I	II	III	
β -lactams									
penicillins	PBPs	1928	27		3				
cephalosporins	PBPs	1948	50	3	5			1	
monobactams	PBPs	1979	2		1		1		
carbapenems	PBPs	1976	4	2	1				
other β -lactams	PBPs	1977	1 ^[d]				1	1	
glycopeptides	peptidoglycan pre- cursors	1953	5	3	2				
fosfomycins									
tetracyclines	Mur A	1969	1		1				
	30S ribosome	1948	15	1	3		3	2	
aminoglycosides	30S ribosome	1943	15		1			1	
macrolides	50S ribosome	1952	16	1	4		1	1 ^[e]	
lincosamide	50S ribosome	1961	2		1				
streptogramins	50S ribosome	1953	2		2				
oxazolidinone ^[a]	50S ribosome	1978	2	1	2			1	
chloramphenicol	50S ribosome	1947	2		1				
fusidic acids	50S ribosome	1961	1		1				
quinolones ^[a,b]	DNA synthesis	1961	26	2	5		2	1	
rifamycins	RNA synthesis	1957	3		1				
sulfonamides ^[a]	folic acid metabolism	1932	15		1				
aminopyrimidines ^[a]	folic acid metabolism	1961	1		1			1	
nitro-heterocycles	DNA interaction	1959	7		1				
polypeptides	membrane	1947	2		1			2	
daptomycin	membrane	1987	1		1				
novel classes							1	3	1

[a] Antibiotic class is not derived from a natural product. [b] Withdrawn compounds are excluded. [c] Therapeutically and/or economically important antibiotics. Not all of these compounds are still actively produced. [d] Faropenem. [e] Beyond phase III, new drug application (NDA) filed.



2) It is hard to perform clinical trials for antibiotic drugs since ethical concerns prohibit comparing compounds to placebos for patients with serious bacterial infections. The only options are non-inferiority studies, which seek to determine if the experimental antibiotic shows similar efficacy compared to a standard drug already on the market.

3) It is challenging to discover new antibiotics. As already outlined, the standard approach in pharmaceutical research is not as suitable for the development of antibiotics. Compounds from chemical libraries often show limited efficacy because of poor bacterial penetration, while potent natural products often have unsuitable ADMET properties.

Today, only 50 research groups with a total of approximately 500 employees are active worldwide in translational antibiotic research.^[282] Nevertheless, the urgent need for new antibacterials has been recognized as a global challenge by the governments. In 2016, more than US\$500 million were globally available to propel antibiotic research and development (R&D). In their report “*Breaking through the wall*”, commissioned by the German health ministry, the Boston Consulting Group suggested that additional research funding should be allocated to antibiotics research.^[282] More importantly, they advised the introduction of a development insurance, the global launch award of US\$1 billion, as a “push-and-pull mechanism” to ensure the development of new last-resort antibiotics. For the development of a new antibiotic, it is generally important to establish a clear target product profile (TPP) that denominates the value of a new antibiotic drug (e.g. number of patients, disease, pathogens, site of infection, level of innovation, competitor drugs, safety, side effects, and form of application). In general, partnerships between private and public institutions can be especially successful for the identification of novel antibiotic classes. The innovation of academia meets the experience of industry on how to move a hit to a lead and into further clinical development.

The key prerequisite for antibiotic development is a clear definition of lead criteria in accordance with the TPP, which brings us to the properties of good antibiotic hit and lead compounds, as depicted in Figure 19.^[284] Optimization of a compound usually takes 2 to 4 years in the preclinical phase, in which more than 400 analogues are synthesized and studied for their activity and ADMET effects. The clinical development consists of three phases with an average duration of 10–14 years until approval.

Most of the drugs in clinical development are derivatives of already approved antibiotic classes. The reasons for moving compounds through development go far beyond overcoming existing resistances, including further aspects such as patentability, price, stability, safety, and advantages in the pharmacokinetic and pharmacodynamic (PK/PD) parameters. However, the design of novel derivatives of known antibiotic classes has become a serious challenge. The current chemical space is already well-covered after more than 60 years of extensive research, which has resulted in almost 200 approved antibiotics divided into 21 different classes. This already excludes all the thousands of derivatives which never made it to the clinic and are either only summarized in patents or fully unpublished. These considerations will especially limit the

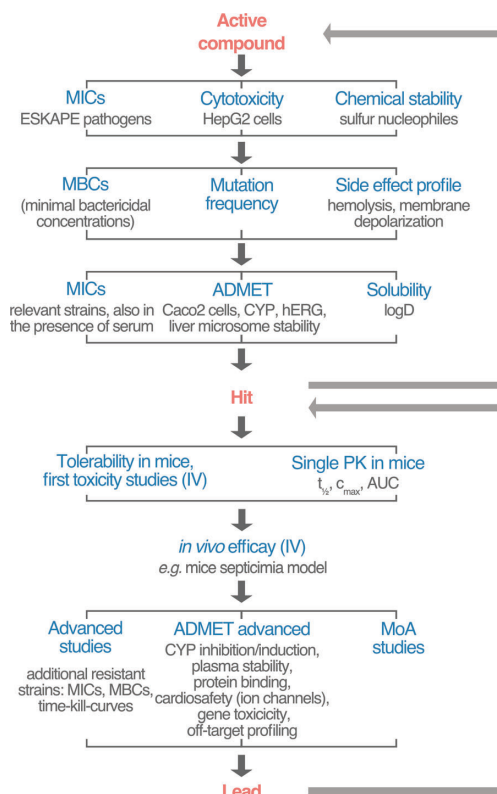


Figure 19. Schematic overview of parameters that are tested for during the industrial development of a drug from an initial active antibiotic candidate to an antibiotic lead compound. Abbreviations: CYP: cytochrome P450, hERG: hERG (human ether-a-go-go-related gene) channel, logD: distribution coefficient, IV: intravenous, PK: pharmacokinetics, $t_{1/2}$: elimination half-life, c_{max} : maximal concentration of drug, AUC: area under the curve.

prospective generation of new penicillin and quinolone antibiotics.

With these general considerations in mind, we now analyze the current clinical pipeline. We will here focus on systemic antibiotics used for the treatment of community-acquired or nosocomial bacterial infections. Topically applied antibiotics (e.g. for skin infections) or orally administered compounds, which are not resorbed (e.g. for treatment of travel diarrhea or antibiotic-associated colitis caused by *C. difficile*), will not be discussed, because of their very different PK/PD profiles. For the same reasons, antibiotics for the treatment of *M. tuberculosis* infections are also excluded. Our overview encompasses all three clinical phases until the end of 2017 and is based upon scientific publications,^[285–287] databases,^[288–290] as well as information collected in personal notes by the authors from oral presentations at international meetings. An overview of all antibiotics currently in clinical trials is depicted in Table 2.

Table 2: Overview of antibacterial compounds currently in clinical development and their application spectrum.

Clinical phase	Compound	Class	Company	Novel structure	Gram-pos. pathogens ^[a]	MDR Ent ^[b]	MDR PsA ^[c]
NDA ^[d] III	solithromycin	ketolide	Cempra		yes		
	cefiderocol	β -lactam	Shionogi	yes ^[e]		yes	yes
	relebactam (with imipenem)	BLI ^[e]	Merck & Co			poss. ^[h,i]	poss. ^[h,i]
	iclaprim	diaminopyrimidine	Motif Bioscience		yes		
	plazomicin	aminoglycoside	Achaogen		yes	yes	
	eravacycline	tetracycline	Tetraphase		yes	yes	
	omadacycline	tetracycline	Paratek Pharmac.		yes		
	contezoli	oxazolidinone	MicRx		yes		
	lascaflaxacin	fluoroquinolone	Kyorin		yes		
	lefamulin	pleuromutilin	Nabriva Therap.	yes	yes		
II	sulopenem	β -lactam	Iterum				
	AAI-101 (with unknown) ^[j]	BLI ^[e]	Allegra Therap.			poss. ^[h,i]	
	naflthromycin	ketolide	Wockhardt		yes		
	alalevonadifloxacin	fluoroquinolone	Wockhardt		yes		
	finafloxacin	fluoroquinolone	MerLion Pharmac.				
	afabacin	FabI inhibitor	Debiopharm	yes	yes		
	brilacidin	peptide	Innovation Pharmac.	yes	yes		
	murepavadin	peptide	Polyphor/ Roche	yes			yes
	gepotidacin	NBTI ^[f]	GlaxoSmithKline	yes	yes		
	zolidodacin	NBTI ^[f]	Entasis Therap.	yes	yes		
I	AIC-499 (with unknown BLI)	β -lactam	AiCuris			poss. ^[h]	poss. ^[h]
	LYS 228	β -lactam	Novartis			yes	
	ETX-2514 (with sulbactam)	BLI ^[e]	Entasis Therap.				
	nacubactam (with unknown)	BLI ^[e]	Roche/Meiji/Fedora			poss. ^[h,i]	poss. ^[h]
	VNRX-5133 (with cefepime)	BLI ^[e]	VenatoRx Pharmac.	yes ^[e]		yes	yes
	zidebactam (with cefepime)	BLI ^[e]	Wockhardt			yes	yes
	contezolid acefosamil ^[k]	oxazolidinone	MicRx		yes		
	TP 271	tetracyclin	Tetraphase Pharmac.		yes		
	KBP-7072	tetracyclin	KBP Biosciences		poss. ^[h]		
	TP-6076	tetracyclin	Tetraphase Pharmac.			poss. ^[h]	poss. ^[h]
SPR741 & SPR 719	peptide & NBTI ^[f]	Spero Therapeutics	yes		poss. ^[h]	poss. ^[h]	

For reasons of clarity, antibiotics lacking novelty or antibiotic application are not denoted with a "no" but with a blank space. [a] MRSA and/or VRE and/or resistant *S. pneumoniae*. [b] Multidrug-resistant Enterobacteriaceae. [c] Multidrug-resistant *P. aeruginosa*. [d] NDA: new drug application.

[e] BLI:

β -lactamase inhibitor. [f] NBTI: novel bacterial topoisomerase inhibitor. [g] Innovative, but not a novel structure. [h] poss.: in vitro data affirm possible application, clinical data pending. [i] Not active for metallo- β -lactamases. [j] The antibiotic partner for combination therapy is not yet reported.

[k] Intravenous administrable prodrug of contezolid (phase III).

5.1 β -Lactam Antibiotics

β -Lactams, first discovered in the 1930s by Fleming,^[291] are the largest and most successful group of antibiotics. β -Lactams target the class of penicillin binding proteins (PBPs) and thereby inhibit peptidoglycan biosynthesis, which itself is essential for biosynthesis of bacterial cell walls. A major problem of β -lactam antibiotics, however, is their susceptibility to chemical breakdown by specific β -lactamases. These resistance-associated enzymes can be classified according to Ambler^[292,293] in four classes: class A, C, and D are serine proteases, whereas class B are metalloproteases. Class A comprises β -lactamases which hydrolyze penicillins and cephalosporins, and includes ESBLs (extended spectrum β -lactamases). Class B covers metallo- β -lactamases (MBL), with the New Delhi metallo- β -lactamase I (NDMI) as a prominent, clinically important member. Class C β -lactamases hydrolyze third-generation cephalosporins and β -lactamase inhibitors. Finally, class D members are able to cleave various β -lactamase inhibitors and also hydrolyze many other β -lactams.

Currently, there are four β -lactams in clinical trials (Figure 20). The monobactam Lys-228 from Novartis is in phase I development. It is stable against MBLs and additionally withstands major resistance-mediating protease classes including ESBLs.^[294,295] It has a broad activity against Gram-negative bacteria, with the exception of *P. aeruginosa*. Sulopenem as well as its orally available prodrug sulopenem etzadroxil are in phase II studies and show activity for *Enterobacteriaceae* that produce ESBLs.^[296,297] Cefiderocol (phase III) from Shionogi is an innovative β -lactam which incorporates a 2-chloro-3,4-dihydroxybenzoyl siderophore.^[298,299] As a "Trojan horse", the antibiotic mimics substrates of cognate iron transport and thereby facilitates penetration of the outer membrane of Gram-negative bacteria. Although it is well-known that rapid resistance development can occur with this mechanism, it is bypassed in this case through the use of additional porin-mediated transport. Importantly, cefiderocol exhibits improved stability towards most β -lactamases, especially towards MBLs, and is therefore one of the most promising antibiotics for multidrug-resistant (MDR) Gram-negative pathogens. Lastly, the β -lactam AIC-

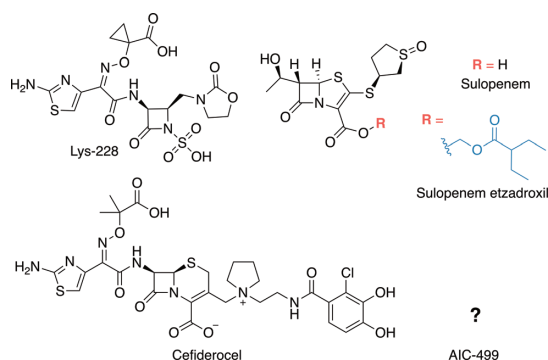


Figure 20. Chemical structures of β -lactam antibiotics currently in clinical development. The structure of AIC-499 has not yet been published.

499 is in phase I development for complicated urinary tract infections (cUTI) in combination with a β -lactamase inhibitor (BLI). Its structure, however, is not revealed and only a limited data set concerning its activity is available.^[300]

5.2. β -Lactamase Inhibitors (BLIs)

β -Lactamase inhibitors (BLIs) act against the enzymatic breakdown of β -lactam antibiotics and thereby counteract antibiotic resistance. Although traditional BLIs are structurally derived from β -lactams, they generally do not have direct antibiotic properties. In recent years, two novel BLI classes which are structurally different from classical β -lactam antibiotics were approved: avibactam and vaborbactam.^[292] Avibactam (Figure 21), a diazabicyclooctane (DBO) derivative, shows increased and broadened potency compared to previous BLIs, and in contrast to the latter it acts by a reversible covalent mechanism. Avibactam targets class A and C β -lactamases, including ESBLs, AmpC, and *Klebsiella pneumoniae* carbapenemase (KPC). Vaborbactam (RPX7009) contains a central cyclic boronic acid pharmacophore. It is mainly a potent inhibitor of class A carbapene-

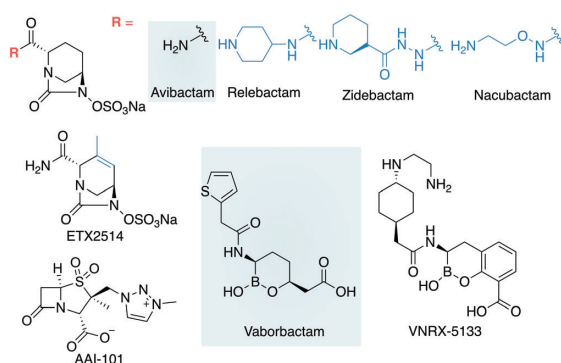


Figure 21. Chemical structure of approved BLIs avibactam and vaborbactam (shown in gray boxes) and current clinically investigated BLIs.

mases, such as KPC, and class C β -lactamases. As vaborbactam does not inhibit class B or D carbapenemases, it is therapeutically combined with the traditional carbapenem meropenem to overcome some of these limitations.^[292,301]

Four DBO-based compounds are currently in development and differ from avibactam by substitution at the amide position 2 (Figure 21). Relebactam, a 4-piperidinylamine from Merck, is under investigation in combination with imipenem in phase III trials. It inhibits class A and C β -lactamases, including KPCs, but does not overcome MBL resistance.^[302,303] Zidebactam, a 3-piperidinylcarbonyl hydrazide from Wockhardt is in phase I in combination with cefepime and targets class A and C β -lactamases. Remarkably for a BLI, the compound also inhibits PBP2 of Gram-negative pathogens and thereby shows antibacterial properties against some *Enterobacteriaceae* and *P. aeruginosa*.^[304,305] The combination with the approved β -lactam antibiotic cefepime enables treatment of carbapenem-resistant *A. baumannii*, *Enterobacteriaceae*, and metallo-carbapenemase-harboring *P. aeruginosa*. Nacubactam, a 2-aminoethoxyamine from Roche in phase I, inhibits class A and C β -lactamases.^[306,307] It also binds to PBP2 and thereby exhibits an antibacterial effect that is weaker than that of zidebactam. Its antibiotic partner for combination therapy is not yet reported but will be critical to decide about the potential of this compound. ETX-2514 from Entasis is a 3-methyl-3-dehydro derivative of avibactam. It is optimized to target class D β -lactamases and restores the activity of sulbactam, which makes it a combination of interest for *A. baumannii* infections.^[308]

A boronate-based compound, VNRX-5133 from VenatoRx is in clinical phase I. Its combination partner is the fourth generation cephalosporin cefepime, so that *Pseudomonas* infections can be included in the therapeutic spectrum. The boronate inhibits serine proteases such as ESBL and KPC by covalent binding, whereas a noncovalent, competitive binding is observed for MBLs.^[309,310] The sulbactam AAI-101 from Allegra is a classical BLI and is currently in phase II.^[311] The drug for combination therapy seems to be cefipim or piperacillin. It has some improved activity for KPCs and class A β -lactamases, including ESBLs.

5.3. Diaminopyrimidine

Trimethoprim (Figure 22), a synthetic diaminopyrimidine antibiotic first marketed in 1962, is—in combination with sulfamethoxazole—still the treatment of choice for community acquired UTI. Trimethoprim, which acts synergistically with sulfamethoxazole, is a selective inhibitor of the bacterial dihydrofolate reductase (DHFR). The main resistance mech-

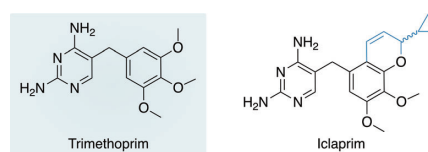


Figure 22. Chemical structures of diaminopyrimidine antibiotics.

anism is based on mutation in the DHFR enzyme. As a major side effect, trimethoprim can cause thrombocytopenia by inhibition of the human DHFR enzyme. Iclaprim, a cyclopropylbenzopyranpyridinopyrimidine, is currently being developed by Motif Biosciences in phase III for acute bacterial skin and skin structure infections (ABSSI).^[312] The compound has a better affinity for DHFR than trimethoprim, but only limited activity for trimethoprim-resistant MRSA strains. It has to be noted that its first phase I study started in 2002 and an NDA to both the FDA and the European Medicines Agency (EMA) was rejected because of concerns regarding efficacy and safety.^[313,314] Another NDA filing based on the present studies is expected in 2018.^[315]

5.4. Aminoglycosides

The inhibition of bacterial protein biosynthesis is one of the main strategies in antibiotic therapy. Today, eight antibiotic classes approved for systemic use target different subunits of the ribosome (Table 1).

Aminoglycosides represent widely used antibiotics that act through binding to the transfer RNA acceptor site of 16S ribosomal RNA. Important members are, for example, the natural product kanamycin and the semisynthetic derivative amikacin (Figure 23). Aminoglycosides have excellent activities against important nosocomial Gram-negative bacteria, including *Pseudomonas*, *Acinetobacter*, and *Enterobacter*. Major side effects are ototoxicity and renal toxicity, which can both be explained by inhibition of protein biosynthesis in human mitochondria.^[316] Resistance is caused by enzymatic transformation of the aminoglycoside, drug efflux, or target modification by methylation of the 16S ribosomal RNA.^[317] Plazomicin (Figure 23) is the only new aminoglycoside in clinical trials. It is currently in phase III for treating cUTI infections.^[318] The compound demonstrates activity against Gram-positive as well as Gram-negative bacterial pathogens, however, with only a weak effect against *Pseudomonas* and *Acinetobacter*, and is stable towards aminoglycoside-modifying enzymes. Nevertheless, it shows cross-resistance in the case of methylation of the 16S ribosomal RNA.

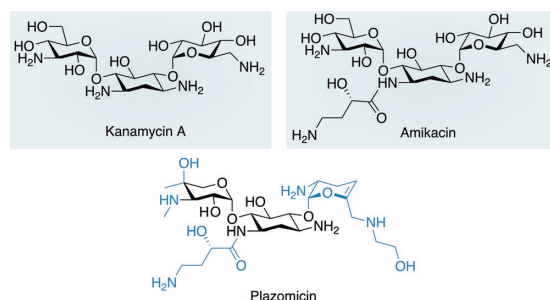


Figure 23. Approved aminoglycosides kanamycin A and amikacin, as well as its clinically tested derivative plazomicin.

5.5. Tetracyclines

Tetracyclines are mainly produced by *Streptomyces* and exhibit broad-spectrum antimicrobial activity by inhibiting the 16S part of the 30S ribosomal subunit.^[319] The major resistance mechanisms are based on efflux or caused by small proteins blocking the tetracycline binding site. Omadacycline (Figure 24, phase III) from Paratek is a novel semisynthetic

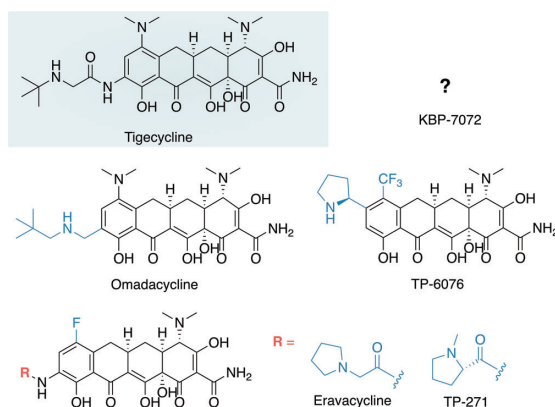


Figure 24. Chemical structures of tetracycline antibiotics. Tigecycline is an approved drug and the chemical structure of KBP-7072 has not yet been published.

aminomethyl tetracycline antibiotic which was developed for the treatment of community-acquired bacterial infections. It overcomes resistance of previous tetracycline generations and has a good activity against MRSA. In studies with patients suffering from complicated skin and skin structure infections, it was comparable to linezolid. Limited possibilities to modify the core structure of tetracyclines nearly resulted in the termination of derivatization projects. However, the group of Myers recently reported a new synthetic access to this scaffold, which now allows the effective and fast synthesis of novel derivatives.^[320] The first compound from this platform, eravacycline, was developed by Tetrphase and is in phase III.^[321] It shows partial or complete cross-resistance to tigecycline, which was approved in 2005, but exhibits lower MIC values in sensitive strains and is both intravenously and orally available. Eravacycline appears to be suitable for treating complicated intraabdominal infections and complicated urinary tract infections, but more clinical efficacy and safety data are required to fully understand its potential. TP-6076 is in clinical phase I with a focus on Gram-negative bacteria.^[322,323] Compared to eravacycline, it shows improved activity against carbapenem-resistant *Enterobacteriaceae*, *A. baumannii*, and *P. aeruginosa*. Notably, TP-6076 represents the most active tetracycline against *Pseudomonas* discovered to date. Two additional tetracycline derivatives, KBP-7072^[324] (structure unknown) and TP-271,^[325] are in phase I and are directed at Gram-positive respiratory pathogens, among others.

5.6. Ketolides

Macrolides, such as erythromycin (Figure 25)—the first member introduced in the 1950s—bind to the 23S part of the RNA of the 50S ribosomal subunit, thereby blocking the exit

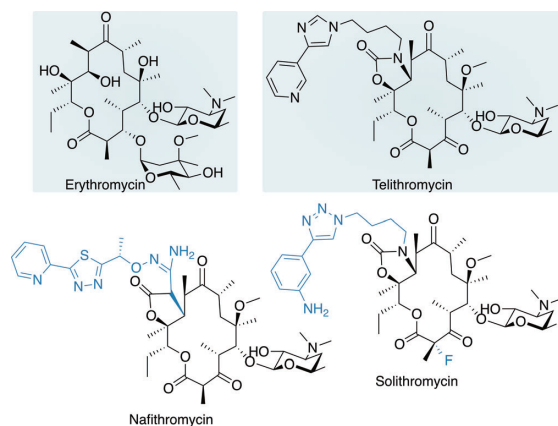


Figure 25. Structures of the approved ketolide antibiotics erythromycin and telithromycin as well as other macrolide antibiotics in clinical development.

tunnel of the synthesized peptide. Macrolides are mainly used for oral treatment of community-acquired respiratory tract infections (RTI) caused for example, by *Streptococcus pneumoniae*. Resistance is a significant problem and can mainly be traced back to dimethylation of the ribosomal binding site or the expression of efflux pumps. Telithromycin, approved in the USA in 2004, was the first derivative of a novel subclass called ketolides for which the cladinose sugar at position 3 is replaced by a ketone, and a substituted cyclic carbamate is introduced at C11–C12. Major resistance mechanisms of previous macrolide antibiotics are thereby overcome. However, serious hepatotoxic side effects have been observed for telithromycin post-approval, which limits its therapeutic use.^[326] Solithromycin (CEM-101, OP-1068)^[327–329] is a 2-fluoroketolide^[330] which shows similar *in vitro* activity as telithromycin and also exhibits no cross-resistance to older approved macrolides in *Streptococci*. Although efficacious in two phase III clinical trials, the compound has not been approved by the FDA yet because of inchoate characterization of potential hepatotoxicity, thus necessitating additional studies.^[331] Nafithromycin (WCK-4873) is a ketolide in which the original carbamate is replaced by a lactone moiety.^[330,332] It is currently under investigation in phase II studies for community-acquired bacterial pneumonia (CABP) by Wockhardt. Its *in vitro* activities are comparable to telithromycin, with advantages against some ketolide-resistant *Pneumococci*. Importantly, nafithromycin does not inhibit any key human CYP isoform even at high concentrations, which is a clear advantage over most macrolides.^[333]

5.7. Oxazolidinones

Linezolid (Figure 26) belongs to one of the two novel antibiotic classes introduced since 2000, the oxazolidinones.^[334] Oxazolidinones inhibit bacterial protein biosynthe-

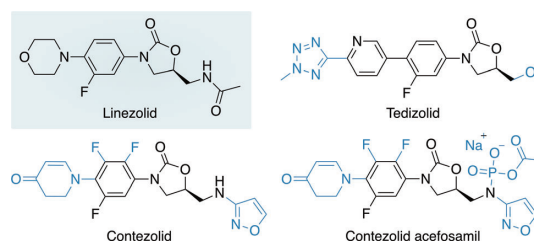


Figure 26. Chemical structures of oxazolidinone antibiotics.

sis by interacting with the A site of the peptidyl transferase center of the ribosomal 50S subunit, although their MoA may be more complex.^[335] Linezolid is active against Gram-positive pathogens, especially for nosocomial infections caused by MRSA and VRE.^[334] Side effects are based on the inhibition of monoamine oxidases, and more importantly also include myelosuppression and neuropathy. These two are observed during prolonged application and are caused by interference with the synthesis of mitochondrial protein. Resistance development is slow, which is mediated by point mutations within the 23S component of rRNA and by the presence of a transmissible cfr ribosomal methyltransferase as major mechanisms.^[336] Tedizolid, originally from Trius and now developed by Merck & Co, is a related compound which *in vitro* is more active than linezolid against sensitive Gram-positive pathogens, and also retains this activity for resistant strains. It has additional advantages over linezolid including single daily dosing, decreased treatment duration, and potentially less adverse affects. ConteZolid (MRX-1) represents an additional, orally available oxazolidinone currently in phase III. Its corresponding intravenous (IV) prodrug contezolid acefosamil (MRX-4) is in phase I.

5.8. Fluoroquinolones

Apart from the inhibition of protein biosynthesis, the interruption of DNA replication is a further efficient strategy for antibiotics. The corresponding enzyme targets are DNA gyrase and/or topoisomerase IV. Fluoroquinolones are an important class of broad-spectrum antibiotics that exhibit excellent tissue penetration, which is advantageous for the treatment of various infections including RTI and UTI. All members inhibit both DNA gyrase and topoisomerase IV. Key fluoroquinolones are ciprofloxacin, which exhibits *P. aeruginosa* activity, and levofloxacin, which is also active against *S. pneumoniae* (Figure 27). Resistances occur mainly by efflux or by mutation of the binding site. Several side effects have been described, including a black box warning by the FDA in 2015 regarding severe tendonitis, including Achilles tendon rupture. With the narrow modification

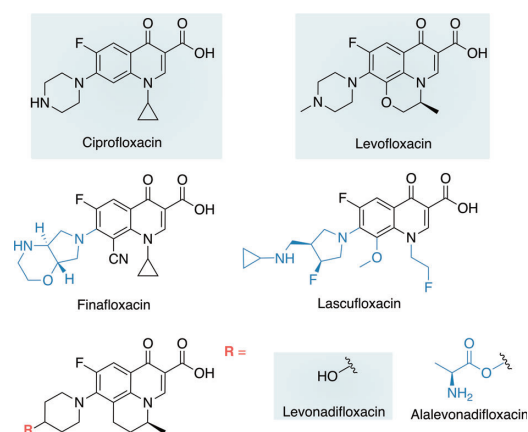


Figure 27. Overview of fluoroquinolone antibiotics. The already approved therapeutics ciprofloxacin, levofloxacin, and levonadifloxacin are shown in gray boxes.

possibilities because of exhaustive prior SAR studies and the need to manage resistance and safety issues in parallel, generating new quinolones with improved properties is a major challenge.^[337] Nevertheless, three fluoroquinolones are in the pipeline with improved activity for resistant Gram-positive pathogens, although Gram-negative resistance could not be overcome so far. Lascufloxacin, an 8-methoxyquinolone from Kyorin, is in phase III and shows improved activity for RTI pathogens. It exerts some activity against MRSA, but with only limited application because of cross-resistance.^[338,339] Finafloxacin, an 8-cyanofluoroquinolone from Merlion which is already marketed for the treatment of ear infections, shows the same spectrum of activity as ciprofloxacin and cross-resistance to it. As a consequence of its higher activity at lower pH values, it is developed for UTI and kidney infections.^[340,341] Alalevonadifloxacin from Wockhard is an L-alanine ester prodrug of levonadifloxacin (*S*-(-)-nadifloxacin) with potential activity for MRSA. Nadifloxacin itself is currently marketed as a topical drug for the treatment of acne.^[342]

5.9. Novel Classes of Antibiotics

Whereas the previously described candidates are all advancements of already approved systemic antibiotics, the clinical pipeline also holds seven promising novel compound classes that are able to overcome existing antimicrobial resistances.

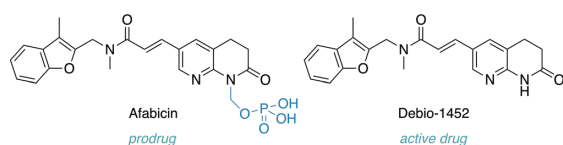


Figure 28. Chemical structures of the prodrug afabacin and the active component Debio-1452.

5.9.1. Afabacin

Afabacin (Figure 28) from DebioPharm inhibits bacterial type I fatty acid biosynthesis and is currently in phase II. Its molecular target in *Staphylococci* is the enoyl-acyl carrier

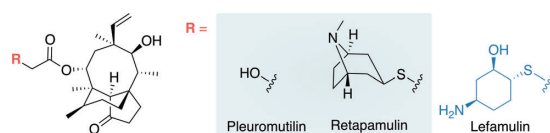


Figure 29. Pleuromutilin-based antibiotics. Structure of the natural product pleuromutilin and its approved derivative retapamulin, as well as lefamulin which is in clinical development.

protein reductase FabI. Afabacin is a methyl phosphate prodrug, while Debio-1452 (AFN-1252) is the active component. Notably, this compound is one of the rare examples originating from big pharma for which a HTS for bacterial targets was successful. The originally weakly active hit was advanced by means of standard medicinal chemistry methods and structure-based design using the crystal structure of FabI to afford the potent antibiotic.^[48,343]

5.9.2. Pleuromutilins

Pleuromutilin (Figure 29), a natural product diterpene produced by the fungus *Pleurotus mutilus*, is an inhibitor of protein biosynthesis which affects substrate binding at both the acceptor and donor sites on the 23S RNA site of the 50S subunit. It contains a rigid tricyclic carbon skeleton with eight stereogenic centers. Retapamulin is a semisynthetic derivative with a thioether acetyl side chain and has been approved for topical *S. aureus* infections since 2007. In addition to its limited applicability, retapamulin, however, shows strong inhibition of cytochrome P450 Cyp3A4 as a major side effect.^[344] Lefamulin (phase III) is a novel thioether derivative, and represents the first systemic pleuromutilin antibiotic. Its PK/PD parameters have been optimized for human application by balancing reduced Cyp interaction with oral availability and the antibacterial spectrum. The compound shows activity for respiratory pathogens and can be formulated for intravenous and oral treatment.^[345,346]

5.9.3. Novel Bacterial Topoisomerase Inhibitors

As discussed in Section 5.8, targeting DNA replication is a very successful antibacterial strategy. Therefore, novel compounds that follow this MoA while omitting cross-resistance to quinolones have been a major focus of many companies.^[347] Based on these efforts, two novel bacterial topoisomerase inhibitors (NBTIs) are currently in phase II. Gepotidacin (Figure 30)^[348] from GSK targets a binding site which is distinctly different from the fluoroquinolone site.^[349] It is active against Gram-positive pathogens and some commonly important Gram-negative bacteria, such as *N. gonorrhoeae*, and is therefore also studied for the treatment of gonorrhoea.^[350] A structurally different motif is found for the

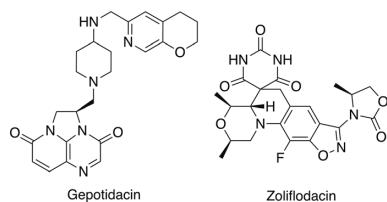


Figure 30. Chemical structures of the novel bacterial topoisomerase inhibitors (NBTIs) gepotidacin and zoliflodacin.

NBTI zoliflodacin (ETX0914, Figure 30) from Astra-Zeneca.^[351] This spiropyrimidinetrione also does not show any cross-resistance to quinolones and exhibits a similar spectrum as described for gepotidacin. Currently it is in phase II with a focus on gonorrhoea.^[350]

5.9.4. Peptides

Peptides of microbial origin such as polymyxins are well-known antibiotics.^[352] Current development focusses on antimicrobial peptides (AMPs) that are naturally a part of the first line defence of higher organisms, such as plants, insects to animals, and humans.^[353,354] These host-defence peptides are produced ribosomally and usually released in high concentration at the infection site. As a consequence of their amphiphilic structure, AMPs are able to interact with both the inner and outer membrane of bacterial cells, thereby resulting in membrane depolarization.^[94] Their systemic application, however, is limited for various reasons, including cell toxicity, physiological stability, and elevated production costs. Nevertheless, two novel peptide antibiotics that have overcome these hurdles in different ways are in phase II clinical trials: Brilacidin (Figure 31) from Cellcutix is a peptidomimetic designed to mimic defence peptides with amphiphilic properties and is currently investigated with a focus on *S. aureus* infections.^[355,356] Murepavidin (Figure 31) from Polyphor is a synthetic macrocyclic peptide based on

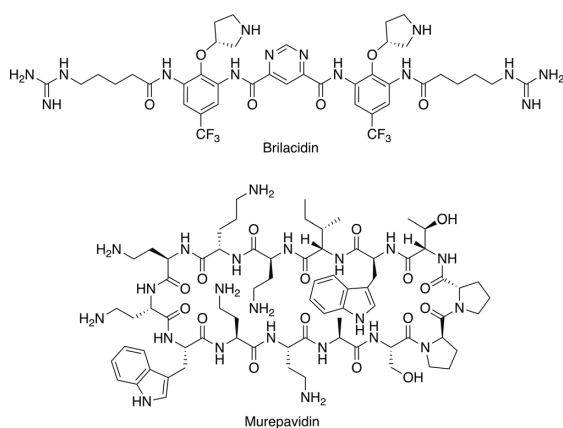


Figure 31. Overview of peptide-based antibiotics currently in clinical development.

protegrin, a linear defensin originally isolated from pigs.^[357] Protegrin induces pore formation in microbial membranes, but itself failed in clinical development because of associated toxicity.^[358] Recently, it was shown that protein epitope mimetics derived from protegrin I appear to kill *P. aeruginosa* through functional inhibition of its lipopolysaccharide-assembly beta-barrel protein LptD, thus preventing synthesis of the cell membrane without a direct lytic mechanism. As a result, the specific *P. aeruginosa* antibiotic murepavidin was developed, which minimizes the toxicity problems usually observed for AMPs.

It is well-known that the cationic AMP polymyxin B₁ (Figure 32) and derivatives which lack the acyl side chain

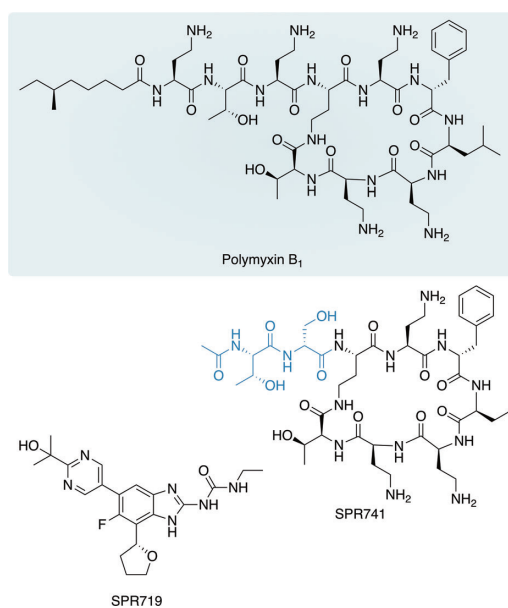


Figure 32. Chemical structures of the NP polymyxin B₁ and its derivative SPR741, which enhances cell penetration of the novel gyrase inhibitor SPR719.

enable the uptake of Gram-positive antibiotics into Gram-negative bacteria. Unfortunately, this rather unspecific membrane depolarization effect causes cytotoxicity in human cells. SPR741 (phase I), developed by Sphero, is a polymyxin B derivative which is expected to be less toxic.^[359] As toxicity is mainly a result of the overall positive charge, two cationic amino groups of polymyxin B were replaced or removed by serine and threonine side chains in SPR741, respectively.^[360] The peptide itself has no intrinsic antibacterial activity, but rather acts as an enhancer of other antibiotics. The clinical combination partner seems to be SPR719, originally from Vertex, which is a novel Gram-positive gyrase inhibitor.^[347,361]

5.10. Biologics

In addition to small-molecule-based antibiotics, biopharmaceuticals (also known as biologics) have emerged as auspicious antibacterial candidates that utilize antibacterial as well as antivirulence strategies.

The immune system is very powerful at fighting infections, and antibodies are a crucial part of this system. Passive immunization in the form of serum therapy was already used to prevent or treat bacterial infections even before the discovery of antibiotics.^[362] Later, antibodies were replaced by the cheaper and safer broad-spectrum small-molecule antibiotics. With the advancement of technology and the availability of monoclonal antibodies (mAbs), including even fully human mAbs, less toxic and immunogenic products are nowadays available. As an additional advantage, a tailored

mAb therapy directed at specific targets of pathogenic bacteria should in this regard also spare the benign human microbiome. In general, adding mAb therapy to the existing standard-of-care needs to demonstrate superiority to justify its higher price. Currently, there are eight mAb-based antibacterials in clinical development (Table 3), which are promising for some key development successes after some major drawbacks.^[362]

The key activity of mAbs is binding to antigens on the bacterial surface, followed by the opsonophagocytic killing (OPK) of the pathogen by the host immune system. Alternatively, the binding of mAbs to virulence factors, which are produced by the pathogen, blocks their activity and in this way prevents the host from further damage or infection (Figure 33 a).

Table 3: Antibacterial monoclonal antibodies in clinical development.

Phase	Name	Class	Type	Company	Target	Pathogen	Clinical design
II	aerumab	mAb	human IgM	Aridis Pharmac.	LPS serotype O11	PsA	adjunctive
	aerucin	mAb	human IgG	Aridis Pharmac.	PsA alginate	PsA	adjunctive
	MEDI3902	mAb	human IgG kappa bispecific Ab	MedImmune	T3SS protein PcrV & Psl exopolysaccharide	PsA	prevention
	514G3	mAb	human IgG	XBiotech	Protein A (SpA)	MRSA	adjunctive
	salvecin	mAb	human IgG	Aridis Pharmac.	α -toxin	MRSA	adjunctive
	suvratoxumab	mAb	human IgG	MedImmune	α -toxin	MRSA	prevention/adjunctive
	ASN-100	two mAbs	human IgG	Arsanis	α -toxin & leukocidin toxins	MRSA	prevention
I	RG-7861	mAb antibiotic conjugate	human IgG- rifamycin conjugate	Genentech/Roche	teichoic acid	MRSA	therapy

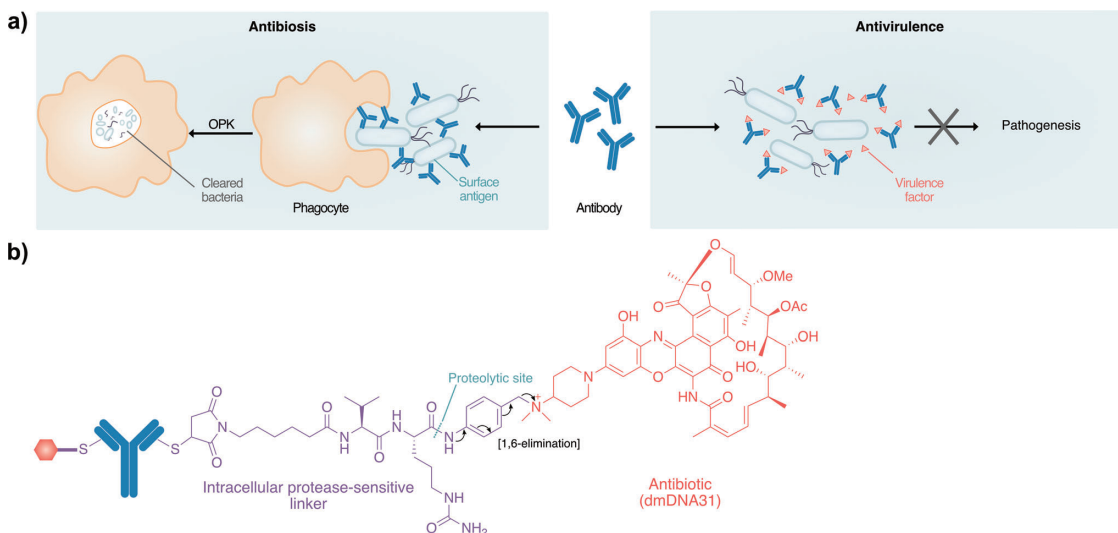


Figure 33. Mode of action of antibacterial antibodies. a) Antibodies either bind to antigens on the bacterial surface, leading to opsonophagocytic killing of the pathogen, or target virulence factors such as toxins which are produced by bacteria. b) Schematic representation of antibody–drug conjugate RG-7861. Each antibody is loaded with two antibiotic units through its light chains. After co-uptake of the conjugate with opsonized bacteria, the proteolytic cleavage of the linker leads to a 1,6-elimination and releases the antibiotic drug inside the immune cells.

Five mAbs that target surface proteins and exhibit OPK are currently in development, three of them in phase II. Aerumab from Aridis, is a fully human anti-*P. aeruginosa* mAb of the LPS serotype O11, originally isolated from a patient. This specific serotype accounts for about 22% of all *P. aeruginosa* hospital-acquired infections worldwide.^[363] A broader coverage is achieved by aerucin from Aridis, a fully human monoclonal IgG1 antibody that binds to alginate, a widely distributed cell-surface polysaccharide of *P. aeruginosa*. Aerucin was shown to bind to more than 90% of *P. aeruginosa* clinical isolates.

The most sophisticated mAb studied is MEDI3902^[364] from Medimmune, which has two bacterial targets: PcrV and PsI. PcrV is a type III secretion system protein which is used by *Pseudomonas* for the injection of toxins and other virulence factors into host cells (Figure 14). PsI is an exopolysaccharide which is part of the glue-like layer that covers the pathogen, and facilitates evasion of the immune system and biofilm formation. MEDI-3902 exerts its antibacterial activity by three mechanisms: 1) obstruction of bacterial cell attachment, 2) PsI-mediated opsonophagocytic killing, and 3) reduced cell toxicity by targeting PcrV.^[365] The mAb 514G3^[366,367] from XBiotech is currently being investigated as an adjunctive therapy for *S. aureus* infections. The antibody is derived from a patient sample and targets the cell-wall moiety Protein A (SpA) which is able to bind immunoglobulins, and in this way is involved in evasion of the immune system. A very different approach is followed by RG-7861 (Figure 33b), a mAb-antibiotic conjugate (AAC) from Roche, which currently is in phase I.^[368] The mAb is loaded with the antibiotic dmdNA31, a rifamycin analogue, and targets teichoic acids of *S. aureus*. The conjugate itself has no antibacterial activity against planktonic *S. aureus* and is not taken up by mammalian cells. However, when it is taken up together with opsonized bacteria by immune cells, such as macrophages or neutrophils, their intracellular proteases release the antibiotic, which then efficiently kills the bacteria.

In antivirulence approaches, mAb therapies are developed to target bacterial toxins. Immunocompromised individuals are at increased risk of *S. aureus* pneumonia, in which α -toxin causes tissue damage, tight junction cleavage, and immune dysregulation. Prophylaxis with mAbs directed against this toxin or use of the mAbs as an adjunctive therapy combined with antibiotics should improve survival rates. Salvecin from Aridis protects against α -toxin-mediated destruction of host cells, thereby preserving the human immune cells. It is a fully human mAb and was discovered by screening B-cell lymphocytes of a patient with confirmed *S. aureus* infection. It is currently being studied in phase II as an adjunctive therapy to standard-of-care antibiotics in patients diagnosed with severe hospital-acquired bacterial pneumonia.^[369,370] Suvratoxumab (MEDI4893), a monoclonal antibody engineered in the Fc region to extend the half-life, targets α -toxin and is also currently being investigated in phase II. However, interstrain diversity and the complex pathogenesis of *S. aureus* bloodstream infections suggest that monotherapy with suvratoxumab will not be sufficient for

adequate protection. Combinations are presently being studied with mAbs for the clumping factor A (ClfA), which is an additional important virulence factor in *S. aureus*.^[371] ASN-100 from Arsanis is a combination of two mAbs that target a total of six different *S. aureus* toxins, which are involved in killing various immune system components, such as macrophages and neutrophils.^[372] One conserved epitope is able to bind five toxins alone. It is currently under investigation in phase II studies.

In addition to mAbs, there are four different biological approaches in clinical development (Table 4). A very innova-

Table 4: Overview of additional antibacterial approaches in clinical development.

Phase	Name	Class	Company	Target	Pathogen
III	reltecomod	peptide	Atox Bio	CD 28 antagonist	<i>S. aureus</i>
II	CF-301	bacteriophage lysin	ContraFect Corp	cell wall (Gram-positive)	MRSA, VRSA
	Sal200	bacteriophage lysin	Intron Biotech.	cell wall (Gram-positive)	MRSA, VRSA
I	CAL02	empty liposomes	Combioxin SA	virulence factors & toxins	<i>S. pneumoniae</i>

tive strategy is being pursued with CAL02, which is a novel empty liposomal drug. It exerts its antivirulence activity by specifically mimicking cell-surface domains that are normally targeted by bacterial toxins.^[373,374] In this regard, CAL02 neutralizes toxins produced by a broad panel of Gram-positive and Gram-negative pathogens and exhibits synergistic effects with antibiotics in in vivo mouse models such as acute pneumonia. CAL02 is currently in phase I for community-acquired bacterial pneumonia (CABP) caused by *Streptococci*.

Alternative therapy strategies cannot be discussed without at least briefly touching on phage therapy. Since the early 20th Century, bacteriophages, that is, viruses that specifically infect bacteria and archaea, have been used to treat a range of bacterial infections. However, since the introduction and success of antibiotics in the mid-20th Century, interest in phages as antimicrobial agents has decreased in Western Europe and the US.^[375] In contrast, they are still actively used in Georgia, Poland, and Russia.^[376] There are major concerns for the systemic application of phages in clinical practice, such as fast resistance development, potential immunogenic reactions, and a limited spectrum of activity. Furthermore, the current approval process is not suitable for phage therapy. This is different for treatment with phage products, such as endolysins. The latter are enzymes used by bacteriophages at the end of their replication cycle to degrade the peptidoglycan of the bacterial host, thereby resulting in cell lysis. As a consequence of the absence of an outer membrane in Gram-positive bacteria, endolysins could be used for the treatment of infections caused by these pathogens. Two active phase II studies are underway that are investigating the potential of phage endolysins for the treatment of *S. aureus* infections. Sal200^[377] is developed by Intron, and CF-301^[378] is developed by ContraFect. Phage endolysins differ from standard-of-care

antibiotics with regards to their elevated potency, speed of bactericidal activity, and high specificity; thus, similar to mAbs they do not harm other bacteria.^[377]

Compared to previous examples, reltecimod (AB103) follows a very different mechanism. It is a novel CD28 antagonistic peptide and is currently in phase III clinical development for necrotizing soft tissue infections. Instead of targeting the pathogen or its virulence factors, this peptide acts in a host-directed manner through modulation of CD28 signaling on T cells, without affecting the normal humoral immune response. Although not solely working against sepsis, reltecimod demonstrates adjuvant activity during the treatment of Gram-positive and Gram-negative bacteria. More importantly, it even clears *S. pyogenes* infections as a stand-alone treatment.^[379,380]

6. Summary and Outlook

Antibiotic resistance still poses a significant threat to human health and the development of new antibacterials that overcome resistance remains a major challenge. Although there are breakthroughs in the clinical development, these are mostly driven by advancements of previous classes, for example, by X-ray structures in the macrolide field^[330] or by new chemistry, for example, in the tetracycline field.^[320] Applying the average attrition rates in pharmaceutical industry,^[381] assuming that 12 % of phase I, 21 % of phase II, and 62 % of phase III compounds will reach the market, we can expect nine to ten compounds from the current pipeline to be approved. Nonetheless, only two to three of them are innovative or novel, characteristics that are urgently required to fight the uphill battle against resistance.

However, novel approaches are being undertaken in both academia and industry to tackle the challenge of bacterial infections. Mining bacterial genomes for new natural products or triggering their expression by altered cultivation conditions may significantly enhance the number of antibiotic candidates with promising therapeutic properties. In this way, potent new antibiotic candidates have been identified in recent years; however, they mainly act through known mechanisms and require further proof of their therapeutic potential. State-of-the-art chemical proteomic and metabolomic deconvolution strategies expand the toolbox for the discovery of new bacterial targets, thereby enabling the development of antibacterials beyond the classical MoA and established resistance pathways. Additionally, although still in its infancy, disarming pathogens without killing (antivirulence) is an intriguing approach with the perspective of impaired resistance development. In addition to standard small-molecule-based treatment, the biological pipeline offers interesting alternatives. However, its attrition rate is hard to predict because there is no benchmark data for approved mAbs, and the recent failures would give a negative impression. Nevertheless, the potential of mAbs for single-agent therapy is unproven and it remains to be seen if these entities are a real “alternative” to traditional antibiotics.

Approaches that think outside the box are, therefore, needed more than ever to identify novel and unconventional

antimicrobial strategies. In this regard, alliances between academia and pharma can be especially beneficial.^[8] Whereas academia is a key driver of innovation, industry has profound experience and resources on how to advance auspicious approaches into translational programs. ADMET and other preclinical tests represent decisive points during this development, however, they are very difficult to get funded and to be performed in an academic setting. To streamline these studies, collaborations with industrial laboratories need to be fostered, or alternatively studies need to be outsourced to a contract research organization (CRO). Contemporary antibacterial funding opportunities such as the Innovative Medicines Initiative (IMI) aim to explicitly foster public-private partnerships (PPP) that bridge the gap between basic and translational research.

A vivid example of such a collaboration is the Natural Product Center of Excellence, a PPP between Fraunhofer and Sanofi, where researchers share common laboratories to identify novel antibacterial natural products among other things. The German Center for Infection Research (DZIF), Infect Control 2020, or CARB-X represent additional integrative and interdisciplinary PPPs that bring together universities, medical centers, and non-university institutes. This kind of research can be highly synergistic, as observed for the recent work of a consortium of academic and industrial scientists on the study and advancement of griselimycin, a potent natural product active against *M. tuberculosis*.^[382]

Given the breadth of innovative ideas and methods, we are confident that research is headed in the right direction and that the described measures will in the near future hopefully streamline the discovery process of novel antibacterial therapeutics.

Acknowledgements

We are grateful to the Deutsche Forschungsgemeinschaft for funding (SI 1096/10-1). M.L. was supported by the German National Academic Foundation. We thank Annabelle Hoegl, Stephan Hacker, and Benedikt Leis for critical revision of the manuscript.

Conflict of interest

The authors declare no conflict of interest.

-
- [1] R. McKie, ““Antibiotic apocalypse”: doctors sound alarm over drug resistance”, **2017**, can be found under <https://www.theguardian.com/society/2017/oct/08/world-faces-antibiotic-apocalypse-says-chief-medical-officer> (accessed March 08, 2018).
 - [2] N. Bagley, K. Outterson, “We Will Miss Antibiotics When They’re Gone”, **2017**, can be found under <https://www.nytimes.com/2017/01/18/opinion/how-to-avoid-a-post-antibiotic-world.html> (accessed March 08, 2018).

- [3] Center for Disease Control and Prevention, "Antibiotic/Antimicrobial Resistance", **2017**, can be found under <https://www.cdc.gov/drugresistance/index.html>, (accessed March 08, 2018).
- [4] U. S. Food & Drug Administration, "New Drugs at FDA: CDER's New Molecular Entities and New Therapeutic Biological Products", **2018**, can be found under <https://www.fda.gov/Drugs/DevelopmentApprovalProcess/DrugInnovation/default.htm> (accessed March 08, 2018).
- [5] K. Lewis, *Annu. Rev. Microbiol.* **2010**, *64*, 357–372.
- [6] S. B. Singh, K. Young, L. Miesel, *Expert Rev. Anti-Infect. Ther.* **2011**, *9*, 589–613.
- [7] V. M. D'Costa, C. E. King, L. Kalan, M. Morar, W. W. L. Sung, C. Schwarz, D. Froese, G. Zazula, F. Calmels, R. Debruyne, G. B. Golding, H. N. Poinar, G. D. Wright, *Nature* **2011**, *477*, 457–461.
- [8] M. F. Chellat, L. Raguž, R. Riedl, *Angew. Chem. Int. Ed.* **2016**, *55*, 6600–6626; *Angew. Chem.* **2016**, *128*, 6710–6738.
- [9] K. M. G. O'Connell, J. T. Hodgkinson, H. F. Sore, M. Welch, G. P. C. Salmond, D. R. Spring, *Angew. Chem. Int. Ed.* **2013**, *52*, 10706–10733; *Angew. Chem.* **2013**, *125*, 10904–10932.
- [10] T. A. Wenczewicz, *Bioorg. Med. Chem.* **2016**, *24*, 6227–6252.
- [11] C. T. Walsh, T. A. Wenczewicz, *J. Antibiot.* **2014**, *67*, 7–22.
- [12] T. S. Crofts, A. J. Gasparrini, G. Dantas, *Nat. Rev. Microbiol.* **2017**, *15*, 422–434.
- [13] P. M. Wright, I. B. Seiple, A. G. Myers, *Angew. Chem. Int. Ed.* **2014**, *53*, 8840–8869; *Angew. Chem.* **2014**, *126*, 8984–9014.
- [14] World Health Organization, "Global priority list of antibiotic-resistant bacteria to guide research, discovery, and development of new antibiotics", **2017**, can be found under <http://www.who.int/medicines/publications/WHO-PPL-Short Summary 25Feb-ET NM WHO.pdf> (accessed March 08, 2018).
- [15] D. T. Hoagland, J. Liu, R. B. Lee, R. E. Lee, *Adv. Drug Delivery Rev.* **2016**, *102*, 55–72.
- [16] A. Zumla, P. Nahid, S. T. Cole, *Nat. Commun.* **2013**, *12*, 388–404.
- [17] K. Lewis, *Nat. Rev. Drug Discovery* **2013**, *12*, 371–387.
- [18] M. A. Farha, E. D. Brown, *Ann. N. Y. Acad. Sci.* **2015**, *1354*, 54–66.
- [19] S. E. Rossiter, M. H. Fletcher, W. M. Wuest, *Chem. Rev.* **2017**, *117*, 12415–12474.
- [20] C. R. Pye, M. J. Bertin, R. S. Lokey, W. H. Gerwick, R. G. Linington, *Proc. Natl. Acad. Sci. USA* **2017**, *114*, 5601–5606.
- [21] G. D. Wright, *Nat. Prod. Rep.* **2017**, *34*, 694–701.
- [22] L. L. Silver, *Clin. Microbiol. Rev.* **2011**, *24*, 71–109.
- [23] K. Ueda, T. Beppu, *J. Antibiot.* **2017**, *70*, 361–365.
- [24] C. Nai, V. Meyer, *Trends Microbiol.* **2017**, *25*, 1–17.
- [25] B. K. Okada, M. R. Seyedsayamdost, *FEMS Microbiol. Rev.* **2017**, *41*, 19–33.
- [26] P. J. Rutledge, G. L. Challis, *Nat. Rev. Microbiol.* **2015**, *13*, 509–523.
- [27] S. Bertrand, N. Bohni, S. Schnee, O. Schumpp, K. Gindro, J.-L. Wolfender, *Biotechnol. Adv.* **2014**, *32*, 1180–1204.
- [28] A. Marmann, A. Aly, W. Lin, B. Wang, P. Proksch, *Mar. Drugs* **2014**, *12*, 1043–1065.
- [29] N. Adnani et al., *ACS Chem. Biol.* **2017**, *12*, 3093–3102.
- [30] Y. Marcy, C. Ouverney, E. M. Bik, T. Losekann, N. Ivanova, H. G. Martin, E. Szeto, D. Platt, P. Hugenholtz, D. A. Relman, S. R. Quake, *Proc. Natl. Acad. Sci. USA* **2007**, *104*, 11889–11894.
- [31] C. Lok, *Nature* **2015**, *522*, 270–273.
- [32] T. Kaerberlein, K. Lewis, S. S. Epstein, *Science* **2002**, *296*, 1127–1129.
- [33] D. Nichols, N. Cahoon, E. M. Trakhtenberg, L. Pham, A. Mehta, A. Belanger, T. Kanigan, K. Lewis, S. S. Epstein, *Appl. Environ. Microbiol.* **2010**, *76*, 2445–2450.
- [34] D. Jung, Y. Aoi, S. S. Epstein, *Microbes Environ.* **2016**, *31*, 456–459.
- [35] B. Berdy, A. L. Spoering, L. L. Ling, S. S. Epstein, *Nat. Protoc.* **2017**, *12*, 2232–2242.
- [36] E. Gavriš et al., *Chem. Biol.* **2014**, *21*, 509–518.
- [37] A. Milshteyn, J. S. Schneider, S. F. Brady, *Chem. Biol.* **2014**, *21*, 1211–1223.
- [38] M. Katz, B. M. Hover, S. F. Brady, *J. Ind. Microbiol. Biotechnol.* **2015**, *43*, 1–13.
- [39] N. Ziemert, M. Alanjary, T. Weber, *Nat. Prod. Rep.* **2016**, *33*, 988–1005.
- [40] M. H. Medema, M. A. Fischbach, *Nat. Chem. Biol.* **2015**, *11*, 639–648.
- [41] H. A. Iqbal, L. Low-Beinart, J. U. Obiajulu, S. F. Brady, *J. Am. Chem. Soc.* **2016**, *138*, 9341–9344.
- [42] K. N. Lam, J. Cheng, K. Engel, J. D. Neufeld, T. C. Charles, *Front. Microbiol.* **2015**, *6*, 149–148.
- [43] B. Adu-Oppong, A. J. Gasparrini, G. Dantas, *Ann. N. Y. Acad. Sci.* **2017**, *1388*, 42–58.
- [44] M. S. Donia, P. Cimermancic, C. J. Schulze, L. C. W. Brown, J. Martin, M. Mitreva, J. Clardy, R. G. Linington, M. A. Fischbach, *Cell* **2014**, *158*, 1402–1414.
- [45] J. Chu et al., *Nat. Chem. Biol.* **2016**, 1–5.
- [46] C.-J. Guo et al., *Cell* **2017**, *168*, 517–526.
- [47] A. J. Waldman, E. P. Balskus, *ACS Infect. Dis.* **2018**, *4*, 14–26.
- [48] D. J. Payne, M. N. Gwynn, D. J. Holmes, D. L. Pompliano, *Nat. Rev. Drug Discovery* **2007**, *6*, 29–40.
- [49] A. Fabbretti, C. O. Gualerzi, L. Brandi, *FEBS Lett.* **2011**, *585*, 1673–1681.
- [50] D. G. Brown, T. L. May-Dracka, M. M. Gagnon, R. Tommasi, *J. Med. Chem.* **2014**, *57*, 10144–10161.
- [51] L. L. Silver, *Bioorg. Med. Chem.* **2016**, *24*, 6379–6389.
- [52] M. Masi, M. Réfregiers, K. M. Pos, J.-M. Pagès, *Nat. Microbiol.* **2017**, *2*, 17001–17007.
- [53] R. Tommasi, D. G. Brown, G. K. Walkup, J. I. Manchester, A. A. Miller, *Nature* **2015**, *529*, 529–542.
- [54] J.-P. Ebejer, M. H. Charlton, P. W. Finn, *J. Cheminf.* **2016**, 1–9.
- [55] G. Krishnamoorthy, I. V. Leus, J. W. Weeks, D. Wolloscheck, V. V. Rybenkov, H. I. Zgurskaya, *mBio* **2017**, *8*, e01172-17.
- [56] S. Hong, T. J. Moritz, C. M. Rath, P. Tamrakar, P. Lee, T. Krucker, L. P. Lee, *ACS Nano* **2017**, *11*, 6959–6967.
- [57] H. Tian, D. A. Six, T. Krucker, J. A. Leeds, N. Winograd, *Anal. Chem.* **2017**, *89*, 5050–5057.
- [58] K. Takroui, H. D. Cooper, A. Spaulding, P. Zucchi, B. Koleva, D. C. Cleary, W. Tear, P. J. Beuning, E. B. Hirsch, J. B. Aggen, *ACS Infect. Dis.* **2016**, *2*, 405–426.
- [59] M. F. Richter, B. S. Drown, A. P. Riley, A. Garcia, T. Shirai, R. L. Svec, P. J. Hergenrother, *Nature* **2017**, *545*, 299–304.
- [60] M. F. Richter, P. J. Hergenrother, *Ann. N. Y. Acad. Sci.* **2018**, *24*, 71–21.
- [61] E. Comer, J. R. Duvall, M. duPont Lee IV, *Future Med. Chem.* **2014**, *6*, 1927–1942.
- [62] J. R. Duvall et al., *ACS Infect. Dis.* **2017**, *3*, 349–359.
- [63] I. B. Seiple et al., *Nature* **2016**, *533*, 338–345.
- [64] R. Fleeman, T. M. LaVoi, R. G. Santos, A. Morales, A. Nefzi, G. S. Welmaker, J. L. Medina-Franco, M. A. Giulianotti, R. A. Houghten, L. N. Shaw, *J. Med. Chem.* **2015**, *58*, 3340–3355.
- [65] D. A. Nichols, A. R. Renslo, Y. Chen, *Future Med. Chem.* **2014**, *6*, 413–427.
- [66] B. Casu, T. Arya, B. Bessette, C. Baron, *Sci. Rep.* **2017**, *7*, 14907.
- [67] L. A. Adams, et al., *Angew. Chem. Int. Ed.* **2015**, *54*, 2179–2184; *Angew. Chem.* **2015**, *127*, 2207–2212.
- [68] N. Velikova, S. Fulle, A. S. Manso, M. Mechkarska, P. Finn, J. M. Conlon, M. R. Oggioni, J. M. Wells, A. Marina, *Sci. Rep.* **2017**, *6*, 1–16.
- [69] D. J. Dwyer, J. J. Collins, G. C. Walker, *Annu. Rev. Pharmacol. Toxicol.* **2015**, *55*, 313–332.

- [70] J. H. Yang, S. C. Bening, J. J. Collins, *Curr. Opin. Microbiol.* **2017**, *39*, 73–80.
- [71] J.-P. Côté, S. French, S. S. Gehrke, C. R. MacNair, C. S. Mangat, A. Bharat, E. D. Brown, *mBio* **2016**, *7*, e01714-16.
- [72] G. Sakoulas, M. Kumaraswamy, A. Kousha, V. Nizet, *mSphere* **2017**, *2*, e00410-17.
- [73] L. Lin et al., *EBioMedicine* **2015**, *2*, 690–698.
- [74] J. Z. Kubicek-Sutherland, D. M. Heithoff, S. C. Ersoy, W. R. Shimp, J. K. House, J. D. Marth, J. W. Smith, M. J. Mahan, *EBioMedicine* **2015**, *2*, 1169–1178.
- [75] S. Zlitni, L. F. Ferruccio, E. D. Brown, *Nat. Chem. Biol.* **2013**, *9*, 796–804.
- [76] K. C. Fahnoe, M. E. Flanagan, G. Gibson, V. Shanmugasundaram, Y. Che, A. P. Tomaras, *PLoS ONE* **2012**, *7*, e51732-7.
- [77] S. C. Ersoy, D. M. Heithoff, L. Barnes V, G. K. Tripp, J. K. House, J. D. Marth, J. W. Smith, M. J. Mahan, *EBioMedicine* **2017**, *20*, 173–181.
- [78] M. A. Farha, S. French, J. M. Stokes, E. D. Brown, *ACS Infect. Dis.* **2018**, *4*, 382–390.
- [79] A. E. Clatworthy, K. P. Romano, D. T. Hung, *Nat. Chem. Biol.* **2018**, *14*, 331–341.
- [80] W. J. Veneman, O. W. Stockhammer, L. de Boer, S. A. J. Zaai, A. H. Meijer, H. P. Spaink, *BMC Genomics* **2013**, *14*, 255.
- [81] H. Hamamoto et al., *Nat. Chem. Biol.* **2015**, *11*, 127–133.
- [82] A. Paudel, S. Panthee, M. Urai, H. Hamamoto, T. Ohwada, K. Sekimizu, *Sci. Rep.* **2018**, 1578.
- [83] C. J.-Y. Tsai, J. M. S. Loh, T. Proft, *Virulence* **2016**, *7*, 214–229.
- [84] J. M. Loh, N. Adenwalla, S. Wiles, T. Proft, *Virulence* **2013**, *4*, 419–428.
- [85] W. Kim, G. L. Hendricks, K. Lee, E. Mylonakis, *Expert Opin. Drug Discovery* **2017**, *12*, 625–633.
- [86] E. Jayamani, R. Rajamuthiah, J. Larkins-Ford, B. B. Fuchs, A. L. Conery, A. Vilcinskas, F. M. Ausubel, E. Mylonakis, *Antimicrob. Agents Chemother.* **2015**, *59*, 1728–1737.
- [87] R. Rajamuthiah, B. B. Fuchs, E. Jayamani, Y. Kim, J. Larkins-Ford, A. Conery, F. M. Ausubel, E. Mylonakis, *PLoS ONE* **2014**, *9*, e89189-11.
- [88] H. Wang et al., *Chem. Biol.* **2013**, *20*, 272–284.
- [89] A. S. Nayar et al., *J. Bacteriol.* **2015**, *197*, 1726–1734.
- [90] I. A. Osterman et al., *Antimicrob. Agents Chemother.* **2016**, *20*, 7481–7489.
- [91] J. Fan et al., *Antimicrob. Agents Chemother.* **2014**, *58*, 7264–7272.
- [92] U. K. Bageshwar, L. VerPlank, D. Baker, W. Dong, S. Hamsanathan, N. Whitaker, J. C. Sacchettini, S. M. Musser, *PLoS ONE* **2016**, *11*, e0149659-25.
- [93] A. T. Tucker, S. P. Leonard, C. D. DuBois, G. A. Knauf, A. L. Cunningham, C. O. Wilke, M. S. Trent, B. W. Davies, *Cell* **2018**, *172*, 618–628.
- [94] R. M. Eband, C. Walker, R. F. Eband, N. A. Magarvey, *Biochim. Biophys. Acta Biomembr.* **2016**, *1858*, 980–987.
- [95] E. K. Sully et al., *PLoS Pathog.* **2014**, *10*, e1004174-14.
- [96] C. L. Quave, J. T. Lyles, J. S. Kavanaugh, K. Nelson, C. P. Parlet, H. A. Crosby, K. P. Heilmann, A. R. Horswill, *PLoS ONE* **2015**, *10*, e0136486-32.
- [97] W. Tegge, M. D. Mihovilovic, R. K. Nandy, S. Roy, G. Bolger, D. E. Kaufmann, M. Schnürch, V. A. Zapol'skii, *J. Med. Microbiol.* **2016**, *65*, 678–687.
- [98] K. P. Smith, J. E. Kirby, *Assay Drug Dev. Technol.* **2016**, *14*, 194–206.
- [99] M. Starkey et al., *PLoS Pathog.* **2014**, *10*, e1004321-17.
- [100] D. Colli, T. D. Bannister, H. Tan, S. Jin, T. Langae, J. Shumate, L. Scampavia, T. P. Spicer, *SLAS Discov.* **2018**, *23*, 55–64.
- [101] G. Pegoraro, T. Misteli, *Trends Genet.* **2017**, *33*, 604–615.
- [102] T. J. Mitchison, *ChemBioChem* **2005**, *6*, 33–39.
- [103] M. L. T. Ang, K. Pethe, *Cytometry* **2016**, *89*, 755–760.
- [104] A. Lamsa, J. Lopez-Garrido, D. Quach, E. P. Riley, J. Pogliano, K. Pogliano, *ACS Chem. Biol.* **2016**, *11*, 2222–2231.
- [105] C. W. Johnston et al., *Nat. Chem. Biol.* **2016**, *12*, 233–239.
- [106] M. A. Wambaugh, V. P. S. Shakya, A. J. Lewis, M. A. Mulvey, J. C. S. Brown, *PLoS Biol.* **2017**, *15*, e2001644-33.
- [107] A. Gurevich, A. Mikheenko, A. Shlemov, A. Korobeynikov, H. Mohimani, P. A. Pevzner, *Nat. Microbiol.* **2018**, *3*, 319–327.
- [108] A. Y. Lee et al., *Science* **2014**, *344*, 208–211.
- [109] S. Chandrasekaran, M. Cokol Cakmak, N. Sahin, K. Yilancioglu, H. Kazan, J. J. Collins, M. Cokol, *Mol. Syst. Biol.* **2016**, *12*, 872–12.
- [110] M. Schenone, V. Dančik, B. K. Wagner, P. A. Clemons, *Nat. Chem. Biol.* **2013**, *9*, 232–240.
- [111] M. A. Farha, E. D. Brown, *Nat. Prod. Rep.* **2016**, *33*, 668–680.
- [112] “Antibacterial New Target Discovery: Sentinel Examples, Strategies, and Surveying Success”: H. A. Sutterlin, J. C. Malinverni, S. H. Lee, C. J. Balibar, T. Roemer, in *Top. Med. Chem.* Springer, Berlin, Heidelberg, **2017**, pp. 1–29.
- [113] K. M. Wetmore et al., *mBio* **2015**, *6*, e00306-15.
- [114] M. Santiago, L. M. Matano, S. H. Moussa, M. S. Gilmore, S. Walker, T. C. Meredith, *BMC Genomics* **2015**, *16*, 252.
- [115] K. Klobucar, E. D. Brown, *FEMS Microbiol. Rev.* **2018**, *42*, 4159.
- [116] M. Jost, J. S. Weissman, *ACS Chem. Biol.* **2018**, *13*, 366–375.
- [117] M. Fonović, M. Bogyo, *Expert Rev. Proteomics* **2008**, *5*, 721–730.
- [118] B. F. Cravatt, A. T. Wright, J. W. Kozarich, *Annu. Rev. Biochem.* **2008**, *77*, 383–414.
- [119] M. H. Wright, S. A. Sieber, *Nat. Prod. Rep.* **2016**, *33*, 681–708.
- [120] M. J. Niphakis, B. F. Cravatt, *Annu. Rev. Biochem.* **2014**, *83*, 341–377.
- [121] M. Garland, S. Loscher, M. Bogyo, *Chem. Rev.* **2017**, *117*, 4422–4461.
- [122] C. W. Tornøe, C. Christensen, M. Meldal, *J. Org. Chem.* **2002**, *67*, 3057–3064.
- [123] V. V. Rostovtsev, L. G. Green, V. V. Fokin, K. B. Sharpless, *Angew. Chem. Int. Ed.* **2002**, *41*, 2596–2599; *Angew. Chem.* **2002**, *114*, 2708–2711.
- [124] L. N. Anderson, P. K. Koch, A. E. Plymale, E. V. Landorf, A. Konopka, F. R. Collart, M. S. Lipton, M. F. Romine, A. T. Wright, *ACS Chem. Biol.* **2016**, *11*, 345–354.
- [125] N. C. Sadler, A. T. Wright, *Curr. Opin. Chem. Biol.* **2015**, *24*, 139–144.
- [126] D. J. Lapinsky, D. S. Johnson, *Future Med. Chem.* **2015**, *7*, 2143–2171.
- [127] C. E. Keohane, A. D. Steele, C. Fetzer, J. Khowsathit, D. Van Tyne, L. Moynié, M. S. Gilmore, J. Karanicolas, S. A. Sieber, W. M. Wuest, *J. Am. Chem. Soc.* **2018**, *140*, 1774–1782.
- [128] Z. Li, P. Hao, L. Li, C. Y. J. Tan, X. Cheng, G. Y. J. Chen, S. K. Sze, H.-M. Shen, S. Q. Yao, *Angew. Chem. Int. Ed.* **2013**, *52*, 8551–8556; *Angew. Chem.* **2013**, *125*, 8713–8718.
- [129] G. Andolina et al., *ACS Chem. Biol.* **2018**, *13*, 666–675.
- [130] M. H. Wright, C. Fetzer, S. A. Sieber, *J. Am. Chem. Soc.* **2017**, *139*, 6152–6159.
- [131] X. Luo et al., *Proc. Natl. Acad. Sci. USA* **2016**, *113*, 3615–3620.
- [132] M. Zampieri, M. Zimmermann, M. Claassen, U. Sauer, *Cell Rep.* **2017**, *19*, 1214–1228.
- [133] M. Zampieri et al., *Sci. Transl. Med.* **2018**, *10*, eaal3973.
- [134] M. M. Savitski et al., *Science* **2014**, *346*, 1255784.
- [135] R. Jafari, H. Almqvist, H. Axelsson, M. Ignatushchenko, T. Lundbäck, P. Nordlund, D. Martinez Molina, *Nat. Protoc.* **2014**, *9*, 2100–2122.
- [136] A. Mateus, T. A. Määttä, M. M. Savitski, *Proteome Sci.* **2017**, *15*, 13.
- [137] I. Becher et al., *Nat. Chem. Biol.* **2016**, *12*, 908–910.
- [138] X. Liao, F. Yang, R. Wang, X. He, H. Li, R. Y. T. Kao, W. Xia, H. Sun, *Chem. Sci.* **2017**, *8*, 8061–8066.

- [139] Y. Wang, et al., *Chem. Sci.* **2017**, *8*, 4626–4633.
- [140] H. Peng, H. Guo, O. Pogoutse, C. Wan, L. Z. Hu, Z. Ni, A. Emili, *Environ. Sci. Technol.* **2016**, *50*, 11329–11336.
- [141] M. Wegener, M. J. Hansen, A. J. M. Driessen, W. Szymanski, B. L. Feringa, *J. Am. Chem. Soc.* **2017**, *139*, 17979–17986.
- [142] J. Chang, Y. Chen, Z. Xu, Z. Wang, Q. Zeng, H. Fan, *Bioconjugate Chem.* **2018**, *29*, 74–82.
- [143] P. Klahn, M. Brönstrup, *Nat. Prod. Rep.* **2017**, *34*, 832–885.
- [144] L. L. Ling et al., *Nature* **2015**, *517*, 455–459.
- [145] T. Homma, A. Nuxoll, A. B. Gandt, P. Ebner, I. Engels, T. Schneider, F. Götz, K. Lewis, B. P. Conlon, *Antimicrob. Agents Chemother.* **2016**, *60*, 6510–6517.
- [146] A. Müller, A. Klöckner, T. Schneider, *Nat. Prod. Rep.* **2017**, *34*, 909–932.
- [147] C. Guo, D. Mandalapu, X. Ji, J. Gao, Q. Zhang, *Chem. Lett.* **2017**, *74*, 417–418.
- [148] W. D. Fiers, M. Craighead, I. Singh, *ACS Infect. Dis.* **2017**, *3*, 688–690.
- [149] K. H. Chen, S. P. Le, X. Han, J. M. Frias, J. S. Nowick, *Chem. Commun.* **2017**, *53*, 11357–11359.
- [150] A. Parmar et al., *Chem. Sci.* **2017**, *8*, 8183–8192.
- [151] K. Jin, K. H. L. Po, W. Y. Kong, C. H. Lo, C. W. Lo, H. Y. Lam, A. Sirinimal, J. A. Reuven, S. Chen, X. Li, *Bioorg. Med. Chem.* **2018**, *26*, 1062–1068.
- [152] A. Parmar et al., *J. Med. Chem.* **2018**, *61*, 2009–2017.
- [153] B. M. Hover et al., *Nat. Microbiol.* **2018**, *3*, 415–422.
- [154] L. H. J. Kleijn, H. C. Vlieg, T. M. Wood, J. Sastre Torano, B. J. C. Janssen, N. I. Martin, *Angew. Chem. Int. Ed.* **2017**, *56*, 16546–16549; *Angew. Chem.* **2017**, *129*, 16773–16776.
- [155] L. Vértesy, E. Ehlers, H. Kogler, M. Kurz, J. Meiwes, G. Seibert, M. Vogel, P. Hammann, *J. Antibiot.* **2000**, *53*, 816–827.
- [156] R. Uchida, M. Iwatsuki, Y.-P. Kim, S. Ohte, S. O. Mura, H. Tomoda, *J. Antibiot.* **2010**, *63*, 151–155.
- [157] H. Hamamoto, K. Kurokawa, C. Kaito, K. Kamura, I. Manitra Razanajatovo, H. Kusuhara, T. Santa, K. Sekimizu, *Antimicrob. Agents Chemother.* **2004**, *48*, 774–779.
- [158] M. Murai, T. Kaji, T. Kuranaga, H. Hamamoto, K. Sekimizu, M. Inoue, *Angew. Chem. Int. Ed.* **2015**, *54*, 1556–1560; *Angew. Chem.* **2015**, *127*, 1576–1580.
- [159] T. Kaji, M. Murai, H. Itoh, J. Yasukawa, H. Hamamoto, K. Sekimizu, M. Inoue, *Chem. Lett.* **2016**, *22*, 16912–16919.
- [160] M. Santiago et al., *Nat. Chem. Biol.* **2018**, *14*, 601–608.
- [161] S. Baumann, J. Herrmann, R. Raju, H. Steinmetz, K. I. Mohr, S. Hüttel, K. Harmrolfs, M. Stadler, R. Müller, *Angew. Chem. Int. Ed.* **2014**, *53*, 14605–14609; *Angew. Chem.* **2014**, *126*, 14835–14839.
- [162] S. Cociancich et al., *Nat. Chem. Biol.* **2015**, *11*, 195–197.
- [163] S. Hüttel, G. Testolin, J. Herrmann, T. Planke, F. Gille, M. Moreno, M. Stadler, M. Brönstrup, A. Kirschning, R. Müller, *Angew. Chem. Int. Ed.* **2017**, *56*, 12760–12764; *Angew. Chem.* **2017**, *129*, 12934–12938.
- [164] B. Cheng, R. Müller, D. Trauner, *Angew. Chem. Int. Ed.* **2017**, *56*, 12755–12759; *Angew. Chem.* **2017**, *129*, 12929–12933.
- [165] Y. J. Kim, H.-J. Kim, G.-W. Kim, K. Cho, S. Takahashi, H. Koshino, W.-G. Kim, *J. Nat. Prod.* **2016**, *79*, 2223–2228.
- [166] J. Kretz, D. Kerwat, V. Schubert, S. Grätz, A. Pesic, S. Semsary, S. Cociancich, M. Royer, R. D. Süßmuth, *Angew. Chem. Int. Ed.* **2015**, *54*, 1969–1973; *Angew. Chem.* **2015**, *127*, 1992–1996.
- [167] S. Grätz, D. Kerwat, J. Kretz, L. von Eckardstein, S. Semsary, M. Seidel, M. Kunert, J. B. Weston, R. D. Süßmuth, *ChemMedChem* **2016**, *11*, 1499–1502.
- [168] D. Kerwat, S. Grätz, J. Kretz, M. Seidel, M. Kunert, J. B. Weston, R. D. Süßmuth, *ChemMedChem* **2016**, *11*, 1899–1903.
- [169] L. von Eckardstein et al., *Chem. Lett.* **2017**, *23*, 15316–15321.
- [170] W. Kim et al., *Nature* **2018**, *111*, 8907–8107.
- [171] P. I. O'Daniel et al., *J. Am. Chem. Soc.* **2014**, *136*, 3664–3672.
- [172] Q. Xiao, S. Vakulenko, M. Chang, S. Mobashery, *Antimicrob. Agents Chemother.* **2014**, *58*, 5841–5847.
- [173] E. Spink et al., *J. Med. Chem.* **2015**, *58*, 1380–1389.
- [174] J. Janardhanan, M. Chang, S. Mobashery, *Curr. Opin. Microbiol.* **2016**, *33*, 13–17.
- [175] N. Koppel, V. Maini Rekdal, E. P. Balskus, *Science* **2017**, *356*, eaag2770.
- [176] A. Zipperer et al., *Nature* **2016**, *535*, 511–516.
- [177] E. M. Aghdam, M. S. Hejazi, A. Barzegar, *Gene* **2016**, *592*, 244–259.
- [178] I. H. Rekdal, R. Brenk, *Future Med. Chem.* **2017**, *9*, 1649–1662.
- [179] S. Langer, M. Hashimoto, B. Hobl, T. Mathes, M. Mack, *J. Bacteriol.* **2013**, *195*, 4037–4045.
- [180] K. F. Blount, et al., *Antimicrob. Agents Chemother.* **2015**, *59*, 5736–5746.
- [181] J. A. Howe et al., *Nature* **2015**, *526*, 672–677.
- [182] J. A. Howe, L. Xiao, T. O. Fischmann, H. Wang, H. Tang, A. Villafania, R. Zhang, C. M. Barbieri, T. Roemer, *RNA Biol.* **2016**, *13*, 946–954.
- [183] H. Wang et al., *Cell Chem. Biol.* **2017**, *24*, 576–588.
- [184] B. K. Johnson, R. B. Abramovitch, *Trends Pharmacol. Sci.* **2017**, *38*, 339–362.
- [185] R. C. Allen, R. Papat, S. P. Diggle, S. P. Brown, *Nat. Rev. Microbiol.* **2014**, *12*, 300–308.
- [186] M. Whiteley, S. P. Diggle, E. P. Greenberg, *Nature* **2017**, *551*, 313–320.
- [187] S. W. Dickey, G. Y. C. Cheung, M. Otto, *Nat. Rev. Drug Discovery* **2017**, *16*, 457–471.
- [188] J. R. Brannon, M. Hadjifrangiskou, *Drug Des. Dev. Ther.* **2016**, *10*, 1795–1806.
- [189] L. N. Silva, K. R. Zimmer, A. J. Macedo, D. S. Trentin, *Chem. Rev.* **2016**, *116*, 9162–9236.
- [190] “Antivirulence Strategies to Target Bacterial Infections”: S. Mühlen, P. Dersch, in *How to Overcome the Antibiotic Crisis: Facts, Challenges, Technologies and Future Perspectives*, Springer International Publishing, Cham, **2016**, pp. 147–183.
- [191] S. T. Rutherford, B. L. Bassler, *Cold Spring Harbor Perspect. Med.* **2012**, *2*, a012427.
- [192] C. Baron, *Curr. Opin. Microbiol.* **2010**, *13*, 100–105.
- [193] E. Ó. Muimhneacháin, F. J. Reen, F. O’Gara, G. P. McGlacken, *Org. Biomol. Chem.* **2018**, *16*, 169–179.
- [194] M. A. Welsh, N. R. Eibergen, J. D. Moore, H. E. Blackwell, *J. Am. Chem. Soc.* **2015**, *137*, 1510–1519.
- [195] C. T. O’Loughlin, L. C. Miller, A. Siryaporn, K. Drescher, M. F. Semmelhack, B. L. Bassler, *Proc. Natl. Acad. Sci. USA* **2013**, *110*, 17981–17986.
- [196] J. T. Hodgkinson, W. R. J. D. Galloway, M. Wright, I. K. Mati, R. L. Nicholson, M. Welch, D. R. Spring, *Org. Biomol. Chem.* **2012**, *10*, 6032–6044.
- [197] A. M. Salam, C. L. Quave, *mSphere* **2018**, *3*, e00500-17.
- [198] E. Geisinger, J. Chen, R. P. Novick, *J. Bacteriol.* **2012**, *194*, 2854–2864.
- [199] P. Mayville, G. Ji, R. Beavis, H. Yang, M. Goger, R. P. Novick, T. W. Muir, *Proc. Natl. Acad. Sci. USA* **1999**, *96*, 1218–1223.
- [200] B. Wang, T. W. Muir, *Cell Chem. Biol.* **2016**, *23*, 214–224.
- [201] J. S. Wright, G. J. Lyon, E. A. George, T. W. Muir, R. P. Novick, *Proc. Natl. Acad. Sci. USA* **2004**, *101*, 16168–16173.
- [202] Y. Tal-Gan, M. Ivancic, G. Cornilescu, H. E. Blackwell, *Org. Biomol. Chem.* **2016**, *14*, 113–121.
- [203] Y. Tal-Gan, D. M. Stacy, M. K. Foegen, D. W. Koenig, H. E. Blackwell, *J. Am. Chem. Soc.* **2013**, *135*, 7869–7882.
- [204] Y. Tal-Gan, M. Ivancic, G. Cornilescu, T. Yang, H. E. Blackwell, *Angew. Chem. Int. Ed.* **2016**, *55*, 8913–8917; *Angew. Chem.* **2016**, *128*, 9059–9063.
- [205] S. M. Daly et al., *Antimicrob. Agents Chemother.* **2015**, *59*, 2223–2235.

- [206] T. Defoirdt, *Trends Microbiol.* **2018**, *26*, 313–328.
- [207] K. C. Collins, K. Tsuchikama, C. A. Lowery, J. Zhu, K. D. Janda, *Tetrahedron* **2016**, *72*, 3593–3598.
- [208] M. Kadirvel, F. Fanimarvasti, S. Forbes, A. McBain, J. M. Gardiner, G. D. Brown, S. Freeman, *Chem. Commun.* **2014**, *50*, 5000–5002.
- [209] M. Guo, S. Gamby, Y. Zheng, H. O. Sintim, *Int. J. Mol. Sci.* **2013**, *14*, 17694–17728.
- [210] C. A. Lowery, J. Park, G. F. Kaufmann, K. D. Janda, *J. Am. Chem. Soc.* **2008**, *130*, 9200–9201.
- [211] K. Tsuchikama, J. Zhu, C. A. Lowery, G. F. Kaufmann, K. D. Janda, *J. Am. Chem. Soc.* **2012**, *134*, 13562–13564.
- [212] W. Zhao, N. Lorenz, K. Jung, S. A. Sieber, *Angew. Chem. Int. Ed.* **2016**, *55*, 1187–1191; *Angew. Chem.* **2016**, *128*, 1203–1207.
- [213] T. Zang, B. W. K. Lee, L. M. Cannon, K. A. Ritter, S. Dai, D. Ren, T. K. Wood, Z. S. Zhou, *Bioorg. Med. Chem. Lett.* **2009**, *19*, 6200–6204.
- [214] A. A. M. Kamal, L. Petrera, J. Eberhard, R. W. Hartmann, *Org. Biomol. Chem.* **2017**, *15*, 4620–4630.
- [215] T. Sams, Y. Baker, J. Hodgkinson, J. Gross, D. Spring, M. Welch, *Isr. J. Chem.* **2016**, *56*, 282–294.
- [216] D. Szamosvári, V. F. Reichle, M. Jureschi, T. Böttcher, *Chem. Commun.* **2016**, *52*, 13440–13443.
- [217] C. Lu, B. Kirsch, C. Zimmer, J. C. de Jong, C. Henn, C. K. Maurer, M. Müsken, S. Häußler, A. Steinbach, R. W. Hartmann, *Chem. Biol.* **2012**, *19*, 381–390.
- [218] C. Lu, C. K. Maurer, B. Kirsch, A. Steinbach, R. W. Hartmann, *Angew. Chem. Int. Ed.* **2014**, *53*, 1109–1112; *Angew. Chem.* **2014**, *126*, 1127–1130.
- [219] E. R. Green, J. Mecsas, *Microbiol. Spectr.* **2016**, *4*, 215–239.
- [220] B. Coburn, I. Sekirov, B. B. Finlay, *Clin. Microbiol. Rev.* **2007**, *20*, 535–549.
- [221] N. C. Marshall, B. B. Finlay, *Expert Opin. Ther. Targets* **2014**, *18*, 137–152.
- [222] L. Gu, S. Zhou, L. Zhu, C. Liang, X. Chen, *Molecules* **2015**, *20*, 17659–17674.
- [223] N. Charro, L. J. Mota, *Expert Opin. Drug Discovery* **2015**, *10*, 373–387.
- [224] A. Anantharajah, M.-P. Mingeot-Leclercq, F. Van Bambeke, *Trends Pharmacol. Sci.* **2016**, *37*, 734–749.
- [225] N. Sunduru, O. Salin, Å. Gylfe, M. Elofsson, *Eur. J. Med. Chem.* **2015**, *101*, 595–603.
- [226] D. L. Hudson, A. N. Layton, T. R. Field, A. J. Bowen, H. Wolf-Watz, M. Elofsson, M. P. Stevens, E. E. Galyov, *Antimicrob. Agents Chemother.* **2007**, *51*, 2631–2635.
- [227] A. Anantharajah, J. M. Buyck, C. Sundin, P. M. Tulkens, M. P. Mingeot-Leclercq, F. Van Bambeke, *Antimicrob. Agents Chemother.* **2017**, *61*, e02566-16.
- [228] P. Uusitalo, U. Hägglund, E. Rhöös, H. Scherman Norberg, M. Elofsson, C. Sundin, *J. Antibiot.* **2017**, *70*, 937–943.
- [229] R. Zambelloni, J. P. R. Connolly, A. Huerta Uribe, K. Burgess, R. Marquez, A. J. Roe, *Mol. Microbiol.* **2017**, *105*, 606–619.
- [230] A. C. McShan, R. N. De Guzman, *Chem. Biol. Drug Des.* **2015**, *85*, 30–42.
- [231] D. Aiello, J. D. Williams, H. Majgier-Baranowska, I. Patel, N. P. Peet, J. Huang, S. Lory, T. L. Bowlin, D. T. Moir, *Antimicrob. Agents Chemother.* **2010**, *54*, 1988–1999.
- [232] N. O. Bowlin et al., *Antimicrob. Agents Chemother.* **2014**, *58*, 2211–2220.
- [233] B. J. Berube, K. R. Murphy, M. C. Torhan, N. O. Bowlin, J. D. Williams, T. L. Bowlin, D. T. Moir, A. R. Hauser, *Antimicrob. Agents Chemother.* **2017**, *61*, e01202-17.
- [234] J. D. Williams et al., *Bioorg. Med. Chem.* **2015**, *23*, 1027–1043.
- [235] C. L. Shaffer, J. A. Good, S. Kumar, K. S. Krishnan, J. A. Gaddy, J. T. Loh, J. Chappell, F. Almqvist, T. L. Cover, M. Hadjifrangiskou, *mBio* **2016**, *7*, e00221-16.
- [236] I. Olsen, *Eur. J. Clin. Microbiol. Infect. Dis.* **2015**, *34*, 877–886.
- [237] Y.-H. Li, X. Tian, *Sensors* **2012**, *12*, 2519–2538.
- [238] C. Solano, M. Echeverez, I. Lasa, *Curr. Opin. Microbiol.* **2014**, *18*, 96–104.
- [239] C. D. Boyd, G. A. O'Toole, *Annu. Rev. Cell Dev. Biol.* **2012**, *28*, 439–462.
- [240] B. M. Prüß, *J. Bacteriol.* **2017**, *199*, e00259-17.
- [241] T. H. Jakobsen, T. Tolker-Nielsen, M. Givskov, *Int. J. Mol. Sci.* **2017**, *18*, 1970.
- [242] D. Fleming, K. P. Rumbaugh, *Microorganisms* **2017**, *5*, 15.
- [243] K. C. Costa, N. R. Glasser, S. J. Conway, D. K. Newman, *Science* **2017**, *355*, 170–173.
- [244] Z. Chen, H. Ji, C. Liu, W. Bing, Z. Wang, X. Qu, *Angew. Chem. Int. Ed.* **2016**, *55*, 10732–10736; *Angew. Chem.* **2016**, *128*, 10890–10894.
- [245] X.-H. Li, J.-H. Lee, *J. Microbiol.* **2017**, *55*, 753–766.
- [246] R. Sommer et al., *J. Am. Chem. Soc.* **2018**, *140*, 2537–2545.
- [247] A. T. Garrison, Y. Abouelhassan, D. Kallifidas, F. Bai, M. Ukhanova, V. Mai, S. Jin, H. Luesch, R. W. Huigens III, *Angew. Chem. Int. Ed.* **2015**, *54*, 14819–14823; *Angew. Chem.* **2015**, *127*, 15032–15036.
- [248] M. C. Jennings, L. E. Ator, T. J. Paniak, K. P. C. Minbiole, W. M. Wuest, *ChemBioChem* **2014**, *15*, 2211–2215.
- [249] R. Joseph, A. Naugolny, M. Feldman, I. M. Herzog, M. Fridman, Y. Cohen, *J. Am. Chem. Soc.* **2016**, *138*, 754–757.
- [250] A. E. Solinski et al., *J. Am. Chem. Soc.* **2017**, *139*, 7188–7191.
- [251] S. R. Park et al., *Nat. Commun.* **2016**, *7*, 10710.
- [252] W. Siala, S. Kuchariková, A. Braem, J. Vleugels, P. M. Tulkens, M.-P. Mingeot-Leclercq, P. Van Dijck, F. Van Bambeke, *Nat. Commun.* **2016**, *7*, 13286.
- [253] I. Di Bonaventura, et al., *Chem. Sci.* **2017**, *8*, 6784–6798.
- [254] A. D. Steele, K. W. Knouse, C. E. Keohane, W. M. Wuest, *J. Am. Chem. Soc.* **2015**, *137*, 7314–7317.
- [255] D. Frees, K. Sørensen, H. Ingmer, *Infect. Immun.* **2005**, *73*, 8100–8108.
- [256] J. Krysiak, M. Stahl, J. Vomacka, C. Fetzer, M. Lakemeyer, A. Fux, S. A. Sieber, *J. Proteome Res.* **2017**, *16*, 1180–1192.
- [257] D. Frees, S. N. A. Qazi, P. J. Hill, H. Ingmer, *Mol. Microbiol.* **2003**, *48*, 1565–1578.
- [258] O. Gaillot, S. Bregenholt, F. Jaubert, J. P. Di Santo, P. Berche, *Infect. Immun.* **2001**, *69*, 4938–4943.
- [259] H.-Y. Kwon, A. D. Ogunniyi, M.-H. Choi, S.-N. Pyo, D.-K. Rhee, J. C. Paton, *Infect. Immun.* **2004**, *72*, 5646–5653.
- [260] F. Ye, J. Li, C.-G. Yang, *Mol. Biosyst.* **2017**, *13*, 23–31.
- [261] E. Culp, G. D. Wright, *J. Antibiot.* **2017**, *70*, 366–377.
- [262] T. Böttcher, S. A. Sieber, *J. Am. Chem. Soc.* **2008**, *130*, 14400–14401.
- [263] M. W. Hackl et al., *J. Am. Chem. Soc.* **2015**, *137*, 8475–8483.
- [264] A. Pahl et al., *Angew. Chem. Int. Ed.* **2015**, *54*, 15892–15896; *Angew. Chem.* **2015**, *127*, 16121.
- [265] F. Weinandy, K. Lorenz-Baath, V. S. Korotkov, T. Böttcher, S. Sethi, T. Chakraborty, S. A. Sieber, *ChemMedChem* **2014**, *9*, 710–713.
- [266] C. Fetzer, V. S. Korotkov, R. Thänert, K. M. Lee, M. Neuenschwander, J. P. von Kries, E. Medina, S. A. Sieber, *Angew. Chem. Int. Ed.* **2017**, *56*, 15746–15750; *Angew. Chem.* **2017**, *129*, 15952–15957.
- [267] H. Brötz-Oesterhelt, P. Sass, *Int. J. Med. Microbiol.* **2014**, *304*, 23–30.
- [268] B. P. Conlon, E. S. Nakayasu, L. E. Fleck, M. D. LaFleur, V. M. Isabella, K. Coleman, S. N. Leonard, R. D. Smith, J. N. Adkins, K. Lewis, *Nature* **2013**, *503*, 365–370.
- [269] H. A. Crosby, P. M. Schlievert, J. A. Merriman, J. M. King, W. Salgado-Pabón, A. R. Horswill, *PLoS Pathog.* **2016**, *12*, e1005604.
- [270] R. K. Gupta, T. T. Luong, C. Y. Lee, *Proc. Natl. Acad. Sci. USA* **2015**, *112*, 14036–14041.



- [271] W. Zheng, Y. Liang, H. Zhao, J. Zhang, Z. Li, *ChemBioChem* **2015**, *16*, 1035–1040.
- [272] F. Sun et al., *Proc. Natl. Acad. Sci. USA* **2012**, *109*, 15461–15466.
- [273] F. Sun et al., *Chem. Biol.* **2011**, *18*, 1032–1041.
- [274] M. H. Kunzmann, N. C. Bach, B. Bauer, S. A. Sieber, *Chem. Sci.* **2014**, *5*, 1158–1176.
- [275] J. S. Matson, J. H. Withey, V. J. DiRita, *Infect. Immun.* **2007**, *75*, 5542–5549.
- [276] D. T. Hung, E. A. Shakhnovich, E. Pierson, J. J. Mekalanos, *Science* **2005**, *310*, 670–674.
- [277] J. H. Withey, D. Nag, S. C. Plecha, R. Sinha, H. Koley, *Antimicrob. Agents Chemother.* **2015**, *59*, 7471–7476.
- [278] S. C. Plecha, J. H. Withey, *J. Bacteriol.* **2015**, *197*, 1716–1725.
- [279] A. K. Woodbrey, E. O. Onyango, M. Pellegrini, G. Kovacicova, R. K. Taylor, G. W. Gribble, F. J. Kull, *Sci. Rep.* **2017**, *7*, 45011.
- [280] R. Anthonard, V. J. DiRita, *mBio* **2013**, *4*, e00403-13.
- [281] J. Rex, “Enabling drug discovery & development to address the crisis of antibacterial resistance: New tools, new pathways & remaining challenges at IFPMA—New pathways for antibiotics”, **2014**, can be found under <http://drive-ab.eu/wp-content/uploads/2014/09/Rex-JH-2015-04-30-IFPMA-New-pathways-for-antibiotics-v1.3.pdf> (accessed March 08, 2018).
- [282] Boston Consulting Group, “Breaking through the wall”, **2017**, can be found under https://www.bundesgesundheitsministerium.de/fileadmin/Dateien/5_Publikationen/Gesundheit/Berichte/GUARD_Follow_Up_Report_Full_Report_final.pdf (accessed March 08, 2018).
- [283] R. G. Finch, D. Greenwood, S. R. Norrby, R. J. Whaley, *Antibiotic and Chemotherapy*, Saunders Elsevier, Edinburgh, **2010**.
- [284] A. J. O'Neill, I. Chopra, *Expert Opin. Invest. Drugs* **2004**, *13*, 1045–1063.
- [285] M. S. Butler, M. A. Blaskovich, M. A. Cooper, *J. Antibiot.* **2017**, *70*, 3–24.
- [286] P. Fernandes, E. Martens, *Biochem. Pharmacol.* **2017**, *133*, 152–163.
- [287] K. Bush, M. G. P. Page, *J. Pharmacokinet. Pharmacodyn.* **2017**, *44*, 113–132.
- [288] Springer International Publishing AG, Adis Insight, can be found under: <http://adis.springer.com/> (accessed March 08, 2018).
- [289] National Institute of Health, “ClinicalTrials.gov,” can be found under <http://ClinicalTrials.gov> (accessed January 18, 2018).
- [290] The PEW Charitable Trust, “Antibiotics currently in global clinical development”, **2014**, can be found under <http://www.pewtrusts.org/en/multimedia/data-visualizations/2014/antibiotics-currently-in-clinical-development> (accessed January 10, 2018).
- [291] A. Fleming, *Br. J. Exp. Pathol.* **1929**, *10*, 226–236.
- [292] K. Bush, *Int. J. Antimicrob. Agents* **2015**, *46*, 483–493.
- [293] R. P. Amber Bush, G. A. Jacoby, *Philos. Trans. R. Soc. Lond., B Biol. Sci.* **1980**, *289*, 321–331.
- [294] F. Reck, A. Bermingham, J. Blais, V. Capka, T. Cariaga, A. Casarez, R. Colvin, C. R. Dean, A. Fekete, W. Gong, et al., *Bioorg. Med. Chem. Lett.* **2018**, *28*, 748–755.
- [295] R. E. Mendes, P. R. Rhomberg, B. Schaefer, M. D. Huband, R. K. Flamm, “In Vitro Activity of LYS228 against *Enterobacteriaceae*, Including Molecularly Characterized Multidrug-Resistant Isolates”, *Poster at ASM Microbe*, **2017**, can be found under: <https://www.jmilabs.com/data/posters/ASMMicrobe17-LYS228.pdf> (accessed January 18, 2018).
- [296] J. M. T. Hamilton-Miller, *Pharmacotherapy* **2003**, *23*, 1497–1507.
- [297] M. Nagashima, S. Goto, T. Yoshida, T. Matsunaga, H. Shimohira, M. Ogawa, *Jpn. J. Antibiot.* **1996**, *49*, 303–323.
- [298] C. C. C. R. de Carvalho, P. Fernandes, *Front. Microbiol.* **2014**, *5*, 290.
- [299] A. Ito, T. Nishikawa, S. Matsumoto, H. Yoshizawa, T. Sato, R. Nakamura, M. Tsuji, Y. Yamano, *Antimicrob. Agents Chemother.* **2016**, *60*, 7396–7401.
- [300] DGAP, “AiCuris startet klinische Entwicklung mit AIC499”, **2017**, can be found under <http://www.dgap.de/dgap/News/corporate/aicuris-startet-klinische-entwicklung-mit-aic-einem-neuartigen-resistenzbrechenden-antibiotikum-gegen-multiresistente-gramnegative-bakterien/?newsID=980605> (accessed January 18, 2018).
- [301] A. Lapuebla, M. Abdallah, O. Olafisoye, C. Cortes, C. Urban, J. Quale, D. Landman, *Antimicrob. Agents Chemother.* **2015**, *59*, 4856–4860.
- [302] E. J. C. Goldstein, D. M. Citron, K. L. Tyrrell, E. Leoncio, C. V. Merriam, *Antimicrob. Agents Chemother.* **2018**, *62*, e01992-17.
- [303] S. Lob, K. Young, M. Motyl, S. Hawser, I. Morrissey, S. Magnet, D. Sahn, “Activity of imipenem-relebactam against *Enterobacteriaceae* and *Pseudomonas aeruginosa* from respiratory tract infections in Europe, SMART 2015”, *Presentation at ECCMID*, Vienna **2017**, information can be found under https://www.escmid.org/escmid/publications/escmid_eLibrary/material/?mid=40327 (accessed January 18, 2018).
- [304] D. M. Livermore, S. Mushtaq, M. Warner, A. Vickers, N. Woodford, *J. Antimicrob. Chemother.* **2017**, *72*, 1373–1385.
- [305] B. Moya, I. M. Barcelo, S. Bhagwat, M. Patel, G. Bou, K. M. Papp-Wallace, R. A. Bonomo, A. Oliver, *Antimicrob. Agents Chemother.* **2017**, *61*, e02529-16.
- [306] D. M. Livermore, M. Warner, S. Mushtaq, N. Woodford, *Antimicrob. Agents Chemother.* **2016**, *60*, 554–560.
- [307] A. Morinaka et al., *J. Antimicrob. Chemother.* **2015**, *70*, 2779–2786.
- [308] T. F. Durand-Réville et al., *Nat. Microbiol.* **2017**, *2*, 17104.
- [309] M. Hackel, D. Pevear, D. Sahn, “In Vitro Activity of Cefepime in Combination with VNRX-5133 against Gram-Negative Uti Isolates”, *Poster at ASM Microbe*, Atlanta, **2018**, information can be found under <http://www.abstractsonline.com/pp8/#/4623/presentation/7380>.
- [310] R. Bushey, “Startup Raises \$42M for Breakthrough Antibiotic Resistance R&D”, **2017**, can be found under <https://www.ddmag.com/article/2017/07/startup-raises-42m-breakthrough-antibiotic-resistance-r-d> (accessed January 18, 2018).
- [311] J. L. Crandon, D. P. Nicolau, *Pathogens* **2015**, *4*, 620–625.
- [312] L. A. Sorbera, J. Castañer, X. Rabassada, *Drugs Future* **2004**, *29*, 220–225.
- [313] FDA, “FDA data sheet Bactrim,” **2012**, can be found under https://www.accessdata.fda.gov/drugsatfda_docs/label/2012/017377s071lbl.pdf (accessed January 18, 2018).
- [314] Bioworld, “FDA Rejects Arpida’s Iclaprim as Company Seeks a Partner”, **2009**, can be found under <http://www.bioworld.com/content/fda-rejects-arpidas-iclaprim-company-seeks-partner> (accessed January 18, 2018).
- [315] WHO, “Antibacterial agents in clinical development, WHO report”, **2017**, can be found under http://www.who.int/medicines/news/2017/IAU_AntibacterialAgentsClinicalDevelopment_webfinal_2017_09_19.pdf (accessed January 18, 2018).
- [316] M. E. Huth, A. J. Ricci, A. G. Cheng, *Int. J. Otolaryngol.* **2011**, *2011*, 937861.
- [317] M. P. Mingeot-Leclercq, Y. Glupczynski, P. M. Tulkens, *Antimicrob. Agents Chemother.* **1999**, *43*, 727–737.
- [318] J. B. Aggen et al., *Antimicrob. Agents Chemother.* **2010**, *54*, 4636–4642.
- [319] P. A. Bradford, C. H. Jones, in *Antibiotic Discovery and Development*, Springer US, Boston, MA, **2011**, pp. 147–179.
- [320] F. Liu, A. G. Myers, *Curr. Opin. Chem. Biol.* **2016**, *32*, 48–57.
- [321] G. G. Zhan et al., *Drugs* **2016**, *76*, 567–588.
- [322] H. Seifert, D. Stefanik, J. A. Sutcliffe, P. G. Higgins, “In-vitro activity of the novel fluorocycline TP-6076 against carbapenem

- non-susceptible *Acinetobacter baumannii*" Presentation at ECCMID, Vienna 2017, information can be found under https://www.escmid.org/escmid_publications/escmid_elibrary/material/?mid=42365 (accessed January 18, 2018).
- [323] Y. Deng, C. Sun, D. K. Hunt, C. Fyfe, C.-L. Chen, T. H. Grossman, J. A. Sutcliffe, X.-Y. Xiao, *J. Med. Chem.* **2017**, *60*, 2498–2512.
- [324] B. Zhang, Y. Wang, Y. Chen, F. Yang, *Open Forum Infectious Diseases* **2016**, *3*, <https://doi.org/10.1093/ofid/ofw172.1544> (accessed January 18, 2018).
- [325] T. H. Grossman et al., *mSphere* **2017**, *2*, e00004-17.
- [326] J. M. Zuckerman, F. Qamar, B. R. Bono, *Infect. Dis. Clin. North Am.* **2009**, *23*, 997–1026.
- [327] P. McGhee, C. Clark, K. M. Kosowska-Shick, K. Nagai, B. Dewasse, L. Beachel, P. C. Appelbaum, *Antimicrob. Agents Chemother.* **2010**, *54*, 230–238.
- [328] D. J. Farrell, R. E. Mendes, R. N. Jones, *Antimicrob. Agents Chemother.* **2015**, *59*, 2432–2434.
- [329] P. Fernandes, E. Martens, D. Bertrand, D. Pereira, *Bioorg. Med. Chem.* **2016**, *24*, 6420–6428.
- [330] P. Fernandes, E. Martens, D. Pereira, *J. Antibiot.* **2017**, *70*, 527–533.
- [331] B. Owens, *Nat. Biotechnol.* **2017**, *35*, 187–188.
- [332] R. K. Flamm, P. R. Rhomberg, H. S. Sader, *Antimicrob. Agents Chemother.* **2017**, *61*, e01230-17.
- [333] R. Chavan, V. Zope, R. Yeole, M. Patel, *Open Forum Infectious Diseases* **2016**, *3*, <https://doi.org/10.1093/ofid/ofw172.1356> (accessed January 18, 2018).
- [334] M. R. Barbachyn, C. W. Ford, *Angew. Chem. Int. Ed.* **2003**, *42*, 2010–2023; *Angew. Chem.* **2003**, *115*, 2056–2070.
- [335] J. A. Ippolito, Z. F. Kanyo, D. Wang, F. J. Franceschi, P. B. Moore, T. A. Steitz, E. M. Duffy, *J. Med. Chem.* **2008**, *51*, 3353–3356.
- [336] O. A. Phillips, L. H. Sharaf, *Expert Opin. Ther. Pat.* **2016**, *26*, 591–605.
- [337] L. A. Mitscher, *Chem. Rev.* **2005**, *105*, 559–592.
- [338] Pharmacodia, "Synthesis of lasifloxacin," can be found under http://en.pharmacodia.com/web/drug/1_1585.html (accessed January 18, 2018).
- [339] R. Kishii, Y. Yamaguchi, M. Takei, *Antimicrob. Agents Chemother.* **2017**, *61*, e00120-17.
- [340] W. Stubbings, P. Leow, G. C. Yong, F. Goh, B. Körber-Irrgang, M. Kresken, R. Endermann, H. Labischinski, *Antimicrob. Agents Chemother.* **2011**, *55*, 4394–4397.
- [341] S. E. Wohlert, T. Jaetsch, B. Gallenkamp, H. J. Knops, N. Lui, M. Preiss, D. Haberich, H. Labischinski, "Synthesis of Finafloxacin", Poster at the 48th ICAAC, Washington, 2008, can be found under http://www.merlionpharma.com/sites/default/files/file/PPS/F1-2036_Wohlert.pdf (accessed: January 18, 2018).
- [342] R. K. Flamm, D. J. Farrell, H. S. Sader, P. R. Rhomberg, R. N. Jones, "New Fluoroquinolone Finafloxacin HCl (FIN): Route of Synthesis Physicochemical Characteristics and Activity under Neutral and Acid Conditions", Poster at the 48th ICAAC, Washington, 2008, can be found under http://www.merlionpharma.com/sites/default/files/file/PPS/F1-2036_Wohlert.pdf (accessed January 18, 2018).
- [343] D. J. Payne et al., *Antimicrob. Agents Chemother.* **2002**, *46*, 3118–3124.
- [344] R. Novak, D. M. Shlaes, *Curr. Opin. Invest. Drugs* **2010**, *11*, 182–191.
- [345] R. E. Mendes, D. J. Farrell, R. K. Flamm, G. H. Talbot, Z. Ivezic-Schoenfeld, S. Paukner, H. S. Sader, *Antimicrob. Agents Chemother.* **2016**, *60*, 4407–4411.
- [346] K. B. Waites, D. M. Crabb, L. B. Duffy, J. S. Jensen, Y. Liu, S. Paukner, *Antimicrob. Agents Chemother.* **2016**, e02008-16.
- [347] M. Hackel, T. Lister, T. R. Parr, Jr., M. Vaara, D. Sahn, "In Vitro Activity of SPR741 Combined with Three Novel Com-
- pounds Against Recent Clinical Isolates of *Acinetobacter baumannii* and *Enterobacteriaceae*", Poster at ASM Microbe, New Orleans 2017, can be found under https://www.ihma.com/app/uploads/Spero_P80_3-combos-with-741_Microbe-2017_v04_final.pdf (accessed January 18, 2018).
- [348] B. D. Bax et al., *Nature* **2010**, *466*, 935–940.
- [349] J. A. Jones, K. G. Virga, G. Gumina, K. E. Hevener, *Medchem-comm* **2016**, *7*, 1694–1715.
- [350] M. Powell, "Gonorrhoea—the current antibiotic pipeline and the need for new drugs," can be found under <https://www.idhub.com/2017/07/07/gonorrhoea-current-antibiotic-pipeline-need-new-drugs> (accessed January 18, 2018).
- [351] R. A. Alm et al., *Antimicrob. Agents Chemother.* **2015**, *59*, 1478–1486.
- [352] A. Kwa, S. K. Kasiakou, V. H. Tam, M. E. Falagas, *Expert Rev. Anti-Infect. Ther.* **2007**, *5*, 811–821.
- [353] H.-K. Kang, C. Kim, C. H. Seo, Y. Park, *J. Microbiol.* **2017**, *55*, 1–12.
- [354] M. Mahlapuu, J. Håkansson, L. Ringstad, C. Björn, *Front. Cell. Infect. Microbiol.* **2016**, *6*, 194.
- [355] I. Morrisey, J. Dallow, A. Siegwart, A. Smith, R. Scott, B. Korczak, "The activity of PMX-30063 against *Staphylococci* and *Streptococci*" Presentation at ECCMID, Vienna, 2017, information can be found under https://www.escmid.org/escmid_publications/escmid_elibrary/material/?mid=5115 (accessed January 18, 2018).
- [356] B. Mensa, G. L. Howell, R. Scott, W. F. DeGrado, *Antimicrob. Agents Chemother.* **2014**, *58*, 5136–5145.
- [357] Pharmacodia, "Structure of murepavadin," can be found under <http://en.pharmacodia.com/web/basic/query?page=1&text.field=text&text.field.ShowName=Keyword&text.val=murepavadin&text.val.ShowName=Murepavadin> (accessed January 18, 2018).
- [358] K.-J. Lou, *Science-Business eXchange* **2010**, *3*, 479.
- [359] D. V. Zurawski, A. A. Reinhart, Y. A. Alameh, M. J. Pucci, Y. Si, R. Abu-Taleb, J. P. Shearer, S. T. Demons, S. D. Tyner, T. Lister, *Antimicrob. Agents Chemother.* **2017**, *61*, e01239-17-6.
- [360] T. P. Zabawa, M. J. Pucci, T. R. Parr, Jr., T. Lister, *Curr. Opin. Microbiol.* **2016**, *33*, 7–12.
- [361] R. E. Mendes, P. R. Rhomberg, A. Lee, T. Lister, T. R. Parr, Jr., M. Vaara, R. K. Flamm, "Antimicrobial Synergistic Effect of a New Anti-Gram-Positive Agent Tested In Combination with Polymyxin Derivative against Gram-Negative Pathogens, Including ESKAPE Group Organisms" Poster at ASM Microbe, New Orleans, 2017, can be found under <https://www.jmilabs.com/data/posters/ASMMicrobe17-SPR719-SPR741.pdf> (accessed January 18, 2018).
- [362] A. DiGiandomenico, B. R. Sellman, *Curr. Opin. Microbiol.* **2015**, *27*, 78–85.
- [363] Q. Lu et al., *J. Antimicrob. Chemother.* **2011**, *66*, 1110–1116.
- [364] I. J. Haq, A. Gardner, M. Brodli, *Ann. Transl. Med.* **2016**, *4*, 12.
- [365] C. Morrison, *Nat. Rev. Drug Discovery* **2015**, *14*, 737–738.
- [366] T. Huynh, M. Stecher, J. Mckinnon, N. Jung, M. E. Rupp, *Open Forum Infectious Diseases* **2016**, *3*, <https://doi.org/10.1093/ofid/ofw172.1057> (accessed January 18, 2018).
- [367] A. K. Varshney et al., *PLoS ONE* **2018**, *13*, e0190537-22.
- [368] S. M. Lehar et al., *Nature* **2015**, *527*, 323–328.
- [369] C. Vuong, A. J. Yeh, G. Y. C. Cheung, M. Otto, *Expert Opin. Invest. Drugs* **2016**, *25*, 73–93.
- [370] Aridis Pharmaceuticals "AR-301: Fully Human mAb Against *Staphylococcus aureus*," can be found under <http://aridispharma.com/ar-101/> (accessed January 18, 2018).
- [371] C. Tkaczyk et al., *Antimicrob. Agents Chemother.* **2017**, *61*, e00629-17.
- [372] Z. Magyarics et al., *Open Forum Infectious Diseases* **2017**, *4*, S310.

- [373] K. A. Gräfe, "Liposomen statt Antibiotika gegen bakterielle Infektionen", **2014**, can be found under <https://www.pharmazeutische-zeitung.de/index.php?id=54969> (accessed January 18, 2018).
- [374] B. Francois, G. Colin, P. F. Dequin, P. F. Laterre, A. Perez, "CAL02: a liposomal adjunctive anti-toxin therapy in infections. A new therapeutic approach for severe community-acquired pneumonia", *Presentation at ECCMID*, Vienna, **2017**, information can be found under https://www.escmid.org/escmid_publications/escmid_elibrary/material/?mid=40357 (accessed January 18, 2018).
- [375] C. J. Cooper, M. Khan Mirzaei, A. S. Nilsson, *Front. Microbiol.* **2016**, *7*, 1209.
- [376] S. T. Abedon, P. García, P. Mullany, R. Aminov, *Front. Microbiol.* **2017**, *8*, 981.
- [377] S. Y. Jun, I. J. Jang, S. Yoon, K. Jang, K.-S. Yu, J. Y. Cho, M.-W. Seong, G. M. Jung, S. J. Yoon, S. H. Kang, *Antimicrob. Agents Chemother.* **2017**, *61*, e02629-16.
- [378] R. Schuch, B. K. Khan, A. Raz, J. A. Rotolo, M. Wittekind, *Antimicrob. Agents Chemother.* **2017**, *61*, e02666-16.
- [379] G. Ramachandran et al., *J. Infect. Dis.* **2013**, *207*, 1869–1877.
- [380] G. Ramachandran et al., *J. Infect. Dis.* **2015**, *211*, 995–1003.
- [381] "Survive the Valley of Death and De-risk Your Pipeline," can be found under <https://www.lonza.com/custom-manufacturing/development-technologies/protein-and-vaccine-development-services/developability-services/about-developability-assessment.aspx> (accessed January 18, 2018).
- [382] A. Kling et al., *Science* **2015**, *348*, 1106–1112.

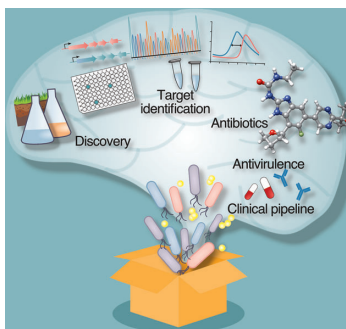
Manuscript received: April 28, 2018
Accepted manuscript online: June 25, 2018
Version of record online: ■ ■ ■ ■ ■ ■ ■ ■ ■ ■

Reviews

Antibacterial Drugs

M. Lakemeyer, W. Zhao, F. A. Mandl,
P. Hammann,
S. A. Sieber* ————— ■■■■-■■■■

Thinking Outside the Box—Novel
Antibacterials To Tackle the Resistance
Crisis



Fit for the future: The discovery of novel antibacterials is a highly interdisciplinary field which relies on input from various research areas. This Review encompasses several aspects of antibiotic development—from very early strategies to mature drugs in clinical trials. An overview is given of methods suitable for mining novel antibacterials and for the elucidation of their bacterial targets.



JOHN WILEY AND SONS LICENSE TERMS AND CONDITIONS

Oct 11, 2018

This Agreement between Lichtenbergstr 4 ("You") and John Wiley and Sons ("John Wiley and Sons") consists of your license details and the terms and conditions provided by John Wiley and Sons and Copyright Clearance Center.

License Number	4445891339724
License date	Oct 11, 2018
Licensed Content Publisher	John Wiley and Sons
Licensed Content Publication	Angewandte Chemie International Edition
Licensed Content Title	Thinking Outside the Box—Novel Antibacterials To Tackle the Resistance Crisis
Licensed Content Author	Markus Lakemeyer, Weining Zhao, Franziska A. Mandl, et al
Licensed Content Date	Oct 11, 2018
Licensed Content Volume	0
Licensed Content Issue	0
Licensed Content Pages	38
Type of use	Dissertation/Thesis
Requestor type	Author of this Wiley article
Format	Print and electronic
Portion	Full article
Will you be translating?	No
Title of your thesis / dissertation	Probing the catalytic activity and oligomeric assembly of S. aureus ClpXP
Expected completion date	Nov 2018
Expected size (number of pages)	160
Requestor Location	Lichtenbergstr 4 Organische Chemie II Lichtenbergstr. 4 Garching, Bavaria 85748 Germany Attn: Lichtenbergstr 4
Publisher Tax ID	EU826007151
Total	0.00 EUR

Terms and Conditions

TERMS AND CONDITIONS

This copyrighted material is owned by or exclusively licensed to John Wiley & Sons, Inc. or one of its group companies (each a "Wiley Company") or handled on behalf of a society with which a Wiley Company has exclusive publishing rights in relation to a particular work

Part IV

APPENDIX

7

Experimental Section for Chapter 4

7.1 CHEMICAL SYNTHESIS

7.1.1 MATERIALS AND METHODS

All reagents were purchased in reagent grade or higher purity from commercial suppliers (Sigma-Aldrich, Thermo Fisher Scientific, TCI Europe, Alfa Aesar, Acros Organics, Merck) and were used without further purifications. Solvents used for chemical reactions were HPLC grade or of higher purity. Distilled technical solvents were used for reaction workup and chromatography. All reactions sensitive to air or moisture were performed in flame-dried glassware under positive pressure of argon using anhydrous solvents. All temperatures were measured externally.

Analytical thin-layer chromatography was carried out on silica gel 60 F254 plates (Merck), with visualization by short-wave UV light ($\lambda = 254, 366 \text{ nm}$) and/or staining with KMnO_4 or cerium ammonium molybdate (CAM) stain. Flash column chromatography was performed on silica gel (Geduran Si 60, 40-63 μm , Merck).

Reversed-phase HPLC-HR-ESI-MS, HPLC-HR-APCI-MS mass spectra were recorded on a Thermo LTQ FT Ultra coupled to a Dionex UltiMate 3000 HPLC system. A Waters XBridge C18 column (3.5 μm , 4.6 x 100 mm, flow rate = 1.1 ml/min) was used for separation of analytes. The column temperature was maintained at 30 °C. The mobile phase for elution consisted of a gradient mixture of 0.1% (v/v) formic acid in water (buffer A) and 0.1% (v/v) formic acid in acetonitrile:water 90:10 (buffer B).

Preparative reversed-phase HPLC separation was performed on a Waters 2695 quaternary gradient module, equipped with an X-Bridge™ Prep C18 5 μm OBD™ (30 x 150 mm) column, a Waters 2998 PDA detector and a Waters Fraction Collector III. Eluents for analytical and preparative RP-HPLC were 0.1% (v/v) TFA in water (buffer A) and 0.1% (v/v) TFA in acetonitrile (buffer B).

Enantiopurity was determined by analytical HPLC (Dionex P580 pump, ASI-100 automated sample injector, UVD 340 U photodiode array detector) using a chiral stationary phase (Daicel Chiralpak AD-H 250x4.6 mm, 5 μm , Chemical Industries). Runs were performed isocratically (*n*-heptan/*i*PrOH, 50/50 (v/v), 20min; flow rate: 1.0 mL/min,) at 20 °C with UV detection ($\lambda = 254 \text{ nm}$).

^1H - and ^{13}C -NMR spectra of small molecules were recorded on Bruker instruments (300 MHz, 400 MHz, 500 MHz or 500 MHz cryo) and referenced to the residual proton signal of the deuterated solvent. ^{19}F -NMR spectra were recorded on a 400 MHz Bruker instrument and were not referenced to an internal standard.

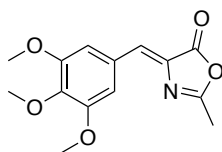
Chemical shifts are reported in parts per million (ppm). Coupling constants (J) are given in Hertz and multiplicity is reported as followed: s = singlet, brs = broad singlet, d = doublet, t = triplet, q = quartet, m = multiplet or unresolved.

7.1.2 SYNTHETIC PROTOCOLS

Synthesis of the unnatural amino acid Tmo

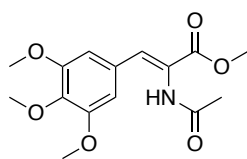
The synthesis of both enantiomers of the unnatural amino acid 3,4,5-trimethoxy-phenylalanine was performed based on known procedures.^[1,2]

(Z)-2-Methyl-4-(3,4,5-trimethoxybenzylidene)oxazol-5(4H)-one (1)



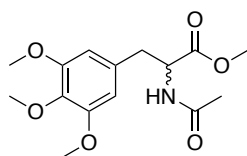
To a mixture of 3,4,5-trimethoxybenzaldehyde (44.0 g, 224 mmol, 1.00 eq), *N*-acetyl glycine (28.8 g, 246 mmol, 1.10 eq) and sodium acetate (20.6 g, 251 mmol, 1.12 eq) was added acetic anhydride (112 mL). The suspension was stirred at 125 °C for 5 h until RP-HPLC-MS showed no residual aldehyde. After cooling to room temperature, a solution of water/ethanol (2/1 (v/v), 3 L) was added and stirred for 30 min. The precipitate was filtered and washed with water/ethanol (2/1, (v/v)). Lyophilization yielded the product (40.0 g, 144 mmol, 64%). **TLC**: R_f = 0.66 (0.5% MeOH, DCM). **$^1\text{H-NMR}$** (400 MHz, CDCl_3): δ [ppm] = 7.39 (s, 2H), 7.04 (s, 1H), 3.90-3.91 (m, 9H), 2.39 (s, 3H). **$^{13}\text{C-NMR}$** (75 MHz, CDCl_3): δ [ppm] = 68.0, 165.8, 153.3, 141.2, 131.8, 131.5, 128.7, 109.7, 77.6, 77.2, 76.7, 61.2, 56.3, 15.9. **HRMS** (ESI): m/z calcd for $\text{C}_{14}\text{H}_{15}\text{NO}_5$: 278.1023 $[\text{M} + \text{H}]^+$, found: 278.1021.

Methyl (Z)-2-acetamido-3-(3,4,5-trimethoxyphenyl)acrylate (2)



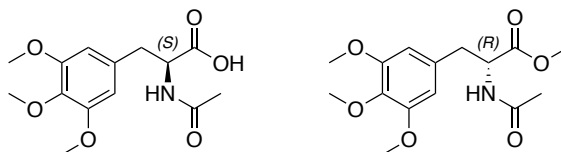
To a suspension of **1** (39.8 g, 144 mmol, 1.00 eq) in MeOH (400 mL) at 0 °C was added sodium methanolate (10.1 g, 187 mmol, 1.30 eq). The mixture was allowed to warm to room temperature and stirred for additional 1.5 h. The solvent was removed under reduced pressure and the residue was dissolved in semi-saturated ammonium chloride (200 mL) and extracted with DCM (3 x 250 mL). The combined organic extracts were dried over MgSO₄ and concentrated under reduced pressure. For further purification, the residue was dissolved in 40% DCM in hexanes (300 mL) and precipitated by addition of hexanes (100 mL). Filtration yielded the product as a pale-yellow solid (38.2 g, 123 mmol, 86%). **TLC**: R_f = 0.34 (2% MeOH, DCM). **¹H-NMR** (400 MHz, CDCl₃): δ [ppm] = 7.89 (s, 1H), 7.21 (s, 1H), 6.91 (s, 2H), 3.81 (s, 6H), 3.75 (d, J = 1.7 Hz, 6H), 2.05 (s, 3H). **¹³C-NMR** (126 MHz, CDCl₃): δ [ppm] = 170.3, 166.6, 154.0, 139.9, 133.0, 129.9, 126.1, 108.2, 60.8, 56.6, 52.8, 22.9. **HRMS** (ESI): m/z calcd for C₁₅H₁₉NO₆: 310.1285 [M + H]⁺, found: 310.1285.

rac-Methyl 2-acetamido-3-(3,4,5-trimethoxyphenyl)propanoate (3)



To a solution of **3** (14.9 g, 48.1 mmol) in methanol (400 mL) was added Pd/C (10%, 1.6 g). The mixture was stirred under an atmosphere of H₂ at room temperature for 16 h and filtered over a pad of Celite. The solvent was reduced under removed pressure, yielding the product as a white solid (14.8 g, 47.6 mmol). **TLC**: R_f = 0.33 (2% MeOH, DCM). **¹H-NMR** (400 MHz, CD₃CN): δ [ppm] = 6.66 (brs, 1H), 6.47 (s, 2H), 4.61 (td, J = 7.9, 5.5 Hz, 1H), 3.78 (s, 6H), 3.68 (s, 3H), 3.67 (s, 3H), 3.05 – 2.84 (m, 2H), 1.86 (s, 3H). **¹³C-NMR** (126 MHz, CD₃CN): δ [ppm] = 173.0, 170.5, 154.1, 137.5, 133.6, 107.3, 60.6, 56.5, 54.6, 52.6, 38.2, 22.7. **HRMS** (ESI): m/z calcd for C₁₅H₂₁NO₆: 312.1442 [M + H]⁺, found: 312.1442.

(S)-2-Acetamido-3-(3,4,5-trimethoxyphenyl)propanoic acid (5) and (R)-Methyl 2-acetamido-3-(3,4,5-trimethoxyphenyl)propanoate (4)



To a suspension of pulverized **3** (9.80 g, 31.5 mmol) in aqueous NaHCO₃ solution (0.2 M, pH = 8.4, 340 mL) was added Alcalase (protease from *B. licheniformis* >2.4 U/g, Sigma-Aldrich, 2.5 mL). The solution was stirred at room temperature while maintaining the pH value. When RP-HPLC-MS showed full conversion (*i.e.* 50%, 6 h), the pH was adjusted to 9. For the purification of **4**, the solution was extracted with DCM (3 x 400 mL). The combined organic fractions were washed with brine (200 mL), dried over MgSO₄ and concentrated under reduced pressure. **4** was obtained as a white solid (4.94 g, 15.9 mmol, 50%). For the purification of **5**, the aqueous layer was adjusted to pH = 1 and saturated with sodium chloride. The aqueous layer was extracted with EtOAc (3 x 400 mL). The combined organic extracts were dried over MgSO₄ and concentrated under reduced pressure and additionally dried under high vacuum. Compound **5** was obtained as an off-white solid (4.34 g, 14.6 mmol, 46%).

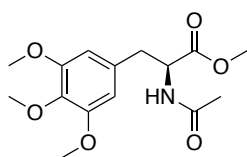
(S)-2-acetamido-3-(3,4,5-trimethoxyphenyl)propanoic acid (5):

TLC: R_f = 0.17 (4% MeOH, 0.5% AcOH, DCM). **¹H-NMR** (500 MHz, CDCl₃): δ [ppm] = 6.38 (s, 2H), 6.26 (d, *J* = 7.6 Hz, 1H), 5.86 (brs, 1H), 4.81 (dt, *J* = 7.5, 6.0 Hz, 1H), 3.81 (s, 3H), 3.81 (s, 6H), 3.09 (ddd, *J* = 49.1, 14.1, 6.0 Hz, 2H), 2.01 (s, 3H). **¹³C-NMR** (101 MHz, CDCl₃): δ [ppm] = 174.2, 171.3, 153.4, 137.1, 131.7, 106.4, 61.0, 56.2, 53.5, 37.6, 23.1. **HRMS** (ESI): *m/z* calcd for C₁₄H₂₀NO₆: 298.1285 [M + H]⁺, found: 298.1284.

(R)-methyl 2-acetamido-3-(3,4,5-trimethoxyphenyl)propanoate (4):

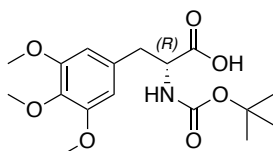
TLC: R_f = 0.33 (2% MeOH, DCM). **¹H-NMR** (400 MHz, CDCl₃): δ [ppm] = 6.30 (s, 2H), 5.93 (d, *J* = 7.8 Hz, 1H), 4.86 (dt, *J* = 7.8, 5.8 Hz, 1H), 3.82 (s, 3H), 3.82 (s, 6H), 3.74 (s, 3H), 3.07 (dd, *J* = 5.8, 1.4 Hz, 2H), 2.00 (s, 3H). **¹³C-NMR** (75 MHz, CDCl₃): δ [ppm] = 172.2, 169.6, 153.4, 137.2, 131.6, 106.3, 61.0, 56.2, 53.3, 52.5, 38.2, 23.4. **HRMS** (ESI): *m/z* calcd for C₁₅H₂₁NO₆: 312.1442 [M + H]⁺, found: 312.1442.

Methyl (*S*)-2-acetamido-3-(3,4,5-trimethoxyphenyl)propanoate (6)



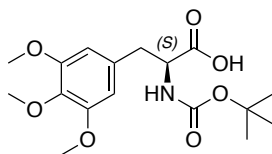
Compound **5** (4.32 g, 14.5 mmol, 1.00 eq) and *p*-toluenesulfonic acid (0.28 g, 1.45 mmol, 0.10 eq) in methanol (150 mL) was stirred at 80 °C for 6 h and cooled to room temperature. The solvent was removed under reduced pressure, the residue was dissolved in DCM (180 mL) and washed with 5% NaHCO₃ (3 x 50 mL), brine (30 mL). The organic phase was dried over MgSO₄ and the solvent was removed under reduced pressure. The product (4.14 g, 13.3 mmol, 92%) was used for the next step without further purification.

(*R*)-2-((*tert*-Butoxycarbonyl)amino)-3-(3,4,5-trimethoxyphenyl)propanoic acid (7)



To a solution of **4** (4.89 g, 15.7 mmol, 1.00 eq) and DMAP (0.38 g, 3.14 mmol, 0.20 eq) in THF (100 mL) was added di-*tert*-butyl dicarbonate (7.22 mL, 6.86 g, 31.4 mmol, 2.00 eq). The solution was stirred at 75 °C for 3 h and cooled to room temperature. 2 M LiOH (80 mL) was added and stirred at room temperature for 5 h until full ester hydrolysis. THF was evaporated under reduced pressure, the aqueous layer was adjusted to pH = 11 and washed with hexanes (2 x 70 mL). The aqueous layer was then adjusted to pH = 2-3 and cooled to 0 °C. A white precipitate formed, which was collected by filtration and washed with ice-cold water. Lyophilization of the residue yielded the product as a white solid (5.36 g, 15.1 mmol, 96%). **TLC**: R_f = 0.27 (3% MeOH, 0.5% AcOH, DCM). **¹H-NMR** (400 MHz CD₃CN): δ [ppm] = 6.51 (s, 2H), 5.50 (s, 1H), 4.41 – 4.27 (m, 1H), 3.79 (s, 6H), 3.68 (s, 3H), 3.08 (dd, *J* = 13.9, 4.9 Hz, 1H), 2.81 (dd, *J* = 14.0, 9.3 Hz, 1H), 1.35 (s, 9H). **¹³C-NMR** (101 MHz, CD₃CN): δ [ppm] = 173.6, 156.4, 154.1, 137.6, 133.9, 107.5, 79.9, 60.7, 56.6, 55.5, 38.2, 28.4. **HRMS** (ESI): *m/z* calcd for C₁₇H₂₅NO₇: 717.3422 [2M + Li]⁺, found: 717.3407.

(S)-2-((*tert*-Butoxycarbonyl)amino)-3-(3,4,5-trimethoxyphenyl)propanoic acid (8)

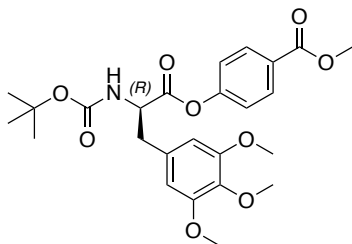


To a solution of **6** (4.05 g, 13.0 mmol, 1.00 eq) and DMAP (0.32 g, 2.60 mmol, 0.20 eq) in THF (90 mL) was added di-*tert*-butyl dicarbonate (5.96 mL, 5.67 g, 26.0 mmol, 2.00 eq). The solution was stirred at 75 °C for 3 h and cooled to room temperature. 2 M LiOH (50 mL) was added and stirred at room temperature for 3 h until full ester hydrolysis. THF was evaporated under reduced pressure and the aqueous layer was adjusted to pH = 11 and washed with hexanes (2 x 50 mL). The aqueous layer was then adjusted to pH = 2-3 and cooled to 0 °C. A white precipitate formed, which was collected by filtration and washed with ice-cold water. Lyophilization of the residue yielded the product as a white solid (4.03 g, 11.3 mmol, 87%). **TLC**: $R_f = 0.27$ (3% MeOH, 0.5% AcOH, DCM). **¹H-NMR** (400 MHz, CD₃CN): δ [ppm] = 6.53 (s, 2H), 5.56 (s, 1H), 4.37 (s, 1H), 3.79 (d, $J = 0.7$ Hz, 6H), 3.68 (d, $J = 0.8$ Hz, 3H), 3.17 – 3.05 (m, 1H), 2.85 – 2.75 (m, 1H), 1.35 (s, 9H). **¹³C-NMR** (126 MHz, CD₃CN): δ [ppm] = 174.4, 156.4, 154.0, 137.4, 133.9, 107.4, 79.9, 60.6, 56.5, 55.7, 38.2, 28.4. **HRMS** (ESI): m/z calcd for C₁₇H₂₅NO₇: 717.3422 [2M + Li]⁺, found: 717.3410.

General procedure 1: Synthesis of phenyl esters (GP1)

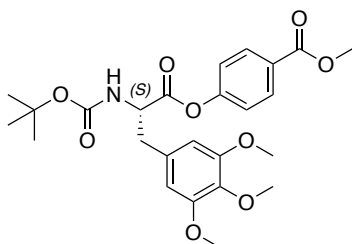
Under an argon atmosphere, the amino acid (1.00 eq) and methyl-4-hydroxybenzoate (1.05 eq) were dissolved in minimal amounts of anhydrous DCM/DMF and cooled to 0 °C. 1-Ethyl-3-(3-dimethylaminopropyl)carbodiimide-hydrochloride (EDC · HCl, 1.05 eq), hydroxybenzotriazole (HOBT · xH₂O, 1.50 eq) and DIPEA (2.00 eq) were added. The solution was stirred and allowed to warm to room temperature overnight. If DMF was used, the solvent was removed under reduced pressure. For workup, the residue/reaction mixture was diluted with DCM and washed with 5% citric acid (3x), 5% NaHCO₃ (3x) and brine (1x). The organic phase was dried over MgSO₄ and the solvent was removed under reduced pressure. Purification was performed by column chromatography or preparative RP-HPLC.

Methyl (*R*)-4-((2-((*tert*-butoxycarbonyl)amino)-3-(3,4,5-trimethoxyphenyl)propanoyl)oxy)-benzoate (9)



The compound was synthesized according to GP1, starting from **7** (2.68 g, 7.54 mmol, 1.00 eq), methyl-4-hydroxybenzoate (1.20 g, 7.92 mmol, 1.05 eq), EDC·HCl (2.17 g, 11.3 mmol, 1.50 eq), HOBT·xH₂O (1.53 g, 11.3 mmol, 1.50 eq) and DIPEA (2.63 mL, 1.95 g, 15.1 mmol, 2.00 eq) in DCM (100 mL). Column chromatography (hexanes/EtOAc, 4/1 → 1/1) yielded the product as a white solid (2.95 g, 6.02 mmol, 80%). **TLC**: R_f = 0.27 (hexanes/EtOAc, 3/1, v/v). **¹H-NMR** (500 MHz, CDCl₃): δ [ppm] = 8.05 (d, *J* = 8.4 Hz, 2H), 7.09 (d, *J* = 8.4 Hz, 2H), 6.42 (s, 2H), 5.11 – 5.04 (m, 1H), 4.82 – 4.74 (m, 1H), 3.91 (s, 3H), 3.84 (s, 3H), 3.81 (s, 6H), 3.16 (d, *J* = 6.2 Hz, 2H), 1.45 (s, 9H). **¹³C-NMR** (101 MHz, CDCl₃): δ [ppm] = 170.3, 166.3, 155.2, 154.0, 153.5, 137.4, 131.3, 131.3, 128.2, 121.4, 106.4, 80.6, 61.0, 56.2, 54.9, 52.4, 38.8, 28.4. **HRMS** (ESI): *m/z* calcd for C₂₅H₃₁NO₉: 531.2337 [M + MeCN + H]⁺, found: 531.2340. Chiral HPLC: t_R = 7.39 min (major), t_R = 8.98 min (minor); er: 97.2:2.8, 94% ee.

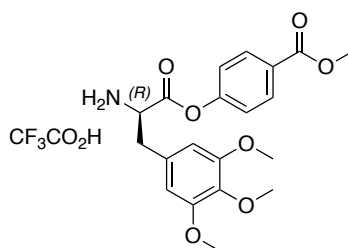
Methyl (*S*)-4-((2-((*tert*-butoxycarbonyl)amino)-3-(3,4,5-trimethoxyphenyl)propanoyl)oxy)-benzoate (10)



The compound was synthesized according to GP1, starting from **8** (2.33 g, 6.56 mmol, 1.00 eq), methyl-4-hydroxybenzoate (1.05 g, 6.88 mmol, 1.05 eq), EDC·HCl (1.89 g, 9.83 mmol, 1.50 eq), HOBT·xH₂O (1.33 g, 9.83 mmol, 1.50 eq) and DIPEA (2.28 mL, 1.69 g, 15.1 mmol, 2.00 eq) in DCM (100 mL). Column chromatography (hexanes/EtOAc, 4/1 → 1/1) yielded the product as a white solid (2.56 g, 5.22 mmol, 80%). **TLC**: R_f = 0.27 (hexanes/EtOAc, 3/1, v/v). **¹H-NMR** (500 MHz, CDCl₃): δ [ppm] = 8.06 (d,

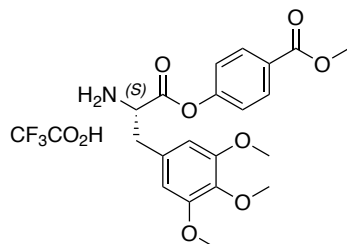
$J = 8.7$ Hz, 2H), 7.09 (d, $J = 8.7$ Hz, 2H), 6.42 (s, 2H), 5.07 (d, $J = 8.2$ Hz, 1H), 4.79 (d, $J = 7.2$ Hz, 1H), 3.91 (s, 3H), 3.84 (s, 3H), 3.81 (s, 6H), 3.17 (d, $J = 5.8$ Hz, 2H), 1.45 (s, 9H). **$^{13}\text{C-NMR}$** (75 MHz, CDCl_3): δ [ppm] = 170.3, 166.3, 155.2, 153.9, 153.5, 137.3, 131.3, 131.3, 128.2, 121.4, 106.3, 80.6, 61.0, 56.2, 54.9, 52.4, 38.8, 28.4. **HRMS** (ESI): m/z calcd for $\text{C}_{25}\text{H}_{31}\text{NO}_9$: 531.2337 [$\text{M} + \text{MeCN} + \text{H}$] $^+$, found: 531.2340. Chiral HPLC: $t_R = 8.96$ min (major), $t_R = 7.39$ min (minor); er: 98.8:1.2, 97% ee.

Methyl (*R*)-4-((2-amino-3-(3,4,5-trimethoxyphenyl)propanoyl)oxy)benzoate • TFA (11)



For deprotection, **9** (1.50 g, 3.06 mmol) was dissolved in anhydrous DCM (20 mL) and cooled to 0°C. TFA (5 mL) was added and the reaction was stirred at 0°C for 5 h. The solvent was removed under reduced pressure and the residue was co-evaporated with toluene to remove residual TFA. The residue was dissolved in a mixture of MeCN/water and lyophilized to yield the product as a white solid (1.52 g, 3.02 mmol, 98%). For subsequent synthesis, the compound was used without further purification. For biochemical testing and analytics, a small portion of the compound was purified by RP-HPLC. **TLC**: $R_f = 0.56$ (2% MeOH, 2% Triethylamine, DCM). **$^1\text{H-NMR}$** (500 MHz, CDCl_3): δ [ppm] = 7.99 (d, $J = 8.8$ Hz, 2H), 7.08 (d, $J = 8.8$ Hz, 2H), 6.51 (s, 2H), 4.43 (dd, $J = 7.9, 5.8$ Hz, 1H), 3.89 (s, 3H), 3.75 (s, 6H), 3.71 (s, 3H), 3.29 (qd, $J = 14.3, 6.8$ Hz, 2H). **$^{13}\text{C-NMR}$** (101 MHz, CDCl_3): δ [ppm] = 167.5, 166.0, 153.6, 153.2, 137.4, 131.4, 128.8, 128.8, 121.1, 106.6, 60.9, 56.1, 54.5, 52.5, 36.7. **HRMS** (ESI): m/z calcd for $\text{C}_{20}\text{H}_{23}\text{NO}_7$: 390.1547 [$\text{M} + \text{H}$] $^+$, found: 390.1548. Chiral HPLC: $t_R = 12.87$ min (major), $t_R = 8.22$ min (minor); er: 97.2:2.8, 94% ee.

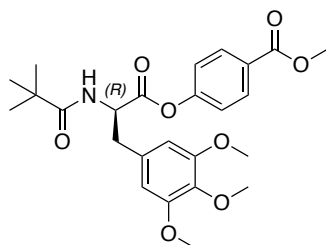
Methyl (*S*)-4-((2-amino-3-(3,4,5-trimethoxyphenyl)propanoyl)oxy)benzoate • TFA (12)



For deprotection, **10** (1.28 g, 2.61 mmol) was dissolved in anhydrous DCM (20 mL) and cooled to 0 °C. TFA (5 mL) was added and the reaction was stirred at 0 °C for 5 h. The solvent was removed under reduced pressure and the residue was co-evaporated with toluene to remove residual TFA. The residue was dissolved in a mixture of MeCN/water and lyophilized to yield the product as a white solid in quantitative yield. For subsequent synthesis, the compound was used without further purification. For biochemical testing and analytics, a small portion of the compound was purified by RP-HPLC. **TLC**: $R_f = 0.56$ (2% MeOH, 2% Triethylamine, DCM). **$^1\text{H-NMR}$** (400 MHz, CDCl_3): δ [ppm] = 8.00 (d, $J = 8.8$ Hz, 2H), 7.08 (d, $J = 8.8$ Hz, 2H), 6.51 (s, 2H), 4.44 (dd, $J = 8.1, 5.7$ Hz, 1H), 3.89 (s, 3H), 3.75 (s, 6H), 3.70 (s, 3H), 3.30 (qd, $J = 14.3, 6.8$ Hz, 2H). **$^{13}\text{C-NMR}$** (101 MHz, CDCl_3): δ [ppm] = 167.5, 166.0, 153.6, 153.2, 137.4, 131.5, 128.8, 128.8, 121.1, 106.5, 77.5, 77.2, 76.8, 60.9, 56.1, 54.6, 52.5, 36.7. **HRMS** (ESI): m/z calcd for $\text{C}_{20}\text{H}_{23}\text{NO}_7$: 390.1547 [$\text{M} + \text{H}$] $^+$, found: 390.1546. Chiral HPLC: $t_R = 8.16$ min (major), $t_R = 13.18$ min (minor); er: 99.0:1.0, 98% ee.

Methyl

(*R*)-4-((2-pivalamido-3-(3,4,5-trimethoxyphenyl)propanoyl)oxy)benzoate (13)

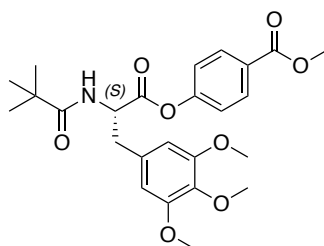


Compound **11** (80 mg, 0.16 mmol, 1.00 eq) was dissolved in DCM (3 mL) and cooled to 0 °C. Pivaloyl chloride (23 μL , 23 mg, 0.19 mmol, 1.20 eq) and triethylamine (44 μL , 32 mg, 0.32 mmol, 2.00 eq) were added and the solution was stirred at 0 °C for 2 h. The solution was warmed to room temperature, diluted with DCM (10 mL) and washed

with 5% citric acid (3 x 2 mL) and brine (5 mL), dried. The organic phase was dried over MgSO₄ and the solvent was removed under reduced pressure. The crude product was purified by RP-HPLC and column chromatography (0.5% MeOH in DCM), yielding the product as a white solid (30 mg, 63 μmol, 40%). **TLC**: R_f = 0.54 (1.5% MeOH in DCM). **¹H-NMR** (500 MHz, CDCl₃): δ [ppm] = 8.10 – 8.02 (m, 2H), 7.15 – 7.08 (m, 2H), 6.41 (s, 2H), 6.24 (d, *J* = 7.5 Hz, 1H), 5.06 (dt, *J* = 7.4, 6.2 Hz, 1H), 3.92 (s, 3H), 3.84 (s, 3H), 3.80 (s, 6H), 3.30 – 3.16 (m, 2H), 1.20 (s, 9H). **¹³C-NMR** (126 MHz, CDCl₃): δ [ppm] = 178.4, 170.2, 166.3, 153.9, 153.5, 137.4, 131.4, 131.2, 128.2, 121.3, 106.3, 61.0, 56.2, 53.4, 52.4, 38.8, 38.3, 27.5. **HRMS** (ESI): *m/z* calcd for C₂₅H₃₁NO₈: 474.2122 [M + H]⁺, found: 474.2124. Chiral HPLC: t_R = 5.43 min (major), tt_R = 4.90 min (minor); er: 99.1:0.9, 98% ee.

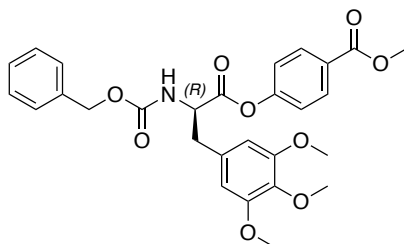
Methyl

(*S*)-4-((2-pivalamido-3-(3,4,5-trimethoxyphenyl)propanoyl)oxy)benzoate (**14**)



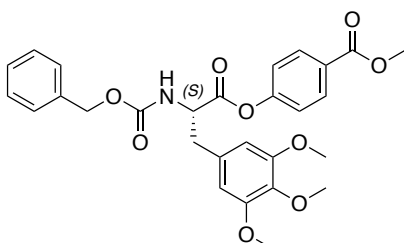
Compound **12** (100 mg, 0.20 mmol, 1.00 eq) was dissolved in DCM (4 mL) and cooled to 0 °C. Pivaloyl chloride (29 μL, 29 mg, 0.24 mmol, 1.20 eq) and triethylamine (54 μL, 40 mg, 0.40 mmol, 2.00 eq) were added and the solution was stirred at 0 °C for 2 h. The solution was warmed to room temperature, diluted with DCM (10 mL) and washed with 5% citric acid (3 x 2 mL) and brine (5 mL), dried. The organic phase was dried over MgSO₄ and the solvent was removed under reduced pressure. The crude product was purified by RP-HPLC, yielding the product as a white solid (86 mg, 0.18 mmol, 92%). **TLC**: R_f = 0.54 (1.5% MeOH in DCM). **¹H-NMR** (500 MHz, CDCl₃): δ [ppm] = 8.06 (d, *J* = 8.7 Hz, 2H), 7.12 (d, *J* = 8.7 Hz, 2H), 6.41 (s, 2H), 6.20 (d, *J* = 7.5 Hz, 1H), 5.08 – 5.03 (m, 1H), 3.92 (s, 3H), 3.84 (s, 3H), 3.80 (s, 6H), 3.22 (s, 2H), 1.20 (s, 9H). **¹³C-NMR** (126 MHz, CDCl₃): δ [ppm] = 178.8, 170.1, 166.3, 153.9, 153.6, 137.4, 131.4, 131.2, 128.3, 121.3, 106.3, 61.1, 56.2, 53.4, 52.5, 38.9, 38.3, 27.5. **HRMS** (ESI): *m/z* calcd for C₂₅H₃₁NO₈: 474.2122 [M + H]⁺, found: 474.2124. Chiral HPLC: t_R = 4.90 min (major), t_R = 5.45 min (minor); er: 98.8:1.2, 97% ee.

Methyl (*R*)-4-((2-(((benzyloxy)carbonyl)amino)-3-(3,4,5-trimethoxyphenyl)propanoyl)oxy)-benzoate (15)



Compound **11** (10 mg, 0.10 mmol, 1.00 eq) was dissolved in DCM (2 mL) and cooled to 0 °C. Benzyl chloroformate (29 μ L, 35 mg, 0.20 mmol, 2.00 eq) and triethylamine (28 μ L, 21 mg, 0.20 mmol, 2.0 eq) were added and the solution was stirred at 0 °C for 5 h. The solution was warmed to room temperature, diluted with DCM (10 mL) and washed with 5% citric acid (3 x 2 mL) and brine (5 mL). The organic phase was dried over MgSO_4 and the solvent was removed under reduced pressure. The crude product was purified by column chromatography (0.3% MeOH in DCM) and RP-HPLC, yielding the product as a white solid (20 mg, 38 μ mol, 38%). **TLC**: $R_f = 0.25$ (1% MeOH in DCM). **$^1\text{H-NMR}$** (500 MHz, CDCl_3): δ [ppm] = 8.06 (d, $J = 8.3$ Hz, 2H), 7.39 – 7.29 (m, 5H), 7.08 (d, $J = 8.3$ Hz, 2H), 6.39 (s, 2H), 5.30 (d, $J = 8.1$ Hz, 1H), 5.15 (q, $J = 12.2$ Hz, 2H), 4.88 (q, $J = 6.7$ Hz, 1H), 3.92 (s, 3H), 3.83 (s, 3H), 3.76 (s, 6H), 3.26 – 3.11 (m, 2H). **$^{13}\text{C-NMR}$** (126 MHz, CDCl_3): δ [ppm] = 169.9, 166.3, 155.8, 153.9, 153.6, 137.4, 136.1, 131.4, 130.9, 128.8, 128.5, 128.4, 128.3, 121.4, 106.3, 67.4, 61.0, 56.2, 55.2, 52.5, 38.7. **HRMS** (ESI): m/z calcd for $\text{C}_{28}\text{H}_{29}\text{NO}_9$: 524.1915 $[\text{M} + \text{H}]^+$, found: 524.1917.

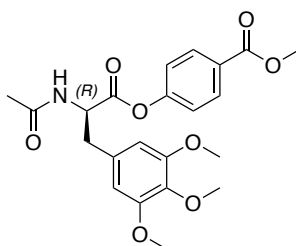
Methyl (*S*)-4-((2-(((benzyloxy)carbonyl)amino)-3-(3,4,5-trimethoxyphenyl)propanoyl)oxy)-benzoate (16)



Compound **12** (75 mg, 0.15 mmol, 1.00 eq) was dissolved in DCM (3 mL) and cooled to 0 °C. Benzyl chloroformate (53 μ L, 64 mg, 0.37 mmol, 2.50 eq) and triethylamine (42 μ L, 30 mg, 0.30 mmol, 2.00 eq) were added and the solution was stirred at 0 °C for 8 h. The solution was warmed to room temperature, diluted with DCM (10 mL) and washed

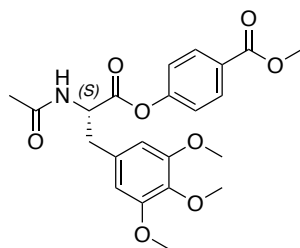
with 5% citric acid (3 x 2 mL) and brine (5 mL), dried. The organic phase was dried over MgSO_4 and the solvent was removed under reduced pressure. The crude product was purified by column chromatography (0.5% MeOH in DCM) and RP-HPLC, yielding the product as a white solid (36 mg, 69 μmol , 46%). **TLC:** $R_f = 0.25$ (1% MeOH in DCM). **$^1\text{H-NMR}$** (500 MHz, CDCl_3): δ [ppm] = 8.06 (d, $J = 8.4$ Hz, 2H), 7.39 – 7.30 (m, 5H), 7.08 (d, $J = 8.3$ Hz, 2H), 6.39 (s, 2H), 5.34 – 5.28 (m, 1H), 5.15 (q, $J = 12.2$ Hz, 2H), 4.88 (q, $J = 6.7$ Hz, 1H), 3.92 (s, 3H), 3.83 (s, 3H), 3.76 (s, 6H), 3.26 – 3.14 (m, 2H). **$^{13}\text{C-NMR}$** (126 MHz, CDCl_3): δ [ppm] = 169.9, 166.3, 155.8, 153.9, 153.5, 137.4, 136.1, 131.4, 130.9, 128.8, 128.5, 128.4, 128.3, 121.4, 106.3, , 67.4, 61.0, 56.2, 55.2, 52.4, 38.7. **HRMS** (ESI): m/z calcd for $\text{C}_{28}\text{H}_{29}\text{NO}_9$: 524.1915 $[\text{M} + \text{H}]^+$, found: 524.1917.

Methyl (*R*)-4-((2-acetamido-3-(3,4,5-trimethoxyphenyl)propanoyl)oxy)-benzoate (49)



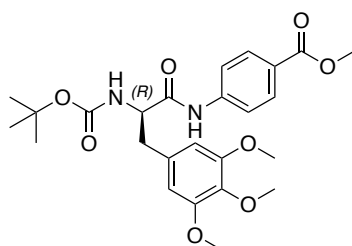
Compound **11** (50 mg, 0.10 mmol, 1.00 eq) was dissolved in DCM (2.5 mL) and cooled to 0 °C. Acetic anhydride (28 μL , 30 mg, 0.30 mmol, 1.50 eq) and DIPEA (42 μL , 31 mg, 0.24 mmol, 1.20 eq) were added and the solution was warmed to room temperature and stirred for 2 h. The solvent was removed under reduced pressure. The crude product was purified by RP-HPLC, yielding the product as a white solid (37 mg, 86 μmol , 86%). **TLC:** $R_f = 0.12$ (1% MeOH in DCM). **$^1\text{H-NMR}$** (400 MHz, CD_3CN): δ [ppm] = 8.03 (d, $J = 8.7$ Hz, 2H), 7.12 (d, $J = 8.8$ Hz, 2H), 6.90 (d, $J = 7.0$ Hz, 1H), 6.58 (s, 2H), 4.77 (dt, $J = 7.9, 6.6$ Hz, 1H), 3.87 (s, 3H), 3.78 (s, 6H), 3.70 (s, 3H), 3.21 – 3.02 (m, 2H), 1.92 (s, 3H). **$^{13}\text{C-NMR}$** (126 MHz, CDCl_3): δ [ppm] = 171.2, 171.0, 166.9, 155.3, 154.3, 137.9, 133.3, 131.9, 129.1, 122.7, 107.6, 60.8, 56.7, 55.4, 52.8, 38.0, 22.6. **HRMS** (ESI): m/z calcd for $\text{C}_{22}\text{H}_{25}\text{NO}_8$: 432.1653 $[\text{M} + \text{H}]^+$, found: 432.1652.

Methyl (*S*)-4-((2-acetamido-3-(3,4,5-trimethoxyphenyl)propanoyl)oxy)-benzoate (51)



Compound **12** (50 mg, 0.10 mmol, 1.00 eq) was dissolved in DCM (2.5 mL) and cooled to 0 °C. Acetic anhydride (28 μ L, 30 mg, 0.30 mmol, 1.50 eq) and DIPEA (42 μ L, 31 mg, 0.24 mmol, 1.2 eq) were added and the solution was warmed to room temperature and stirred for 2 h. The solvent was removed under reduced pressure. The crude product was purified by RP-HPLC, yielding the product as a white solid (28 mg, 65 μ mol, 65%). **TLC:** R_f = 0.12 (1% MeOH in DCM)₂ **¹H-NMR** (400 MHz, CDCl₃): δ [ppm] = 8.06 (d, J = 8.7 Hz, 2H), 7.09 (d, J = 8.8 Hz, 2H), 6.41 (s, 2H), 5.98 (d, J = 7.3 Hz, 1H), 5.08 (dt, J = 7.6, 6.3 Hz, 1H), 3.92 (s, 3H), 3.84 (s, 3H), 3.80 (s, 6H), 3.20 (qd, J = 13.9, 6.3 Hz, 2H), 2.06 (s, 3H). **¹³C-NMR** (126 MHz, CDCl₃): δ [ppm] = 170.1, 170.0, 166.3, 153.9, 153.6, 137.6, 131.4, 131.1, 128.4, 121.4, 106.4, 61.0, 56.3, 53.7, 52.4, 38.4, 23.3. **HRMS** (ESI): m/z calcd for C₂₂H₂₅NO₈: 432.1653 [M + H]⁺, found: 432.1652.

Methyl (*R*)-4-(2-((*tert*-butoxycarbonyl)amino)-3-(3,4,5-trimethoxyphenyl)propanamido)benzoate (17)

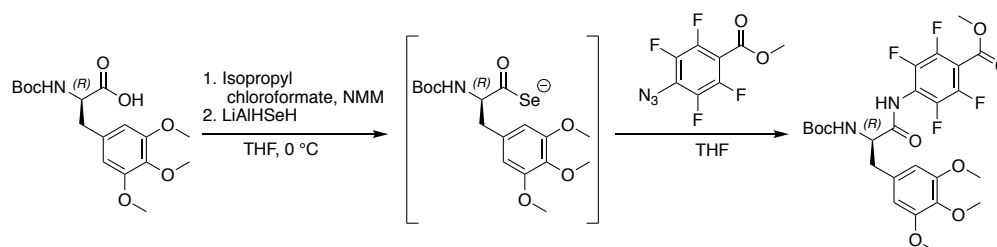


Compound **7** (500 mg, 1.41 mmol, 1.00 eq) and methyl-4-aminobenzoate (230 mg, 1.55 mmol, 1.10 eq) were dissolved in DMF (10 mL) and cooled to 0 °C. COMU (1.41 g, 3.38 mmol, 2.40 eq) and DIPEA (980 μ L, 0.73 g, 5.63 mmol, 4.00 eq) were added and the solution was stirred at room temperature for 48 h. The solvent was removed under reduced pressure and the residue was dissolved in DCM (20 mL). The organic phase was washed with 5% citric acid (3 x 5 mL), 5% NaHCO₃ (3 x 5 mL) and brine (10 mL). The

solvent was removed under reduced pressure and the crude product was purified using RP-HPLC, yielding the product (300 mg, 0.61 mmol, 44%) as an off-white solid. **TLC**: $R_f = 0.13$ (hexanes/EtOAc, 3/1, v/v). **$^1\text{H-NMR}$** (500 MHz, CD_3CN): δ [ppm] = 8.65 (brs, 1H), 7.93 (d, $J = 8.4$ Hz, 2H), 7.64 (d, $J = 8.4$ Hz, 2H), 6.52 (s, 2H), 5.68 (brs, 1H), 4.42 – 4.31 (m, 1H), 3.85 (s, 3H), 3.72 (s, 6H), 3.66 (s, 3H), 3.06 (dd, $J = 13.7, 6.1$ Hz, 1H), 2.88 (dd, $J = 13.7, 8.5$ Hz, 1H), 1.37 (s, 9H). **$^{13}\text{C-NMR}$** (101 MHz, CD_3CN): δ [ppm] = 171.8, 167.1, 156.5, 154.1, 143.5, 137.7, 133.8, 131.3, 126.3, 119.8, 107.5, 80.2, 60.7, 57.8, 56.5, 52.5, 39.0, 28.5. **HRMS** (ESI): m/z calcd for $\text{C}_{25}\text{H}_{32}\text{N}_2\text{O}_8$: 489.2231 $[\text{M} + \text{H}]^+$, found: 489.2229.

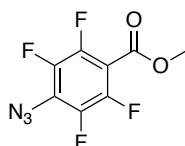
Synthesis of aryl amides via selenocarboxylates

Fluorinated aromatic amide **18** was synthesized according to Supporting Scheme 1, based on the protocol from Wu *et al.*^[3] LiAlHSeH was freshly prepared for each reaction, following the literature.^[3] In brief, to a suspension of LiAlH_4 (44.0 mg, 1.10 mmol) in anhydrous THF (10 mL) under argon was added selenium powder (88.0 mg, 1.10 mmol) in one portion at 0 °C. The mixture was stirred at 0 °C for 20 min and then directly used for the amidation reaction.



Supporting Scheme 1. Synthesis of **18** via selenocarboxylates.

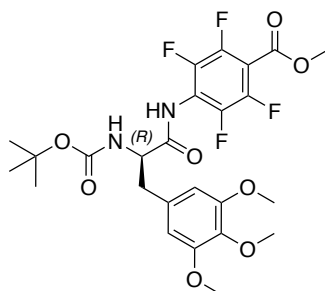
Methyl 4-azido-2,3,5,6-tetrafluorobenzoate (**52**)



The compound was synthesized according to Xi *et al.*, starting from methyl pentafluorobenzoate.^[4]

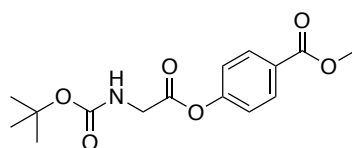
Methyl (*R*)-4-(2-((*tert*-butoxycarbonyl)amino)-3-(3,4,5-trimethoxyphenyl)propanamido)-2,3,5,6-tetrafluorobenzoate

(18)



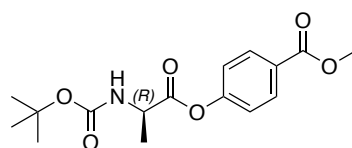
Under an argon atmosphere, a solution of **4** (391 mg, 1.10 mmol, 1.10 eq) and *N*-methylmorpholine (120 μ L, 1.10 mmol, 1.10 eq) in anhydrous THF (10 mL) was cooled to 0 °C. A solution of 1 M isopropyl chloroformate in toluene (1.10 mL, 1.10 mmol, 1.10 eq) was added and the mixture was stirred at 0 °C for 20 min. Then, the obtained mixed anhydride solution was added to a freshly prepared LiAlHSeH solution over 5 min. The mixture was stirred for additional 30 min while maintaining the temperature below 5 °C. Next, a solution of methyl 4-azido-2,3,5,6-tetrafluorobenzoate **52** (249 mg, 1.00 mmol, 1.00 eq) in anhydrous THF (1 mL) was added to the selenocarboxylate solution. The mixture was allowed to warm to room temperature and stirred for another 18 h. For workup, the solution was filtered over a pad of celite, which was subsequently rinsed with EtOAc (3 x 25 mL). The organic layer was washed with 5% NaHCO₃ (2 x 25 mL), water (2 x 25 mL), and brine (30 mL). The organic layer was dried over MgSO₄ and treated with activated charcoal which was subsequently filtered off over a pad of celite. The solvent was removed under reduced pressure. Column chromatography (hexanes/EtOAc, 10/1 \rightarrow 2/1) and RP-HPLC yielded the product as a white solid (175 mg, 0.31 mmol, 31%). **TLC**: R_f = 0.20 (1% MeOH in DCM). **¹H-NMR** (500 MHz, CD₃CN): δ [ppm] = 8.55 (s, 1H), 6.57 (s, 2H), 5.72 (d, *J* = 8.2 Hz, 1H), 4.53 – 4.43 (m, 1H), 3.94 (s, 3H), 3.79 (s, 6H), 3.69 (s, 3H), 3.14 (dd, *J* = 14.2, 5.4 Hz, 1H), 2.87 (dd, *J* = 13.9, 9.2 Hz, 1H), 1.36 (s, 9H). **¹³C-NMR** (126 MHz, CD₃CN): δ [ppm] = 171.3, 160.7, 156.5, 154.1, 145.9 (“d”*, *J* = 254 Hz), 143.2 (“d”*, *J* = 254 Hz), 137.6, 133.7, 120.9 – 120.5 (m), 110.8 – 110.5 (m), 107.5, 80.3, 60.6, 57.1, 56.5, 53.9, 38.3, 28.4. **¹⁹F-NMR** (471 MHz, CD₃CN): δ [ppm] = -141.9 – -142.2 (m, 2F), -145.0 – -145.5 (m, 2F). **HRMS** (ESI): *m/z* calcd for C₂₅H₂₈F₄N₂O₈: 561.1855 [M + H]⁺, found: 561.1852. *Splitting of the signal due to C-F-correlation.

Methyl 4-(((*tert*-butoxycarbonyl)glycyl)oxy)benzoate (19)



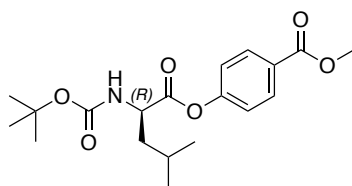
The compound was synthesized according to GP1, starting from Boc-Gly-OH (198 mg, 1.13 mmol, 1.00 eq), methyl-4-hydroxybenzoate (180 mg, 1.19 mmol, 1.05 eq), EDC · HCl (325 mg, 1.70 mmol, 1.50 eq), HOBT · xH₂O (230 mg, 1.70 mmol, 1.50 eq) and DIPEA (394 μL, 292 mg, 2.26 mmol, 2.00 eq) in DCM (20 mL). Preparative RP-HPLC yielded the product as a white solid (204 mg, 0.66 mmol, 58%). **TLC:** R_f = 0.58 (0.5% MeOH in DCM). **¹H-NMR** (500 MHz, CD₃CN): δ [ppm] = 8.04 (d, *J* = 8.1 Hz, 2H), 7.22 (d, *J* = 8.5 Hz, 2H), 5.76 (brs, 1H), 4.05 (d, *J* = 6.2 Hz, 2H), 3.87 (s, 3H), 1.43 (s, 9H). **¹³C-NMR** (126 MHz, CD₃CN): δ [ppm] = 170.2, 166.8, 156.9, 155.2, 131.9, 129.0, 122.8, 80.2, 52.8, 43.2, 28.4. **HRMS** (ESI): *m/z* calcd for C₂₂H₂₅NO₇: 619.2498 [2M + H]⁺, found: 619.2498.

Methyl 4-(((*tert*-butoxycarbonyl)-(*R*)-alanyl)oxy)benzoate (20)



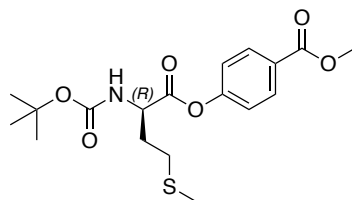
The compound was synthesized according to GP1, starting from Boc-(*R*)-Ala-OH (214 mg, 1.13 mmol, 1.00 eq), methyl-4-hydroxybenzoate (180 mg, 1.19 mmol, 1.05 eq), EDC · HCl (325 mg, 1.70 mmol, 1.50 eq), HOBT · xH₂O (230 mg, 1.70 mmol, 1.50 eq) and DIPEA (394 μL, 292 mg, 2.26 mmol, 2.00 eq) in DCM (12 mL). Column chromatography (0.5% MeOH in DCM) yielded the product as a white solid (203 mg, 0.63 mmol, 56%). **TLC:** R_f = 0.45 (0.5% MeOH in DCM). **¹H-NMR** (500 MHz, CDCl₃): δ [ppm] = 8.07 (d, *J* = 8.7 Hz, 2H), 7.18 (d, *J* = 8.7 Hz, 2H), 5.07 (s, 1H), 4.58 – 4.49 (m, 1H), 3.91 (s, 3H), 1.55 (d, *J* = 7.4 Hz, 3H), 1.46 (s, 9H). **¹³C-NMR** (101 MHz, CDCl₃): δ [ppm] = 171.7, 166.4, 155.3, 154.3, 131.4, 128.1, 121.5, 80.4, 52.4, 49.7, 28.5, 18.4. **HRMS** (ESI): *m/z* calcd for C₁₆H₂₁NO₆: 324.1442 [M + H]⁺, found: 324.1442.

Methyl 4-(((*tert*-butoxycarbonyl)-(*R*)-leucyl)oxy)benzoate (21)



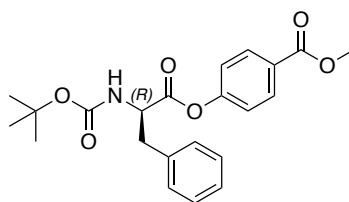
The compound was synthesized according to GP1, starting from Boc-(*R*)-Leu-OH (261 mg, 1.13 mmol, 1.00 eq), methyl-4-hydroxybenzoate (180 mg, 1.19 mmol, 1.05 eq), EDC · HCl (325 mg, 1.70 mmol, 1.50 eq), HOBT · xH₂O (230 mg, 1.70 mmol, 1.50 eq) and DIPEA (394 μL, 292 mg, 2.26 mmol, 2.00 eq) in DCM/DMF (12 mL/0.5 mL). Column chromatography (1.0% MeOH in DCM) yielded the product as a colorless oil which solidified upon standing (283 mg, 0.77 mmol, 68%). **TLC:** R_f = 0.51 (1% MeOH in DCM). **¹H-NMR** (500 MHz, CDCl₃): δ [ppm] = 8.07 (d, *J* = 8.7 Hz, 2H), 7.18 (d, *J* = 8.7 Hz, 2H), 4.93 (d, *J* = 8.5 Hz, 1H), 4.58 – 4.47 (m, 1H), 3.91 (s, 3H), 1.87 – 1.75 (m, 2H), 1.71 – 1.62 (m, 1H), 1.46 (s, 9H), 1.02 (d, *J* = 6.3 Hz, 6H). **¹³C-NMR** (126 MHz, CDCl₃): δ [ppm] = 171.9, 166.4, 155.6, 154.3, 131.3, 128.0, 121.6, 80.4, 52.5, 52.4, 41.5, 28.4, 25.1, 23.1, 22.0. **HRMS** (ESI): *m/z* calcd for C₁₉H₂₇NO₆: 366.1911 [M + H]⁺, found: 366.1912.

Methyl 4-(((*tert*-butoxycarbonyl)-(*R*)-methionyl)oxy)benzoate (22)



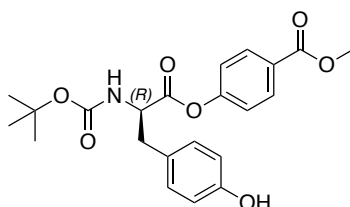
The compound was synthesized according to GP1, starting from Boc-(*R*)-Met-OH (282 mg, 1.13 mmol, 1.00 eq), methyl-4-hydroxybenzoate (180 mg, 1.19 mmol, 1.05 eq), EDC · HCl (325 mg, 1.70 mmol, 1.50 eq), HOBT · xH₂O (230 mg, 1.70 mmol, 1.50 eq) and DIPEA (394 μL, 292 mg, 2.26 mmol, 2.00 eq) in DCM (20 mL). Column chromatography (1.5% MeOH in DCM) yielded the product as a white solid (273 mg, 0.71 mmol, 63%). **TLC:** R_f = 0.47 (1.5% MeOH in DCM). **¹H-NMR** (300 MHz, CDCl₃): δ [ppm] = 8.13 – 7.99 (m, 2H), 7.24 – 7.13 (m, 2H), 5.19 (d, *J* = 8.1 Hz, 1H), 4.65 (s, 1H), 3.91 (s, 3H), 2.72 – 2.58 (m, 2H), 2.30 (dt, *J* = 8.6, 4.8 Hz, 1H), 2.19 – 2.00 (m, 4H), 1.46 (s, 9H). **¹³C-NMR** (126 MHz, CDCl₃): δ [ppm] = 170.8, 166.3, 155.5, 154.1, 131.4, 131.3, 128.2, 121.5, 121.5, 53.1, 52.4, 31.8, 30.2, 28.4, 15.7. **HRMS** (ESI): *m/z* calcd for C₁₈H₂₅NO₆S: 384.1475 [M + H]⁺, found: 384.1472.

Methyl 4-(((*tert*-butoxycarbonyl)-(*R*)-phenylalanyl)oxy)benzoate (23)



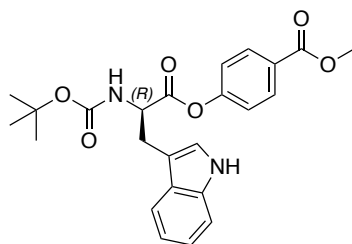
The compound was synthesized according to GP1, starting from Boc-(*R*)-Phe-OH (300 mg, 1.13 mmol, 1.00 eq), methyl-4-hydroxybenzoate (180 mg, 1.19 mmol, 1.05 eq), EDC·HCl (325 mg, 1.70 mmol, 1.50 eq), HOBT·xH₂O (230 mg, 1.70 mmol, 1.50 eq) and DIPEA (394 μL, 292 mg, 2.26 mmol, 2.00 eq) in DCM (20 mL). Column chromatography (hexanes/EtOAc, 4/1) yielded the product as a white solid (384 mg, 0.96 mmol, 85%). **TLC:** R_f = 0.47 (hexanes/EtOAc, 4/1, v/v). **¹H-NMR** (300 MHz, CDCl₃): δ [ppm] = 8.10 – 8.00 (m, 2H), 7.40 – 7.27 (m, 3H), 7.28 – 7.20 (m, 3H), 7.12 – 7.00 (m, 2H), 5.04 (s, 1H), 4.82 (t, *J* = 6.9 Hz, 1H), 3.91 (s, 3H), 3.23 (d, *J* = 6.3 Hz, 2H), 1.44 (s, 9H). **¹³C-NMR** (126 MHz, CDCl₃): δ [ppm] = 170.2, 166.2, 155.2, 153.9, 135.6, 131.2, 129.4, 128.8, 128.0, 127.4, 121.4, 80.5, 54.7, 52.3, 38.3, 28.3. **HRMS** (ESI): *m/z* calcd for C₂₂H₂₅NO₆: 400.1755 [M + H]⁺, found: 400.1735.

Methyl 4-(((*tert*-butoxycarbonyl)-(*R*)-tyrosyl)oxy)benzoate (24)



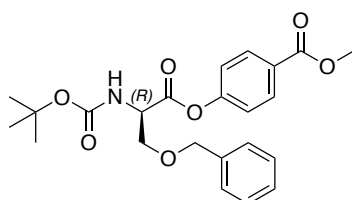
The compound was synthesized (without prior protection of tyrosine) according to GP1, starting from Boc-(*R*)-Tyr-OH (159 mg, 0.57 mmol, 1.00 eq), methyl-4-hydroxybenzoate (258 mg, 1.70 mmol, 3.00 eq), EDC·HCl (163 mg, 0.85 mmol, 1.50 eq), HOBT·xH₂O (115 mg, 0.85 mmol, 1.50 eq) and DIPEA (197 μL, 146 mg, 1.13 mmol, 2.00 eq) in DCM (8 mL). RP-HPLC yielded the product as a white solid (5 mg, 12.0 μmol, 2%). **TLC:** R_f = 0.22 (1% MeOH in DCM). **¹H-NMR** (500 MHz, CDCl₃): δ [ppm] = 8.03 (d, *J* = 8.7 Hz, 2H), 7.16 – 7.09 (m, 4H), 6.78 (d, *J* = 8.5 Hz, 2H), 5.75 – 5.67 (m, 1H), 4.50 (q, *J* = 7.5 Hz, 1H), 3.87 (s, 3H), 3.17 – 2.96 (m, 2H), 1.39 (s, 9H). **¹³C-NMR** (101 MHz, CDCl₃): δ [ppm] = 171.7, 166.8, 156.9, 156.4, 155.2, 131.9, 131.4, 129.0, 128.6, 122.7, 116.1, 80.2, 56.6, 52.8, 37.0, 28.4. **HRMS** (ESI): *m/z* calcd for C₂₂H₂₅NO₇: 415.1704 [M + H]⁺, found: 416.1705.

Methyl 4-(((*tert*-butoxycarbonyl)-(*R*)-tryptophyl)oxy)benzoate (25)



The compound was synthesized according to GP1, starting from Boc-(*R*)-Trp-OH (300 mg, 1.13 mmol, 1.00 eq), methyl-4-hydroxybenzoate (180 mg, 1.19 mmol, 1.05 eq), EDC·HCl (325 mg, 1.70 mmol, 1.50 eq), HOBT·xH₂O (230 mg, 1.70 mmol, 1.50 eq) and DIPEA (394 μL, 292 mg, 2.26 mmol, 2.00 eq) in DCM (20 mL). Column chromatography (hexanes/EtOAc, 4/1) yielded the product as a white solid (384 mg, 0.96 mmol, 85%). **TLC**: R_f = 0.14 (hexanes/EtOAc, 4/1, v/v). **¹H-NMR** (500 MHz, CDCl₃): δ [ppm] = 8.18 (brs, 1H), 8.04 – 7.98 (m, 2H), 7.63 (d, *J* = 7.9 Hz, 1H), 7.39 (d, *J* = 7.8 Hz, 1H), 7.25 – 7.21 (m, 1H), 7.16 – 7.08 (m, 2H), 6.98 – 6.93 (m, 2H), 5.16 (s, 1H), 4.88 (q, *J* = 6.4 Hz, 1H), 3.91 (s, 3H), 3.49 – 3.38 (m, 2H), 1.45 (s, 9H). **¹³C-NMR** (101 MHz, CDCl₃): δ [ppm] = 170.7, 166.4, 155.4, 154.2, 136.4, 131.3, 128.0, 127.7, 123.0, 122.7, 121.5, 120.1, 119.0, 111.4, 110.1, 80.4, 54.7, 52.3, 28.5, 28.1. **HRMS** (ESI): *m/z* calcd for C₂₄H₂₆N₂O₆: 439.1864 [M + H]⁺, found: 439.1858.

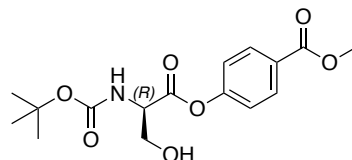
Methyl 4-((O-benzyl-N-(*tert*-butoxycarbonyl)-(*R*)-seryl)oxy)benzoate (26)



The compound was synthesized according to GP1, starting from Boc-(*R*)-Ser(Bzl)-OH (334 mg, 1.13 mmol, 1.00 eq), methyl-4-hydroxybenzoate (180 mg, 1.19 mmol, 1.05 eq), EDC·HCl (325 mg, 1.70 mmol, 1.50 eq), HOBT·xH₂O (230 mg, 1.70 mmol, 1.50 eq) and DIPEA (394 μL, 292 mg, 2.26 mmol, 2.00 eq) in DCM/DMF (12 mL/ 0.2 mL). Column chromatography (0.75% MeOH in DCM → 1.0% MeOH in DCM) yielded the product as a colorless oil which solidified upon standing (350 mg, 0.81 mmol, 72%). **TLC**: R_f = 0.58 (1% MeOH in DCM). **¹H-NMR** (500 MHz, CDCl₃): δ [ppm] = 8.09 – 8.02 (m, 2H), 7.39 – 7.26 (m, 5H), 7.13 – 7.09 (m, 2H), 5.49 (d, *J* = 8.9 Hz, 1H), 4.70 (dt, *J* = 9.2, 3.1 Hz, 1H), 4.66 – 4.51 (m, 2H), 4.09 (dd, *J* = 9.4, 3.2 Hz, 1H), 3.92 (s, 3H), 3.80

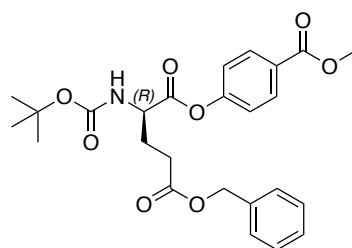
(dd, $J = 9.3, 3.2$ Hz, 1H), 1.47 (s, 9H). $^{13}\text{C-NMR}$ (126 MHz, CDCl_3): δ [ppm] = 169.1, 166.3, 155.5, 154.2, 137.3, 131.2, 128.6, 128.1, 128.0, 127.8, 121.5, 80.4, 73.5, 70.0, 54.3, 52.3, 28.3. **HRMS** (ESI): m/z calcd for $\text{C}_{23}\text{H}_{27}\text{NO}_7$: 430.1860 $[\text{M} + \text{H}]^+$, found: 430.1861.

Methyl 4-(((*tert*-butoxycarbonyl)-(*R*)-seryl)oxy)benzoate (27)



To a solution of **26** (100 mg, 0.23 mmol) in EtOAc (7 mL) was added Pd/C (30 mg). The suspension was flushed with H_2 for 2 min and stirred under an H_2 -atmosphere (balloon) at room temperature for 16 h. The mixture was filtered over a pad of celite, which was subsequently washed with EtOAc. The solvent was removed under reduced pressure and the residue was purified by column chromatography (2% MeOH in DCM), yielding the product as a white solid (78 mg, 0.23 mmol, 99%). **TLC**: $R_f = 0.32$ (2% MeOH in DCM). $^1\text{H-NMR}$ (500 MHz, CDCl_3): δ [ppm] = 8.08 (d, $J = 8.7$ Hz, 2H), 7.20 (d, $J = 8.7$ Hz, 2H), 5.50 (s, 1H), 4.63 (s, 1H), 4.19 (dd, $J = 11.1, 3.7$ Hz, 1H), 4.06 (dd, $J = 11.0, 3.5$ Hz, 1H), 3.92 (s, 3H), 1.48 (s, 9H). $^{13}\text{C-NMR}$ (101 MHz, CDCl_3): δ [ppm] = 169.3, 166.4, 155.8, 154.2, 131.4, 128.3, 121.6, 80.8, 63.6, 56.1, 52.4, 28.4. **HRMS** (ESI): m/z calcd for $\text{C}_{16}\text{H}_{21}\text{NO}_7$: 340.1391 $[\text{M} + \text{H}]^+$, found: 340.1391.

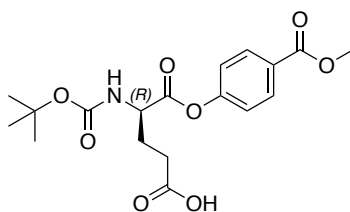
5-benzyl 1-(4-(methoxycarbonyl)phenyl) (*tert*-butoxycarbonyl)-(*R*)-glutamate (28)



The compound was synthesized according to GP1, starting from Boc-(*R*)-Glu(OBzl)-OH (381 mg, 1.13 mmol, 1.00 eq), methyl-4-hydroxybenzoate (180 mg, 1.19 mmol, 1.05 eq), EDC \cdot HCl (325 mg, 1.70 mmol, 1.50 eq), HOBT \cdot $x\text{H}_2\text{O}$ (230 mg, 1.70 mmol, 1.50 eq) and DIPEA (394 μL , 292 mg, 2.26 mmol, 2.00 eq) in DCM (12 mL). Column chromatography (0.6% MeOH in DCM) yielded the product as a white solid (392 mg, 0.83 mmol, 73%). **TLC**: $R_f = 0.24$ (1% MeOH in DCM). $^1\text{H-NMR}$ (500 MHz, CDCl_3):

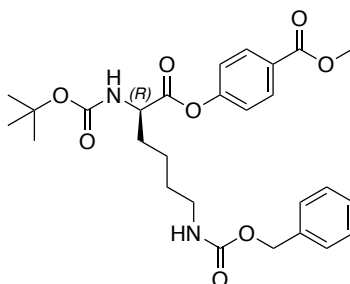
δ [ppm] = 8.07 (d, J = 8.8 Hz, 2H), 7.40 – 7.30 (m, 5H), 7.20 – 7.16 (m, 2H), 5.18 (brs, 1H), 5.14 (s, 2H), 4.57 (q, J = 8.6, 7.5 Hz, 1H), 3.92 (s, 3H), 2.64 – 2.51 (m, 2H), 2.44 – 2.34 (m, 1H) 2.14 (dtd, J = 14.5, 8.1, 6.6 Hz, 1H), 1.45 (s, 9H). **$^{13}\text{C-NMR}$** (101 MHz, CDCl_3): δ [ppm] = 172.6, 170.6, 166.3, 155.6, 154.1, 135.8, 131.4, 128.8, 128.5, 128.5, 128.2, 121.5, 80.6, 66.8, 53.4, 52.4, 30.4, 28.4, 27.5. **HRMS** (ESI): m/z calcd for $\text{C}_{25}\text{H}_{29}\text{NO}_8$: 472.1966 $[\text{M} + \text{H}]^+$, found: 472.1969.

(*R*)-4-((*tert*-butoxycarbonyl)amino)-5-(4-(methoxycarbonyl)phenoxy)-5-oxopentanoic acid (29)



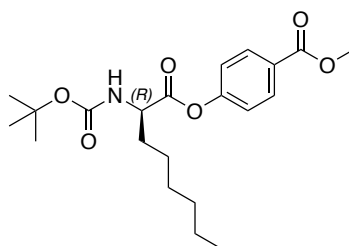
To a solution of **28** (118 mg, 0.25 mmol) in EtOAc (6 mL) was added Pd/C (30 mg). The suspension was flushed with H_2 for 2 min and stirred under an H_2 -atmosphere (balloon) at room temperature for 16 h. The mixture was filtered over a pad of celite, which was subsequently washed with EtOAc. The solvent was removed under reduced pressure and the residue was purified by column chromatography (hexanes/EtOAc, 1/1, then 5% MeOH in DCM), yielding the product as a white solid (56 mg, 0.15 mmol, 59%). **TLC**: R_f = 0.29 (5% MeOH in DCM). **$^1\text{H-NMR}$** (500 MHz, CDCl_3): δ [ppm] = 8.07 (d, J = 8.7 Hz, 2H), 7.19 (d, J = 8.7 Hz, 2H), 5.22 (brs, 1H), 4.60 (brs, 1H), 3.92 (s, 3H), 2.66 – 2.54 (m, 2H), 2.42 – 2.35 (m, 1H), 2.17 – 2.09 (m, 1H), 1.46 (s, 9H). **$^{13}\text{C-NMR}$** (101 MHz, CDCl_3): δ [ppm] = 177.3, 170.6, 166.3, 155.7, 154.1, 131.4, 128.3, 121.5, 80.8, 53.2, 52.4, 30.0, 28.4, 27.5. **HRMS** (ESI): m/z calcd for $\text{C}_{18}\text{H}_{23}\text{NO}_8$: 382.1496 $[\text{M} + \text{H}]^+$, found: 382.1498.

Methyl 4-((N^6 -((benzyloxy)carbonyl)- N^2 -(*tert*-butoxycarbonyl)-(*R*)-lysyl)-oxy)benzoate (30)



The compound was synthesized according to GP1, starting from Boc-(*R*)-Lys(Cbz)-OH (430 mg, 1.13 mmol, 1.00 eq), methyl-4-hydroxybenzoate (180 mg, 1.19 mmol, 1.05 eq), EDC·HCl (325 mg, 1.70 mmol, 1.50 eq), HOBT·xH₂O (230 mg, 1.70 mmol, 1.50 eq) and DIPEA (394 μL, 292 mg, 2.26 mmol, 2.00 eq) in DCM (12 mL). Column chromatography (hexanes/EtOAc, 3/1 → 2/1) yielded the product as a white solid (429 mg, 0.83 mmol, 74%). **TLC**: R_f = 0.21 (hexanes/EtOAc, 3/1, v/v). **¹H-NMR** (400 MHz, CDCl₃): δ [ppm] = 8.11 – 8.03 (m, 2H), 7.40 – 7.27 (m, 5H), 7.21 – 7.13 (m, 2H), 5.10 (s, 2H), 5.20 – 5.13 (m, 1H), 4.85 – 4.79 (m, 1H), 4.54 – 4.46 (m, 1H), 3.92 (s, 3H), 3.24 (d, *J* = 6.2 Hz, 2H), 2.04 – 1.91 (m, 1H), 1.84 (dt, *J* = 14.2, 7.6 Hz, 1H), 1.63 – 1.49 (m, 4H), 1.46 (s, 9H). **¹³C-NMR** (126 MHz, CDCl₃): δ [ppm] = 171.2, 166.4, 156.7, 155.7, 154.2, 136.6, 131.4, 128.7, 128.3, 128.3, 128.1, 121.6, 80.4, 66.9, 53.7, 52.4, 40.6, 32.1, 29.6, 28.5, 22.6. **HRMS** (ESI): *m/z* calcd for C₂₇H₃₄N₂O₈: 515.2388 [M + H]⁺, found: 515.2387.

Methyl (*R*)-4-((2-((*tert*-butoxycarbonyl)amino)octanoyl)oxy)benzoate (31)

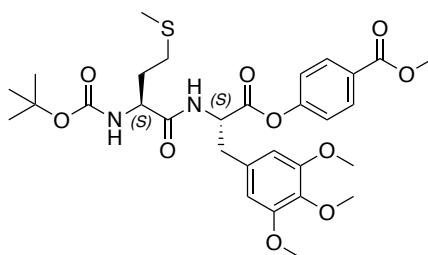


The compound was synthesized according to GP1, starting from Boc-(*R*)-2-amino-octanoic acid (Boc-(*R*)-2-Aoc-OH, 235 mg, 0.91 mmol, 1.00 eq), methyl-4-hydroxybenzoate (144 mg, 0.95 mmol, 1.05 eq), EDC·HCl (261 mg, 1.36 mmol, 1.50 eq), HOBT·xH₂O (184 mg, 1.36 mmol, 1.50 eq) and DIPEA (316 μL, 234 mg, 1.81 mmol, 2.00 eq) in DCM (10 mL). Prior to reaction, the DCHA of the commercially available Boc-(*R*)-2-Aoc-OH·DCHA form was removed by extraction between EtOAc and 5% KHSO₄ according to the protocol of the supplier. Column chromatography (hexanes/EtOAc, 7/1) yielded the product as a colorless oil (0.28 g, 0.58 mmol, 64%). **TLC**: R_f = 0.33 (hexanes/EtOAc, 7/1). **¹H-NMR** (500 MHz, CDCl₃): δ [ppm] = 8.07 (d, *J* = 8.7 Hz, 2H), 7.17 (d, *J* = 8.7 Hz, 2H), 5.02 (d, *J* = 8.3 Hz, 1H), 4.55 – 4.47 (m, 1H), 3.92 (s, 3H), 2.02 – 1.90 (m, 1H), 1.79 (dt, *J* = 14.8, 7.8 Hz, 1H), 1.46 (s, 10H), 1.45 – 1.24 (m, 8H), 0.89 (t, *J* = 6.8 Hz, 3H). **¹³C-NMR** (101 MHz, CDCl₃): δ [ppm] = 171.4, 166.4, 155.6, 154.3, 131.4, 128.1, 121.6, 80.3, 53.9, 52.4, 32.6, 31.7, 29.0, 28.5, 25.5, 22.7, 14.2. **HRMS** (ESI): *m/z* calcd for C₂₁H₃₁NO₆: 394.224 [M + H]⁺, found: 394.226.

General procedure 2: Synthesis of dipeptide phenyl esters (GP2)

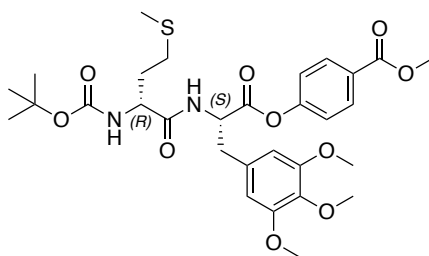
Under an argon atmosphere, (*R*)-**11** or (*S*)-**12** (1.00 eq) and the Boc-protected amino acid (1.10 eq) were dissolved in minimal amounts of anhydrous DMF and cooled to 0 °C. (1-Cyano-2-ethoxy-2-oxoethylideneaminoxy)dimethylamino-morpholinocarbenium hexafluorophosphate (COMU, 1.10 eq) and DIPEA (2.00 eq) were added. The solution was stirred and allowed to warm to room temperature overnight. The solvent was removed under reduced pressure. For workup, the residue was diluted with DCM and washed with 5% citric acid (3x), 5% NaHCO₃ (3x) and brine (1x). The organic phase was dried over MgSO₄ and the solvent was removed under reduced pressure. Purification was performed by column chromatography and/or preparative RP-HPLC.

Methyl 4-(((*S*)-2-((*S*)-2-((*tert*-butoxycarbonyl)amino)-4-(methylthio)butanamido)-3-(3,4,5-trimethoxyphenyl)propanoyl)oxy)benzoate (**32**)



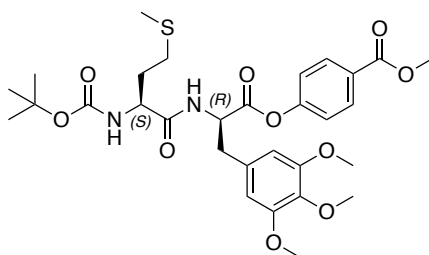
The compound was synthesized according to GP2, starting from phenyl ester **12** (100 mg, 0.20 mmol, 1.00 eq), Boc-(*S*)-Met-OH (55 mg, 0.22 mmol, 1.10 eq), COMU (94 mg, 0.22 mmol, 1.10 eq) and DIPEA (69 μ L, 51 mg, 0.40 mmol, 2.00 eq) in DMF (3 mL). RP-HPLC yielded the product as a white solid (42 mg, 68 μ mol, 34%). **TLC**: R_f = 0.29 (1% MeOH in DCM). **¹H-NMR** (500 MHz, CD₃CN): δ [ppm] = 8.04 (d, J = 8.8 Hz, 2H), 7.15 (d, J = 8.7 Hz, 2H), 7.14 (brs, 1H), 6.58 (s, 2H), 5.62 (d, J = 7.6 Hz, 1H), 4.84 (td, J = 7.7, 5.8 Hz, 1H), 4.15 (d, J = 7.2 Hz, 1H), 3.87 (s, 3H), 3.79 (s, 6H), 3.69 (s, 3H), 3.25 – 3.09 (m, 2H), 2.54 – 2.38 (m, 2H), 2.01 (s, 3H), 1.94 – 1.87 (m, 1H), 1.85 – 1.74 (m, 1H), 1.37 (s, 9H). **¹³C-NMR** (126 MHz, CD₃CN): δ [ppm] = 173.0, 170.7, 166.8, 156.5, 155.2, 154.2, 137.7, 133.1, 131.9, 129.0, 122.6, 107.4, 80.0, 60.7, 56.6, 54.9, 54.5, 52.8, 37.8, 32.5, 30.6, 28.4, 15.2. **HRMS** (ESI): m/z calcd for C₃₀H₄₀N₂O₁₀S: 621.2476 [M + H]⁺, found: 621.2477.

Methyl 4-(((S)-2-((R)-2-((tert-butoxycarbonyl)amino)-4-(methylthio)butanamido)-3-(3,4,5-trimethoxyphenyl)propanoyl)oxy)benzoate (33)



The compound was synthesized according to GP2, starting from phenyl ester **12** (100 mg, 0.20 mmol, 1.00 eq), Boc-(*R*)-Met-OH (55 mg, 0.22 mmol, 1.10 eq), COMU (94 mg, 0.22 mmol, 1.10 eq) and DIPEA (69 μ L, 51 mg, 0.40 mmol, 2.00 eq) in DMF (3 mL). RP-HPLC yielded the product as a white solid (74 mg, 0.12 mmol, 60%). **TLC**: R_f = 0.35 (1% MeOH in DCM). **¹H-NMR** (500 MHz, CD₃CN): δ [ppm] = 8.04 (d, J = 8.7 Hz, 2H), 7.20 – 7.15 (m, 2H), 7.13 (br s, 1H), 6.57 (s, 2H), 5.62 (d, J = 8.2 Hz, 1H), 4.81 (q, J = 7.4, 6.9 Hz, 1H), 4.15 (brs, 1H), 3.87 (s, 3H), 3.79 (s, 6H), 3.69 (s, 3H), 3.24 (dd, J = 13.9, 5.5 Hz, 1H), 3.08 (dd, J = 13.9, 8.9 Hz, 1H), 2.47– 2.35 (m, 2H), 2.00 (s, 3H), 1.92 – 1.83 (m, 1H), 1.80 – 1.70 (m, 1H), 1.36 (s, 9H). **¹³C-NMR** (100 MHz, CD₃CN): δ [ppm] = 173.1, 170.8, 166.8, 156.6, 155.3, 154.3, 137.9, 133.2, 131.9, 129.1, 122.7, 107.5, 80.1, 60.8, 56.7, 55.0, 54.4, 52.8, 37.9, 32.4, 30.6, 28.4, 15.2. **HRMS** (ESI): m/z calcd for C₃₀H₄₀N₂O₁₀S: 621.2476 [M + H]⁺, found: 621.2471.

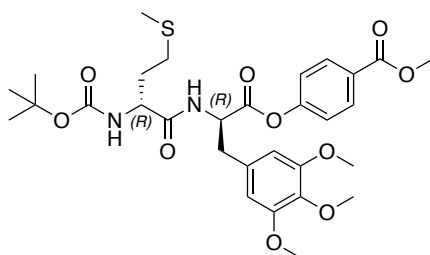
Methyl 4-(((R)-2-((S)-2-((tert-butoxycarbonyl)amino)-4-(methylthio)butanamido)-3-(3,4,5-trimethoxyphenyl)propanoyl)oxy)benzoate (34)



The compound was synthesized according to GP2, starting from phenyl ester **11** (100 mg, 0.20 mmol, 1.00 eq), Boc-(*S*)-Met-OH (55 mg, 0.22 mmol, 1.10 eq), COMU (94 mg, 0.22 mmol, 1.10 eq) and DIPEA (69 μ L, 51 mg, 0.40 mmol, 2.00 eq) in DMF (3 mL). RP-HPLC yielded the product as a white solid (107 mg, 0.17 mmol, 87%). **TLC**: R_f = 0.36 (1% MeOH in DCM). **¹H-NMR** (500 MHz, CD₃CN): δ [ppm] = 8.07 – 8.02 (m, 2H), 7.20 – 7.15 (m, 2H), 7.15 – 7.11 (m, 1H), 6.58 (s, 2H), 5.63 (d, J = 8.3 Hz, 1H), 4.80

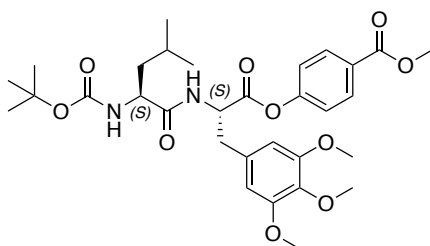
(q, $J = 7.4$ Hz, 1H), 4.18 – 4.08 (m, 1H), 3.87 (s, 3H), 3.79 (s, 6H), 3.69 (s, 3H), 3.24 (dd, $J = 13.9, 5.5$ Hz, 1H), 3.08 (dd, $J = 13.9, 8.9$ Hz, 1H), 2.46 – 2.34 (m, 2H), 2.00 (s, 3H), 1.92 – 1.83 (m, 1H), 1.81 – 1.70 (m, 1H), 1.36 (s, 9H). $^{13}\text{C-NMR}$ (126 MHz, CD_3CN): δ [ppm] = 173.0, 170.8, 166.8, 156.6, 155.2, 154.2, 137.7, 133.2, 131.9, 129.0, 122.7, 107.3, 80.0, 60.7, 56.6, 55.0, 54.3, 52.8, 37.8, 32.4, 30.5, 28.4, 15.2. **HRMS** (ESI): m/z calcd for $\text{C}_{30}\text{H}_{40}\text{N}_2\text{O}_{10}\text{S}$: 621.2476 $[\text{M} + \text{H}]^+$, found: 621.2472.

Methyl 4-(((*R*)-2-((*R*)-2-((*tert*-butoxycarbonyl)amino)-4-(methylthio)-butanamido)-3-(3,4,5-trimethoxyphenyl)propanoyl)oxy)benzoate (35)



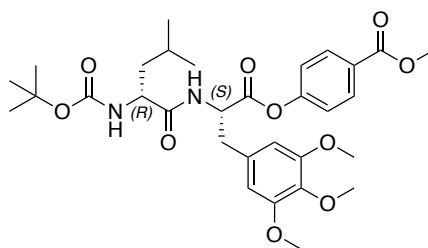
The compound was synthesized according to GP2, starting from phenyl ester **11** (100 mg, 0.20 mmol, 1.00 eq), Boc-(*R*)-Met-OH (55 mg, 0.22 mmol, 1.10 eq), COMU (94 mg, 0.22 mmol, 1.10 eq) and DIPEA (69 μL , 51 mg, 0.40 mmol, 2.00 eq) in DMF (3 mL). RP-HPLC yielded the product as a white solid (0.10 g, 0.17 mmol, 84%). **TLC**: $R_f = 0.29$ (1% MeOH in DCM). $^1\text{H-NMR}$ (500 MHz, CD_3CN): δ [ppm] = 8.04 8.04 (d, $J = 8.7$ Hz, 2H), 7.15 (d, $J = 8.7$ Hz, 2H), 7.14 (brs, 1H), 6.58 (s, 2H), 5.62 (d, $J = 8.0$ Hz, 1H), 4.85 (td, $J = 7.7, 5.8$ Hz, 1H), 4.15 (d, $J = 9.7$ Hz, 1H), 3.87 (s, 3H), 3.79 (s, 6H), 3.69 (s, 3H), 3.28 – 3.09 (m, 2H), 2.54 – 2.38 (m, 2H), 2.02 (s, 3H), 1.94 – 1.89 (m, 1H), 1.84 – 1.76 (m, 1H), 1.37 (s, 9H). $^{13}\text{C-NMR}$ (126 MHz, CD_3CN): δ [ppm] = 173.0, 170.7, 166.8, 156.5, 155.2, 154.2, 137.7, 133.1, 131.9, 129.0, 122.6, 107.4, 80.0, 60.7, 56.6, 54.9, 54.5, 52.8, 37.8, 32.5, 30.5, 28.4, 15.2. **HRMS** (ESI): m/z calcd for $\text{C}_{30}\text{H}_{40}\text{N}_2\text{O}_{10}\text{S}$: 621.2476 $[\text{M} + \text{H}]^+$, found: 621.2475.

Methyl 4-(((*S*)-2-((*S*)-2-((*tert*-butoxycarbonyl)amino)-4-methylpentanamido)-3-(3,4,5-trimethoxyphenyl)propanoyl)oxy)benzoate (36)



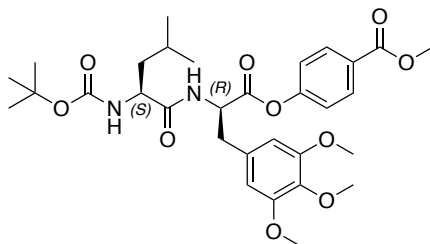
The compound was synthesized according to GP2, starting from phenyl ester **12** (50 mg, 0.10 mmol, 1.00 eq), Boc-(*S*)-Leu-OH (25 mg, 0.11 mmol, 1.10 eq), COMU (47 mg, 0.11 mmol, 1.10 eq) and DIPEA (52 μ L, 38 mg, 0.30 mmol, 3.00 eq) in DMF (2 mL). RP-HPLC yielded the product as a white solid (49 mg, 81 μ mol, 82%). **TLC**: R_f = 0.22 (1% MeOH in DCM). **¹H-NMR** (500 MHz, CD₃CN): δ [ppm] = 8.09 – 8.00 (m, 2H), 7.17 – 7.13 (m, 2H), 7.12 (brs, 1H), 6.57 (s, 2H), 5.50 (d, J = 8.3 Hz, 1H), 4.81 (td, J = 7.8, 5.9 Hz, 1H), 4.08 – 3.99 (m, 1H), 3.87 (s, 3H), 3.79 (s, 6H), 3.69 (s, 3H), 3.27 – 3.02 (m, 2H), 1.62 (dt, J = 13.8, 6.8 Hz, 1H), 1.42 (d, J = 10.8 Hz, 2H), 1.36 (s, 9H), 0.88 (dd, J = 11.7, 6.6 Hz, 6H). **¹³C-NMR** (126 MHz, CD₃CN): δ [ppm] 173.9, 170.8, 166.8, 156.5, 155.2, 154.2, 137.7, 133.2, 131.8, 129.0, 122.6, 107.4, 79.8, 60.7, 56.6, 54.8, 53.9, 52.8, 41.8, 37.8, 28.4, 25.4, 23.2, 21.7. **HRMS** (ESI): m/z calcd for C₃₁H₄₂N₂O₁₀: 603.2912 [M + H]⁺, found: 603.2903.

Methyl 4-(((*S*)-2-((*R*)-2-((*tert*-butoxycarbonyl)amino)-4-methylpentanamido)-3-(3,4,5-trimethoxyphenyl)propanoyl)oxy)benzoate (37**)**



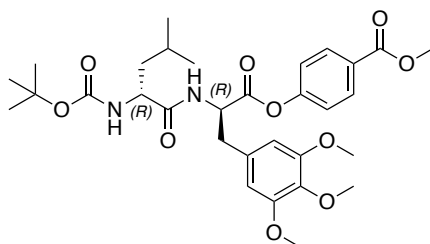
The compound was synthesized according to GP2, starting from phenyl ester **12** (100 mg, 0.20 mmol, 1.00 eq), Boc-(*R*)-Leu-OH (51 mg, 0.22 mmol, 1.10 eq), COMU (94 mg, 0.22 mmol, 1.10 eq) and DIPEA (69 μ L, 51 mg, 0.40 mmol, 2.00 eq) in DMF (3 mL). RP-HPLC yielded the product as a white solid (35 mg, 58 μ mol, 29%). **TLC**: R_f = 0.47 (2% MeOH in DCM). **¹H-NMR** (500 MHz, CDCl₃): δ [ppm] = 8.05 (d, J = 8.6 Hz, 2H), 7.17 (d, J = 8.7 Hz, 2H), 7.09 (brs, 1H), 6.58 (s, 2H), 5.49 (s, 1H), 4.79 (d, J = 8.0 Hz, 1H), 4.08 – 3.98 (m, 1H), 3.88 (s, 3H), 3.80 (s, 6H), 3.70 (s, 3H), 3.24 (dd, J = 13.9, 5.5 Hz, 1H), 3.07 (dd, J = 13.9, 9.1 Hz, 1H), 1.68 – 1.57 (m, 1H), 1.41 – 1.37 (m, 2H), 1.36 (m, 9H), 0.85 (dd, J = 6.6, 2.9 Hz, 6H). **¹³C-NMR** (126 MHz, CD₃CN): δ [ppm] 174.0, 170.9, 166.8, 156.5, 155.2, 154.2, 137.7, 133.2, 131.8, 129.0, 122.7, 122.6, 107.4, 79.8, 60.7, 56.6, 55.0, 53.7, 52.8, 41.7, 37.8, 28.4, 25.3, 23.1, 21.8. **HRMS** (ESI): m/z calcd for C₃₁H₄₂N₂O₁₀: 603.2912 [M + H]⁺, found: 603.2913.

Methyl 4-(((S)-2-((R)-2-((tert-butoxycarbonyl)amino)-4-methylpentanamido)-3-(3,4,5-trimethoxyphenyl)propanoyl)oxy)benzoate (38)



The compound was synthesized according to GP2, starting from phenyl ester **11** (150 mg, 0.30 mmol, 1.00 eq), Boc-(S)-Leu-OH (76 mg, 0.33 mmol, 1.10 eq), COMU (140 mg, 0.33 mmol, 1.10 eq) and DIPEA (104 μ L, 77 mg, 0.60 mmol, 2.00 eq) in DMF (4 mL). RP-HPLC yielded the product as a white solid (85 mg, 0.14 mmol, 47%). **TLC**: R_f = 0.48 (2% MeOH in DCM). **¹H-NMR** (500 MHz, CDCl₃): δ [ppm] = 8.04 (d, J = 8.6 Hz, 2H), 7.17 (d, J = 8.7 Hz, 2H), 7.12 (brs, 1H), 6.58 (s, 2H), 5.49 (s, 1H), 4.85 – 4.75 (m, 1H), 4.09 – 3.99 (m, 1H), 3.87 (s, 3H), 3.79 (s, 6H), 3.69 (s, 3H), 3.24 (dd, J = 13.9, 5.5 Hz, 1H), 3.07 (dd, J = 13.9, 9.1 Hz, 1H), 1.57 – 1.48 (m, 1H), 1.41 – 1.37 (m, 2H), 1.36 (s, 9H), 0.85 (dd, J = 6.6, 2.7 Hz, 6H). **¹³C-NMR** (126 MHz, CD₃CN): δ [ppm] = 174.0, 170.8, 166.8, 156.5, 155.2, 154.2, 137.7, 133.2, 131.9, 129.0, 122.7, 122.6, 107.4, 79.8, 60.7, 56.6, 55.0, 53.7, 52.8, 41.8, 37.8, 28.4, 25.3, 23.1, 21.8. **HRMS** (ESI): m/z calcd for C₃₁H₄₂N₂O₁₀: 603.2912 [M + H]⁺, found: 603.2910.

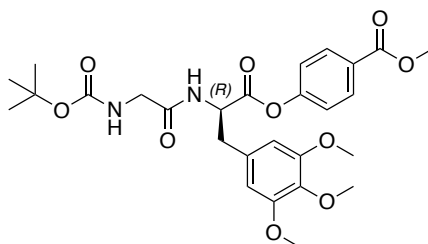
Methyl 4-(((R)-2-((R)-2-((tert-butoxycarbonyl)amino)-4-methylpentanamido)-3-(3,4,5-trimethoxyphenyl)propanoyl)oxy)benzoate (39)



The compound was synthesized according to GP2, starting from phenyl ester **11** (100 mg, 0.20 mmol, 1.00 eq), Boc-(R)-Leu-OH (51 mg, 0.22 mmol, 1.10 eq), COMU (94 mg, 0.22 mmol, 1.10 eq) and DIPEA (69 μ L, 51 mg, 0.40 mmol, 2.00 eq) in DMF (3 mL). RP-HPLC yielded the product as a white solid (64 mg, 0.11 mmol, 53%). **TLC**: R_f = 0.21 (1% MeOH in DCM). **¹H-NMR** (500 MHz, CD₃CN): δ [ppm] = 8.04 (d, J = 8.7 Hz, 2H), 7.14 (d, J = 8.8 Hz, 2H), 7.11 (brs, 1H), 6.57 (s, 2H), 5.49 (d, J = 8.0 Hz,

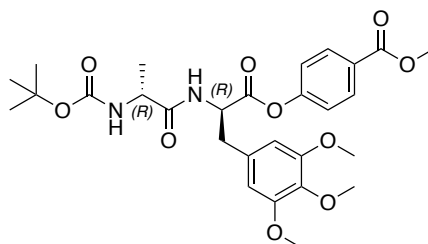
iH), 4.82 (td, $J = 7.7, 5.8$ Hz, 1H), 4.08 – 3.98 (m, 1H), 3.87 (s, 3H), 3.79 (s, 6H), 3.69 (s, 3H), 3.28 – 3.06 (m, 2H), 1.68 – 1.57 (m, 1H), 1.43 (d, $J = 7.9$ Hz, 2H), 1.36 (s, 9H), 0.88 (dd, $J = 11.6, 6.6$ Hz, 6H). **$^{13}\text{C-NMR}$** (126 MHz, CD_3CN): δ [ppm] 173.9, 170.8, 166.8, 156.5, 155.2, 154.2, 137.7, 133.2, 131.8, 129.0, 122.6, 107.4, 79.8, 60.7, 56.6, 54.8, 53.9, 52.8, 41.8, 37.8, 28.4, 25.4, 23.2, 21.7. **HRMS** (ESI): m/z calcd for $\text{C}_{31}\text{H}_{42}\text{N}_2\text{O}_{10}$: 603.2912 $[\text{M} + \text{H}]^+$, found: 603.2907.

Methyl (*R*)-4-((2-(2-((*tert*-butoxycarbonyl)amino)acetamido)-3-(3,4,5-trimethoxyphenyl)propanoyl)oxy)benzoate (40)



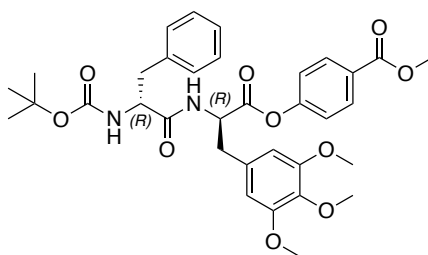
The compound was synthesized according to GP2, starting from phenyl ester **11** (100 mg, 0.20 mmol, 1.00 eq), Boc-Gly-OH (38 mg, 0.22 mmol, 1.10 eq), COMU (94 mg, 0.22 mmol, 1.10 eq) and DIPEA (69 μL , 51 mg, 0.40 mmol, 2.00 eq) in DMF (3 mL). RP-HPLC yielded the product as a white solid (70 mg, 0.13 mmol, 64%). **TLC**: $R_f = 0.15$ (1% MeOH in DCM) **$^1\text{H-NMR}$** (500 MHz, CD_3CN): δ [ppm] = 8.04 (d, $J = 8.5$ Hz, 2H), 7.15 (d, $J = 8.6$ Hz, 2H), 7.04 (brs, 1H), 6.57 (s, 2H), 5.62 (brs, 1H), 4.82 (q, $J = 7.3$ Hz, 1H), 3.87 (s, 3H), 3.79 (s, 6H), 3.70 (s, 3H), 3.67 (d, $J = 6.2$ Hz, 2H), 3.24 – 3.06 (m, 2H), 1.38 (s, 9H). **$^{13}\text{C-NMR}$** (126 MHz, CD_3CN): δ [ppm] = 170.9, 170.8, 166.8, 157.0, 155.1, 154.2, 137.7, 133.1, 131.8, 129.0, 122.6, 107.4, 80.0, 60.7, 56.6, 55.0, 52.8, 44.3, 37.9, 28.4. **HRMS** (ESI): m/z calcd for $\text{C}_{27}\text{H}_{34}\text{N}_2\text{O}_{10}$: 547.2286 $[\text{M} + \text{H}]^+$, found: 547.2285.

Methyl 4-(((*R*)-2-((*R*)-2-((*tert*-butoxycarbonyl)amino)propanamido)-3-(3,4,5-trimethoxyphenyl)propanoyl)oxy)benzoate (41)



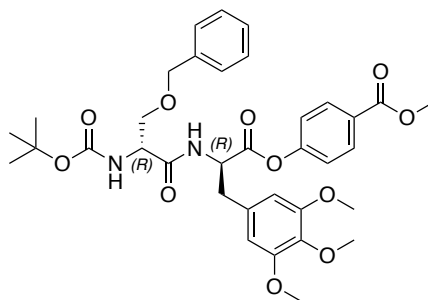
The compound was synthesized according to GP2, starting from phenyl ester **11** (100 mg, 0.20 mmol, 1.00 eq), Boc-(*R*)-Ala-OH (41 mg, 0.22 mmol, 1.10 eq), COMU (94 mg, 0.22 mmol, 1.10 eq) and DIPEA (69 μ L, 51 mg, 0.40 mmol, 2.00 eq) in DMF (3 mL) RP-HPLC yielded the product as a white solid (83 mg, 0.15 mmol, 74%). **TLC**: R_f = 0.35 (1% MeOH in DCM). **$^1\text{H-NMR}$** (500 MHz, CD_3CN): δ [ppm] = 8.04 (d, J = 8.8 Hz, 2H), 7.15 (d, J = 8.7 Hz, 2H), 7.09 (brs, 1H), 6.58 (s, 2H), 5.56 (brs, 1H), 4.83 (td, J = 7.6, 5.9 Hz, 1H), 4.11 – 4.01 (m, 1H), 3.87 (s, 3H), 3.79 (s, 6H), 3.69 (s, 3H), 3.24 – 3.08 (m, 2H), 1.37 (s, 9H), 1.22 (d, J = 7.2 Hz, 3H). **$^{13}\text{C-NMR}$** (126 MHz, CD_3CN): δ [ppm] = 174.1, 170.8, 166.8, 156.3, 155.2, 154.2, 137.7, 133.1, 131.8, 129.0, 107.5, 79.9, 60.7, 56.6, 54.9, 52.8, 51.0, 37.9, 28.4, 18.3. **HRMS** (ESI): m/z calcd for $\text{C}_{28}\text{H}_{36}\text{N}_2\text{O}_{10}$: 561.2443 $[\text{M} + \text{H}]^+$, found: 561.2442.

Methyl 4-(((*R*)-2-((*R*)-2-((*tert*-butoxycarbonyl)amino)-3-phenylpropanamido)-3-(3,4,5-trimethoxyphenyl)propanoyl)oxy)benzoate (42**)**



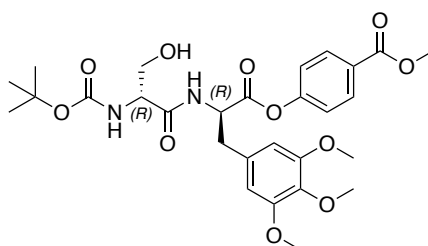
The compound was synthesized according to GP2, starting from phenyl ester **11** (100 mg, 0.20 mmol, 1.00 eq), Boc-(*R*)-Phe-OH (58 mg, 0.22 mmol, 1.10 eq), COMU (94 mg, 0.22 mmol, 1.10 eq) and DIPEA (69 μ L, 51 mg, 0.40 mmol, 2.00 eq) in DMF (3 mL). Column chromatography (hexanes/EtOAc, 2/1) yielded the product as a white solid (68 mg, 0.11 mmol, 54%). **TLC**: R_f = 0.25 (hexanes/EtOAc, 2/1, v/v). **$^1\text{H-NMR}$** (400 MHz, CD_3CN): δ [ppm] = 8.07 – 8.02 (m, 2H), 7.30 – 7.17 (m, 6H), 7.16 – 7.12 (m, 2H), 6.58 (s, 2H), 5.48 (d, J = 8.3 Hz, 1H), 4.84 (td, J = 7.5, 6.0 Hz, 1H), 4.30 (brs, 1H), 3.87 (s, 3H), 3.78 (s, 6H), 3.69 (s, 3H), 3.22 – 3.04 (m, 3H), 2.85 – 2.73 (m, 1H), 1.29 (s, 9H). **$^{13}\text{C-NMR}$** (101 MHz, CD_3CN): δ [ppm] = 172.7, 170.7, 166.8, 156.3, 155.1, 154.3, 154.2, 138.4, 137.8, 133.1, 131.9, 130.2, 129.2, 129.0, 127.5, 122.7, 122.7, 107.5, 80.0, 60.7, 56.6, 56.5, 55.0, 52.8, 38.5, 37.9, 28.3. **HRMS** (ESI): m/z calcd for $\text{C}_{34}\text{H}_{40}\text{N}_2\text{O}_{10}$: 637.2756 $[\text{M} + \text{H}]^+$, found: 637.2752.

Methyl 4-(((*R*)-2-((*R*)-3-(benzyloxy)-2-((*tert*-butoxycarbonyl)-amino)propanamido)-3-(3,4,5-trimethoxyphenyl)propanoyl)oxy)benzoate (43)



The compound was synthesized according to GP2, starting from phenyl ester **11** (150 mg, 0.30 mmol, 1.00 eq), Boc-(*R*)-Ser(Bzl)-OH (97 mg, 0.33 mmol, 1.10 eq), COMU (140 mg, 0.33 mmol, 1.10 eq) and DIPEA (104 μ L, 77 mg, 0.60 mmol, 2.00 eq) in DMF (4 mL). RP-HPLC yielded the product as a white solid (155 mg, 0.23 mmol, 78%). **TLC**: R_f = 0.35 (2% MeOH in DCM). **¹H-NMR** (500 MHz, CD₃CN): δ [ppm] = 8.05 – 8.00 (m, 2H), 7.33 – 7.24 (m, 5H), 7.22 (brs, 1H), 7.13 (d, J = 8.7 Hz, 2H), 6.56 (s, 2H), 5.63 (brs, 1H), 4.86 (q, J = 7.2 Hz, 1H), 4.46 (d, J = 2.5 Hz, 2H), 4.26 (brs, 1H), 3.87 (s, 3H), 3.77 (s, 6H), 3.69 – 3.65 (m, 4H), 3.61 (dd, J = 9.7, 5.1 Hz, 1H), 3.24 – 3.07 (m, 2H), 1.38 (s, 9H). **¹³C-NMR** (126 MHz, CD₃CN): δ [ppm] = 171.3, 170.6, 166.8, 156.4, 155.1, 154.2, 139.0, 137.8, 133.0, 131.8, 129.2, 129.0, 128.6, 128.5, 122.6, 107.4, 80.2, 73.6, 70.6, 60.7, 56.6, 55.2, 55.0, 52.8, 37.9, 28.4. **HRMS** (ESI): m/z calcd for C₃₅H₄₂N₂O₁₁: 667.2861 [M + H]⁺, found: 667.2860.

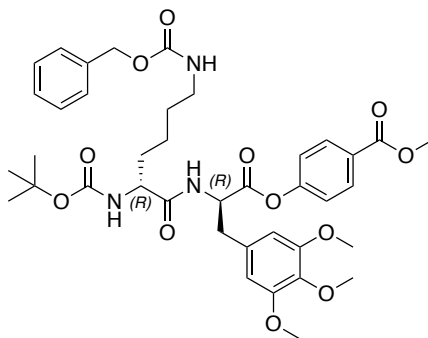
Methyl 4-(((*R*)-2-((*R*)-2-((*tert*-butoxycarbonyl)amino)-3-hydroxypropanamido)-3-(3,4,5-trimethoxyphenyl)propanoyl)oxy)benzoate (44)



To a solution of **43** (70 mg, 0.11 mmol) in EtOAc (5 mL) was added Pd/C (15 mg). The suspension was flushed with H₂ for 2 min and stirred under an H₂-atmosphere (balloon) at room temperature for 45 h. The mixture was filtered over a pad of celite, which was subsequently washed with EtOAc. The solvent was removed under reduced pressure and the residue was purified by column chromatography (2% MeOH in DCM)

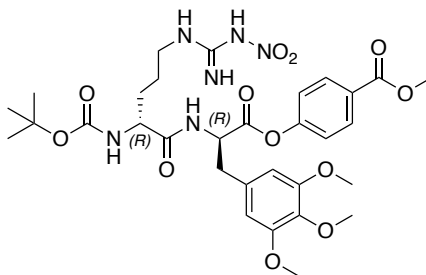
and RP-HPLC, yielding the product as a white solid (51 mg, 88 μ mol, 84%). **TLC**: R_f = 0.38 (3% MeOH in DCM). **$^1\text{H-NMR}$** (500 MHz, CD_3CN): δ [ppm] = 8.08 – 8.00 (m, 2H), 7.26 (d, J = 7.3 Hz, 1H), 7.18 – 7.13 (m, 2H), 6.57 (s, 2H), 5.61 (brs, 1H), 4.86 (td, J = 7.5, 5.9 Hz, 1H), 4.10 (brs, 1H), 3.87 (s, 3H), 3.78 (s, 6H), 3.74 – 3.67 (m, 4H), 3.64 (dd, J = 11.0, 5.3 Hz, 1H), 3.24 – 3.07 (m, 2H), 1.38 (s, 9H). **$^{13}\text{C-NMR}$** (126 MHz, CD_3CN): δ [ppm] = 166.8, 156.5, 155.1, 155.1, 154.2, 137.7, 133.0, 131.8, 129.0, 122.6, 107.5, 80.1, 62.9, 60.7, 57.0, 56.6, 55.0, 52.8, 37.9, 28.4. **HRMS** (ESI): m/z calcd for $\text{C}_{28}\text{H}_{36}\text{N}_2\text{O}_{11}$: 577.2392 [M+H]⁺, found: 577.2392.

Methyl 4-(((*R*)-2-(((*R*)-6-(((benzyloxy)carbonyl)amino)-2-((*tert*-butoxycarbonyl)-amino)hexanamido)-3-(3,4,5-trimethoxyphenyl)propanoyl)oxy)benzoate (46)



The compound was synthesized according to GP2, starting from phenyl ester **11** (150 mg, 0.30 mmol, 1.00 eq), Boc-*(R)*-Lys(Cbz)-OH (125 mg, 0.33 mmol, 1.10 eq), COMU (140 mg, 0.33 mmol, 1.10 eq) and DIPEA (104 μ L, 77 mg, 0.60 mmol, 2.00 eq) in DMF (4 mL). Column chromatography (hexanes/EtOAc, 1/1 \rightarrow 1/2) yielded the product as a white solid (184 mg, 0.24 mmol, 82%). **TLC**: R_f = 0.33 (2% MeOH in DCM). **$^1\text{H-NMR}$** (500 MHz, CD_3CN): δ [ppm] = 8.06 – 8.00 (m, 2H), 7.39 – 7.27 (m, 5H), 7.18 – 7.12 (m, 2H), 7.10 (d, J = 7.3 Hz, 1H), 6.58 (s, 2H), 5.64 – 5.52 (m, 1H), 5.03 (s, 2H), 4.84 (ddd, J = 8.1, 7.3, 5.9 Hz, 1H), 4.02 – 3.93 (m, 1H), 3.87 (s, 3H), 3.78 (s, 6H), 3.69 (s, 3H), 3.24 – 3.07 (m, 2H), 3.06 – 2.99 (m, 2H), 1.70 – 1.48 (m, 2H), 1.47 – 1.24 (m, 14H). **$^{13}\text{C-NMR}$** (126 MHz, CD_3CN): δ [ppm] = 173.5, 170.8, 166.8, 157.4, 156.5, 155.2, 154.2, 138.4, 137.7, 133.1, 131.9, 129.4, 129.0, 128.7, 128.6, 122.6, 107.5, 79.8, 66.6, 60.7, 56.6, 55.3, 54.8, 52.8, 40.9, 37.9, 32.4, 30.1, 28.4, 23.3. **HRMS** (ESI): m/z calcd for $\text{C}_{39}\text{H}_{49}\text{N}_3\text{O}_{12}$: 752.3389 [M + H]⁺, found: 752.3389.

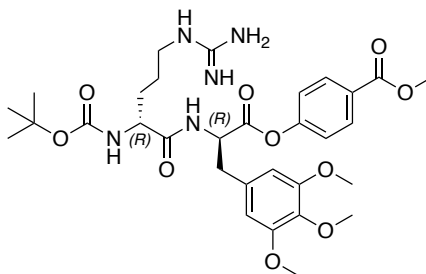
Methyl 4-(((R)-2-((R)-2-((tert-butoxycarbonyl)amino)-5-(3-nitroguanidino)-pentanamido)-3-(3,4,5-trimethoxyphenyl)propanoyl)oxy)benzoate (47)



The compound was synthesized according to GP2, starting from phenyl ester **11** (150 mg, 0.30 mmol, 1.00 eq), Boc-(R)-Arg(NO₂)-OH (105 mg, 0.33 mmol, 1.10 eq), COMU (140 mg, 0.33 mmol, 1.10 eq) and DIPEA (104 μL, 77 mg, 0.60 mmol, 2.00 eq) in DMF (4 mL). RP-HPLC yielded the product as a white solid (122 mg, 0.18 mmol, 66%). **TLC**: R_f = 0.22 (2% MeOH, 2% triethylamine in DCM). **¹H-NMR** (500 MHz, CD₃CN): δ [ppm] = 8.08 – 8.01 (m, 2H), 7.18 (d, *J* = 11.0 Hz, 2H), 7.18 – 7.12 (m, 2H), 6.58 (s, 2H), 5.60 (brs, 1H), 4.88 (q, *J* = 7.4 Hz, 1H), 4.06 (s, 1H), 3.87 (s, 3H), 3.79 (s, 6H), 3.69 (s, 3H), 3.27 – 3.01 (m, 4H), 1.68 (brs, 1H), 1.60 – 1.48 (m, 3H), 1.37 (s, 9H). **¹³C-NMR** (126 MHz, CD₃CN): δ [ppm] = 173.2, 170.7, 166.8, 160.6, 156.6, 155.1, 154.2, 137.6, 133.2, 131.9, 129.0, 122.6, 118.3, 107.5, 80.0, 60.7, 56.6, 54.8, 54.7, 52.8, 41.4, 37.9, 30.2, 28.4. *One carbon from a methylene group, expected at ca. 25 ppm, is not visible in the ¹³C-spectrum. It probably is superimposed with the peak at 28.4 ppm.* **HRMS** (ESI): *m/z* calcd for C₃₁H₄₂N₆O₁₂: 691.2934 [M + H]⁺, found: 691.2923.

Methyl

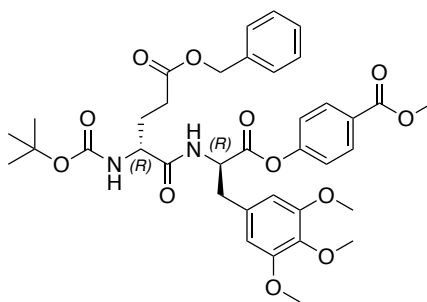
4-(((R)-2-((R)-2-((tert-butoxycarbonyl)amino)-5-guanidinopentanamido)-3-(3,4,5-trimethoxyphenyl)propanoyl)oxy)benzoate (48)



To a solution of **47** (50 mg, 72 μmol) in EtOAc (5 mL) was added Pd/C (20 mg). The suspension was flushed with H₂ for 2 min and stirred under an H₂-atmosphere (balloon) at room temperature for 45 h. The mixture was filtered over a pad of celite, which

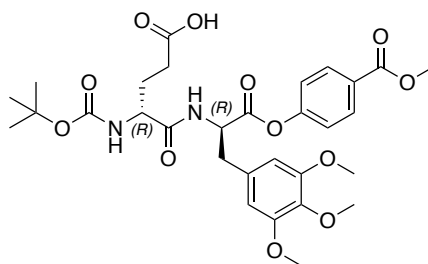
was subsequently washed with EtOAc. The solvent was removed under reduced pressure and the residue was purified by RP-HPLC, yielding the product as a white solid (8 mg, 12 μ mol, 17%). **¹H-NMR** (500 MHz, CD₃CN): δ [ppm] = 8.06 – 8.02 (m, 2H), 7.96 (brs, 1H), 7.51 (brs, 1H), 7.20 – 7.13 (m, 2H), 7.18 – 7.12 (m, 2H), 6.60 (s, 2H), 4.90 – 4.81 (m, 1H), 4.04 (s, 1H), 3.87 (s, 3H), 3.78 (s, 6H), 3.69 (s, 3H), 3.30 – 3.02 (m, 4H), 1.70 (brs, 1H), 1.60 – 1.48 (m, 3H), 1.36 (s, 9H). **¹³C-NMR** (126 MHz, CD₃CN): δ [ppm] = 173.4, 170.8, 166.8, 158.3, 156.7, 155.2, 154.2, 137.6, 133.3, 131.9, 129.0, 125.7, 122.7, 107.5, 79.9, 60.7, 56.6, 54.9, 54.7, 52.8, 41.4, 37.8, 29.9, 28.4, 25.3. **HRMS** (ESI): *m/z* calcd for C₃₁H₄₃N₅O₁₀: 646.3083 [M + H]⁺, found: 646.3079.

Methyl 4-(((*R*)-2-(((*R*)-5-(benzyloxy)-2-((*tert*-butoxycarbonyl)amino)-5-oxopentanamido)-3-(3,4,5-trimethoxyphenyl)propanoyl)oxy)benzoate (50)



The compound was synthesized according to GP2, starting from phenyl ester **11** (150 mg, 0.30 mmol, 1.00 eq), Boc-*(R)*-Glu(OBzl)-OH (111 mg, 0.33 mmol, 1.10 eq), COMU (140 mg, 0.33 mmol, 1.10 eq) and DIPEA (104 μ L, 77 mg, 0.60 mmol, 2.00 eq) in DMF (4 mL). Column chromatography (hexanes/EtOAc, 2/1) yielded the product as a white solid (175 mg, 0.25 mmol, 83%). **TLC**: R_f = 0.25 (hexanes/EtOAc, 2/1, v/v). **¹H-NMR** (500 MHz, CD₃CN): δ [ppm] = 8.05 – 8.00 (m, 2H), 7.40 – 7.28 (m, 5H), 7.17 – 7.11 (m, 3H), 6.58 (s, 2H), 5.61 (d, *J* = 6.0 Hz, 1H), 5.07 (s, 2H), 4.84 (td, *J* = 7.7, 5.9 Hz, 1H), 4.13 – 4.04 (m, 1H), 3.88 (s, 3H), 3.78 (s, 6H), 3.69 (s, 3H), 3.26 – 3.07 (m, 2H), 2.39 (t, *J* = 7.6 Hz, 2H), 2.04 – 1.96 (m, 1H), 1.86 – 1.78 (m, 1H), 1.37 (s, 9H). **¹³C-NMR** (126 MHz, CD₃CN): δ [ppm] = 173.5, 172.8, 170.7, 166.8, 156.4, 155.1, 154.2, 137.7, 137.3, 133.1, 131.9, 129.4, 129.0, 129.0, 128.9, 107.4, 80.0, 66.8, 60.7, 56.6, 54.9, 54.6, 52.8, 37.8, 30.9, 28.4, 28.1. **HRMS** (ESI): *m/z* calcd for C₃₇H₄₄N₂O₁₂: 709.2967 [M + H]⁺, found: 709.2970.

(R)-4-((tert-butoxycarbonyl)amino)-5-(((R)-1-(4-(methoxycarbonyl)phenoxy)-1-oxo-3-(3,4,5-trimethoxyphenyl)propan-2-yl)amino)-5-oxopentanoic acid (45)



To a solution of **50** (70 mg, 99 μ mol) in EtOAc (5 mL) was added Pd/C (15 mg). The suspension was flushed with H₂ for 2 min and stirred under an H₂-atmosphere (balloon) at room temperature for 18 h. The mixture was filtered over a pad of celite, which was subsequently washed with EtOAc. The solvent was removed under reduced pressure and the residue was purified by RP-HPLC, yielding the product as a white solid (51 mg, 82 μ mol, 83%). **TLC**: R_f = 0.26 (2% MeOH, 0.5% AcOH in DCM). **¹H-NMR** (500 MHz, CD₃CN): δ [ppm] = 8.06 – 8.01 (m, 2H), 7.19 – 7.12 (m, 3H), 6.58 (s, 2H), 5.64 (d, J = 7.4 Hz, 1H), 4.88 – 4.81 (m, 1H), 4.10 – 4.02 (m, 1H), 3.87 (s, 3H), 3.79 (s, 6H), 3.69 (s, 3H), 3.26 – 3.07 (m, 2H), 2.32 (t, J = 7.4 Hz, 2H), 2.02 – 1.95 (m, 1H), 1.83 – 1.72 (m, 1H), 1.37 (s, 9H). **¹³C-NMR** (126 MHz, CD₃CN): δ [ppm] = 174.4, 172.9, 170.7, 166.8, 156.5, 155.1, 154.2, 137.7, 133.1, 131.8, 129.0, 122.6, 107.4, 80.0, 60.7, 56.6, 54.9, 54.6, 52.8, 37.8, 30.3, 28.4, 28.0. **HRMS** (ESI): m/z calcd for C₃₀H₃₈N₂O₁₂: 619.2498 [M + H]⁺, found: 619.2499.

7.2 BIOCHEMICAL METHODS

7.2.1 PROTEIN PURIFICATION

C-terminal STREP-II affinity tagged *S. aureus* ClpP were cloned in pET301 expression vectors via Gateway[®] cloning system (Life Technologies) and purified as described previously.^[5,6] In short, ClpP was expressed overnight at 25 °C in *E. coli* BL21(DE3) cells after induction at OD₆₀₀ = 0.6 with 0.5 mM IPTG. Cells were harvested, resuspended in binding buffer (100 mM Tris/HCl, pH = 8.0, 150 mM NaCl, 1 mM EDTA) and lysed by sonication (2 x (7 min, 30% int.; 3 min, 80% int.), Bandelin Sonopuls) under constant cooling with ice. The lysate was cleared by centrifugation (38,000 rpm, 30 min, 4 °C) and the soluble fraction was loaded on an equilibrated 5 mL StrepTrap HP column (GE Healthcare) using an Äkta purifier 10 system (GE Healthcare). The column was washed with binding buffer. Elution was performed over four column volumes (CV) of binding buffer + 2.5 mM desthiobiotin. The fractions containing ClpP were pooled, concentrated using a 50 kDa MWCO centrifugal filter (Merck) and subjected to preparative size-exclusion chromatography (HiLoad 16/60 Superdex 200 pg (GE Healthcare)) using ClpP storage buffer (20 mM HEPES, pH = 7.0, 100 mM NaCl). The identity and purity of the protein was validated by intact-protein MS and SDS-PAGE. Fractions containing ClpP were pooled, concentrated and stored at -80 °C.

Untagged *S. aureus* ClpP was used for experiments concerning the de-oligomerization during the catalytic cycle of ClpP. The protein was kindly provided by Dr. Mathias Hackl and was purified through anion exchange, hydrophobic interaction and size-exclusion chromatograph, as described previously.^[7]

S. aureus ClpX was cloned in pET300 expression vectors with an N-terminal His₆-tag and a TEV cleavage site and purified as described previously.^[8,9] In short, ClpX was expressed in *E. coli* BL21(DE3) cells at 25 °C overnight after induction at OD₆₀₀ = 0.6 with 0.5 mM IPTG. The cells were harvested and lysed in ClpX lysis buffer (25 mM HEPES pH = 7.6, 200 mM KCl, 0.5 mM ATP, 1 mM DTT, 5 mM MgCl₂, 5% glycerol) by sonication (2 x (7 min, 30% int.; 3 min, 80% int.), Bandelin Sonopuls) under constant cooling with ice. The lysate was cleared by centrifugation (38,000 rpm, 30 min, 4 °C) and the soluble fraction was loaded on a pre-equilibrated HisTrap HP column

(GE Healthcare) using an ÄKTA purifier 10 system (GE Healthcare). The column was washed with 10 CV lysis buffer + 40 mM imidazole. Elution was carried out using 4 CV lysis buffer + 500 mM imidazole. EDTA (2 mM) and TEV protease (500 μ L, 2.0 mg/mL) were added to the pooled elution fractions and incubated at 10 °C overnight. Full cleavage of the purification tag was verified by intact-protein mass spectrometry. The sample was concentrated using a 50 kDa MWCO centrifugal filter (Merck) and subjected to preparative size-exclusion chromatography (HiLoad 16/60 Superdex 200 pg (GE Healthcare)) using ClpX storage buffer (25 mM HEPES, pH = 7.6, 200 mM KCl, 5 mM MgCl₂, 1 mM DTT, 0.5 M ATP, 5 % glycerol). The identity and purity of the protein was validated by intact-protein MS and SDS-PAGE. Fractions containing ClpX were pooled, concentrated and stored at -80 °C.

The Walker-B point mutant of SaClpX (E183Q) was generated by QuickChange II site-directed mutagenesis protocol (Stratagene) using the pET300 ClpX expression vector as a template, as previously described.^[9] Expression and purification were performed under the same conditions as for the pET300-wt expression vector.

Enhanced GFP which is C-terminally tagged for ClpXP degradation by a short SsrA sequence (AANDENYALAA), *i.e.* eGFP-SsrA, was purified by a N-terminal His₆-tag. In previous studies the Strep-tagged version was used.^[6,8] As this, however, would have been co-purified during the analytical Strep-purification of ClpP in context of the experiments concerning the de-oligomerization during ClpP's catalytic cycle, the purification tag was altered. We used the Gateway[®] cloning system (Life Technologies) for cloning. The eGFP-SsrA gene from the previously cloned pDest007 expression vector was transferred into a pDONR201 vector via BP reaction. After amplification of the vector in *E. coli* Top10 cells and DNA-purification, LR reaction was used to transfer the eGFP-SsrA gene into the pET300 expression vector which holds an N-terminal His₆-tag. The correct DNA sequence was verified by Sanger sequencing and the vector was transformed into *E. coli* SG1146a cells. Expression was carried out in 1 L LB Media (0.1 mg/mL ampicillin), which was inoculated with an overnight culture (1:100). After reaching OD₆₀₀ = 0.6, and induction by addition of 1 mM IPTG, expression was performed at 37 °C for 6 h. The cells were harvested, resuspended in 25 mL lysis buffer (20 mM TRIS, pH = 8.0, 150 mM NaCl, 10 mM imidazole, 2 mM β -mercaptoethanol) + 0.2% NP-40 and lysed by sonication (2 x (7 min, 30% int.; 3 min, 80% int.), Bandelin Sonopuls) under constant cooling with ice. The lysate was cleared by centrifugation

(38,000 rpm, 30 min, 4 °C) and the soluble fraction was loaded on a equilibrated 5 mL HisTrap HP column (GE Healthcare) using an ÄKTA purifier 10 system (GE Healthcare). The column was washed with 8 CV lysis-buffer, 8 CV lysis-buffer + 850 mM NaCl (total 1 M NaCl) and 8 CV lysis-buffer + 10 mM imidazole (total 20 mM imidazole). Elution was performed by 5 CV of lysis-buffer + 490 mM imidazole (total 500 mM). All fractions containing protein were concentrated using a 10 kDa MWCO centrifugal filter (Merck) and subjected to preparative size-exclusion chromatography (HiLoad 16/60 Superdex 200 pg (GE Healthcare)) using eGFP-SsrA-storage buffer (20 mM Tris, pH = 8, 100 mM NaCl, 10% glycerol). The identity and purity of the protein was validated by intact-protein MS and SDS-PAGE. Fractions containing eGFP-SsrA were pooled, concentrated and stored at -80 °C.

7.2.2 INTACT-PROTEIN MASS SPECTROMETRY

High-resolution intact-protein mass spectrometry was performed to validate the identity of expressed proteins, to measure the degree of covalent modification of ClpP by small-molecules and for analysis of the pull-down experiments in respect to ClpP's de-oligomerization during the catalytic cycle (see below). Measurements were performed on a Dionex Ultimate 3000 HPLC system coupled to an LTQ FT Ultra (Thermo) mass spectrometer with an electrospray ionization source (spray voltage 4.0 kV, tube lens 110 V, capillary voltage 48 V, sheath gas 60 a.u., aux gas 10 a.u., sweep gas 0.2 a.u.). Reaction mixtures containing a total of about 1 – 10 pmol protein were desalted with a Massprep desalting cartridge (Waters) before measurement. The mass spectrometer was operated in positive ion mode collecting full scans at high resolution ($R = 200,000$) from m/z 600 to m/z 2000. The protein spectra were deconvoluted using the Thermo Xcalibur Xtract algorithm.

7.2.3 *IN VITRO* ACTIVITY ASSAYS

In vitro inhibition of *S. aureus* ClpXP protease activity was measured by monitoring the degradation of eGFP-SsrA, a fluorescent substrate which is tagged for ClpXP-mediated degradation by a short SsrA-sequence.^[10,11] 0.60 μ L of compound (100x stocks in DMSO) or DMSO as a control were added to a black flat bottom 96-well plate (Greiner). 58.4 μ L of enzyme-mix (final concentrations: 0.10 μ M ClpP₁₄, 0.20 μ M ClpX₆, ATP-regeneration system: 4 mM ATP, 16 mM creatine phosphate, 20 U/mL creatine phosphokinase in PZ buffer (25 mM HEPES, pH = 7.6, 200 mM KCl, 5 mM MgCl₂, 1 mM DTT, 10% glycerol)) was added and the mixture was incubated at 32 °C for 15 min. The reaction was started by addition of 1 μ L of eGFP-SsrA (18 μ M in PZ buffer, final concentration: 0.3 μ M). GFP fluorescence (λ_{ex} = 465 nm, λ_{em} = 535 nm) was monitored at 32 °C with an Infinite M200 Pro plate reader (Tecan). The slope of the curve in the linear range was determined via linear regression using GraphPad Prism. DMSO-treated control samples were normalized to 100% activity and samples without ClpXP were used as a negative control. Data were recorded in triplicates and at least two independent experiments were performed. For measurement of the protease activity in the presence of activating compounds, the eGFP-SsrA-concentration was tripled (final concentration: 0.9 μ M) in order to properly fit the linear range.

In vitro ATPase activity of *S. aureus* ClpX in the presence/absence of inhibitors and/or ClpP was measured using an enzyme-coupled assay.^[12] The assay was performed in ATPase buffer (final concentrations: 100 mM HEPES, 200 mM KCl, 20 mM MgCl₂, 1 mM DTT, 1 mM NADH, 2 mM phosphoenolpyruvate, 50 U/mL lactate dehydrogenase, 50 U/mL pyruvate kinase, 10% glycerol) using a final concentration of 0.33 μ M ClpX₆ (and 0.17 μ M ClpP₁₄ if applicable). Inhibition experiments were performed in a total volume of 100 μ L. 1.0 μ L of compound (100x stocks in DMSO) or DMSO as a control were pipetted in transparent flat bottom 96-well plate (Greiner). 89 μ L of ClpX in ATPase buffer were added and the mixture was incubated at 32 °C for 10 min. The reaction was started by addition of 10 μ L ATP (20 mM in PZ buffer, pH = 7.6, final concentration 2 mM). Absorbance (λ = 340 nm) was monitored at 32° C with an Infinite M200 Pro plate reader (Tecan). The slope of the curve in the linear range was determined via linear regression using GraphPad Prism. DMSO treated control samples

were normalized to 100% activity and samples without ClpX were used as a negative control. Data were recorded in triplicates and at least two independent experiments were performed. For measurement of the ATPase activity in the presence of activating compounds or upon activation by ClpP, the concentrations of NADH and phosphoenolpyruvate were doubled (final concentration: 2 mM and 4 mM, respectively) in order to properly fit the linear range. Measurements for the determination of the apparent affinity constant were performed in a volume of 60 μ L. The slope of the curve in the linear range was determined via linear regression using GraphPad Prism. Samples without ClpX were used as a negative control. For determination of the affinity constants, data were fitted using a Hill Fit.

7.2.4 ANALYTICAL SIZE-EXCLUSION CHROMATOGRAPHY

Analytical size-exclusion chromatography experiments were performed at 4 °C on an ÄKTA purifier 10 system (GE Healthcare) using a calibrated Superdex 200 10/300 GL (GE Healthcare) or a calibrated Superose 6 Increase 10/300 GL (GE Healthcare) column. PZ buffer supplemented with 0.5 mM ATP was used for all runs. We used a mutant of ClpX, ClpX(E183Q), which cannot hydrolyze ATP for the experiments.^[9] Samples (depending on the experiment: 0.71 μ M ClpP₁₄, 2.86 μ M ClpX(E183Q)₆ and/or 200 μ M compound, V = 200 μ L) were mixed, incubated for 15 min at 32 °C and loaded into a 500 μ L loop. Elution was monitored at 280 nm. Runs were referenced against the salt peak of the conductivity trace and normalized to the highest peak for easier comparison.

7.2.5 NEGATIVE-STAIN ELECTRON MICROSCOPY

For recording of negative-stain TEM images, the ClpX₆P₇ complex was formed by incubation of ClpXP with **9** (0.71 μ M ClpP₁₄, 2.86 μ M ClpX(E183Q)₆, 200 μ M **9**, V = 200 μ L) and isolated by analytical size-exclusion chromatography. A sample of the complex peak (0.035 mg/mL) was adsorbed on glow-discharged formvar-supported carbon-coated Cu₄₀₀ TEM grids (Science Services, Munich, Germany) and stained with an aqueous uranyl formate solution (2%) containing sodium hydroxide (25 mM).

Imaging was performed with a Tecnai 120 electron microscope (FEI, Thermo Fisher Scientific) operated at 120 kV. Images were acquired with a TVIPS TemCam-F416, CMOS detector. Micrograph scale bars were calibrated by imaging 2D catalase crystals and using the lattice constants as length reference. Imaging was performed at $\times 67,000$ magnification. For image processing, libraries of individual particle micrographs were created by particle picking by use of the Relion 2.1 routine.^[13] In total, 33374 particles were picked from 414 micrographs. 2D classes were generated in three runs (100 classes each). 18382 particles were selected from the 2D classes and 3D classes were calculated. Particles were classified in four 3D classes and the most populated class was chosen for refinement. The final refinement was based on 5593 particles and the final resolution was 30.5 Å.

7.2.6 DETERMINATION OF DISSOCIATION CONSTANTS BY SWITCHSENSE

All measurements were performed on a dual-color DRX² instrument using a standard switchSENSE® chip (order no. MPC2-96-2-G1R1, Dynamic Biosensors GmbH), which provides two differently labeled DNA sequences on each electrode (green fluorescent NL-A96, red fluorescent NL-B96). The chip was functionalized by hybridization of the ClpP₁₄-cNL-B96-conjugate and bare cNL-A96 DNA (each 200 nM, HE40 buffer, Dynamic Biosensors GmbH). In this way, the red fluorescence yields the desired signal, while the green fluorescence provides an on-spot reference for unspecific effects. The conjugate was prepared by coupling the complementary nanolever sequence cNL-B96 sequence to ClpP₁₄ using the amine-coupling kit (order no. CK-NH₂-1-B96, Dynamic Biosensors GmbH). To analyze the ClpX₆ - ClpP₇ interaction, the ClpP₁₄-cNL-B96-conjugate (200 nM) was preincubated with **35** (200 μM) in the presence of 0.5 mM ATP for at least 2 h before functionalization. The titration experiments were performed in HEPES buffer (25 mM HEPES, pH = 7.6, 200 mM KCl, 5 mM MgCl₂, 0.5 mM TCEP, 0.5 mM ATP, 10% glycerol). In a 1:1 dilution series, 14 ClpX samples were prepared starting at a concentration of 600 μM. After functionalization of the chip, increasing concentrations of ClpX were injected and the dynamic response was measured in stopped-flow after 2 min of equilibration. To ensure that the observed effect is not due to aging of the conjugate, a control experiment was performed. For this, the chip was regenerated and freshly functionalized before each measurement of the titration series and the

dynamic response of the conjugate was checked to be constant before injection of ClpX. During regeneration, the chip is exposed to a high-pH regeneration solution (order no. SOL-REG-12-1, Dynamic Biosensors GmbH). This procedure denatures the double-stranded DNA by disrupting hydrogen bonds between the base pairs. The conjugate is washed away while the covalently attached single-stranded nanolevers remain on the surface and can be reused for a new functionalization step. Dynamic responses were normalized, resulting in fraction-bound values. For determination of the affinity constants, data were fitted using a Langmuir Fit.

7.2.7 INTACT-PROTEIN MS-BASED PULLDOWN-ASSAY

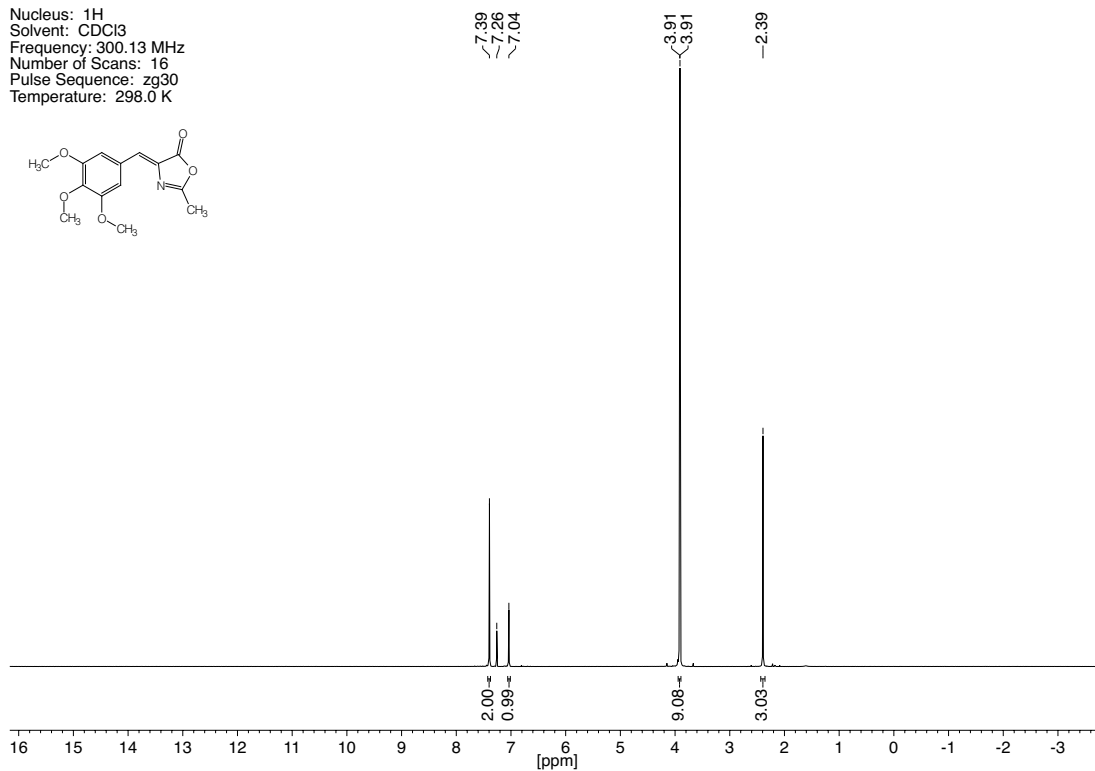
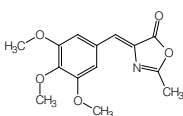
In order to investigate if de-oligomerization of Clp(X)P is associated with its catalytic activity, we performed pulldown-experiments with Strep-tagged ClpP and untagged ClpP. Experiments were performed in PZ buffer (25 mM HEPES, pH = 7.6, 200 mM KCl, 5 mM MgCl₂, 1 mM DTT, 10% glycerol). For peptidase assay conditions, 0.1 μM Strep-tagged ClpP₁₄, 0.1 μM untagged ClpP₁₄, and 100 μM Ac-Ala-hArg-2-Aoc-ACC were incubated at 32 °C for 6 h. As a control, DMSO was added instead of substrate. For protease assay conditions, 0.1 μM Strep-tagged ClpP₁₄, 0.1 μM untagged ClpP₁₄, 0.2 μM ClpX₆, and 0.9 μM eGFP-SsrA were incubated for 2 h at 32 °C. As a control, DMSO was added instead of eGFP-SsrA. After incubation, affinity purification was performed using self-packed gravity-flow Strep-Tactin Sepharose (50% suspension, iba) affinity columns. Columns were equilibrated with PZ buffer (600 μL). Samples (350 μL) were loaded onto columns and washed with PZ buffer (800 μL). Elution was performed using PZ buffer + 10 mM desthiobiotin (600 μL). Samples from each fraction were diluted with PZ buffer and subjected to intact-protein mass spectrometry (see above). The intensities of both ClpP species within the deconvoluted spectra were compared relatively. For control experiments, 1 μM Strep-tagged ClpP₁₄ and 1 μM untagged ClpP₁₄ in 400 μL PZ buffer were incubated with 25 μM **9** or DMSO at 32 °C for 24 h. Full hydrolysis was verified by intact-protein mass spectrometry and samples were subjected to analytical gel filtration to verify re-oligomerization, and affinity purification–mass spectrometry, as described above.

7.3 REFERENCES

- [1] P. Furet, P. Imbach, M. Noorani, J. Koeppler, K. Laumen, M. Lang, V. Guagnano, P. Fuerst, J. Roesel, J. Zimmermann, C. García-Echeverría, *J. Med. Chem.* **2004**, *47*, 4810–4813.
- [2] C. E. Humphrey, M. Furegati, K. Laumen, L. La Vecchia, T. Leutert, J. C. D. Müller-Hartweg, M. Vögtle, *Org. Process Res. Dev.* **2007**, *11*, 1069–1075.
- [3] X. Wu, L. Hu, *J. Org. Chem.* **2007**, *72*, 765–774.
- [4] S. Xie, S. A. Lopez, O. Ramström, M. Yan, K. N. Houk, *J. Am. Chem. Soc.* **2015**, *137*, 2958–2966.
- [5] M. Gersch, A. List, M. Groll, S. A. Sieber, *J. Biol. Chem.* **2012**, *287*, 9484–9494.
- [6] M. W. Hackl, M. Lakemeyer, M. Dahmen, M. Glaser, A. Pahl, K. Lorenz-Baath, T. Menzel, S. Sievers, T. Böttcher, I. Antes, H. Waldmann, S. A. Sieber, *J. Am. Chem. Soc.* **2015**, *137*, 8475–8483.
- [7] M. Gersch, R. Kolb, F. Alte, M. Groll, S. A. Sieber, *J. Am. Chem. Soc.* **2014**, *136*, 1360–1366.
- [8] M. Gersch, K. Famulla, M. Dahmen, C. Göbl, I. Malik, K. Richter, V. S. Korotkov, P. Sass, H. Rübsamen-Schaeff, T. Madl, H. Brötz-Oesterhelt, S. A. Sieber, *Nat. Commun.* **2015**, *6*, 6320.
- [9] C. Fetzer, V. S. Korotkov, R. Thänert, K. M. Lee, M. Neuenschwander, J. P. von Kries, E. Medina, S. A. Sieber, *Angew. Chem. Int. Ed.* **2017**, *56*, 15746–15750.
- [10] Y. I. Kim, R. E. Burton, B. M. Burton, R. T. Sauer, T. A. Baker, *Mol. Cell.* **2000**, *5*, 639–648.
- [11] G. L. Hersch, T. A. Baker, R. T. Sauer, *Proc. Natl. Acad. Sci. U.S.A.* **2004**, *101*, 12136–12141.
- [12] J. G. Nørby, *Meth. Enzymol.* **1988**, *156*, 116–119.
- [13] R. Fernandez-Leiro, S. H. W. Scheres, *Acta Cryst* **2017**, *76*, 496–502.

7.4 NMR SPECTRA

Nucleus: ^1H
Solvent: CDCl_3
Frequency: 300.13 MHz
Number of Scans: 16
Pulse Sequence: zg30
Temperature: 298.0 K



Nucleus: ^{13}C
Solvent: CDCl_3
Frequency: 75.48 MHz
Number of Scans: 256
Pulse Sequence: zgpg30
Temperature: 298.0 K

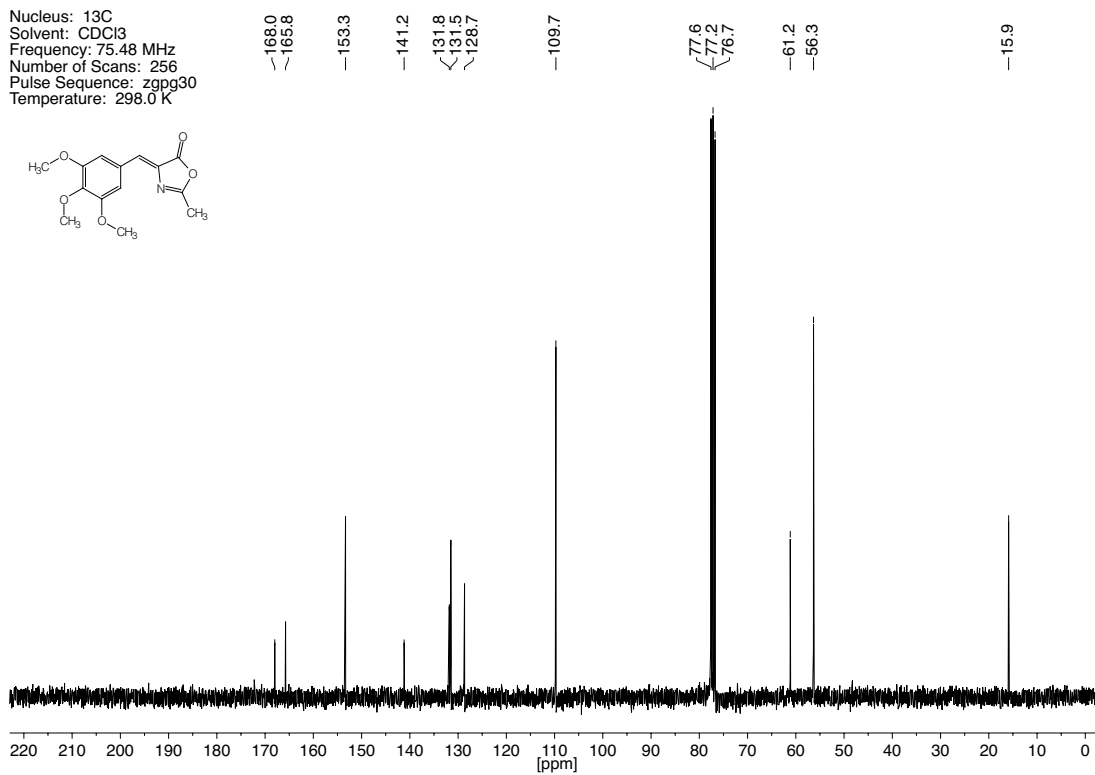
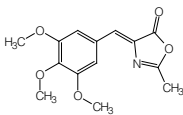
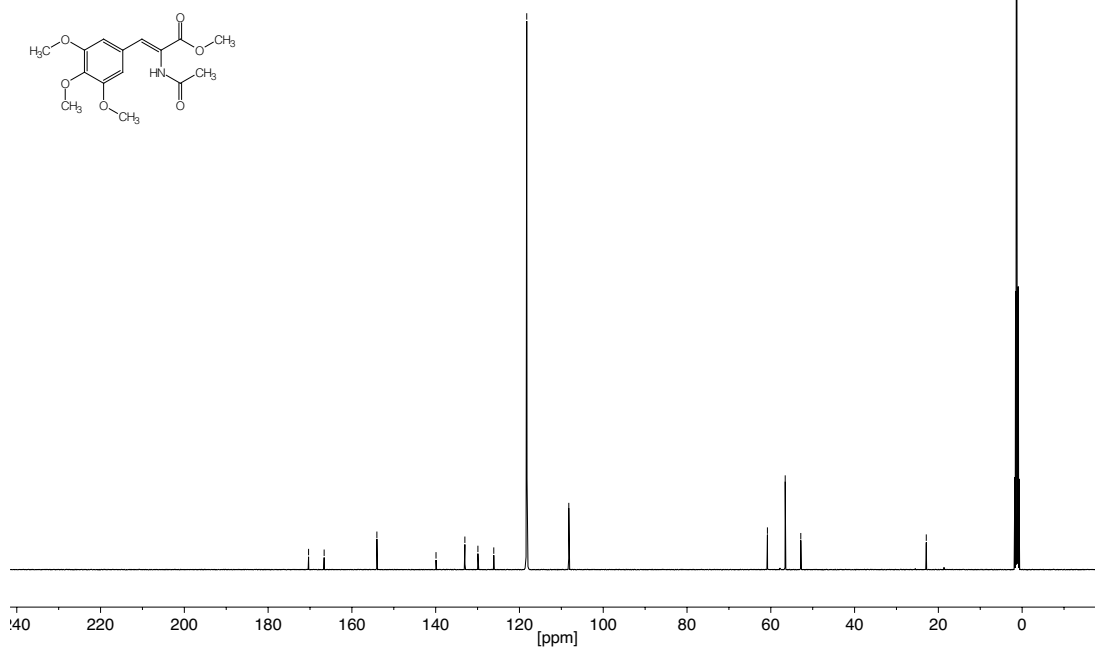


Figure 7.1. ^1H - and ^{13}C -NMR spectra of compound 1.

Nucleus: ^{13}C
Solvent: CD_3CN
Frequency: 125.83 MHz
Number of Scans: 256
Pulse Sequence: zgpg30
Temperature: 299.9 K



Nucleus: ^{13}C
Solvent: CD_3CN
Frequency: 125.83 MHz
Number of Scans: 256
Pulse Sequence: zgpg30
Temperature: 299.9 K

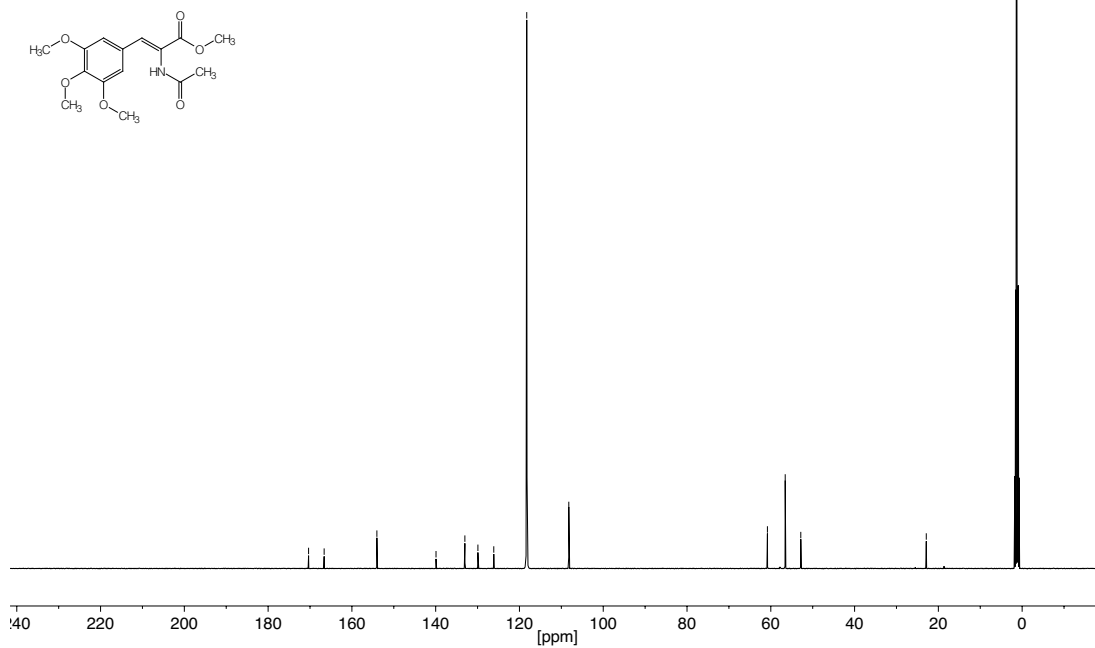
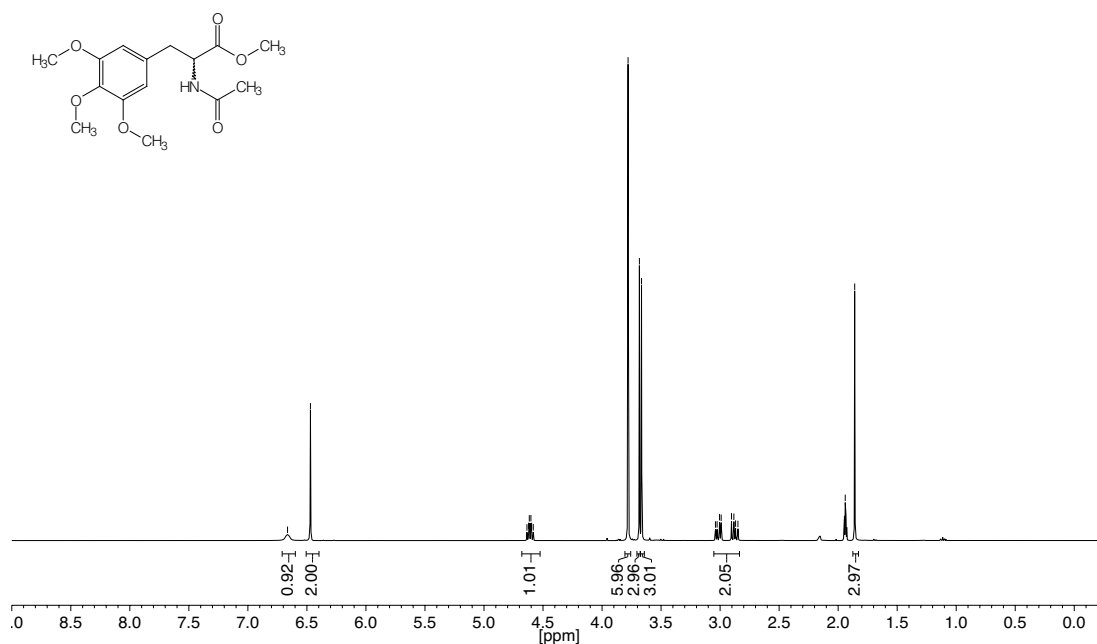


Figure 7.2. ^1H - and ^{13}C -NMR spectra of compound 2.

Nucleus: ^1H
 Solvent: CD_3CN
 Frequency: 400.13 MHz
 Number of Scans: 16
 Pulse Sequence: zg30
 Temperature: 298.0 K



Nucleus: ^{13}C
 Solvent: CD_3CN
 Frequency: 125.83 MHz
 Number of Scans: 256
 Pulse Sequence: zgpg30
 Temperature: 299.8 K

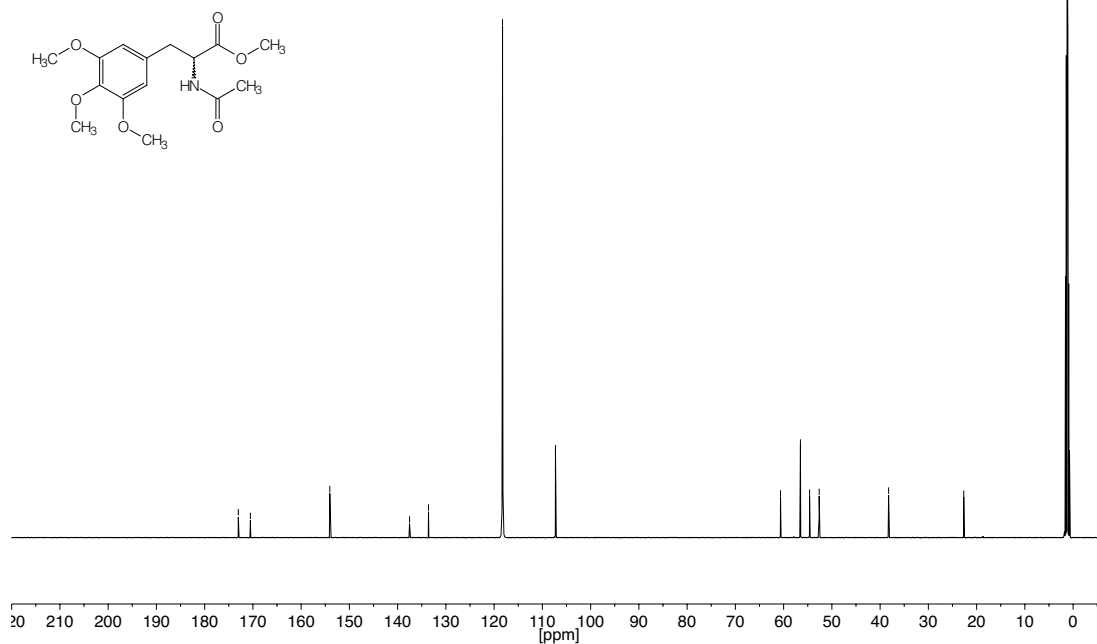
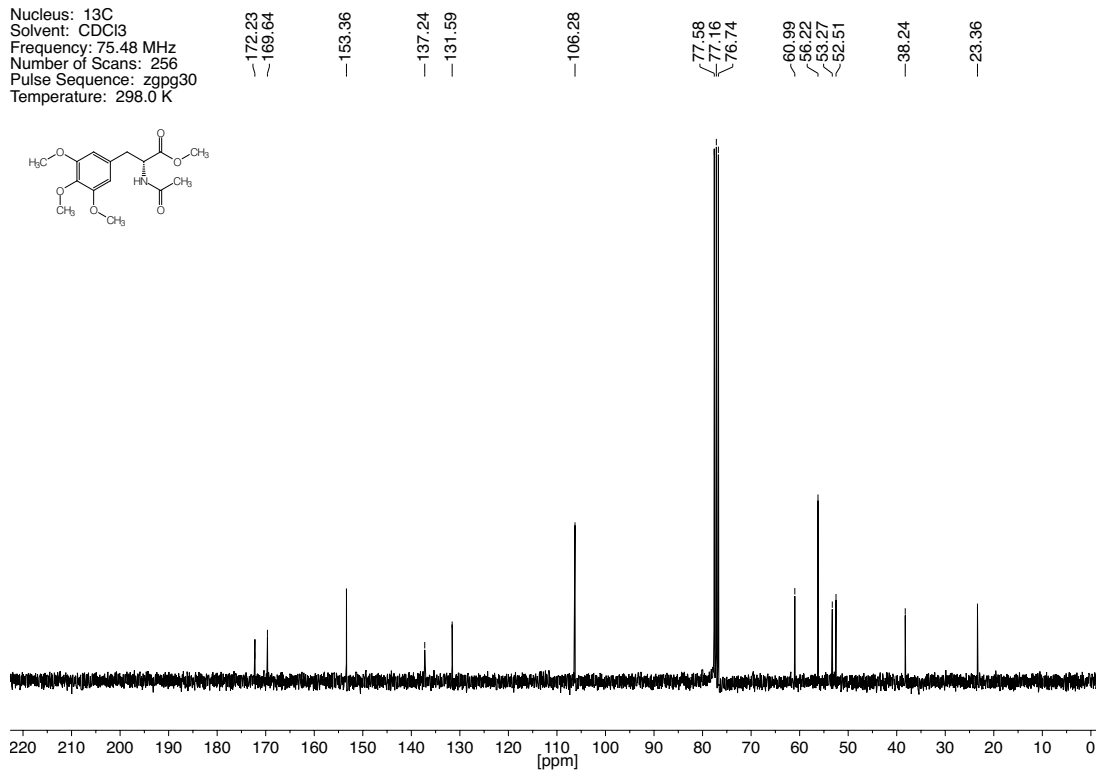


Figure 7.3. ^1H - and ^{13}C -NMR spectra of compound 3.

Nucleus: ^{13}C
Solvent: CDCl_3
Frequency: 75.48 MHz
Number of Scans: 256
Pulse Sequence: zgpg30
Temperature: 298.0 K



Nucleus: ^{13}C
Solvent: CDCl_3
Frequency: 75.48 MHz
Number of Scans: 256
Pulse Sequence: zgpg30
Temperature: 298.0 K

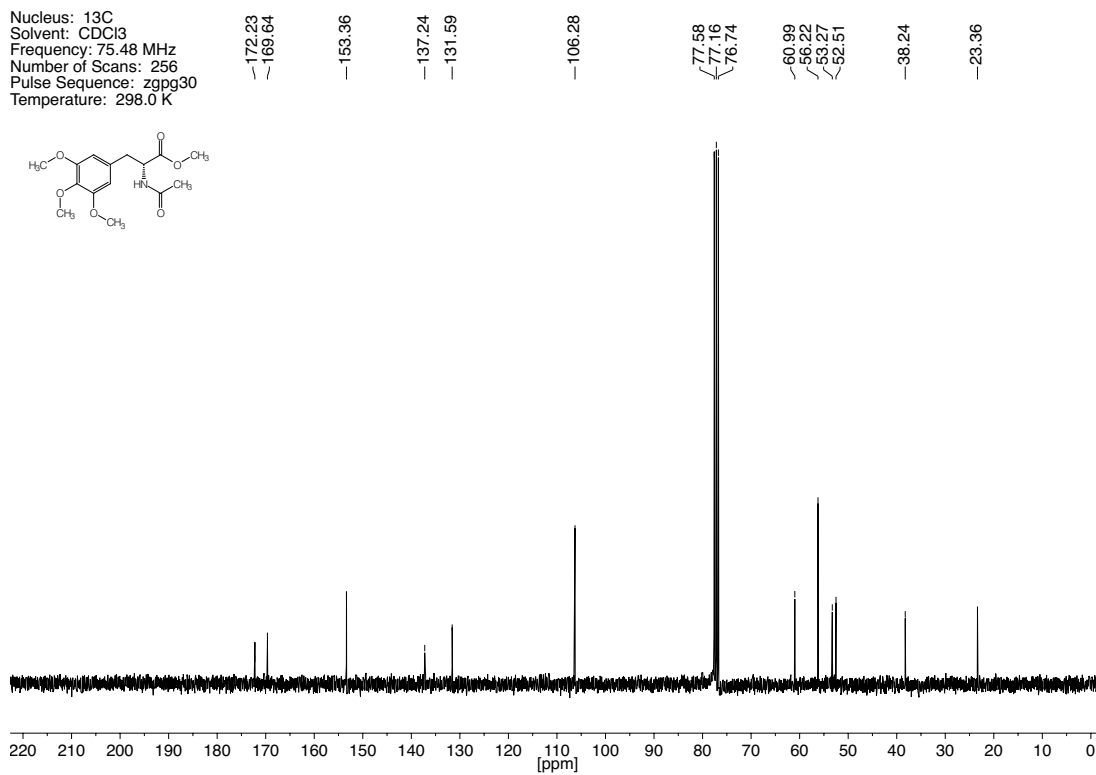
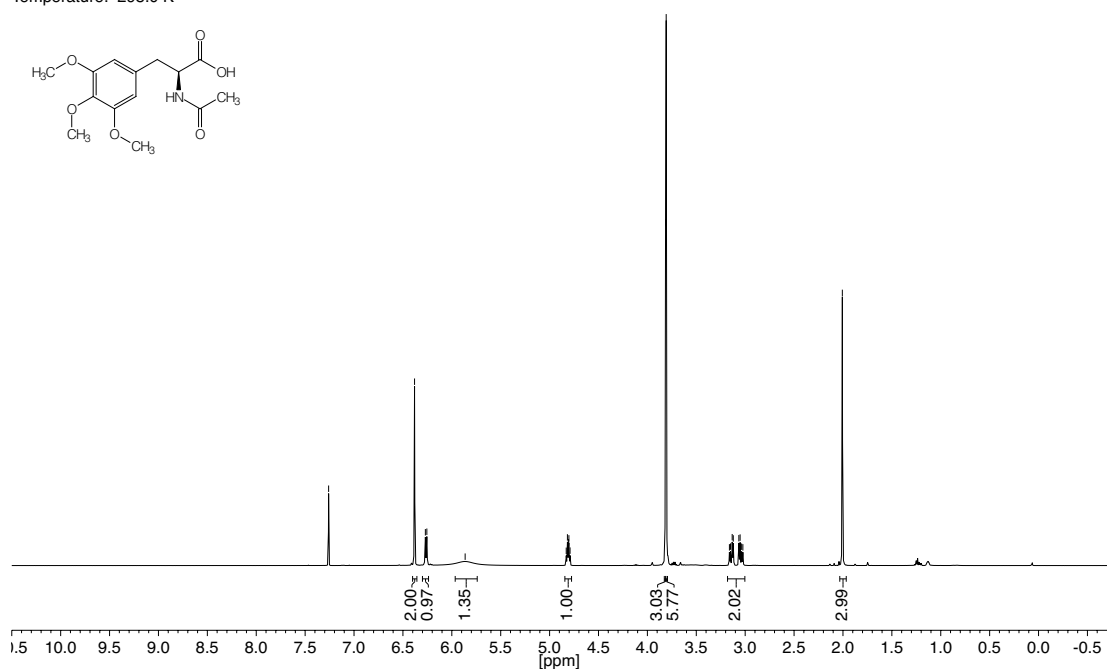


Figure 7.4. ^1H - and ^{13}C -NMR spectra of compound 4.

Nucleus: ^1H
 Solvent: CDCl_3
 Frequency: 500.13 MHz
 Number of Scans: 16
 Pulse Sequence: zg30
 Temperature: 298.0 K



Nucleus: ^{13}C
 Solvent: CDCl_3
 Frequency: 100.62 MHz
 Number of Scans: 1024
 Pulse Sequence: zgpg30
 Temperature: 298.0 K

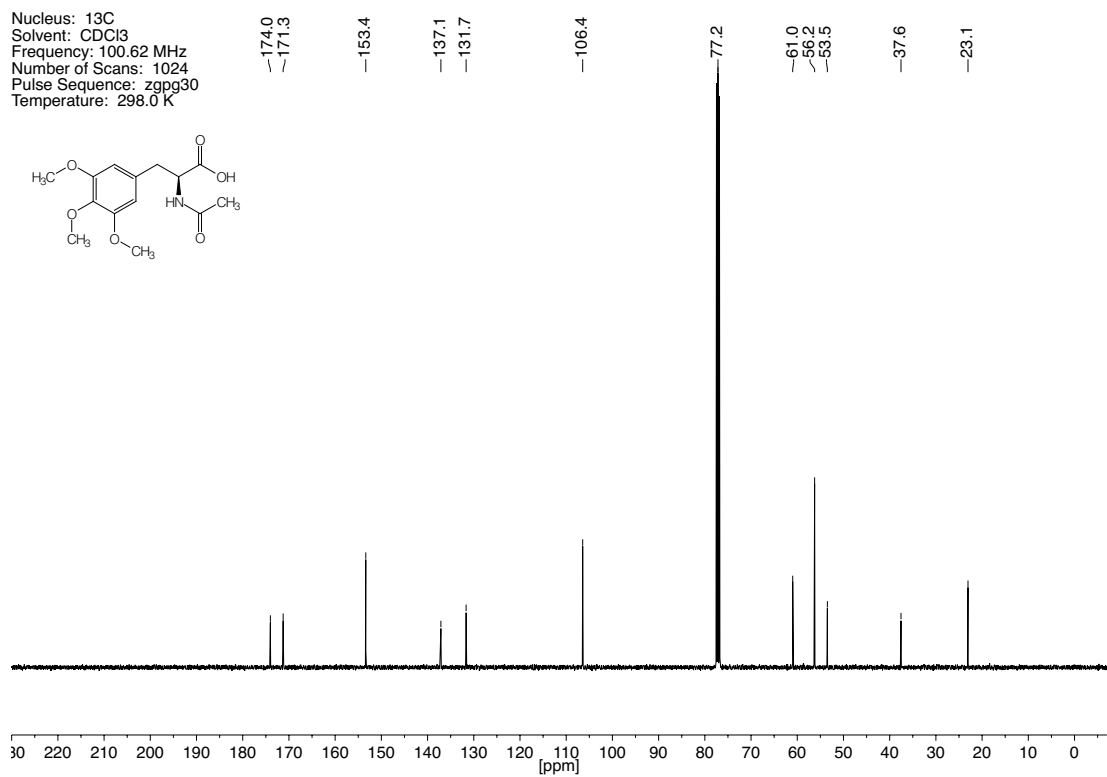
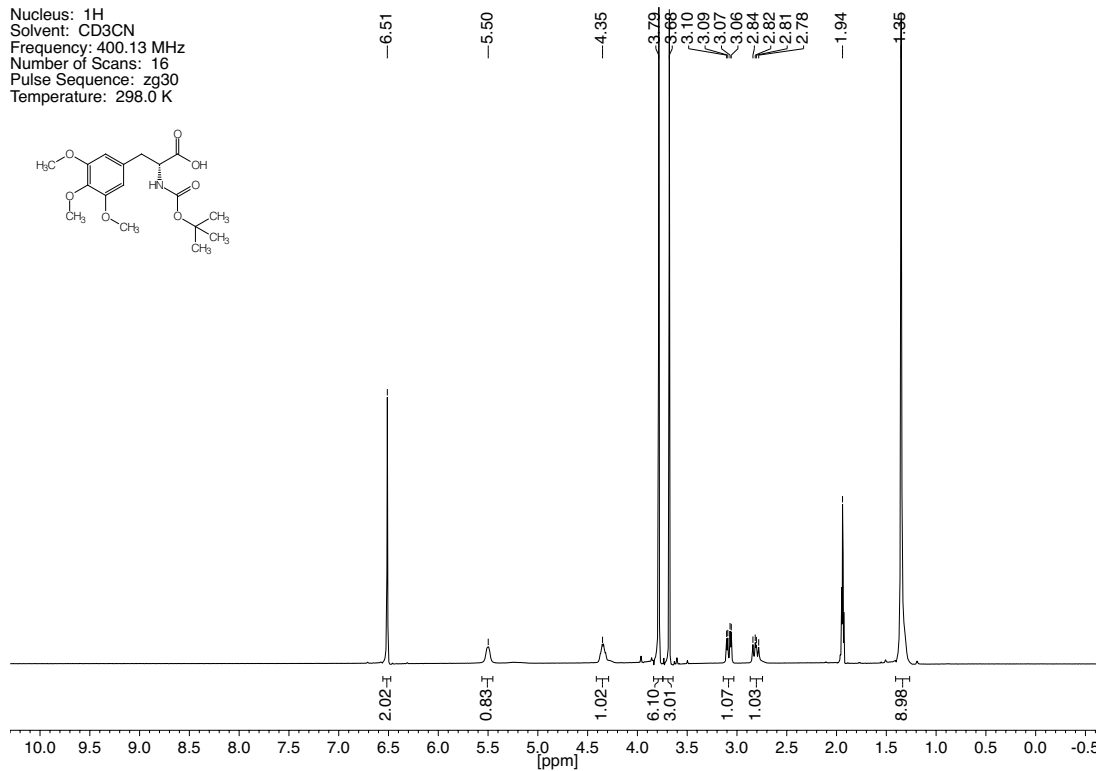
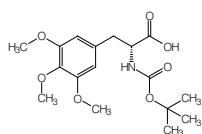


Figure 7.5. ^1H - and ^{13}C -NMR spectra of compound 5.

Nucleus: ^1H
 Solvent: CD_3CN
 Frequency: 400.13 MHz
 Number of Scans: 16
 Pulse Sequence: zg30
 Temperature: 298.0 K



Nucleus: ^{13}C
 Solvent: CD_3CN
 Frequency: 100.62 MHz
 Number of Scans: 1024
 Pulse Sequence: zgpg30
 Temperature: 298.0 K

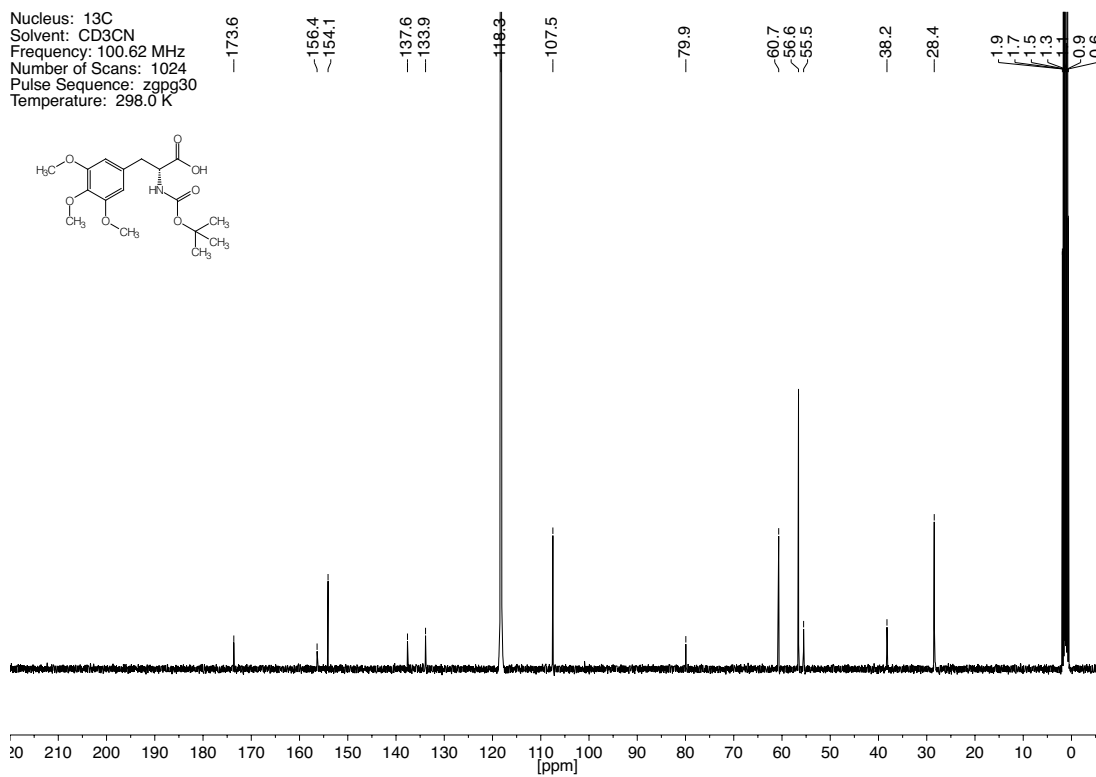
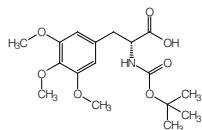


Figure 7.6. ^1H - and ^{13}C -NMR spectra of compound 7.

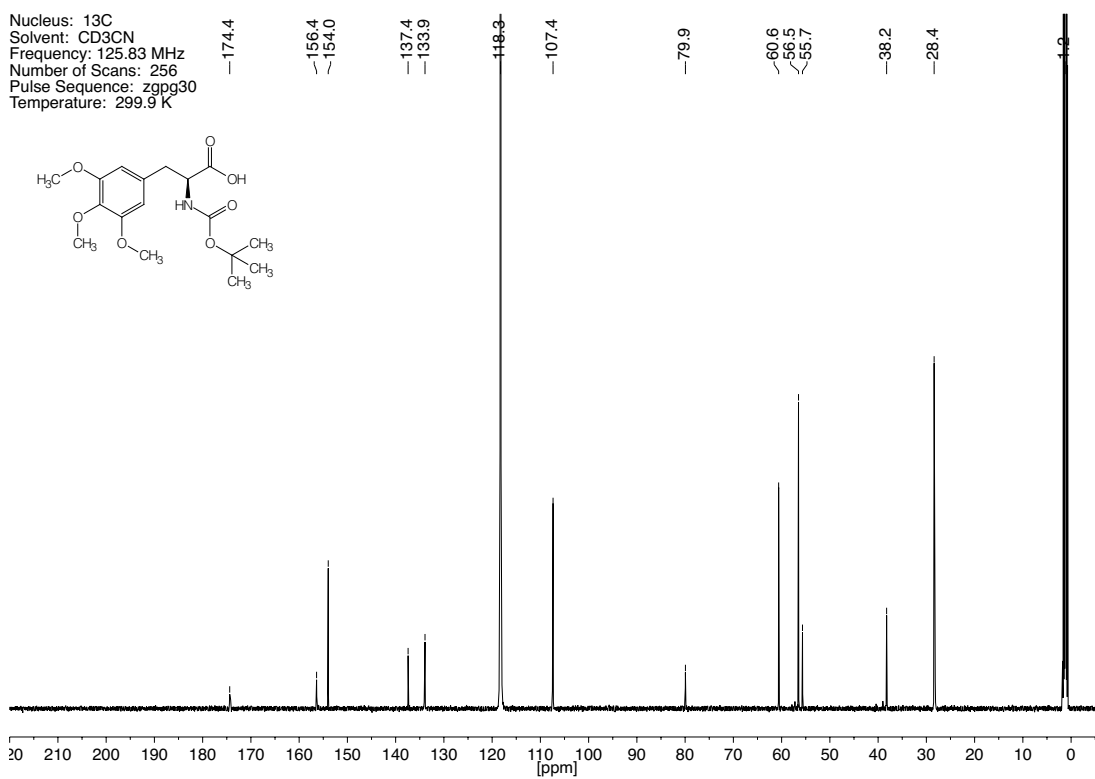
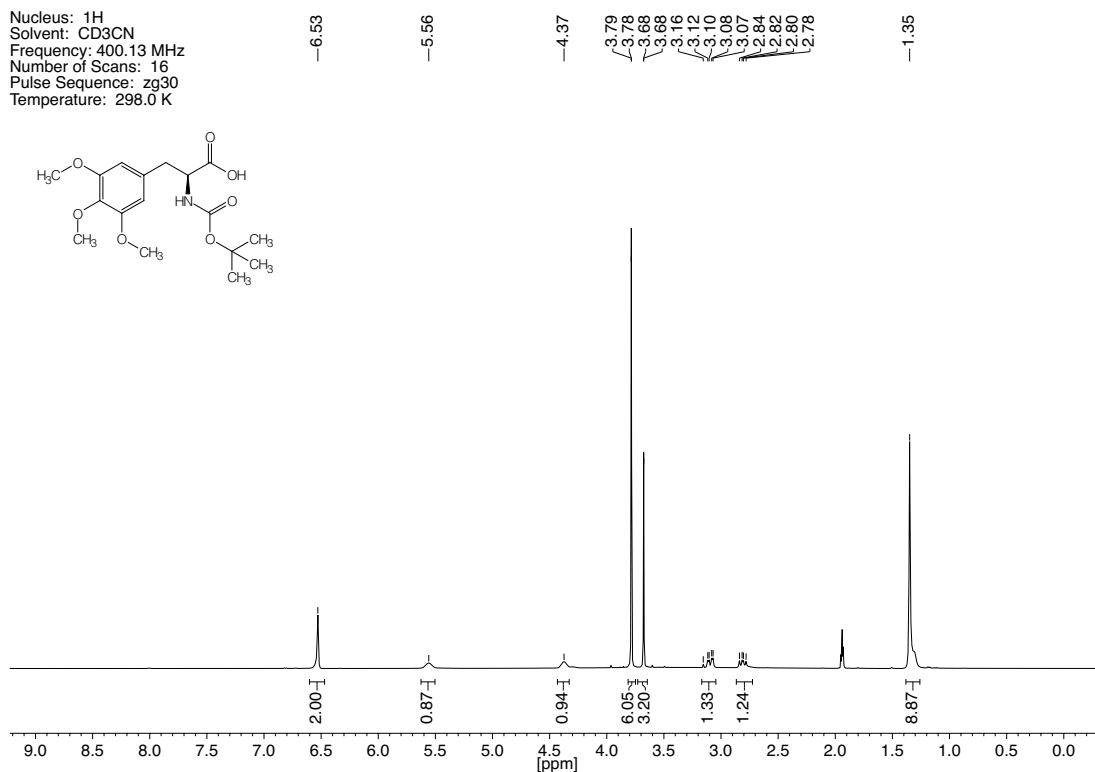
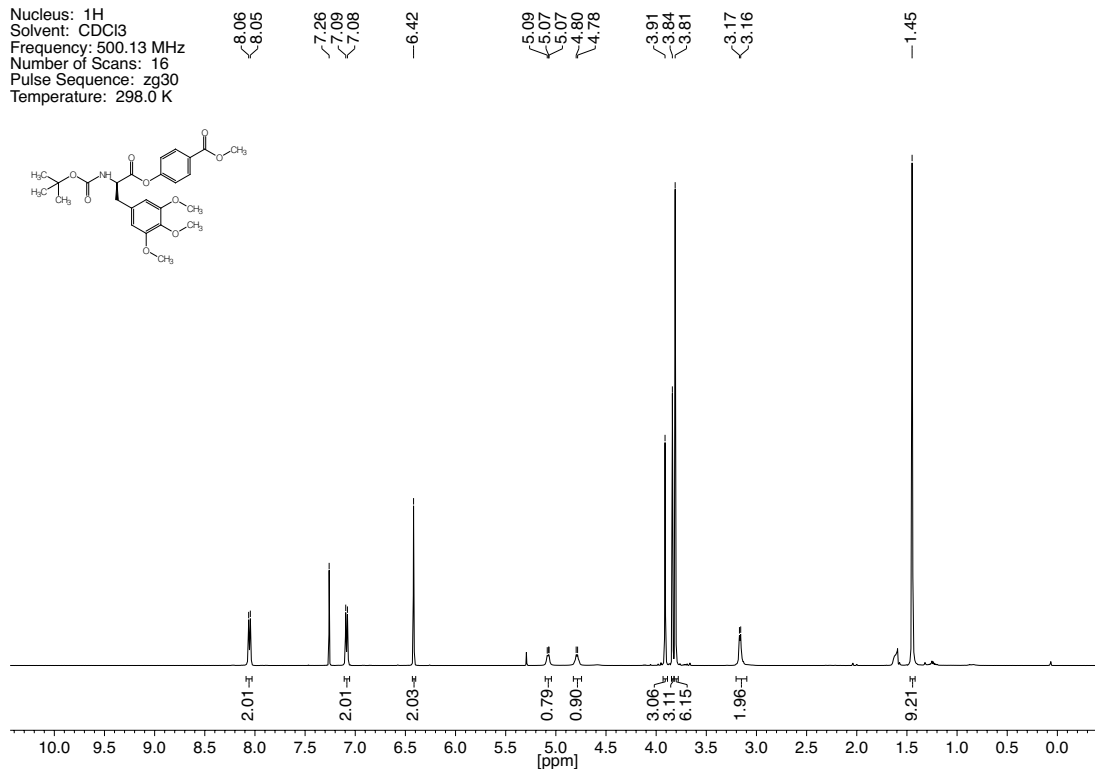


Figure 7.7. ^1H - and ^{13}C -NMR spectra of compound **8**.

Nucleus: ^1H
 Solvent: CDCl_3
 Frequency: 500.13 MHz
 Number of Scans: 16
 Pulse Sequence: zg30
 Temperature: 298.0 K



Nucleus: ^{13}C
 Solvent: CDCl_3
 Frequency: 100.62 MHz
 Number of Scans: 1024
 Pulse Sequence: zgpg30
 Temperature: 298.0 K

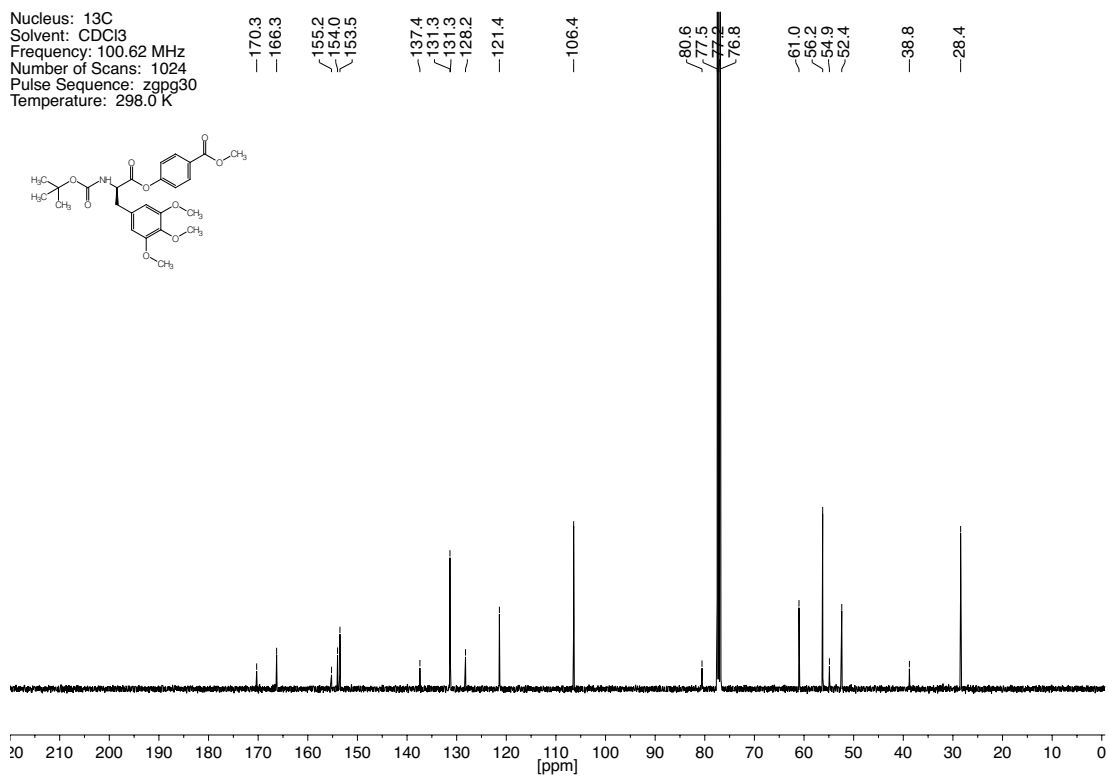


Figure 7.8. ^1H - and ^{13}C -NMR spectra of compound 9.

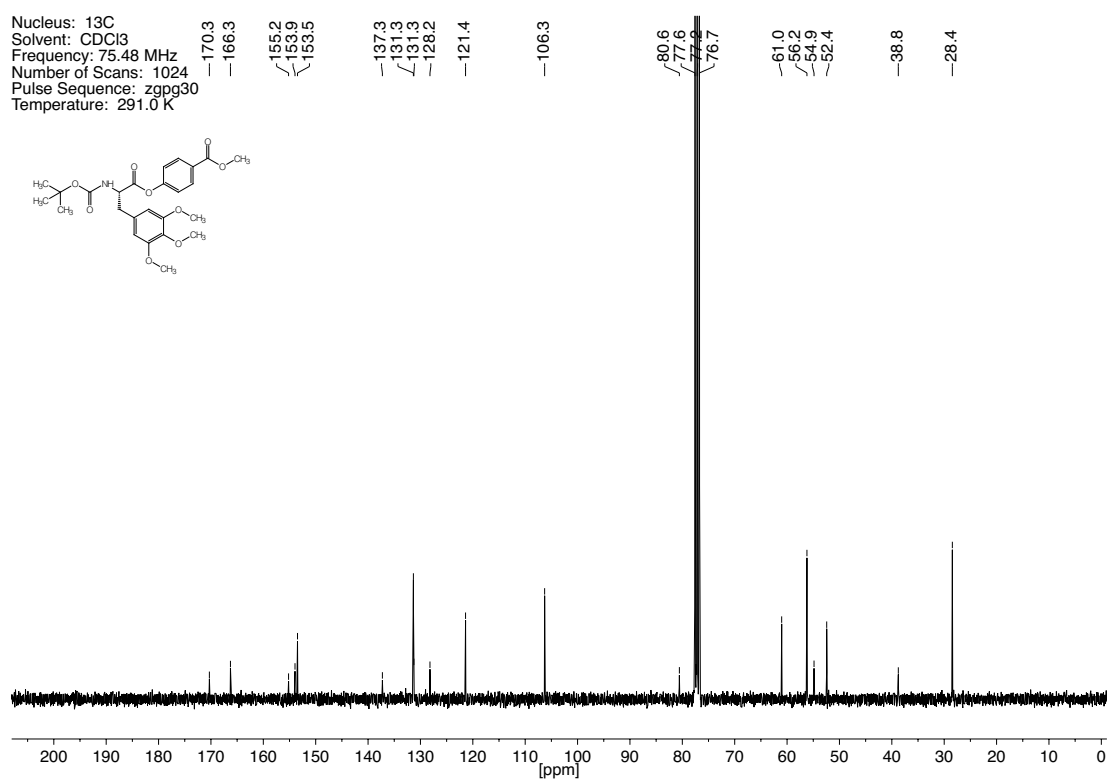
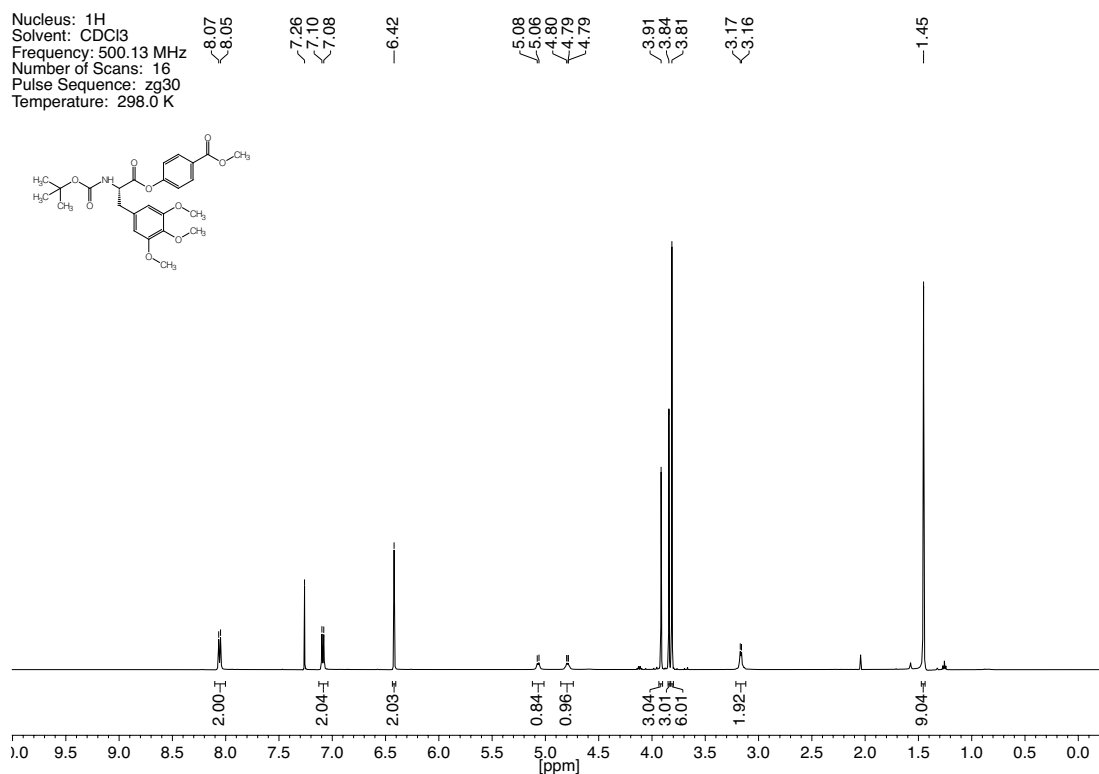
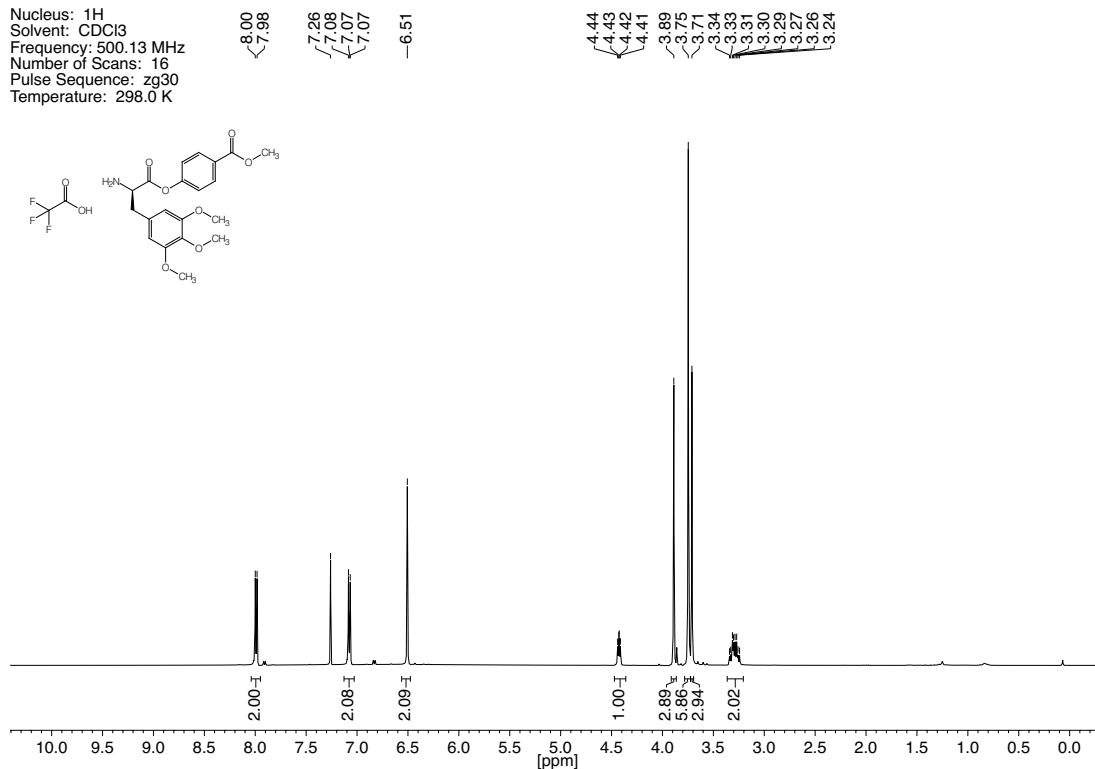


Figure 7.9. ^1H - and ^{13}C -NMR spectra of compound **10**.

Nucleus: ^1H
 Solvent: CDCl_3
 Frequency: 500.13 MHz
 Number of Scans: 16
 Pulse Sequence: zg30
 Temperature: 298.0 K



Nucleus: ^{13}C
 Solvent: CDCl_3
 Frequency: 100.62 MHz
 Number of Scans: 256
 Pulse Sequence: zgpg30
 Temperature: 298.0 K

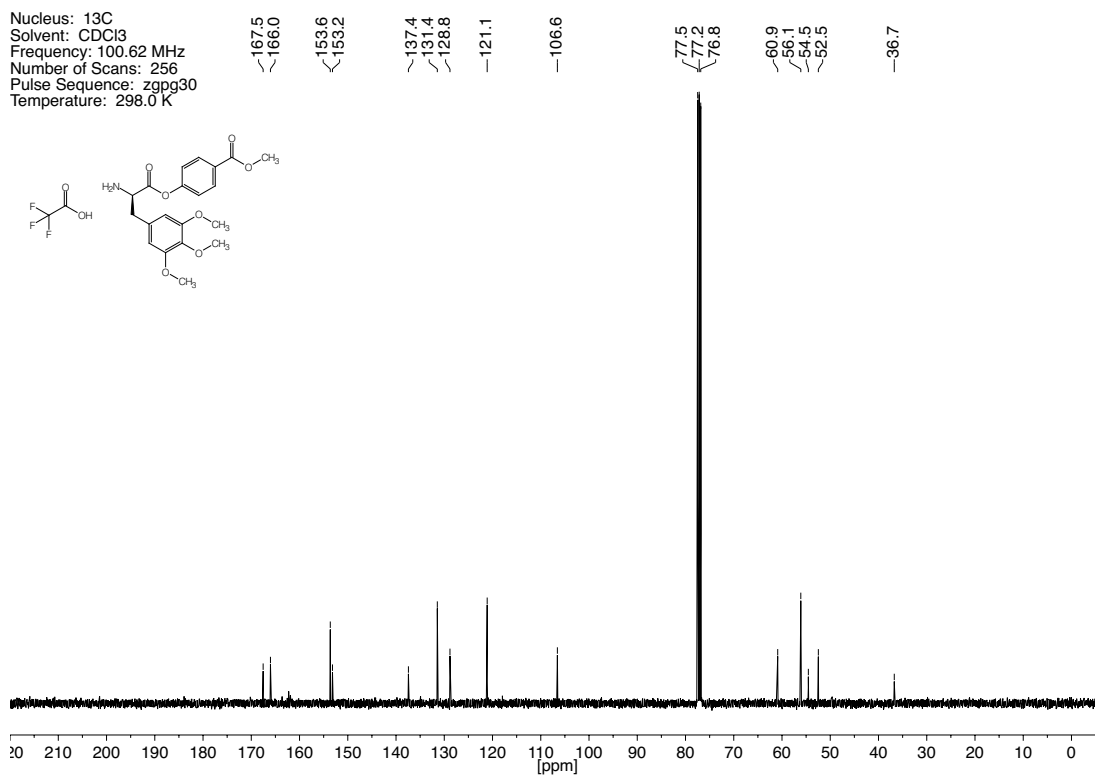
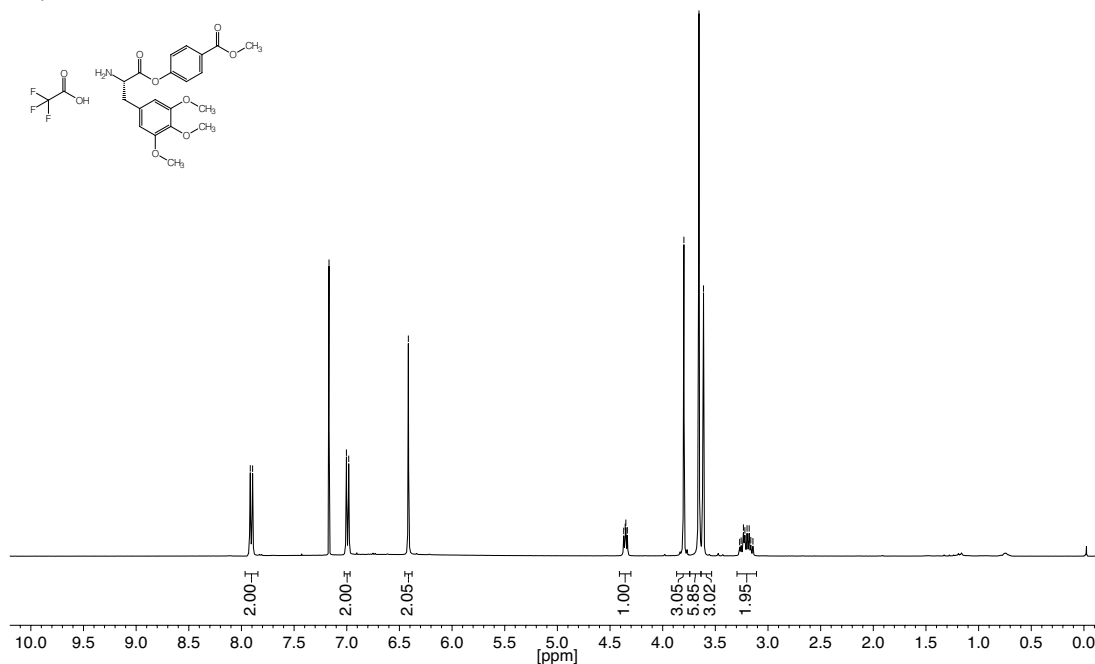


Figure 7.10. ^1H - and ^{13}C -NMR spectra of compound 11.

Nucleus: ^1H
 Solvent: CDCl_3
 Frequency: 400.13 MHz
 Number of Scans: 16
 Pulse Sequence: zg30
 Temperature: 298.0 K



Nucleus: ^{13}C
 Solvent: CDCl_3
 Frequency: 100.62 MHz
 Number of Scans: 256
 Pulse Sequence: zgpg30
 Temperature: 298.0 K

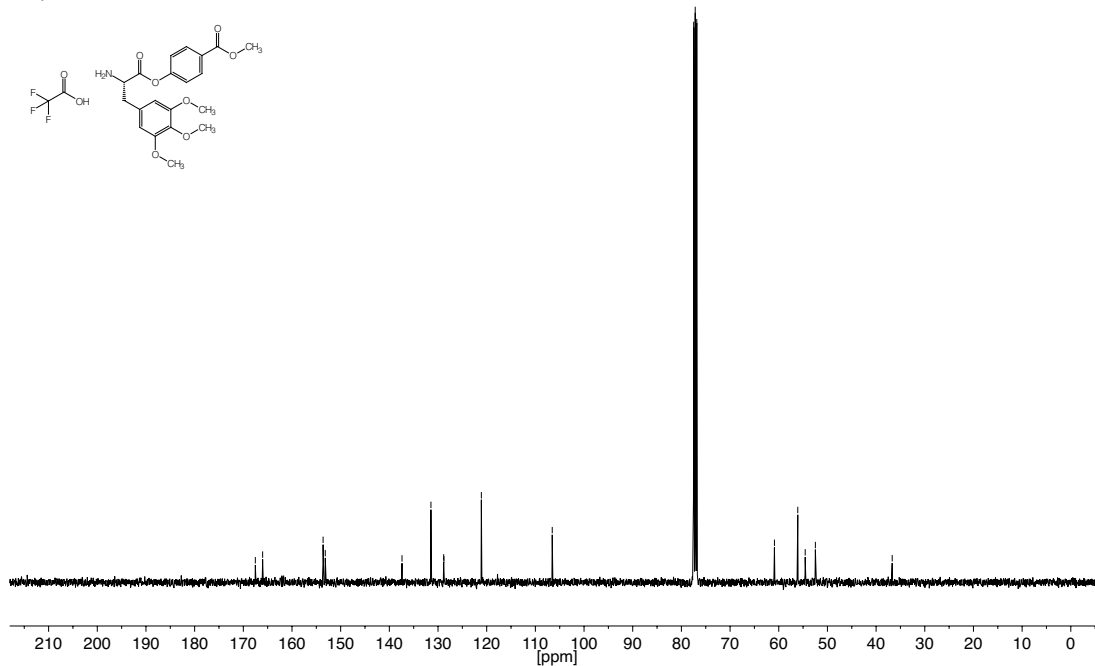


Figure 7.11. ^1H - and ^{13}C -NMR spectra of compound 10.

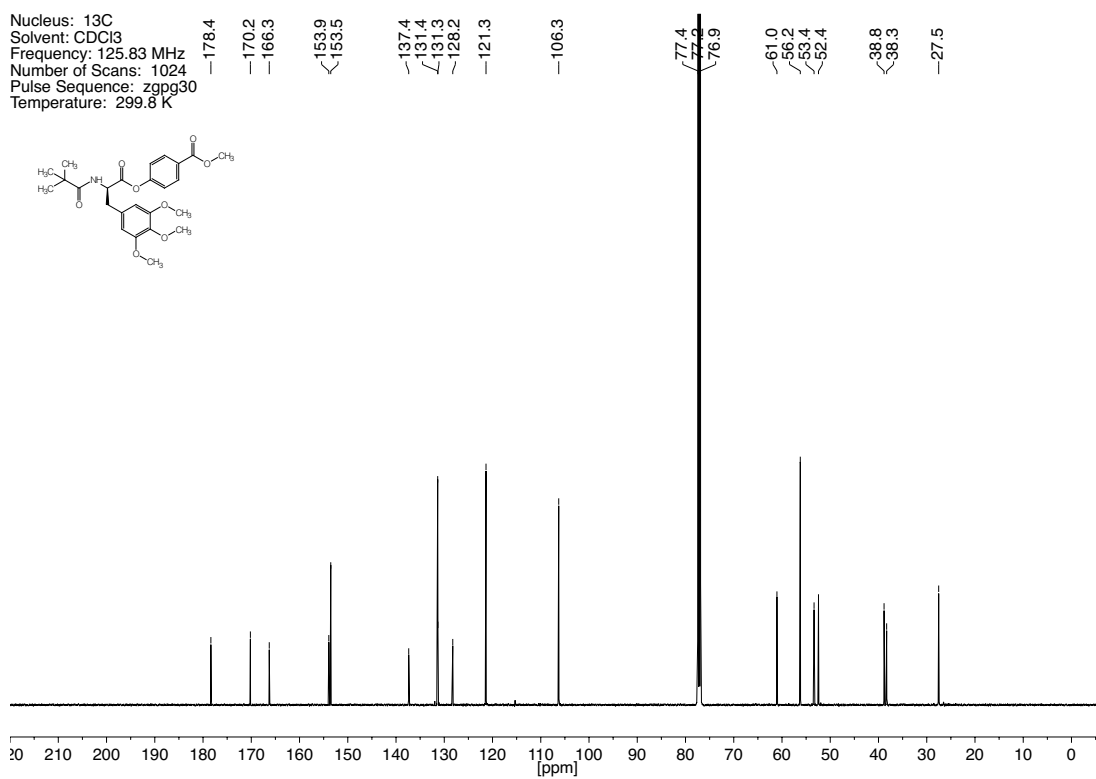
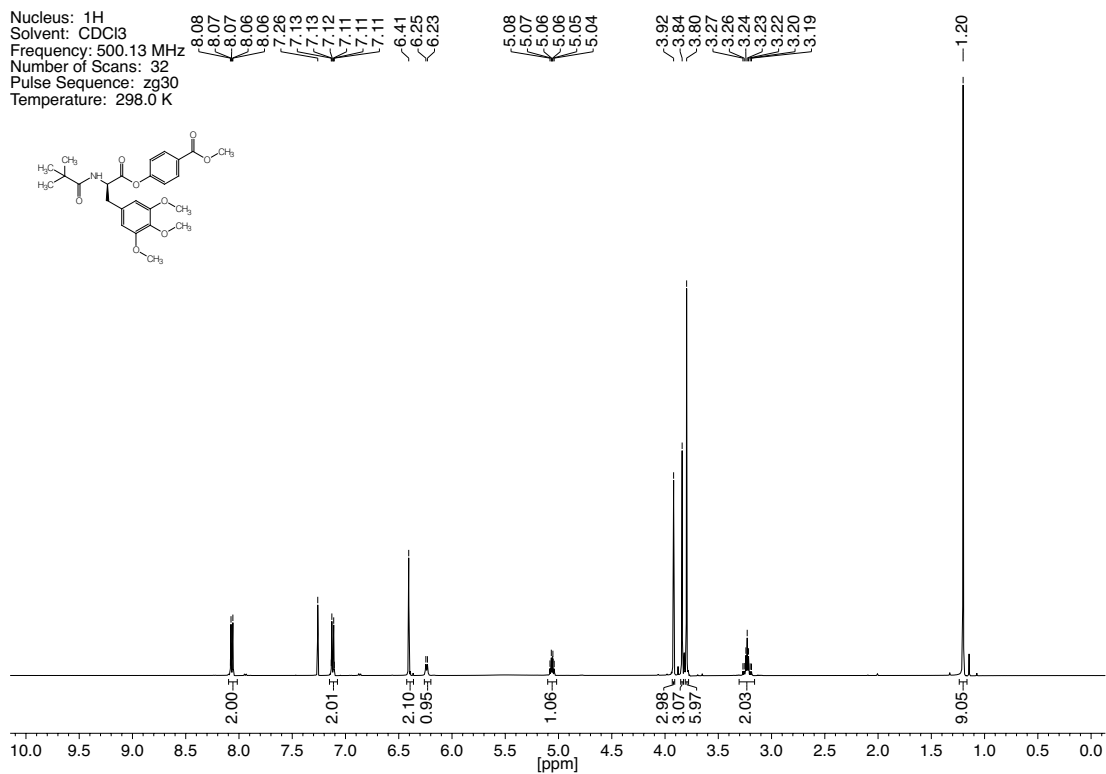


Figure 7.12. ^1H - and ^{13}C -NMR spectra of compound 13.

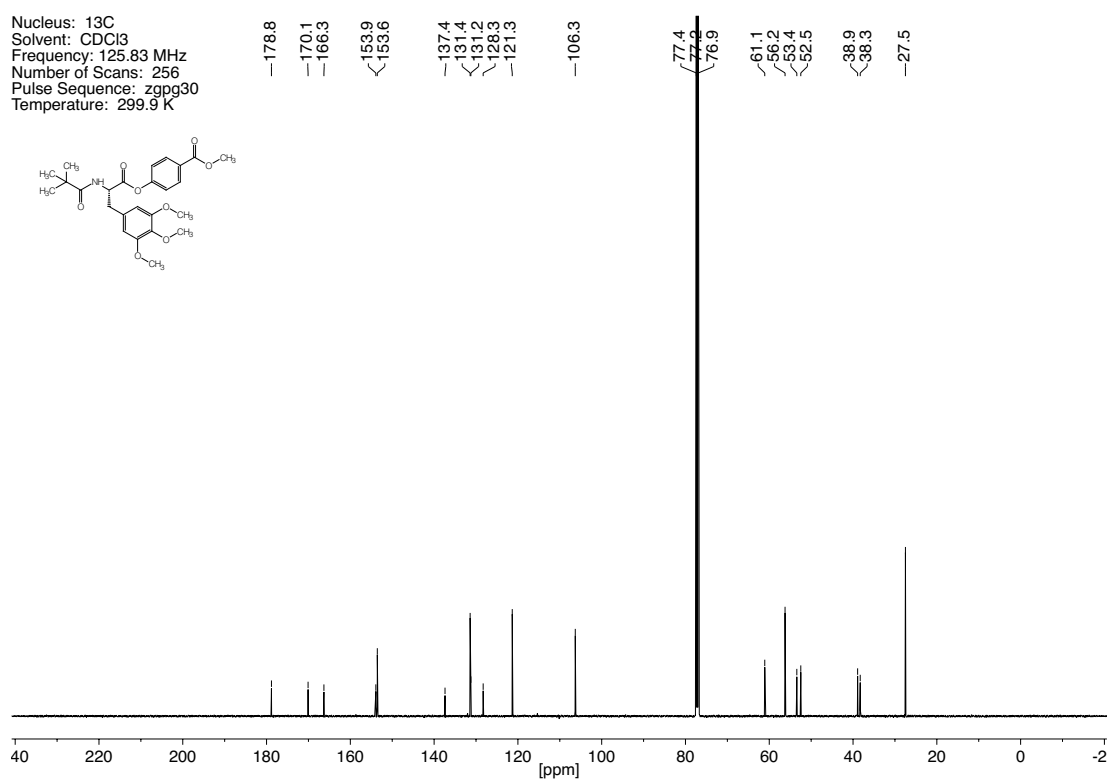
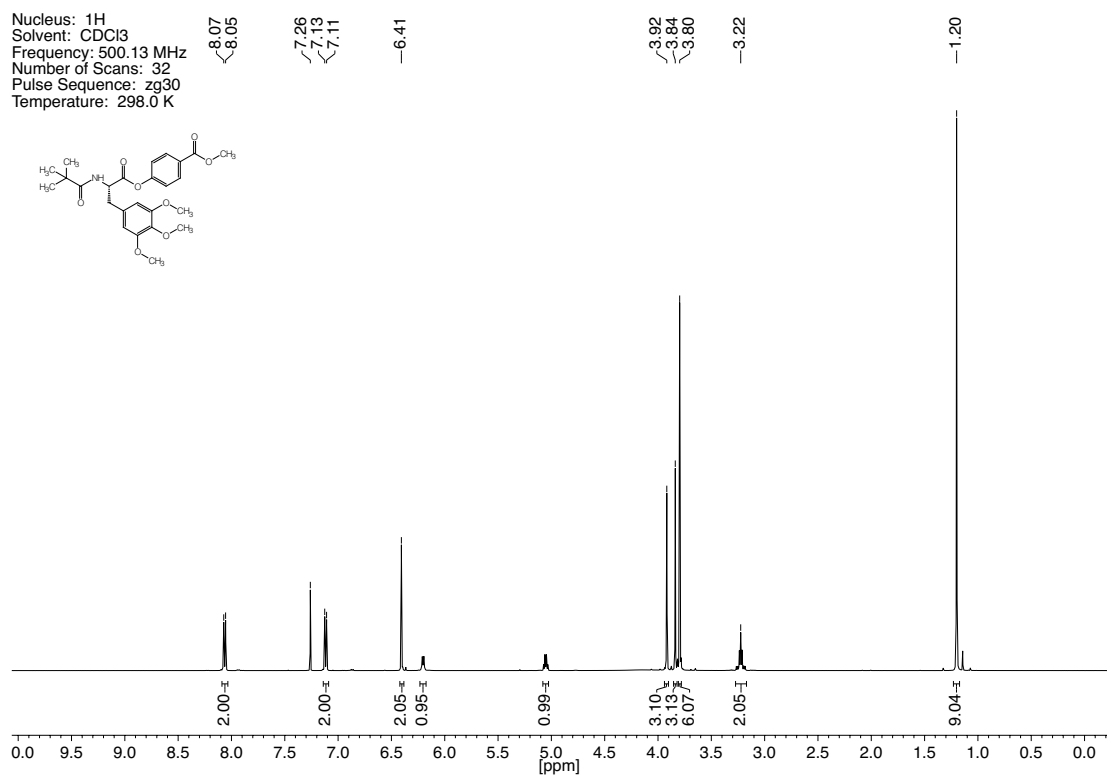
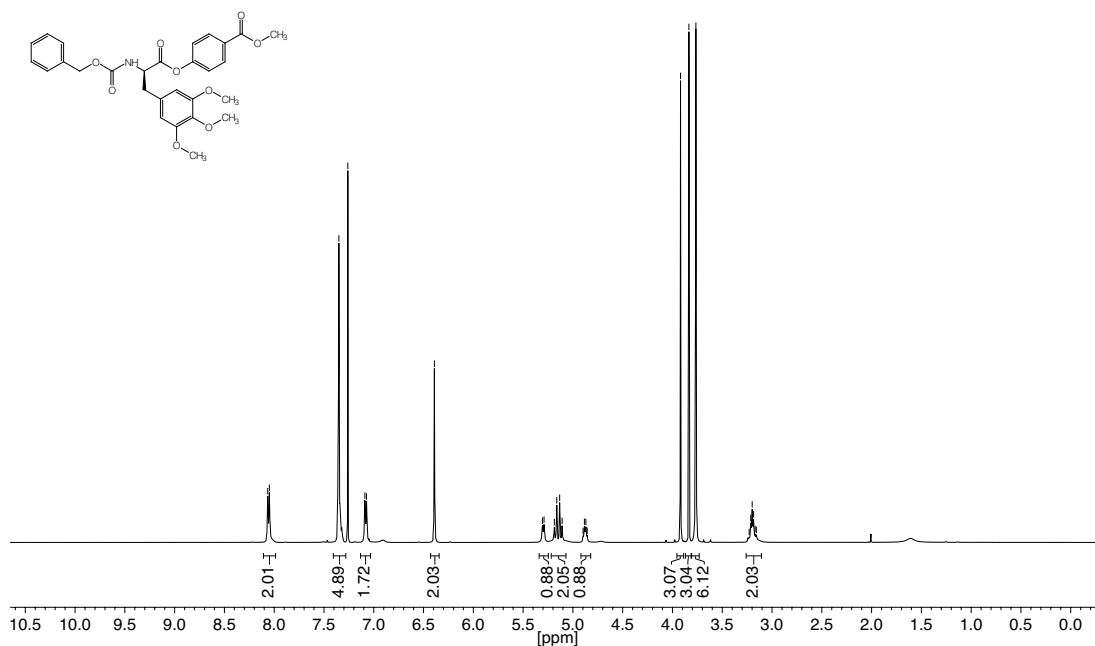


Figure 7.13. ^1H - and ^{13}C -NMR spectra of compound **14**.

Nucleus: ^1H
 Solvent: CDCl_3
 Frequency: 500.13 MHz
 Number of Scans: 64
 Pulse Sequence: zg30
 Temperature: 298.0 K



Nucleus: ^{13}C
 Solvent: CDCl_3
 Frequency: 125.83 MHz
 Number of Scans: 256
 Pulse Sequence: zgpg30
 Temperature: 299.9 K

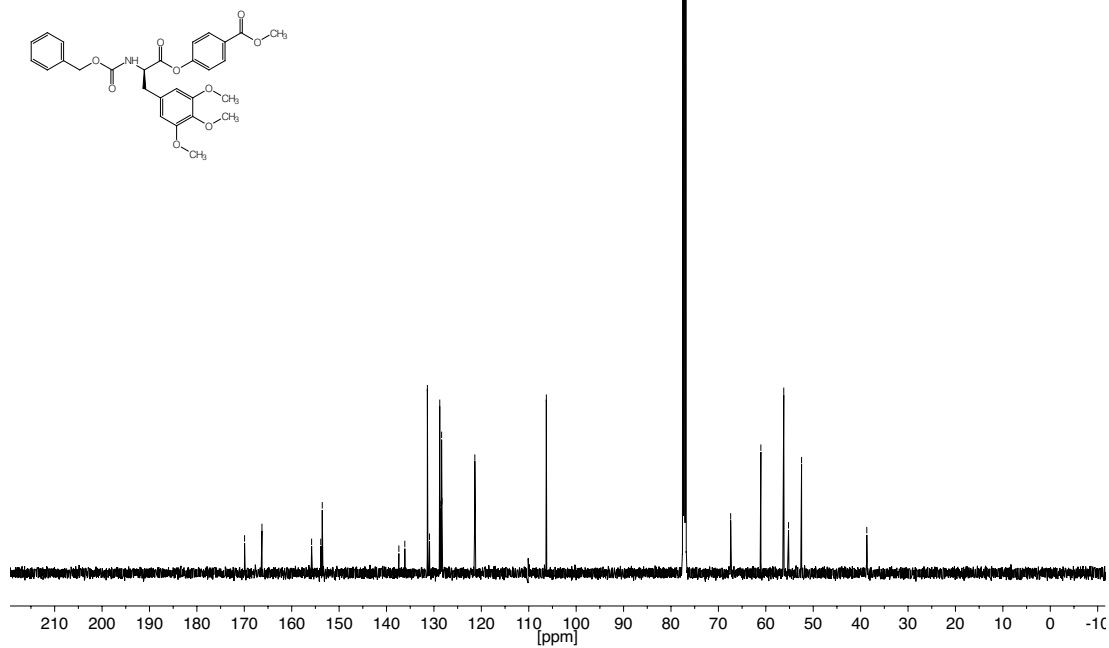


Figure 7.14. ^1H - and ^{13}C -NMR spectra of compound 15.

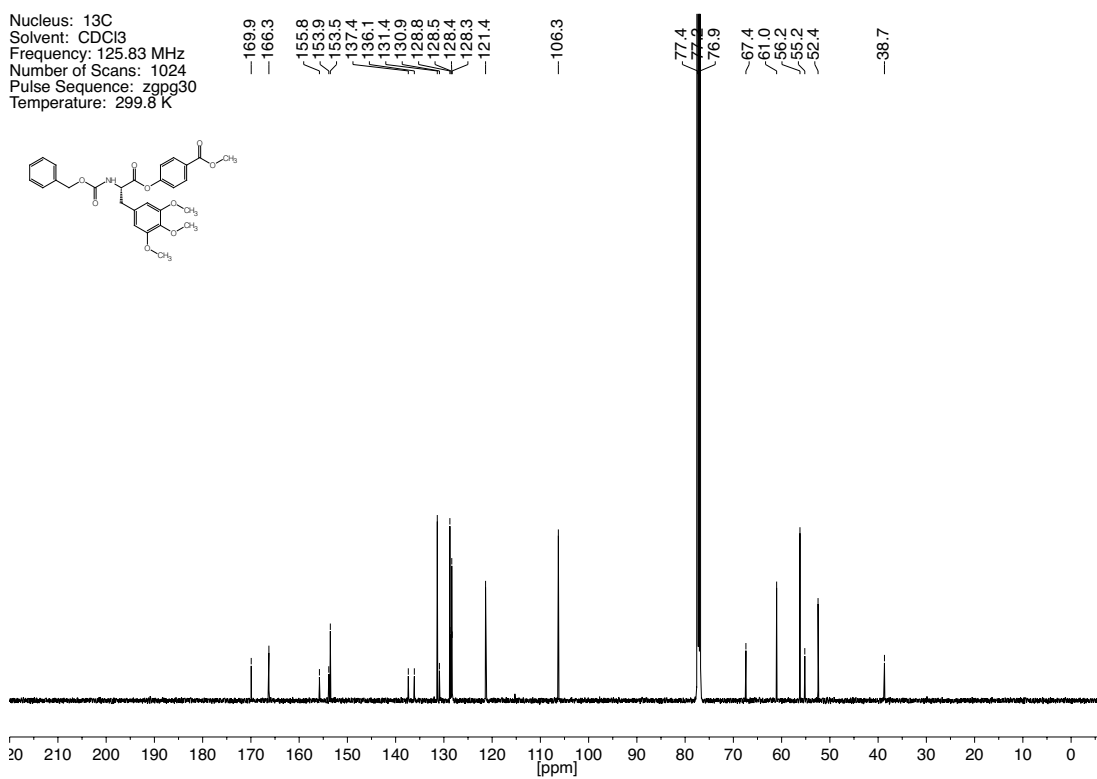
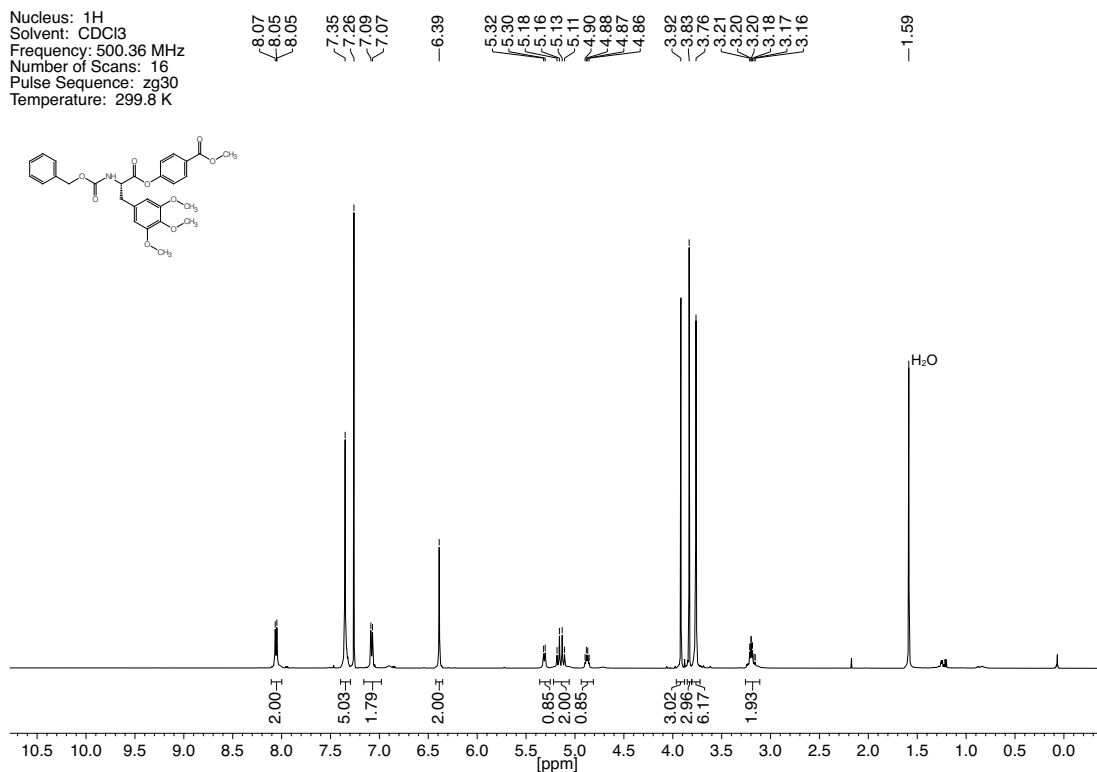


Figure 7.15. ^1H - and ^{13}C -NMR spectra of compound **16**.

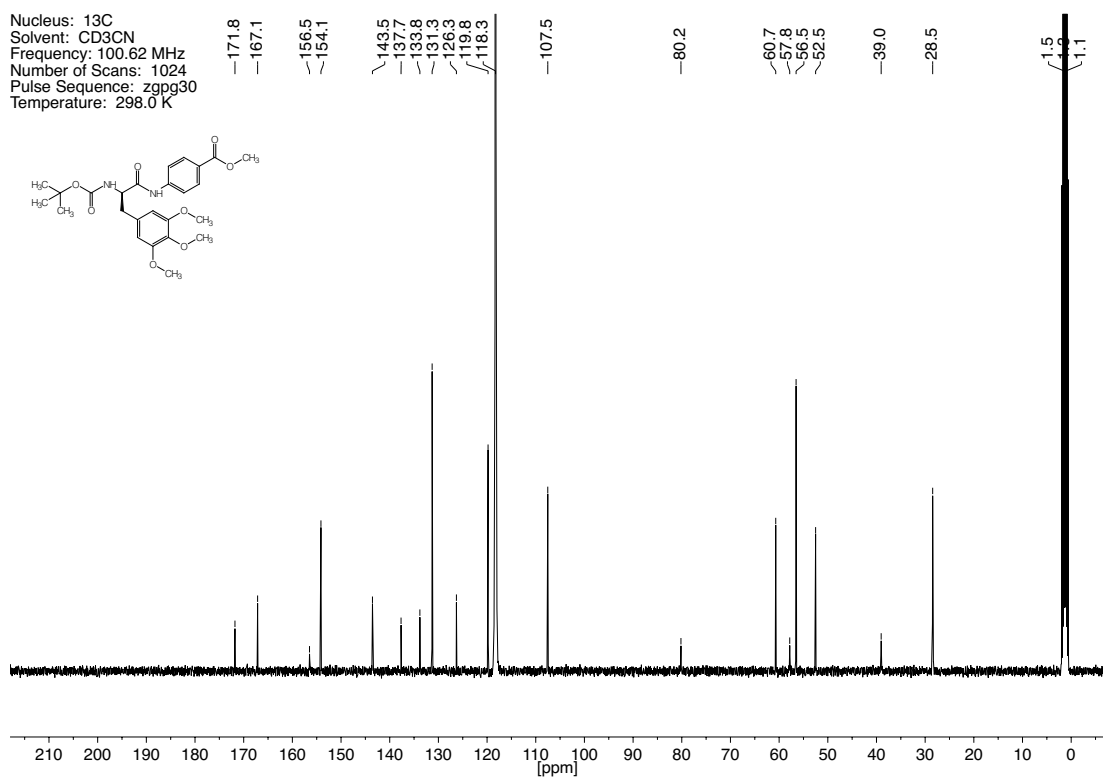
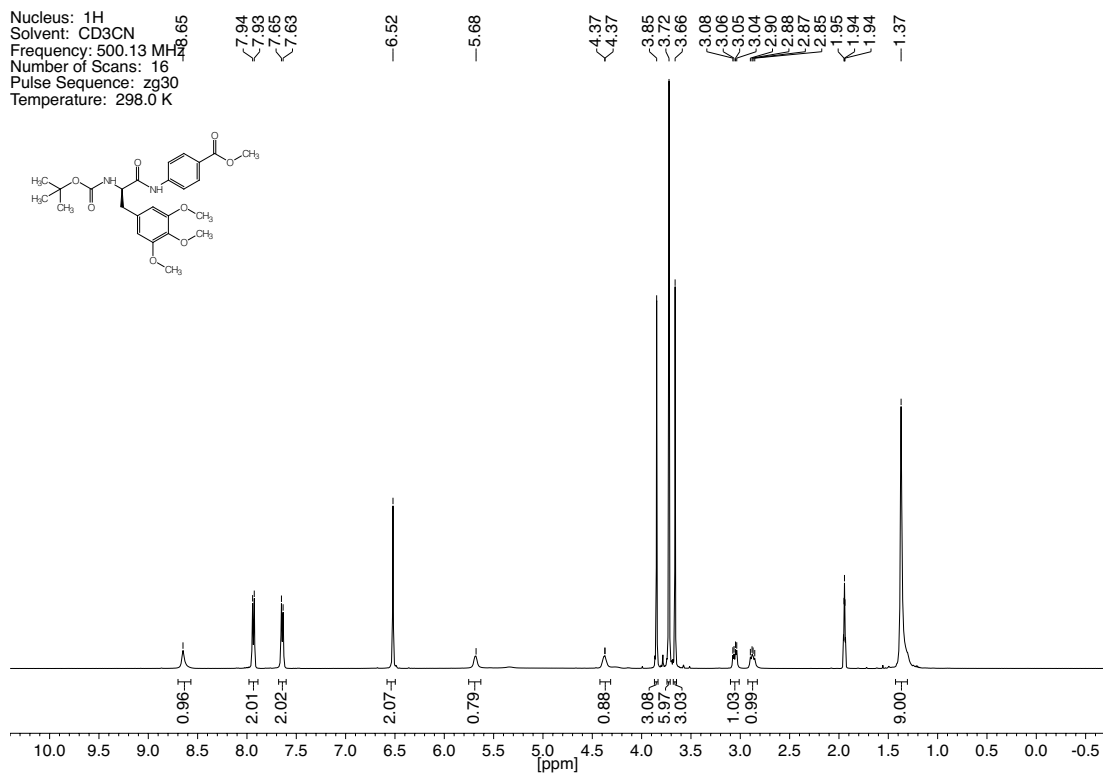


Figure 7.16. ^1H - and ^{13}C -NMR spectra of compound 17.

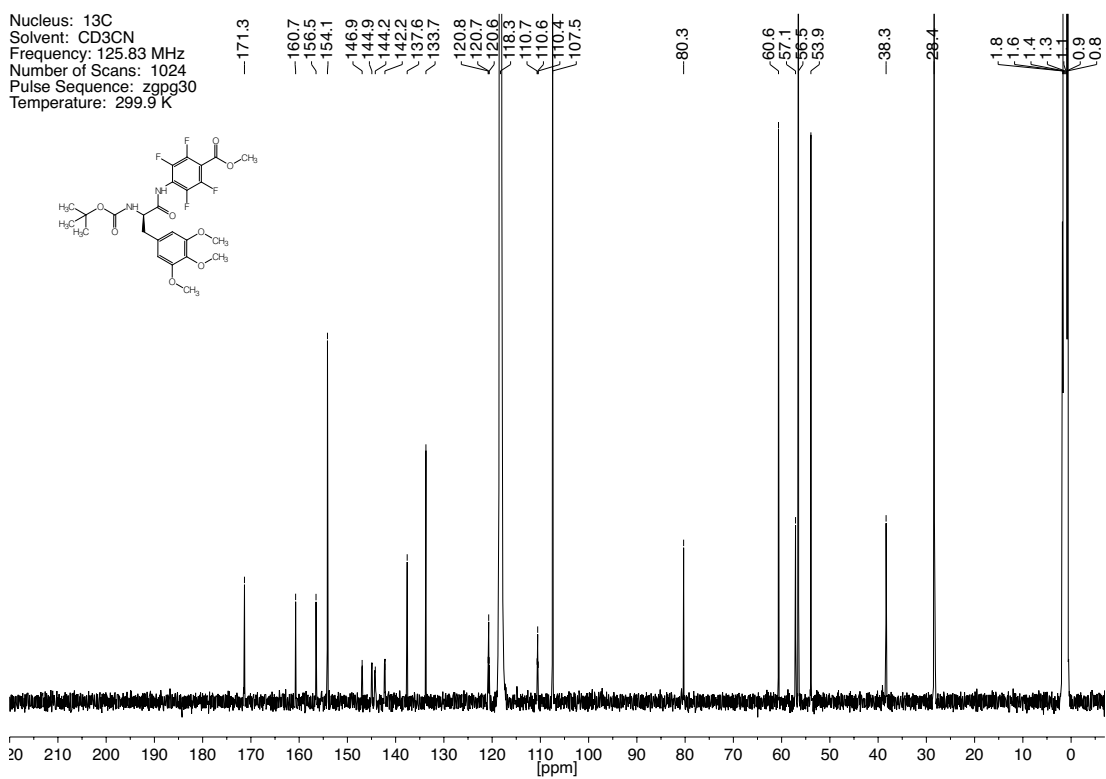
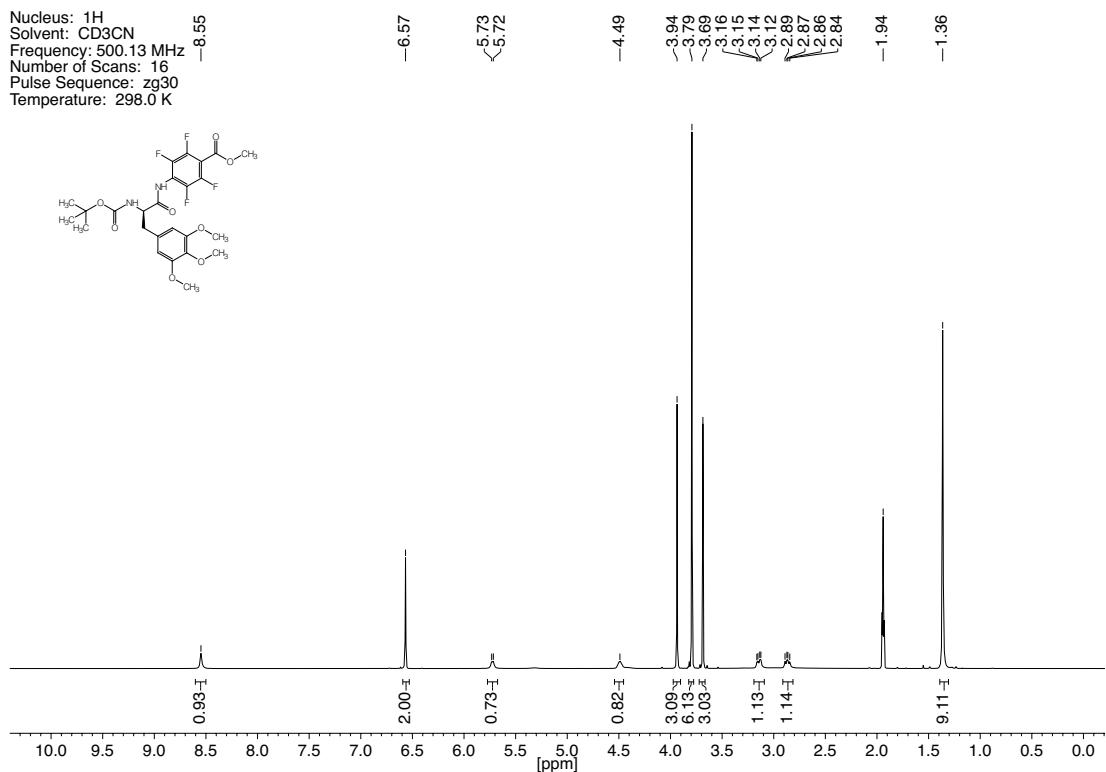


Figure 7.17. ^1H - and ^{13}C -NMR spectra of compound 18.

Nucleus: ^{19}F
Solvent: CD_3CN
Frequency: 470.77 MHz
Number of Scans: 16
Pulse Sequence: zgpg30
Temperature: 299.9 K

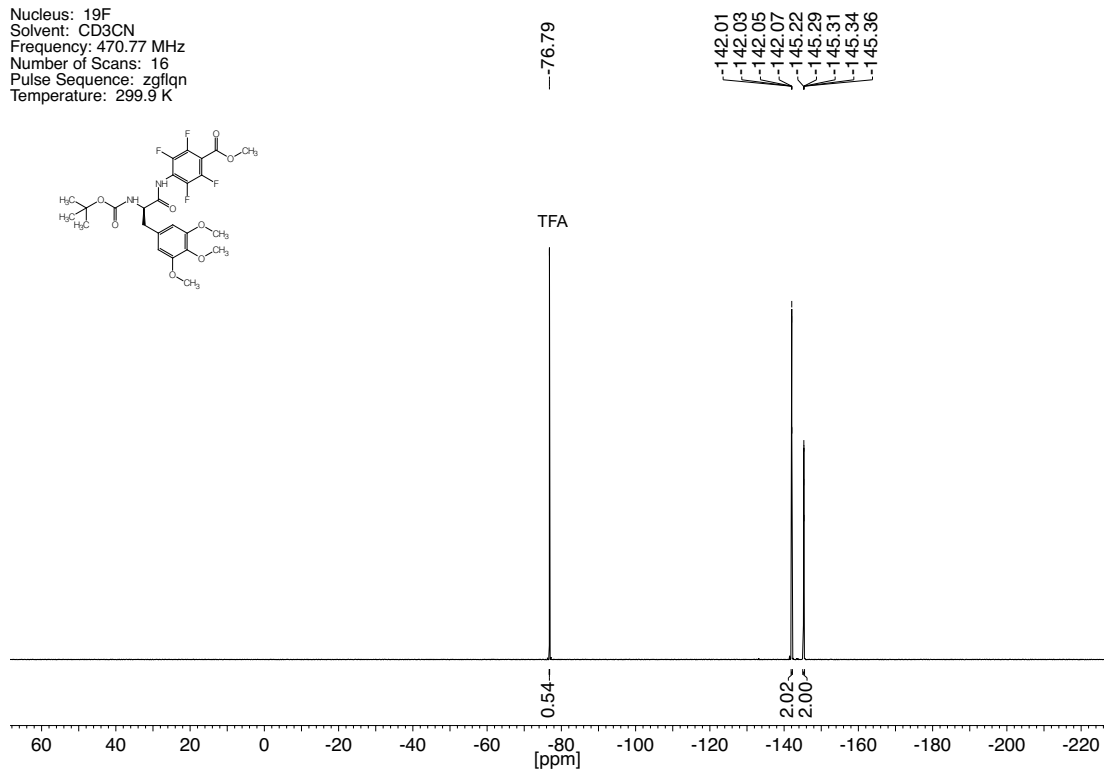


Figure 7.18. ^{19}F -NMR spectrum of compound **18**.

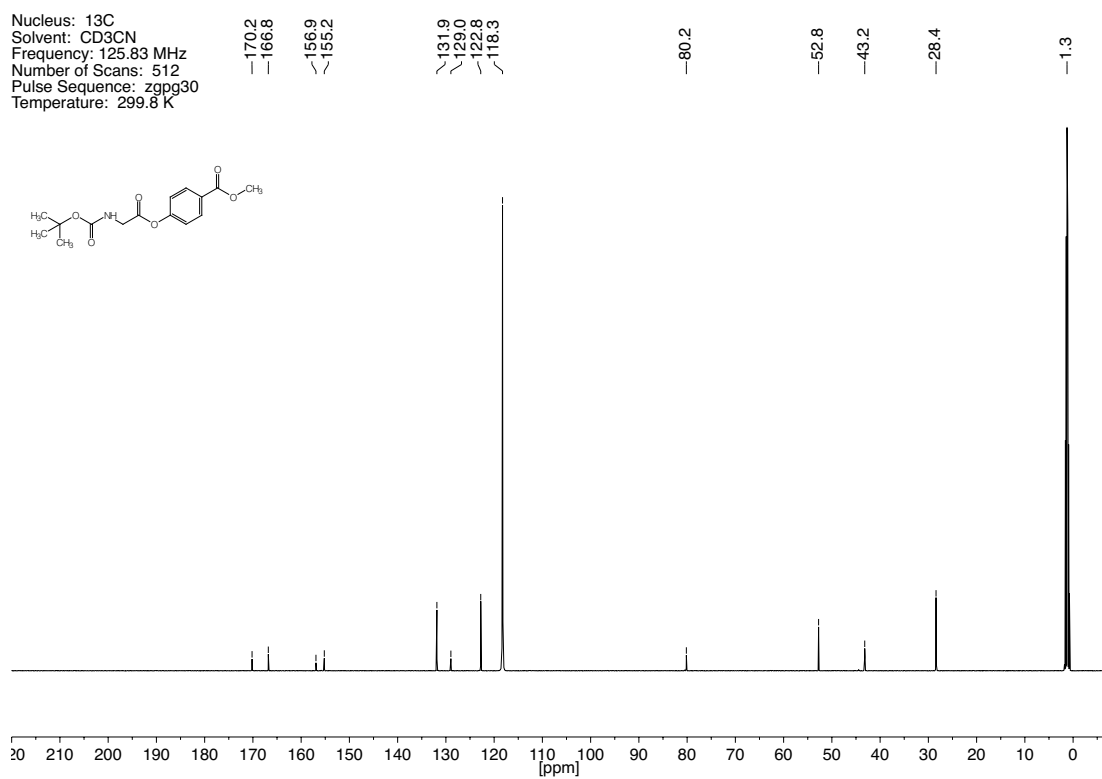
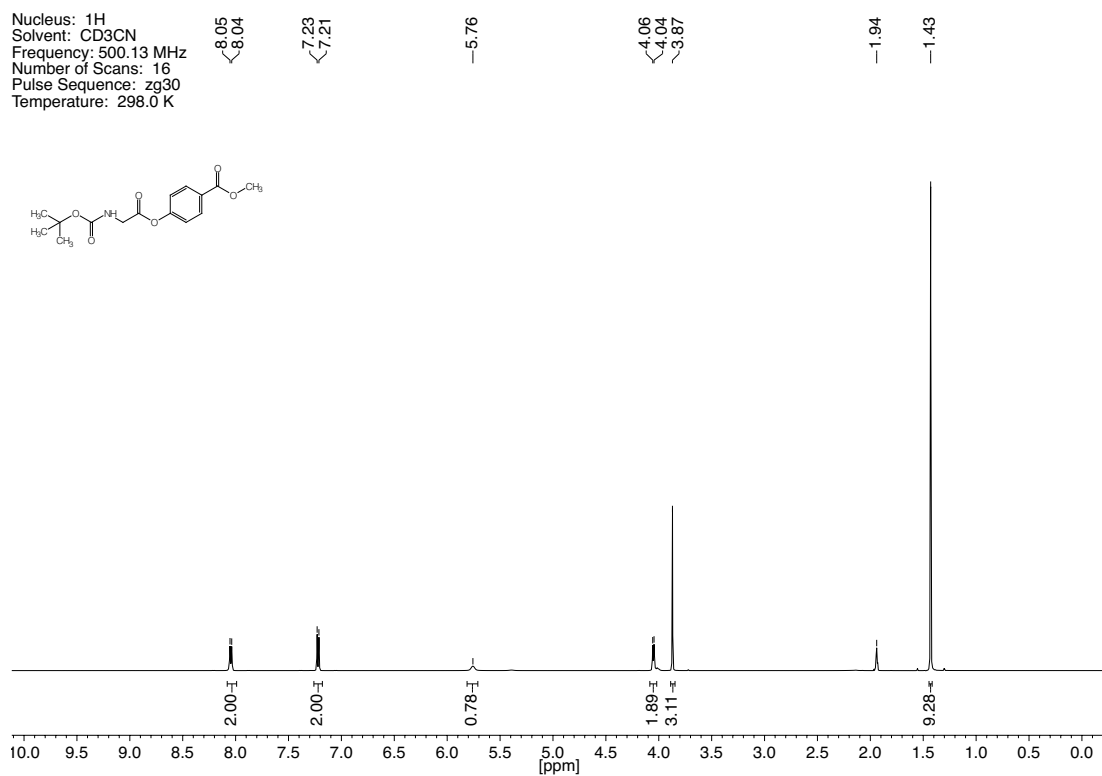


Figure 7.19. ^1H - and ^{13}C -NMR spectra of compound **19**.

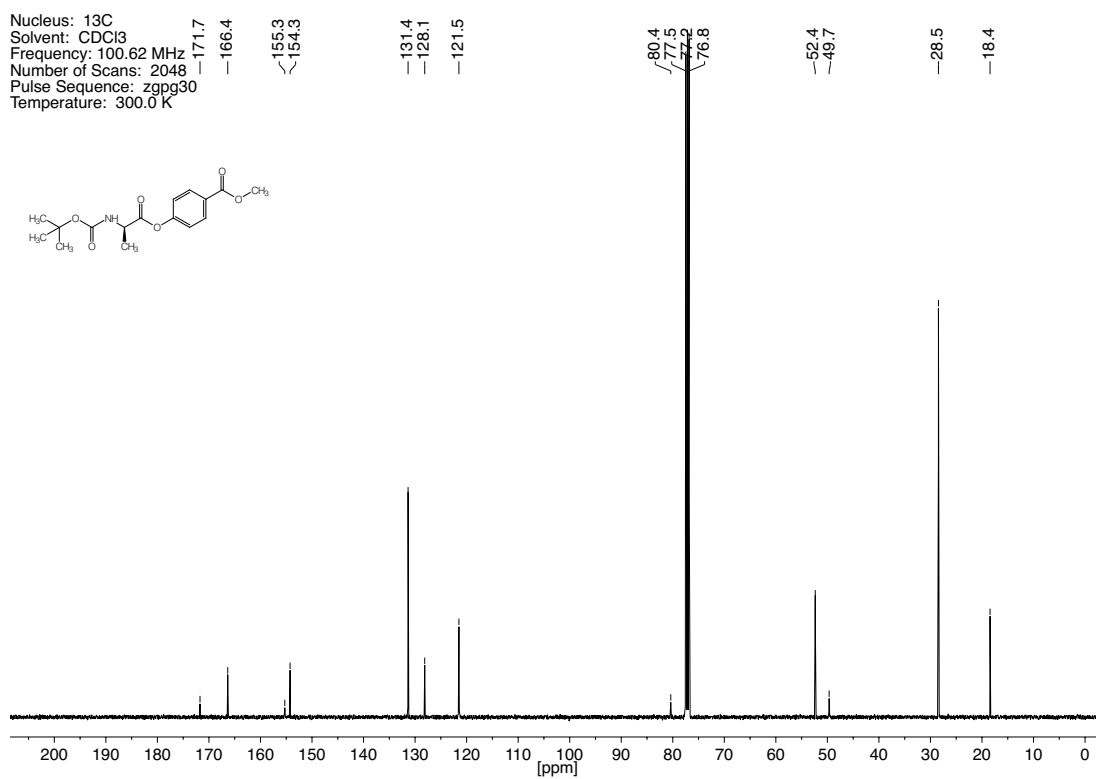
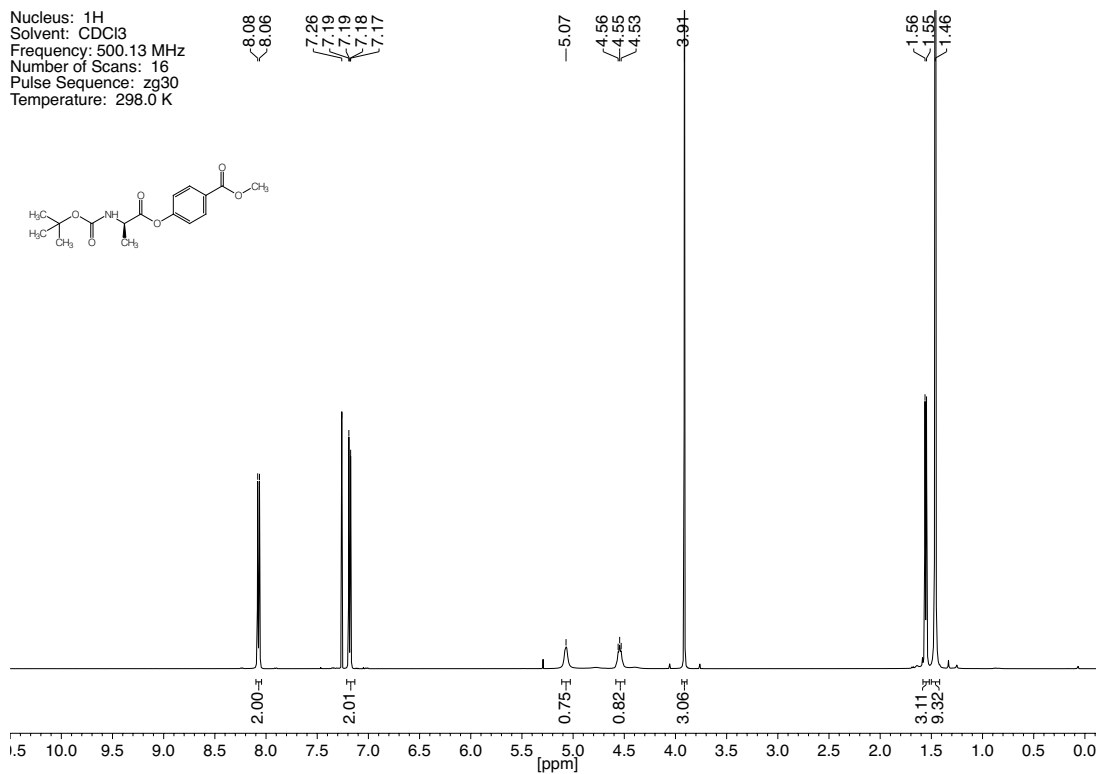
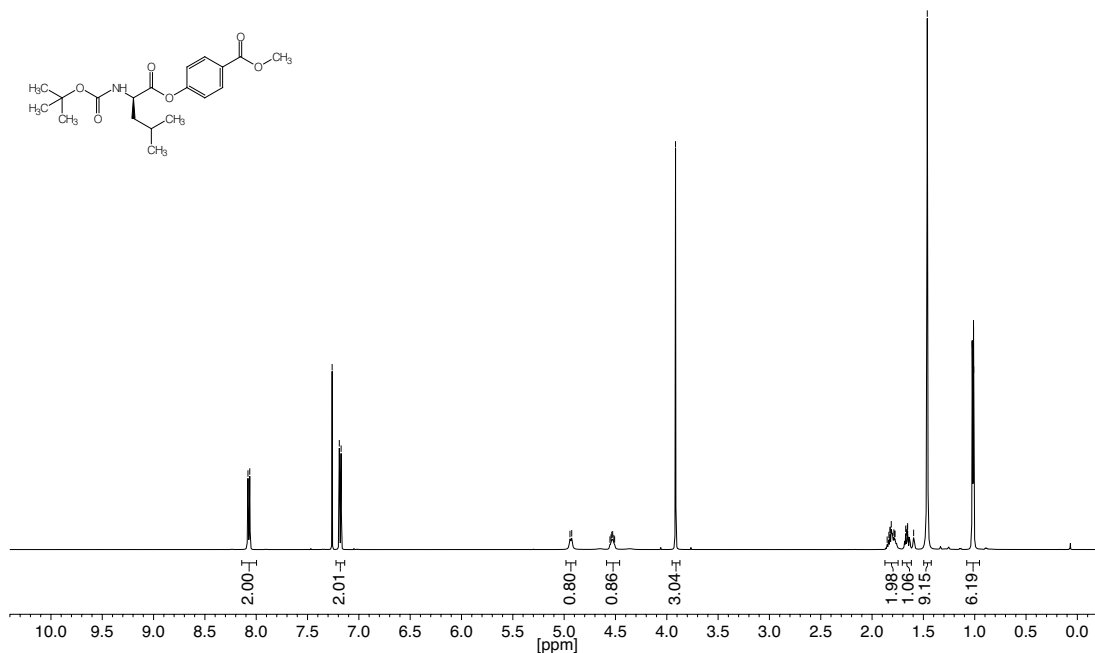


Figure 7.20. ^1H - and ^{13}C -NMR spectra of compound 20.

Nucleus: ^1H
 Solvent: CDCl_3
 Frequency: 500.13 MHz
 Number of Scans: 16
 Pulse Sequence: zg30
 Temperature: 298.0 K



Nucleus: ^{13}C
 Solvent: CDCl_3
 Frequency: 125.83 MHz
 Number of Scans: 256
 Pulse Sequence: zgpg30
 Temperature: 299.8 K

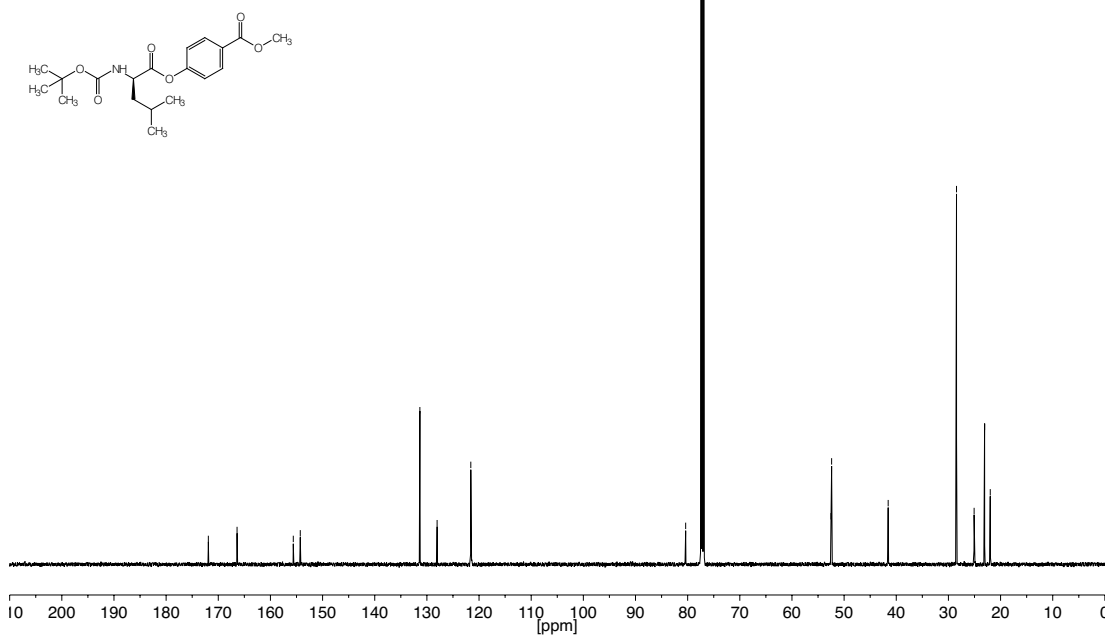
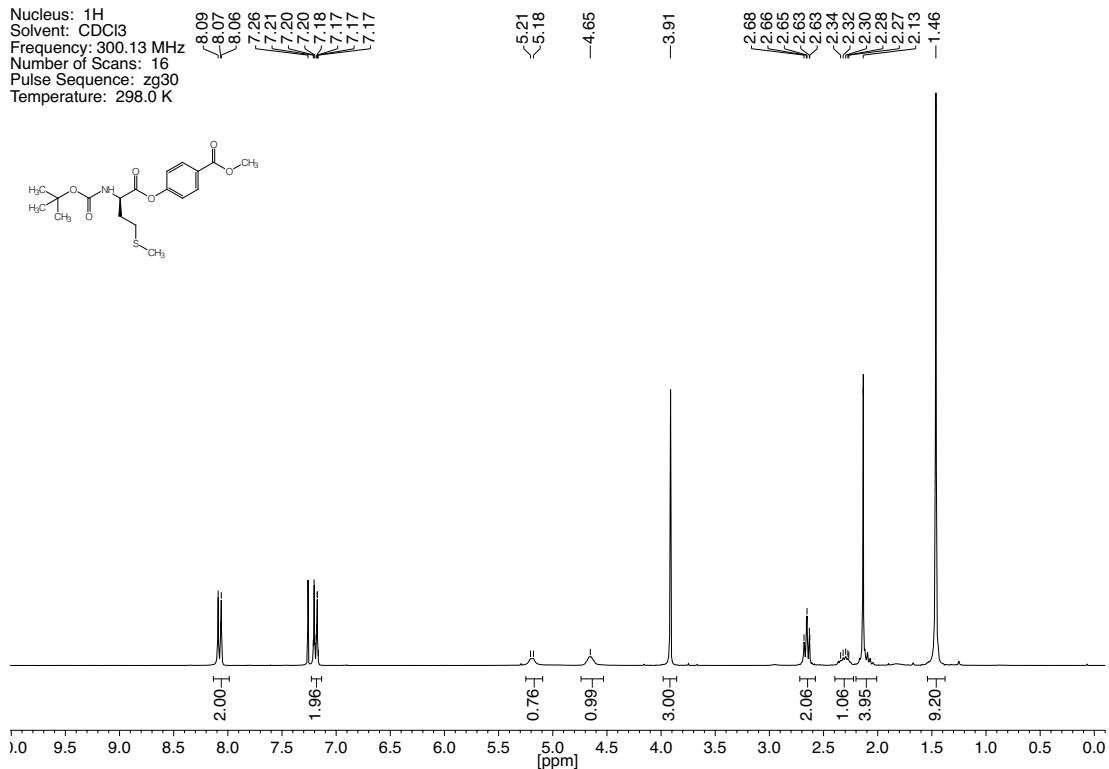


Figure 7.21. ^1H - and ^{13}C -NMR spectra of compound **21**.

Nucleus: ^1H
 Solvent: CDCl_3
 Frequency: 300.13 MHz
 Number of Scans: 16
 Pulse Sequence: zg30
 Temperature: 298.0 K



Nucleus: ^{13}C
 Solvent: CDCl_3
 Frequency: 125.83 MHz
 Number of Scans: 256
 Pulse Sequence: zgpg30
 Temperature: 299.9 K

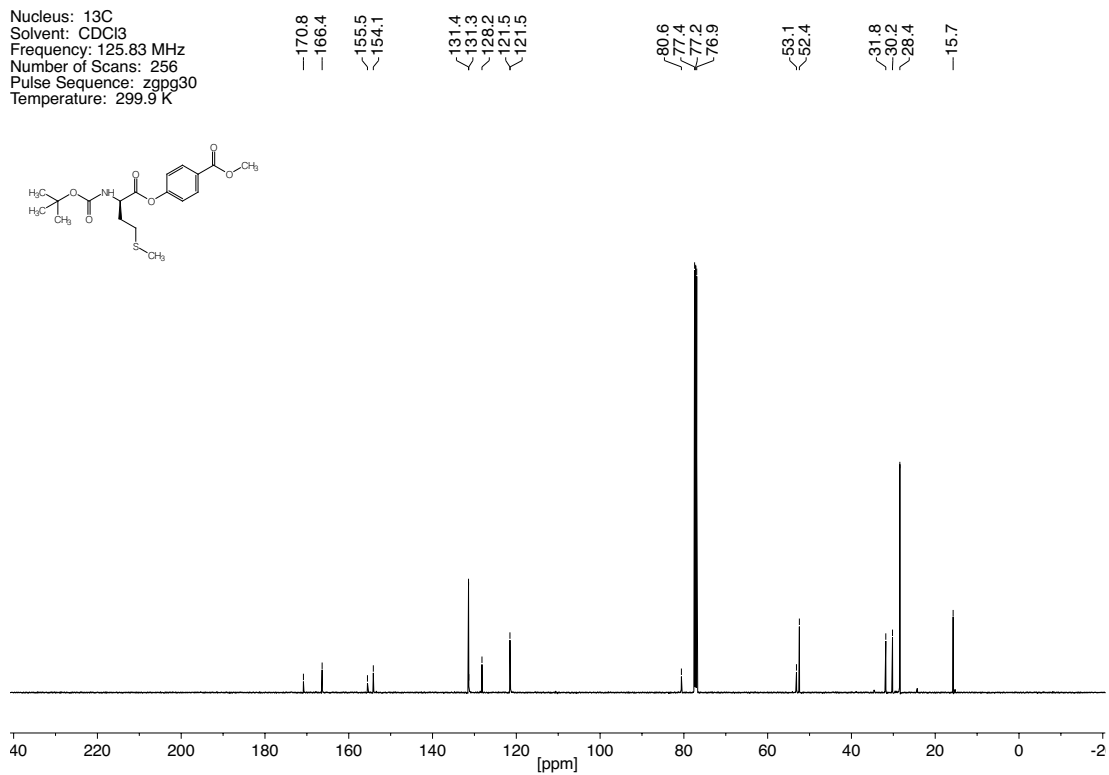


Figure 7.22. ^1H - and ^{13}C -NMR spectra of compound 22.

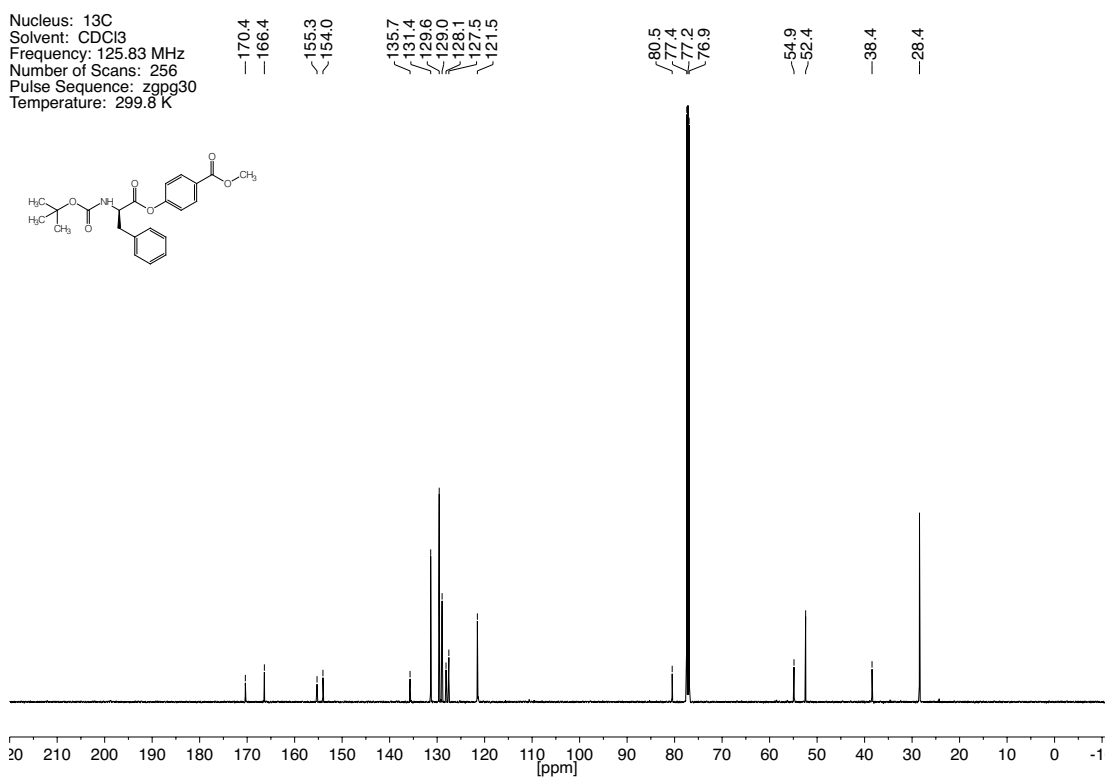
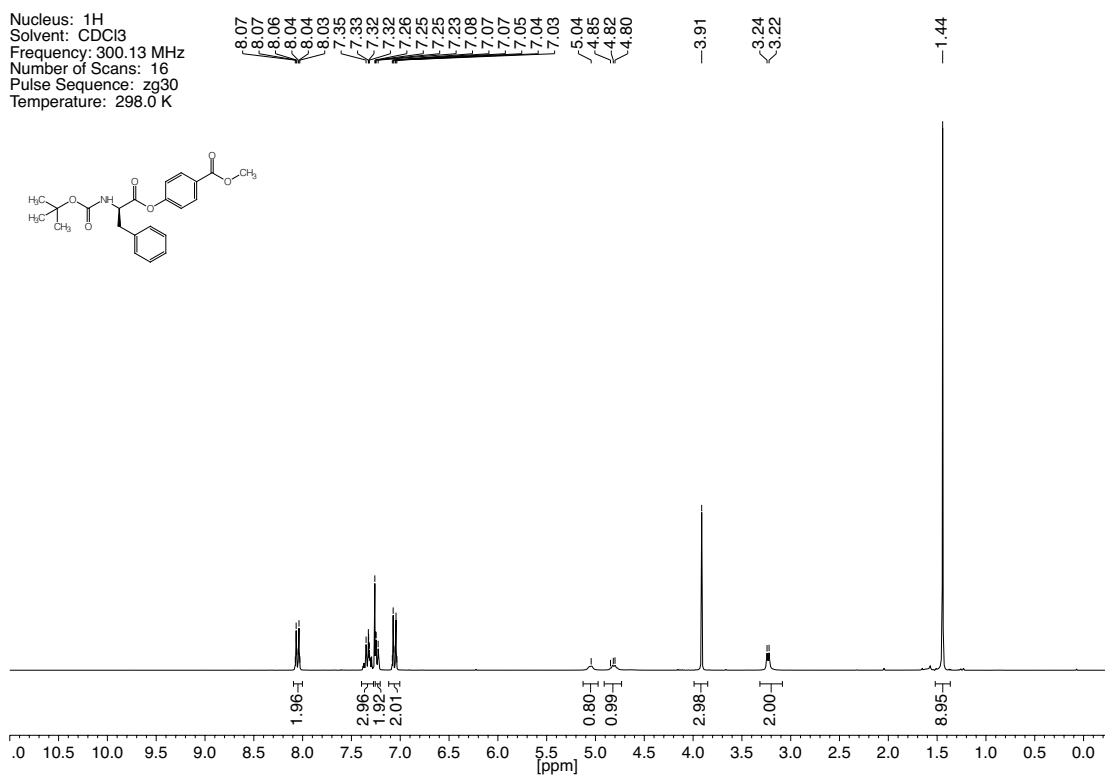
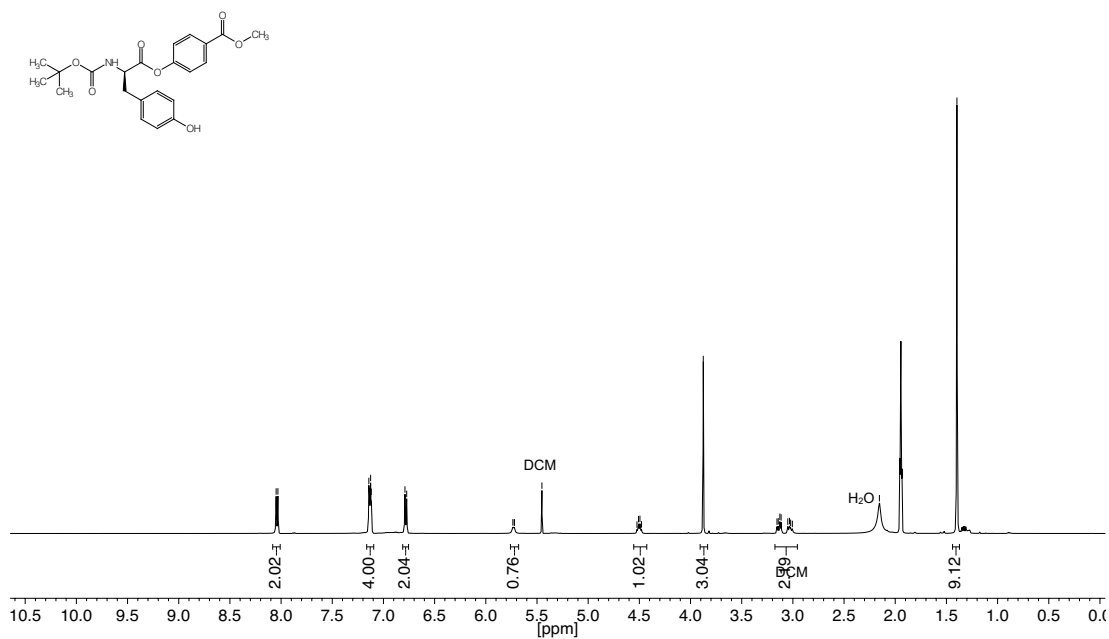


Figure 7.23. ^1H - and ^{13}C -NMR spectra of compound **23**.

Nucleus: ^1H
 Solvent: CD_3CN
 Frequency: 500.13 MHz
 Number of Scans: 64
 Pulse Sequence: zg30
 Temperature: 298.0 K



Nucleus: ^{13}C
 Solvent: CD_3CN
 Frequency: 125.83 MHz
 Number of Scans: 1024
 Pulse Sequence: zgpg30
 Temperature: 299.9 K

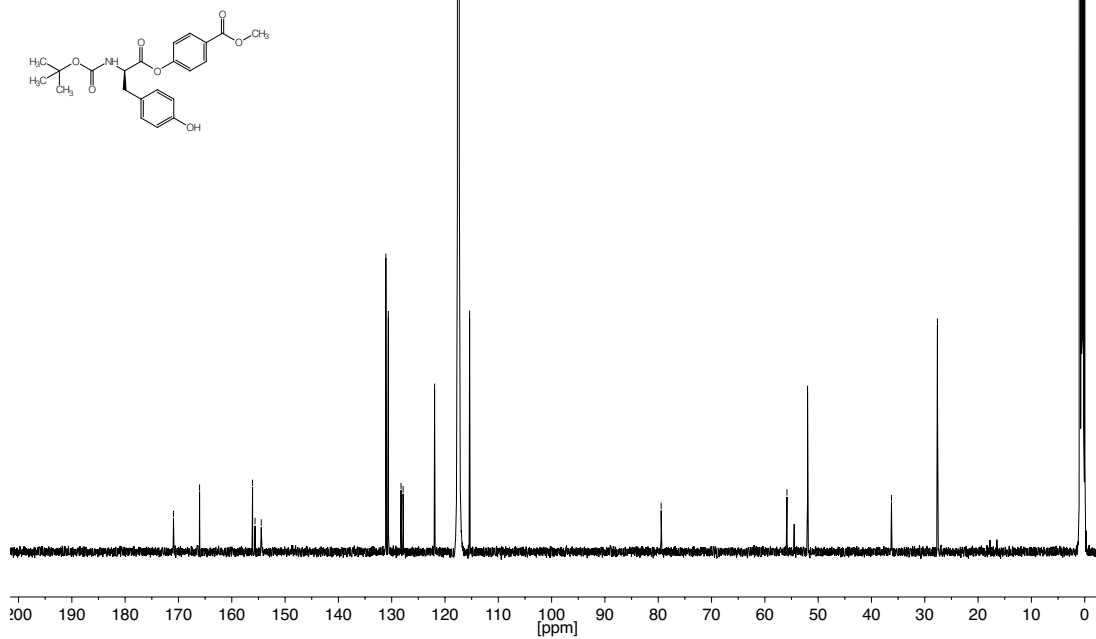


Figure 7.24. ^1H - and ^{13}C -NMR spectra of compound 24.

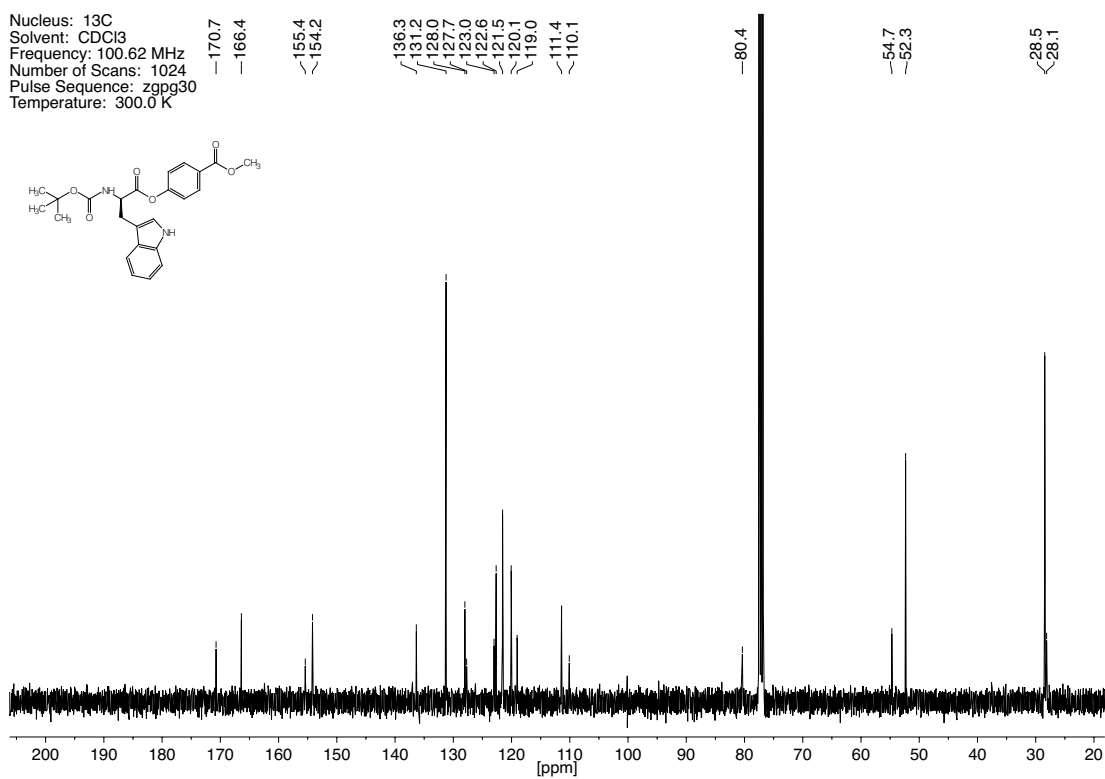
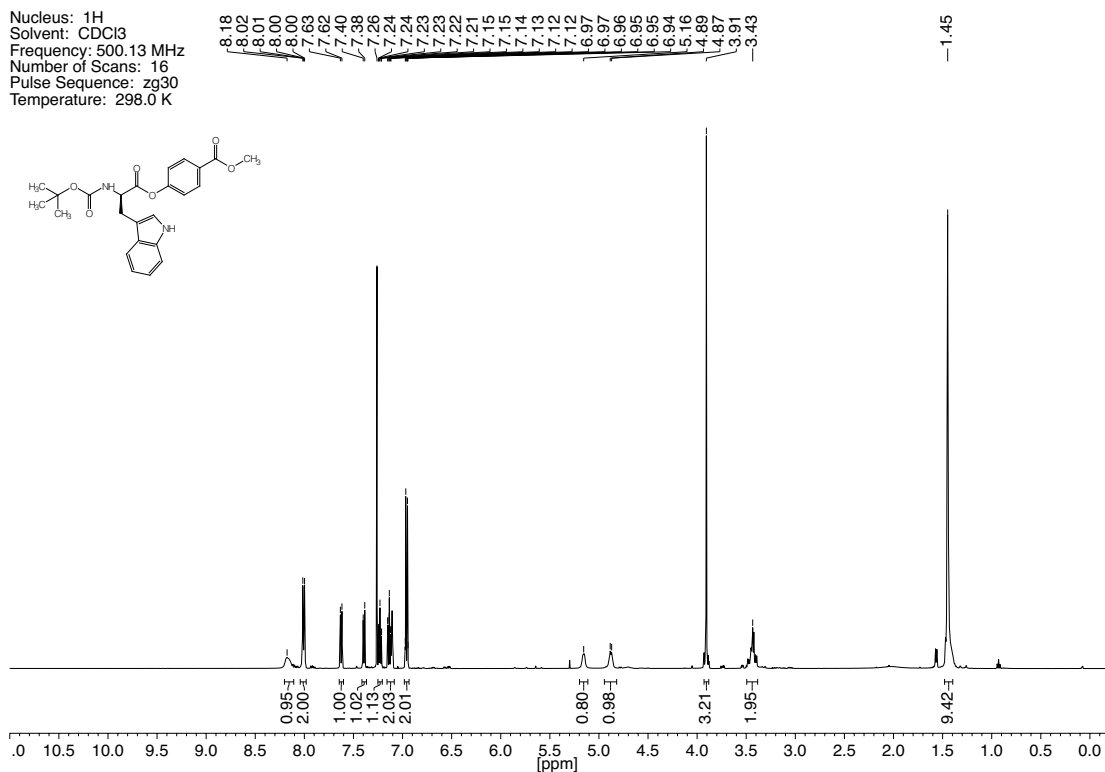


Figure 7.25. ^1H - and ^{13}C -NMR spectra of compound 25.

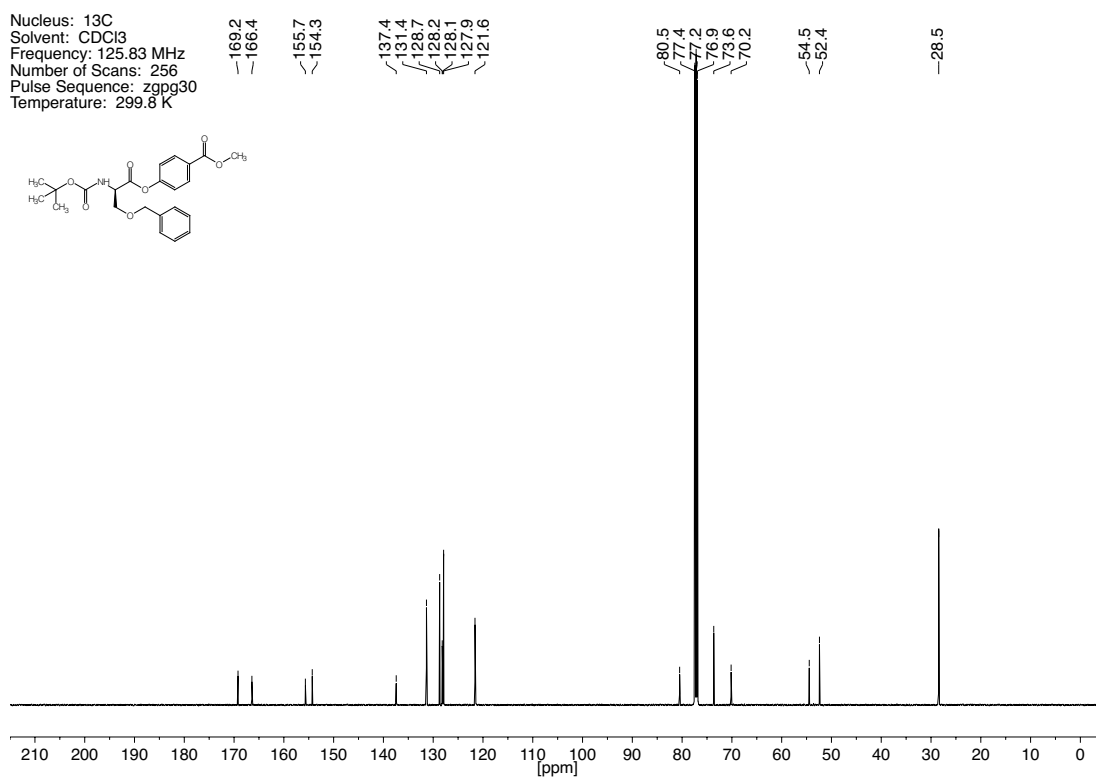
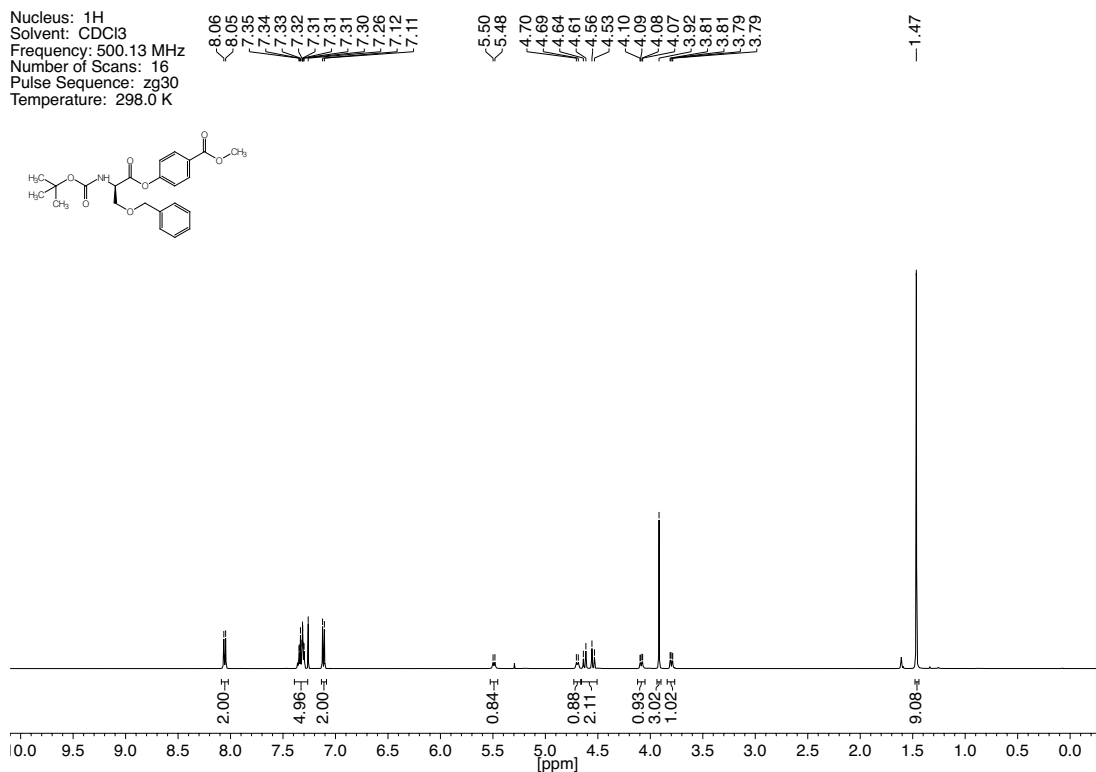


Figure 7.26. ^1H - and ^{13}C -NMR spectra of compound 26.

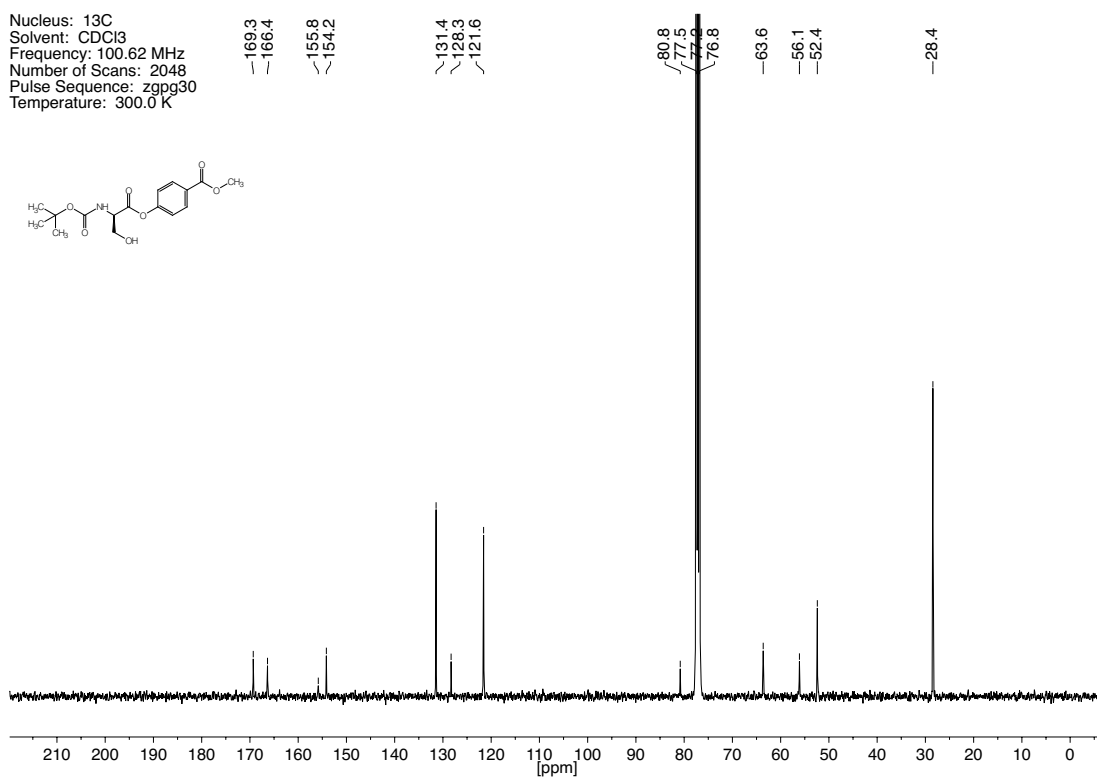
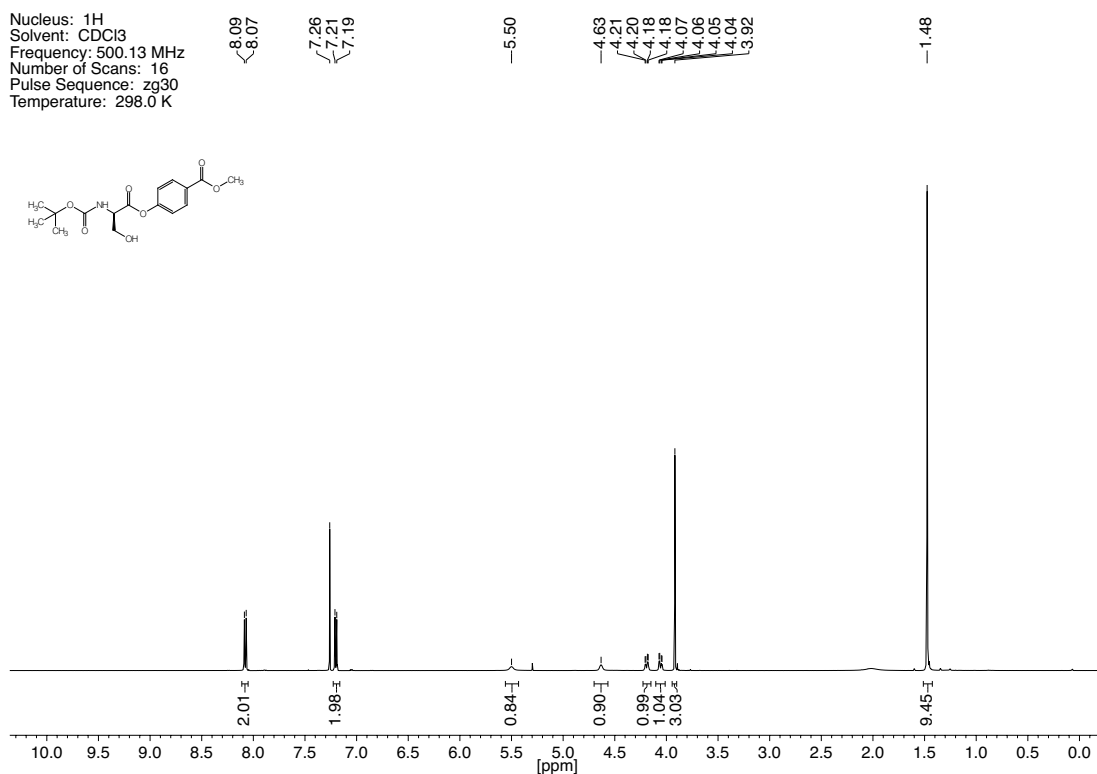


Figure 7.27. ^1H - and ^{13}C -NMR spectra of compound **27**.

Nucleus: ^1H
 Solvent: CDCl_3
 Frequency: 500.13 MHz
 Number of Scans: 16
 Pulse Sequence: zg30
 Temperature: 298.0 K

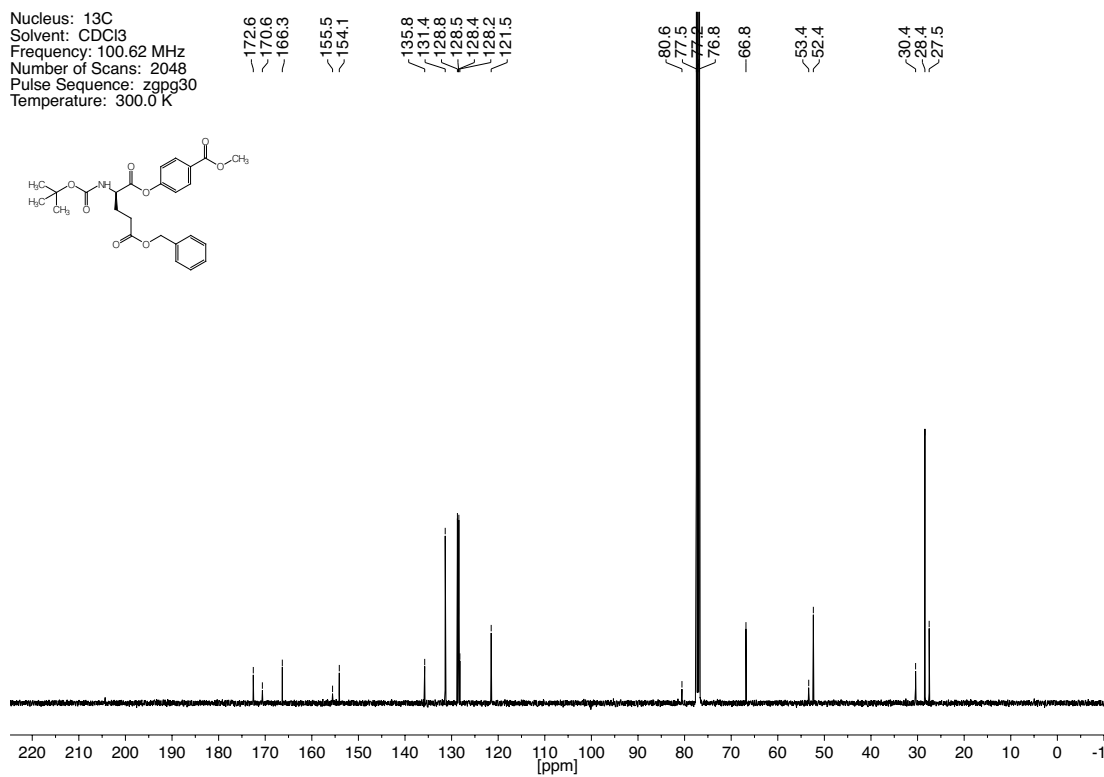
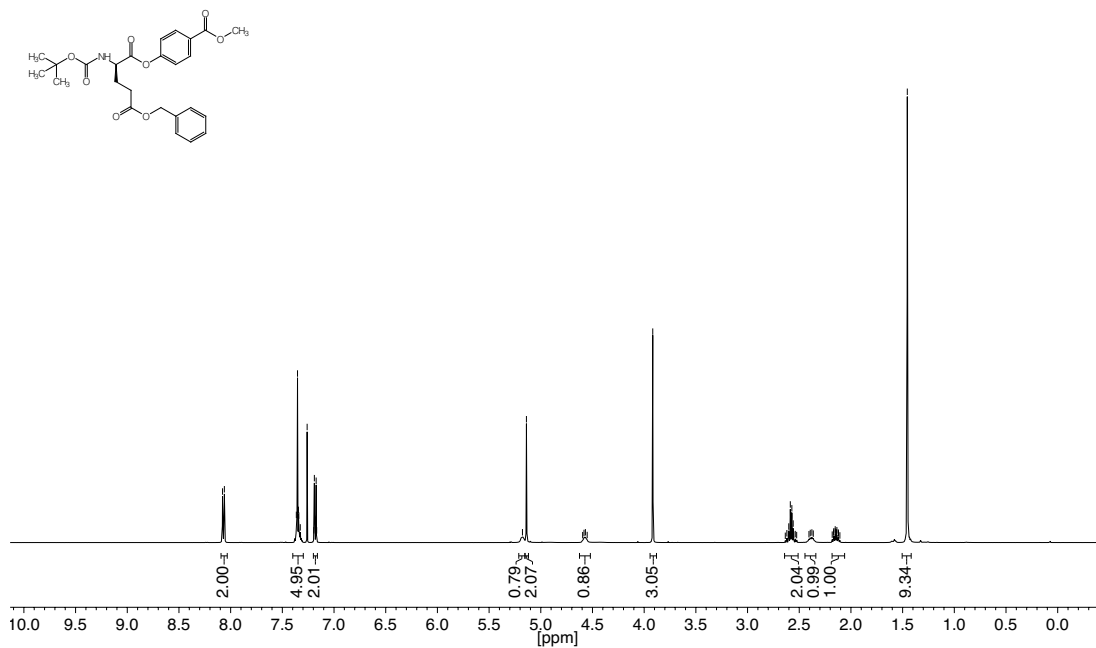


Figure 7.28. ^1H - and ^{13}C -NMR spectra of compound 28.

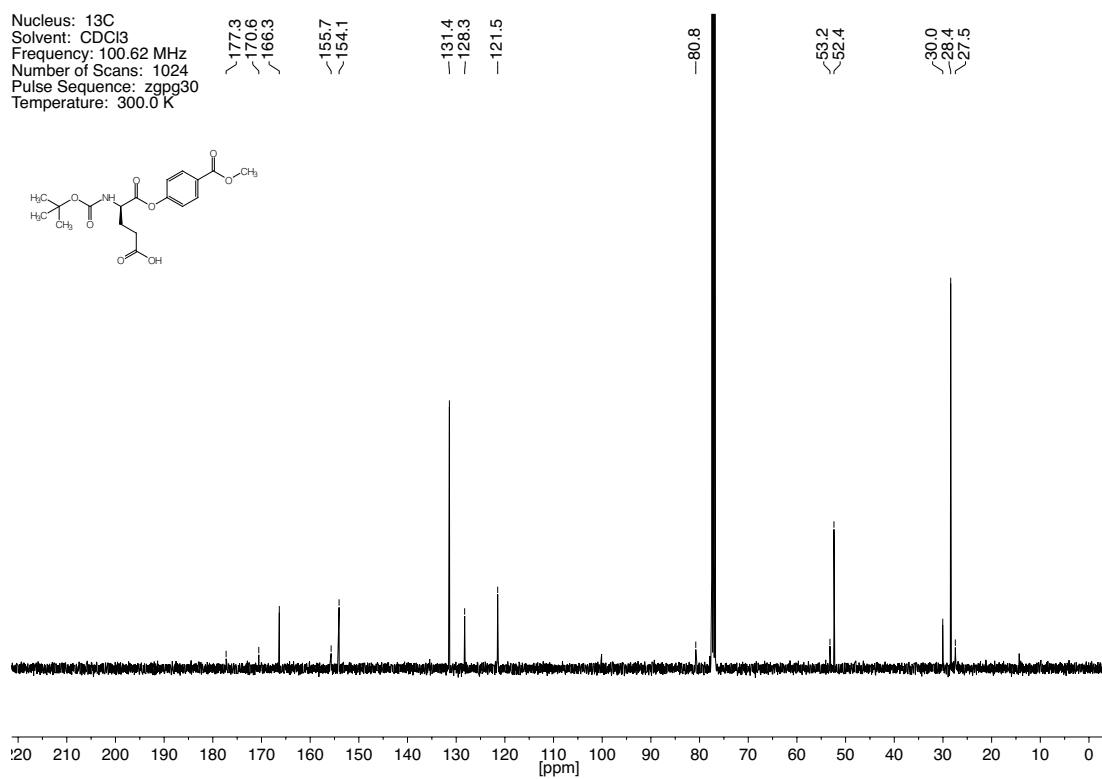
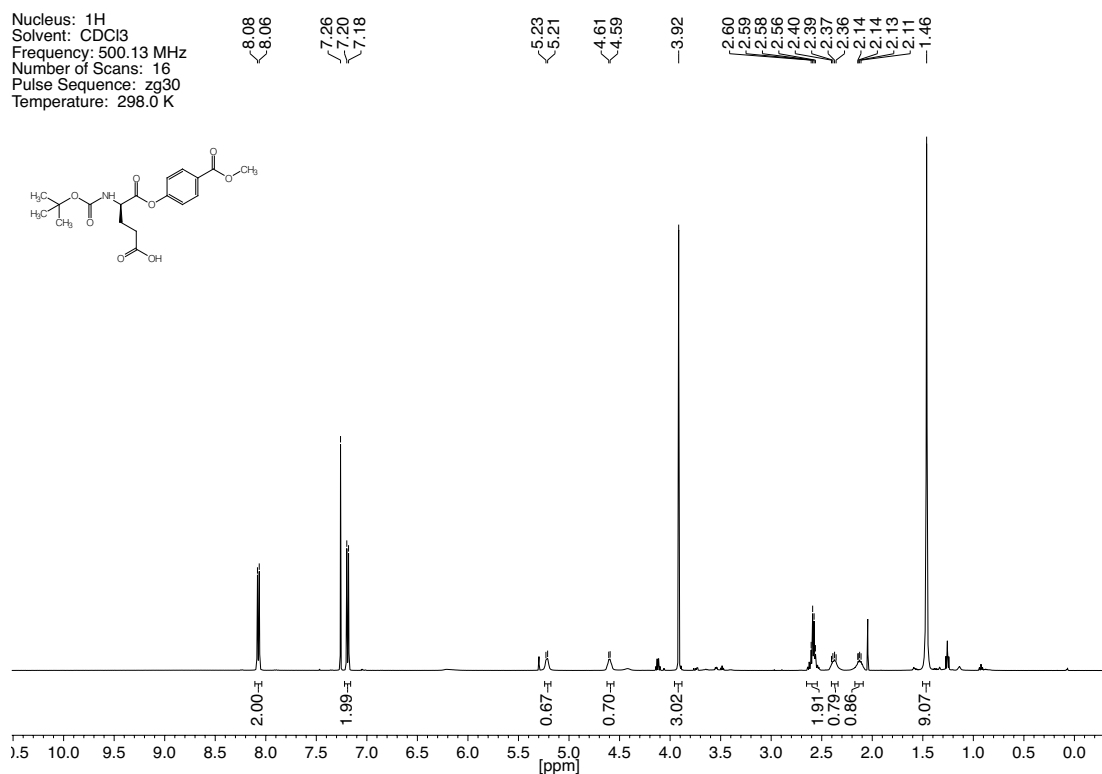
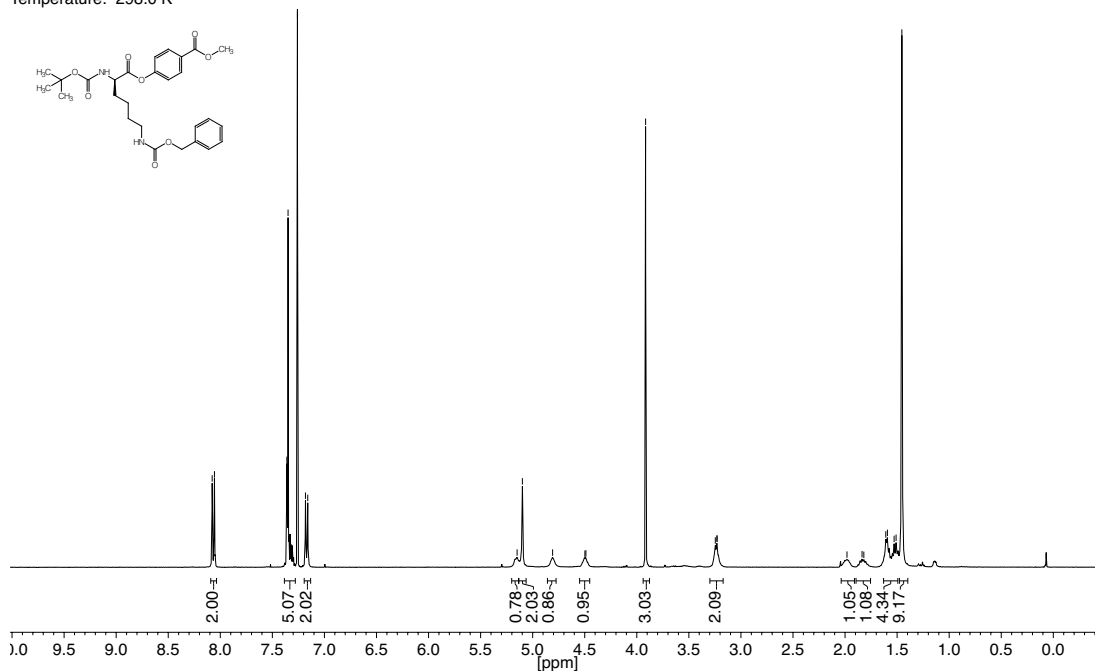


Figure 7.29. ^1H - and ^{13}C -NMR spectra of compound **29**.

Nucleus: ^1H
 Solvent: CDCl_3
 Frequency: 400.13 MHz
 Number of Scans: 16
 Pulse Sequence: zg30
 Temperature: 298.0 K



Nucleus: ^{13}C
 Solvent: CDCl_3
 Frequency: 125.83 MHz
 Number of Scans: 256
 Pulse Sequence: zgpg30
 Temperature: 299.9 K

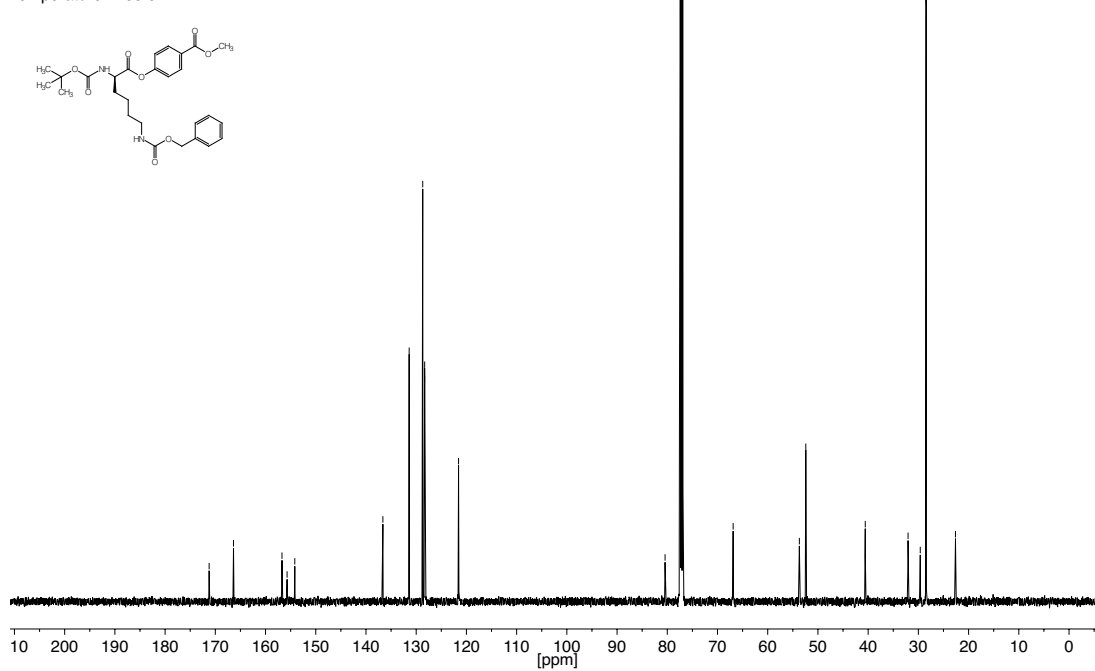


Figure 7.30. ^1H - and ^{13}C -NMR spectra of compound 30.

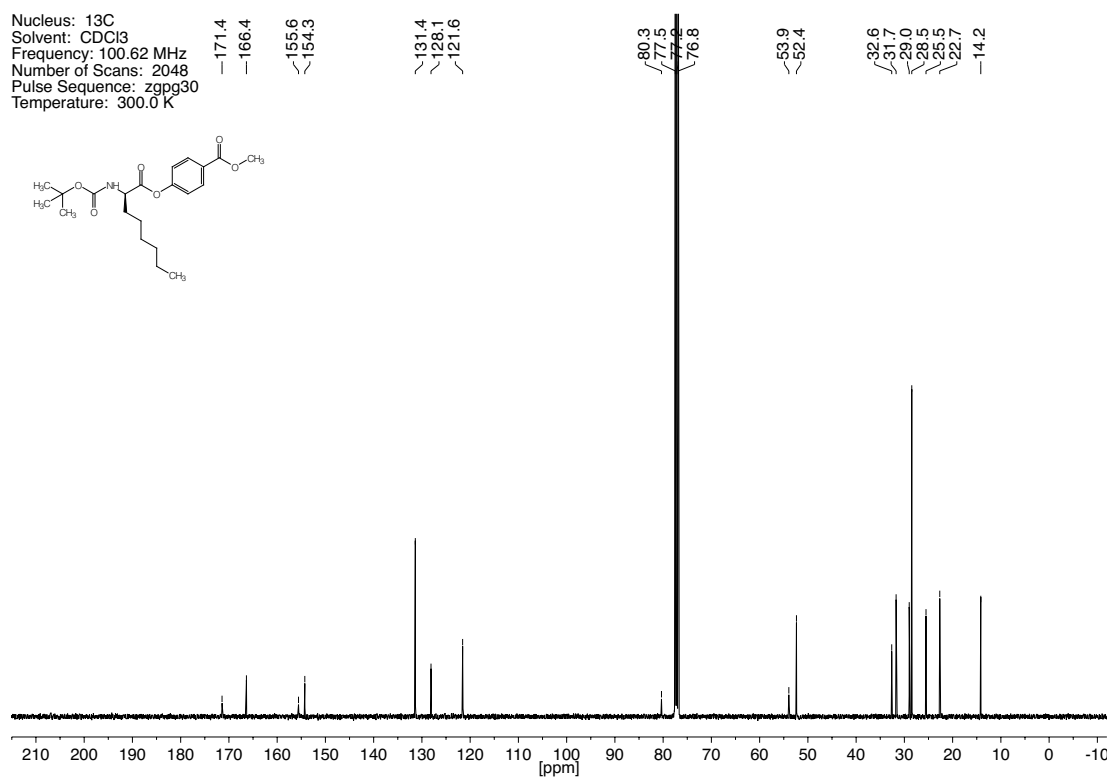
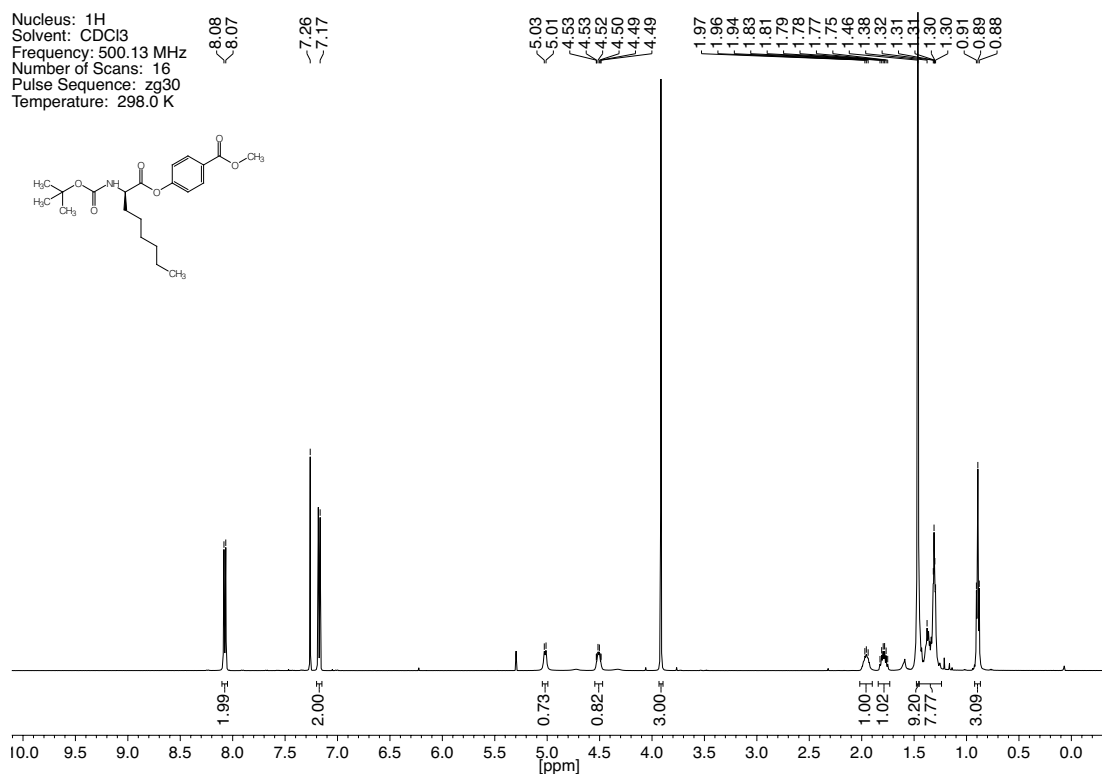


Figure 7.31. ^1H - and ^{13}C -NMR spectra of compound **31**.

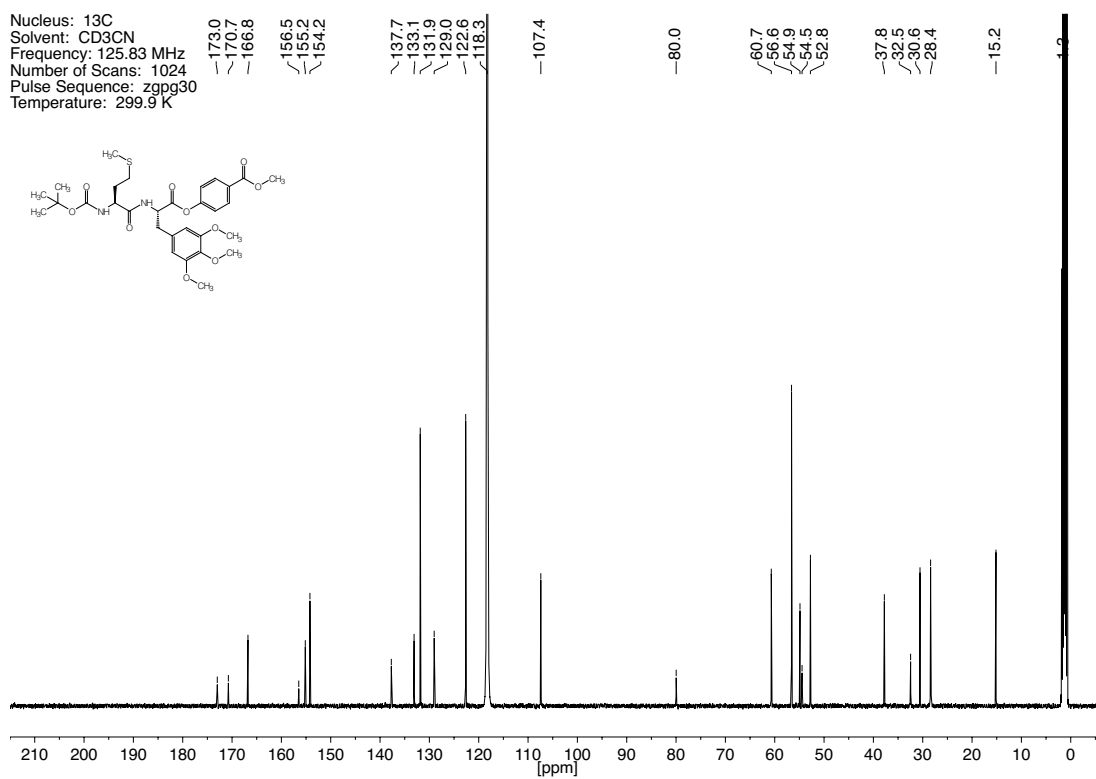
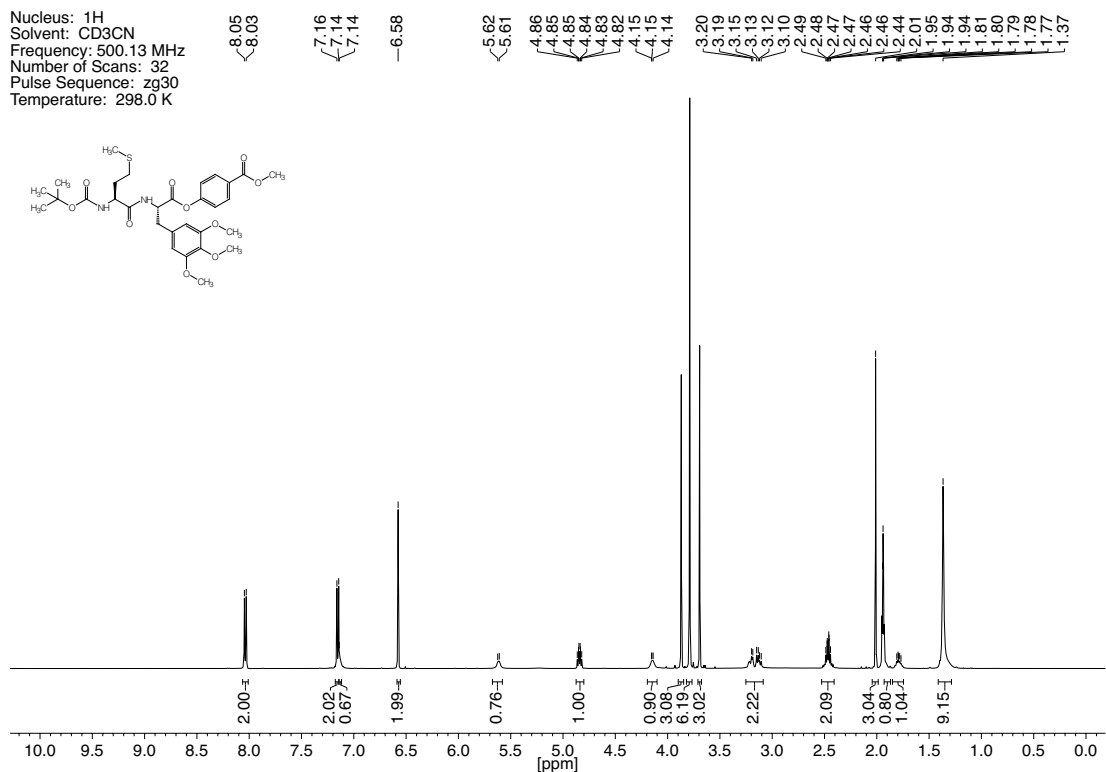


Figure 7.32. ^1H - and ^{13}C -NMR spectra of compound 32.

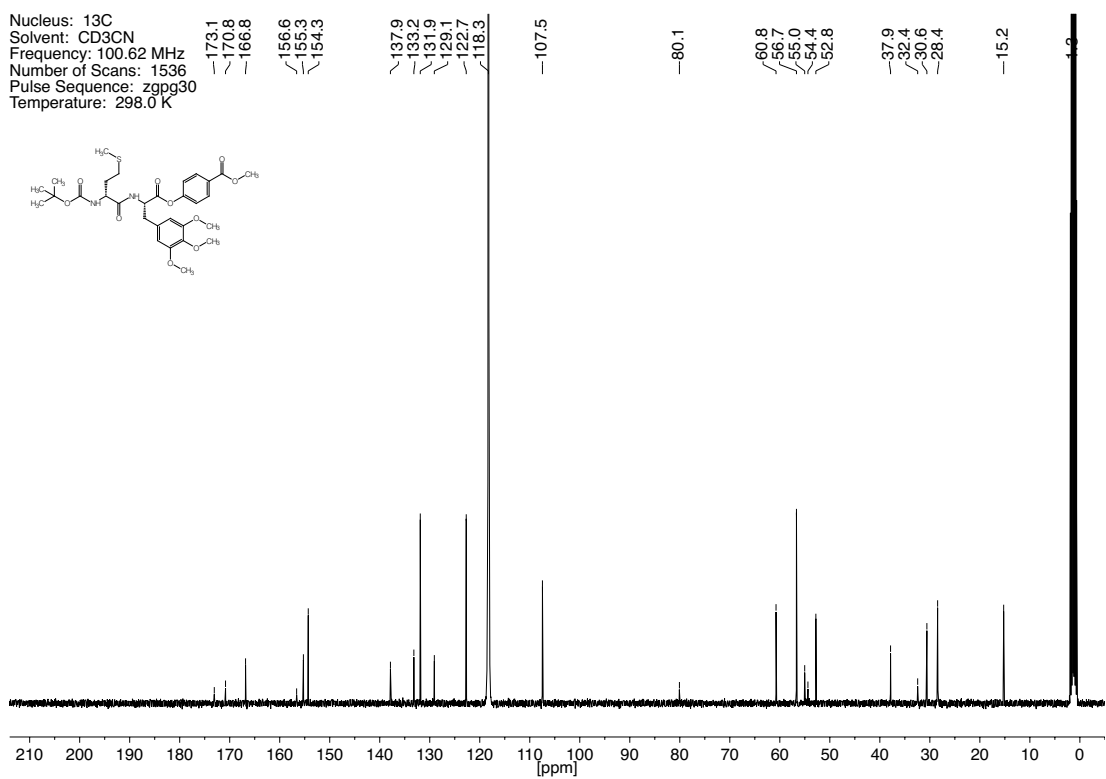
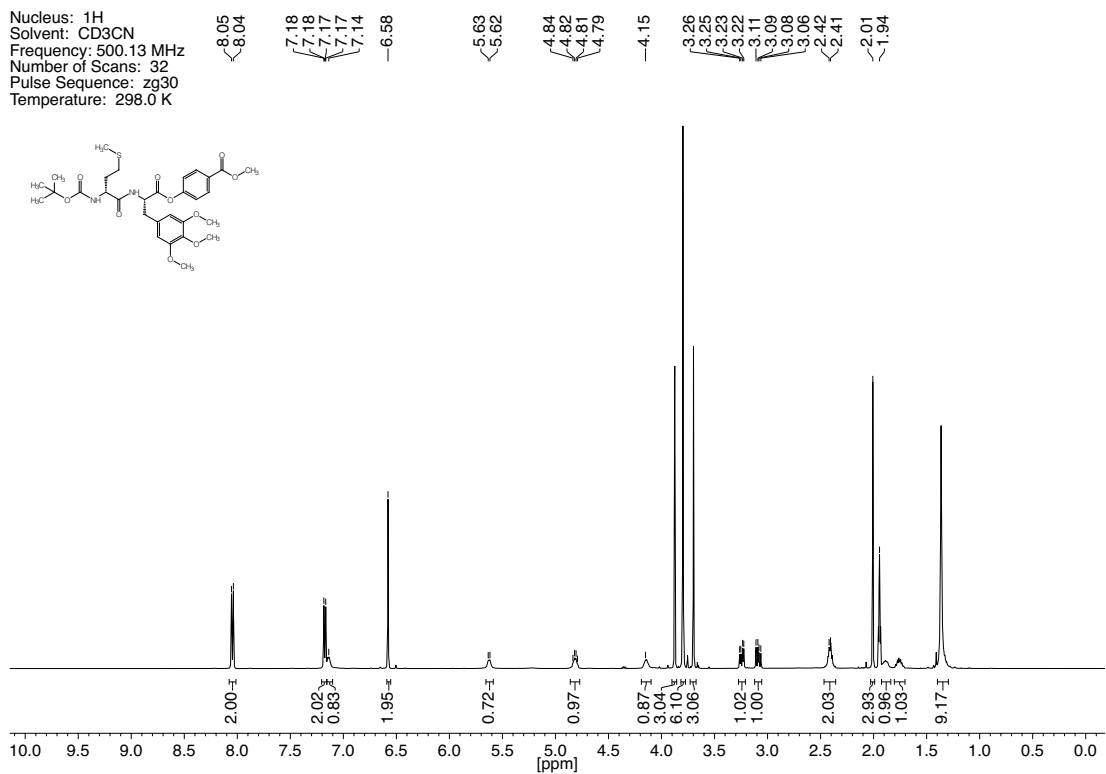
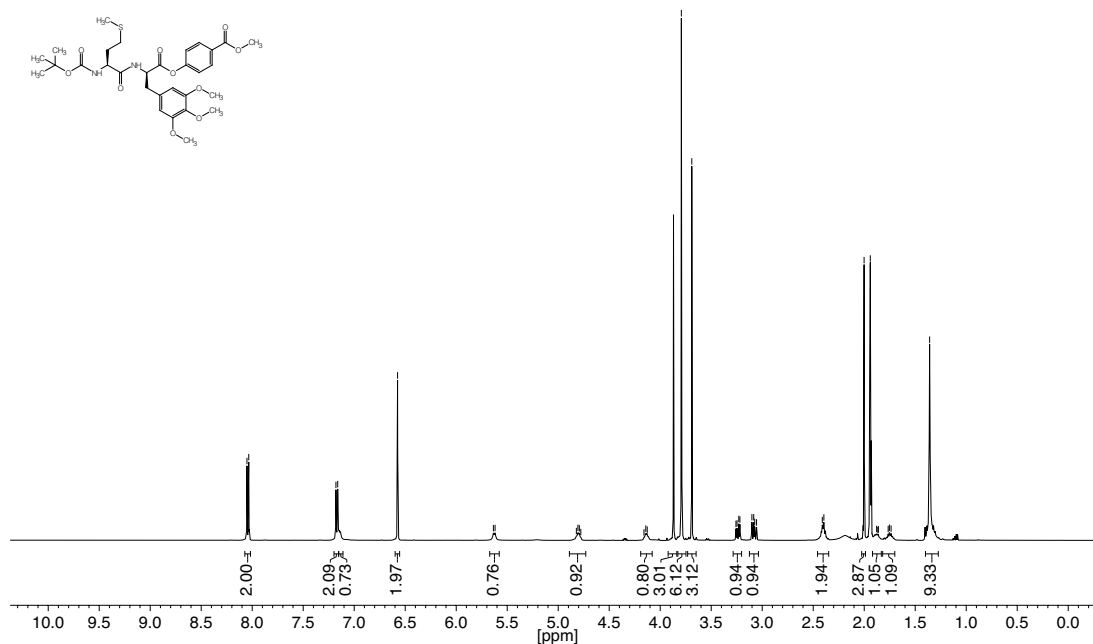


Figure 7.33. ^1H - and ^{13}C -NMR spectra of compound 33.

Nucleus: ^1H
 Solvent: CD_3CN
 Frequency: 500.36 MHz
 Number of Scans: 16
 Pulse Sequence: zg30
 Temperature: 299.8 K

8.05
8.05
8.04
8.03
7.18
7.16
6.58
5.64
5.62
4.82
4.81
4.79
4.78
4.16
4.14
4.13
3.87
3.79
3.69
3.26
3.25
3.22
3.10
3.09
3.07
3.06
2.41
2.40
2.00
1.94
1.88
1.86
1.77
1.75
1.74
1.36



Nucleus: ^{13}C
 Solvent: CD_3CN
 Frequency: 125.83 MHz
 Number of Scans: 1024
 Pulse Sequence: zgpg30
 Temperature: 299.8 K

173.0
170.8
166.8
156.6
155.2
154.2
137.7
133.2
131.9
129.0
122.7
118.3
107.3
80.0
60.7
56.6
55.0
54.3
52.8
37.8
32.4
30.5
28.4
15.2

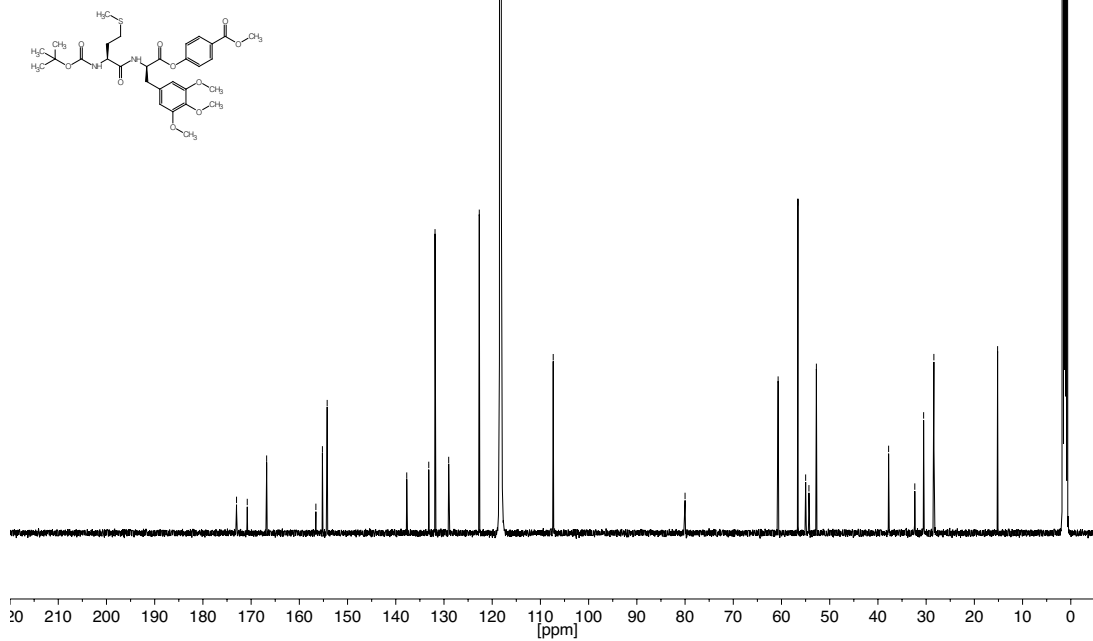


Figure 7.34. ^1H - and ^{13}C -NMR spectra of compound 34.

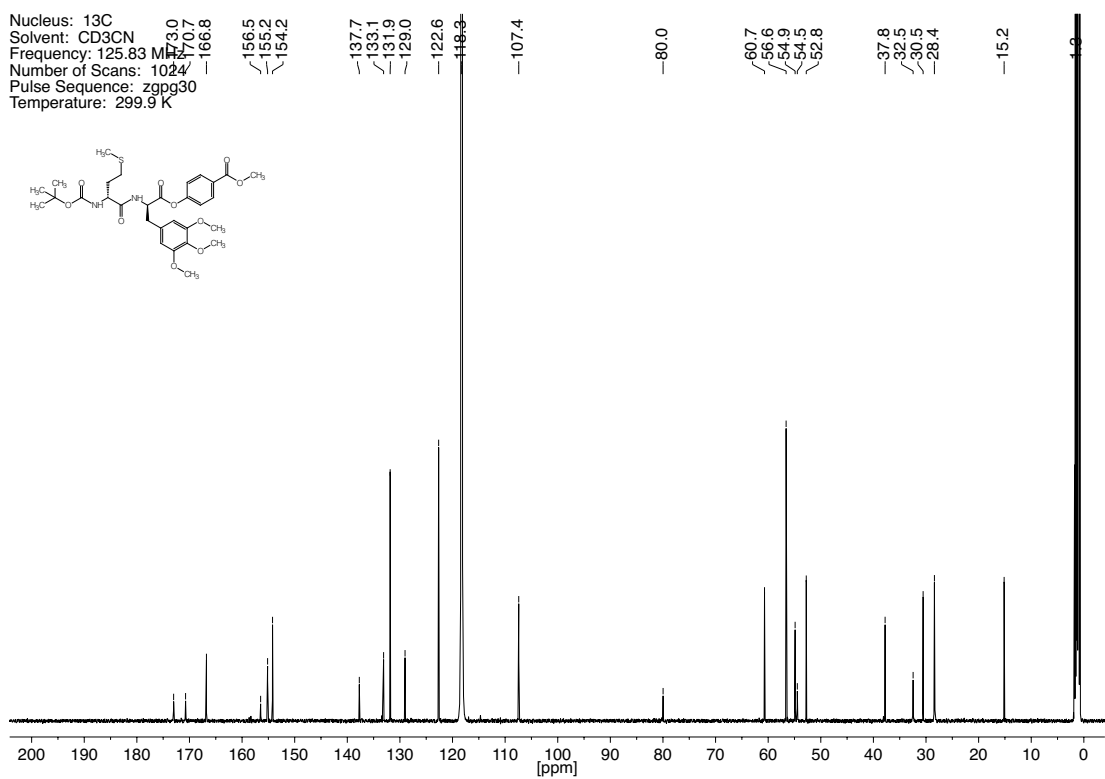
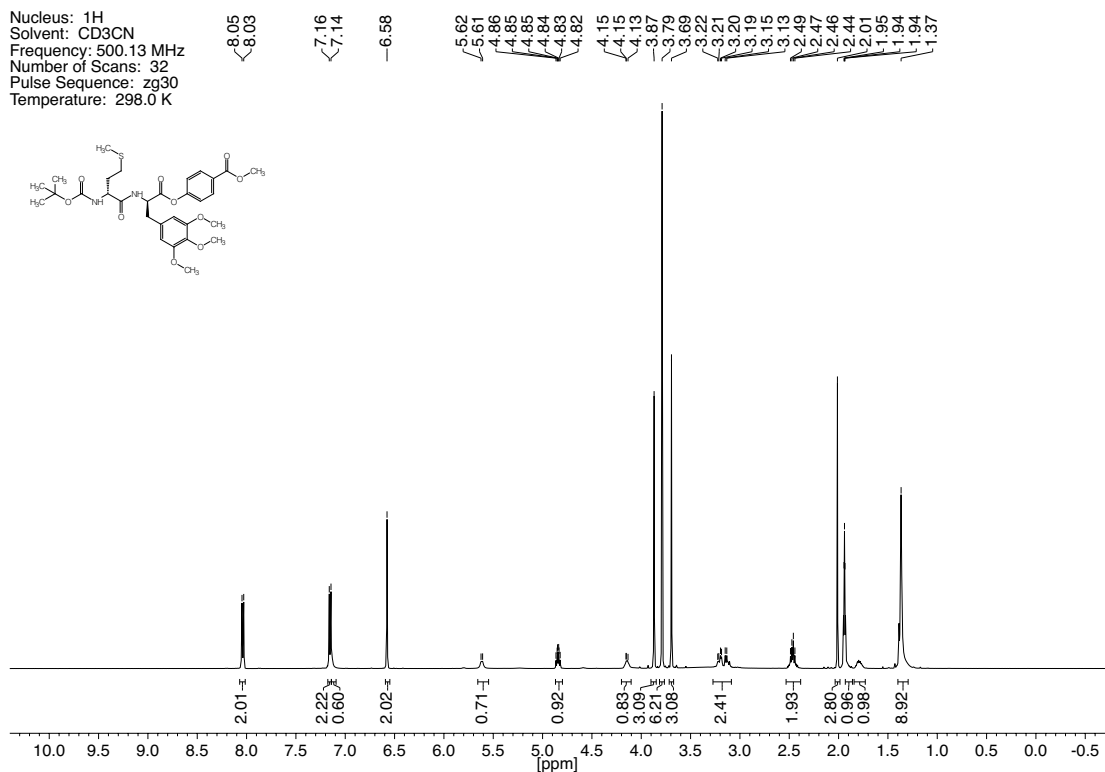
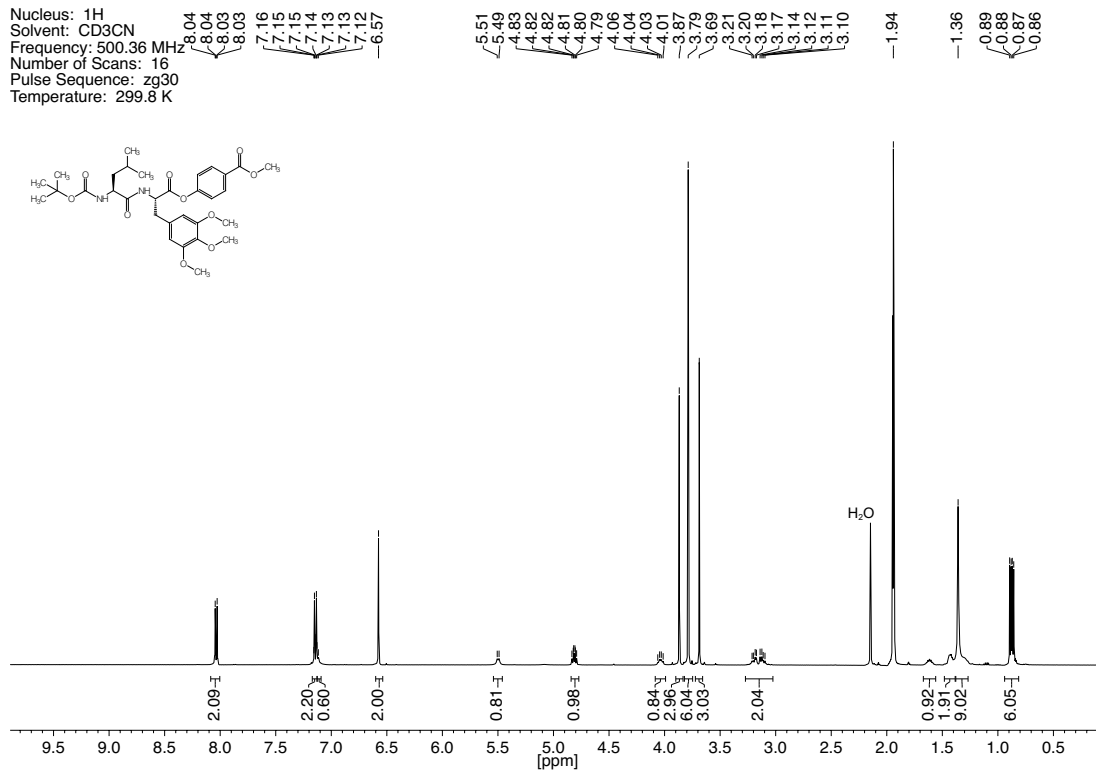


Figure 7.35. ^1H - and ^{13}C -NMR spectra of compound 35.

Nucleus: ^1H
 Solvent: CD_3CN
 Frequency: 500.36 MHz
 Number of Scans: 16
 Pulse Sequence: zg30
 Temperature: 299.8 K



Nucleus: ^{13}C
 Solvent: CD_3CN
 Frequency: 125.83 MHz
 Number of Scans: 1024
 Pulse Sequence: zgpg30
 Temperature: 299.8 K

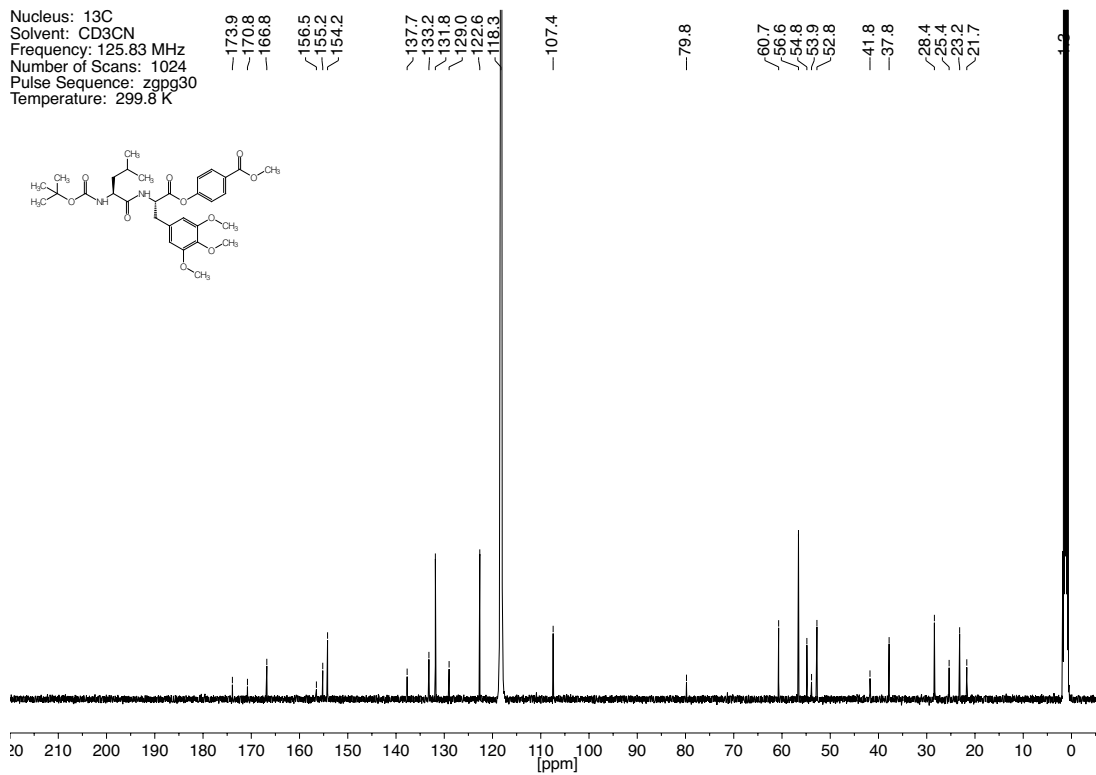


Figure 7.36. ^1H - and ^{13}C -NMR spectra of compound 36.

Nucleus: ^1H
 Solvent: CD_3CN
 Frequency: 500.13 MHz
 Number of Scans: 16
 Pulse Sequence: zg30
 Temperature: 298.0 K

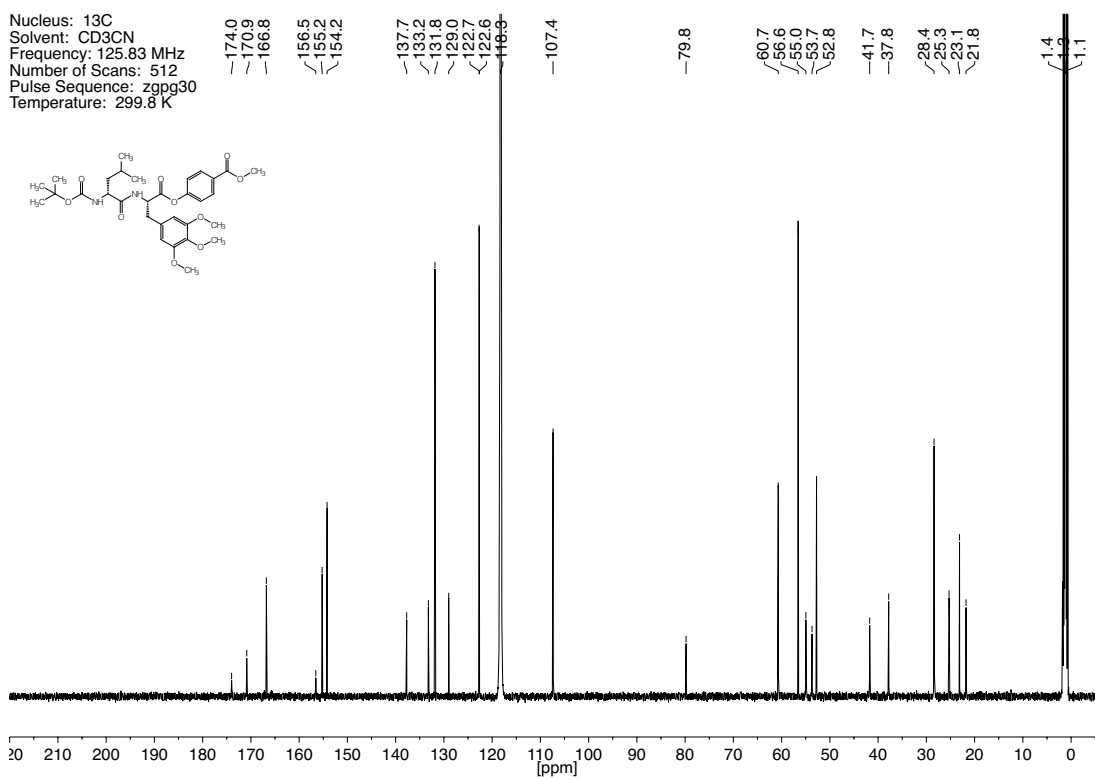
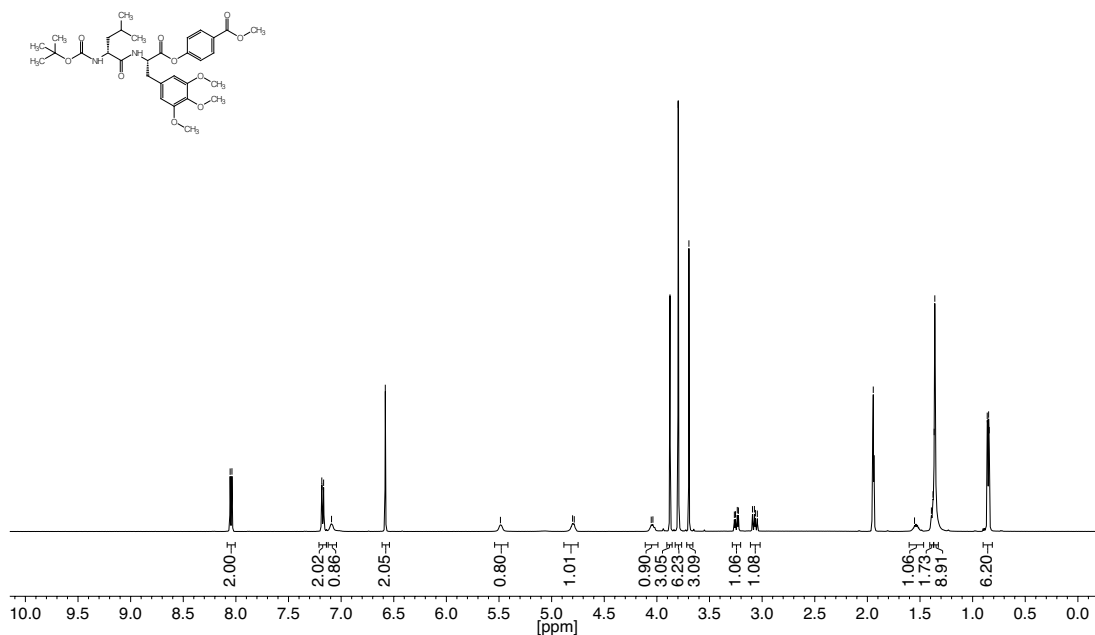


Figure 7.37. ^1H - and ^{13}C -NMR spectra of compound 37.

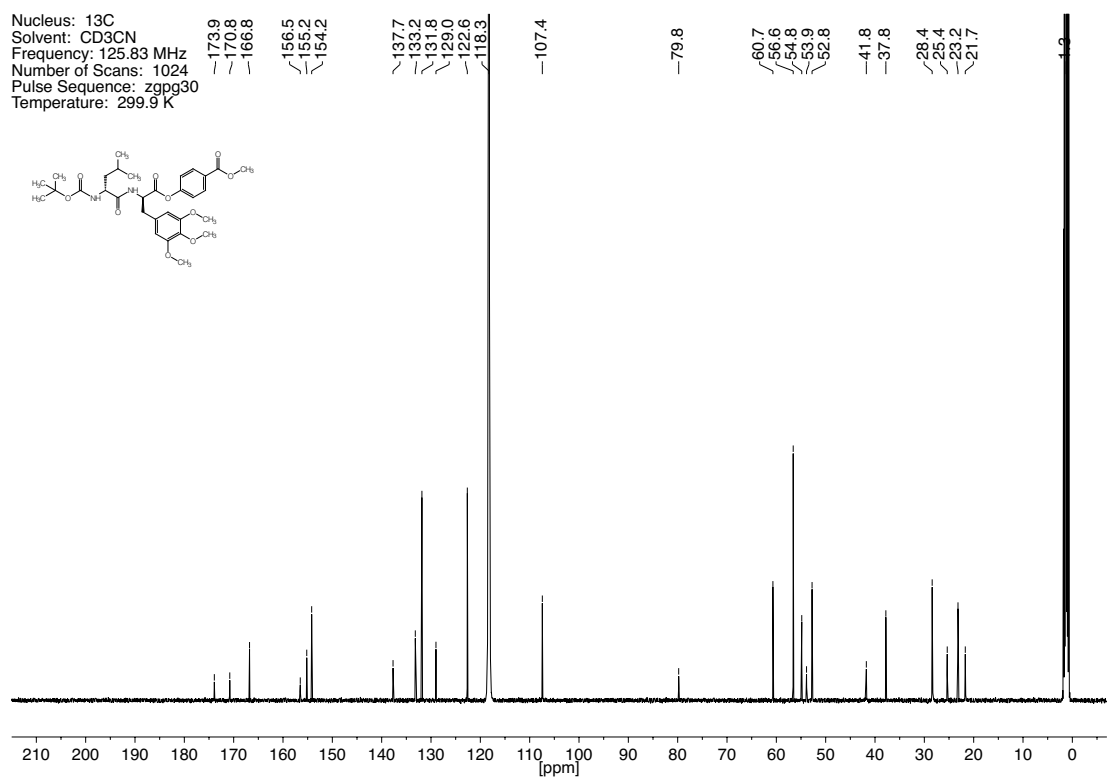
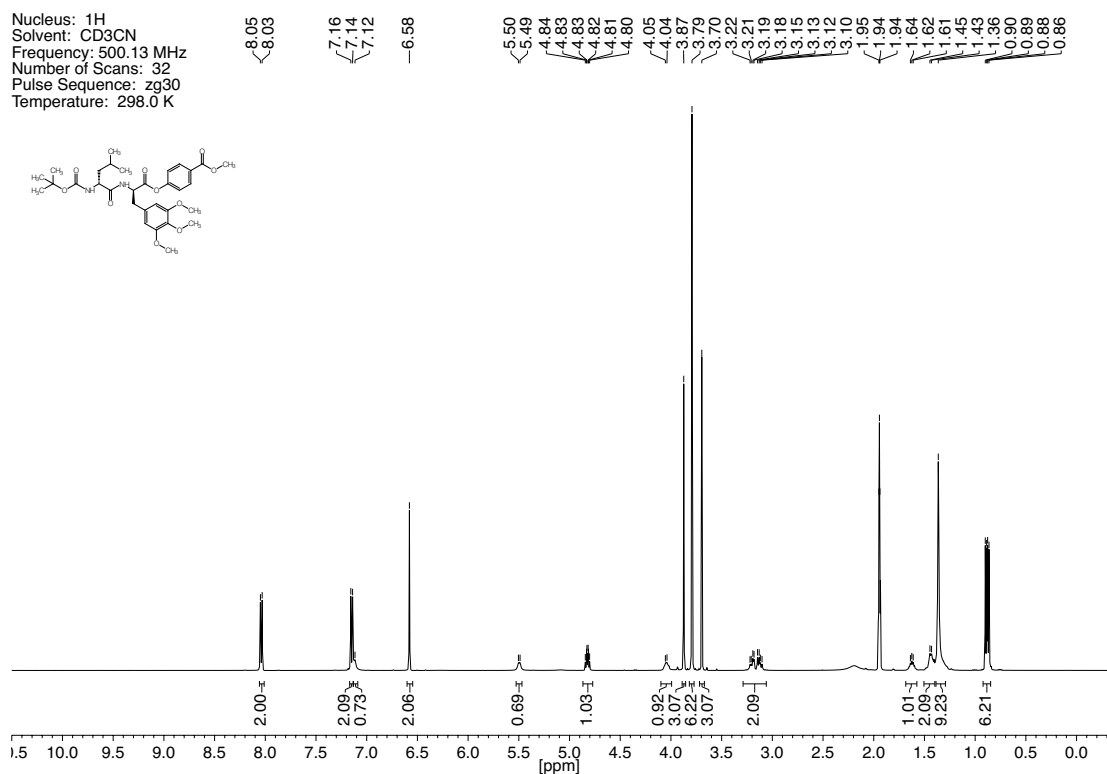
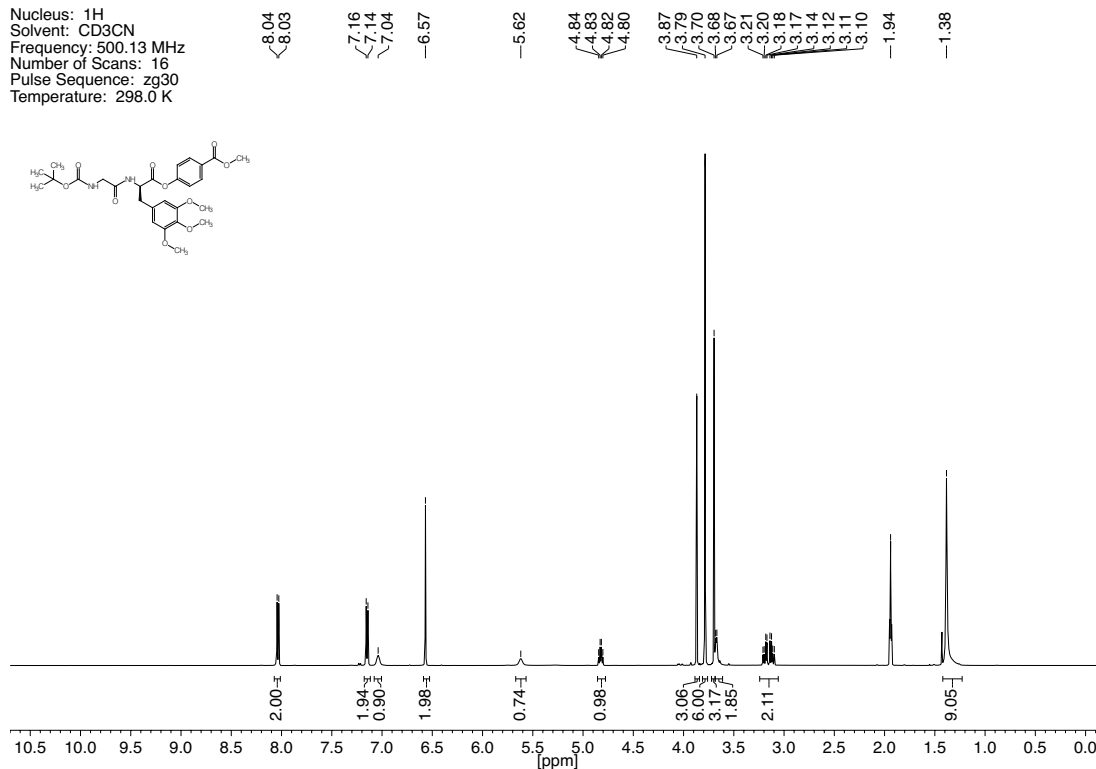


Figure 7.39. ^1H - and ^{13}C -NMR spectra of compound 39.

Nucleus: ^1H
 Solvent: CD_3CN
 Frequency: 500.13 MHz
 Number of Scans: 16
 Pulse Sequence: zg30
 Temperature: 298.0 K



Nucleus: ^{13}C
 Solvent: CD_3CN
 Frequency: 125.83 MHz
 Number of Scans: 512
 Pulse Sequence: zgpg30
 Temperature: 299.8 K

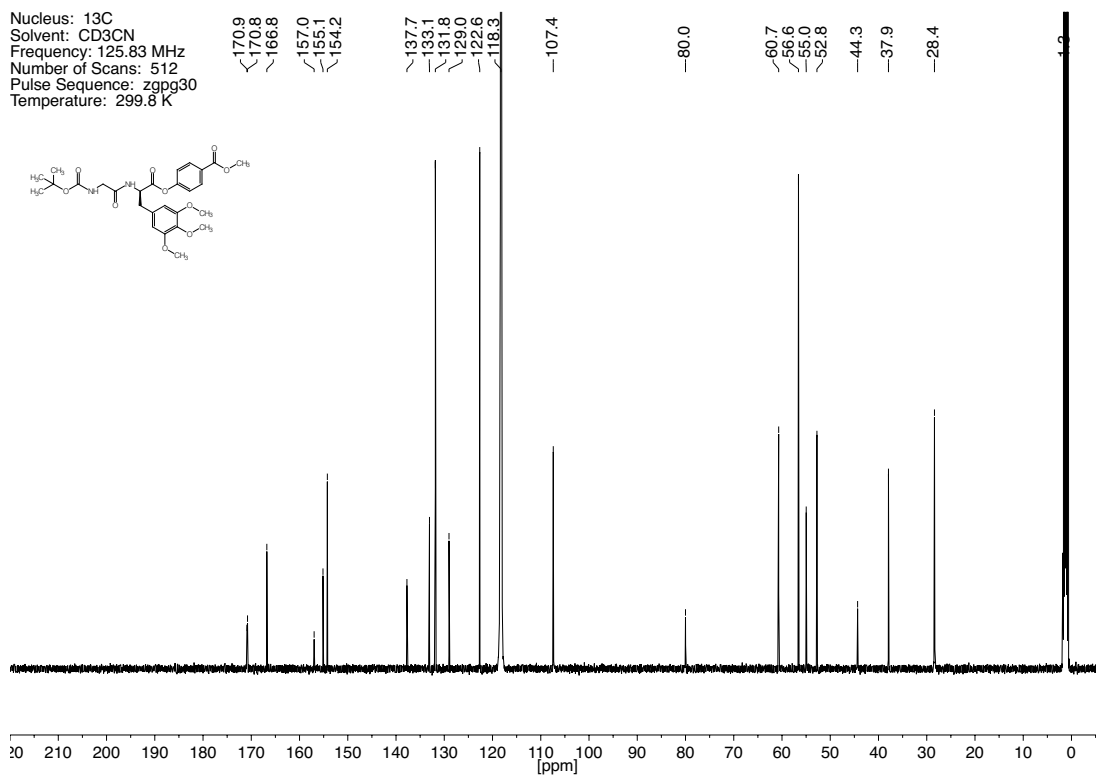
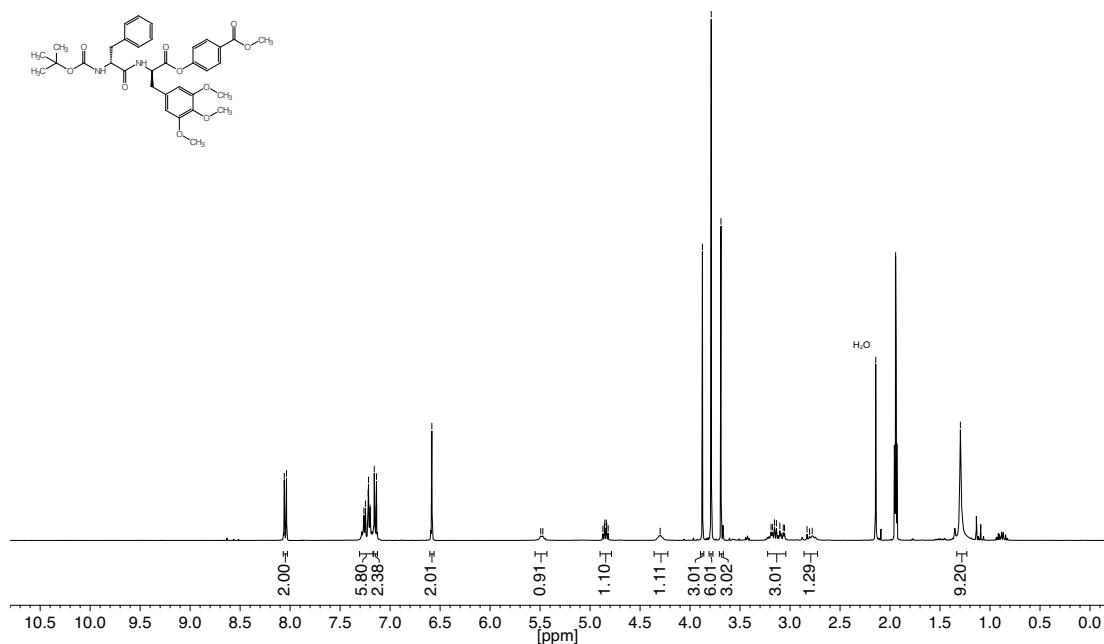


Figure 7.40. ^1H - and ^{13}C -NMR spectra of compound 40.

Nucleus: ^1H
Solvent: CD_3CN
Frequency: 400.13 MHz
Number of Scans: 16
Pulse Sequence: zg30
Temperature: 298.0 K



Nucleus: ^{13}C
Solvent: CD_3CN
Frequency: 125.83 MHz
Number of Scans: 256
Pulse Sequence: zgpg30
Temperature: 299.9 K

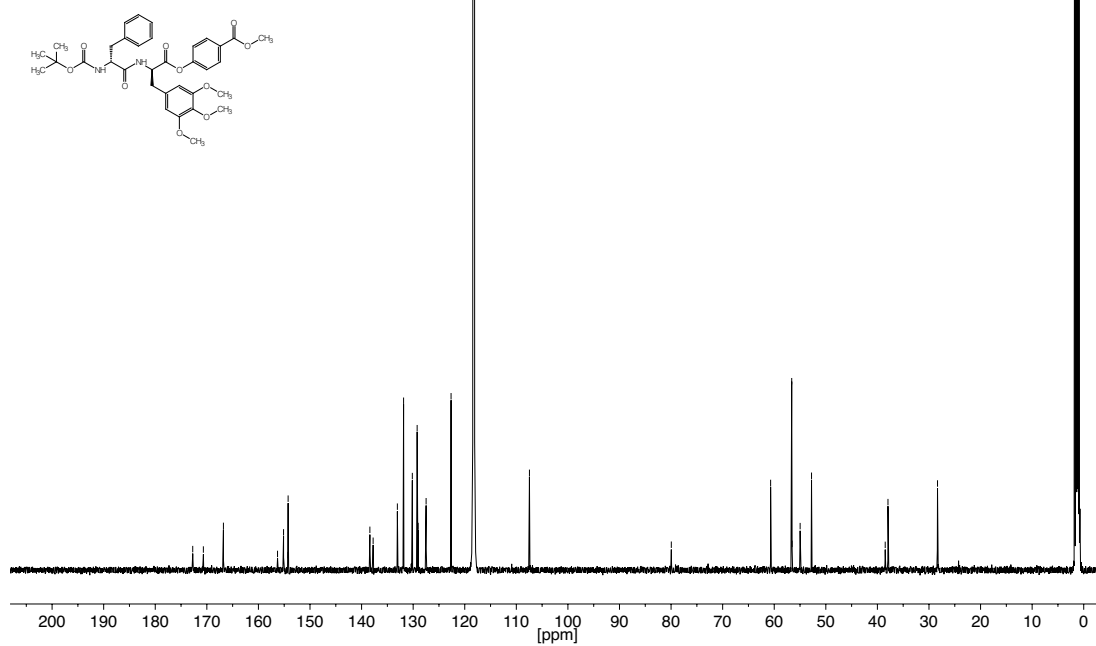


Figure 7.42. ^1H - and ^{13}C -NMR spectra of compound 42.

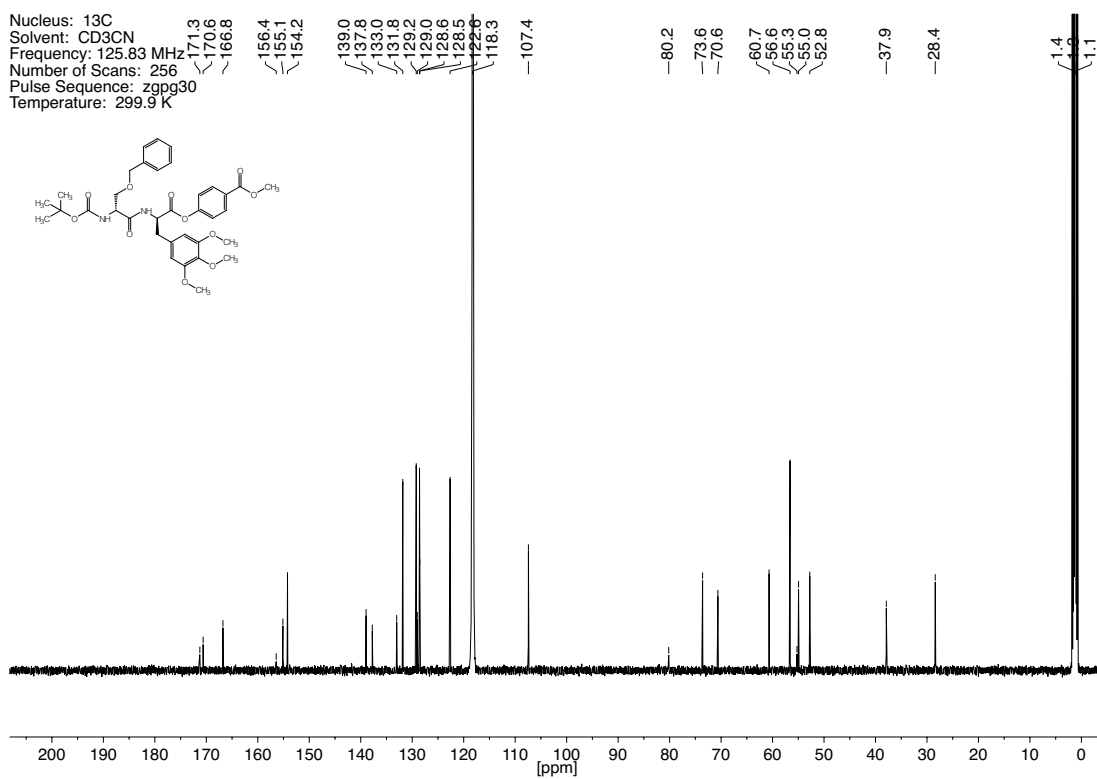
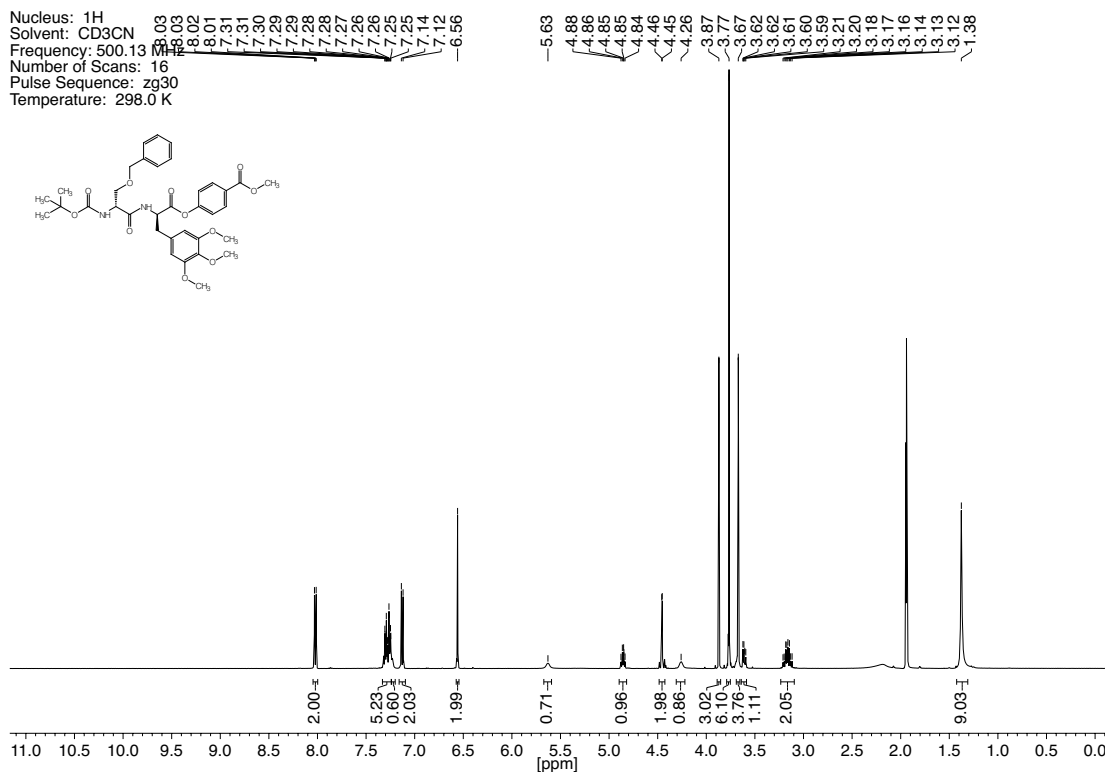


Figure 7.43. ^1H - and ^{13}C -NMR spectra of compound 43.

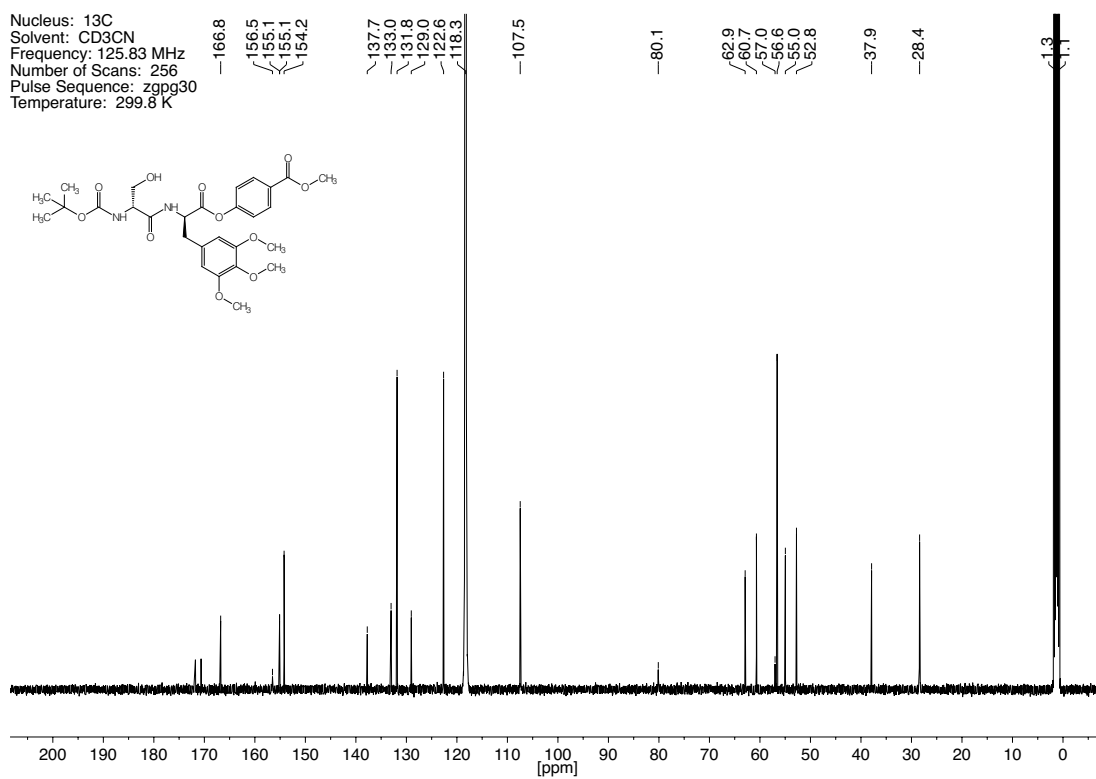
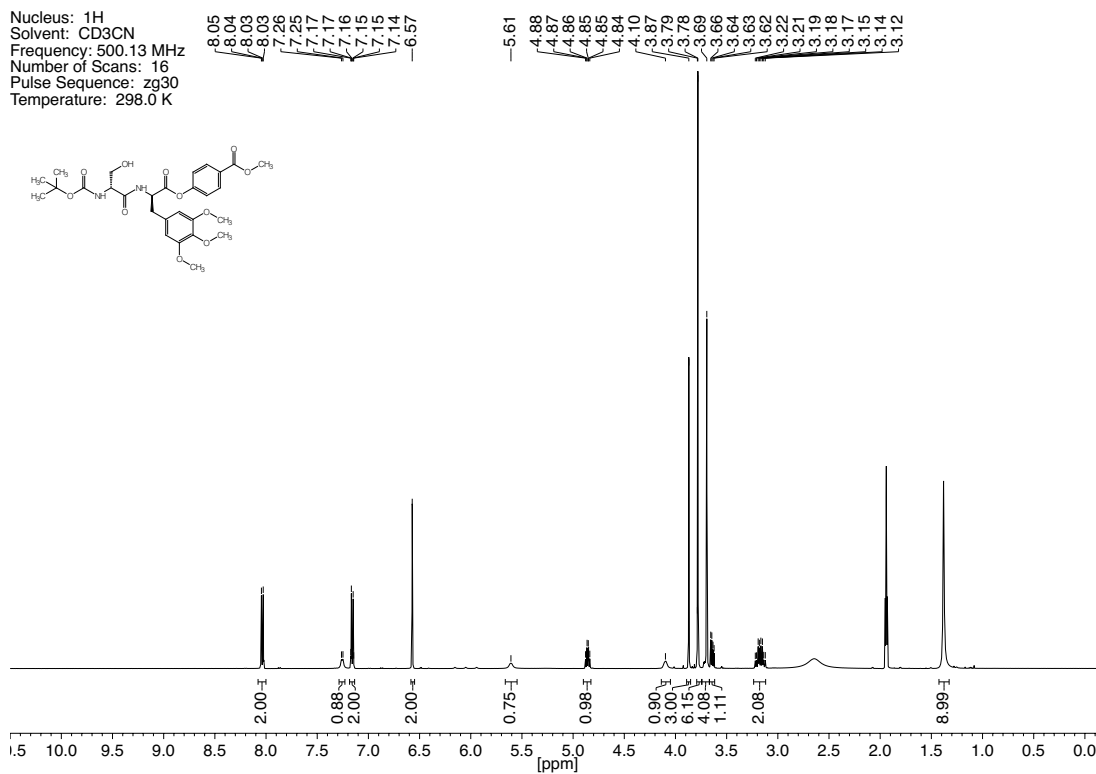


Figure 7.44. ^1H - and ^{13}C -NMR spectra of compound 44.

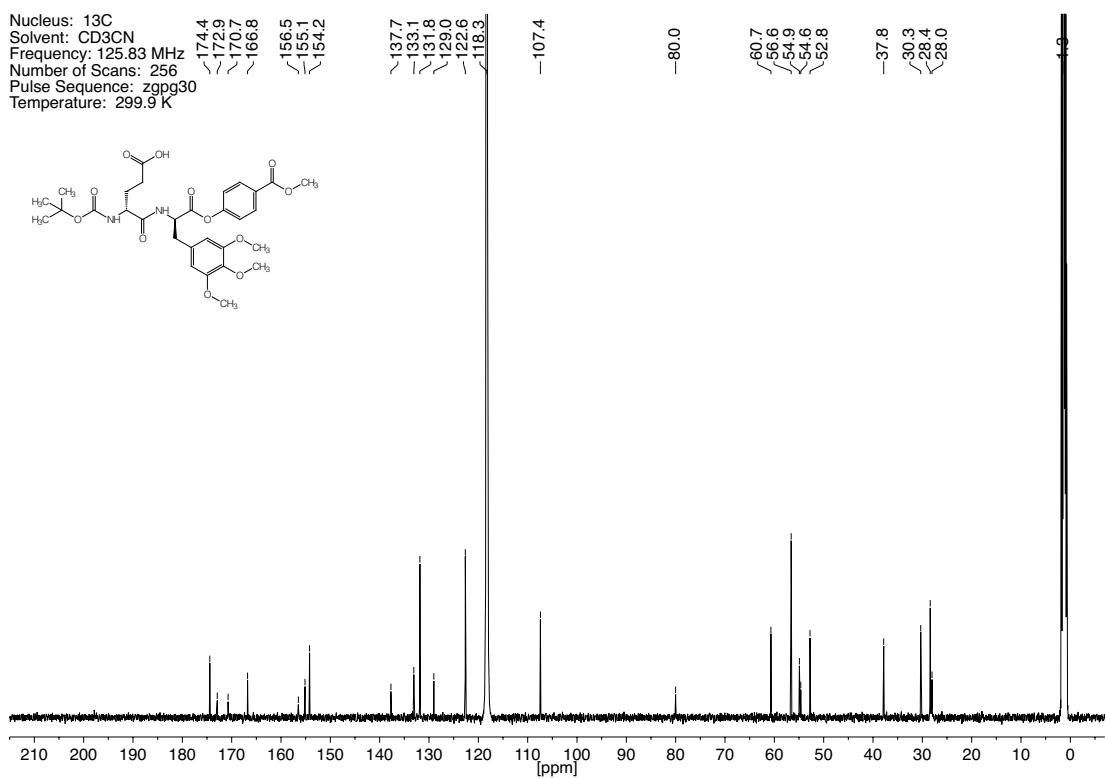
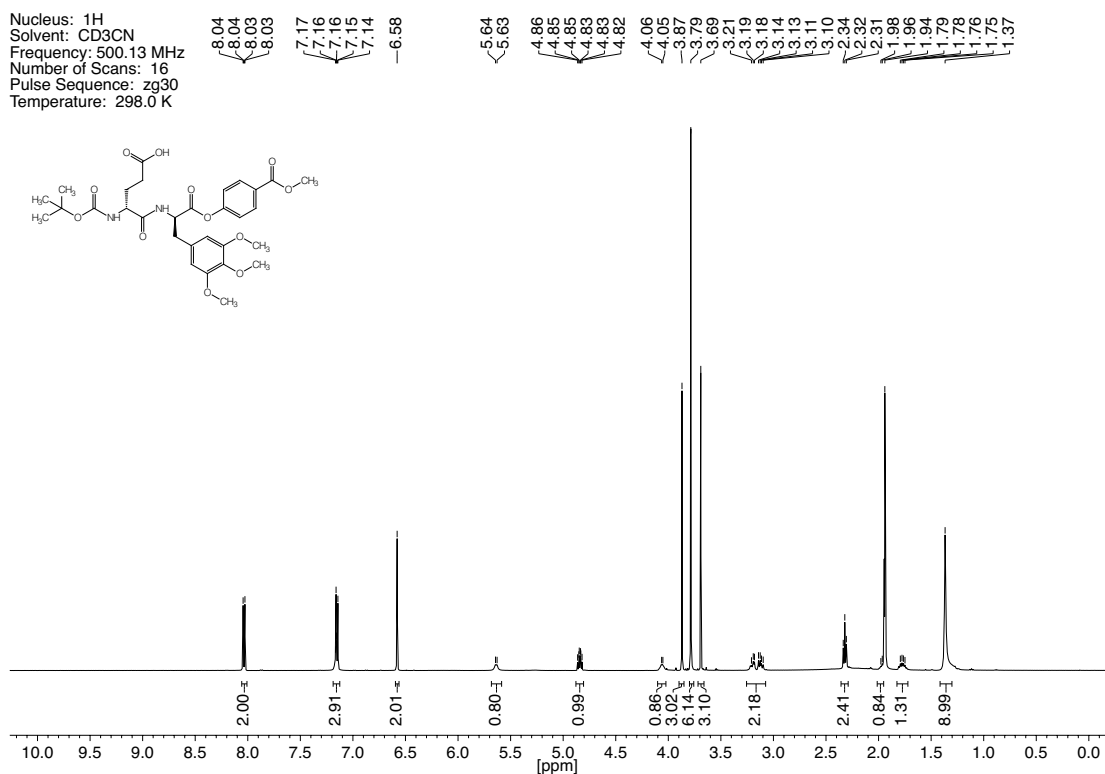


Figure 7.45. ^1H - and ^{13}C -NMR spectra of compound 45.

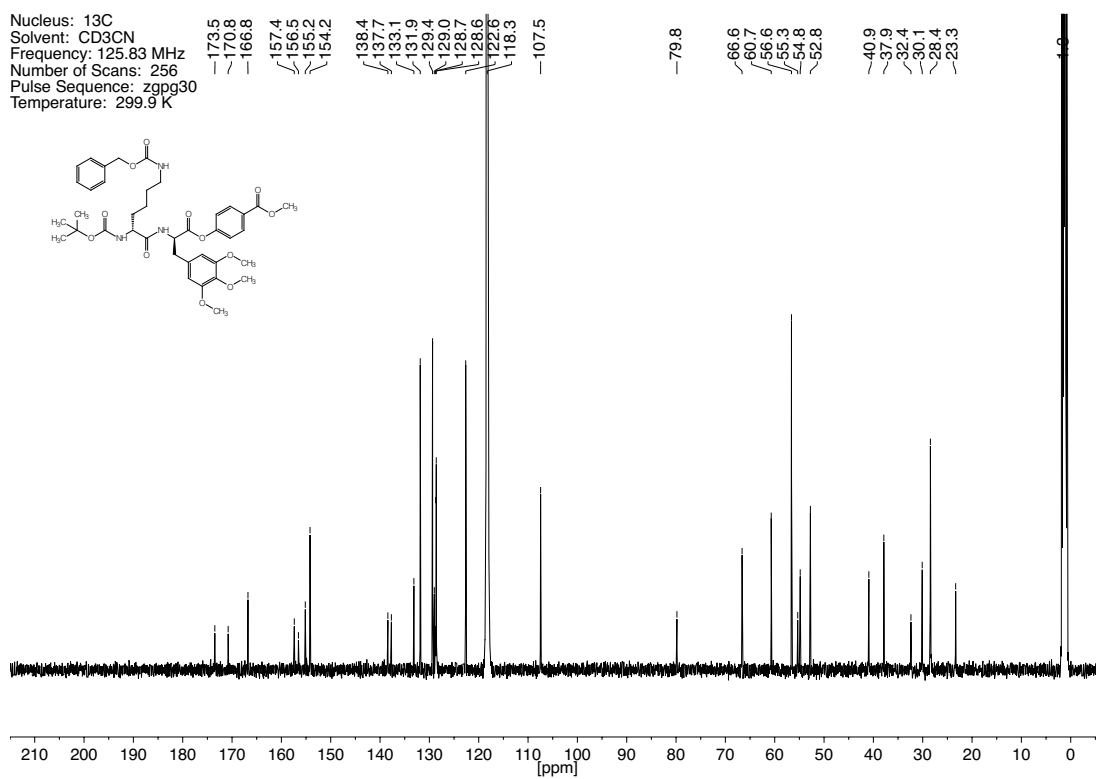
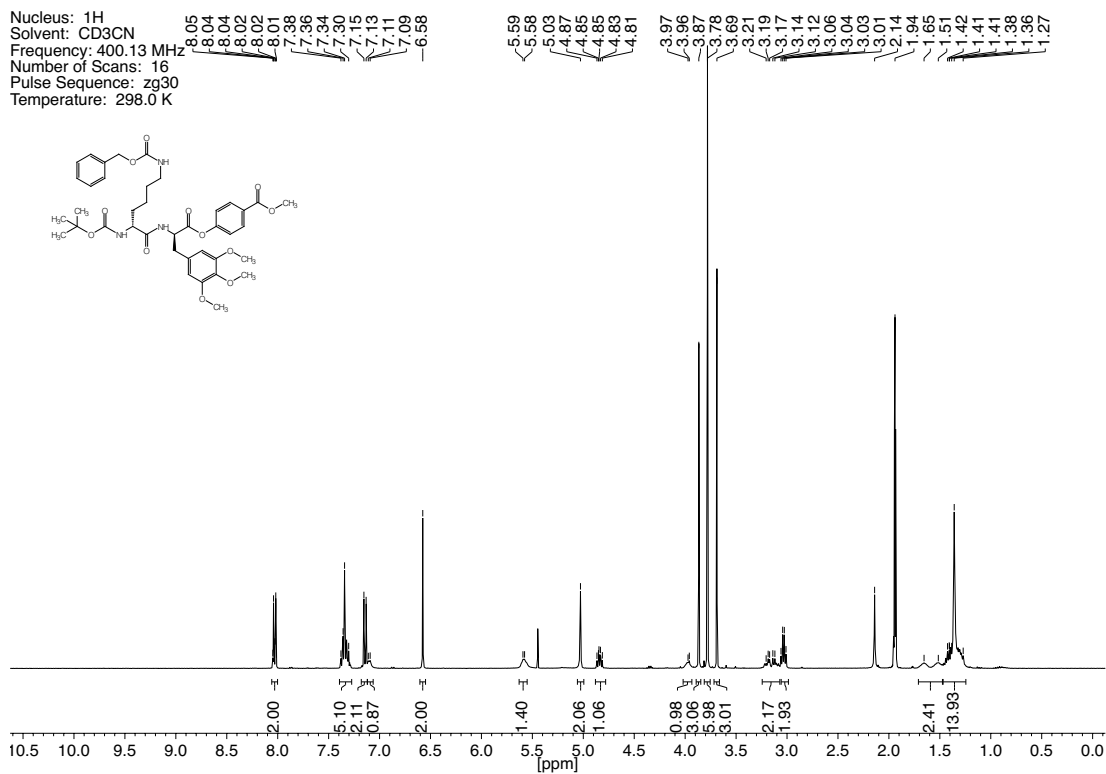


Figure 7.46. ^1H - and ^{13}C -NMR spectra of compound 46.

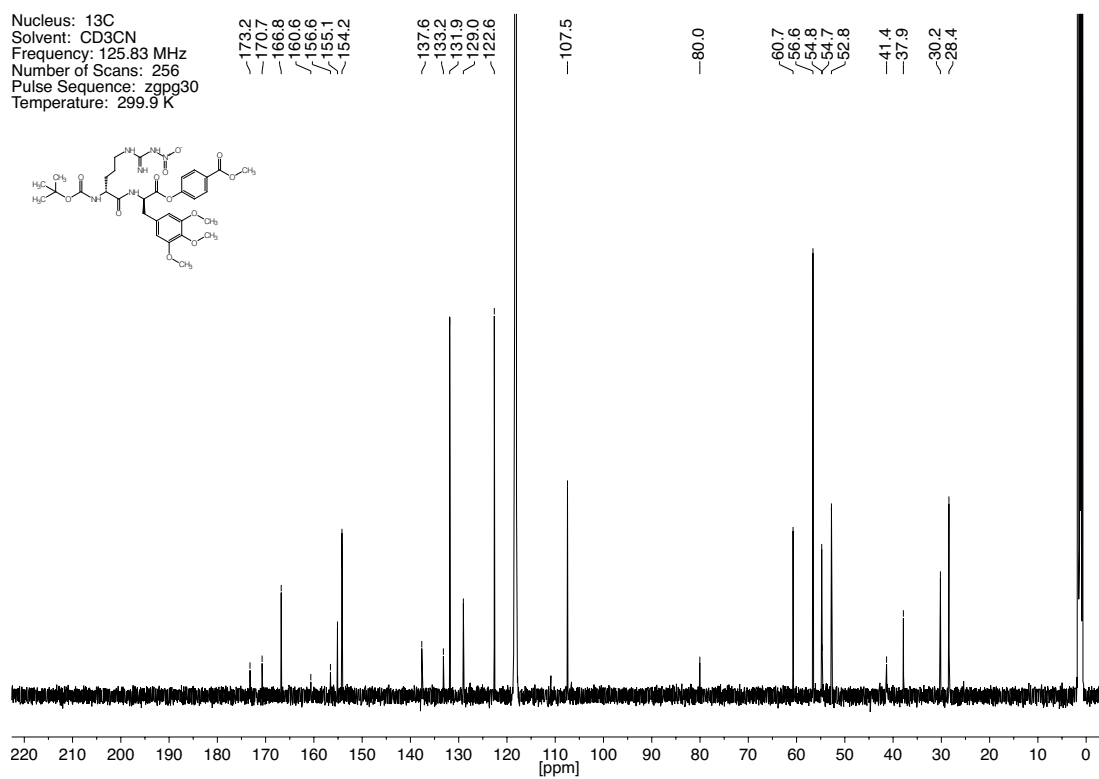
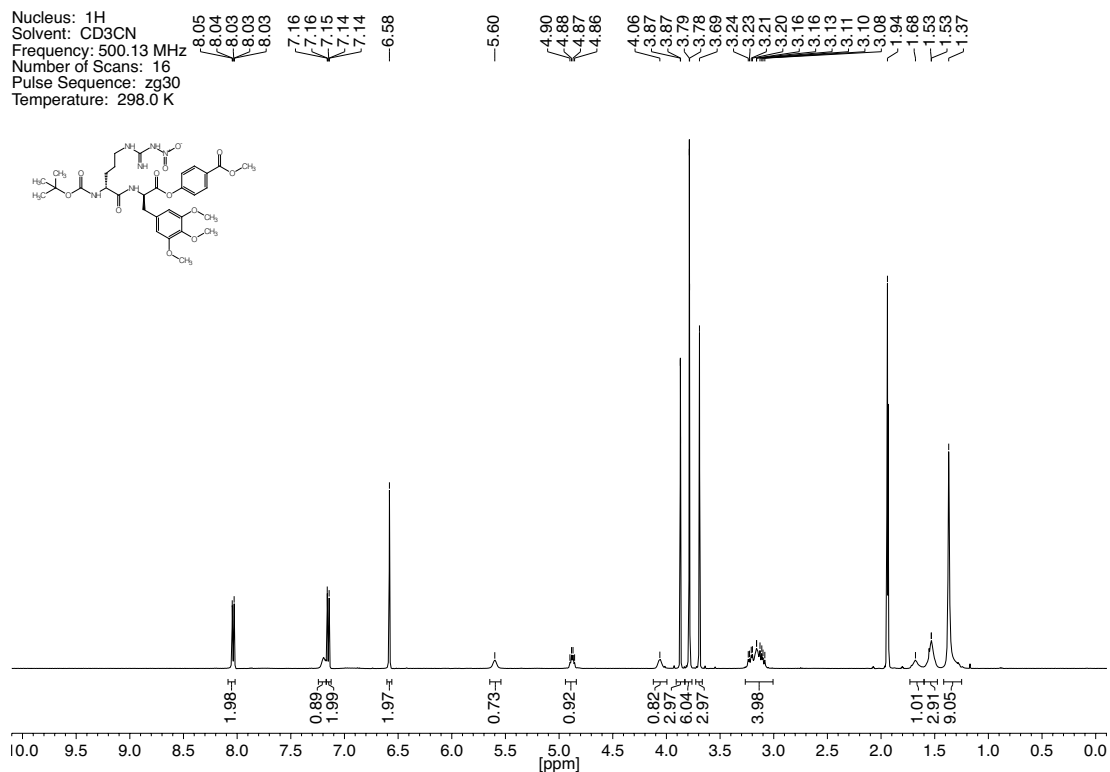
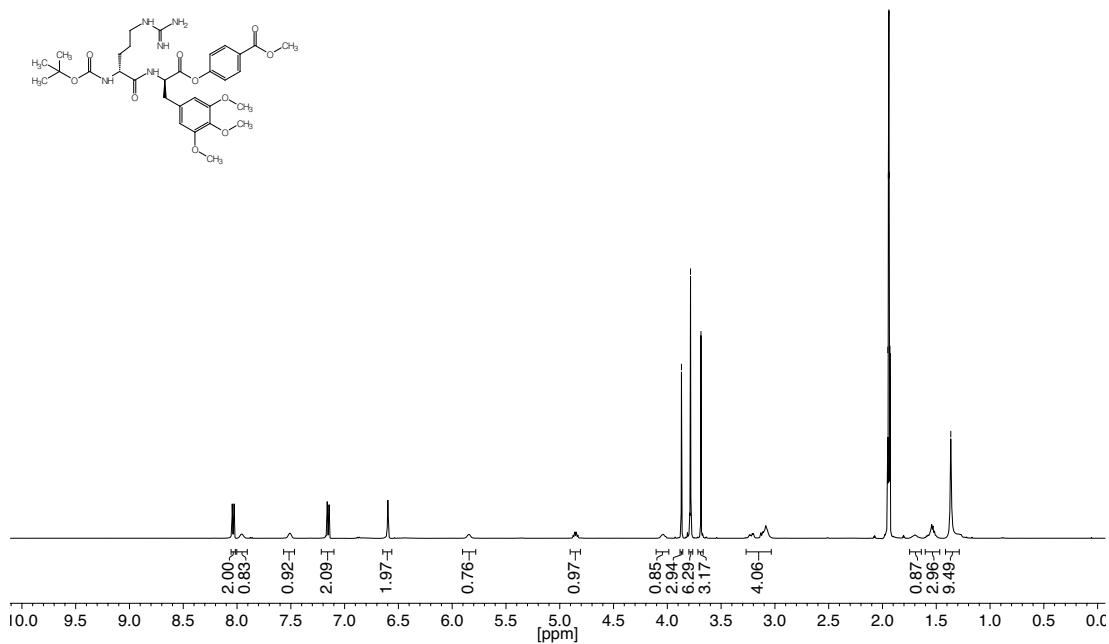


Figure 7.47. ^1H - and ^{13}C -NMR spectra of compound 47.

Nucleus: ^1H
 Solvent: CD_3CN
 Frequency: 500.36 MHz
 Number of Scans: 16
 Pulse Sequence: zg30
 Temperature: 299.8 K



Nucleus: ^{13}C
 Solvent: CD_3CN
 Frequency: 125.83 MHz
 Number of Scans: 512
 Pulse Sequence: zgpg30
 Temperature: 299.9 K

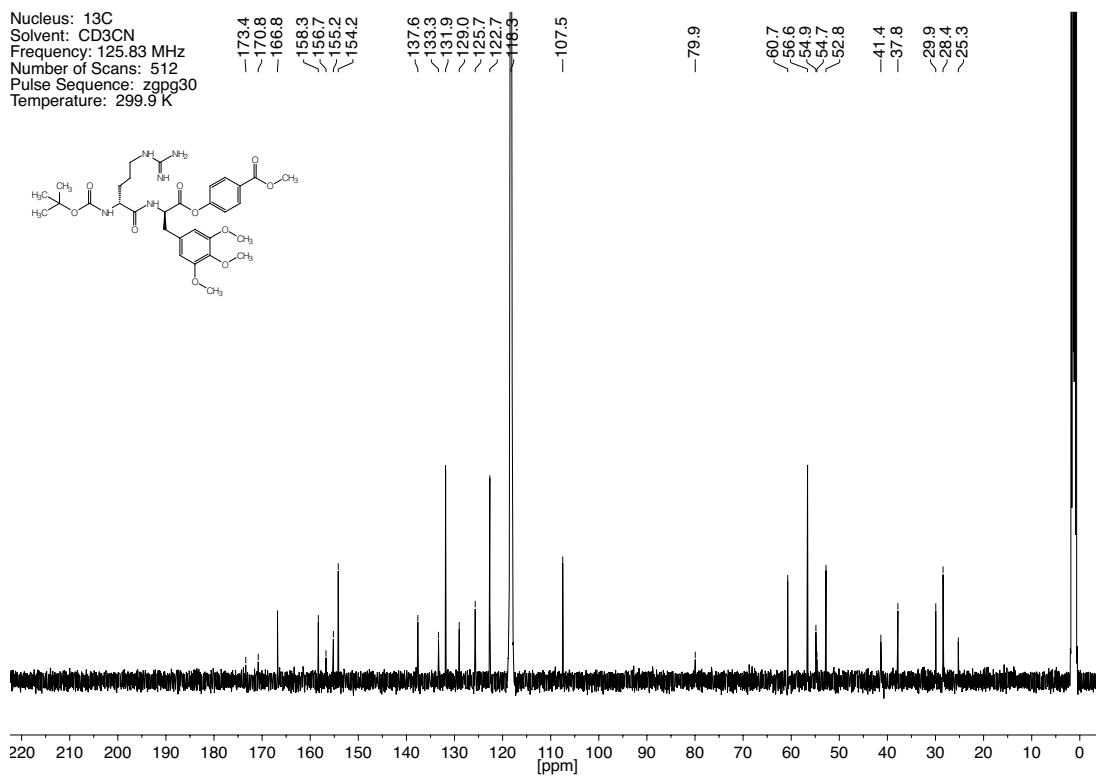


Figure 7.48. ^1H - and ^{13}C -NMR spectra of compound 48.

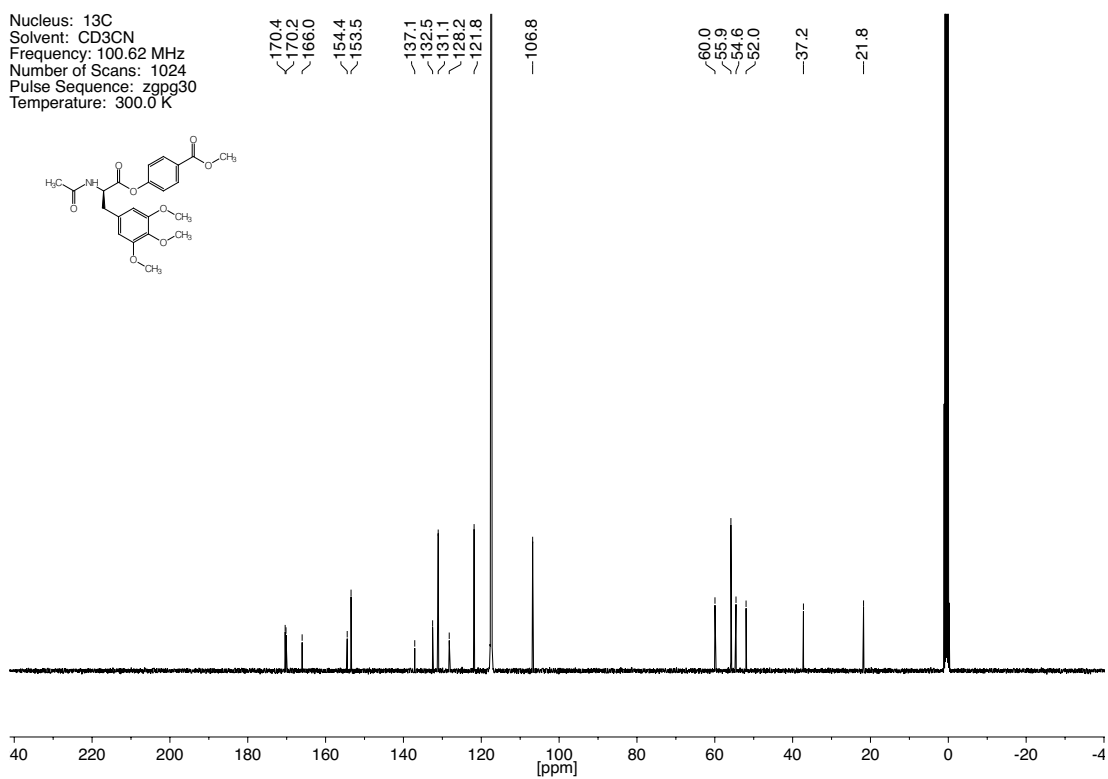
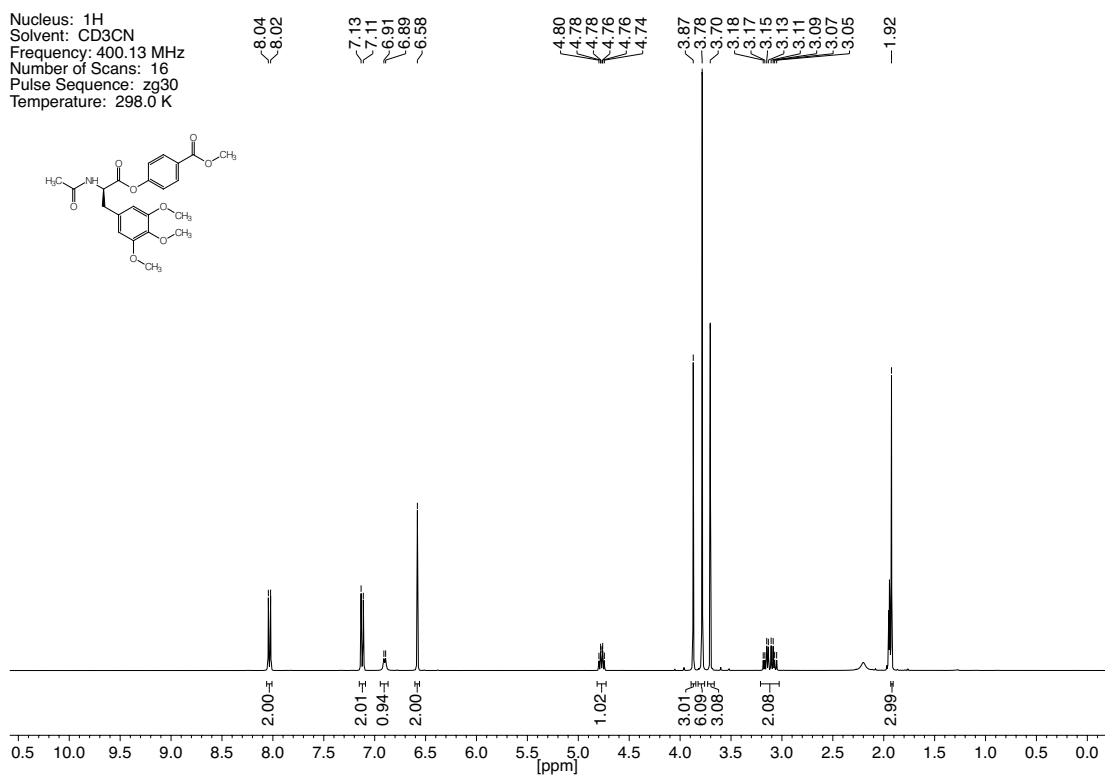
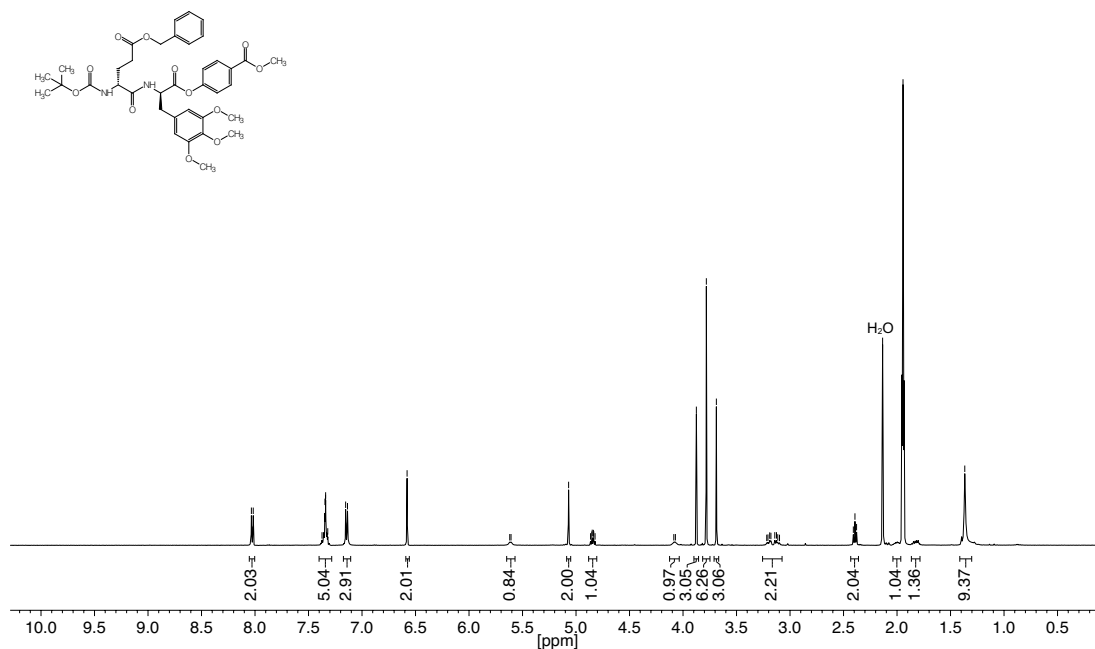


Figure 7.49. ^1H - and ^{13}C -NMR spectra of compound **49**.

Nucleus: ^1H
 Solvent: CD_3CN
 Frequency: 500.13 MHz
 Number of Scans: 32
 Pulse Sequence: zg30
 Temperature: 298.0 K



Nucleus: ^{13}C
 Solvent: CD_3CN
 Frequency: 125.83 MHz
 Number of Scans: 1024
 Pulse Sequence: zgpg30
 Temperature: 299.8 K

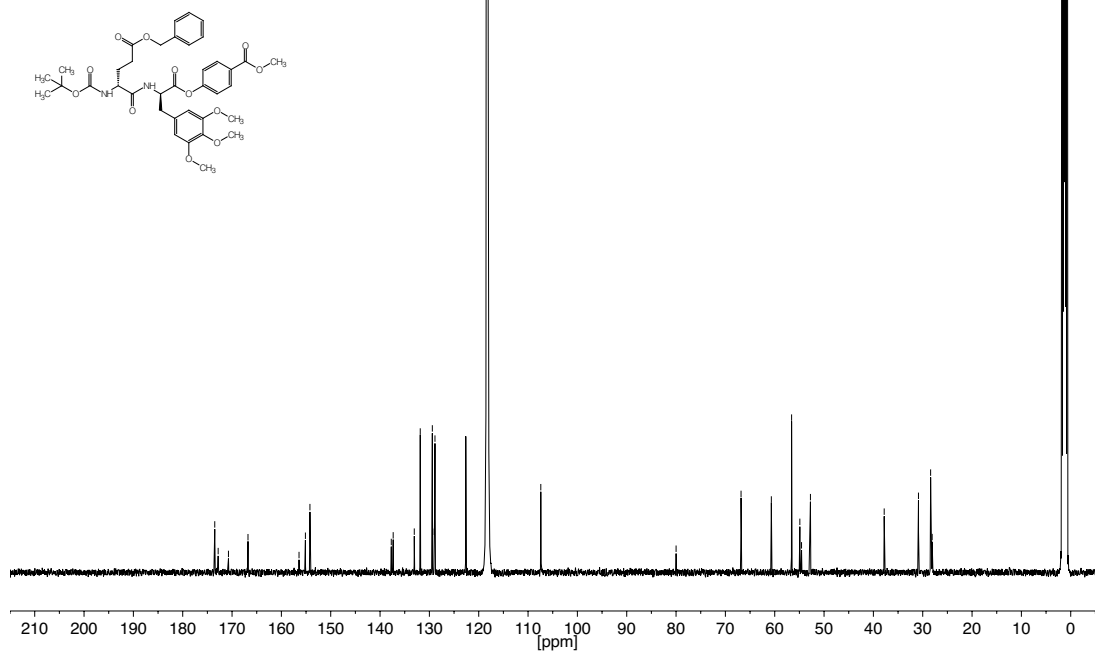


Figure 7.50. ^1H - and ^{13}C -NMR spectra of compound 50.

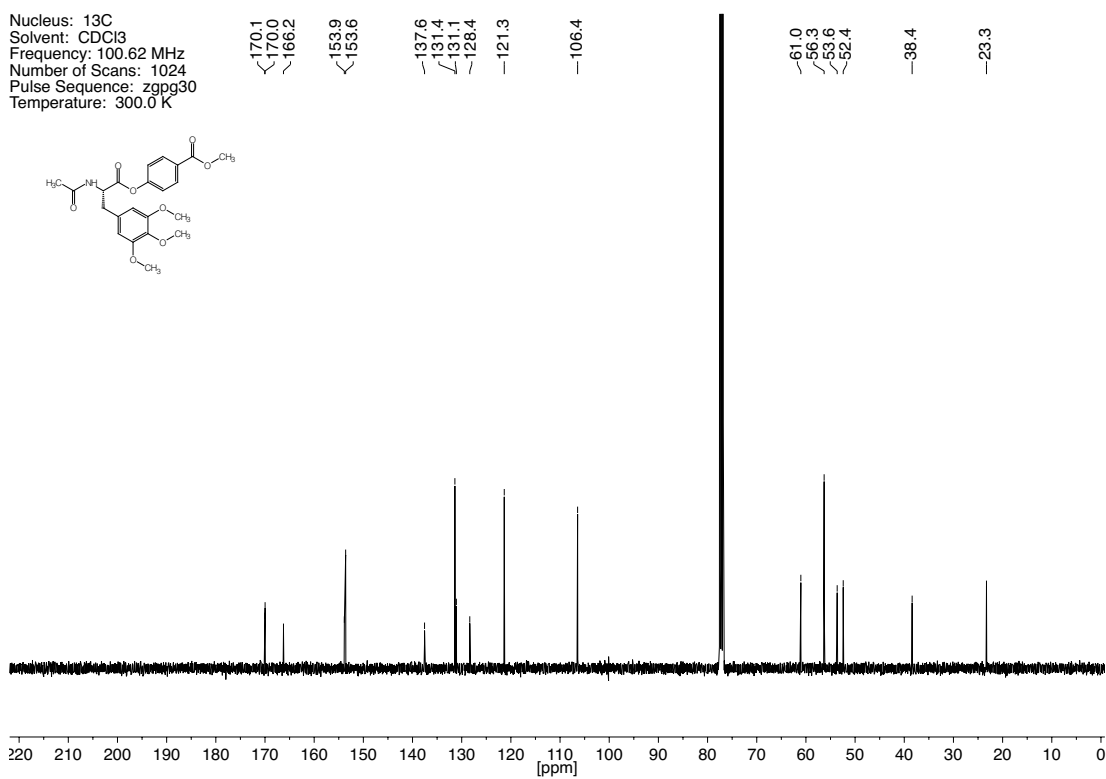
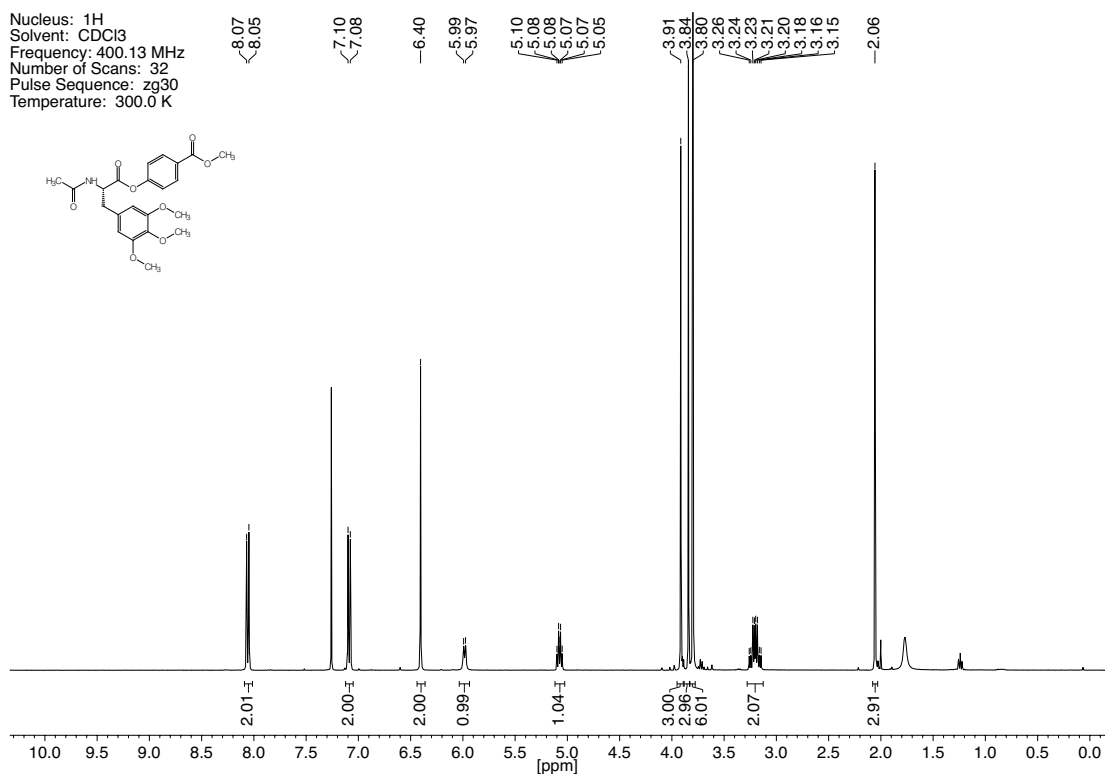


Figure 7.51. ^1H - and ^{13}C -NMR spectra of compound **51**.

Markus Lakemeyer

Lebenslauf

- 04.2014 - 11.2018 **Promotion**
bei Prof. Dr. Stephan A. Sieber
Lehrstuhl für Organische Chemie II
Technische Universität München
- 10.2011 – 02.2014 **Master of Science, Chemie**
Philipps-Universität Marburg
- 04.2013 – 11.2013 **Masterarbeit**
bei Prof. Dr. Matthew Bogyo
Department of Pathology, Stanford University (USA)
*Titel: Characterization of Fibroblast Activation Protein α
with activity-based probes*
- 10.2008 – 07.2011 **Bachelor of Science, Chemie**
Rheinisch-Westfälische Technische Hochschule Aachen
Bachelorarbeit bei Prof. Dr. Elmar Weinhold
*Titel: Synthese eines spaltbaren Linkers für die
Klickreaktion auf Oberflächen*
- 08.2007 – 04.2008 **Zivildienst**
Förderschule „Schule unterm Regenbogen“ in Nieheim-Eversen
- 08.1998 – 06.2007 **Städtisches Gymnasium, Steinheim (Westf.)**
Abitur
- 09.1994 – 07.1998 **Grundschule Sommersell, Nieheim**

DANKSAGUNG

Diese Promotion wäre ohne die Unterstützung vieler Menschen nicht möglich gewesen. Mein erster Dank gilt meinem Doktorvater Stephan Sieber. Vielen Dank für die spannenden Projekte und für die außerordentliche Betreuung.

Für die Bereitschaft, meine Promotion auch recht kurzfristig zu begutachten, gilt mein herzlicher Dank den weiteren Mitgliedern der Prüfungskommission, Michael Groll, Kathrin Lang, Markus Kaiser und Franz Hagn.

Im Laboralltag konnte ich auf den Rückhalt meiner Kolleginnen und Kollegen setzen. Vielen Dank an Katja Bäuml, Christina Brumer, Katja Gliesche, Mona Wolff und unsere Auszubildenden – sie haben stets dafür gesorgt, dass sowohl administrativ als auch im Laboralltag alles reibungslos läuft. Die Arbeitsatmosphäre in meinem Labor D habe ich immer sehr genossen. Dafür danke ich Volker Kirsch, Anja Fux, Ines Hübner, Robert Masics und meinen ehemaligen Kollegen Max Koch, Maria Dahmen und Johannes Lehmann. Ich hoffe, meinem Nachfolger Till Reinhardt wird es ebenso ergehen.

Für zahlreiche fruchtbare Diskussionen danke ich dem ClpP-Team: Mathias Hackl, Christian Fetzer, Patrick Allihn, Dóra Balogh und Matthias Stahl. Die beiden letztgenannten waren insbesondere immer dann zur Stelle, wenn ein Inhibitor plötzlich zum Aktivator wurde und Diskussionbedarf bestand. Des Weiteren danke ich für die gute Atmosphäre innerhalb und außerhalb des Labors meinen Kollegen Pavel Kielkowski, Annabelle Hoegl, Philipp Le, Martin Pfanzelt, Theresa Rauh, Jonas Drechsel, Carolin Gleißner, Barbara Hofbauer, Kyu Myung Lee, Angela Weigert Muñoz, Wolfgang Heydenreuter und Megan Wright.

Vielen Dank an Franziska Mandl, Christian Fetzer und Mathias Hackl für die Aufnahme in das aBACTER-Büro und zusammen mit Stephan Hacker und Lena Kunold für die fortwährende Unterstützung.

Meine Praktikantinnen und Praktikanten (Andreas Voll, Dominik Essig, Korbinian Köhler, Marcel Genge, Philip Böhm, Xu Zhou, Stefanie Ludwig, Waldemar Schmidt), sowie die von mir betreuten Master-Studenten (Ines Hübner, Johannes Rößler und Konstantin Eckel) haben großartige Arbeit geleistet und ich habe gerne mein Wissen mit ihnen geteilt. Viel Erfolg auf Eurem weiteren Weg!

Die einzelnen Kapitel dieser Arbeit sind in Zusammenarbeit mit begabten Kooperationspartnern entstanden. Besonders hervorheben möchte ich dabei Mathias Hackl, Axel Pahl, Katrin Lorenz-Baath, Thomas Menzel, Thomas Böttcher, Sonja Sievers und Herbert Waldmann für den High-Throughput Screen und das darauf basierende Phenylester-Projekt. Das Oxazol-Projekt entstand ebenfalls auf Grundlage des HTS in Kooperation u.a. mit Axel Pahl, Marie-Theres Vielberg, Michael Groll, Jan Vomacka, Vadim Korotkov und Christian Fetzer. Eva Bertosin und Hendrik Dietz konnten den neu identifizierten ClpXP-Komplex per Elektronenmikroskopie verifizieren, und Friederike Möller von Dynamic Biosensors ermöglichte die Messungen der ClpX-ClpP-Affinitäten. Der Review-Artikel entstand in erfolgreicher Zusammenarbeit mit Weining Zhao, Franziska Mandl und Peter Hammann.

Ich danke der Studienstiftung des deutschen Volkes für die finanzielle und ideelle Unterstützung während des Studiums und der Promotion, aber auch für die großartigen Menschen, die ich im Rahmen von Sommerakademien und Seminaren kennenlernen konnte.

Wichtige Freunde außerhalb des Labors haben mich auf meinem bisherigen Weg begleitet und unterstützt. Insbesondere zu nennen sind hierbei Ketii Piradashvili, Moriz Habigt, Lena Unterberg, David Murphy, Katharina Väh, Moritz Waltenberger, Valentina Goldmann, Katharina Löffler, Christian „Grischdl“ Wiedermann, Sarah-Maria Hartmann und Peter Baumann.

Zuletzt möchte ich mich zutiefst bei meiner Familie für den Rückhalt während des Studiums und der Promotion bedanken. Ihr habt mich immer bedingungslos unterstützt – auch, wenn zum Beispiel mal wieder ein Umzug quer durch Deutschland anstand.

Herzlichen Dank Euch allen!